1980

Effects of reduced inertia on the transient stability of a power system

Siwanan Na Nakorn
Iowa State University

INFORMATION TO USERS

This was produced from a copy of a document sent to us for microfilming. While the most advanced technological means to photograph and reproduce this document have been used, the quality is heavily dependent upon the quality of the material submitted.

The following explanation of techniques is provided to help you understand markings or notations which may appear on this reproduction.

1. The sign or "target" for pages apparently lacking from the document photographed is "Missing Page(s)". If it was possible to obtain the missing page(s) or section, they are spliced into the film along with adjacent pages. This may have necessitated cutting through an image and duplicating adjacent pages to assure you of complete continuity.

2. When an image on the film is obliterated with a round black mark it is an indication that the film inspector noticed either blurred copy because of movement during exposure, or duplicate copy. Unless we meant to delete copyrighted materials that should not have been filmed, you will find a good image of the page in the adjacent frame.

3. When a map, drawing or chart, etc., is part of the material being photographed the photographer has followed a definite method in "sectioning" the material. It is customary to begin filming at the upper left hand corner of a large sheet and to continue from left to right in equal sections with small overlaps. If necessary, sectioning is continued again—beginning below the first row and continuing on until complete.

4. For any illustrations that cannot be reproduced satisfactorily by xerography, photographic prints can be purchased at additional cost and tipped into your xerographic copy. Requests can be made to our Dissertations Customer Services Department.

5. Some pages in any document may have indistinct print. In all cases we have filmed the best available copy.

University
Microfilms
International

300 N. ZEEB ROAD, ANN ARBOR, MI 48106
18 BEDFORD ROW, LONDON WC1R 4EJ, ENGLAND

NAKORN, SIWANAN NA

EFFECTS OF REDUCED INERTIA ON THE TRANSIENT STABILITY OF A POWER SYSTEM

Iowa State University PH.D. 1980

Effects of reduced inertia on the transient stability of a power system

by

Siwanan Na Nakorn

A Dissertation Submitted to the
Graduate Faculty in Partial Fulfillment of the
Requirements for the Degree of
DOCTOR OF PHILOSOPHY

Major: Electrical Engineering

Approved:

Signature was redacted for privacy.

In Charge of Major Work

Signature was redacted for privacy.

For the Major Department

Signature was redacted for privacy.

For the Graduate College

Iowa State University
Ames, Iowa

1980

TABLE OF CONTENTS

LIST OF FIGURES

LIST OF TABLES

LIST OF SYMBOLS AND DEFINITIONS

$\bar{A}$	Characteristic matrix
d	Subscript, denoting d-axis component of a variable
$\frac{d}{dt}$	Time derivative operator
Δ	Subscript, denoting incremental value of a variable
$\bar{\delta}$	Inertial center of the machines in the existing system
δ_i	Torque angle of machine i, indicates the position of the quadrature axis with respect to a synchronous frame
E_i	Voltage behind transient reactance of machine i
$\bar{E}'$	Voltage behind equivalent transient reactance of the classical model of an induction machine
H_i	Inertia constant of machine i
$\bar{H}$	Inertia constant of the existing system
$\bar{I}$	Identity matrix
k	Subscript, denoting remote generator
λ	Eigenvalue
$\bar{\mu}$	Eigenvector
ω_i	Angular speed deviation of machine i from synchronous speed
ω_R	Synchronous speed (377 radian/second)
P_{ei}	Electrical power of machine i
P_{mi}	Mechanical power of machine i
q	Subscript, denoting q-axis component of a variable

r_1	Stator resistance
r_2	Rotor resistance
S	Per unit slip
V	Terminal voltage
X_1	Stator reactance
X_2	Rotor reactance @ 60 Hz
X_m	Magnetizing reactance
X'	Equivalent transient reactance of an induction machine
X'_d	d-axis transient reactance of a synchronous machine
$Y_{ii}\underline{/\theta_{ii}}$	Driving point admittance at node i
$Y_{ij}\underline{/\theta_{ij}}$	Transfer admittance between nodes i and j

I. INTRODUCTION

A. Purpose

Due to the scarceness and rapidly rising price of conventional fossil fuels, considerable attention is currently being given to the development of small hydro sites. It is often suggested that a large number of these sites, either the ones that can be newly developed or the ones that can be improved upon, exist in the western, northeastern (New England), and southern part of the United States, and that these sites can be developed economically [1-5]. It is also assumed that the electric power generated at these sites will be delivered to existing power networks. In addition, induction generation is sometimes suggested for these sites [3-5].

If low-head hydro sites are developed in large numbers, substantial low inertia generation in remote locations will be connected to existing power networks. Planning engineers have expressed some concern as to the possible adverse effects this may cause to the power system dynamic performance. The effect that this low inertia may have on the transient stability of the generators of the existing system as well as the remote generation itself is the focus of the investigation reported upon in this study.

The remote generation, representing low-head hydro units, can be synchronous, induction, or a combination of both types. The study was conducted on a variety of system configurations and conditions.

B. Scope of the Work

The objective of this research is to investigate the effect of the inertia of a remote generation on the transient stability of an existing power network, to which it is connected, as well as on the transient stability of the remote generation itself.

For this study, a simple three-generator power system is selected as the existing system. The remote generation, represented by a fourth generator, is connected to the existing system by a suitable double-circuit transmission line. This remote generation is to have unusually low inertia, characteristic of low-head hydro generators. The four-generator network comprises the study system.

First swing transient stability studies are made on the study system. The same disturbance is used for analysis in all the studies, namely, a three-phase fault cleared at 6 cycles by removing the faulted line. About 150 studies are selected for detailed analysis. The studies cover a variety of system configurations and conditions concerning:

- the initial load flow (including load level),
- the connection of the remote generation to the existing system (point of connection, length of line),
- the location of the fault (inside the existing system, in the transmission line joining the remote generation to the existing power network),
- the type of remote generation (synchronous, induction, and combination of synchronous and induction),

- the inertia of the remote generator,
- the parameters of the remote generator (induction case only),
- the penetration level, i.e., the fraction of the existing system load supplied by the remote generation.

The results of the transient stability studies are subjected to detailed analysis, using a special computer program developed for this purpose. The influence of the above system parameters and conditions on the system transient behavior are examined. Conclusions are then drawn concerning the potential effect of substantial low-head hydro generation on the existing system as well as on the remote generation.

In addition to the transient stability analysis, and to gain insight into the inherent dynamic characteristic of the power system, eigenvalues and eigenvectors analysis using small perturbation technique on the selected power network is also conducted (this type of analysis is also known in the literature as normal mode and mode shape analysis). The range of parameters covered is similar to that of the transient stability studies, except that studies concerning induction generation are not included.

II. LITERATURE REVIEW

Since the energy crisis of 1973, a lot of attention has been given to the increased production of electric energy from hydro sources. About 15 percent of the nation's electric-generating capacity is hydro electric and about 40 percent of this hydro electric capacity is federally owned [1]. The majority of these hydro plants are of medium-head and high-head types. The capacity at some of these plants can be improved upon (up to 10 percent increase) by changing old turbine runners with the more efficient ones and by rewinding generators [1,2]. Even though this improvement is welcome, it does not change the level of electric energy production significantly.

One form of hydro electric generation that can add significantly to the electric energy production is the low-head type. Generally, the low-head hydro sites are limited to the ones having heads up to 50 feet and capacity less than 5,000 kW. According to the Federal Power Commission and the Corps of Engineers, there exists 305.5 million kW of undeveloped hydro capacity [3]. About one-third (105.5 million kW) of this undeveloped capacity belongs to sites having potential capacity more than 5,000 kW each. The remaining two-thirds (200 million kW) is of the low-head type.

About one-eighth (26.6 million kW) of the electrically undeveloped low-head capacity already exists at small, low-head dams all over the country with the majority of them located in the northeastern states. The federal government, through the Department of Energy, initiated a

low-head hydro electric program in May 1977. The goals of this program are to put 1.5 million kW on line by 1985, another 20 million kW by 2000 and another 50 million kW by 2020 [3]. The escalating price and the uncertainty of supply of conventional fossil fuels made this form of electricity generation economically competitive. It is also non-depletable, pollution free, and environmentally acceptable.

The existing technology in low-head hydro generation is to use a tube-turbine or bulb-turbine as a prime mover and the generator can be either synchronous or [illegible]duction [3-5]. Even though bulb-turbines can be superior to the other types of turbines in terms of efficiency and economics due to its compactness, self-containing, and operationally-flexible installation, there are still some limitations to its use. One disadvantage is that its inertia is less than that [illegible] types including vertical-shaft Kaplan turbines, so that its use is limited to systems where there are other power sources available to maintain an electrically stable system.

Historically, the turbine-generator units in low-head installations have had low inertia constants (H). Most of the existing low-head units, operated by the U.S. Bureau of Reclamation, have inertia constants of 1 second (MWS/MVA) or less on machine rating base.

Investigations concerning the effect of synchronous machines' inertia on the transient stability of a power system have appeared in the literature in the past. The results of these investigations which are relevant to this research topic are summarized below.

Due to advances in metallurgy, generator cooling methods, and insulation systems, the trends in designing steam turbine-generator units have continually shown an increase in power output per pound of material as well as per physical dimensions. Two significant parameters are adversely affected by these trends, namely, the direct axis transient reactance (X_d') which increases, and the inertia constant "H" which decreases. According to the authors of references [6,7], these trends result in lower transient stability limits, as evidenced by the decrease in critical fault clearing times by 2-3 cycles. They maintain that the shift in the two parameters will be significant enough to require considerable improvements in relay protection, higher response excitation, improved turbine valve control, and other changes.

The trends for hydro generator units tend to be opposite to those of steam units, however. As hydro machines with larger MVA ratings and higher speeds are undertaken, their direct axis transient reactance (X_d') values will decrease and their inertia constant "H" will increase [8].

Basu and Nanda [9] investigated a two-machine power system, one of them being a remote hydro unit. They reported that if the ratio of the inertia constants of the remote machine to the existing machine is much different from unity, the response, due to disturbance, will be more oscillatory and will require longer settling time than when the inertia ratio is close to unity.

Most of the transient stability studies conducted so far treated the energy stored in the rotating masses per unit power (H) as a

constant, rather than as a function of speed. According to reference [10] this can lead to optimistic results.

Many investigators [11-13] reported on the means to identify groups of machines that tend to swing together following a disturbance. Once these groups are identified, equivalent machines can be constructed. To save computing time and cost, the machines remote from the disturbance need not be represented in detail. In addition, each coherent group of machines is represented by an equivalent machine. References [14,15] propose means of constructing equivalents to represent a power area.

Another important area in the study of power system dynamic performance is power system damping. Reference [16] suggested different methods of power system damping. Reference [17] reports that even though the general practice is to distribute damping among several machines, the optimum distribution would be to place all of the damping in the machine with smaller inertia. This is especially true if the inertia of the receiving end source is large compared with that of the remote generation, damping of the remote generation will be of prime importance.

E. W. Kimbark, in the discussion in reference [16], suggested that although there are several sources of positive damping in a power system, there are also sources of negative damping, notably voltage-regulating and speed-governing systems. Ordinarily the inherent positive damping predominates, although in some unusual circumstances, the net damping is negative.

The conventional method of studying transient stability, assuming constant voltage behind transient reactance for each generator (classical representation), neglects damping. In an undamped two-machine system, the amplitudes of successive swings remain approximately constant. In a system of three or more machines this is no longer so, and there is a possibility of losing synchronism on the second swing or even the third. With adequate damping, this is very unlikely, and the first swing criterion may be applied with confidence.

The influence of generator model complexity on the accuracy of stability study results varies with many factors. The dynamic behavior of a real generator varies in a nonlinear way with the electrical load on the generator; therefore, a model chosen to represent the generator must be accurate over a wide range of operating conditions [18]. However, if we are only interested in the qualitative assessment of the system's first swing transient, then the classical model representations for all of the synchronous machines are quite accurate [19,20].

A real generator's dynamic performance also varies with the transmission system to which it is connected and also with the electrical proximity between it and others of comparable size in the system. If it is closely coupled to the other generators of near equal size, its observed dynamic behavior, when subjected to a test disturbance, will be different from its behavior when electrically remote from other generators [18]. The effect of inertia on the coupling of generators of near equal size will also be observed in this research project.

Many investigators have reported on the use of induction generators in low-head hydro generation [3-5]. This is due to its ruggedness and simplicity, which contribute to the low operating and maintenance costs. Unlike the synchronous generator, the induction generator does not develop continuous current at its short circuited terminals, since the induction generator loses its excitation at short circuit. However, an induction generator develops an instantaneous short circuit current which decays rapidly [21,22]. The effect that this characteristic may have on the dynamic performance of the power system will also be observed in this research project.

Linearized analysis has been used as a means of gaining insight into the dynamic behavior of a power system. In the literature, sometimes it is known as normal mode and mode shape analysis. This is the study of the eigenvalues and eigenvectors of a power system using small perturbation techniques. Byerly et al. [23] reported on such a study. When classical representations are used, a power system of n generators has (n-1) normal modes of oscillation (natural frequencies). The frequencies of oscillation are primarily determined by generator inertias, generation and network reactances, and average angular differences between generators. In the interconnected power network of North America, interarea inertial modes of oscillation fall in the range of 0.2 - 0.5 Hz. These modes are often poorly damped [23]. Frequencies of oscillation of individual machines are usually in the range of 1 - 2 Hz. The influence of low inertia of the remote, low-head, hydro generation on the power system's modes of oscillation will be investigated in this research project.

III. STABILITY ANALYSIS

A. The Power System Investigated

1. Existing system

The existing power system used in this study is the nine-bus, three-generator, and three-load system shown in Figure 1 (known in the literature as the WSCC test system) [19]. It has been modified from the original WSCC system to avoid excessive var situation by reducing the voltage level from 230 KV to 161 KV. The capacity of the existing generation is 520 MW and the base, or reference, case used is one with a total load of 315 MW. Under heavy load condition, the total load of the system is 630 MW. Generator data for this system are given in Table 1.

Table 1. Generator data

Generator	1	2	3
Rated MVA	247.5	192.0	128.0
KV	16.5	18.0	13.8
P.F.	1.0	0.85	0.85
Type	hydro	steam	steam
Speed	180 r/min	3600 r/min	3600 r/min
X_d', pu [a]	0.0608	0.1198	0.1813
τ_{do}, S	8.96	6.00	5.89
H, S [a]	23.6	6.40	3.01

[a] On 100 MVA base.

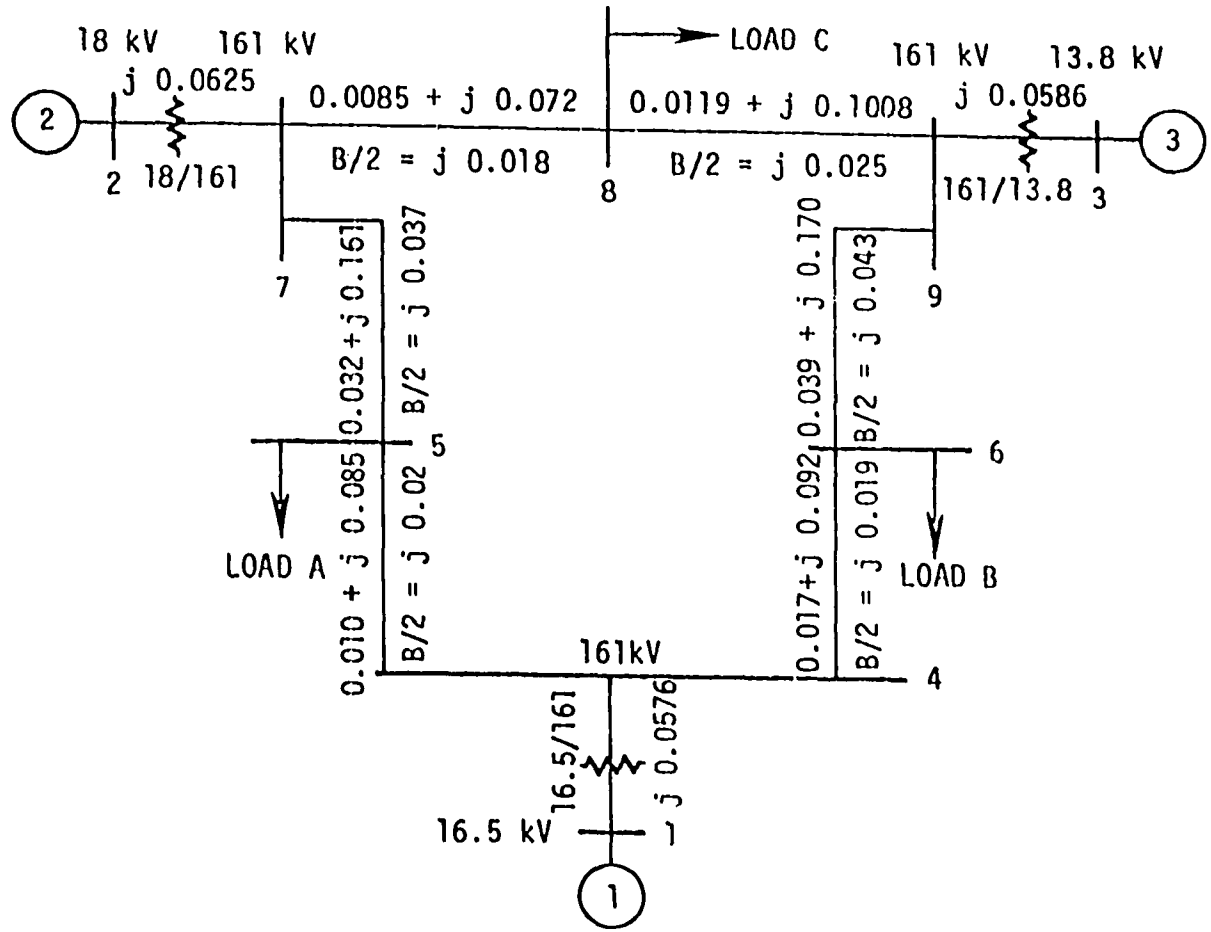

Figure 1. Nine bus system impedance diagram. All impedances in pu on 100 MVA base.

The base case (normal) loads are:

Load A = 125 MW, 50 MVAR

Load B = 90 MW, 30 MVAR

Load C = 100 MW, 35 MVAR

Under heavy load conditions, the three loads are given by:

Load A = 200 MW, 80 MVAR

Load B = 230 MW, 77 MVAR

Load C = 200 MW, 70 MVAR

2. Remote generation

The remote generation is connected to the nine-bus system by a double circuit 161 kV transmission line to one of the load buses (bus 6 or bus 8), forming a four-generator, eleven-bus system. This transmission line is either 40 miles long (short line case) or 120 miles long (long line case). Two connections are used as shown in Figures 2 and 3 for bus 6 and 8 respectively. This basic plan is changed only to accommodate the needs for the mix of induction and synchronous generation at the remote location as shown in Figure 4.

3. Choice of inertia for remote generation

Generator No. 2 of the existing system, which is rated at 192 MVA, has an inertial stored energy, at rated speed, of 640 MW.S. This corresponds to an inertia constant H = 3.33 S on the machine rating base, and 6.40 S on the system base of 100 MVA used in the study. This value of inertia constant is reasonable for a fossil fuel generator of this size, but is somewhat large for a hydro machine.

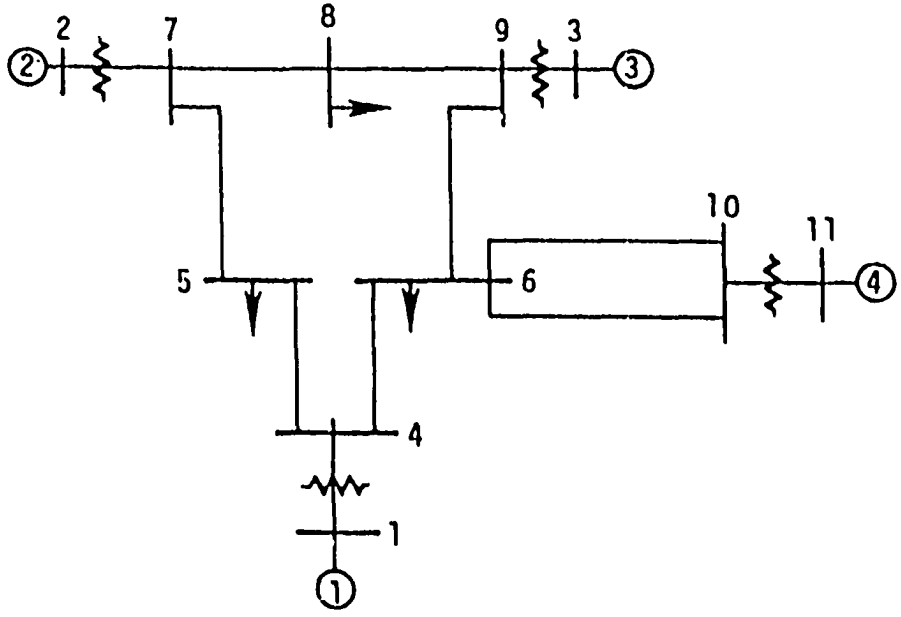

Figure 2. Four-generator system for bus-6 connection.

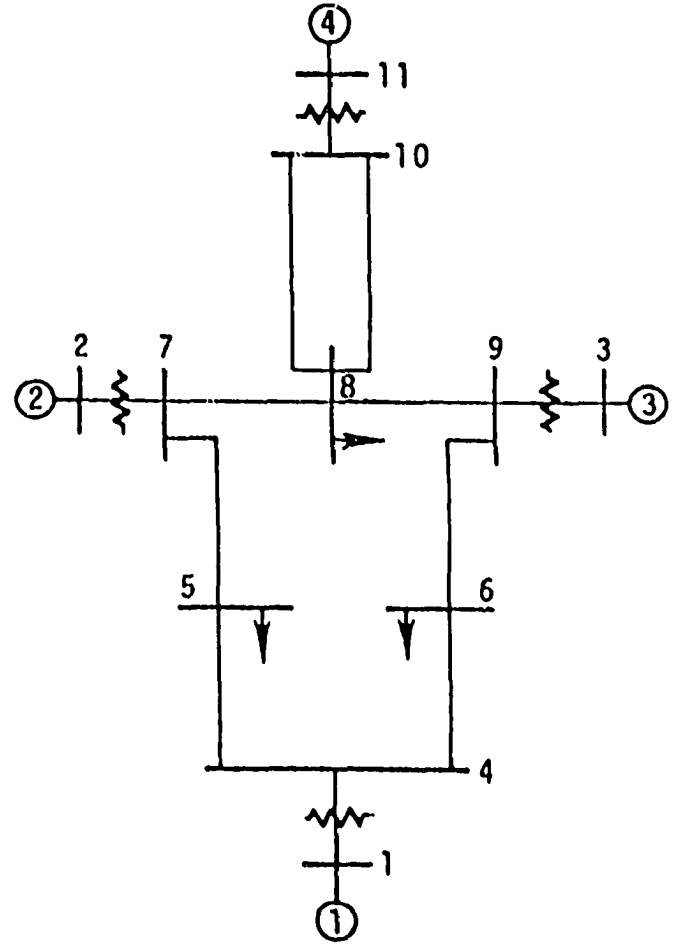

Figure 3. Four-generator system for bus-8 connection.

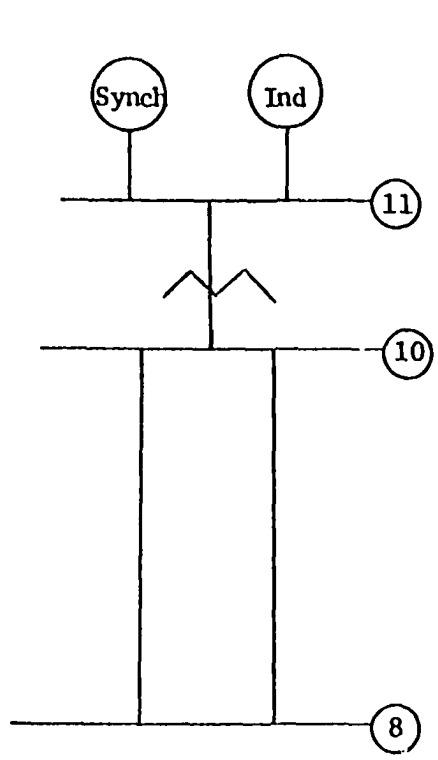

a) LF-5

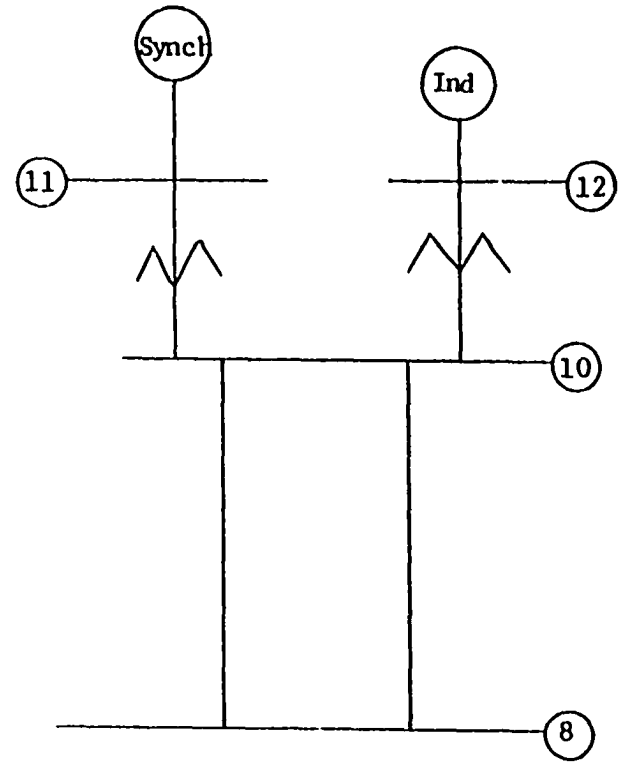

b) LF-10 → LF-16

Figure 4. Connections for synchronous and induction generation at remote locations.

When a synchronous generator is used at the remote location, the same value of H as that of generator No. 2 is assigned to it, i.e., H = 6.40 S on a 100 MVA base (or 3.33 S on machine rating base). This value of H is considered high and is designated as such in the study. This value is selected as a reference to which low inertias are compared. For the low inertia cases, at the remote synchronous machine, a value of H = 1.0 S is used (which corresponds to 0.52 S on the generator rating base). This value of H, while being on the low side, is not too unrealistic for small low-head hydro generators. In some studies, intermediate values of H (e.g., H = 4.0 S) are used.

When induction generation is used at the remote location, a 100 MVA generator is used with the normal load studies. A value of H = 1.0 S (on machine rating base) is assigned to it, which is consistent with the little data available to us on induction generators. For the heavy load conditions, two of those generators are assumed to be in use (even though they appear as one in the study), and thus the same value of H (on machine rating base) is assigned to them. For studies where H is different from the normal, H = 0.5 S (on machine rating base, for low H) and H = 2.0 S (on machine rating base, for high H) are used.

When a mix of synchronous and induction generation is used at the remote location, the induction machine is exactly as described above, i.e., normally rated 100 MVA, H = 1.0 S. For the synchronous machine, however, a machine similar to that of generator No. 3 is used. The latter is rated 128 MVA, with a value of H = 3.01 S on 100 MVA base (or 2.35 S on its own base). This value is not varied in this series of studies.

B. Transient Stability Analysis

1. Initial conditions

Before the transient stability studies are conducted, the initial system conditions are established using a load flow computer solution. The basic combinations of load level, line length, and bus connection are given in the load flow cases and are used for purely synchronous or purely induction remote generation cases. A summary of these cases is given in Table 2.

Table 2. Load flow cases for remote synchronous or induction generation

Case Number	Load Level[a]	Line Length[b]	Bus Connection	Remote Gen. Power MW	Penetration Level %
1	N	S	5	85	27
2	H	S	6	160	25
3	N	L	6	85	27
4	H	L	6	160	25
5	N	S	8	85	27
6	N	L	8	85	27
7	H	S	8	160	25
8	H	L	8	160	25
9	The same as LF-5 except for reduced voltage at bus 11				

[a] N = normal, H = heavy.

[b] S = short line, L = long line.

For the studies where the remote generation is made up of a mix of induction and synchronous generation, variations of load flow cases 5-8 are used to obtain the desired initial conditions. Seven additional load flow cases are needed for the range of induction generator parameters, and for the configuration and mix of the induction and synchronous generation. These are summarized in Table 3.

Table 3. Additional load flow cases for configuration of Figure 5(b)

Case Number	Load Level	Induction Gen.		Synchronous Gen.		Total Penetration Level &
		Bus Connection	Power MW	Bus Connection	Power MW	
10	N	12	42.5	11	42.5	27
11	H	12	160.0	11	0	25
12	H	12	80.0	11	80.0	25
13	N	12	85.0	11	0	27
14	N	12	42.5	11	42.5	27
15	H	12	160.0	11	0	25
16	H	12	80.0	11	80.0	25

Tc study the effect of varying the penetration level, namely, the fraction of the existing load supplied by the remote generation, additional load flow cases are needed. These are summarized in Table 4 and are for remote synchronous or induction generation.

Table 4. Load flow cases for remote synchronous or induction generation

Case Number	Load Level	Line Length	Bus Connection	Remote Gen. Power MW	Penetration Level %
17	N	S	8	40	13
18	N	L	8	40	13
19	N	S	8	120	38
20	N	L	8	120	38
21	H	S	8	120	19
22	H	L	8	120	19
23	H	S	8	120+120[a]	38
24	H	L	8	120+120	38
25	H	S	5	160	25
26	H	L	5	160	25

[a]Two identical generating units are assumed to be in use.

2. The model used

For transient stability analysis, a classical representation of synchronous generation is used throughout the project. This simple model is adequate for this study because only qualitative comparison is needed to conduct the desired investigation. The transient behavior of interest is the first swing inertial transient. The synchronous machine is thus represented by a constant voltage behind a transient reactance such as shown in Figure 5.

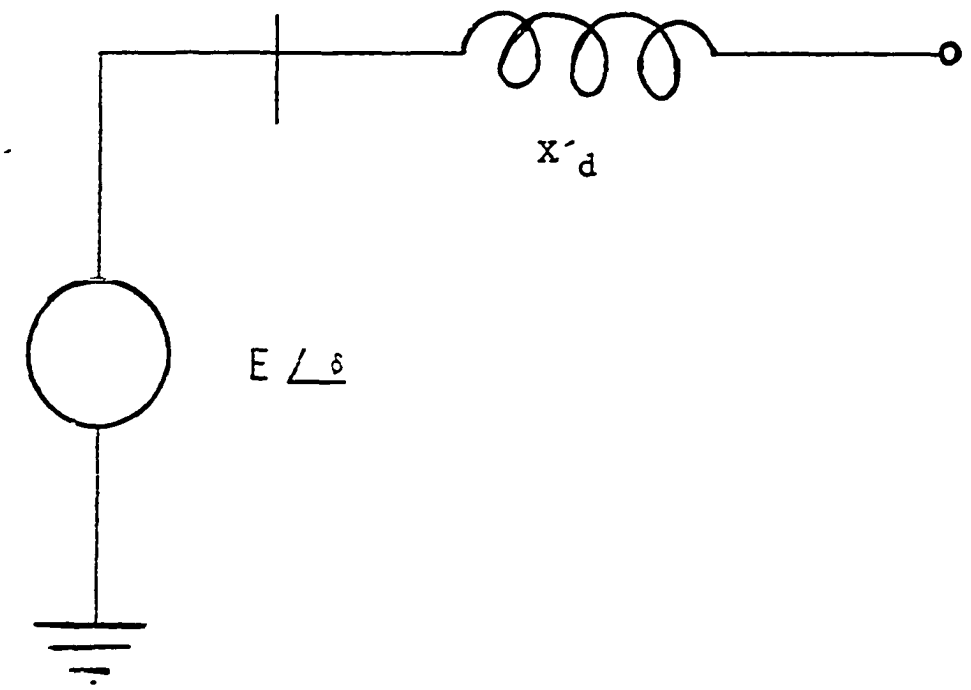

Figure 5. Synchronous machine model.

All the loads are represented by constant impedances and the transmission networks are represented by their steady-state, 60 Hz, parameters (R, X, and B).

The corresponding classical model for the induction generator is shown in Figure 6(a), where

r_1, r_2 = stator and rotor resistances (0.015 pu each)

X_1, X_2 = stator and 60 Hz rotor reactances (0.09 pu each)

X_m = magnetizing reactance (4.0 pu)

V = the terminal voltage

s = per unit (pu) slip

To incorporate the induction generator model in the stability program, the initial slip and terminal voltage used are calculated to

match the initial conditions of the network and the induction machine's initial torque and power. For convenience, the circuit of Figure 6(a) is converted to the equivalent circuit shown in Figure 6(b), where

$$X' = X_1 + \frac{X_2 X_m}{X_2 + X_m} \tag{3.1}$$

$$\bar{E}' = \bar{V} + \bar{I}_1 (V_1 + jX') \tag{3.2}$$

The induction machine is now represented by an equivalent circuit similar to that of the synchronous machine except that the voltage E' (behind the transient reactance X') is not constant.

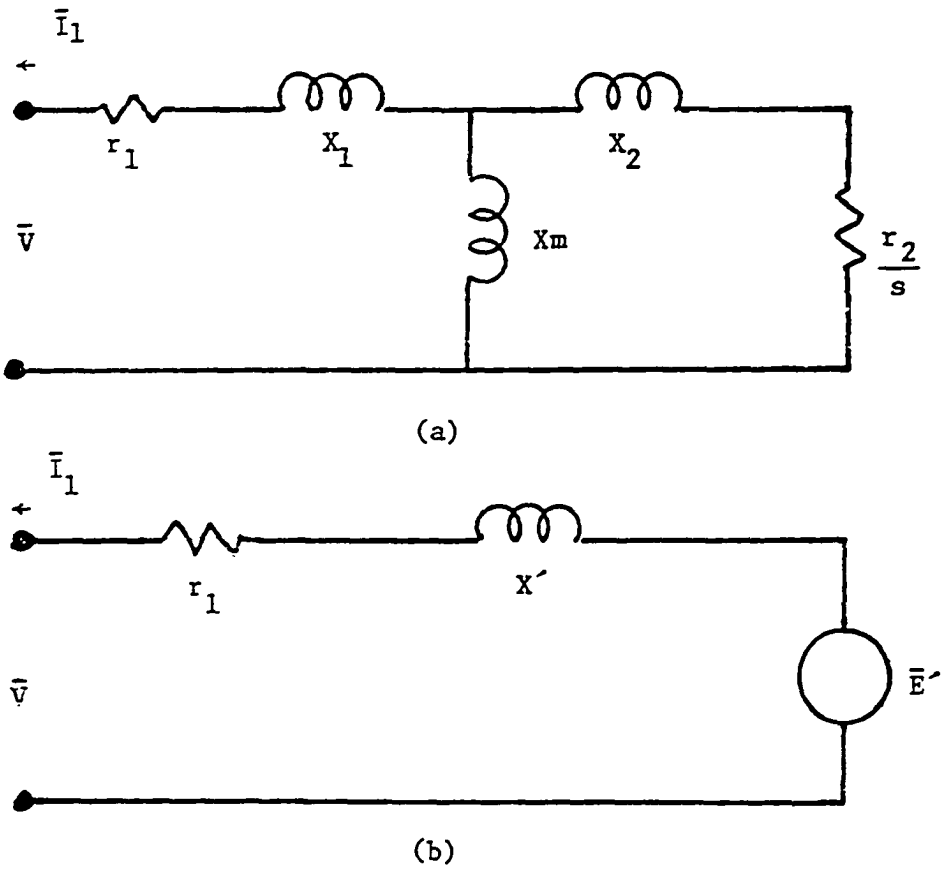

Figure 6. Induction machine model.

3. Power network disturbance

In all of the transient stability studies conducted, the same disturbance is used, namely, a three-phase fault cleared at six cycles by removing the faulted line with no reclosing.

4. Parameters under investigation

The effects of various parameters on the dynamic performance of the selected power network are observed. These parameters are:

- the inertia of the remote generation,
- the type of remote generation (synchronous, induction, and combination of synchronous and induction),
- the parameters of the remote generator (induction case only)
- the location of the fault (inside the existing power network or in the transmission line joining the remote generation to the existing power network),
- load level (normal or heavy),
- penetration level,
- the connection of the remote generation to the existing system (point of connection, length of line).

C. Normal Mode and Mode Shape Analysis

To gain better insight and understanding of the dynamic performance of the selected power network, a portion of this research is devoted to the study of the system's natural frequencies of oscillation, especially the dominant modes of oscillation. The technique used is the small

perturbation approached [19,23], from which the system's eigenvalues and eigenvectors, for a given operating condition, are computed.

The study of normal modes and mode shapes is the direct analysis of the system's inherent dynamic characteristic. It is a valuable aid to the interpretation of simulations, giving valuable insight as to the origin of the phenomena observed.

This portion of the study will cover only the remote synchronous generation. The parameters under investigation are the same as those covered in part B except that the cases concerning remote induction generation are omitted.

IV. MATHEMATICAL MODELS

A. Transient Stability Analysis

Since our interest is in the so-called "first swing inertial transient," a simple representation of the synchronous machines, i.e., constant voltage behind transient reactance, is used. The system configuration is schematically shown in Figure 7.

Figure 7 shows, in addition to the reference node 0, n-nodes representing the n-generators in the existing system, plus node k where the new generation is to be located. The network interconnects these

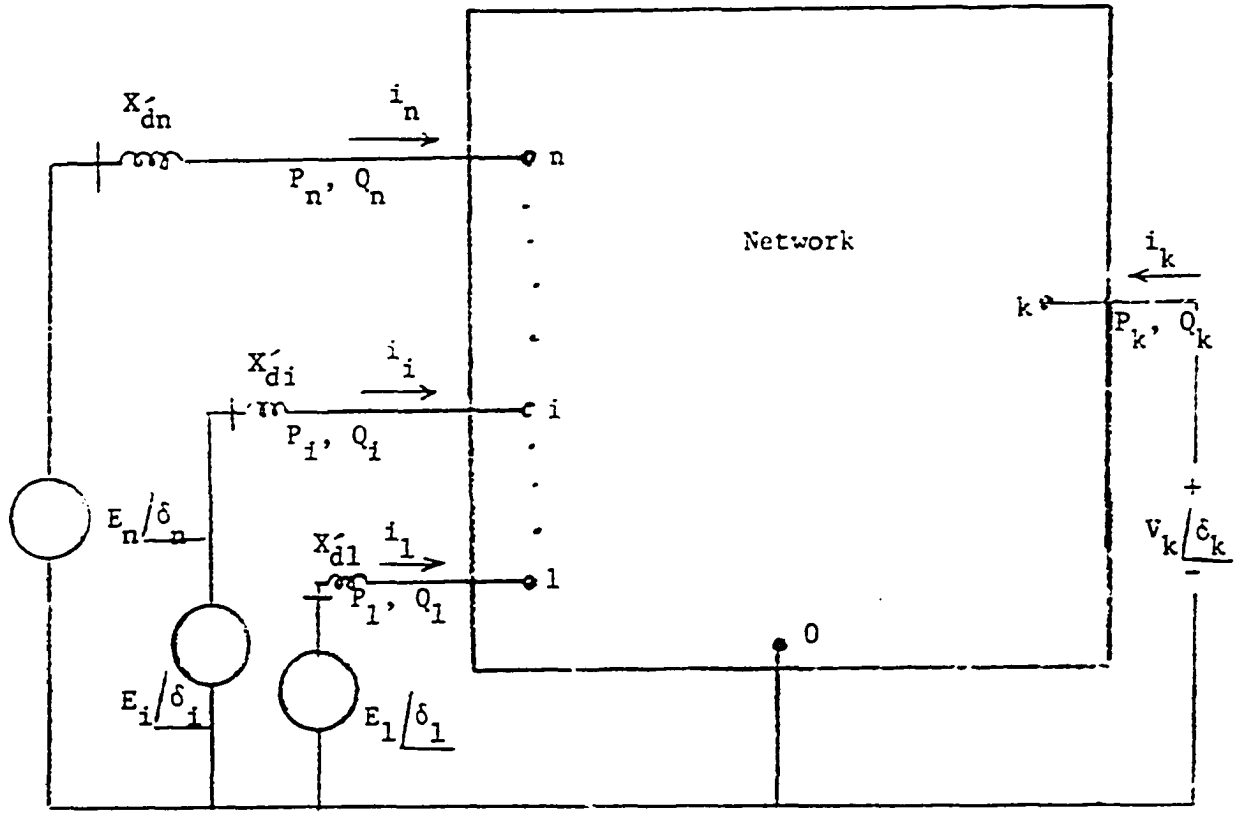

Figure 7. Schematic representation of the network.

nodes and includes the load buses. For generator i the terminal voltage is V_i, the current is I_i, the power and reactive power are P_i and Q_i, the direct axis transient reactance is X'_{di}, and the internal voltage behind the transient reactance is $E_i \angle \delta_i$.

An admittance matrix representing the whole system is formed for a particular operating condition and network configuration. All the nodes in Figure 7, except the generator internal nodes, are then eliminated and the Y-bus admittance matrix is formed.

1. The models

a. The synchronous machine The basic equation to be solved, for machine i, is of the form [19,24]:

$$\frac{2H_i}{\omega_R}\frac{d\omega_i}{dt} + d_i\omega_i = P_{mi} - P_{ei} \qquad (4.1)$$

where H_i = inertia constant in per unit MW.S/system MVA base

ω_i = angular speed deviation from synchronous speed in radian/second

ω_R = rated angular speed in radian/second

P_{mi}, P_{ei} = mechanical and electrical power in per unit

d_i = damping constant

In this study, the damping d_i is neglected and the mechanical power P_{mi} is assumed constant. The electrical power P_{ei} is calculated at a

given instant from the load flow solution of the network knowing the network constraints and the machine angle, δ_i. For the case of constant impedance loads, we can show that [19,24]

$$P_{ei} = E_i^2 G_{ii} + E_i E_k Y_{ik} \cos (\theta_{ik} - \delta_i + \delta_k) + \sum_{\substack{j=1 \\ j \neq i}}^{n} E_i E_j Y_{ij} \cos (\theta_{ij} - \delta_i + \delta_j) \qquad (4.2)$$

where $Y_{ii} \angle\theta_{ii} = G_{ii} + j B_{ii}$

= driving point admittance at node i

$Y_{ij} \angle\theta_{ij} = G_{ij} + j B_{ij}$

= transfer admittance between nodes i and j

For the induction generator, the equivalent circuit shown in Figure 6(b) is similar to the model used for synchronous machines, i.e., a voltage source behind a transient reactance. The only difference is that the voltage E′ behind the transient reactance X′ of the induction machine is not constant, i.e., it varies with the slip s. Since s varies with time, the value of E′ has to be computed and updated for every time step of calculation. Thus we can use the same form of equations that has been developed for the synchronous machine, i.e., equations (4.1) and (4.2).

2. Relative motion of new generation with respect to the existing system

In conventional stability studies, time solutions of the generator angles, δ_i, are obtained. This is augmented with the investigation of

the relative motion of the new generator with respect to the motion of the inertial center of the machines in the existing system ($\bar{\delta}$).

By examining this relative motion, greater insight can be obtained as to the effect of the various factors on the first swing stability.

The position of the inertial center $\bar{\delta}$ is given by

$$\bar{\delta} = \frac{1}{\bar{H}} \sum_{i=1}^{n} H_i \delta_i \tag{4.3}$$

where $\bar{H} = \sum_{i=1}^{n} H_i$

Using equation (4.2) in equation (4.1) with $d_i = 0$, $\omega_i = \frac{d\delta_i}{dt}$, $P_{ci} = P_{mi} - E_i^2 G_{ii}$, $A_{ij} = E_i E_j Y_{ij}$, $\delta_{ij} = \delta_i - \delta_j$, we have

$$\frac{2H_i}{\omega_R} \frac{d^2\delta_i}{dt^2} = P_{ci} - A_{ik} \cos(\theta_{ik} - \delta_{ik}) - \sum_{\substack{j=1 \\ j\neq i}}^{n} A_{ij} \cos(\theta_{ij} - \delta_{ij}) \tag{4.4}$$

By adding the set of equations (4.4) for i=1,2,...,n, and using equation (4.3), the equation of motion of the inertial center is obtained

$$\frac{2\bar{H}}{\omega_R} \frac{d^2\bar{\delta}}{dt^2} = \sum_{i=1}^{n} P_{ci} - \sum_{i=1}^{n} A_{ik} \cos(\theta_{ik} - \delta_{ik}) - \sum_{i=1}^{n} \sum_{\substack{j=1 \\ j\neq i}}^{n} A_{ij} \cos(\theta_{ij} - \delta_{ij}) \tag{4.5}$$

The equation of motion of the remote machine at node k can be written as

$$\frac{2H_k}{\omega_R}\frac{d^2\delta_k}{dt^2} = P_{ck} - \sum_{j=1}^{n} A_{kj} \cos(\theta_{kj} - \delta_{kj}) \tag{4.6}$$

By subtracting equation (4.5) from equation (4.6) and rearranging, we have

$$\begin{aligned}\frac{2}{\omega_R}\frac{d^2}{dt^2}(\delta_k - \bar{\delta}) = &\left(\frac{P_{ck}}{H_k} - \frac{1}{\bar{H}}\sum_{i=1}^{n} P_{ci}\right) - \frac{1}{H_k}\sum_{j=1}^{n} A_{kj}\cos(\theta_{kj} - \delta_{kj}) \\ &+ \frac{1}{\bar{H}}\sum_{j=1}^{n} A_{jk}\cos(\theta_{jk} - \delta_{jk}) \\ &+ \frac{1}{\bar{H}}\sum_{i=1}^{n}\sum_{\substack{j=1 \\ j\neq i}}^{n} A_{ij}\cos(\theta_{ij} - \delta_{ij})\end{aligned} \tag{4.7}$$

Since $A_{ij} = A_{ji}$, $\theta_{ij} = \theta_{ji}$, and $\delta_{ij} = -\delta_{ji}$, equation (4.7) can be rearranged as

$$\begin{aligned}\frac{2}{\omega_R}\frac{d^2}{dt^2}(\delta_k - \bar{\delta}) = &\left(\frac{P_{ck}}{H_k} - \frac{1}{\bar{H}}\sum_{i=1}^{n} P_{ci}\right) \\ &- \sum_{j=1}^{n}\left[\frac{1}{H_k}A_{kj}\cos(\theta_{kj} - \delta_{kj}) - \frac{1}{\bar{H}}A_{kj}\cos(\theta_{kj} + \delta_{kj})\right] \\ &+ \frac{1}{\bar{H}}\sum_{i=1}^{n}\sum_{\substack{j=1 \\ j\neq i}}^{n} A_{ij}(\cos\theta_{ij}\cos\delta_{ij} + \sin\theta_{ij}\sin\delta_{ij})\end{aligned} \tag{4.8}$$

For any square, symmetric matrix having dimensions $(n \times n)$, $\sum_{i=1}^{n}\sum_{\substack{j=1 \\ j\neq i}}^{n}$ is the sum of the off-diagonal elements and the subscripts i and j

of these elements are reversed in values, i.e., A_{ij} vs. A_{ji}, therefore

$$
\begin{aligned}
& A_{ij} (\cos \theta_{ij} \cos \delta_{ij} + \sin \theta_{ij} \sin \delta_{ij}) \\
& + A_{ji} (\cos \theta_{ji} \cos \delta_{ji} + \sin \theta_{ji} \sin \delta_{ji}) \\
& = A_{ij} (\cos \theta_{ij} \cos \delta_{ij} + \sin \theta_{ij} \sin \delta_{ij}) \\
& + A_{ij} (\cos \theta_{ij} \cos \delta_{ij} - \sin \theta_{ij} \sin \delta_{ij}) \\
& = 2 A_{ij} \cos \theta_{ij} \cos \delta_{ij} \\
& = 2 \hat{A}_{ij} \cos \delta_{ij}
\end{aligned}
$$

where $\hat{A}_{ij} = A_{ij} \cos \theta_{ij}$

Therefore

$$
\frac{1}{\bar{H}} \sum_{i=1}^{n} \sum_{\substack{j=1 \\ j \neq i}}^{n} A_{ij} \cos (\theta_{ij} - \delta_{ij}) = \frac{1}{\bar{H}} \sum_{i=1}^{n-1} \sum_{j=i+1}^{n} 2 \hat{A}_{ij} \cos \delta_{ij} \qquad (4.9)
$$

The right hand side of equation (4.9) is the summation of the off-diagonal elements by row-order.

By using equation (4.9) in equation (4.8) we have

$$
\begin{aligned}
\frac{2}{\omega_R} \frac{d^2}{dt^2} (\delta_k - \bar{\delta}) = & \left(\frac{P_{ck}}{H_k} - \frac{1}{\bar{H}} P_{ci} \right) \\
& - \sum_{j=1}^{n} \left[\frac{1}{H_k} A_{kj} \cos (\theta_{kj} - \delta_{kj}) + \frac{1}{\bar{H}} A_{kj} \cos (\theta_{kj} + \delta_{kj}) \right] \\
& + \sum_{i=1}^{n-1} \sum_{j=i+1}^{n} \frac{2}{\bar{H}} \hat{A}_{ij} \cos \delta_{ij} \qquad (4.10)
\end{aligned}
$$

Examining the various terms in equation (4.10) we note that:

1. The last term in equation (4.10) represents the synchronizing forces among the machines in the existing system. Its size is indicative of the influence of the disturbance on these machines. The smaller the term, the more coherent the motion of this group of machines with respect to the motion of the remote machine.
2. The size of the swing $(\delta_k - \bar{\delta})$ is a better indication of the stability of the new generation, with respect to the existing system, for a given disturbance. The third term (involving A_{kj}) represents the synchronizing forces between the remote machine and the machines in the existing system. It is indicative of the interaction between the two groups of machines.
3. The various influences can be analyzed for different values of the parameters under investigation, i.e., H_k, load level, penetration level, etc.

We note that in both equations (4.5) and (4.10) there are terms indicative of the interaction between the new and the old generation; these have parameters with subscripts k,j or k,i. The terms with i,j subscripts, however, are indicative of the impact of the disturbance on the machines of the existing system.

If the remote generation consists of two generating units, such as the case of mixed synchronous and induction generation, we can write the equations of motion of the two machines as

$$\frac{2H_{k1}}{\omega_R}\frac{d^2\delta_{k1}}{dt^2} = P_{ck1} - A_{k1\,k2}\cos(\theta_{k1\,k2} - \delta_{k1\,k2}) - \sum_{j=1}^{n} A_{k1j}\cos(\theta_{k1j} - \delta_{k1j}) \qquad (4.11.a)$$

and

$$\frac{2H_{k2}}{\omega_R}\frac{d^2\delta_{k2}}{dt^2} = P_{ck2} - A_{k2\,k1}\cos(\theta_{k2\,k1} - \delta_{k2\,k1}) - \sum_{j=1}^{n} A_{k2j}\cos(\theta_{k2j} - \delta_{k2j}) \qquad (4.11.b)$$

From equation (4.5), the equation of motion of the inertial center can be written as

$$\frac{2\bar{H}}{\omega_R}\frac{d^2\bar{\delta}}{dt^2} = \sum_{i=1}^{n} P_{ci} - \sum_{i=1}^{n} A_{ik1}\cos(\theta_{ik1} - \delta_{ik1}) - \sum_{i=1}^{n} A_{ik2}\cos(\theta_{ik2} - \delta_{ik2}) - \sum_{i=1}^{n}\sum_{\substack{j=1 \\ j\neq i}}^{n} A_{ij}\cos(\theta_{ij} - \delta_{ij}) \qquad (4.12)$$

By subtracting equation (4.12) from equations (4.11.a) and (4.11.b) and rearranging, we can show that

$$\frac{2}{\omega_R}\frac{d^2}{dt^2}(\delta_{k1}-\bar{\delta}) = \left(\frac{P_{ck1}}{H_{k1}} - \frac{1}{\bar{H}}\sum_{i=1}^{n} P_{ci}\right)$$

$$- \sum_{j=1}^{n}\left[\frac{1}{H_{k1}} A_{k1j}\cos(\theta_{k1j}-\delta_{k1j}) - \frac{1}{\bar{H}} A_{k1j}\cos(\theta_{k1j}+\delta_{k1j})\right]$$

$$+ \frac{1}{\bar{H}}\sum_{i=1}^{n-1}\sum_{j=i+1}^{n} 2\hat{A}_{ij}\cos\delta_{ij}$$

$$- \frac{1}{H_{k1}} A_{k1\,k2}\cos(\theta_{k1\,k2}-\delta_{k1\,k2})$$

$$+ \frac{1}{\bar{H}}\sum_{i=1}^{n} A_{ik2}\cos(\theta_{ik2}-\delta_{ik2}) \qquad (4.13)$$

and

$$\frac{2}{\omega_R}\frac{d^2}{dt^2}(\delta_{k2}-\bar{\delta}) = \left(\frac{P_{ck2}}{H_{k2}} - \frac{1}{\bar{H}}\sum_{i=1}^{n} P_{ci}\right)$$

$$- \sum_{j=1}^{n}\left[\frac{1}{H_{k2}} A_{k2j}\cos(\theta_{k2j}-\delta_{k2j}) - \frac{1}{\bar{H}} A_{k2j}\cos(\theta_{k2j}+\delta_{k2j})\right]$$

$$+ \frac{1}{\bar{H}}\sum_{i=1}^{n-1}\sum_{j=i+1}^{n} 2\hat{A}_{ij}\cos\delta_{ij}$$

$$- \frac{1}{H_{k2}} A_{k2\,k1}\cos(\theta_{k2\,k1}-\delta_{k2\,k1})$$

$$+ \frac{1}{\bar{H}}\sum_{i=1}^{n} A_{ik1}\cos(\theta_{ik1}-\delta_{ik1}) \qquad (4.14)$$

B. Linearized Equations for Eigenvalue Analysis

The swing equation of machine i in an n-machine power system can be written as

$$\frac{2H_i}{\omega_R}\frac{d^2\delta_i}{dt^2} = P_{mi} - P_{ei} \tag{4.15}$$

$$= P_{mi} - E_i^2 Y_{ii} \cos\theta_{ii} - \sum_{\substack{j=1 \\ j\neq i}}^{n} E_i E_j Y_{ij} \cos(\theta_{ij} - \delta_{ij})$$

$$= P_{mi} - E_i^2 G_{ii} - \sum_{\substack{j=1 \\ j\neq i}}^{n} E_i E_j G_{ij} \cos\delta_{ij}$$

$$- \sum_{\substack{j=1 \\ j\neq i}}^{n} E_i E_j B_{ij} \sin\delta_{ij}$$

$$i,j=1,2,\ldots,n \tag{4.16}$$

where n is the total number of machines, including the remote machine.

If the system is subjected to a small perturbation, the generator rotor positions will be slightly displaced from their quiescent values. Denoting the quiescent rotor position by subscript o, and the change in that position by the subscript Δ, the new rotor angles are then given by

$$\delta_i = \delta_{io} + \delta_{i\Delta} \tag{4.17}$$

and

$$\delta_{ij} = (\delta_{io} - \delta_{jo}) + (\delta_{i\Delta} - \delta_{j\Delta}) \tag{4.18}$$

From equation (4.18), and using the approximations

$$\cos(\delta_{i\Delta} - \delta_{j\Delta}) \simeq 1 \tag{4.19}$$

and

$$\sin(\delta_{i\Delta} - \delta_{j\Delta}) \simeq (\delta_{i\Delta} - \delta_{j\Delta}) \tag{4.20}$$

we can show that

$$\cos \delta_{ij} \simeq \cos (\delta_{io} - \delta_{jo}) - (\delta_{i\Delta} - \delta_{j\Delta}) \sin (\delta_{io} - \delta_{jo}) \tag{4.21}$$

and

$$\sin \delta_{ij} \simeq \sin (\delta_{io} - \delta_{jo}) + (\delta_{i\Delta} - \delta_{j\Delta}) \cos (\delta_{io} - \delta_{jo}) \tag{4.22}$$

substituting equations (4.21) and (4.22) in equation (4.16), we get

$$\frac{2H_i}{\omega_R} \frac{d^2\delta_{i\Delta}}{dt^2} = P_{mi} - E_i^2 G_{ii}$$

$$- \sum_{\substack{j=1 \\ j\neq i}}^{n} E_i E_j G_{ij} \left[\cos (\delta_{io} - \delta_{jo}) - (\delta_{i\Delta} - \delta_{j\Delta}) \sin (\delta_{io} - \delta_{jo})\right]$$

$$- \sum_{\substack{j=1 \\ j\neq i}}^{n} E_i E_j B_{ij} \left[\sin (\delta_{io} - \delta_{jo}) + (\delta_{i\Delta} - \delta_{j\Delta}) \cos (\delta_{i_o} - \delta_{jo})\right]$$

$$i=1,2,\ldots,n \tag{4.23}$$

From steady-state condition,

$$P_{mi} - E_i^2 G_{ii} - \sum_{\substack{j=1 \\ j\neq i}}^{n} E_i E_j G_{ij} \cos (\delta_{io} - \delta_{jo})$$

$$- \sum_{\substack{j=1 \\ j\neq i}}^{n} E_i E_j B_{ij} \sin (\delta_{io} - \delta_{jo}) = 0 \tag{4.24}$$

Consequently equation (4.23) is simplified to

$$\frac{2H_i}{\omega_R}\frac{d^2\delta_{i\Delta}}{dt^2} = \sum_{\substack{j=1\\ j\neq i}}^{n} E_i E_j G_{ij} \sin(\delta_{io}-\delta_{jo})(\delta_{i\Delta}-\delta_{j\Delta})$$

$$- \sum_{\substack{j=1\\ j\neq i}}^{n} E_i E_j B_{ij} \cos(\delta_{io}-\delta_{jo})(\delta_{i\Delta}-\delta_{j\Delta})$$

$$i=1,2,\ldots,n \qquad (4.25)$$

Equation (4.25) can be rewritten as

$$\frac{2H_i}{\omega_R}\frac{d^2\delta_{i\Delta}}{dt^2} = \left[\sum_{\substack{j=1\\ j\neq i}}^{n} E_i E_j G_{ij} \sin(\delta_{io}-\delta_{jo}) - \sum_{\substack{j=1\\ j\neq i}}^{n} E_i E_j B_{ij} \cos(\delta_{io}-\delta_{jo})\right]\delta_{i\Delta}$$

$$- \sum_{\substack{j=1\\ j\neq i}}^{n} E_i E_j G_{ij} \sin(\delta_{io}-\delta_{jo})\delta_{j\Delta} + \sum_{\substack{j=1\\ j\neq i}}^{n} E_i E_j B_{ij} \cos(\delta_{io}-\delta_{jo})\delta_{j\Delta}$$

$$i=1,2,\ldots,n \qquad (4.26)$$

which can be written in matrix form as

$$\left\{\left[g_{ij}\right] + \left[b_{ij}\right]\right\}\left[\delta_{i\Delta}\right] = \left[\frac{2H_i}{\omega_R}\ddot{\delta}_{i\Delta}\right] \qquad (4.27)$$

where $[g_{ij}]$ = (n x n) matrix having elements g_{ij}

$$g_{ij} = -E_i E_j G_{ij} \sin(\delta_{io}-\delta_{jo}) \qquad (4.27.a)$$

$$g_{ii} = \sum_{\substack{j=1\\ j\neq i}}^{n} E_i E_j G_{ij} \sin(\delta_{io}-\delta_{jo}) = -\sum_{\substack{j=1\\ j\neq i}}^{n} g_{ij} \qquad (4.27.b)$$

$[\ b_{ij}]$ = (n x n) matrix having elements b_{ij}

$$b_{ij} = E_i E_j B_{ij} \cos (\delta_{io} - \delta_{jo}) \tag{4.27.c}$$

$$b_{ii} = - \sum_{\substack{j=1 \\ j \neq i}}^{n} E_i E_j B_{ij} \cos (\delta_{io} - \delta_{jo}) = - \sum_{\substack{j=1 \\ j \neq i}}^{n} b_{ij} \tag{4.27.d}$$

For the system without phase shifters,

$$G_{ij} = G_{ji}$$

and

$$B_{ij} = B_{ji}$$

Also $\sin (\delta_{io} - \delta_{jo}) = -\sin (\delta_{jo} - \delta_{ic})$

and

$$\cos (\delta_{io} - \delta_{jo}) = \cos (\delta_{jo} - \delta_{io})$$

Hence $g_{ij} = -g_{ji}$

and

$$b_{ij} = b_{ji} \tag{4.28}$$

It follows that $[g_{ij}]$ is a skew-symmetric matrix and $[b_{ij}]$ is a symmetric matrix. Since the conductance terms of a power system are usually small compared to the susceptance terms, $[g_{ij}]$ can be neglected, which simplifies the calculation considerably.

Equation (4.27) can be simplified to

$$[b_{ij}]\ [\delta_{i\Delta}] = \left[\frac{2H_i}{\omega_R}\ \ddot{\delta}_{i\Delta}\right] \tag{4.29}$$

Dividing each indivisual equation by the corresponding $\frac{2H_i}{\omega_R}$ gives

$$\bar{A}\,\bar{\delta}_\Delta = \ddot{\bar{\delta}}_\Delta \tag{4.30}$$

where

$$a_{ij} = \frac{\omega_R}{2H_i}\, b_{ij} \tag{4.30a}$$

Equation (4.30) is in the proper form of an eigenvalue problem. Now the calculation of normal modes and mode shapes can be expressed as an eigenvalue problem by using the technique described in references [19,23].

Let the incremental rotor angle oscillations be described by

$$\bar{\delta}_\Delta = \bar{\mu} \sin(\omega t) \tag{4.31}$$

where $\bar{\delta}$ and $\bar{\mu}$ are vectors of dimension n, then

$$\dot{\bar{\delta}}_\Delta = \bar{\mu}\,\omega \cos(\omega t) \tag{4.32}$$

and

$$\ddot{\bar{\delta}}_\Delta = -\bar{\mu}\,\omega^2 \sin(\omega t) \tag{4.33}$$

Substituting equations (4.31) and (4.33) in equation (4.30)

$$\bar{A}\,\bar{\mu} \sin(\omega t) = -\bar{\mu}\,\omega^2 \sin(\omega t)$$

or

$$(\bar{A} + \omega^2 \bar{I})\,\bar{\mu} \sin(\omega t) = 0 \tag{4.34}$$

where $\bar{I}$ is an (n x n) identity matrix.

If equation (4.34) is to be valid for all values of t, then

$$(\bar{A} + \omega^2 \bar{I})\ \bar{\mu} = 0 \tag{4.35}$$

must be satisfied.

If the eigenvalues λ_j and the eigenvectors $\bar{\mu}^j$ are found such that

$$(\bar{A} - \lambda_j \bar{I})\ \bar{\mu}^j = 0 \tag{4.36}$$

then the natural frequency of oscillations (normal modes) are given by

$$\omega_j = \sqrt{-\lambda_j} \tag{4.37}$$

The corresponding eigenvectors $\bar{\mu}^j$ indicate the relative amplitudes of the generator rotor oscillations at a given frequency (mode shape) as shown by equation (4.31) and they also indicate the relative velocity deviations as shown by equation (4.32).

The influences of different parameters on the normal modes and mode shapes will be investigated. The parameters under investigation will be similar to those used in the transient stability studies.

V. QUALITATIVE ANALYSIS OF TRANSIENT AND DYNAMIC SYSTEM BEHAVIOR

A. Transient Stability

1. Stability criteria

For the case of all synchronous machines, the stability of the generators is decided by examining their rotor angles, or the angles of their internal voltages. For stability, the angle between each pair of machines reaches a peak value during the transient and then decreases. If any of these angle differences increases indefinitely, the system, by definition, is unstable since at least one machine loses synchronism with the rest of the system.*

When there is an induction generator at the remote location, the stability concept is not applicable. However, it is easy to detect situations of "unfeasible" operation, when the machine slip increases indefinitely and the internal voltage "collapses." These situations will be called "unstable" for easy reference, even though the meaning of instability will be somewhat different from loss of synchronism.

2. Effect of disturbance on remote generation

The effect of disturbance on remote synchronous machines can be observed from the relative position of the rotor of the remote generator with respect to the positions of the rotors of the existing machines, namely, $(\delta_k - \delta_1)$, $(\delta_k - \delta_2)$, and $(\delta_k - \delta_3)$. The relative position and the

---

*In the transient stability program, the run is aborted if the angle exceeds a prescribed value.

relative acceleration of the rotor of the remote machine with respect to the inertial center of the existing machines, namely, $(\delta_k - \bar{\delta})$ and $(\ddot{\delta}_k - \ddot{\bar{\delta}})$, are also good indicators of the effect of disturbance on synchronous remote generation.

For the remote induction machine, the effect of disturbance can be observed from the slip and the internal voltage.

3. Effect of disturbance on existing machines

The terms that are indicative of the effect of disturbance on the existing machines are the motion of the inertial center ($\bar{\delta}$ and $\ddot{\bar{\delta}}$) and the synchronizing forces among the existing machines

$$\sum_{i=1}^{n} \sum_{\substack{j=1 \\ j \neq i}}^{n} A_{ij} \cos (\theta_{ij} - \delta_{ij})$$

4. Interaction between remote and existing generators

The terms that are indicative of the interaction between remote and existing generators are the synchronizing forces between the remote generator and the existing generators

$$\sum_{i}^{n} A_{ik} \cos (\theta_{ik} - \delta_{ik}).$$

By comparing these terms ($(\delta_k - \delta_i)$, $(\delta_k - \bar{\delta})$, $(\ddot{\delta}_k - \ddot{\bar{\delta}})$, $\bar{\delta}$, $\ddot{\bar{\delta}}$, A_{ij}, and A_{ik}) the effects of inertia of the remote generation, as well as other parameters, on the dynamic performance of the power system can be observed and summarized.

B. Tools of Analysis

1. Transient stability analysis

Two main computer programs are used for transient stability analysis: the "transient stability program" and the "stability analysis program." A brief description of the functions of these programs is given below.

a. Transient stability program The transient stability program is a modified version of the Philadelphia Electric Power System Stability Computer Program [25], available at the Iowa State University Power System Computer Service. For a given network configuration and parameters, initial operating conditions, and for a given disturbance, the program obtains a time solution of the generators' rotor positions, powers, voltages, etc., and flows in "monitored" lines. The program permits several models for the machines, loads, and control equipment (only the classical models are used for this project). It can also provide plots of selected quantities obtained in the solution.

b. Stability analysis program ("STANAL") The stability analysis program makes an analysis of the interaction between a selected group of generators (usually one or two remote machines), and the rest of the generators in the system (existing generators). The former group can be synchronous, induction, or both. The latter group is assumed to be made up on synchronous generators.

The Philadelphia Electric Transient Stability Program is modified to output the data required by the stability analysis program. These data include the system bus admittance matrix, machine parameters, and machine rotor angles at each time step.

The STANAL program performs the computer calculations specified by the equations in section A of Chapter IV. The results of these calculations are tabulated and plotted. The STANAL program accomplishes the following:

1. Formation of the system bus admittance matrix and reduction of the matrix to the internal generator nodes.
2. For each time step, calculation of:
   i. The inertial center of the "existing" system and the angle of each generator with respect to that inertial center (equation (4.3)).
   ii. The acceleration of the inertial center of the "existing" system and the relative acceleration of each generator with respect to the inertial center (equations (4.5), (4.10), (4.13), and (4.14)).
   iii. Each term of the previously mentioned equations separately, to show the effect of each term as it relates to the "new" generator.

2. Eigenvalue analysis

For the linearized analysis, a third computer program called "CTLMAT" is used. This program is available at the Iowa State University Power System Computer Service. It can perform several real matrix operations and it can accommodate a (30 x 30) matrix, having up to 900 elements. It is used in this research to find the eigenvalues and eigenvectors of the characteristic matrix $\bar{A}$ (equations (4.30) and (4.35)). The procedure is as follows.

The internal voltages E_i and E_j and the elements Y_{ij} and θ_{ij} of the reduced admittance matrix of the fault cleared network are obtained from the STANAL program, while the initial rotor angles δ_{io} and δ_{jo} are obtained from the transient stability program. These are used to calculate the elements a_{ij} of matrix $\bar{A}$.

$$a_{ij} = \frac{\omega_R}{2H_i} b_{ij}$$

$$= \frac{\omega_R}{2H_i} E_i E_j B_{ij} \cos (\delta_{io} - \delta_{jo})$$

$$= \frac{\omega_R}{2H_i} E_i E_j Y_{ij} \sin \theta_{ij} \cos (\delta_{io} - \delta_{jo})$$

After the matrix $\bar{A}$ is formed, the eigenvalues λ_i and the eigenvectors $\bar{\mu}_i$ are obtainable from the CTLMAT program.

A sample calculation of a_{ij} and the formation of matrix $\bar{A}$ is shown in Appendix A.

VI. TRANSIENT STABILITY ANALYSIS

A. Scope of the Analysis

Three series of studies were conducted, with each series devoted to one type of remote generation, i.e., synchronous, induction, or a mix of synchronous and induction generation. For each series, the system parameters were varied, and their effects on the system transient performance were studied.

The system parameters varied were:

- The existing network bus to which the remote generation is connected (this variation was used only for the synchronous generation case).
- The location of the fault: external to the existing network or inside it, and close to or far from the remote generation.
- The inertia of the remote generation.
- The system load level: normal or heavy.
- The penetration level, i.e., the ratio of the remote generation to the system load.
- The type of remote generation (synchronous, induction, and combination of synchronous and induction).
- The length of the transmission lines connecting the remote generation to the existing network.
- The parameters of the remote generation (this variation was used only in the induction generation case).

The series of studies conducted were:

1. Synchronous generation at remote location

a. Series ST for "external" faults:

- studies ST-1 through ST-16 were conducted for bus 6 connection,
- studies ST-17 through ST-36 were conducted for bus 8 connection,
- studies ST-26A, 30I, 46C, 56, 73, and 80 were conducted to determine the critical inertia required by the remote generation for transient stability,
- studies ST-57 through ST-72 were conducted to determine the effect of variation in penetration level (between 13 and 38 percent).

These studies are listed in Tables 5, 6, and 7.

b. Series SR for "internal" faults:

- studies SR-1 through SR-25B were made for bus 6 connection.

These studies are listed in Table 8.

2. Induction generation at remote location (Series SM):

a. studies SM-1 - SM-16 were made for bus 8 connection,

b. study SM-17 was made for bus 6 connection.

These studies are listed in Table 9.

3. Combination of synchronous and induction generation at remote location (Series SI):

a. studies SI-1 through SI-22 were made for bus 8 connection and for the network configurations shown in Figure 4.

These studies are listed in Table 10.

Table 5. Synchronous generator - ST Series

Case	New Generation Join the Existing System at Bus No.	Load Flow Case	Length of New Transmission Lines	Load Level	H, to 100 MVA Base, sec	Fault Location, Bus No.	Condition
ST-1	6	LF-1	short	normal	high, 6.4	10	stable
ST-2	6	LF-1	short	normal	low, 1.0	10	stable
ST-3	6	LF-1	short	normal	high, 6.4	6	stable
ST-4	6	LF-1	short	normal	low, 1.0	6	stable
ST-5	6	LF-2	short	heavy	high, 6.4	10	stable
ST-6	6	LF-2	short	heavy	low, 1.0	10	unstable
ST-7	6	LF-3	long	normal	high, 6.4	10	stable
ST-8	6	LF-3	long	normal	low, 1.0	10	stable
ST-9	6	LF-3	long	normal	high, 6.4	6	stable
ST-10	6	LF-3	long	normal	low, 1.0	6	stable
ST-11	6	LF-2	short	heavy	high, 6.4	6	stable
ST-12	6	LF-2	short	heavy	low, 1.0	6	unstable
ST-13	6	LF-4	long	heavy	high, 6.4	10	stable
ST-14	6	LF-4	long	heavy	low, 1.0	10	unstable
ST-15	6	LF-4	long	heavy	high, 6.4	6	stable
ST-16	6	LF-4	long	heavy	low, 1.0	6	unstable
ST-17	8	LF-5	short	normal	high, 6.4	10	stable
ST-18	8	LF-5	short	normal	low, 1.0	10	stable

ST-19	8	LF-5	short	normal	high,	6.4	8	stable
ST-20	8	LF-5	short	normal	low,	1.0	8	stable
ST-21	8	LF-6	long	normal	high,	6.4	10	stable
ST-22	8	LF-6	long	normal	low,	1.0	10	stable
ST-23	8	LF-6	long	normal	high,	6.4	8	stable
ST-24	8	LF-6	long	normal	low,	1.0	8	stable
ST-25	8	LF-7	short	heavy	high,	6.4	10	stable
ST-26	8	LF-7	short	heavy	low,	1.0	10	unstable
ST-27	8	LF-7	short	heavy	high,	6.4	8	stable
ST-28	8	LF-7	short	heavy	low,	1.0	8	unstable
ST-29	8	LF-8	long	heavy	high,	6.4	10	stable
ST-30	8	LF-8	long	heavy	low,	1.0	10	unstable
ST-31	8	LF-8	long	heavy	high,	6.4	8	stable
ST-32	8	LF-8	long	heavy	low,	1.0	8	unstable
ST-33	8	LF-8	long	heavy	medium,	4.0	10	stable
ST-34	8	LF-8	long	heavy	medium,	4.0	8	stable
ST-35	8	LF-7	short	heavy	medium,	4.0	10	stable
ST-36	8	LF-7	short	heavy	medium,	4.0	8	stable

Table 6. Synchronous generator - ST Series - critical inertia

Case	New Generation Join the Existing System at Bus No.	Load Flow Case	Length of New Transmission Lines	Load Level	H, to 100 MVA base, sec	Fault Location, Bus No.	Condition
ST-26A	8	LF-7	short	heavy	1.44	10	marginally stable
ST-30I	8	LF-8	long	heavy	3.49	10	marginally stable
ST-46C	6	LF-4	long	heavy	3.69	10	marginally stable
ST-56	6	LF-2	short	heavy	1.44	10	marginally stable
ST-73	5	LF-25	short	heavy	1.44	10	marginally stable
ST-80	5	LF-26	long	heavy	3.58	10	marginally stable

Table 7. Synchronous generator - ST series - variation of penetration level[a]

Case	New Generation Join Existing System @ Bus #	Load Flow Case	Length of New Transmission Lines	Load Level	H, to 100 MVA base, sec	Fault Location, Bus No.	Condition	Penetration Level, Percent
ST-57	8	LF-17	short	normal	high, 6.4	10	stable	13
ST-58	8	LF-17	short	normal	low, 1.0	10	stable	13
ST-59	8	LF-18	long	normal	high, 6.4	10	stable	13
ST-60	8	LF-18	long	normal	low, 1.0	10	stable	13
ST-61	8	LF-19	short	normal	high, 6.4	10	stable	38
ST-61A	8	LF-19	short	normal	1.44	10	stable	38
ST-62	8	LF-19	short	normal	low, 1.0	10	stable	38
ST-63	8	LF-20	long	normal	high, 6.4	10	stable	38
ST-64	8	LF-20	long	normal	low, 1.0	10	unstable	38
ST-64A	8	LF-20	long	normal	3.69	10	stable	38
ST-65	8	LF-21	short	heavy	high, 6.4	10	stable	19
ST-65A	8	LF-21	short	heavy	1.44	10	stable	19
ST-66	8	LF-21	short	heavy	low, 1.0	10	stable	19
ST-67	8	LF-22	long	heavy	high, 6.4	10	stable	19
ST-68	8	LF-22	long	heavy	low, 1.0	10	unstable	19
ST-68A	8	LF-22	long	heavy	3.69	10	stable	19
ST-69	8	LF-23	short	heavy	high, 6.4	10	stable	38
ST-70	8	LF-23	short	heavy	low, 1.0	10	unstable	38
ST-70A	8	LF-23	short	heavy	1.44	10	unstable	38
ST-71	8	LF-24	long	heavy	high, 6.4	10	unstable	38
ST-72	8	LF-24	long	heavy	low, 1.0	10	unstable	38

[a]Penetration level is the fraction of the system load that is supplied by the remote generation.

Table 8. Synchronous generator - SR Series - faults located inside the existing system

Case	New Generation Joins Existing System @ Bus #	Load Flow Case	Length of New Transmission Lines	Load Level	H, to 100 MVA base, sec	Fault Location, Bus No.	Condition
SR-1	6	LF-1	short	normal	high, 6.4	6 (6-4)[a]	stable
SR-2	6	LF-1	short	normal	low, 1.0	6 (6-4)	stable
SR-3	6	LF-2	short	heavy	high, 6.4	6 (6-4)	stable
SR-4	6	LF-2	short	heavy	low, 1.0	6 (6-4)	unstable
SR-4A	6	LF-2	short	heavy	1.44	6 (6-4)	stable
SR-5	6	LF-3	long	normal	high, 6.4	6 (6-4)	stable
SR-6	6	LF-3	long	normal	low, 1.0	6 (6-4)	stable
SR-7	6	LF-4	long	heavy	high, 6.4	6 (6-4)	stable
SR-8	6	LF-4	long	heavy	low, 1.0	6 (6-4)	unstable
SR-8A	6	LF-4	long	heavy	3.69	6 (6-4)	stable
SR-9	6	LF-4	long	heavy	high, 6.4	6 (6-9)	stable
SR-10	6	LF-4	long	heavy	3.69	6 (6-9)	stable
SR-11	6	LF-2	short	heavy	high, 6.4	6 (6-9)	stable
SR-12	6	LF-2	short	heavy	3.69	6 (6-9)	stable
SR-13	6	LF-2	short	heavy	1.44	6 (6-9)	stable
SR-13A	6	LF-2	short	heavy	low, 1.0	6 (6-9)	unstable
SR-14	6	LF-2	short	heavy	high, 6.4	9 (9-6)	stable
SR-15	6	LF-2	short	heavy	3.69	9 (9-6	stable
SR-16	6	LF-2	short	heavy	1.44	9 (9-6)	stable
SR-16A	6	LF-2	short	heavy	low, 1.0	9 (9-6)	stable
SR-17	6	LF-4	long	heavy	high, 6.4	9 (9-6)	stable
SR-17A	6	LF-4	long	heavy	3.69	9 (9-6)	stable
SR-17B	6	LF-4	long	heavy	high, 6.4	9 (9-8)	stable
SR-17C	6	LF-4	long	heavy	3.69	9 (9-8)	stable
SR-17D	6	LF-2	short	heavy	1.44	9 (9-8)	stable
SR-17E	6	LF-2	short	heavy	3.69	9 (9-8)	stable
SR-17F	6	LF-2	short	heavy	high, 6.4	9 (9-8)	stable

SR-17G	6	LF-2	short	heavy	low, 1.0	9 (9-8)	stable
SR-18	6	LF-2	short	heavy	1.44	5 (5-4)	stable
SR-18A	6	LF-2	short	heavy	low, 1.0	5 (5-4)	stable
SR-18B	6	LF-2	short	heavy	high, 6.4	5 (5-4)	stable
SR-19	6	LF-2	short	heavy	1.44	5 (5-7)	stable
SR-19A	6	LF-2	short	heavy	low, 1.0	5 (5-7)	stable
SR-19B	6	LF-2	short	heavy	high, 6.4	5 (5-7)	stable
SR-20	6	LF-2	short	heavy	1.44	7 (7-5)	stable
SR-20A	6	LF-2	short	heavy	low, 1.0	7 (7-5)	stable
SR-20B	6	LF-2	short	heavy	high, 6.4	7 (7-5)	stable
SR-21	6	LF-2	short	heavy	1.44	7 (7-8)	stable
SR-21A	6	LF-2	short	heavy	low, 1.0	7 (7-8)	stable
SR-21B	6	LF-2	short	heavy	high, 6.4	7 (7-8)	stable
SR-22	6	LF-2	short	heavy	1.44	4 (4-5)	stable
SR-22A	6	LF-2	short	heavy	low, 1.0	4 (4-5)	stable
SR-22B	6	LF-2	short	heavy	high, 6.4	4 (4-5)	stable
SR-23	6	LF-2	short	heavy	1.44	4 (4-6)	stable
SR-23A	6	LF-2	short	heavy	low, 1.0	4 (4-6)	stable
SR-23B	6	LF-2	short	heavy	high, 6.4	4 (4-6	stable
SR-24	6	LF-2	short	heavy	1.44	8 (8-7)	stable
SR-24A	6	LF-2	short	heavy	low, 1.0	8 (8-7)	stable
SR-24B	6	LF-2	short	heavy	high, 6.4	8 (8-7)	stable
SR-25	6	LF-2	short	heavy	1.44	8 (8-9)	stable
SR-25A	6	LF-2	short	heavy	low, 1.0	8 (8-9)	stable
SR-25B	6	LF-2	short	heavy	high, 6.4	8 (8-9)	stable

[a]Fault located at Bus 6 in the transmission lines joining Bus 6 to Bus 4.

Table 9. Induction generator - SM Series

Case	New Gen. Joins Existing System at Bus No.	Load Flow Case	Length of New Trans. Line	Load Level	Fault Location at Bus No.	Induction Gen. Parameter			Initial Slip %	Comment
						H, to 100 MVA base, sec	r_2 pu	τ'_{do} sec		
SM-1	8	LF-5	short	normal	10	1.0	0.015	0.7233	1.2605	stable
SM-2	8	LF-5	short	normal	10	0.5	0.015	0.7233	1.2605	unstable
SM-3	8	LF-5	short	normal	10	2.0	0.015	0.7233	1.2605	stable
SM-4	8	LF-5	short	normal	10	1.0	0.045	0.2411	3.7815	stable
SM-5	8	LF-9	short	normal	10	1.0	0.015	0.7233	1.5910	stable
SM-6	8	LF-5	short	normal	10	0.5	0.045	0.2411	1.5910	stable
SM-7	8	LF-5	short	normal	10	2.0	0.045	0.2411	3.7815	stable
SM-8	8	LF-5	short	normal	8	0.5	0.015	0.7233	1.2605	unstable
SM-9	8	LF-5	short	normal	8	1.0	0.015	0.7233	1.2605	stable
SM-10	8	LF-5	short	normal	8	2.0	0.015	0.7233	1.2606	stable
SM-11	8	LF-5	short	normal	8	0.5	0.045	0.2411	3.7815	stable
SM-12	8	LF-5	short	normal	8	1.0	0.045	0.2411	3.7805	stable
SM-13	8	LF-5	short	normal	8	2.0	0.045	0.2411	3.7805	stable
SM-14	8	LF-6	long	normal	10	1.0	0.015	0.7233	1.2605	unstable
SM-15	8	LF-7	short	heavy	10	2.0	0.0075	0.7233	1.1840	unstable
SM-16	8	LF-8	long	heavy	10	2.0	0.0075	0.7233	1.1840	unstable
SM-17	6	LF-1	short	normal	10	1.0	0.015	0.7233	1.2605	stable

Table 10. Synchronous and induction generators - SI Series

Case No.	New Generation Joins the Existing System at Bus No.	Load Flow Cases	Length of New Trans. Line	Load Level	Fault Location at Bus No.
SI-1	8	LF-5	short	normal	10
SI-2	8	LF-5	short	normal	10
SI-3	8	LF-5	short	normal	10
SI-4	8	LF-5	short	normal	10
SI-5	8	LF-10	short	normal	10
SI-6	8	LF-10	short	normal	10
SI-7	8	LF-11	short	heavy	10
SI-8	8	LF-12	short	heavy	10
SI-9	8	LF-13	long	normal	10
SI-10	8	LF-14	long	normal	10
SI-11	8	LF-15	long	heavy	10
SI-12	8	LF-16	long	heavy	10
SI-13	8	LF-11	short	heavy	10
SI-14	8	LF-13	long	normal	10
SI-15	8	LF-15	long	heavy	10
SI-16	8	LF-16	long	heavy	10
SI-17	8	LF-11	short	heavy	10
SI-18	8	LF-15	long	heavy	10
SI-19	8	LF-16	long	heavy	10
SI-20	8	LF-11	short	heavy	10
SI-21	8	LF-15	long	heavy	10
SI-22	8	LF-15	long	heavy	10

Synch. Generator Parameter			Induction Generator Parameter						Condition
H, sec	P, MW	Bus Conn.	H, sec	r_2 pu	τ'_{do} sec	Initial slip, %	P, MW	Bus Conn.	
3.01	0	11	1.0	0.015	0.7233	1.2605	85	11	stable
3.01	42.5	11	1.0	0.015	0.7233	0.6237	42.5	11	stable
3.01	0	11	0.5	0.015	0.7233	1.2605	85	11	stable
3.01	42.5	11	0.5	0.015	0.7233	0.6237	42.5	11	stable
3.01	42.5	11	1.0	0.015	0.7233	0.6751	42.5	12	stable
3.01	42.5	11	0.5	0.015	0.7233	0.6751	42.5	12	stable
3.01	0	11	0.5	0.0075	0.7233	1.4623	160	12	unstable
3.01	80	11	0.5	0.015	0.7233	1.3144	80	12	stable
3.01	0	11	0.5	0.015	0.7233	1.3796	85	12	unstable
3.01	42.5	11	0.5	0.015	0.7233	0.6617	42.5	12	stable
3.01	0	11	0.5	0.0075	0.7233	1.4689	160	12	unstable
3.01	80	11	0.5	0.015	0.7233	1.3089	80	12	unstable
3.01	0	11	1.0	0.0075	0.7233	1.4623	160	12	unstable
3.01	0	11	1.0	0.015	0.7233	1.3796	85	12	stable
3.01	0	11	1.0	0.0075	0.7233	1.4689	160	12	unstable
3.01	80	11	1.0	0.015	0.7233	1.3089	80	12	unstable
3.01	0	11	2.0	0.0075	0.7233	1.4623	160	12	unstable
3.01	0	11	2.0	0.0075	0.7233	1.4689	160	12	unstable
3.01	80	11	2.0	0.015	0.7233	1.3089	80	12	stable
3.01	0	11	4.0	0.0075	0.7233	1.4623	160	12	stable
3.01	0	11	4.0	0.0075	0.7233	1.4689	160	12	unstable
3.01	0	11	8.0	0.0075	0.7233	1.4689	160	12	marginally stable

B. Numerical Results

Typical results from the series of studies listed in Tables 5 through 10 are given in Appendices B - G (Figures 8 - 451). Reference [20] contains a complete set of the series listed in Tables 5, 9, and 10.

The effect of variation of system parameters on the dynamic performance of the power network can be grouped in four main areas for detailed examination:

- The effect of the disturbance on the overall power network, both existing system and added remote generation. The criterion used is transient stability.
- The effect of the disturbance on the remote generation. The factors examined pertain to the relative motion of the rotor(s) of the remote generation, e.g., relative angles and accelerations, and, for the induction generation cases, slip and internal voltage.
- The effect of the disturbance on the generators of the existing system. The factors examined are the collective motion of the generators of the existing system (their inertial centers) and the mutual interaction among those generators.
- The mutual interaction between the new generation and the machines of the existing system, following the disturbance.

A summary of the findings is given below.

1. Transient stability

a. Remote synchronous generation When the remote generation is made up of synchronous machines and the faults are located in the

transmission line joining the remote generation to the existing system and the penetration level is not greater than 27 percent, instability occurs only at heavy load and low inertia situations (Cases ST-6, 12, 14, 16, 26, 28, 30, and 32). From the listing in Table 5, the fault location, the length of the transmission lines to the remote generation, and the point of connection to the existing network have very little influence. When the inertia is increased from H = 1.0 to H = 4.0 or 6.4, for identical network configuration and disturbance, the system becomes stable, as is evident from comparing Case ST-26 to Cases ST-35 and ST-25.

Even though the influence of the length of the transmission lines to the remote generation does not show in Table 5, its influence shows up clearly in Table 6. The data in this table concentrate only on the heavy load level, fault on bus 10, and penetration level of 25 percent. Table 6 clearly shows that, for the same disturbance, long trarsmission line (120 miles) requires much higher inertia constant, H, than short transmission line (40 miles) for stability to be maintained. This is evident from comparing Case ST-26A to Case ST-30I and Cast ST-46C to Case ST-56. Table 6 also confirms the observation made earlier (from discussion of Table 5) that the point of connection to the existing network has very little influence. This is evident from comparing Case ST-26A (bus 8 connection) to Case ST-56 (bus 6 connection) or Case ST-73 (bus 5 connection). These three cases require identical critical inertia of H = 1.44. The critical inertia requirement for the other three remaining cases for long transmission line varies only slightly from

H = 3.49 (Case ST-30I, bus 8 connection) to H = 3.69, (Case ST-46C, bus 6 connection).

The influence of the penetration level can be observed from Table 7. High penetration level (38 percent), long transmission line, and low inertia can cause instability even at normal load level (Case ST-64). By reducing the length of the transmission line, the power network became stable (Case ST-62). Stability can also be maintained by reducing the penetration level, e.g., by comparing Case ST-64 to Case ST-22. This is as expected because the higher the penetration level, the higher the loading of the remote machine and the weaker becomes its synchronizing forces to the existing machines. For example, under normal load condition, when the penetration level is increased from 27 percent to 38 percent, the generation of the remote machine increased from 85 MW (neglecting transmission line loss) to 120 MW.

The combination of heavy load level and low inertia is even more detrimental to the stability of the overall power network and especially to the remote machine itself. At 25 percent penetration level, the output of the remote machine must be 157 MW which is 96 percent of its rating. Under this operating condition, the power network became unstable for this disturbance (Cases ST-26 and ST-30). By reducing the penetration level to 19 percent, the remote machine is operated at 43 MW below its rating. This operating condition is still not enough to maintain stability after the disturbance, if the transmission line to the remote generation is long (Case ST-68). However, the power network became stable if the transmission line is short (Case ST-66). Indeed,

the influence of the transmission line on the stability of the remote generation is clearly shown again.

When the fault is located outside the existing power network, the overall system loses stability under heavy load and low inertia conditions (Table 5). It makes very little difference whether the fault is located at the sending end (bus 10) or at the receiving end (bus 6 or bus 8), e.g., Cases ST-6 and ST-12. Even though the sending-end fault is expected to be more severe than the receiving-end fault, the conclusion cannot be drawn at this point. Faults located inside the existing system but close to the point of connection (bus 6) yielded the same results, e.g., Cases SR-4, SR-8, and SR-13A of Table 8. The overall system became stable when faults were moved further inside the existing system. These are clearly demonstrated by comparing Case SR-4 to Case SR-23A and Case SR-13A to Case SR-16A. Hence, when the inertia of the remote generation is low and the load level is high, faults located electrically far away from the remote generation are less severe than the faults that are electrically close to the remote generation.

b. Remote induction generation For the cases where the remote generation is made up of induction machines, the effect of the remote generator inertia is even more pronounced. Not only were the heavy load cases unstable (Cases SM-15, 16), but also were some of the normal load and low inertia runs (Cases SM-2, 8, and 14). It is interesting to note that for the normal load cases, stability was maintained when either H or the rotor resistance r_2 was increased, as is evident from comparing Case SM-2 to Cases SM-1 and SM-4. The Case SM-14, which is unstable,

indicates that the operation of the induction generation is quite sensitive to the transmission network impedance, since it differs from Case SM-1 (stable) only by the length of the transmission line.

c. Remote synchronous and induction generation Analysis of the cases where there is a mix of synchronous and induction generation at the remote location is more complex because of the relatively large number of variables involved. However, there are certain patterns of behavior that can be detected from Table 10:

- Division of the generation among the induction and synchronous machines improves stability (e.g., compare Cases SI-7, 8).
- Low inertia makes the system vulnerable to instability even at normal load (Case SI-9) but more so at heavy load (Cases SI-7, 11, 12, 13, 15, and 16).
- It appears to be more beneficial to connect the synchronous and induction generation on the same bus.
- For the induction machine, dynamic behavior is influenced by the values of r_2 and the transmission line impedance (Cases SI-17, 18, and 19).
- When "worst" combinations of the above factors are used, even high values of inertia will not be sufficient to maintain stability (Cases SI-20, 21).

2. Effect of disturbance on remote generation

a. Remote synchronous generation Tables 11 through 14 give information on the peak of the relative position of the rotor of the

remote generator with respect to the positions of the rotors of the existing machines and their inertial centers for the synchronous generation case. Examining the data in these tables we note the following.

1) Effect of inertia of remote generation From the data in Table 11, we can easily see the effect of the inertia on the motion of the remote synchronous generator. All the cases where the value of H is low have much higher "swings" (e.g., compare Cases ST-8 with ST-7 and ST-22 with ST-21). This is consistent with the discussion in the previous section.

It was also found that for a given system configuration and operating condition, and for the same disturbance, there is a critical value of the remote machine inertia, for which the system is barely stable. The critical inertia cases, for heavy load condition and 25 percent penetration level, are given in Table 12. Information in this table reveals the following interesting aspects of these cases:

- The maximum relative swings of the rotor of the remote generator with respect to the rotors of the machines in the existing system and its inertial center change very little with various combination of the remote inertia and the impedance of the transmission line, e.g., compare Cases ST-26A to ST-30I.
- The maximum relative swings change very little with different points of connection to the existing system, e.g., compare Cases ST-26A to ST-56 and ST-73.
- Stability limit (maximum relative swing) seems to be governed by the pair of generators having the largest difference in inertia,

e.g., the remote generator and the generator No. 1 in the existing system.

2) Effect of transmission line length The effect of the increase in the length of the transmission line seems to be to increase the angular swings but to lower accelerations (e.g., compare Cases ST-8 with ST-2 and ST-24 with ST-20). It is also evident that these effects are accentuated at heavier loads (e.g., compare Cases ST-1, 5 to ST-7, 13).

3) Effect of fault location When the fault location is moving away from the remote machine toward the existing system, the effect of disturbance on remote machines is reduced, e.g., compare Cases ST-33 and ST-34 of Table 11. The effect of disturbance on the remote machine becomes much less when the fault is located inside the existing system itself which is clearly shown in Table 14. A close observation of this table reveals many interesting points:

- The disturbance on the remote machine is most severe when the fault is located close to the machine with the highest inertia, e.g., fault at bus 4, Cases SR-22A and SR-23A.
- The opposite of the above observation is not true, i.e., fault located close to the machine with the lowest inertia (fault at bus 9) does not produce the least disturbance on the remote machine.
- When the fault is located outside the existing system, the relative swing of the rotor of the remote generator with respect to the existing machine with the highest inertia, i.e.,

$(\delta_k - \delta_1)$, is consistently larger than those with respect to the lighter machines; this is no longer true when the fault is located inside the existing system, e.g., compare Cases SR-16A with SR-17G.

- The lower inertia of the remote machine produces greater swings and accelerations, e.g., Cases SR-14 and SR-16A; this is consistent with earlier observation.

4) Effect of penetration level Table 13 demonstrates that the combination of high penetration level and low inertia, even under normal load condition, can be detrimental to the remote machine especially when the transmission line joining the remote machine to the existing system is long. The relative swings of the rotor of the remote generator with respect to the rotors of the machines in the existing system and its inertial center increase very rapidly with the increase in penetration level. For example, $(\delta_k - \delta_1)$ is 29 degrees when the penetration level is 13 percent (Case ST-58); it jumps to 89 degrees when the penetration level is 27 percent (Case ST-18); it further increases to 156 degrees when the penetration level is 38 percent (Case ST-62). Heavy loads and long transmission lines simply accentuate the problem even more. For this studied system, penetration level greater than 25 percent cannot be tolerated under heavy load and low inertia condition.

b. Remote induction generation In Table 15, a selected number of remote induction generation cases are presented, showing the effect of the disturbance on the remote machine. Again, the effect of the

inertia on the machine's dynamic behavior is easily demonstrated. Low inertia results in a higher maximum slip and lower internal voltage. These effects are reduced when the rotor resistance r_2 is increased. The effects are comparable for receiving-end and sending-end faults.

c. Remote synchronous and induction generation In Table 16, a selected number of cases where the remote machines are made up of a mix of synchronous and induction generators are presented. The same basic case is shown with different induction generator inertia, distribution of load, and load level. Again, we can see that:

- The lower inertia produces greater swings and accelerations of the rotors of both remote generators (e.g., Cases SI-5, 6 and SI-7, 8, 20).
- The same effect is observed with higher load level, as seen when Cases SI-6 and SI-8 are compared.
- The effect of the generation distribution among the remote machines is demonstrated by comparing Cases SI-8 and SI-7. This unstable heavy load condition became stable when the generation was equally distributed among the synchronous and induction machines.

3. Effect of disturbance on existing machines

a. Remote synchronous generation In Tables 17 through 20, terms that are indicative of the effect of the disturbance on the existing machines, as well as on their interaction with the remote synchronous generation, are displayed. These terms give information on the motion of the inertial center ($\bar{\delta}$ and $\ddot{\bar{\delta}}$), the synchronizing forces among the

existing machines (Equation (4.9)) and the synchronizing forces between the remote generator and the existing machines

$$-\sum_{i=1}^{n} A_{ik} \cos (\theta_{ik} - \delta_{ik}).$$

These synchronizing force terms are given in column AIJ and AIK respectively. Examining the data in these tables we note the following.

1) Effect of inertia of remote generation From the data in Table 17, the low inertia at the remote generation causes the rotors of the existing machines to move at a higher pace and acceleration (e.g., compare Cases ST-2 to ST-1 and Cases ST-22 to ST-21). Also, the existing machines are disturbed to a greater extent for heavier loads than for lighter loads, e.g., compare Cases ST-25 and ST-17. It is interesting to note that the term indicative of the synchronizing forces among the existing machines (AIJ column) is not greatly influenced by the inertia of the remote machine (e.g., compare Cases ST-7 and ST-8). Rather, it is more influenced by the load level (e.g., compare Cases ST-5 and ST-1) and the impedance between the remote generation and the existing system (e.g., compare Cases ST-7 to ST-1).

It appears that, when the power network is critically stable under heavy load condition and 25 percent penetration level, the existing machines are disturbed to a greater degree from the combination of short transmission lines and low inertia (H = 1.44) than from the combination of long transmission lines and medium inertia (e.g., compare Cases ST-26A to ST-30I of Table 18).

2) Effect of transmission line length The effect of the increase in the length of the transmission line appears to depend on the system load level. Under normal load condition, the disturbance on the inertial center is more severe for short transmission line cases than for long transmission line cases (e.g., compare Cases ST-1 to ST-7 and ST-2 to ST-8). But, under heavy load condition, the opposite results are observed, i.e., long transmission line has more effect on the motion of the inertial center than short transmission line (e.g., compare Cases ST-5 to ST-13 and ST-35 to ST-33).

3) Effect of fault location Fault locations seem to have great influence on the degree that the existing machines are disturbed. The motion of the inertial center of the existing machines varies widely with different fault locations. It appears that the existing power network is disturbed the least when the fault is located at the machine with the smallest inertia, i.e., fault at bus 9 in the transmission line joining bus 9 to bus 6. The opposite is true when the fault is located at the machine with the largest inertia, i.e., fault at bus 4 in the transmission line joining bus 4 to bus 5. These are shown clearly by Table 20, e.g., compare Cases SR-14 to SR-22B. Low inertia of the remote generation and long transmission line to the remote generation enhance the severity of the disturbance, e.g., compare Cases SR-22A to SR-22B and SR-17 to SR-14. The AIJ term is also influenced considerably by the fault location, e.g., compare Cases SR-14 to SR-24B.

4) Effect of penetration level Table 19 shows that penetration level has a direct influence on the degree that the existing

machines are disturbed, i.e., the higher the penetration level, the more severe the disturbance on the existing machines will be. This observation is true for both normal load condition (e.g., compare Cases ST-57 to ST-61) and heavy load condition (e.g., compare Cases ST-65 to ST-25 (Table 17)). Low inertia of the remote generation accentuates the problem even more (e.g., compare Cases ST-58 and ST-62 with Cases ST-57 and ST-61). The AIJ term is not strongly influenced by the variation of penetration level (e.g., compare Cases ST-57 to ST-61).

b. Remote induction generation Some selected remote induction generation cases are displayed in Table 21. The acceleration of the inertial center of the existing machines is less sensitive to the inertia of the remote generation than in the corresponding remote synchronous generation cases.

c. Remote synchronous and induction generation Similar effects are obtained with a mix of induction and synchronous generation at the remote location, as seen in the data presented in Table 22. The same trends discussed in Part b are observed, but the magnitude of the interaction among the machines of the existing system (AIJ term) is less severe.

4. Interaction between remote and existing generators

The last column of Tables 17 through 20 (AIK term), the last row of Table 21 (AIK term), and the last two columns of Table 22 (AIK1, AIK2 terms) are indicative of the synchronizing forces between the remote generation and the machines in the existing system. From these tables the following conclusion can be reached.

a. Remote synchronous generation

- For stability to be maintained, low inertia of the remote generation requires stronger synchronizing forces between the remote generation and the machines of the existing system than high inertia (e.g., compare Cases ST-2 to ST-1 and Cases ST-18 to ST-17 of Table 17).
- For stability to be maintained, heavy load level requires stronger interaction between remote and existing generators than normal load level (e.g., compare Cases ST-5 to ST-1 and Cases ST-25 to ST-17 of Table 17).
- Short transmission line joining the remote generation to the existing system results in stronger interaction than long transmission line (e.g., compare Cases ST-1 to ST-7 and Cases ST-5 to ST-13 of Table 17).
- When the overall power network is critically stable, the combination of low inertia and short transmission line requires much higher interaction than that of medium inertia and long transmission line (e.g., compare Cases ST-26A to ST-30I of Table 18).
- High penetration level results in stronger interaction than low penetration level (e.g., compare Cases ST-62 to ST-58 and Cases ST-25 to ST-65 of Tables 17 and 19).
- Fault location has strong influence on the synchronizing forces, i.e., the interaction is strongest when the fault is located at the remote machine and getting weaker when the

fault is located inside the existing system (e.g., compare Cases ST-5 and ST-11 of Table 17 to Cases SR-14, 18B, and 22B of Table 20).

b. Remote induction generation When the remote generation is an induction machine or the mix of synchronous and induction machines, the same trends are observed. Since severe disturbances are associated with low inertia and heavy load and the more severe disturbances require greater synchronizing forces to "hold the system together," correspondingly high values of AIK (or AIK1, AIK2) are observed. This is evident in the selected data presented in Tables 21 and 22.

Table 11. The effect of disturbance on remote synchronous machine

Case No.	$(\delta_k - \delta_1)$ max. degree (@ time, sec)	$(\delta_k - \delta_2)$ max. degree (@ time, sec)	$(\delta_k - \delta_3)$ max. degree (@ time, sec)	$(\delta_k - \bar{\delta})$ max. degree (@ time, sec)	$(\ddot{\delta}_k - \ddot{\delta})$ max. rad/sec^2 (@ time, sec)
ST-1	26.86	17.09	-11.64	23.38	22.54
	(0.25)	(0.25)	(0.60)	(0.25)	(0.60)
ST-2	74.11	66.30	69.51	70.93	455.06
	(0.15)	(0.15)	(0.45)	(0.15)	(0.9)
ST-3	24.61	13.08	-12.39	20.59	20.18
	(0.25)	(0.25)	(0.60)	(0.25)	(0.60)
ST-4	79.03	67.67	74.09	74.69	471.75
	(1.65)	(1.65)	(9.35)	(1.65)	(1.8)
ST-5	35.39	31.26	29.72	34.07	34.59
	(0.25)	(0.25)	(0.25)	(0.25)	(0.6)
ST-7	40.21	32.36	27.31	37.48	18.54
	(0.3)	(0.3)	(0.35)	(0.30)	(0.75)
ST-8	93.90	86.15	87.73	90.78	334.11
	(0.2)	(0.2)	(1.35)	(0.2)	(1.95)
ST-9	35.71	30.74	27.85	33.73	16.15
	(1.2)	(1.2)	(1.25)	(1.2)	(1.6)
ST-10	75.78	75.63	65.28	71.43	266.40
	(1.65)	(2.05)	(1.3)	(1.65)	(1.85)
ST-11	30.73	24.92	24.91	28.99	28.71
	(0.25)	(0.25)	(0.30)	(0.25)	(0.6)
ST-13	74.38	72.22	70.76	73.63	30.97
	(0.4)	(0.4)	(0.4)	(0.4)	(0.95)
ST-15	59.53	59.43	62.33	59.72	22.48
	(0.45)	(0.45)	(0.4)	(0.45)	(0.95)
ST-17	33.57	14.26	11.47	27.54	18.00
	(0.25)	(1.95)	(0.35)	(0.25)	(1.55)
ST-18	89.36	72.76	81.33	82.52	511.71
	(1.05)	(1.625)	(1.95)	(1.05)	(2.1)

ST-19	33.34	9.75	16.49	26.75	20.66
	(0.3)	(0.3)	(0.4)	(0.3)	(0.65)
ST-20	70.94	58.12	56.60	63.03	362.22
	(1.0)	(0.7)	(0.45)	(1.0)	(0.85)
ST-21	46.29	30.31	28.36	41.47	15.29
	(0.35)	(0.3)	(0.35)	(0.35)	(1.8)
ST-22	102.77	85.02	78.88	97.16	319.41
	(1.7)	(1.7)	(1.7)	(1.7)	(1.525)
ST-23	44.67	32.08	35.58	40.37	18.11
	(1.25)	(1.15)	(0.4)	(1.25)	(0.8)
ST-24	79.32	59.96	48.17	72.04	220.80
	(0.2)	(0.15)	(0.15)	(0.15)	(1.45)
ST-25	48.05	23.12	29.01	41.28	27.69
	(0.3)	(0.25)	(0.3)	(0.3)	(1.65)
ST-27	46.35	17.28	29.56	38.83	27.56
	(0.3)	(0.35)	(0.35)	(0.3)	(0.7)
ST-29	85.16	64.39	68.89	79.41	31.01
	(0.45)	(0.4)	(0.4)	(0.4)	(2.075)
ST-31	76.14	67.90	70.30	72.14	26.90
	(0.45)	(0.5)	(0.45)	(0.45)	(0.95)
ST-33	113.95	85.62	89.99	106.[illegible]	51.31
	(0.45)	(0.4)	(0.4)	(0.4)	(0.925)
ST-34	91.01	65.74	76.84	84.76	45.92
	(0.4)	(0.45)	(0.4)	(0.4)	(0.85)
ST-35	61.28	36.16	39.30	53.70	54.86
	(0.25)	(0.2)	(0.2)	(0.25)	(1.5)
ST-36	54.88	28.06	28.91	46.44	47.52
	(0.25)	(0.2)	(0.25)	(0.25)	(1.5)

Table 12. The effect of disturbance on remote synchronous machine - critical inertia

Case No.	$(\delta_k - \delta_1)$ max. degree (@ time, sec)	$(\delta_k - \delta_2)$ max. degree (@ time, sec)	$(\delta_k - \delta_3)$ max. degree (@ time, sec)	$(\delta_k - \bar{\delta})$ max. degree (@ time, sec)	$(\ddot{\delta}_k - \ddot{\bar{\delta}})$ max. rad/sec^2 (@ time, sec)
ST-26A	135.57 (0.225)	104.73 (0.2)	105.09 (0.2)	126.04 (0.225)	318.77 (0.45)
ST-30I	137.93 (0.55)	111.66 (0.825)	117.14 (0.7)	129.03 (0.6)	-29.98 (0.2)
ST-46C	121.21 (0.65)	120.94 (0.85)	118.68 (0.7)	120.26 (0.725)	-28.18 (0.2)
ST-56	125.16 (0.225)	119.08 (0.225)	110.68 (0.2)	122.58 (0.225)	412.26 (0.475)
ST-73	126.30 (0.25)	114.10 (0.2)	119.44 (0.2)	122.69 (0.25)	422.71 (0.475)
ST-80	121.35 (0.60)	112.40 (0.7)	120.13 (0.65)	119.23 (0.6)	-30.30 (0.2)

Table 13. The effect of disturbance on remote synchronous machine - variation of penetration level

Case No.	$(\delta_k - \delta_1)$ max. degree (@ time, sec)	$(\delta_k - \delta_2)$ max. degree (@ time, sec)	$(\delta_k - \delta_3)$ max. degree (@ time, sec)	$(\delta_k - \bar{\delta})$ max. degree (@ time, sec)	$(\ddot{\delta}_k - \ddot{\bar{\delta}})$ max. rad/sec^2 (@ time, sec)
ST-57	-11.30 (0.70)	- 8.71 (0.75)	-18.56 (0.65)	-11.11 (0.65)	13.54 (0.65)
ST-58	28.73 (0.15)	19.86 (0.125)	11.32 (0.125)	25.04 (0.15)	-198.57 (0.125)
ST-59	14.51 (0.35)	6.78 (0.40)	7.85 (0.40)	12.25 (0.35)	-8.48 (0.40)
ST-60	35.78 (0.15)	28.56 (0.15)	21.65 (0.15)	33.09 (0.15)	-148.31 (0.15)
ST-61	53.14 (0.25)	27.83 (0.25)	22.29 (0.25)	45.43 (0.25)	-27.71 (0.25)
ST-61A	97.30 (0.15)	76.59 (0.15)	68.26 (0.15)	90.65 (0.15)	-237.57 (0.15)
ST-62	156.24 (0.20)	127.30 (0.20)	114.18 (0.20)	146.81 (0.20)	-329.14 (0.1125)
ST-63	74.68 (0.35)	52.17 (0.35)	48.75 (0.35)	67.96 (0.35)	-20.94 (0.35)
ST-64A	84.86 (0.30)	62.64 (0.25)	57.26 (0.25)	77.80 (0.30)	-39.25 (0.30)

ST-65	25.62 (0.30)	7.92 (0.30)	17.41 (0.35)	21.36 (0.30)	-20.22 (0.30)
ST-65A	69.48 (0.15)	56.37 (0.15)	58.21 (0.15)	65.92 (0.15)	-245.66 (0.15)
ST-66	114.49 (0.175)	96.09 (0.15)	97.34 (0.15)	108.93 (0.175)	-365.50 (0.1125)
ST-67	45.93 (0.35)	34.82 (0.35)	41.32 (0.35)	43.36 (0.35)	-18.99 (0.35)
ST-68A	57.24 (0.30)	43.66 (0.25)	48.16 (0.25)	53.70 (0.30)	-37.19 (0.30)
ST-69	65.76 (0.35)	30.36 (0.35)	37.06 (0.35)	56.29 (0.35)	-18.04 (0.35)

Table 14. The effect of disturbance on remote synchronous machine - faults located inside the existing system

Case No.	$(\delta_k - \delta_1)$ max. degree (@ time, sec)	$(\delta_k - \delta_2)$ max. degree (@ time, sec)	$(\delta_k - \delta_3)$ max. degree (@ time, sec)	$(\delta_k - \bar{\delta})$ max. degree (@ time, sec)	$(\ddot{\delta}_k - \ddot{\bar{\delta}})$ max. rad/sec^2 (@ time, sec)
SR-14	11.21 (0.25) - 4.74 (0.60)	-15.77 (0.35) 27.31 (0.75)	-19.54 (0.20) 27.72 (0.85)	5.40 (0.20) - 2.12 (0.50)	- 5.93 (0.20) 8.03 (0.50)
SR-16A	39.08 (0.125) -22.65 (0.3)	32.17 (0.125) -45.33 (0.3)	20.21 (0.125) -47.21 (0.25)	36.02 (0.125) -29.23 (0.3)	-228.43 (0.125) 261.92 (0.3)
SR-17	21.54 (0.25) 2.84 (0.65)	- 0.99 (0.3) 34.11 (0.7)	- 8.40 (0.2) 35.99 (0.85)	15.39 (0.2) 8.36 (0.55)	- 4.64 (0.25) 5.97 (0.60)
SR-17A	29.47 (0.2) 2.33 (0.55)	- 5.81 (0.4) 43.39 (0.75)	0.49 (0.2) 46.80 (0.825)	24.06 (0.2) 0.40 (0.5)	-20.21 (0.2 23.55 (0.5)
SR-17B	28.79 (0.35) 1.13 (0.70)	46.70 (0.5) 9.47 (0.85)	-11.48 (0.2) 31.74 (0.5)	29.76 (0.40) 2.12 (0.75)	5.91 (0.15) -17.57 (0.45)
SR-17C	35.95 (0.3) - 7.00 (0.625)	40.92 (0.4) 18.53 (0.7)	- 3.54 (0.25) 20.69 (0.5)	32.42 (0.3) - 1.13 (0.65)	-18.66 (0.4) 35.69 (0.675)
SR-17F	21.53 (0.35) -11.80 (0.65)	34.84 (0.45) 6.59 (0.75)	-20.54 (0.20) 18.69 (0.45)	21.43 (0.4) - 8.66 (0.7)	8.73 (0.15) -22.15 (0.40)
SR-17G	39.31 (0.125) - 0.75 (0.25)	32.67 (0.125) - 8.58 (0.25)	-48.15 (0.25) 27.67 (0.4)	36.24 (0.125) - 6.58 (0.25)	-211.84 (0.125) 229.43 (0.25)
SR-18A	34.42 (0.15) -12.46 (0.25)	30.15 (0.15) -13.86 (0.25)	28.53 (0.15) -20.33 (0.25)	33.05 (0.15) -13.45 (0.25)	-215.97 (0.15) 225.00 (0.25)
SR-18B	7.59 (0.25) -10.26 (0.65)	36.74 (0.65) 2.02 (1.125)	18.67 (0.5) 3.03 (1.125)	8.08 (0.3) 1.32 (0.6)	- 5.18 (0.35) 6.15 (0.65)
SR-19A	33.28 (0.15) -15.44 (0.25)	27.65 (0.15) -30.58 (0.25)	26.80 (0.15) -29.24 (0.25)	31.60 (0.15) -19.63 (0.25)	-222.47 (0.15) 245.33 (0.25)

SR-19B	9.22 (0.3)	-13.50 (0.45)	- 2.41 (0.55)	5.50 (0.2)	- 3.39 (0.2)
	0.64 (1.0)	7.06 (0.85)	10.39 (0.85)	1.72 (0.55)	3.56 (0.55)
SR-20A	31.27 (0.15)	-46.71 (0.275)	-34.52 (0.25)	25.83 (0.15)	-173.48 (0.15)
	- 5.86 (0.25)	- 3.63 (0.4)	23.88 (0.4)	-15.97 (0.25)	222.48 (0.25)
SR-20B	16.59 (0.4)	-27.59 (0.3)	- 9.41 (0.25)	7.41 (0.45)	4.13 (0.2)
	- 9.42 (0.85)	15.63 (0.75)	15.04 (0.8)	- 2.96 (0.9)	- 4.87 (0.45)
SR-21A	29.55 (0.125)	-47.64 (0.275)	18.95 (0.125)	25.78 (0.125)	-181.63 (0.125)
	- 9.63 (0.25)	-14.62 (0.4)	-20.81 (0.25)	-17.72 (0.25)	204.51 (0.25)
SR-21B	9.67 (0.25)	-35.36 (0.4)	31.28 (0.4)	-12.32 (0.575)	- 7.55 (0.35)
	-13.72 (0.6)	12.00 (0.8)	- 5.22 (0.675)	14.97 (0.9)	19.05 (0.625)
SR-22A	60.17 (0.15)	59.40 (0.15)	56.89 (0.125)	59.55 (0.15)	-360.62 (0.15)
	-29.95 (0.3125)	-21.60 (0.25)	-25.98 (0.2375)	-28.07 (0.3125)	365.62 (0.3125)
SR-22B	10.03 (0.2)	31.77 (0.675)	16.52 (0.45)	11.04 (0.25)	- 9.55 (0.25)
	-12.23 (0.6)	1.74 (1.125)	17.85 (0.8)	- 1.38 (0.6)	10.18 (0.6)
SR-23A	67.40 (0.15)	64.73 (0.15)	60.14 (0.15)	66.22 (0.15)	-257.17 (0.15)
	-24.96 (0.3)	-41.65 (0.3625)	-54.89 (0.3)	-30.73 (0.3)	272.90 (0.3)
SR-23B	8.45 (0.2)	7.05 (0.15)	8.09 (0.25)	8.06 (0.2)	-11.86 (0.2)
	-39.73 (0.75)	-16.93 (0.7)	- 5.59 (0.65)	-32.07 (0.7)	10.27 (0.65)
SR-24A	31.11 (0.15)	18.15 (0.1)	16.58 (0.1)	26.39 (0.15)	-171.62 (0.15)
	- 5.96 (0.25)	-36.40 (0.25)	-24.03 (0.25)	-13.50 (0.25)	181.53 (0.25)
SR-24B	10.83 (0.25)	-30.69 (0.45)	34.68 (0.45)	4.17 (0.25)	-10.82 (0.35)
	-15.79 (0.60)	11.30 (0.85)	- 9.14 (0.70)	-15.22 (0.60)	24.31 (0.65)
SR-25A	29.95 (0.125)	19.71 (0.125)	16.58 (0.1)	26.65 (0.125)	-153.47 (0.125)
	3.52 (0.25)	-11.07 (0.25)	-34.51 (0.25)	- 2.77 (0.25)	171.31 (0.25)
SR-25B	18.73 (0.35)	- 5.27 (0.15)	-15.54 (0.2)	18.45 (0.4)	9.26 (0.15)
	- 8.24 (0.70	37.34 (0.55)	13.44 (0.45)	- 3.36 (0.7)	-18.29 (0.45)

Table 15. The effect of disturbance on remote induction machine

	Sending End Fault					
	τ'_{d0} = 0.7233 sec r_2 = 0.015 pu s_0 = 0.7563 Hz			τ'_{d0} = 0.2411 sec r_2 = 0.045 pu s_0 = 2.2689 Hz		
	H, MW.S/MVA			H, MW.S/MVA		
	0.5	1.0	2.0	0.5	1.0	2.0
Case No.	SM-2	SM-1	SM-3	SM-6	SM-4	SM-7
Max. slip, Hz	33.82	4.1222	2.6582	8.0352	5.3788	3.8912
Time @ max. slip, sec	1.0	0.2	0.2	0.15	0.15	0.15
Internal voltage @ max. slip, pu	0.0561	0.5727	0.6748	0.7222	0.8035	0.8295
Terminal power @ max. slip, pu	0.0470	1.0871	0.9169	1.2425	0.9802	0.7463
Max. internal voltage, pu	0.3708	0.9922	0.9957	0.9943	0.9945	0.9948
Time @ max. voltage, sec	0.15	1.0	0.95	0.85	0.85	1.45
Slip @ max. voltage, Hz	7.3056	1.2098	1.0797	2.5796	2.5092	2.4716
Terminal power @ max. volt., pu	0.6486	0.8248	0.8048	0.8393	0.8354	0.8320
Max. terminal power, pu	0.6709	1.1005	1.2587	1.2425	1.2602	1.1222
Time @ max. power, sec	0.2	0.25	0.3	0.15	0.2	0.2
Slip @ max. power, Hz	7.3931	3.6328	2.1477	8.0352	4.8719	3.8102
Internal volt. @ max. power, pu	0.6709	0.5373	0.7260	0.7222	0.8313	0.9125
	unstable					

Receiving End Fault					
τ'_{d0} = 0.7233 sec r_2 = 0.015 pu s_0 = 0.7563 Hz			τ'_{d0} = 0.2411 sec r_2 = 0.045 pu s_0 = 2.2689 Hz		
H, MW.S/MVA			H, MW.S/MVA		
0.5	1.0	2.0	0.5	1.0	2.0
SM-8	SM-9	SM-10	SM-11	SM-12	SM-13
33.67	4.0068	2.5983	8.2672	5.5032	3.9574
1.0	0.2	0.2	0.15	0.15	0.15
0.0488	0.5747	0.6801	0.7162	0.8030	0.8306
0.0312	1.0624	0.9013	1.2415	0.9783	0.7342
0.3534	0.9900	0.9939	0.9939	0.9936	0.9969
0.15	1.0	0.95	0.85	0.85	1.45
7.1372	1.2827	1.1462	2.6578	2.5850	2.5224
0.6073	0.8262	0.8047	0.8392	0.8342	0.8163
0.6846	1.1003	1.2467	1.2415	1.2447	1.1091
0.2	0.25	0.3	0.15	0.2	0.2
7.3273	3.5474	2.1225	8.2672	5.0059	3.8841
0.3286	0.5487	0.7315	0.7162	0.8206	0.9056
unstable					

Table 16. The effect of the disturbance on remote machines - synchronous and induction generation mix

Case No.	H, MW.S/MVA	Load Level	Load Distribution	
			Synch. MW	Ind. MW
SI-5	1.0	normal	42.5	42.5
SI-6	0.5	normal	42.5	42.5
SI-7	0.5	heavy	0	160
SI-8	0.5	heavy	80	80
SI-20	4.0	heavy	0	160

$(\delta_{k1} - \bar{\delta})$ max. Degree (@ time, sec)	$(\delta_{k2} - \bar{\delta})$ max. Degree (@ time, sec)	$(\ddot{\delta}_{k1} - \ddot{\bar{\delta}})$ max. Rad/sec^2 (@ time, sec)	$(\ddot{\delta}_{k2} - \ddot{\bar{\delta}})$ max. Rad/sec^2 (@ time, sec)	Max. Slip Hz (@ time, sec)
27.13 (0.3)	35.14 (0.25)	29.53 (0.55)	-99.58 (0.25)	1.9935 (0.15)
30.72 (0.3)	44.99 (0.2)	-49.64 (0.3)	-270.81 (0.2)	3.2331 (0.15)
← Induction Generation unstable →				
48.17 (0.35)	93.91 (0.1)	40.65 (1.6)	246.89 (0.1)	6.6546 (0.15)
32.07 (0.45)	52.84 (0.45)	-53.70 (0.45)	61.79 (0.1)	2.7073 (0.2)

Table 17. Effect of disturbance on existing machines - remote synchronous generation

Case No.	$\bar{\delta}$ max. Degree (@ time, sec)	$\ddot{\bar{\delta}}$ max. Rad/sec^2 (@ time, sec)	AIJ,/sec		AIK,/sec	
			min.	max.	max. (@ time, sec)	min. (@ time, sec)
ST-1	99.60 (2.1)	3.87 (0.25)	.0286	.0297	.0190 (0.6)	-.0198 (0.25)
ST-2	203.95 (2.1)	13.29 (0.15)	.0282	.0297	.0649 (0.9)	-.0697 (0.15)
ST-3	102.91 (2.1)	3.10 (0.25	.0287	.0297	.0170 (0.6)	-.0155 (0.25)
ST-4	196.17 (2.1)	13.64 (1.65)	.0279	.0297	.0669 (1.8)	-.0712 (1.65)
ST-5	304.91 (2.1)	6.89 (0.25)	.0639	.0665	.0396 (0.6)	-0.0231 (0.25)
ST-7	96.89 (2.1)	3.41 (0.35)	.0339	.0347	.0069 (0.75)	-.0256 (0.35)
ST-8	191.10 (2.1)	8.32 (0.2)	.0315	.0347	.0399 (1.95)	-.0514 (0.2)
ST-9	116.24 (2.1)	2.88 (1.2)	.0337	.0347	.0049 (1.6)	-.0229 (1.2)
ST-10	180.72 (2.1)	7.30 (1.65)	.0322	.0347	.0308 (1.85)	-.0458 (2.05)
ST-11	316.18 (2.1)	5.56 (0.25)	.0644	.0665	.0351 (0.6)	-.0159 (0.25)
ST-13	421.24 (2.1)	7.33 (0.4)	.0766	.0776	.0187 (0.95)	-.0430 (0.4)
ST-15	436.87 (2.1)	5.88 (0.45)	.0766	.0776	.0113 (0.95)	-.0354 (0.45)
ST-17	114.51 (2.1)	3.46 (0.25)	.0259	.0281	.0160 (1.55)	-.0160 (0.25)
ST-18	247.77 (2.1)	14.50 (1.95)	.0244	.0281	.0718 (2.1)	-.0756 (1.95)

ST-19	131.82	3.37	.0256	.0282	.0183	-.0158
	(2.1)	(0.35)			(0.65)	(0.35)
ST-20	223.44	11.27	.0245	.0282	.0536	-.0565
	(2.1)	(1.00)			(0.85)	(1.00)
ST-21	105.29	3.36	.0322	.0341	.0043	-.0247
	(2.1)	(0.35)			(1.8)	(0.35)
ST-22	209.87	8.58	.0300	.0341	.0382	-.0519
	(2.1)	(1.7)			(1.525)	(1.7)
ST-23	148.62	3.40	.0316	.0341	.0068	-.0252
	(2.1)	(0.4)			(0.8)	(0.4)
ST-24	223.36	7.02	.0294	.0341	.0247	0.0429
	(2.1)	(0.15)			(1.45)	(0.15)
ST-25	322.26	6.78	.0600	.0672	.0314	-.0224
	(2.1)	(0.3)			(1.65)	(0.25)
ST-27	362.30	6.08	.0612	.0672	.0313	-.0184
	(2.1)	(0.3)			(0.7)	(0.35)
ST-29	418.76	7.44	.0727	.0794	.0161	-.0445
	(2.1)	(0.45)			(2.075)	(0.4)
ST-31	486.07	6.73	.0699	.0794	.0126	-.0429
	(2.1)	(0.45)			(0.95)	(0.5)
ST-33	578.21	9.66	.0628	.0794	.0185	-.0527
	(2.1)	(0.45)			(0.925)	(0.4)
ST-34	551.84	8.06	.0695	.0794	.0155	-.0466
	(2.1)	(0.4)			(0.85)	(0.4)
ST-35	412.30	9.70	.0551	.0669	.0377	-.0383
	(2.1)	(0.25)			(1.5)	(0.2)
ST-36	410.63	7.81	.0592	.0673	.0341	-.0255
	(2.1)	(0.25)			(1.5)	(0.25)

Table 18. Effect of disturbance on existing machines - remote synchronous generation - critical inertia

Case No.	$\bar{\delta}$ max. Degree (@ time, sec)	$\ddot{\bar{\delta}}$ max. Rad/sec^2 (@ time, sec)	AIJ,/sec		AIK,/sec	
			min.	max.	max. (@ time, sec)	min. (@ time, sec)
ST-26A	1007.67 (2.1)	19.33 (0.275)	0.0307	0.0672	0.0821 (0.15)	-0.0663 (0.45)
ST-30I	848.99 (2.1)	10.11 (0.5)	0.0587	0.0792	0.0542 (0.95)	-0.0230 (1.35)
ST-46C	878.09 (2.1)	9.08 (0.4)	0.0747	0.0776	0.0520 (0.4)	-0.0276 (1.5625)
ST-56	978.02 (2.1)	17.78 (0.3)	0.0470	0.0665	0.0796 (0.15)	-0.0777 (0.475)
ST-73	1035.60 (2.1)	17.79 (0.3)	0.0561	0.0688	0.0820 (0.15)	-0.0795 (0.475)
ST-80	797.20 (2.1)	9.0 (0.35)	0.0756	0.0800	0.0538 (0.35)	-0.0292 (1.275)

Table 19. Effect of disturbance on existing machines - remote synchronous generation - variation of penetration level

Case No.	$\bar{\delta}$ max. Degree (@ time, sec)	$\ddot{\bar{\delta}}$ max. Rad/sec^2 (@ time, sec)	AIJ,/sec		AIK,/sec	
			min.	max.	max. (@ time, sec)	min. (@ time, sec)
ST-57	104.81 (2.1)	2.0 (0.35)	0.0270	0.0279	0.0253 (0.65)	0.0041 (0.35)
ST-58	140.49 (2.1)	6.27 (0.125)	0.0266	0.0279	0.0182 (0.125)	-0.0384 (0.25)
ST-59	90.76 (2.1)	1.66 (0.4)	0.0332	0.0337	0.0028 (0.4)	-0.0118 (0.75)
ST-60	121.35 (2.1)	4.97 (0.15)	0.0326	0.0336	0.0201 (0.15)	-0.0231 (0.35)
ST-61	130.87 (2.1)	5.39 (0.25)	0.0242	0.0286	0.0361 (0.25)	-0.0084 (0.60)
ST-61A	277.42 (2.1)	13.07 (0.15)	0.0214	0.0286	0.0773 (0.15)	-0.0542 (0.35)
ST-62	501.11 (2.1)	13.70 (0.2625	0.0164	0.0286	0.0751 (0.2625)	-0.0672 (0.40)
ST-63	136.70 (2.1)	4.63 (0.35)	0.0305	0.0348	0.0414 (0.35)	0.0034 (0.80)
ST-64	155.50 (2.1)	5.56 (0.30)	0.0276	0.0349	0.0462 (0.25)	-0.0014 (0.65)

ST-65	270.43 (2.1)	4.26 (0.30)	0.0647	0.0670	0.0357 (0.65)	0.0001 (0.30)
ST-65A	547.68 (2.1)	15.06 (0.15)	0.0595	0.0667	0.0578 (0.15)	-0.0697 (0.35)
ST-66	926.89 (2.1)	19.78 (0.175)	0.0525	0.0666	0.0813 (0.15)	-0.0780 (0.325)
ST-67	272.31 (2.1)	4.96 (0.35)	0.0763	0.0786	0.0216 (0.35)	-0.0167 (0.80)
ST-68A	316.28 (2.1)	6.40 (0.3)	0.0744	0.0786	0.0287 (0.3)	-0.0189 (0.65)
ST-69	340.69 (2.1)	8.12 (0.35	0.0543	0.0647	0.0221 (0.35)	-0.0075 (0.85)

Table 20. Effect of disturbance on existing machines - remote synchronous generation - faults located inside the existing system

Case No.	$\bar{\delta}$ max. Degree (@ time, sec)	$\ddot{\delta}$ max. Rad/sec^2 (@ time, sec)	AIJ,/sec		AIK,/sec	
			min.	max.	max. (@ time, sec)	min. (@ time, sec)
SR-14	2/9.19 (2.1)	1.91 (0.2) -0.88 (0.5)	0.0534	0.0570	0.0261 (0.5)	0.0139 (0.2)
SR-16A	441.86 (2.1)	8.91 (0.125) -5.60 (0.3)	0.0530	0.0568	0.0252 (0.125)	-0.0532 (0.3)
SR-17	311.09 (2.1)	1.90 (0.25) -0.37 (0.55)	0.0579	0.0620	0.0125 (0.55)	0.0027 (0.25)
SR-17A	341.80 (2.1)	3.57 (0.2) -1.88 (0.5)	0.0583	0.0620	0.0063 (0.2)	-0.0203 (0.5)
SR-17B	461.07 (2.1)	5.50 (0.45) -1.98 (0.775)	0.0461	0.0539	0.0176 (0.45)	-0.0060 (0.15)
SR-17C	508.82 (2.1)	4.64 (0.35) -1.40 (0.675)	0.0492	0.0539	0.0130 (0.35)	-0.0200 (0.675)
SR-17F	450.18 (2.1)	6.02 (0.45) -2.97 (0.70)	0.0417	0.0460	0.0081 (0.40)	-0.0206 (0.15)
SR-17G	603.71 (2.1)	9.65 (0.125) -3.42 (0.25)	0.0377	0.0460	0.0282 (0.125)	-0.0448 (0.25)
SR-18A	871.74 (2.1)	11.89 (0.15) -1.88 (0.25)	0.0390	0.0467	0.0313 (0.15)	-0.0420 (0.25)
SR-18B	697.89 (2.1)	4.87 (0.35) 3.21 (1.20)	0.0403	0.0467	0.0153 (0.65)	0.0063 (0.35)
SR-19A	438.51 (2.1)	8.98 (0.15) -5.44 (0.25)	0.0422	0.0447	0.0222 (0.15)	-0.0548 (0.25)

SR-19B	308.20 (2.1)	1.45 (0.25) 0.38 (0.55)	0.0433	0.0447	0.0239 (0.55)	0.0181 (0.2)
SR-20A	518.23 (2.1)	7.18 (0.15) -3.92 (0.25)	0.0384	0.0445	0.0116 (0.15)	-0.0503 (0.25)
SR-20B	376.84 (2.1)	2.53 (0.4) -0.20 (0.95)	0.0394	0.0447	0.0239 (0.2)	0.0160 (0.45)
SR-21A	689.95 (2.1)	8.64 (0.125) -2.13 (0.25)	0.0327	0.0421	0.0110 (0.125)	-0.0499 (0.25)
SR-21B	558.75 (2.1)	5.12 (0.35) -0.91 (0.625)	0.0330	0.0421	0.0392 (0.625)	0.0154 (0.35)
SR-22A	1059.68 (2.1)	18.57 (0.15) -5.40 (0.3125)	0.0388	0.0467	0.0666 (0.15)	-0.0608 (0.3125)
SR-22B	743.53 (2.1)	5.53 (0.25) 3.23 (0.55)	0.0411	0.0467	0.0190 (0.06)	0.0025 (0.25)
SR-23A	625.76 (2.1)	12.39 (0.15) -4.54 (0.3)	0.0439	0.0549	0.0387 (0.15)	-0.0539 (0.3)
SR-23B	352.86 (2.1)	2.49 (0.2) -0.28 (0.6)	0.0504	0.0549	0.0317 (0.65)	0.0137 (0.2)
SR-24A	673.13 (2.1)	8.44 (0.15) -1.77 (0.25)	0.0308	0.0421	0.0092 (0.15)	-0.0407 (0.25)
SR-24B	531.01 (2.1)	5.52 (0.4) -1.75 (0.65)	0.0323	0.0421	0.0434 (0.65)	0.0126 (0.35)
SR-25A	578.61 (2.1)	7.29 (0.125) -2.17 (0.25)	0.0369	0.0460	0.0158 (0.125)	-0.0370 (0.25)
SR-25B	465.87 (2.1)	5.34 (0.45) -1.33 (0.725)	0.0389	0.0460	0.0043 (0.45)	-0.0213 (0.15)

Table 21. Effect of disturbance on existing machines - remote induction generation

	Sending End Fault					
	τ'_{d0} = 0.7233 sec r_2 = 0.015 pu s_0 = 0.7563 Hz			τ'_{d0} = 0.2411 sec r_2 = 0.045 pu s_0 = 2.2699 Hz		
	H, MW.S/MVA			H, MW.S/MVA		
	0.5	1.0	2.0	0.5	1.0	2.0
Case No.	SM-2	SM-1	SM-3	SM-6	SM-4	SM-7
$\ddot{\bar{\delta}}$, rad/sec^2, first swing,	unstab.					
max.	3.5715	5.0464	4.4379	4.6387	4.0049	2.5914
min.	-0.0116	-0.0486	-0.1908	-0.0865	-0.0720	-0.0198
$(\ddot{\delta}_k - \ddot{\bar{\delta}})$, rad/sec^2, first swing,						
max.	276.13	140.55	73.52	326.01	163.26	81.96
min.	34.85	-63.38	-46.70	-166.17	-85.98	-29.37
AIJ,/sec						
max.	-0.0314	-0.0317	-0.0317	-0.0317	-0.0317	-0.0317
min.	-0.0296	-0.0296	-0.0301	-0.0295	-0.0300	-0.0302
AIK,/sec						
max.	0.0217	0.0294	0.0279	0.0274	0.0241	0.0167
min.	0.0035	0.0031	0.0019	0.0	0.0	0.0

Receiving End Fault					
τ'_{d0} = 0.7233 sec r_2 = 0.015 pu s_0 = 0.7563 Hz			τ'_{d0} = 0.2411 sec r_2 = 0.045 pu s_0 = 2.2689 Hz		
H, MW.S/MVA			H, MW.S/MVA		
0.5	1.0	2.0	0.5	1.0	2.0
SM-8	SM-9	SM-10	SM-11	SM-12	SM-13
unstab.					
3.7816 -0.0115	5.1675 -0.0183	4.7429 -0.1438	4.7475 -0.1316	4.1852 -0.1741	2.7731 -0.1465
237.90 30.82	123.18 -62.85	66.71 -45.43	326.20 -166.22	163.33 -83.25	81.93 -28.30
-0.0314 -0.0285	-0.0317 -0.0288	-0.0317 -0.0291	-0.0317 -0.0286	-0.0317 -0.0290	-0.0317 -0.0292
0.0217 0.0031	0.0289 0.0040	0.0273 0.0024	0.0276 0.0	0.0241 0.0	0.168 0.0

Table 22. Effect of the disturbance on the existing machines - remote synchronous and induction generation mix

Case No.	H MW.S/MVA	Load Level	Load Distribution		$\ddot{\delta}$ max, Rad/sec^2 (@ Time, sec)
			Synch. MW	Ind. MW	
SI-5	1.0	normal	42.5	42.5	4.84 (0.25)
SI-6	0.5	normal	42.5	42.5	5.20 (0.2)
SI-8	0.5	heavy	80	80	10.17 (0.35)
SI-20	4.0	heavy	0	160	9.39 (0.45)

AIJ,/sec		AIK1,/sec		AIK2,/sec	
min.	max.	min. (@ time, sec)	max. (@ time, sec)	min. (@ time, sec)	max. (@ time, sec)
.0252	.0273	-.0086 (0.3)	.0136 (1.5)	-.0139 (0.25)	.0052 (1.5)
.0248	.0273	-.0111 (0.3)	.0150 (1.5)	-.0170 (0.2)	.0066 (0.5)
.0557	.0643	-.0178 (0.3)	.0213 (1.6)	-.0180 (0.2)	.0094 (1.6)
.0600	.0630	-.0097 (0.45)	.0250 (0.2)	-.0240 (0.45)	.0045 (1.95)

VII. EIGENVALUE ANALYSIS OF THE FAULT-CLEARED NETWORK

A. Scope of the Analysis

Eigenvalue analysis of the fault-cleared network of the studied power system is conducted to investigate the effect of the variation of the parameters of interest on the normal modes and mode shapes of this system. These parameters are:

- the inertia of the remote generation,
- load level,
- penetration level,
- length of the new transmission lines,
- the point of connection of the remote generation to the existing system.

Cases NM-1 through NM-12 are conducted to cover these parameters. The results are tabulated in Table 23. From this table, the influence of the above parameters are identified and summarized. For the selected power system, there are three natural modes of oscillation, with each mode associated with the oscillation of one group of machines with respect to another group. The grouping depends on the system configuration, i.e., the impedance between the machines, the machines' inertias, the load levels, the penetration level, the point of connection, etc. This is reflected in the data displayed in Table 23 (in the frequencies of oscillation and the mode shapes).

The response of the power network to severe disturbances, such as displayed by the swing curves of Chapter VI, is influenced by these natural modes of oscillation. One or more of these modes may show up as

the dominating modes. Thus, comparing Table 23 with the swing curves of Chapter VI will help us understand the influence of these parameters on the dynamic performance of the selected power network.

B. Numerical Results

1. Eigenvalue analysis

From Table 23, the influence of various parameters on the normal modes and mode shapes of the fault-cleared network are summarized below.

a. Effect of the inertia of the remote generation High inertia of the remote generation yielded three natural modes of oscillation. The mode shape of the lowest mode of oscillation is such that machines no. 2, 3, and the remote machine are swinging together as one group against machine no. 1 and the remote machine has the largest relative swing. For the next higher mode of oscillation, machines no. 2 and 3 are swinging together as one group against both machine no. 1 and the remote machine as a group. For the highest mode of oscillation, machines no. 1, 2, and the remote machine are swinging together as one group against machine no. 3, e.g., Case NM-1.

Low inertia of the remote generation results in higher frequencies of oscillation and somewhat different grouping of coherent machines. In the lowest mode of oscillation. the grouping of coherent machines is the same as that of the high remote inertia case, i.e., machines no. 2, 3, and the remote machine are swinging together as one group against machine no. 1 (e.g., compare Cases NM-2 to NM-1). The grouping of the coherent machines for the next mode of oscillation is such that machine no. 3

and the remote machine are swinging together as one group against machines no. 1 and 2 which form another group. The highest mode of oscillation is very interesting because the remote machine is swinging against the three existing machines (e.g., Case NM-2) which remain relatively stationary.

b. Effect of load level Load level has a minor influence on the frequencies of oscillation but it has no effect on the grouping of coherent machines. Heavier loads tend to decrease the frequencies of oscillation slightly. This trend is consistent for both high and low inertia cases, e.g., compare Cases NM-3 to NM-5 and NM-4 to NM-6.

c. Effect of penetration level In this study, penetration level seems to have negligible effect on neither the frequencies of oscillation nor the grouping of coherent machines, e.g., compare Cases NM-1 to NM-3 and NM-2 to NM-4.

d. Effect of length of the new transmission lines Long transmission lines (high impedance) between the remote generation and the existing system tends to decrease the frequencies of oscillation slightly, but has no effect on the grouping of the coherent machines. This trend is consistent for both high and low remote inertia cases, e.g., compare Cases NM-5 to NM-7 and NM-6 to NM-8.

e. Effect of the point of connection The effect of the point of connection of the remote generation to the existing system seems to depend on both the inertia of the remote generation and the length of the transmission network joining the remote generation to the existing system. For long transmission line cases, the point of connection affects

Table 23. Normal modes and mode shapes of the fault-cleared network

Case No.	Remote Gen. Joins the Existing System at Bus No.	Length of New Trans-mission Lines	Load Level	Penetra-tion Level, Percent	Remote Inertia, to 100 MVA base, sec
NM-1	8	short	normal	13	6.4
NM-2	8	short	normal	13	1.0
NM-3	8	short	normal	27	6.4
NM-4	8	short	normal	27	1.0
NM-5	8	short	heavy	25	6.4
NM-6	8	short	heavy	25	1.0
NM-7	8	long	heavy	25	6.4
NM-8	8	long	heavy	25	1.0
NM-9	6	long	heavy	25	6.4
NM-10	6	long	heavy	25	1.0
NM-11	6	short	heavy	25	6.4
NM-12	6	short	heavy	25	1.0

Natural Modes		Normalized Mode Shapes (Relative Rotor Angle Deviations)				Group of Coherent Machines	
Frequency, Hz	Period, sec	Bus 1	Bus 2	Bus 3	Bus 11	Group 1, Machines No.	Group 2, Machines No.
1.21	0.82	-0.5003	0.6401	0.4418	1.0	2,3,11	1
1.74	0.57	-0.0720	1.0	0.1497	-0.8043	2,3	1,11
2.20	0.45	-0.0346	-0.1968	1.0	-0.1457	3	1,2,11
1.39	0.72	-0.3706	1.0	0.5944	0.5711	2,3,11	1
2.14	0.47	-0.0407	-0.3556	1.0	0.2277	3,11	1,2
3.67	0.27	-0.0084	-0.0651	-0.1276	1.0	1,2,3	11
1.21	0.83	-0.5037	0.6474	0.4535	1.0	2,3,11	1
1.75	0.57	-0.0701	1.0	0.1429	-0.8083	2,3	1,11
2.20	0.45	-0.0338	-0.1964	1.0	-0.1490	3	1,2,11
1.38	0.72	-0.3722	1.0	0.6040	0.5799	2,3,11	1
2.14	0.47	-0.0397	-0.3595	1.0	0.2296	3,11	1,2
3.68	0.27	-0.0082	-0.0653	-0.1288	1.0	1,2,3	11
1.18	0.85	-0.5068	0.6481	0.4763	1.0	2,3,11	1
1.74	0.57	-0.0704	1.0	0.1625	-0.8163	2,3	1,11
2.17	0.46	-0.0312	-0.2061	1.0	-0.1489	3	1,2,11
1.36	0.74	-0.3784	1.0	0.6432	0.6099	2,3,11	1
2.12	0.47	-0.0356	-0.3729	1.0	0.2171	3,11	1,2
3.65	0.27	-0.0078	-0.0675	-0.1278	1.0	1,2,3	11
1.08	0.93	-0.3712	0.2777	0.1989	1.0	2,3,11	1
1.55	0.65	-0.1759	1.0	0.4482	-0.5609	2,3	1,11
2.14	0.47	-0.0357	-0.2716	1.0	-0.0670	3	1,2,11
1.35	0.74	-0.3771	1.0	0.6179	0.6556	2,3,11	1
2.11	0.47	-0.0385	-0.3750	1.0	0.2976	3,11	1,2
2.94	0.34	-0.0052	-0.0653	-0.1525	1.0	1,2,3	11
1.16	0.86	-0.2871	0.0226	0.0809	1.0	2,3,11	1
1.40	0.72	-0.2545	1.0	0.5384	-0.3130	2,3	1,11
2.14	0.47	-0.0292	-0.3002	1.0	-0.0622	3	1,2,11
1.37	0.73	-0.3562	1.0	0.6009	0.2108	2,3,11	1
2.10	0.48	-0.0465	-0.3558	1.0	0.3661	3,11	1,2
2.83	0.35	-0.0193	-0.0181	-0.1423	1.0	1,2,3	11
1.34	0.75	-0.6194	1.0	0.7192	0.9495	2,3,11	1
1.53	0.65	-0.0032	-0.8770	-0.2361	1.0	1,2,3	11
2.17	0.46	-0.0210	-0.2682	1.0	-0.1244	3	1,2,11
1.39	0.72	-0.3542	1.0	0.5918	0.1914	2,3,11	1
2.12	0.47	-0.0448	-0.3445	1.0	0.2531	3,11	1,2
3.55	0.28	-0.0210	-0.0265	-0.1109	1.0	1,2,3	11

only the frequencies of oscillation, but has no effect on the grouping of the coherent machines. This observation is true for both high and low remote inertia cases, e.g., compare Cases NM-7 to NM-9 and NM-8 to NM-10. Short transmission lines and low remote inertia yield similar results to those obtained for long transmission line, i.e., the frequencies of oscillation may change but the grouping of coherent machines are not altered (e.g., compare Cases NM-6 to NM-12). However, the combination of short transmission line and high remote inertia may influence both the frequencies of oscillation and the grouping of coherent machines, e.g., compare Cases NM-5 to NM-11.

2. Analysis of the swing curves of Chapter VI

The response of the power network due to severe disturbances, such as displayed by the swing curves of Chapter VI, can be analyzed from the understanding of the natural modes of oscillation and the mode shapes discussed in the previous section. The swing curves chosen for analysis are those of the ST-Series.

a. Effect of high inertia of the remote generation High inertia of the remote generation consistently yields one dominating mode of oscillation having the frequency ranging from 1.0 Hz to 1.34 Hz depending upon load level, penetration level, the point of connection, and the length of the transmission line joining the remote generation to the existing system. It is interesting to note that the dominating mode that appears in the swing curves of Chapter VI is always the lowest mode of oscillation predicted by the linear analysis of Chapter VII (Table 23).

The mode shape of this mode of oscillation (as shown in Table 23) is such that machines no. 2, 3, and the remote machine are swinging together as one group against machine no. 1 and that the relative rotor angle deviation of the remote machine is larger than those of machines no. 2 and 3. The swing curves of Chapter VI agree very closely with this prediction.

The other two higher modes may or may not show up as secondary modes superimposed on the dominant mode. If any of these secondary modes do show up noticeably, it is the one dominated by machine no. 3. The effect of this mode is more noticeable if the fault is moved from bus 10 to bus 6 or bus 8, i.e., closer to the existing system. The effect of this secondary mode is more pronounced when the penetration level is low. Higher penetration level or heavier load level appears to suppress this secondary mode.

Long transmission line between the remote generation and the existing system not only reduces the frequencies of oscillation, but also accentuates the relative swings between the remote machine and the machines of the existing system.

Moving the point of connection from bus 8 to bus 6 results in two dominant modes of oscillation. These two modes, which are influenced by machine no. 2 and the remote machine, interact strongly. The result is that machines no. 2, 3, and the remote machine do not swing as a group against machine no. 1.

b. Effect of low inertia of the remote generation For low inertia of the remote generation, the single dominant mode of oscillation

that causes machines no. 2, 3, and the remote machine to swing together against machine no. 1 disappear. In its place, three interacting modes of oscillation can be detected. The result that we can observe in the swing curves of Chapter VI is that the remote machine is swinging at a high frequency (ranging from 2.83 Hz to 3.68 Hz) against machine no. 1 and this high frequency swing is superimposed on a slower swing (ranging from 1.35 Hz to 1.39 Hz) that is dominated by machine no. 2. Since the interaction among the three modes of oscillation is strong, the swing curves of machines no. 2 and 3 against machine no. 1 appear as severely distorted sine curves.

The effects of penetration level, load level, length of the transmission line and point of connection are consistent with those discussed previously under items b through e of Section 1.

VIII. CONCLUSIONS

A. Effect of Various Parameters

From the analysis given in Chapters VI and VII the following conclusion can be reached.

1. Effect of low inertia

Low inertia, at the remote generation, made the system more vulnerable to a disturbance either on a transmission network between the remote generator(s) and the existing network or on a transmission network of the existing system close to the bus to which the remote generation is connected (bus 6 or bus 8). With other factors the same, the inertia at the remote generator(s) means:

- For the remote generator(s), higher rotor angle swings and greater tendency toward instability.
- For the existing system generators, higher rotor swings and greater magnitude of synchronizing forces among the groups of machines to hold the system together.
- The system, due to disturbance, is oscillating at a higher frequency.
- For the fault in the transmission line joining the remote generation to the existing system, stability limit (maximum relative swing) seems to be governed by the remote machine (lowest inertia) and machine no. 1 (highest inertia) of the existing system.
- Coherency among machines no. 2, 3, and the remote machine that exists when the remote machine has high inertia, is gone. Thus,

all three modes of oscillations show up distinctly rather than just one dominant mode to be found.

- With the lack of any one dominant mode of oscillation, the relative swings of machines no. 2, 3, and the remote machine with respect to machine no. 1 appear as severely distorted sine curves, in contrast to the undistorted sinusoidal swings obtained under high remote inertia cases.

2. Induction versus synchronous generation

The remote induction machine is particularly vulnerable to instability when the inertia is low. On the other hand, the existing system generators are less affected by the disturbance for remote induction generation than for the synchronous case.

The effect of the disturbance on the remote induction machine is much reduced when its rotor resistance is increased. This is because the maximum torque occurs at a higher slip, allowing a larger region of "feasible" operation.

A mix of synchronous and induction generators at the remote location appears to improve the system dynamic behavior. To take full advantage of that effect, equal sharing of the remote generation among the synchronous and induction generators appears to be desirable.

3. System load level and penetration level

In the major portion of this study, the remote generation was held to about 27 percent of the total system generation, but the overall load and generation levels were changed. The normal load represented 315 MW

load while in the heavy load condition a 630 MW load was used. The generation capacity was about 683 MW.

At this level of penetration of the remote generation, it is critical that higher (or at least normal) values of inertia constants be used for remote generation. If this is not provided for, poor dynamic behavior at heavy load conditions, including instability, is often encountered.

The effect of the variation of the penetration level (13-38 percent) can be summarized as follows:

- For the overall system, the relative swings of the rotor of the remote generator with respect to the rotors of the machines in the existing system and its inertial center increase very rapidly with the increase in penetration level.
- The effect of disturbance on the existing machines is more severe under high penetration level.
- High penetration level appears to suppress the higher (secondary) modes of oscillation, making the lower, and dominant, mode stand out by itself (this is true only when the remote generation has high inertia).

4. Fault location

Faults external to the existing network are more severe than the internal faults. Thus, faults that are electrically close to the remote generation adversely affect the transient stability of the overall power network. The opposite is true with faults that are electrically far

away from the remote generation. The effect of fault location can be summarized below:

- For an external fault, the relative swing of the rotor of the remote generator with respect to the rotor of the existing machine with the highest inertia is consistently larger than those with respect to the lighter machines; this is not always true for internal fault.
- For an internal fault, the remote machine is most disturbed when the fault is located close to the machine with the highest inertia (machine no. 1). However, the opposite is not true, i.e., a fault located close to the machine with the lowest inertia (machine no. 3) does not necessarily cause the least amount of disturbance to the remote machine.
- For both external and internal faults, lower inertia of the remote machine produces greater swings and accelerations of the remote machine.
- For internal faults, it appears that the existing power network is least disturbed when the fault is located at the machine with the smallest inertia, and it is most disturbed when the fault is located at the machine with the highest inertia.
- Fault location has strong influence on the synchronizing forces between the two groups of machines.

5. Network configuration

The existing network bus to which the remote generation is connected has not been critical in this study; other factors are more important.

The dynamic behavior of the remote induction generation appears to be more sensitive to the impedance (the length) of the transmission network joining the remote generation to the existing system than that of the remote synchronous generation.

For critically stable remote synchronous generation cases, long transmission lines required an inertia constant at the remote machine almost three times as much as that required by short transmission lines.

The effect of the disturbance on both the remote machine and the existing machines is greater when the transmission lines joining them are long. The machines' relative swings are accentuated, but the accelerations appear to be reduced and the frequencies of oscillation are also reduced. The reduction in frequencies of oscillation can be observed from both the swing curves of Chapter VI and the small perturbation analysis of Chapter VII.

When a mix of remote synchronous and induction generators is used, it appears to be more beneficial to connect them to the same bus, i.e., to have them electrically close.

From the above discussion, it is clear that low inertia at the remote generation, long transmission network joining the remote generation to the existing power system, heavy load level, and high penetration level are all detrimental to the dynamic behavior of the power system. Each of these parameters by itself has an adverse effect on the dynamic performance of the power system. The combined effects of these parameters acting together are even worse and should be avoided.

Under transient condition, remote induction generation appears to benefit from higher rotor resistance; but, this means higher losses and lower efficiency under normal operating condition. So, a compromise among these conflicting requirements must be made in the choice of the value of the rotor resistance.

IX. REFERENCES

1. General Accounting Office. "Power Production at Federal Dams Could be Increased by Modernizing Turbines and Generators." Document No. PE-269 254/9SL. Washington, D.C.: General Accounting Office, Energy and Minerals Division, March 1977.

2. Rosko, R. J. "Expanded Opportunities for Hydro Generation." Electric Forum 3 (No. 3, 1977):10-12.

3. Gladwell, J. S.; and Warnick, C. C., eds. Low-Head Hydro: An Examination of an Alternative Energy Source. Moscow, Idaho: Idaho Water Resources Research Institute, 1978.

4. Van Vranken, W. P. "Tube Turbines to Modernize Hydro Plants." Allis Chalmers Engineering Review 40 (No. 3, 1975):14-17.

5. Van Vranken, W. P.; and Wachter, G. F. "A Second Look at Small Hydro Sites." Allis-Chalmers Engineering Review 30 (No. 3, 1965):30-31.

6. Concordia, C.; and Brown, P. G. "Effects of Trends in Large Steam Turbine Driven Generator Parameters on Power System Stability." IEEE Trans., PAS-90 (September/October 1971):2211-2218.

7. Lokay, H. E.; and Thoits, P. O. "Effects of Future Turbine-Generator Characteristics on Transient Stability." IEEE Trans., PAS-90 (November/December 1971):2427-2431.

8. Van Vranken, W. P. "Future Hydrogenerator Design Concepts Favor System Stability." Allis-Chalmers Engineering Review 37 (No. 3, 1972):23-25.

9. Basu, T. K.; and Nanda, J. "Effects of Different Parameters on Transient Stability of Power Systems." Journal of the Institution of Engineers (India), Electrical Engineering Division 58 (April 1978):256-261.

10. Carton, E.; and Ribbens-Pavella, M. "Lyapunov Methods Applied to Multimachine Transient Stability with Variable Inertia Coefficients." Proc. IEE (London) 118, No. 11 (November 1971):1601-1606.

11. Lee, S. T. Y.; and Schweppe, F. C. "Distance Measures and Coherency Recognition for Transient Stability Equivalents." IEEE Trans., PAS-92 (No. 5, 1973):1550-1557.

12. Germond, A. J.; and Podmore, R. "Dynamic Aggregation of Generating Unit Models." IEEE Trans., PAS-97 (July/August 1978):1060-1069.

13. Podmore, R. "Identification of Coherent Generators for Dynamic Equivalents." IEEE Trans., PAS-97 (July/August 1978):1344-1354.

14. Undrill, J. M.; and Turner, A. E. "Construction of Power System Electromechanical Equivalents by Modal Analysis." IEEE Trans., PAS-90 (September/October 1971):2049-2059.

15. Undrill, J. M.; Casazza, J. A.; Gulachenski, E. M.; and Kirchmayer, L. K. "Electromechanical Equivalents for Use in Power System Stability Studies." IEEE Trans., PAS-90 (September/October 1971): 2060-2071.

16. Mittelstadt, W. A. "Four Methods of Power System Damping." IEEE Trans., PAS-87 (May 1968):1323-1329.

17. de Mello, F. P.; and Laskowski, T. F. "Concepts of Power System Dynamic Stability." IEEE Trans., PAS-94 (May/June 1975):827-833.

18. Dandeno, P. L.; Hauth, R. L.; and Schulz, R. P. "Effects of Synchronous Machine Modeling in Large Scale System Studies." IEEE Trans., PAS-92 (March/April 1973):574-582.

19. Anderson, P.M.; and Fouad, A. A. Power System Control and Stability, Vol. 1. Ames, Iowa: Iowa State University Press, 1977.

20. Fouad, A. A.; Kruempel, K. C.; and Na Nakorn, S. "Effect of Reduced Inertia on the Transient Stability of a Power System." Final report submitted to the U.S. Bureau of Reclamation for Contract No. 9-07-83-V0711, 1979.

21. Moore, R. C. "Consider Induction Generators." Allis-Chalmers Electrical Review 28 (No. 4, 1963):18-21.

22. Moore, R. C. "Induction Versus Synchronous Generators." Allis-Chalmers Engineering Review 30 (No. 3, 1965):25-29.

23. Byerly, R. T.; Sherman, D. E.; and McLain, D. K. "Normal Modes and Mode Shapes Applied to Dynamic Stability Analysis." IEEE Trans., PAS-94 (March/April 1975):224-229.

24. Ramey, D. G.; Byerly, R. T.; and Sherman, D. E. "The Application of Transfer Admittances to the Analysis of Power System Stability Studies." IEEE Trans., PAS-90 (May/June 1971):993-999.

25. Philadelphia Electric Company, System Planning Division. "Power System Stability Program User's Guide." Philadelphia Electric Company, Publication No. UG004-2, April 1971.

X. ACKNOWLEDGEMENTS

The author wishes to express his appreciation to all the members of his committee, Dr. R. G. Brown, Dr. R. A. Danofsky, Dr. A. A. Fouad, Dr. J. O. Kopplin, Dr. K. C. Kruempel, and Dr. R. J. Lambert. A special thanks is given to his major advisor, Dr. Fouad, for his sacrifice and valuable guidance and suggestions, and to Dr. Kopplin who took over for Dr. Fouad during the last stage of the author's educational career. Special thanks are given to Dr. Kruempel and Professor J. R. Pavlat for their valuable aid with the computer.

Deepest gratitude is given to the Ananda Mahidol Foundation and the Electricity Generating Authority of Thailand for their generosity and financial support.

A special thanks is given to Jeanne Gehm for her excellent typing and her eagerness to help.

To his wife, her love, patience, understanding, and dedication makes all this worthwhile.

XI. APPENDIX A: COMPUTATION OF THE CHARACTERISTIC MATRIX $\bar{A}$

A. Case NM-3

This case covers the remote synchronous generation series ST-17 through ST-20 (short line, bus 8 connection, normal load, and penetration level = 27%).

From the data of case ST-17, we have

$$\delta_{10} = 2.03^\circ,\ \delta_{20} = 11.67^\circ,\ \delta_{30} = 14.64^\circ,\ \delta_{40} = 13.60^\circ$$

$$A_{12} = 1.325078,\ A_{13} = 1.106276,\ A_{14} = 0.769159$$

$$\hat{A}_{12} = 0.200157,\ \hat{A}_{13} = 0.143811,\ \hat{A}_{14} = 0.095433$$

$$\theta_{12} = 81.31^\circ,\ \theta_{13} = 82.53^\circ,\ \theta_{14} = 82.87^\circ$$

$$H_1 = 23.64\,S,\quad H_2 = 6.40\,S,\quad H_3 = 3.01\,S,\quad H_4 = 6.40\,S.$$

From equation (4.27.a),

$$g_{ij} = -\hat{A}_{ij} \sin (\delta_{io} - \delta_{jo})$$

Also from equation (4.27.b),

$$g_{ii} = -\sum_{\substack{j=1 \\ j\neq i}}^{n} g_{ij}$$

Thus the first row of matrix $[g_{ij}]$ can be calculated as follows.

$$g_{12} = -0.200157 \sin (2.03 - 11.67^\circ) = 0.033518$$

$$g_{13} = -0.143811 \sin (2.03^\circ - 14.64^\circ) = 0.031396$$

$$g_{14} = -0.095439 \sin (2.03^\circ - 13.60^\circ) = 0.019141$$

$$g_{11} = -(g_{12} + g_{13} + g_{14}) \qquad = -0.084054$$

From equation (4.27.c)

$$b_{ij} = A_{ij} \sin \theta_{ij} \cos (\delta_{io} - \delta_{jo})$$

and from equation (4.27.d),

$$b_{ii} = - \sum_{\substack{j=1 \\ j \neq i}}^{n} b_{ij}$$

Thus the first row of matrix $[b_{ij}]$ can be calculated as follows.

$$b_{12} = 1.325078 \sin 81.31^{\circ} \cos (2.03^{\circ} - 11.67^{\circ}) = 1.291377$$

$$b_{13} = 1.106276 \sin 82.53^{\circ} \cos (2.03^{\circ} - 14.64^{\circ}) = 1.070430$$

$$b_{14} = 0.769159 \sin 82.87^{\circ} \cos (2.03^{\circ} - 13.60^{\circ}) = 0.747707$$

$$b_{11} = -(b_{12} + b_{13} + b_{14}) \qquad = -3.109515$$

From the above calculations, it is clearly shown that g_{ij} is very small compared to b_{ij}. The effect of omitting g_{ij} from the characteristic matrix $\bar{A}$ will be shown below.

First, the matrix $\bar{A}$ is formed with $[g_{ij}]$ included. The ith row of matrix $\bar{A}$ is then given by an adapted form of equation (4.30.a),

$$a_{ij} = \frac{\omega_R}{2H_i} (g_{ij} + b_{ij})$$

For example, the elements of the first row of matrix $\bar{A}$ are:

$$a_{11} = \frac{377}{2 \times 23.64} (-0.084054 - 3.109515) = -25.464795$$

$$a_{12} = \frac{377}{2 \times 23.64} (0.033518 + 1.291377) = 10.564412$$

$$a_{13} = \frac{377}{2 \times 23.64} (0.031396 + 1.070430) = 8.785711$$

$$a_{14} = \frac{377}{2 \times 23.64} (0.019141 + 0.747707) = 6.114672$$

The matrix A (including $[g_{ij}]$) is given by

$$\bar{A} = \begin{bmatrix} -25.4648 & 10.5644 & 8.78571 & 6.11467 \\ 37.0478 & -94.5144 & 25.1249 & 32.3416 \\ 65.0690 & 52.6337 & -168.446 & 50.7437 \\ 21.4585 & 32.1067 & 23.9643 & -77.5295 \end{bmatrix}$$

The corresponding matrix $\bar{A}$ neglecting $[g_{ij}]$ is given by

$$\bar{A} = \begin{bmatrix} -24.7946 & 10.2971 & 8.53536 & 5.96204 \\ 38.0350 & -95.1988 & 24.9396 & 32.2242 \\ 67.0352 & 53.0277 & -170.912 & 50.8488 \\ 22.0223 & 32.2242 & 23.9148 & -78.1613 \end{bmatrix}$$

The effects of $[g_{ij}]$ on the normal modes and mode shapes of the characteristic matrix $\bar{A}$ are summarized in Table 24. As is evident in this table, the effects of $[g_{ij}]$ on the normal modes (natural frequencies) and mode shapes (normalized generator relative rotor angle deviations) of matrix $\bar{A}$ are extremely small. Indeed, the information concerning the normal modes and mode shapes has not been lost at all by

omitting $[g_{ij}]$. Hence, the assumption made earlier in Chapter IV that $[g_{ij}]$ is negligible is valid. The direct benefit of this assumption is a substantial saving in computation.

Table 24. Normal modes and mode shapes - Case NM-3

$[g_{ij}]$ Included					$[g_{ij}]$ Not Included				
Natural Modes, in Hz	Normalized Mode Shapes (Relative Rotor Angle Deviations)				Natural Modes, in Hz	Normalized Mode Shapes (Relative Rotor Angle Deviations)			
	Bus 1	Bus 2	Bus 3	Bus 11		Bus 1	Bus 2	Bus 3	Bus 11
1.21	-0.5308	0.6464	0.4520	1.0	1.21	-0.5037	0.6474	0.4535	1.0
1.74	-0.0732	1.0	0.1432	-0.8058	1.75	-0.0701	1.0	0.1429	-0.8083
2.19	-0.0351	-0.2008	1.0	-0.1505	2.20	-0.0338	-0.1964	1.0	-0.1490

XII. APPENDIX B: OUTPUT OF STABILITY ANALYSIS COMPUTER PROGRAM FOR CASE ST-1

Case ST-1 is representative of the original ST-series. The complete list of this series (ST-1 through ST-36) is shown in Table 5. The output of STANAL computer program for this series is shown in the appendix of reference [20]. As a sample, only Case ST-1 will be shown in this chapter via Figures 8 through 17. The variables chosen for demonstration in this series are listed below.

1. Angles δ_1, δ_2, δ_3, and $\bar{\delta}$ (Figure 8).
2. Angles δ_k and $\bar{\delta}$ (Figure 9).
3. Relative angles $(\delta_1 - \bar{\delta})$, $(\delta_2 - \bar{\delta})$, and $(\delta_3 - \bar{\delta})$ (Figure 10).
4. Relative angle $(\delta_k - \bar{\delta})$ (Figure 11).
5. Accelerations $\ddot{\delta}_1$, $\ddot{\delta}_2$, $\ddot{\delta}_3$, and $\ddot{\bar{\delta}}$ (Figure 12).
6. Accelerations $\ddot{\delta}_k$ and $\ddot{\bar{\delta}}$ (Figure 13).
7. Relative accelerations $(\ddot{\delta}_1 - \ddot{\bar{\delta}})$, $(\ddot{\delta}_2 - \ddot{\bar{\delta}})$, and $(\ddot{\delta}_3 - \ddot{\bar{\delta}})$ (Figure 14).
8. Relative acceleration $(\ddot{\delta}_k - \ddot{\bar{\delta}})$ (Figure 15).
9. Terms of equation (4.10) (Figure 16):

$$SSPC = \left(\frac{P_{ck}}{H_k} - \frac{1}{\bar{H}} \sum_{i=1}^{n} P_{ci} \right),$$

$$SSUMA = \sum_{j=1}^{n} \left[\frac{1}{H_k} A_{kj} \cos (\theta_{kj} - \delta_{kj}) + \frac{1}{\bar{H}} A_{kj} \cos (\theta_{kj} + \delta_{kj}) \right],$$

$$SSUMAH = \sum_{i=1}^{n-1} \sum_{j=i+1}^{n} \frac{2}{\bar{H}} \hat{A}_{ij} \cos \delta_{ij}.$$

10. Terms of equation (4.5) (Figure 17):

$$SPCP = \sum_{i=1}^{n} \frac{P_{ci}}{\bar{H}} ,$$

$$SUMK = - \sum_{i=1}^{n} \frac{A_{ik}}{\bar{H}} \cos (\theta_{ik} - \delta_{ik}) ,$$

$$SUMIJ = - \sum_{i=1}^{n} \sum_{\substack{j=1 \\ j \neq i}}^{n} A_{ij} \cos (\theta_{ij} - \delta_{ij}) .$$

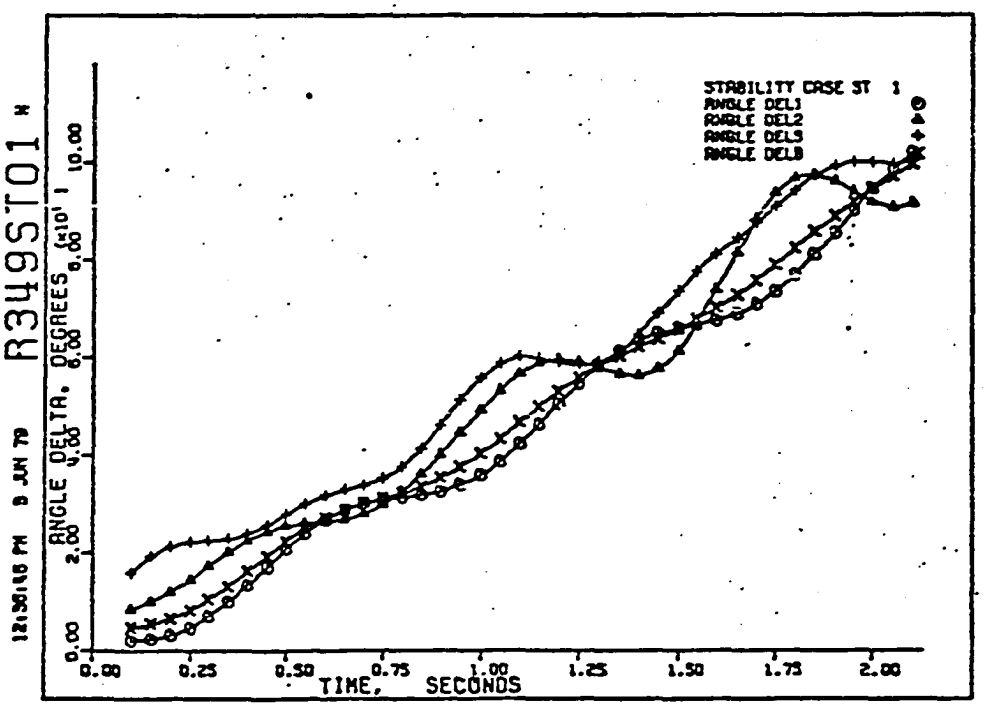

Figure 8. Case ST-1: angles δ_1, δ_2, δ_3, and $\bar{\delta}$.

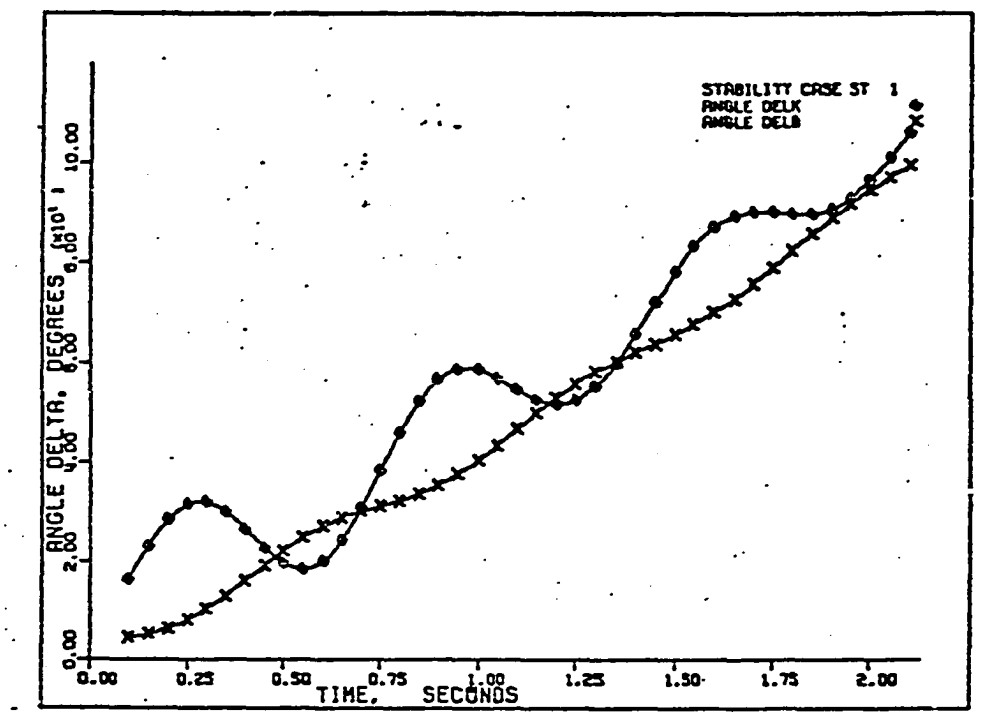

Figure 9. Case ST-1: angles δ_k and $\bar{\delta}$.

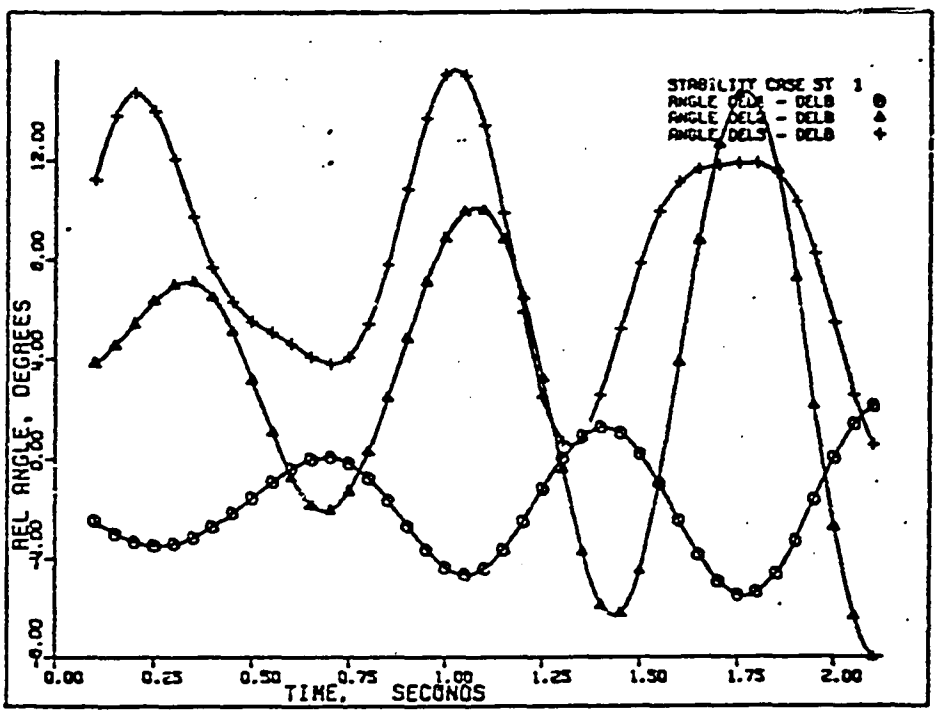

Figure 10. Case ST-1: relative angles $(\delta_1 - \bar{\delta})$, $(\delta_2 - \bar{\delta})$, and $(\delta_3 - \bar{\delta})$.

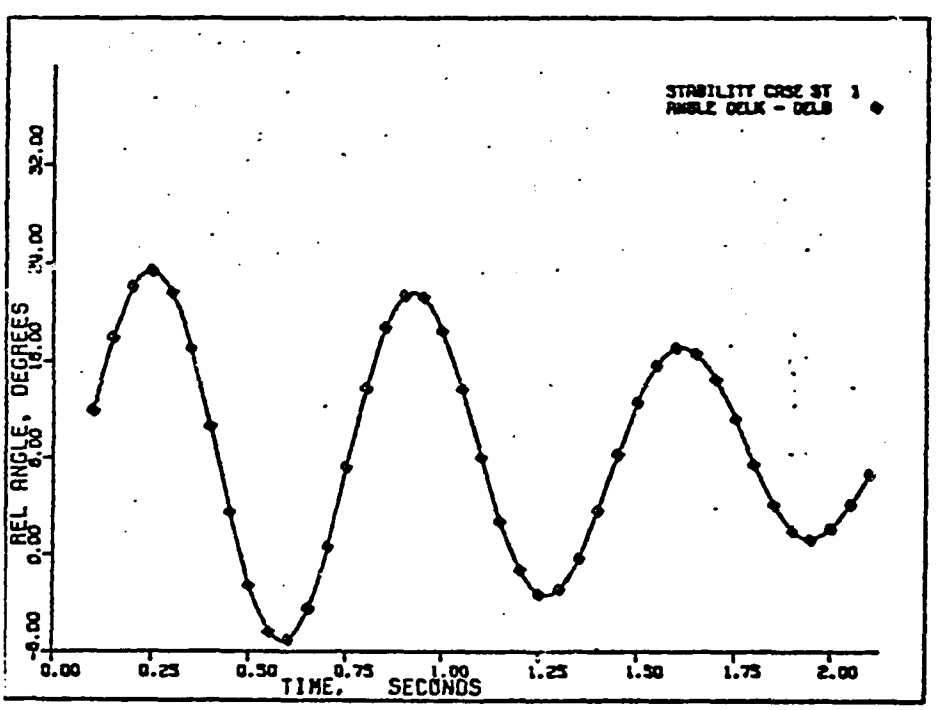

Figure 11. Case ST-1: relative angle $(\delta_k - \bar{\delta})$.

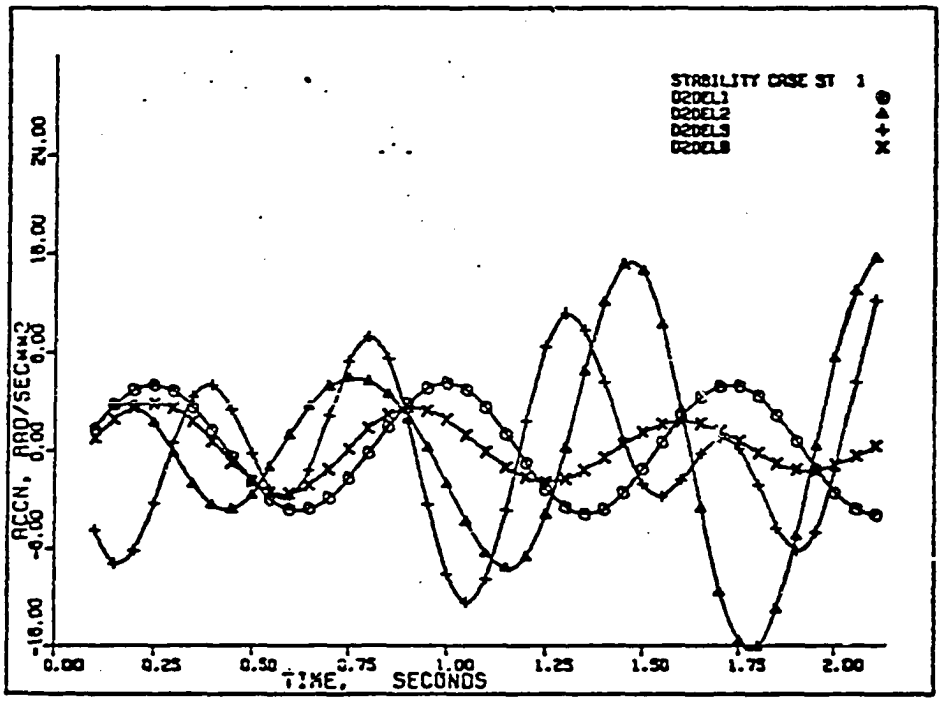

Figure 12. Case ST-1: accelerations $\ddot{\delta}_1$, $\ddot{\delta}_2$, $\ddot{\delta}_3$, and $\bar{\ddot{\delta}}$.

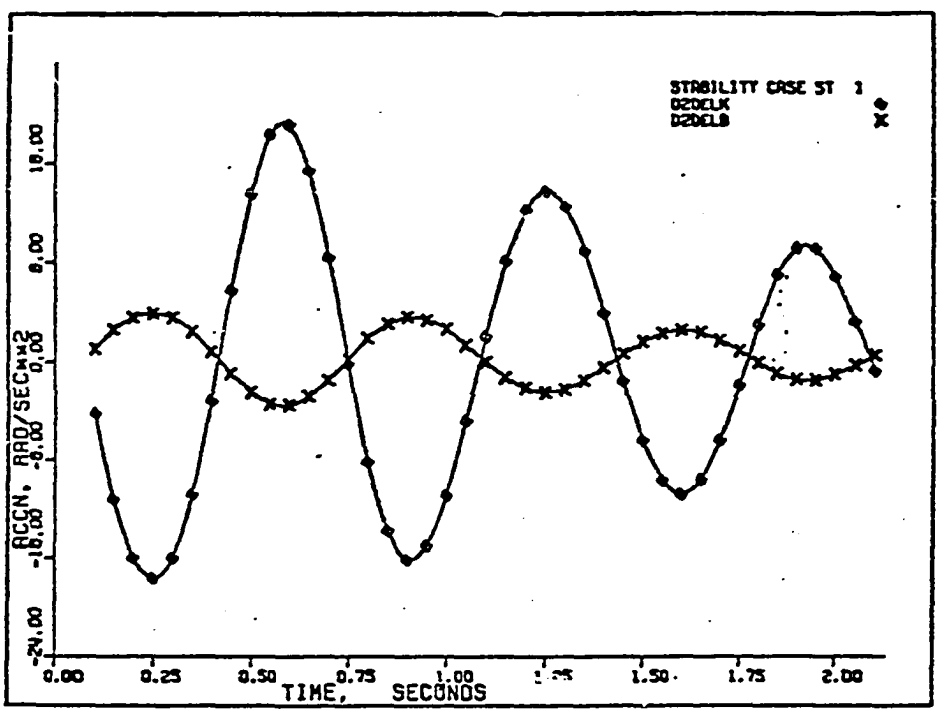

Figure 13. Case ST-1: accelerations $\ddot{\delta}_k$ and $\bar{\ddot{\delta}}$.

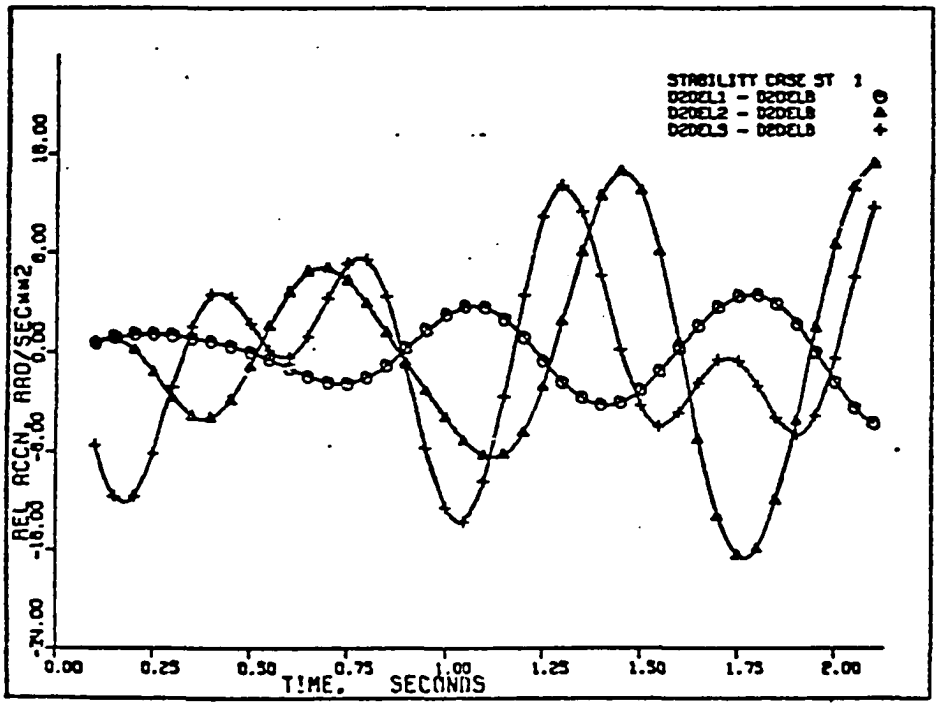

Figure 14. Case ST-1: relative accelerations $(\ddot{\delta}_1 - \ddot{\bar{\delta}})$, $(\ddot{\delta}_2 - \ddot{\bar{\delta}})$, and $(\ddot{\delta}_3 - \ddot{\bar{\delta}})$.

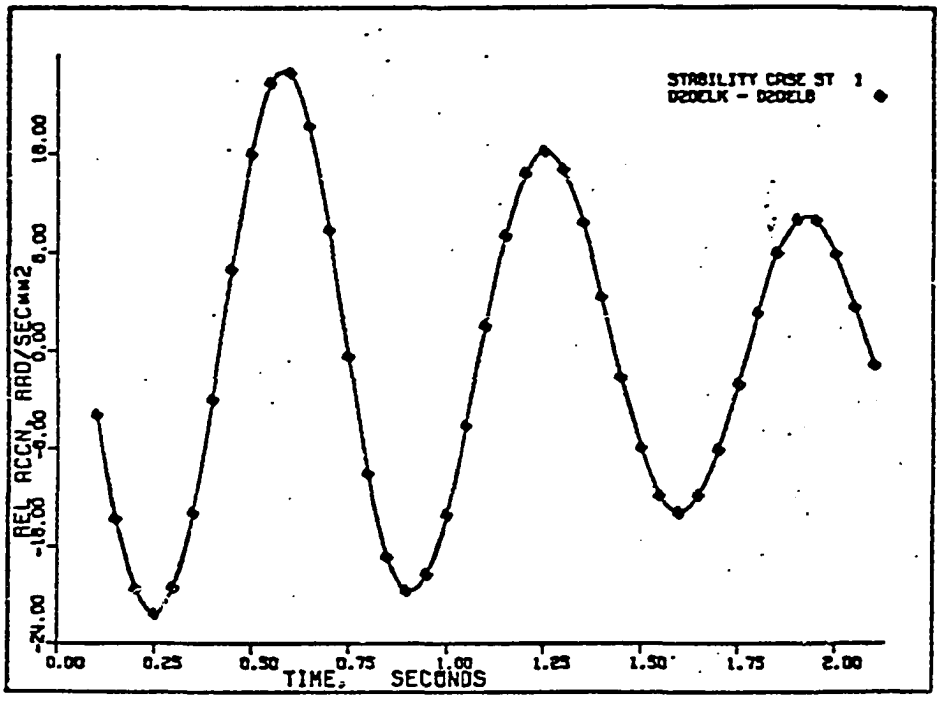

Figure 15. Case ST-1: relative acceleration $(\ddot{\delta}_k - \ddot{\bar{\delta}})$.

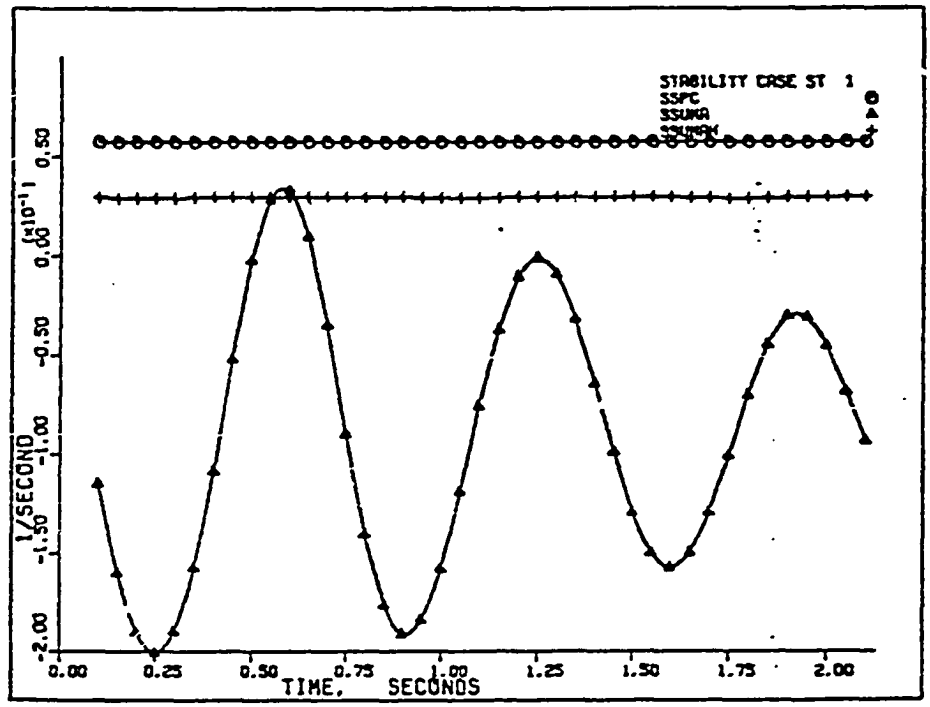

Figure 16. Case ST-1: terms of equation (4.10).

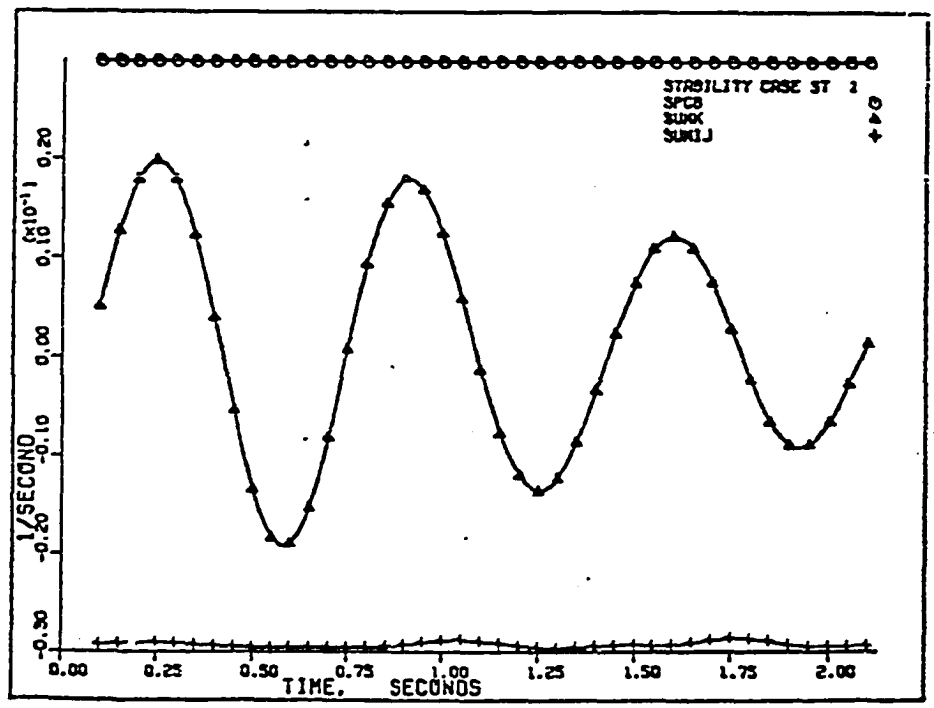

Figure 17. Case ST-1: terms of equation (4.5).

XIII. APPENDIX C: OUTPUT OF STABILITY ANALYSIS COMPUTER PROGRAM FOR CASE SM-1

Case SM-1 is representative of the SM-series. The complete list of this series (SM-1 through SM-17) is shown in Table 9. The output of STANAL computer program for this series is shown in the appendix of reference [20]. As a sample, only Case SM-1 will be shown in this chapter via Figures 18 through 28. The variables chosen for demonstration in this series are listed below.

1. Angles δ_1, δ_2, δ_3, and $\bar{\delta}$ (Figure 18).
2. Angles δ_k and $\bar{\delta}$ (Figure 19).
3. Relative angles $(\delta_1 - \bar{\delta})$, $(\delta_2 - \bar{\delta})$, and $(\delta_3 - \bar{\delta})$ (Figure 20).
4. Relative angle $(\delta_k - \bar{\delta})$ (Figure 21).
5. Accelerations $\ddot{\delta}_1$, $\ddot{\delta}_2$, $\ddot{\delta}_3$, and $\ddot{\bar{\delta}}$ (Figure 22).
6. Accelerations $\ddot{\delta}_k$ and $\ddot{\bar{\delta}}$ (Figure 23).
7. Relative accelerations $(\ddot{\delta}_1 - \ddot{\bar{\delta}})$, $(\ddot{\delta}_2 - \ddot{\bar{\delta}})$, and $(\ddot{\delta}_3 - \ddot{\bar{\delta}})$ (Figure 24).
8. Relative acceleration $(\ddot{\delta}_k - \ddot{\bar{\delta}})$ (Figure 25).
9. Terms of equation (4.10) (Figure 26):

$$SSPC = \left(\frac{P_{ck}}{H_k} - \frac{1}{\bar{H}} \sum_{i=1}^{n} P_{ci} \right),$$

$$SSUMA = - \sum_{j=1}^{n} \left[\frac{1}{H_k} A_{kj} \cos (\theta_{kj} - \delta_{kj}) + \frac{1}{\bar{H}} A_{kj} \cos (\theta_{kj} + \delta_{kj}) \right],$$

$$SSUMAH = \sum_{i=1}^{n-1} \sum_{j=i+1}^{n} \frac{2}{\bar{H}} \hat{A}_{ij} \cos \delta_{ij} .$$

10. Terms of equation (4.5) (Figure 27):

$$SPCP = \sum_{i=1}^{n} \frac{P_{ci}}{\bar{H}} ,$$

$$SUMK = - \sum_{i=1}^{n} \frac{A_{ik}}{\bar{H}} \cos (\theta_{ik} - \delta_{ik}) ,$$

$$SUMIJ = - \sum_{i=1}^{n} \sum_{\substack{j=1 \\ j \neq i}}^{n} A_{ij} \cos (\theta_{ij} - \delta_{ij}) .$$

11. Internal voltage, slip, terminal power, and terminal reactive power (Figure 28).

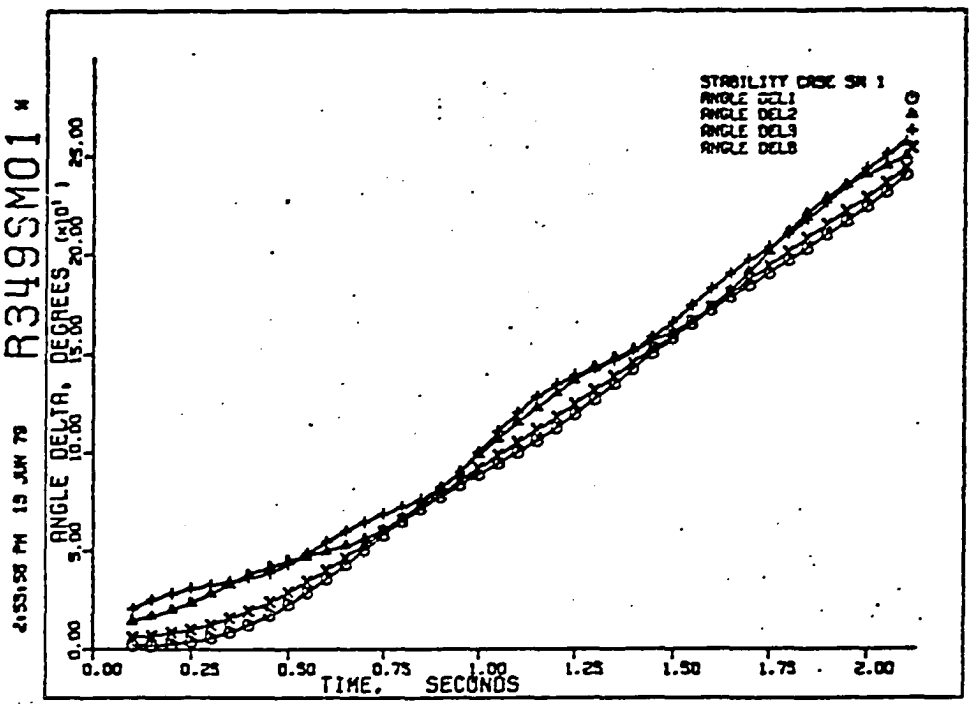

Figure 18. Case SM-1: angles δ_1, δ_2, δ_3, and $\bar{\delta}$.

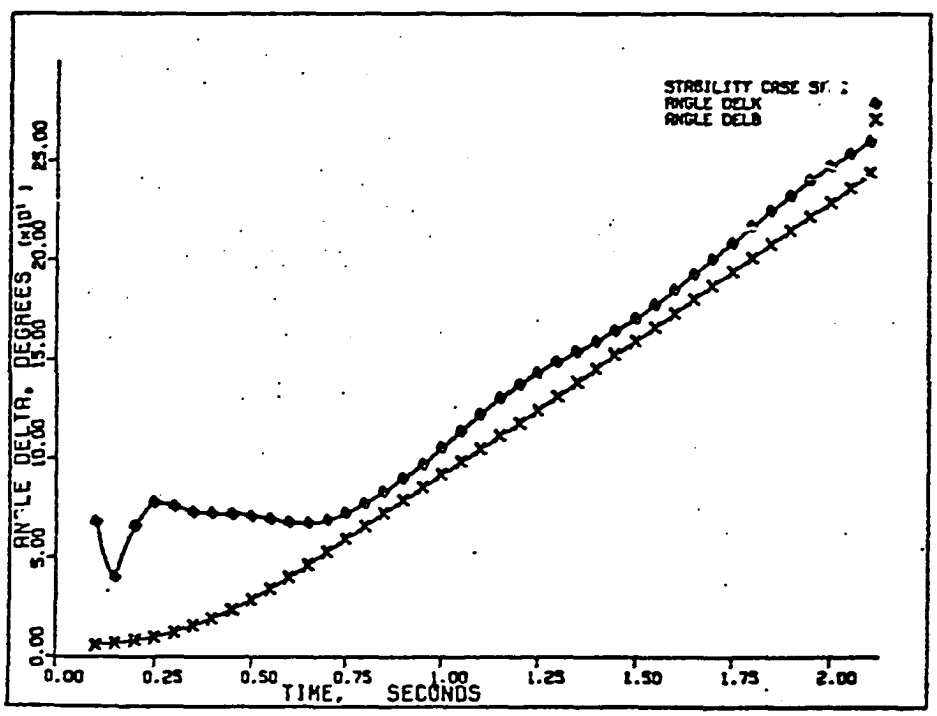

Figure 19. Case SM-1: angles δ_k and $\bar{\delta}$.

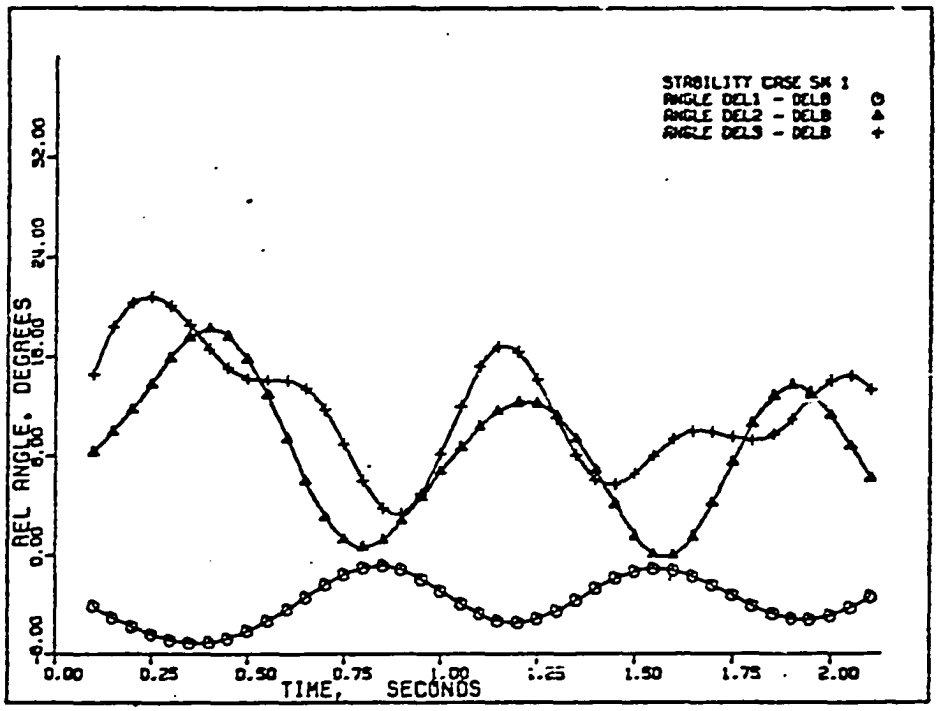

Figure 20. Case SM-1: relative angles $(\delta_1 - \bar{\delta})$, $(\delta_2 - \bar{\delta})$, and $(\delta_3 - \bar{\delta})$.

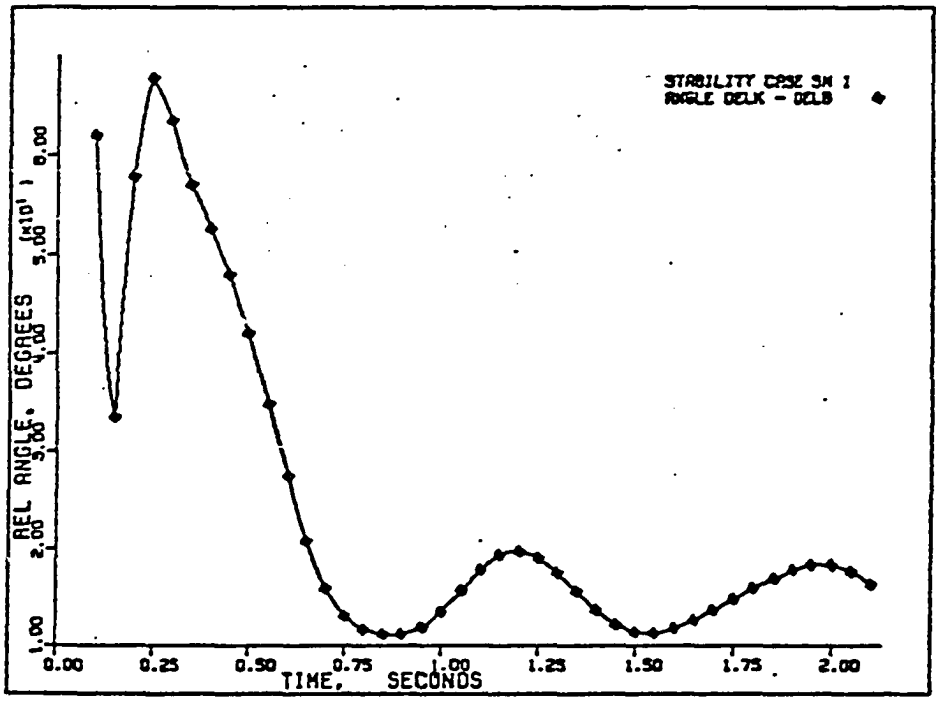

Figure 21. Case SM-1: relative angle $(\delta_k - \bar{\delta})$.

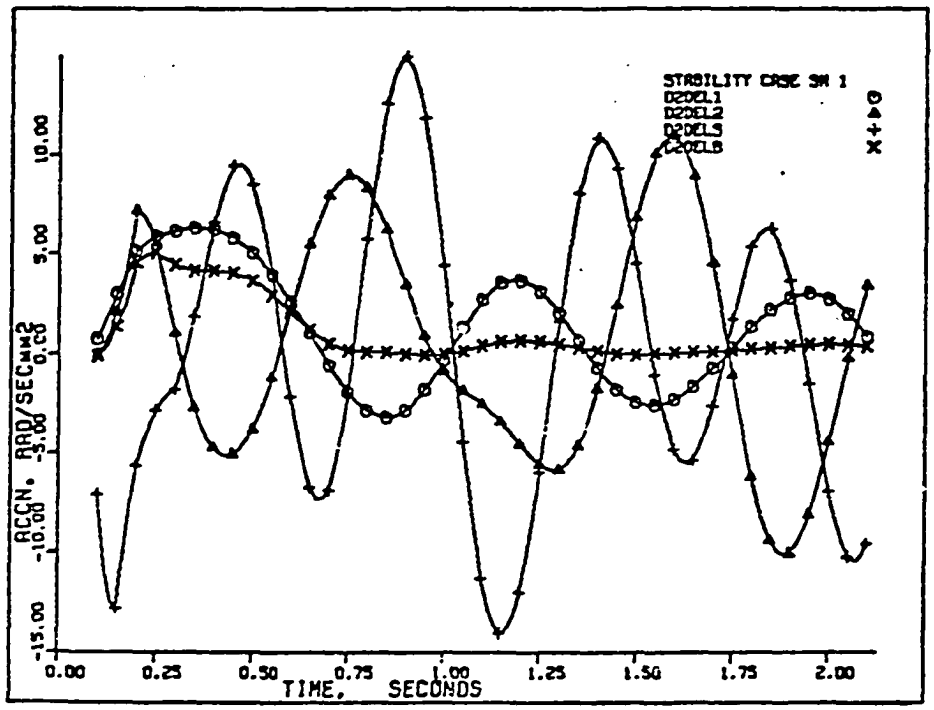

Figure 22. Case SM-1: accelerations $\ddot{\delta}_1$, $\ddot{\delta}_2$, $\ddot{\delta}_3$, and $\ddot{\bar{\delta}}$.

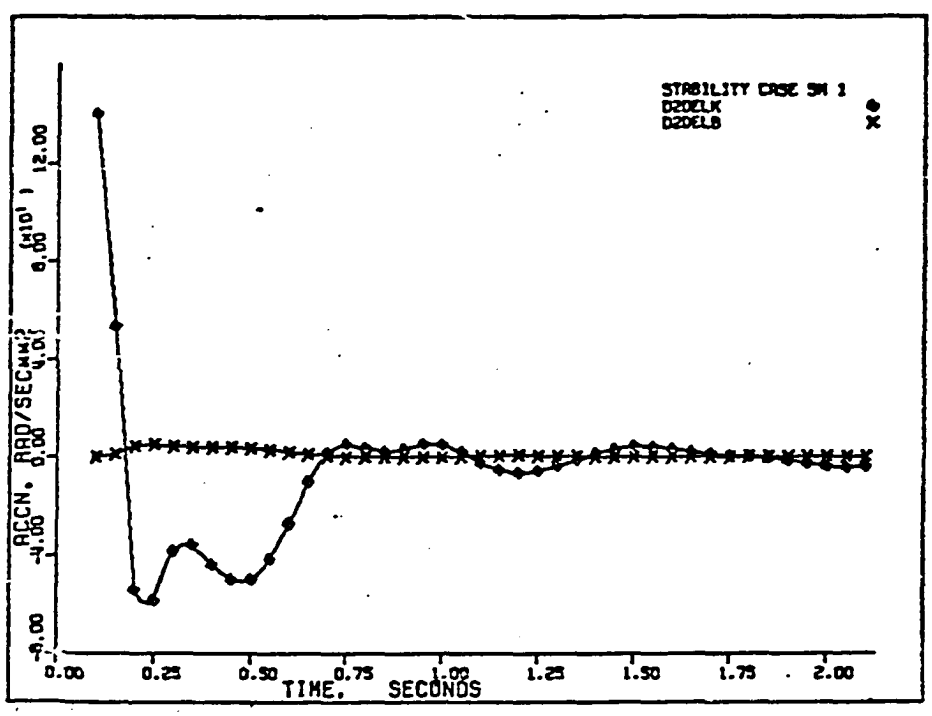

Figure 23. Case SM-1: accelerations $\ddot{\delta}_k$ and $\ddot{\bar{\delta}}$.

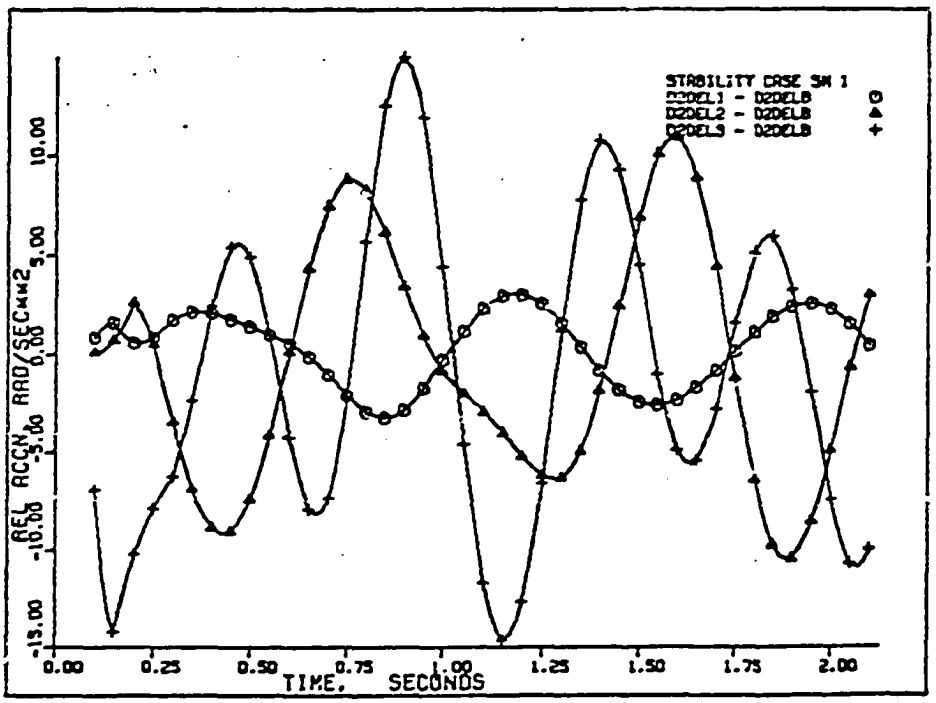

Figure 24. Case SM-1: relative accelerations $(\ddot{\delta}_1 - \ddot{\bar{\delta}})$, $(\ddot{\delta}_2 - \ddot{\bar{\delta}})$, and $(\ddot{\delta}_3 - \ddot{\bar{\delta}})$.

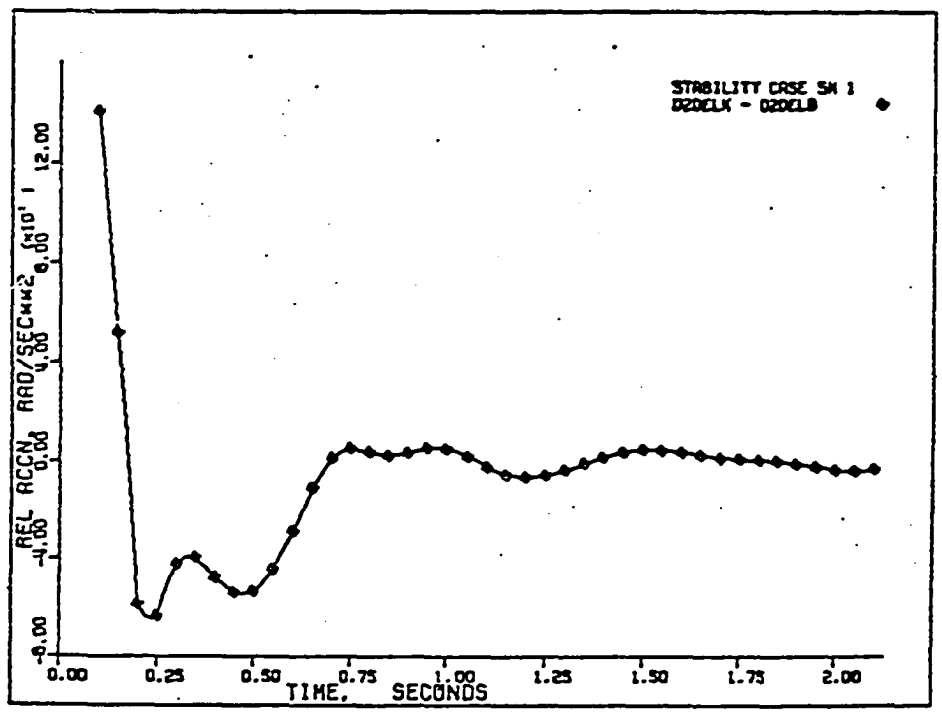

Figure 25. Case SM-1: relative acceleration $(\ddot{\delta}_k - \ddot{\bar{\delta}})$.

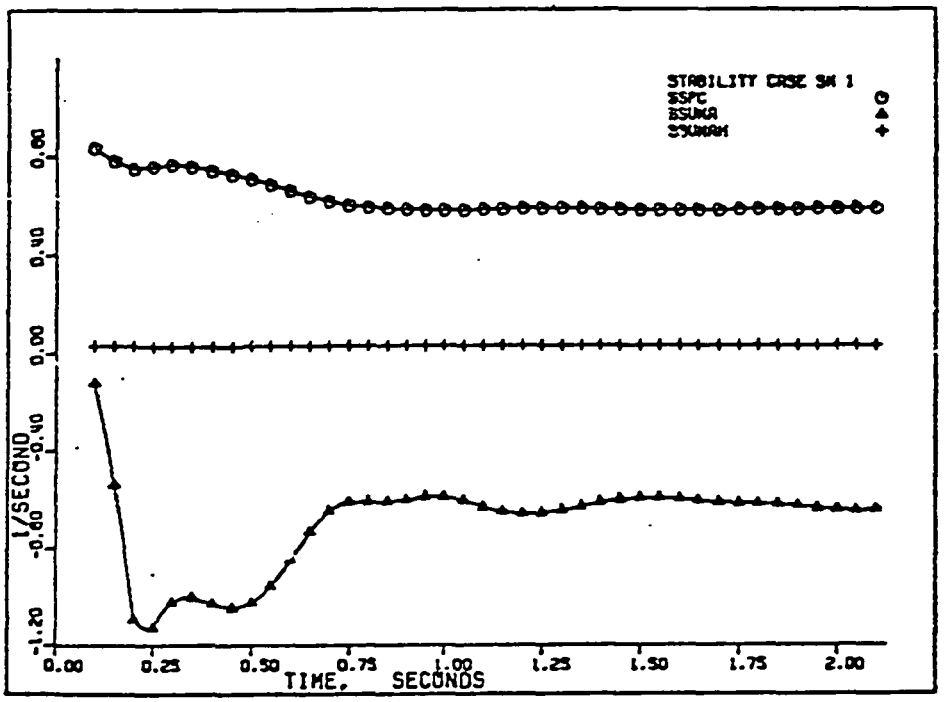

Figure 26. Case SM-1: terms of equation (4.10).

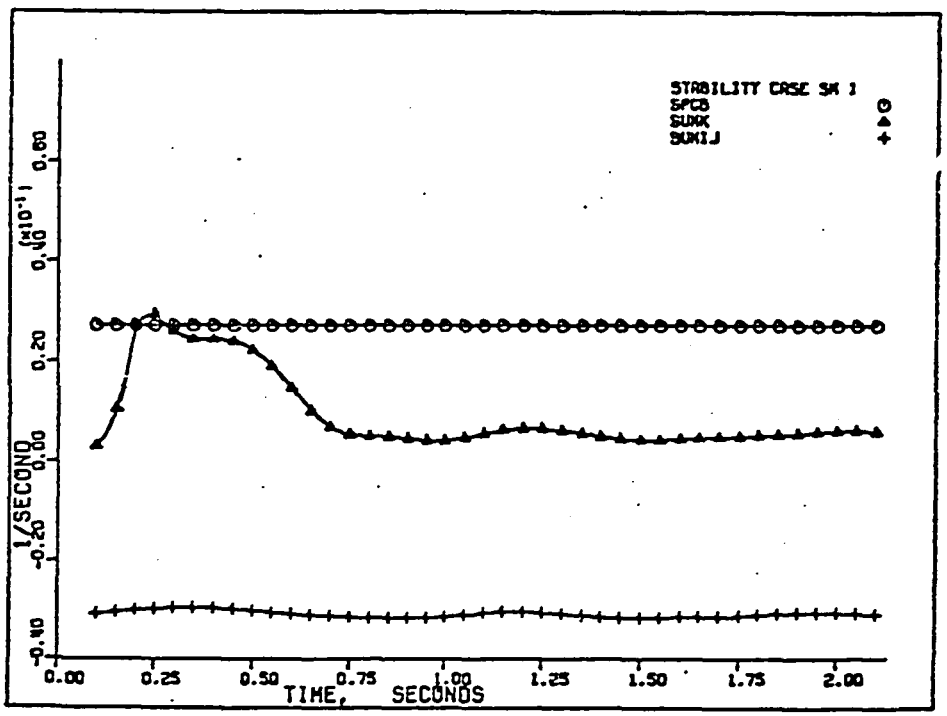

Figure 27. Case SM-1: terms of equation (4.5).

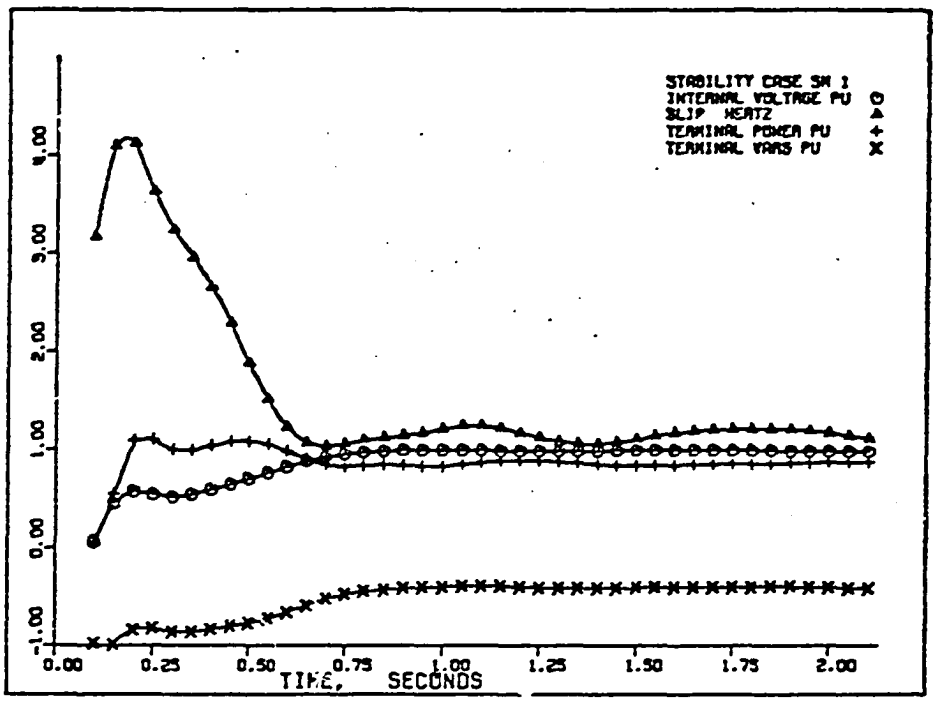

Figure 28. Case SM-1: internal voltage, slip, terminal power, and terminal reactive power.

XIV. APPENDIX D: OUTPUT OF STABILITY ANALYSIS COMPUTER PROGRAM FOR CASE SI-1

Case SI-1 is representative of the SI-series. The complete list of this series (SI-1 through SI-22) is shown in Table 10. The output of STANAL computer program for this series is shown in the appendix of reference [20]. As a sample, only Case SI-1 will be shown in this chapter via Figures 29 through 40. The variables chosen for demonstration in this series are listed below.

1. Angles δ_1, δ_2, δ_3, and $\bar{\delta}$ (Figure 29).
2. Angles δ_{k1}, δ_{k2}, $\bar{\delta}$ (Figure 30).
3. Relative angles $(\delta_1 - \bar{\delta})$, $(\delta_2 - \bar{\delta})$, and $(\delta_3 - \bar{\delta})$ (Figure 31).
4. Relative angles $(\delta_{k1} - \bar{\delta})$ and $(\delta_{k2} - \bar{\delta})$ (Figure 32).
5. Accelerations $\ddot{\delta}_1$, $\ddot{\delta}_2$, $\ddot{\delta}_3$, and $\ddot{\bar{\delta}}$ (Figure 33).
6. Accelerations $\ddot{\delta}_{k1}$, $\ddot{\delta}_{k2}$, and $\ddot{\bar{\delta}}$ (Figure 34).
7. Relative accelerations $(\ddot{\delta}_1 - \ddot{\bar{\delta}})$, $(\ddot{\delta}_2 - \ddot{\bar{\delta}})$, and $(\ddot{\delta}_3 - \ddot{\bar{\delta}})$ (Figure 35).
8. Relative accelerations $(\ddot{\delta}_{k1} - \ddot{\bar{\delta}})$ and $(\ddot{\delta}_{k2} - \ddot{\bar{\delta}})$ (Figure 36).
9. Terms of equation (4.13) (Figure 37):

$$\text{SSPCI} = \left(\frac{P_{ck1}}{H_{k1}} - \frac{1}{\bar{H}} \sum_{i=1}^{n} P_{ci} \right),$$

$$\text{SSUMA1} = - \sum_{j=1}^{n} \left[\frac{1}{H_{k1}} A_{klj} \cos (\theta_{klj} - \delta_{klj}) - \frac{1}{\bar{H}} A_{klj} \cos (\theta_{klj} + \delta_{klj}) \right],$$

$$\text{SSUMAH} = \frac{1}{\bar{H}} \sum_{i=1}^{n-1} \sum_{j=i+1}^{n} 2 \hat{A}_{ij} \cos \delta_{ij} ,$$

$$SK1K2 = -\frac{1}{H_{k1}} A_{k1k2} \cos(\theta_{k1k2} - \delta_{k1k2}) ,$$

$$SUMIK2 = \frac{1}{\bar{H}} \sum_{i=1}^{n} A_{ik2} \cos(\theta_{ik2} - \delta_{ik2}) .$$

10. Terms of equation (4.14) (Figure 38):

$$SSPC2 = \left(\frac{P_{ck2}}{H_{k2}} - \frac{1}{\bar{H}} \sum_{i=1}^{n} P_{ci} \right) ,$$

$$SSUMA2 = -\sum_{j=1}^{n} \left[\frac{1}{H_{k2}} A_{k2j} \cos(\theta_{k2j} - \delta_{k2j}) - \frac{1}{\bar{H}} A_{k2j} \cos(\theta_{k2j} + \delta_{k2j}) \right] ,$$

$$SSUMAH = \frac{1}{\bar{H}} \sum_{i=1}^{n-1} \sum_{j=i+1}^{n} 2 \hat{A}_{ij} \cos \delta_{ij} ,$$

$$SK2K1 = -\frac{1}{H_{k2}} A_{k2k1} \cos(\theta_{k2k1} - \delta_{k2k1}) ,$$

$$SUMIK1 = \frac{1}{\bar{H}} \sum_{i=1}^{n} A_{ik1} \cos(\theta_{ik1} - \delta_{ik1}) .$$

11. Terms of equation (4.12) (Figure 39):

$$SPCB = \frac{1}{\bar{H}} \sum_{i=1}^{n} P_{ci} ,$$

$$SUMK1 = -\frac{1}{\bar{H}} \sum_{i=1}^{n} A_{ik1} \cos(\theta_{ik1} - \delta_{ik1}) ,$$

$$SUMK2 = -\frac{1}{\bar{H}} \sum_{i=1}^{n} A_{ik2} \cos(\theta_{ik2} - \delta_{ik2}) ,$$

$$SUMIJ = -\frac{1}{\bar{H}} \sum_{i=1}^{n} \sum_{\substack{j=1 \\ j \neq i}}^{n} A_{ij} \cos(\theta_{ij} - \delta_{ij}) .$$

12. Internal voltage, slip, terminal power, and terminal reactive power (Figure 40).

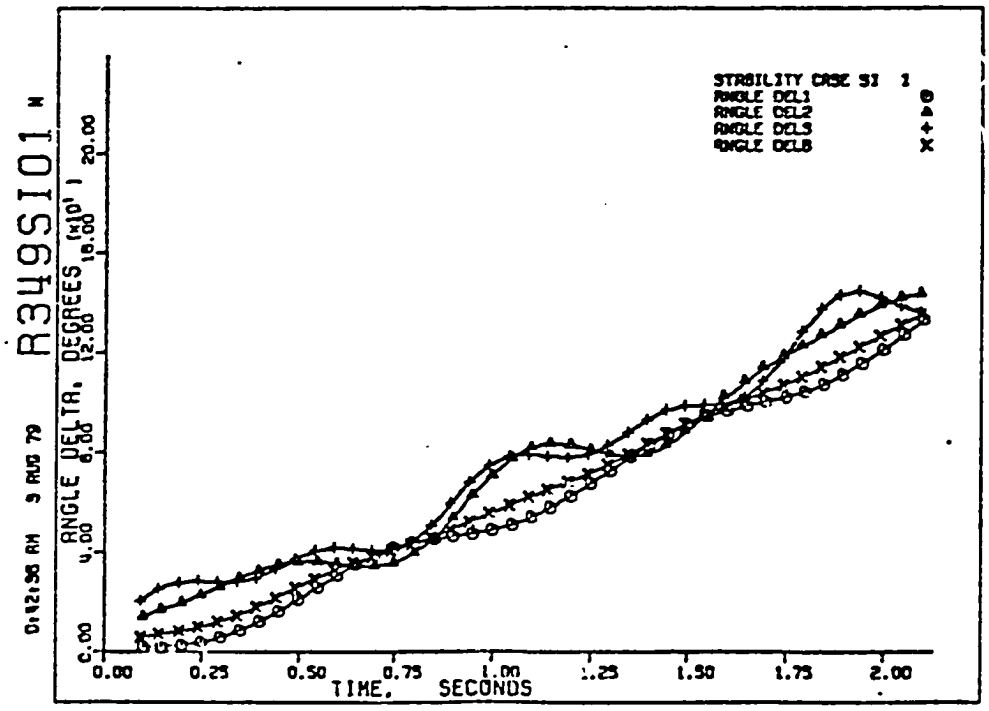

Figure 29. Case SI-1: angles δ_1, δ_2, δ_3, and $\bar{\delta}$.

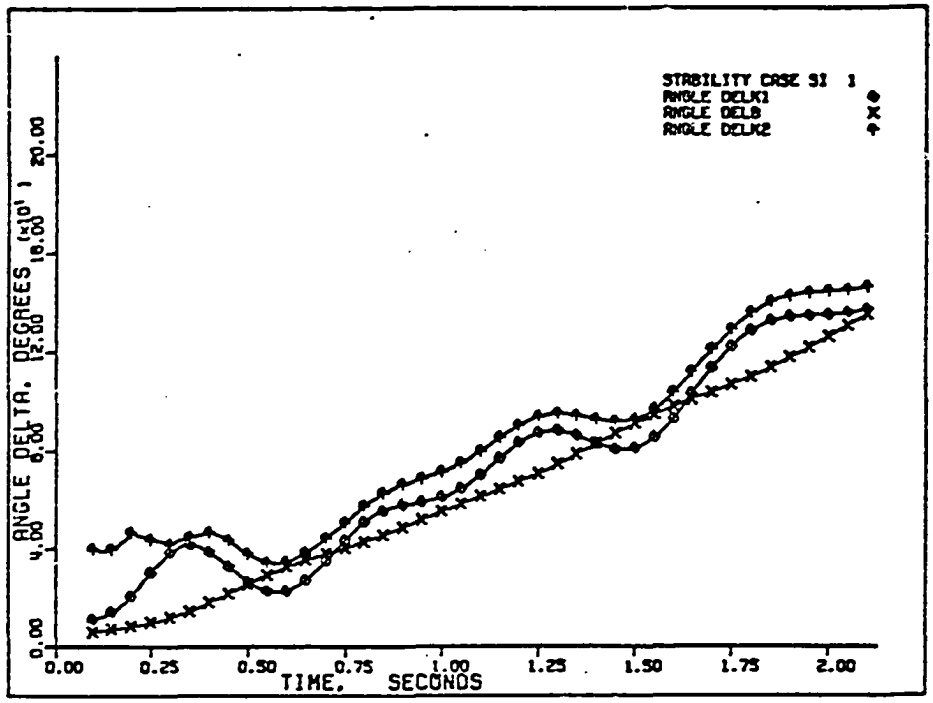

Figure 30. Case SI-1: angles δ_{k1}, δ_{k2}, and $\bar{\delta}$.

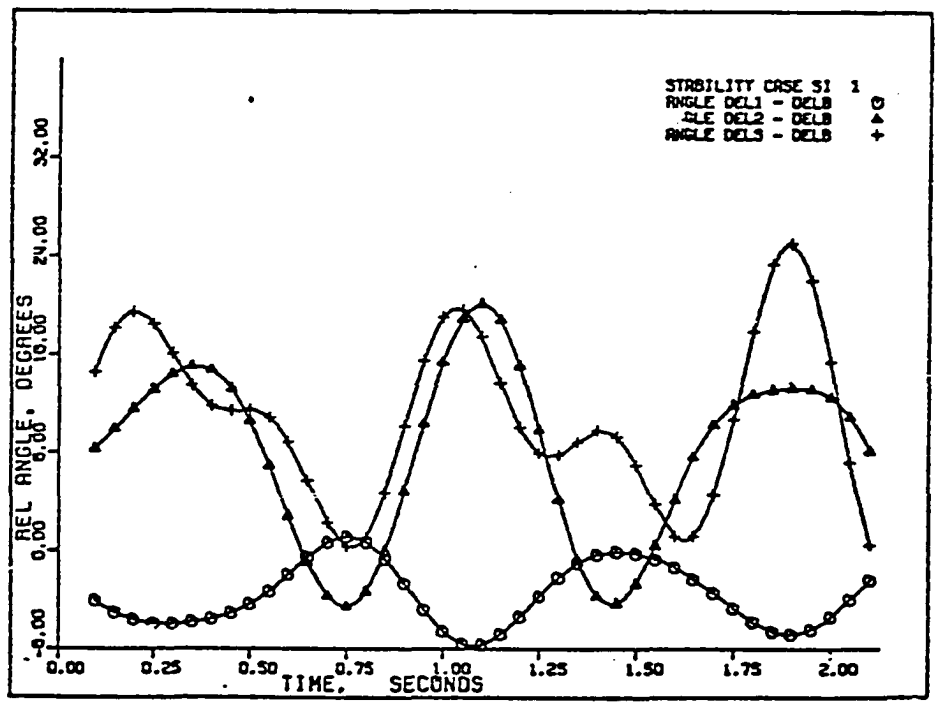

Figure 31. Case SI-1: relative angles $(\delta_1 - \bar{\delta})$, $(\delta_2 - \bar{\delta})$, and $(\delta_3 - \bar{\delta})$.

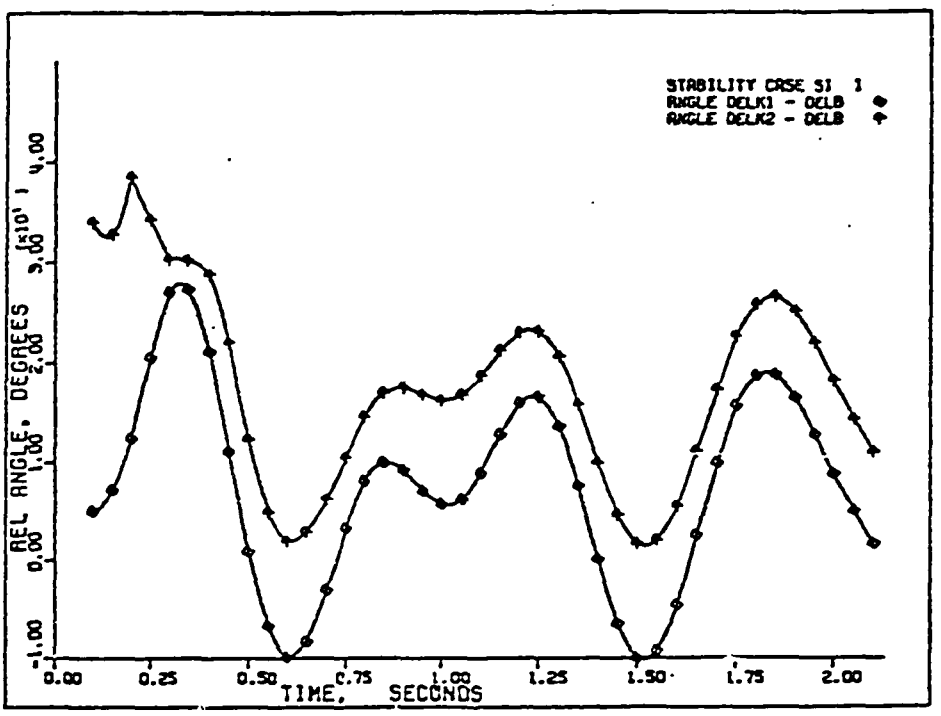

Figure 32. Case SI-1: relative angles $(\delta_{k1} - \bar{\delta})$ and $(\delta_{k2} - \bar{\delta})$.

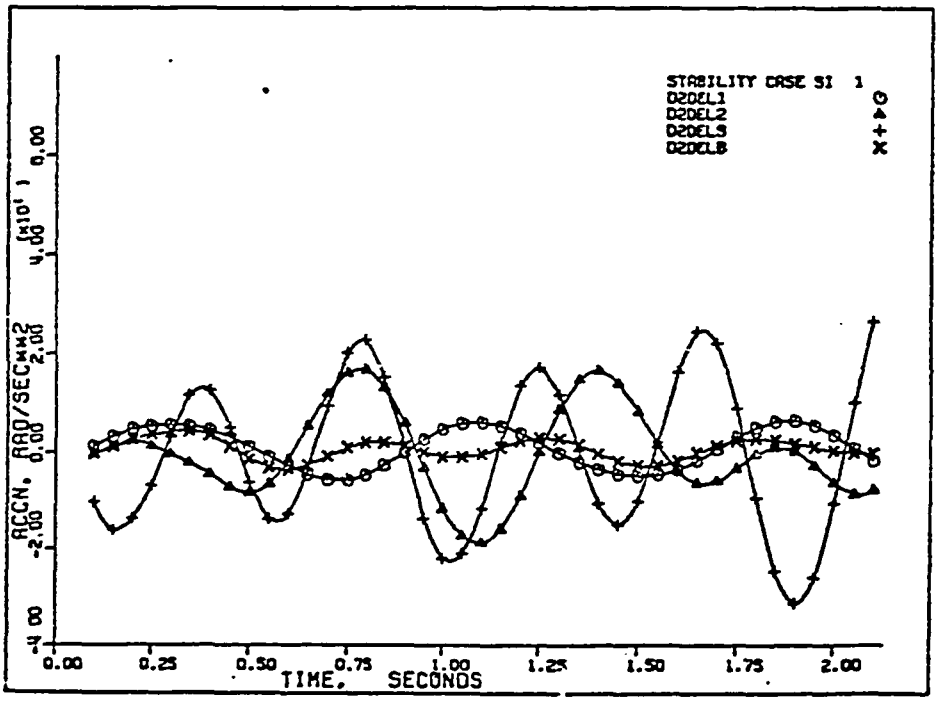

Figure 33. Case SI-1: accelerations $\ddot{\delta}_1$, $\ddot{\delta}_2$, $\ddot{\delta}_3$, and $\ddot{\bar{\delta}}$.

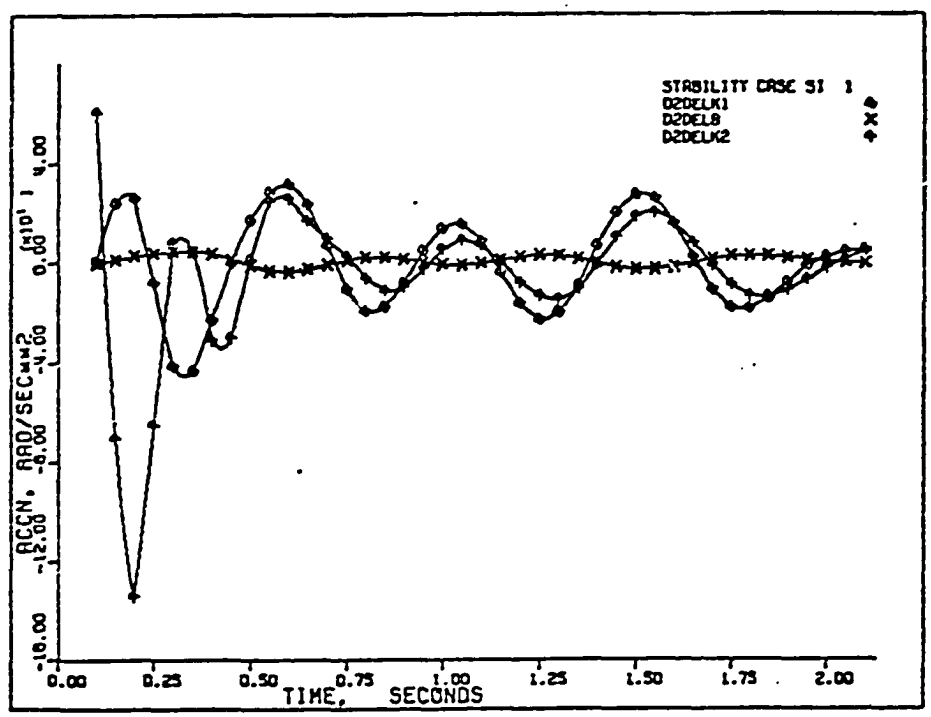

Figure 34. Case SI-1: accelerations $\ddot{\delta}_{k1}$, $\ddot{\delta}_{k2}$, and $\ddot{\bar{\delta}}$.

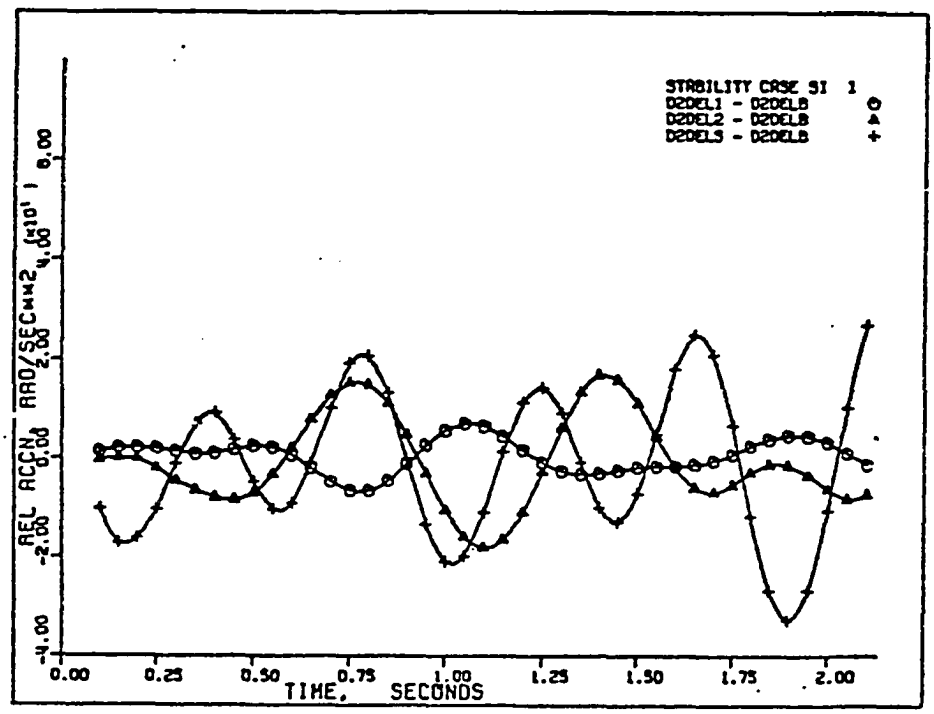

Figure 35. Case SI-1: relative accelerations $(\ddot{\delta}_1 - \ddot{\bar{\delta}})$, $(\ddot{\delta}_2 - \ddot{\bar{\delta}})$, and $(\ddot{\delta}_3 - \ddot{\bar{\delta}})$.

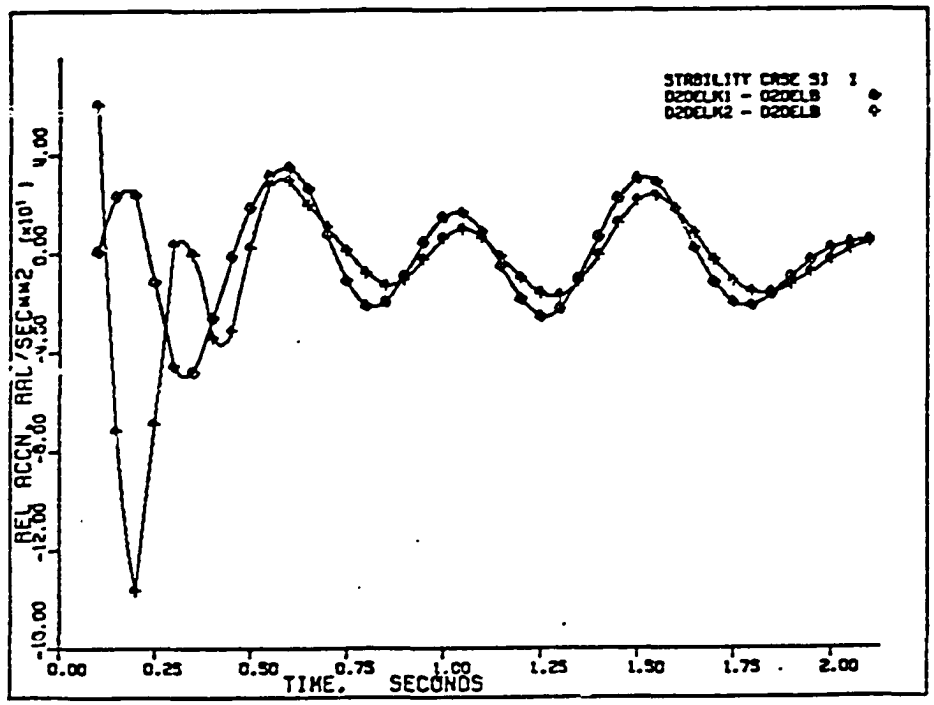

Figure 36. Case SI-1: relative accelerations $(\ddot{\delta}_{k1} - \ddot{\delta})$ and $(\ddot{\delta}_{k2} - \ddot{\delta})$.

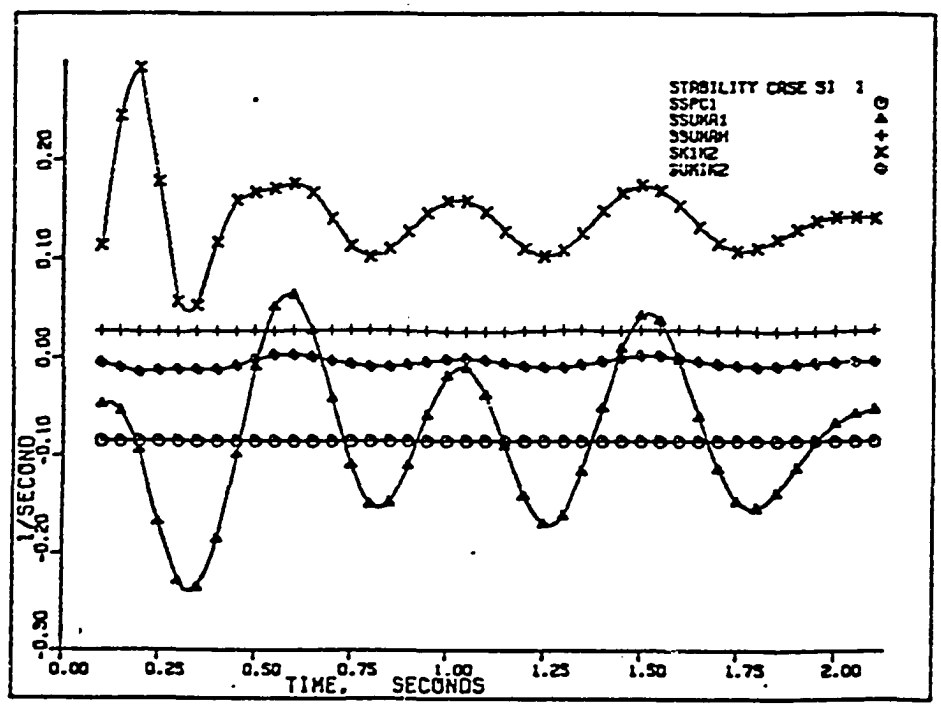

Figure 37. Case SI-1: terms of equation (4.13).

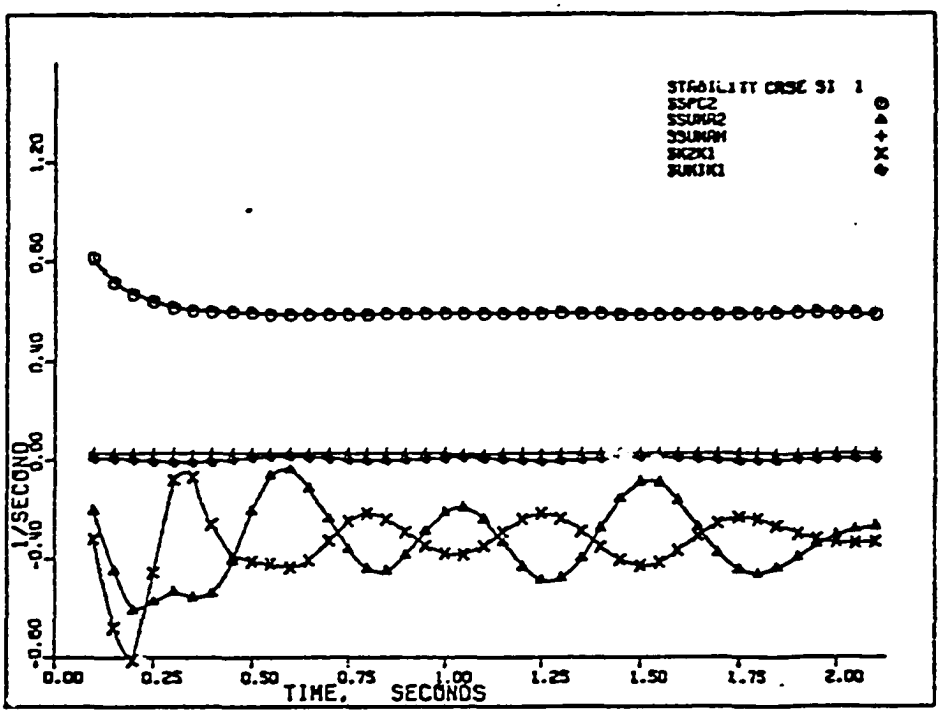

Figure 38. Case SI-1: terms of equation (4.14).

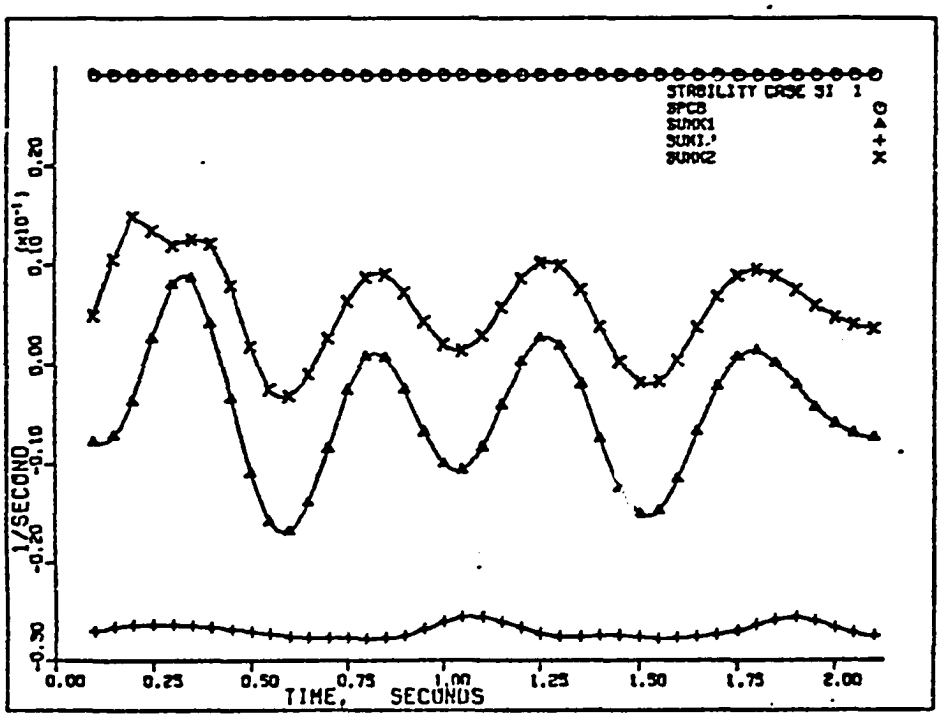

Figure 39. Case SI-1: terms of equation (4.12).

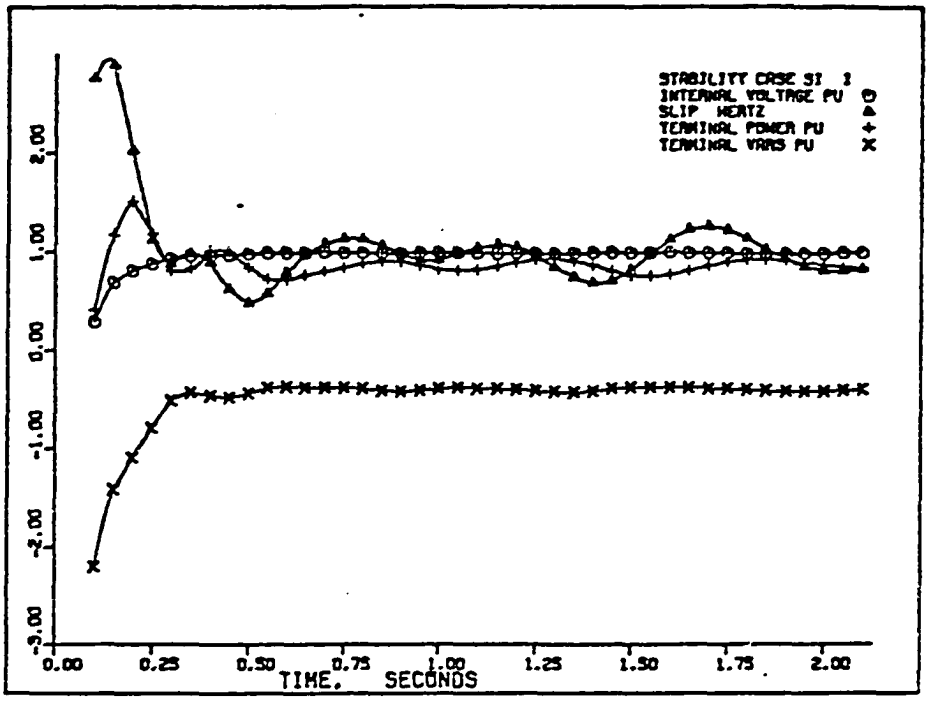

Figure 40. Case SI-1: internal voltage, slip, terminal power, and terminal reactive power.

XV. APPENDIX E: OUTPUT OF STABILITY ANALYSIS COMPUTER PROGRAM FOR REMOTE SYNCHRONOUS GENERATION - CRITICAL INERTIA

This portion of runs is an addition to the original ST-series (Cases ST-1 through ST-36). The purpose of these runs is to find the minimum inertia constant "H" of the remote synchronous machine required for stable transient response due to the specified disturbance (three-phase fault at bus 10, cleared at six cycles by removing the faulted line). The power system is assumed to be under heavy load condition with the penetration level of 25 percent. Critical inertia constants for various power system configurations (point of connection, length of line) are determined. The complete list of these runs is listed in Table 6. The complete output of STANAL computer program for this series is shown via Figures 41 through 100. The variables chosen for demonstration in this series are listed below.

1. Angles δ_1, δ_2, δ_3, and $\bar{\delta}$ (Figures 41 through 46).
2. Angles δ_k and $\bar{\delta}$ (Figures 47 through 52).
3. Relative angles $(\delta_1 - \bar{\delta})$, $(\delta_2 - \bar{\delta})$, and $(\delta_3 - \bar{\delta})$ (Figures 53 through 58).
4. Relative angle $(\delta_k - \bar{\delta})$ (Figures 59 through 64).
5. Accelerations $\ddot{\delta}_1$, $\ddot{\delta}_2$, $\ddot{\delta}_3$, and $\ddot{\bar{\delta}}$ (Figures 65 through 70).
6. Accelerations $\ddot{\delta}_k$ and $\ddot{\bar{\delta}}$ (Figures 71 through 76).
7. Relative accelerations $(\ddot{\delta}_1 - \ddot{\bar{\delta}})$, $(\ddot{\delta}_2 - \ddot{\bar{\delta}})$, and $(\ddot{\delta}_3 - \ddot{\bar{\delta}})$ (Figures 77 through 82).
8. Relative acceleration $(\ddot{\delta}_k - \ddot{\bar{\delta}})$ (Figures 83 through 88).

9. Terms of equation (4.10) (Figure 89 through 94):

$$SSPC = \left(\frac{P_{ck}}{H_k} - \frac{1}{\bar{H}} \sum_{i=1}^{n} P_{ci} \right),$$

$$SSUMA = - \sum_{j=1}^{n} \left[\frac{1}{H_k} A_{kj} \cos (\theta_{kj} - \delta_{kj}) + \frac{1}{\bar{H}} A_{kj} \cos (\theta_{kj} + \delta_{kj}) \right],$$

$$SSUMAH = \sum_{i=i}^{n-1} \sum_{j=i+1}^{n} \frac{2}{\bar{H}} \hat{A}_{ij} \cos \delta_{ij} .$$

10. Terms of equation (4.5) (Figures 95 through 100):

$$SPCP = \sum_{i=1}^{n} \frac{P_{ci}}{\bar{H}}$$

$$SUMK = - \sum_{i=i}^{n} \frac{A_{ik}}{\bar{H}} \cos (\theta_{ik} - \delta_{ik}) ,$$

$$SUMIJ = - \sum_{i=1}^{n} \sum_{\substack{j=1 \\ j \neq i}}^{n} A_{ij} \cos (\theta_{ij} - \delta_{ij}) .$$

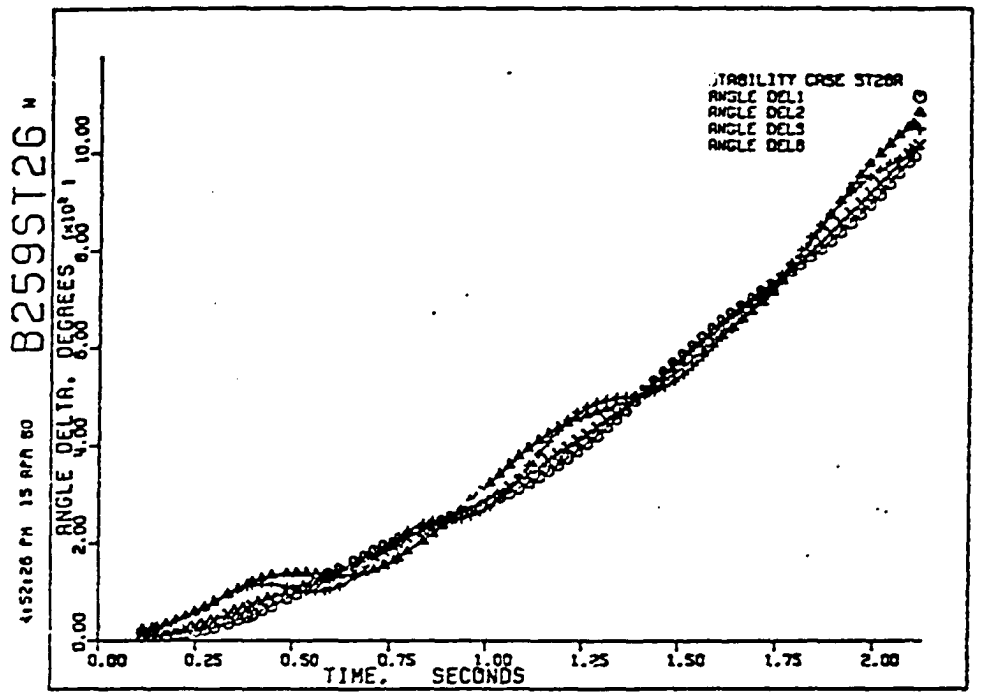

Figure 41. Case ST-26A: angles δ_1, δ_2, δ_3, and $\bar{\delta}$.

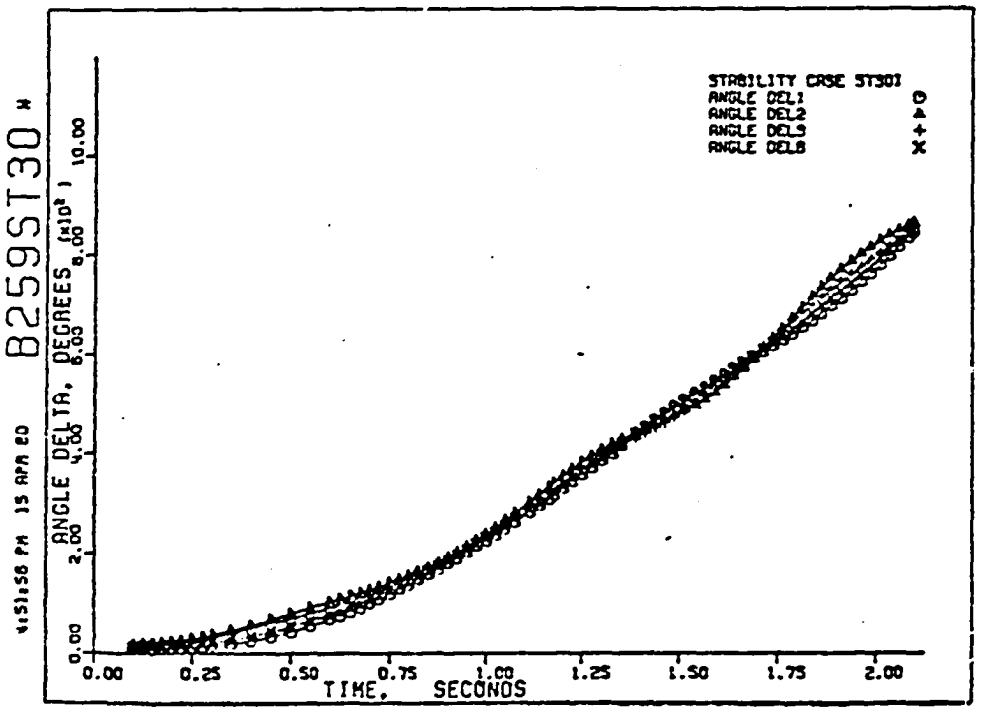

Figure 42. Case ST-30I: angles δ_1, δ_2, δ_3, and $\bar{\delta}$.

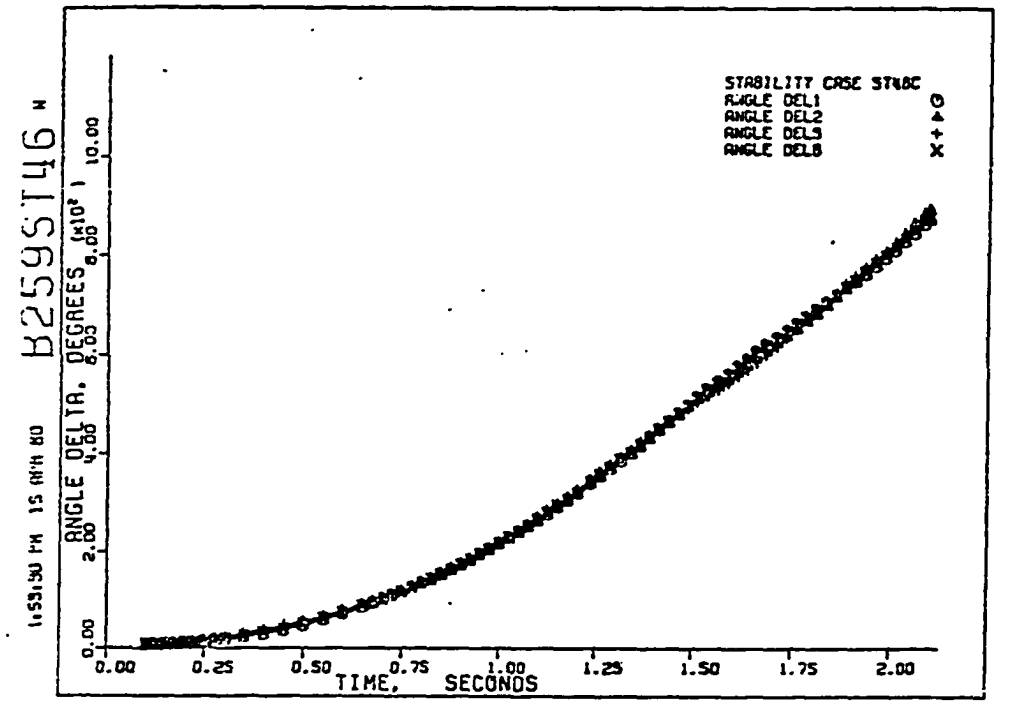

Figure 43. Case ST-46C: angles δ_1, δ_2, δ_3, and $\bar{\delta}$.

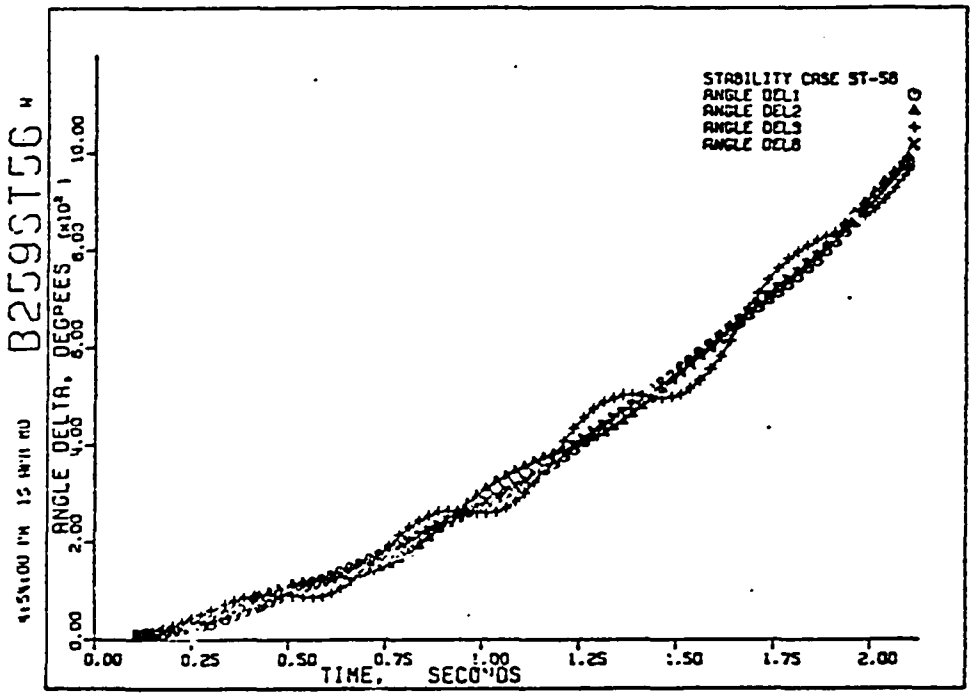

Figure 44. Case ST-56: angles δ_1, δ_2, δ_3, and $\bar{\delta}$.

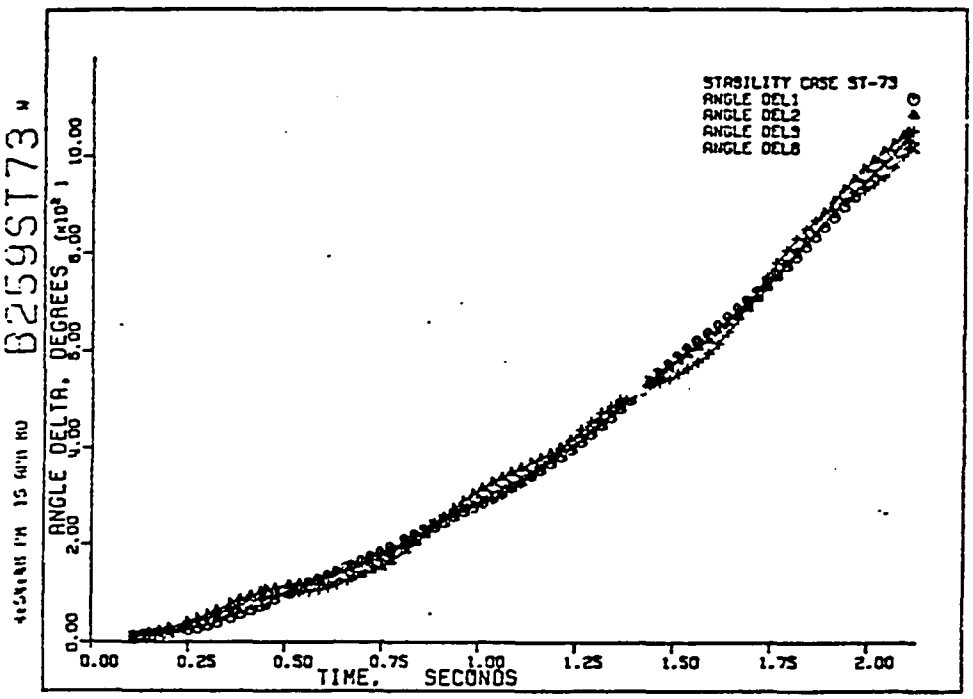

Figure 45. Case ST-73: angles δ_1, δ_2, δ_3, and $\bar{\delta}$.

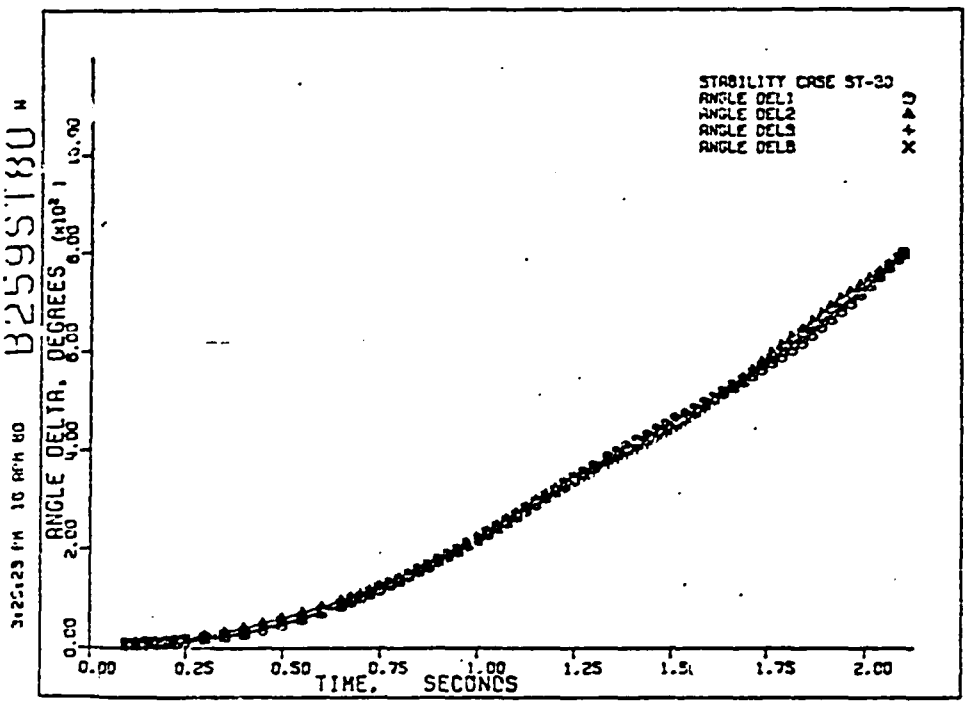

Figure 46. Case ST-80: angles δ_1, δ_2, δ_3, and $\bar{\delta}$.

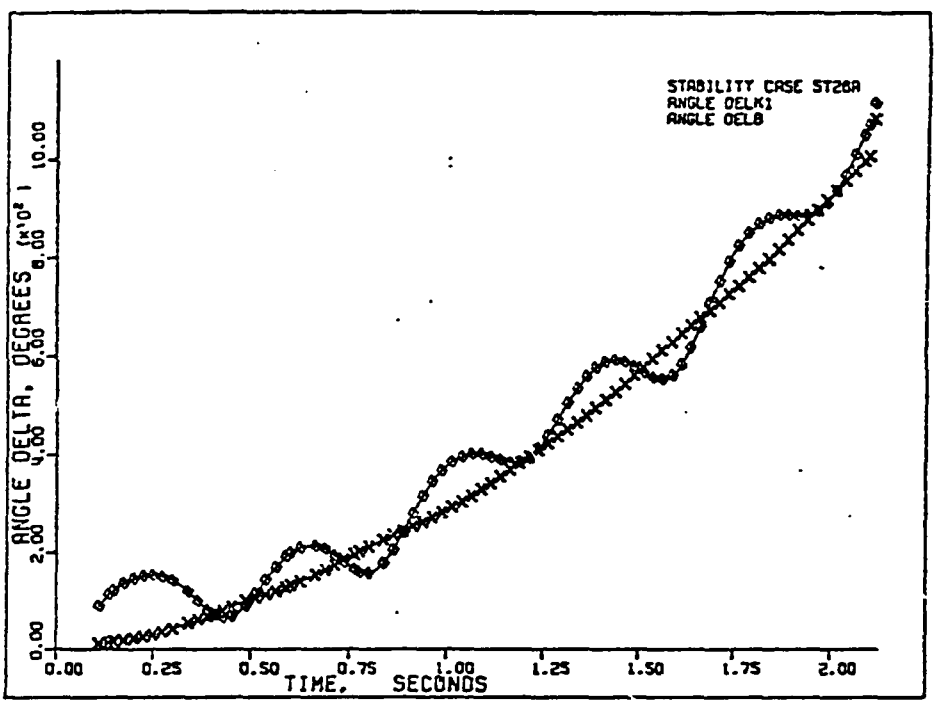

Figure 47. Case ST-26A: angles δ_k and $\bar{\delta}$.

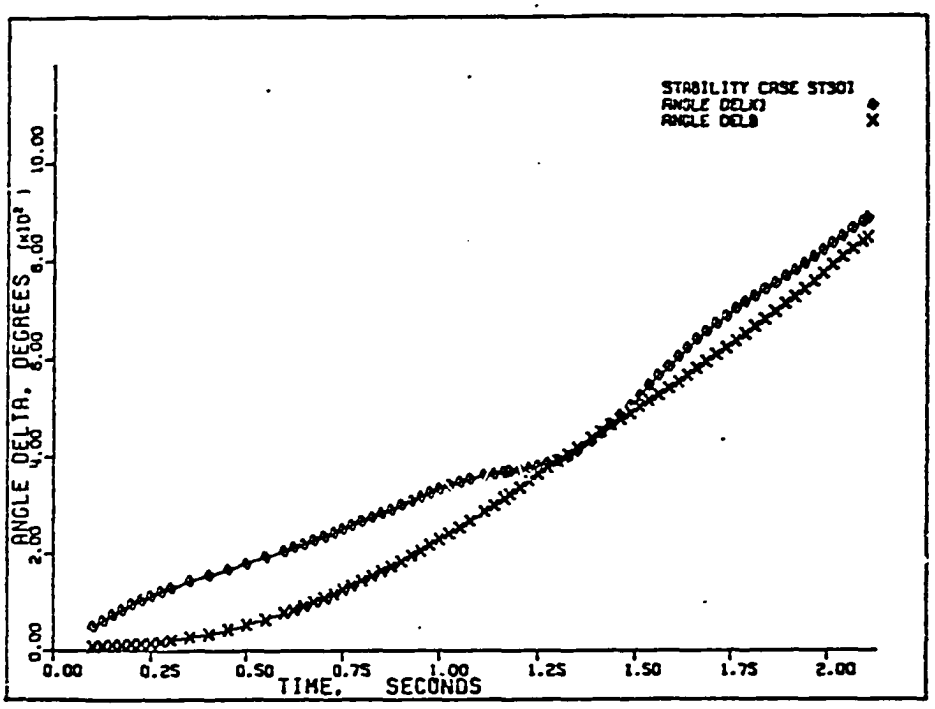

Figure 48. Case ST-30I: angles δ_k and $\bar{\delta}$.

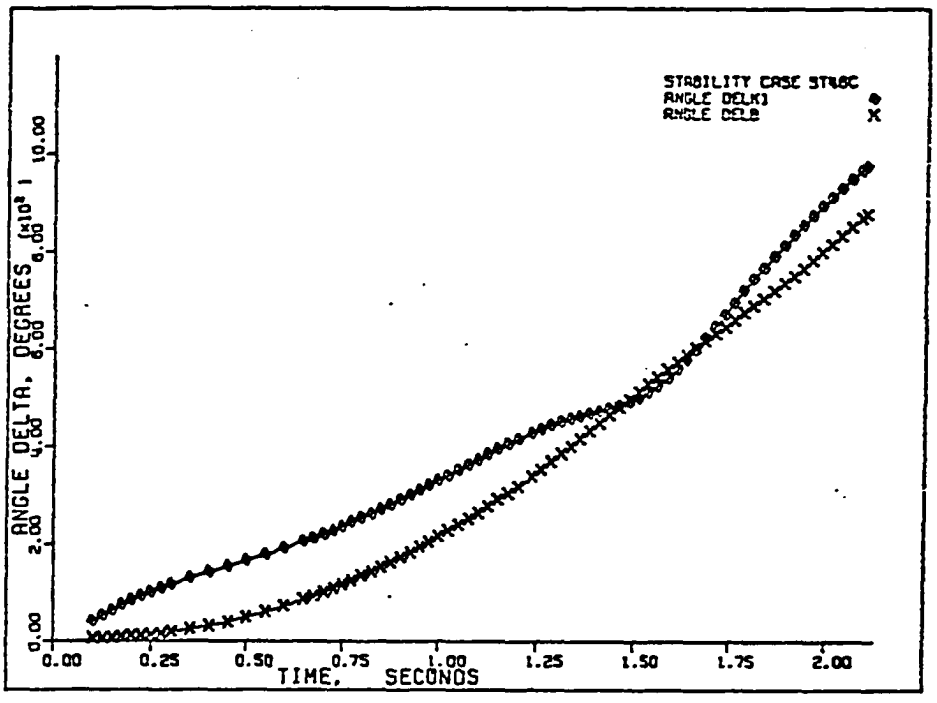

Figure 49. Case ST-46C: angles δ_k and $\bar{\delta}$.

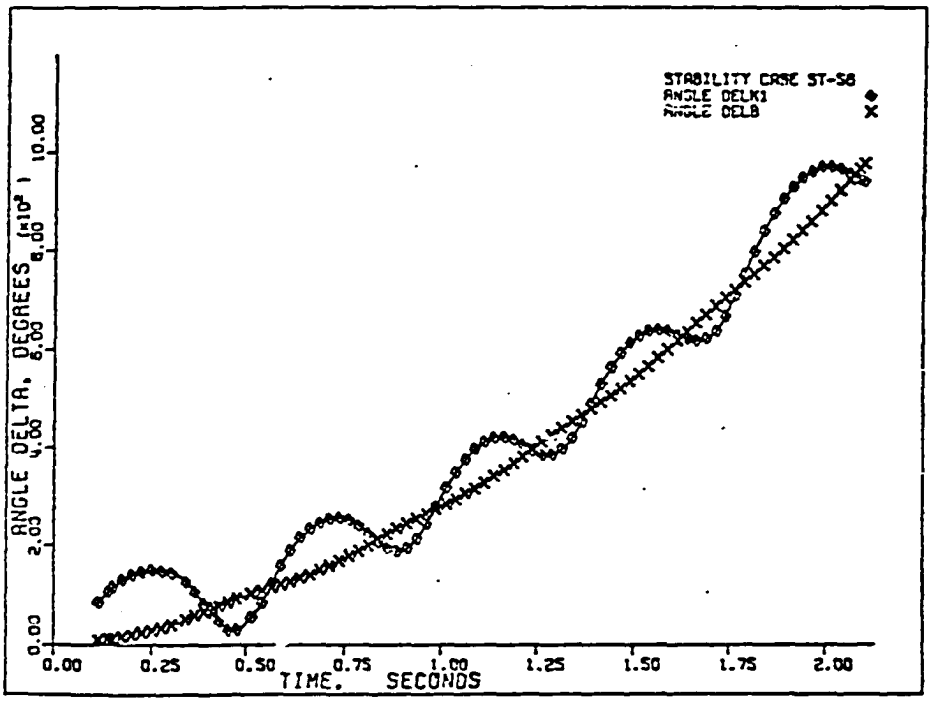

Figure 50. Case ST-56: angles δ_k and $\bar{\delta}$.

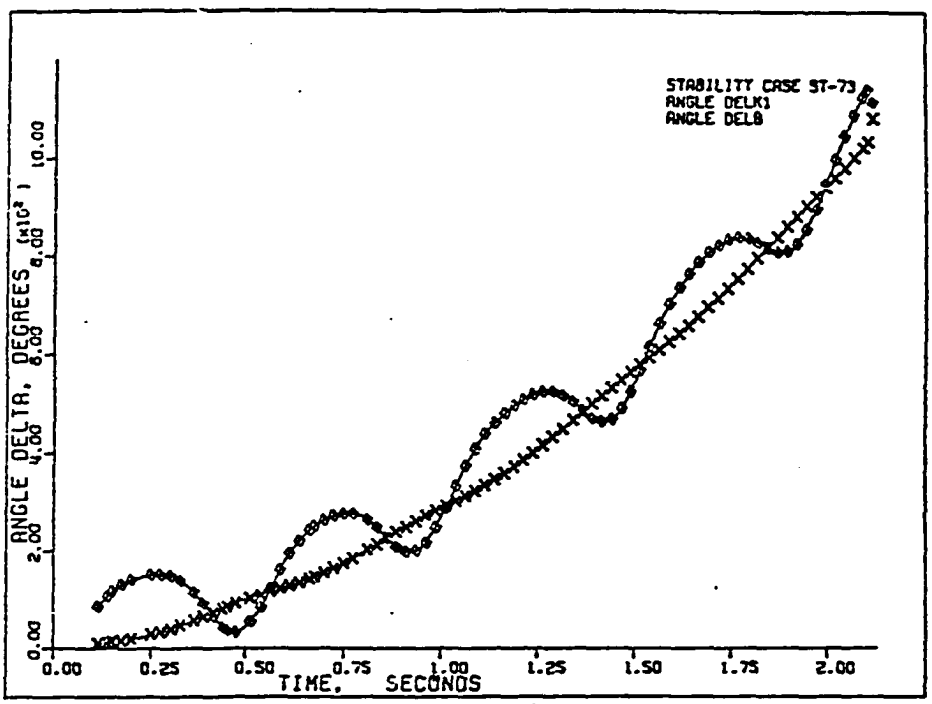

Figure 51. Case ST-73: angles δ_k and $\bar{\delta}$.

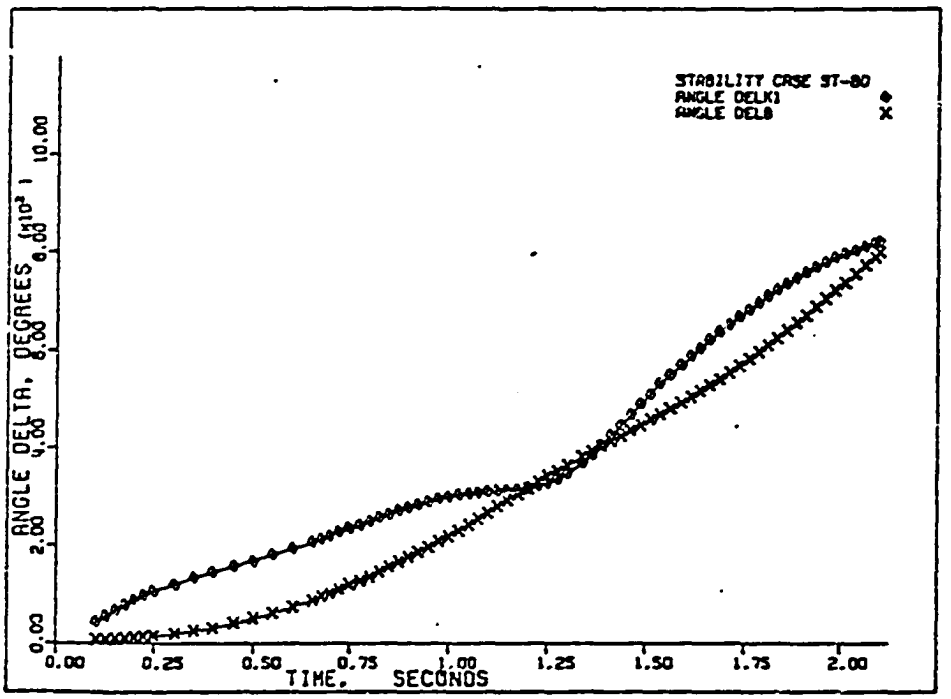

Figure 52. Case ST-80: angles δ_k and $\bar{\delta}$.

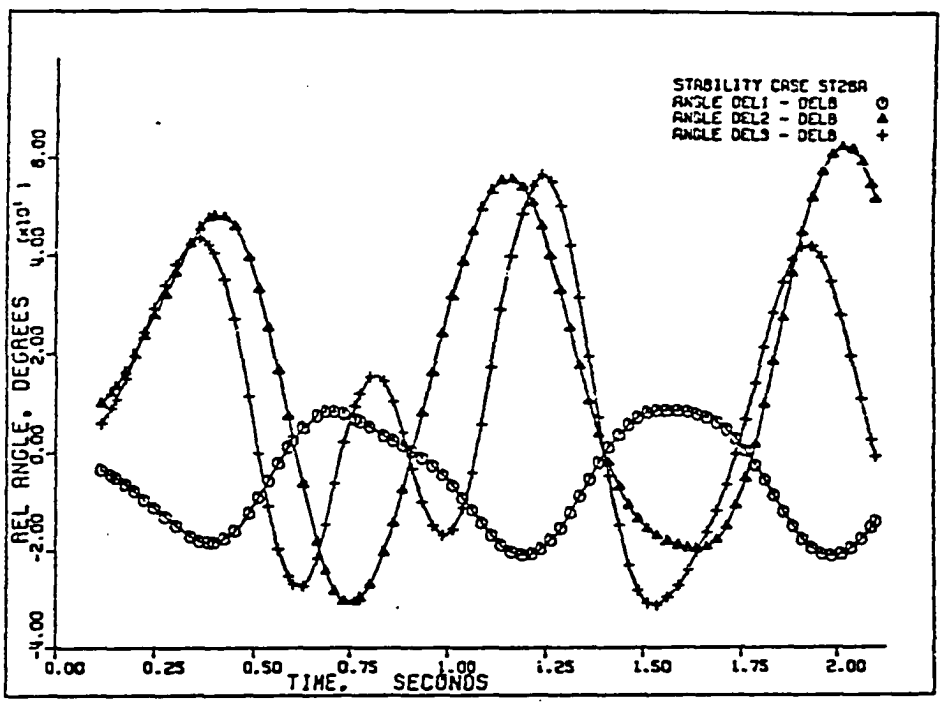

Figure 53. Case ST-26A: relative angles $(\delta_1 - \bar{\delta})$, $(\delta_2 - \bar{\delta})$, and $(\delta_3 - \bar{\delta})$.

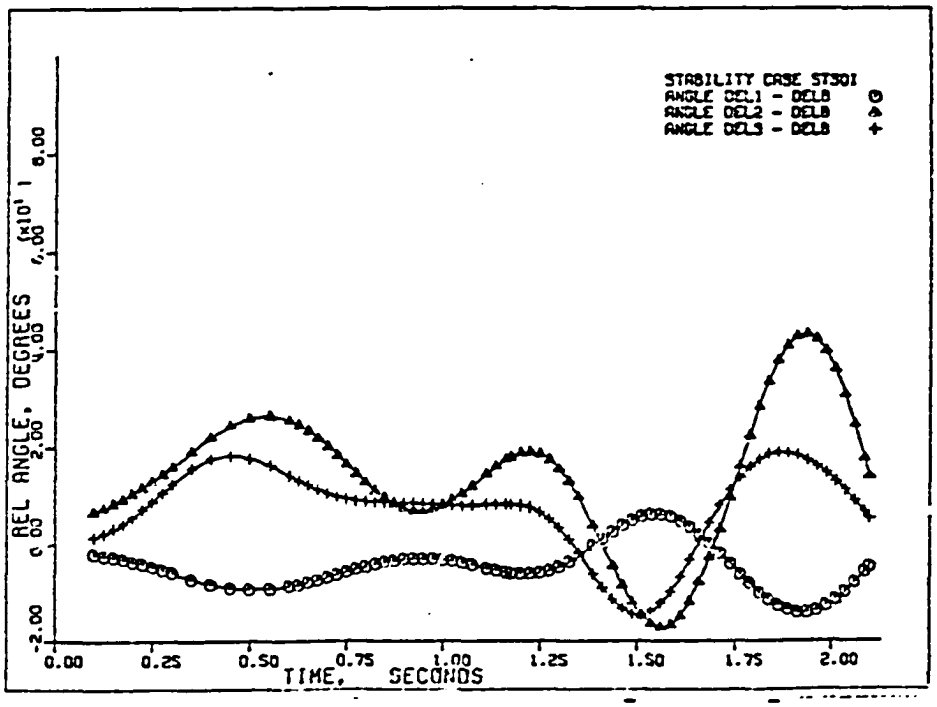

Figure 54. Case ST-30I: relative angles $(\delta_1 - \bar{\delta})$, $(\delta_2 - \bar{\delta})$, and $(\delta_3 - \bar{\delta})$.

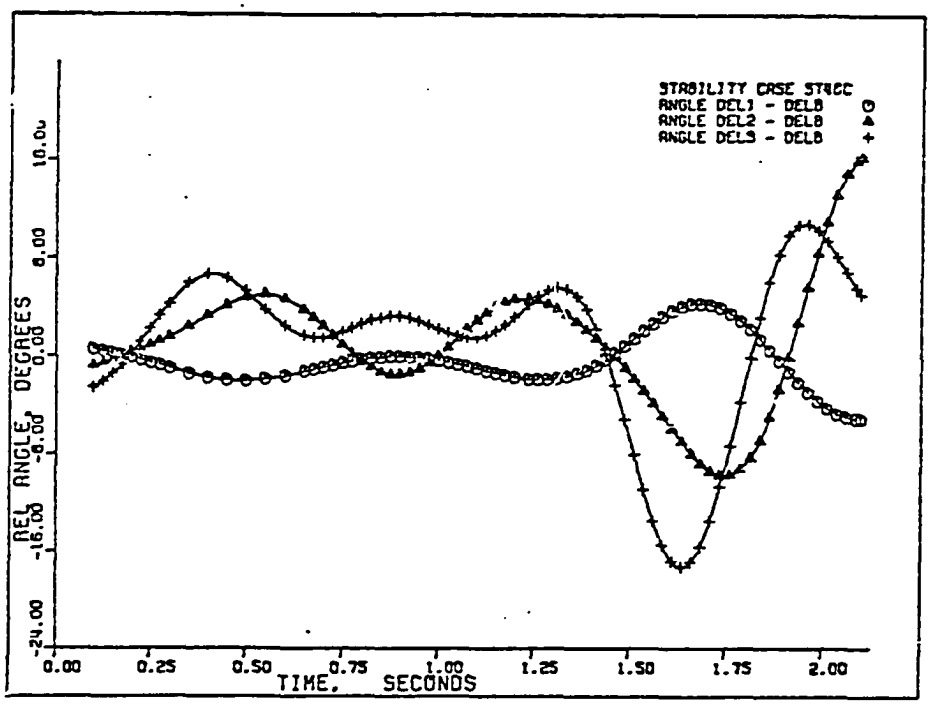

Figure 55. Case ST-46C: relative angles $(\delta_1 - \bar{\delta})$, $(\delta_2 - \bar{\delta})$, and $(\delta_3 - \bar{\delta})$.

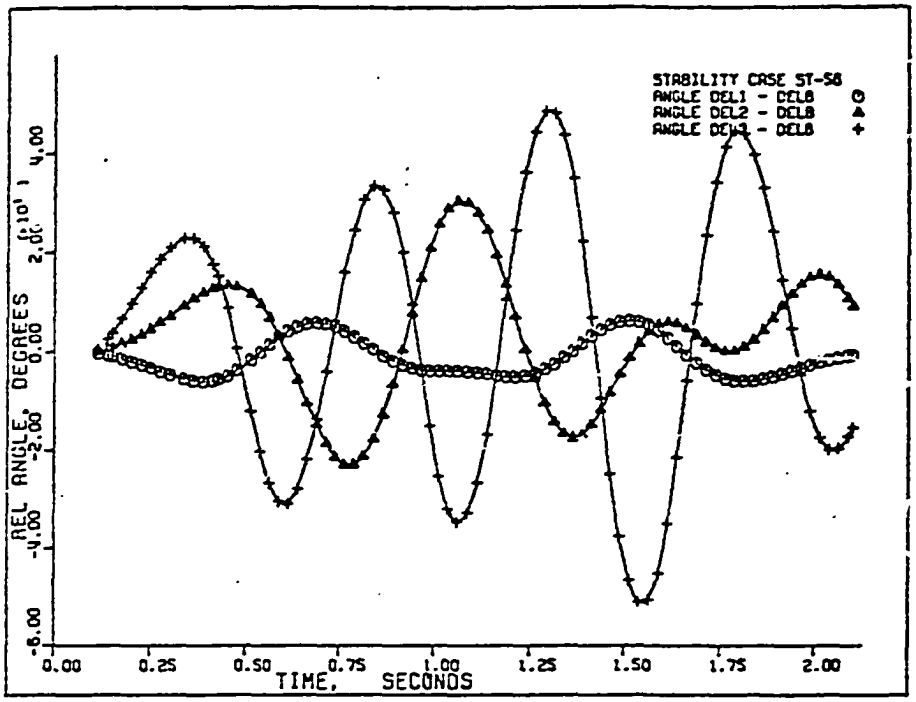

Figure 56. Case ST-56: relative angles $(\delta_1 - \bar{\delta})$, $(\delta_1 - \bar{\delta})$, and $(\delta_3 - \bar{\delta})$.

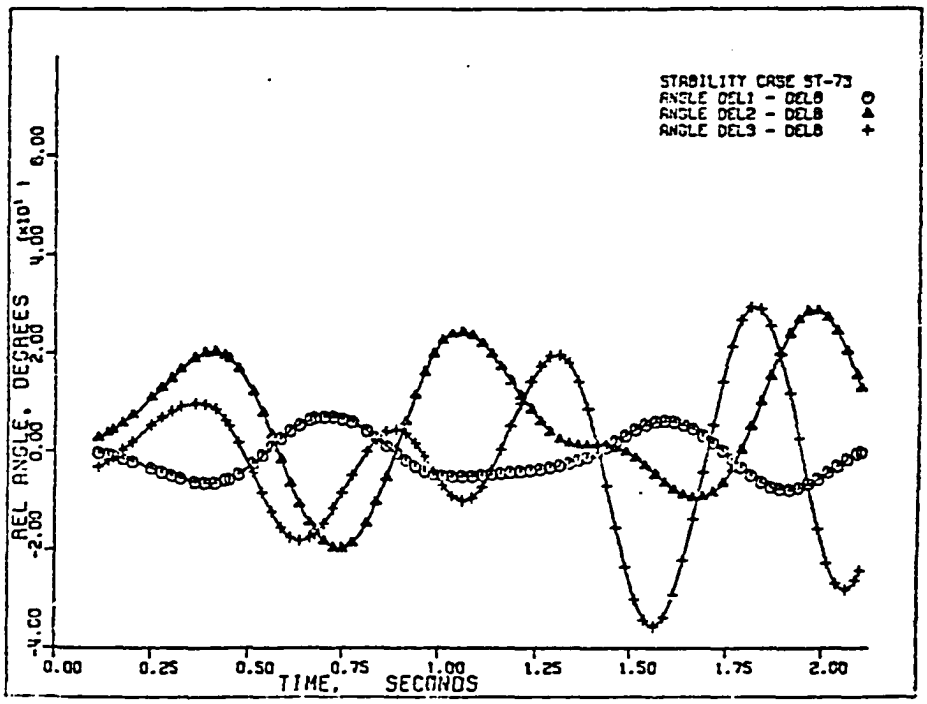

Figure 57. Case ST-73: relative angles $(\delta_1 - \bar{\delta})$, $(\delta_2 - \bar{\delta})$, and $(\delta_3 - \bar{\delta})$.

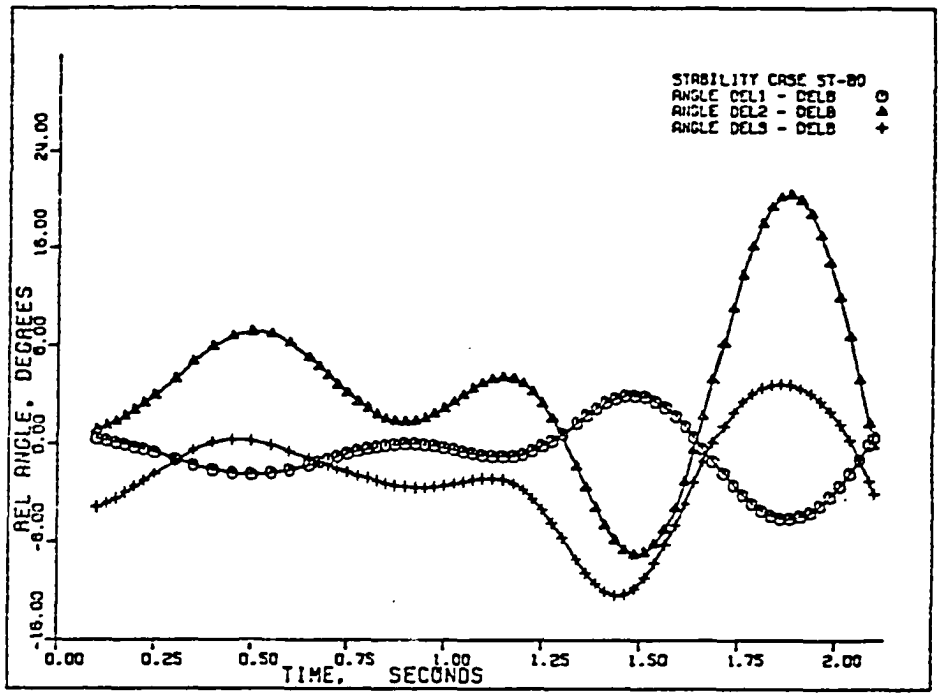

Figure 58. Case ST-80: relative angles $(\delta_1 - \bar{\delta})$, $(\delta_2 - \bar{\delta})$, and $(\delta_3 - \bar{\delta})$.

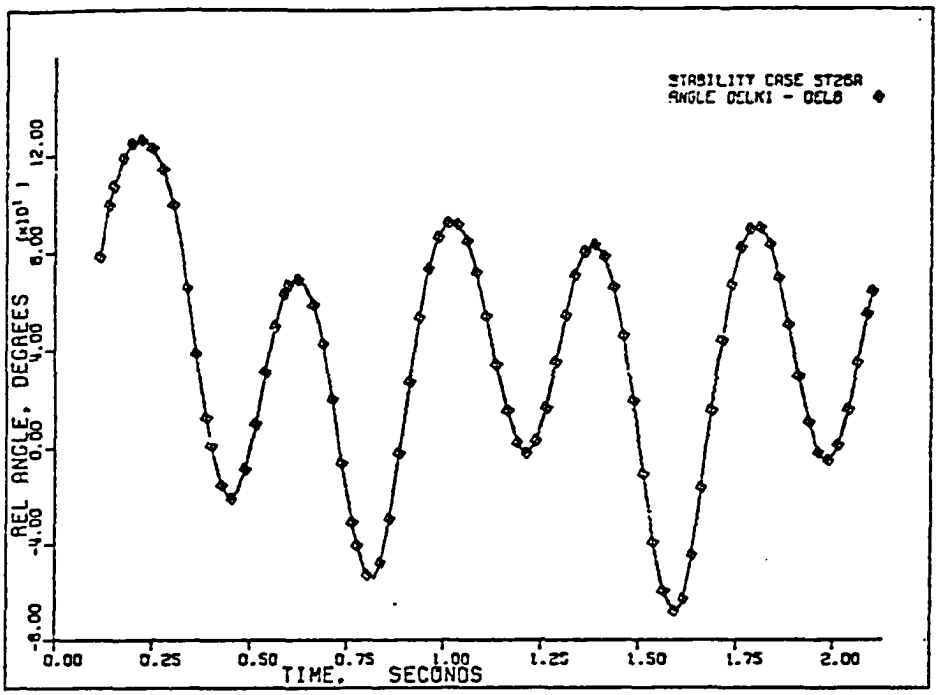

Figure 59. Case ST-26A: relative angle $(\delta_k - \bar{\delta})$.

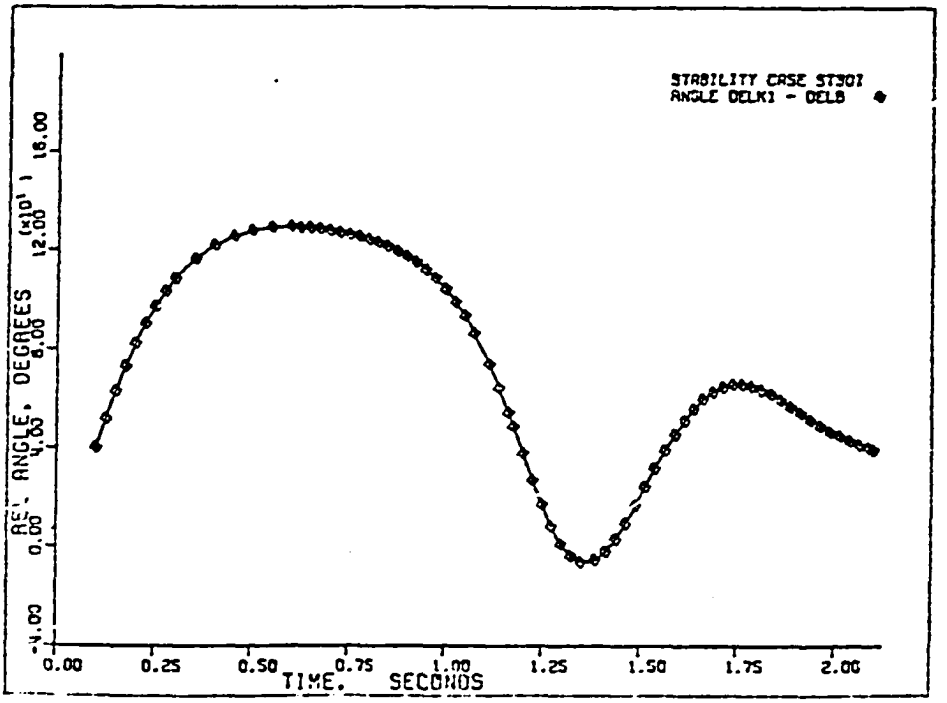

Figure 60. Case ST-30I: relative angle $(\delta_k - \bar{\delta})$.

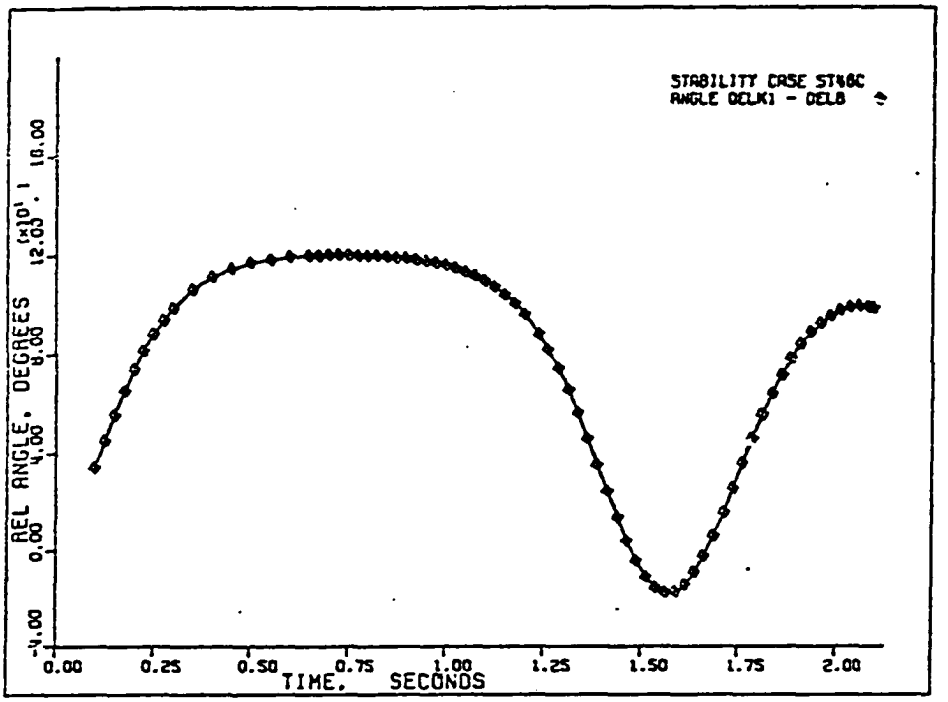

Figure 61. Case ST-46C: relative angle $(\delta_k - \bar{\delta})$.

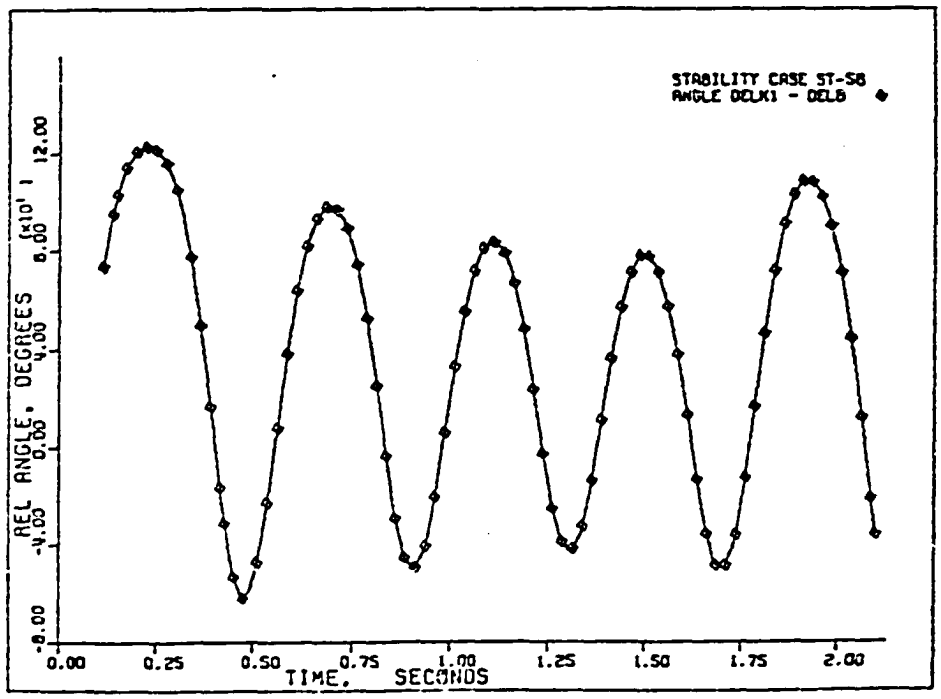

Figure 62. Case ST-56: relative angle $(\delta_k - \bar{\delta})$.

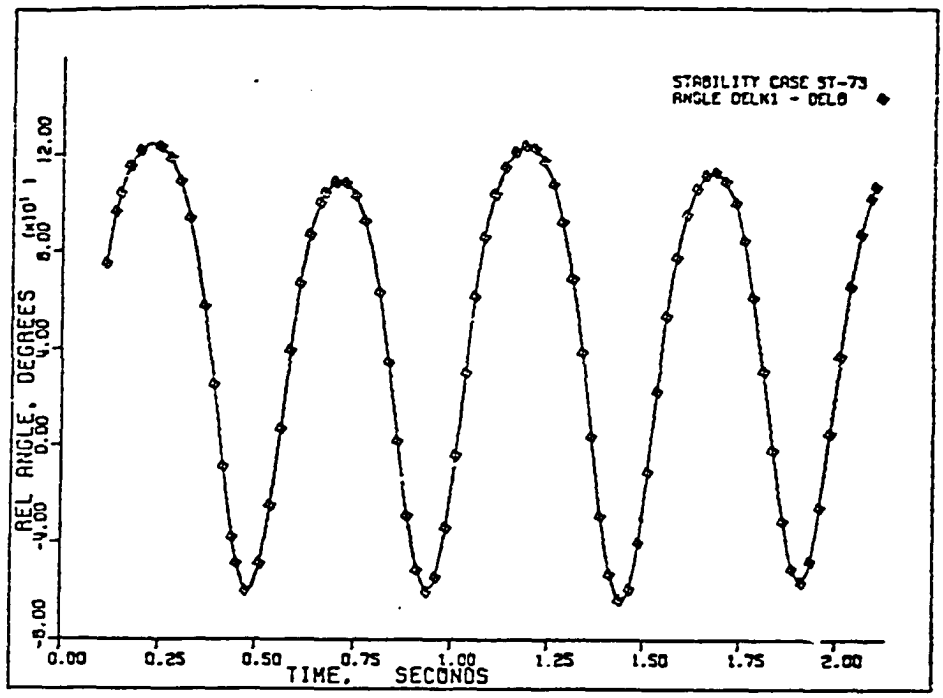

Figure 63. Case ST-73: relative angle $(\delta_k - \bar{\delta})$.

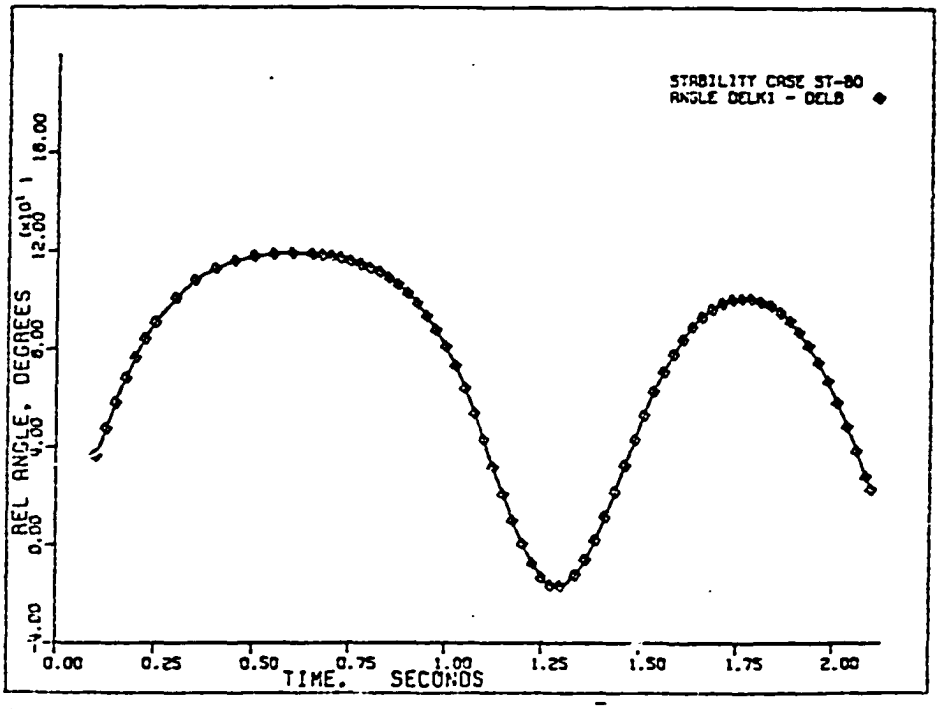

Figure 64. Case ST-80: relative angle $(\delta_k - \bar{\delta})$.

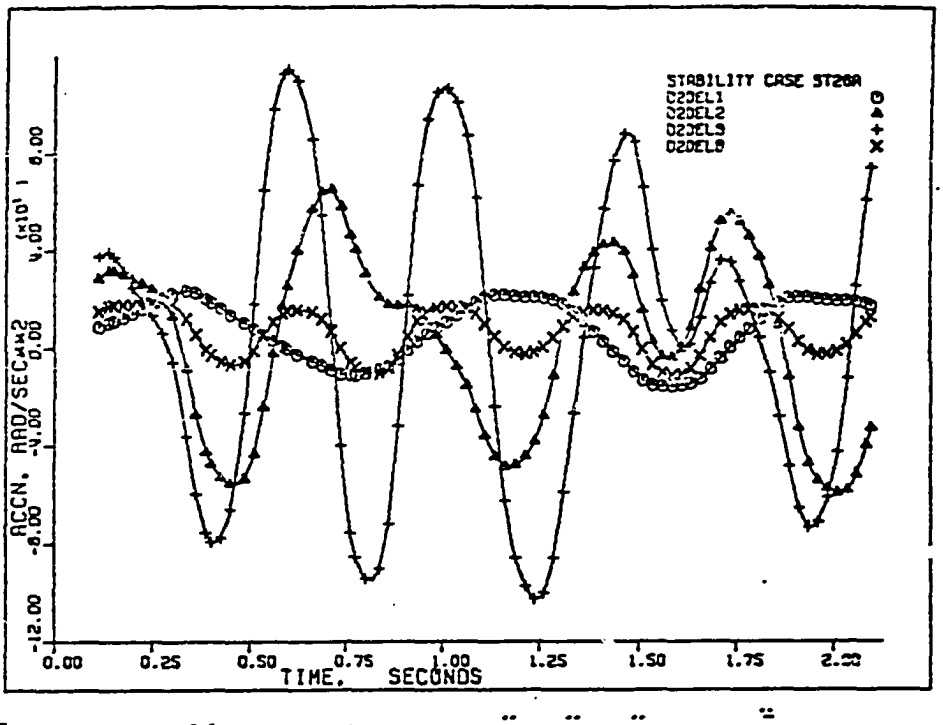

Figure 65. Case ST-26A: accelerations $\ddot{\delta}_1$, $\ddot{\delta}_2$, $\ddot{\delta}_3$, and $\ddot{\bar{\delta}}$.

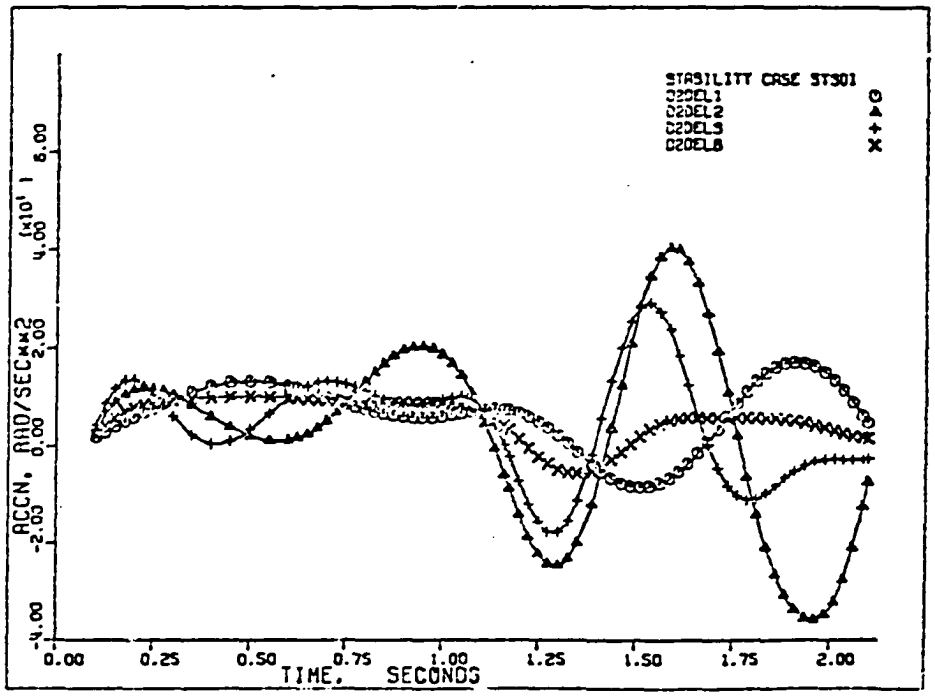

Figure 66. Case ST-30I: accelerations $\ddot{\delta}_1$, $\ddot{\delta}_2$, $\ddot{\delta}_3$, and $\ddot{\bar{\delta}}$.

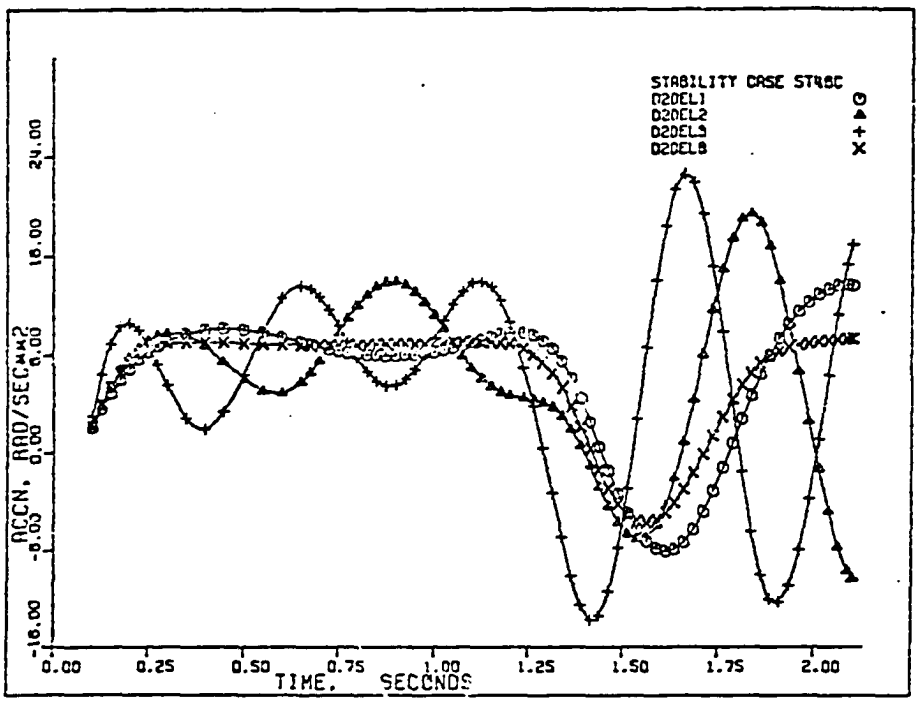

Figure 67. Case ST-46C: accelerations $\ddot{\delta}_1$, $\ddot{\delta}_2$, $\ddot{\delta}_3$, and $\ddot{\bar{\delta}}$.

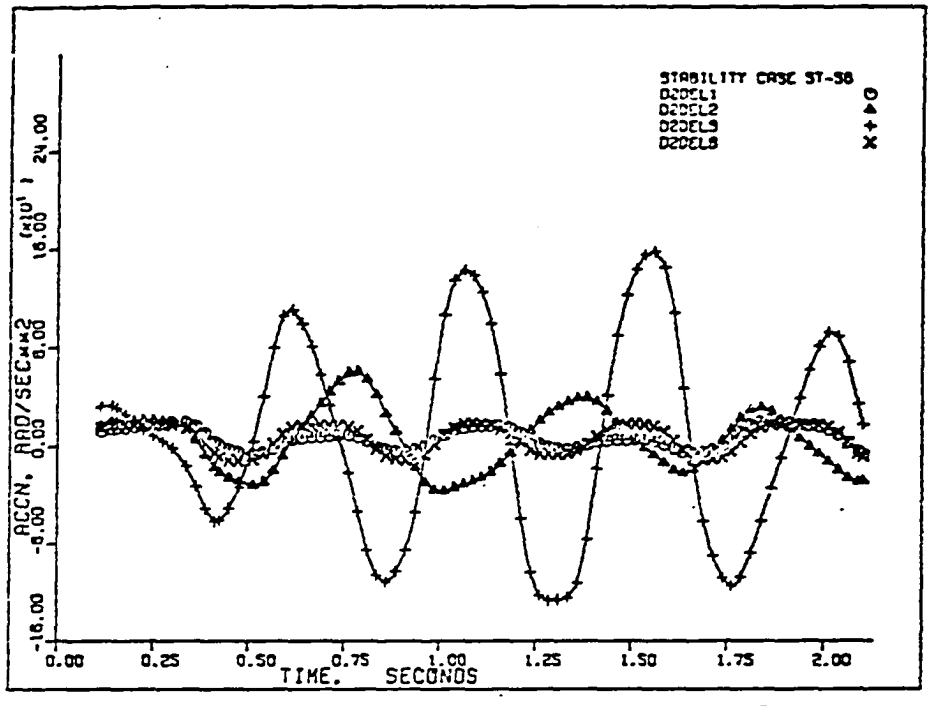

Figure 68. Case ST-56: accelerations $\ddot{\delta}_1$, $\ddot{\delta}_2$, $\ddot{\delta}_3$, and $\bar{\delta}$.

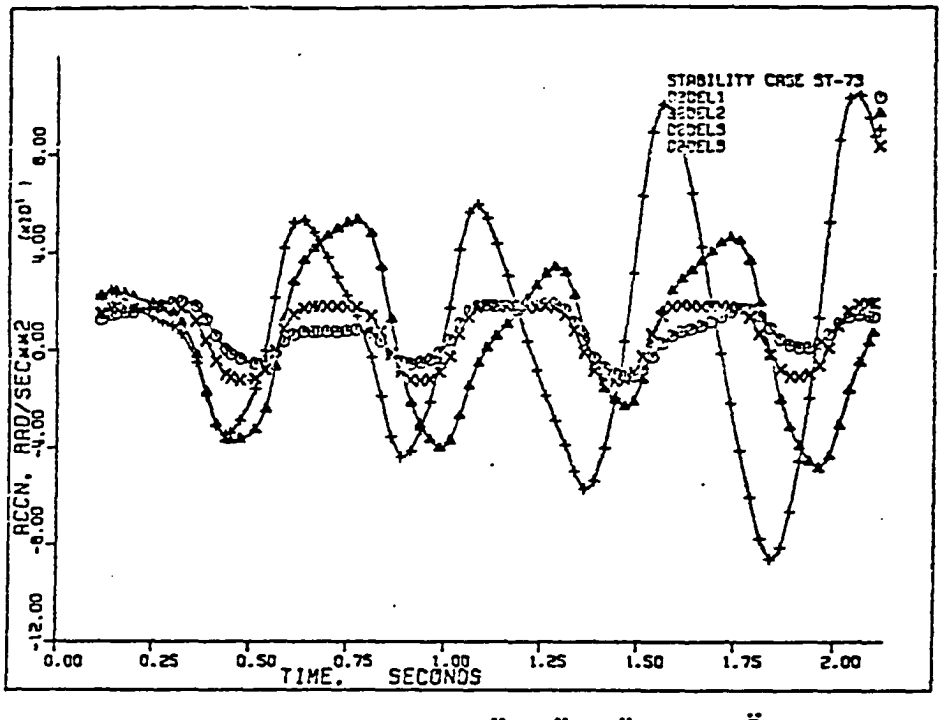

Figure 69. Case ST-73: accelerations $\ddot{\delta}_1$, $\ddot{\delta}_2$, $\ddot{\delta}_3$, and $\ddot{\bar{\delta}}$.

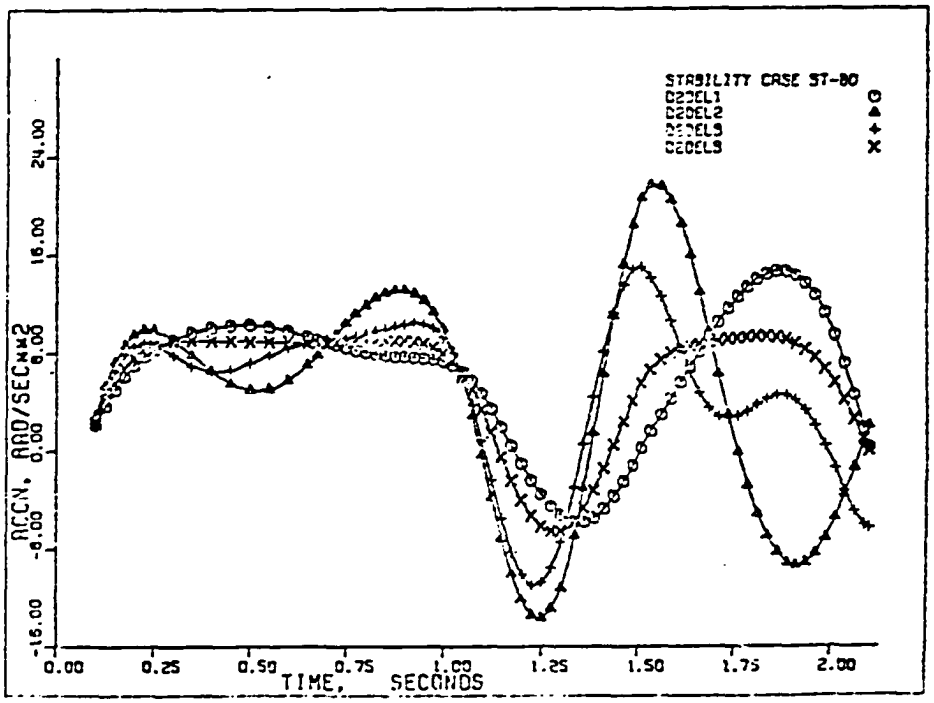

Figure 70. Case ST-80: accelerations $\ddot{\delta}_1$, $\ddot{\delta}_2$, $\ddot{\delta}_3$, and $\ddot{\bar{\delta}}$.

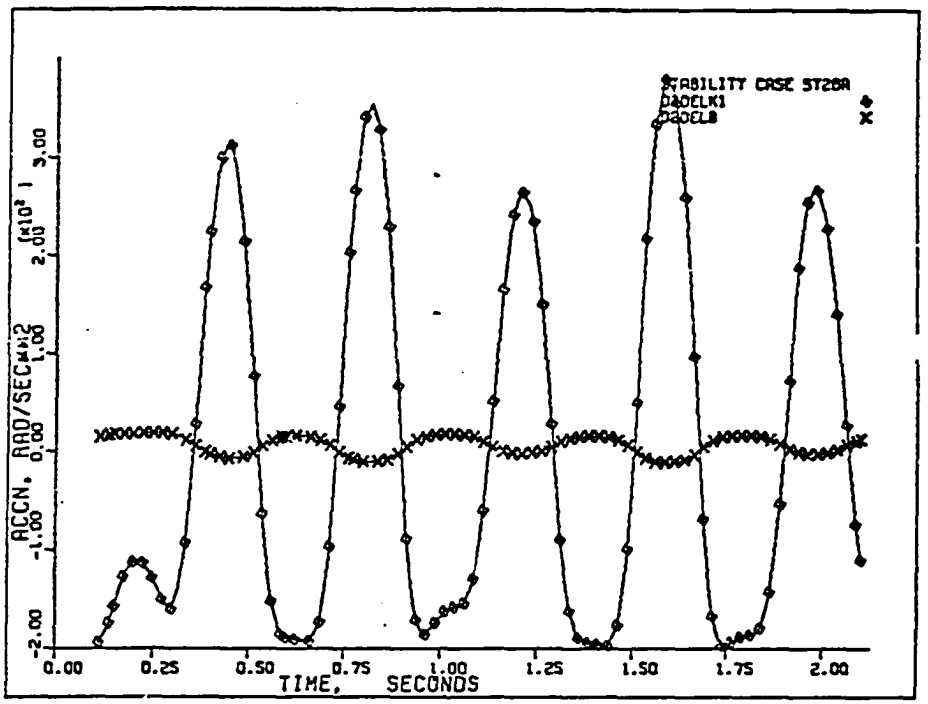

Figure 71. Case ST-26A: accelerations $\ddot{\delta}_k$ and $\ddot{\bar{\delta}}$.

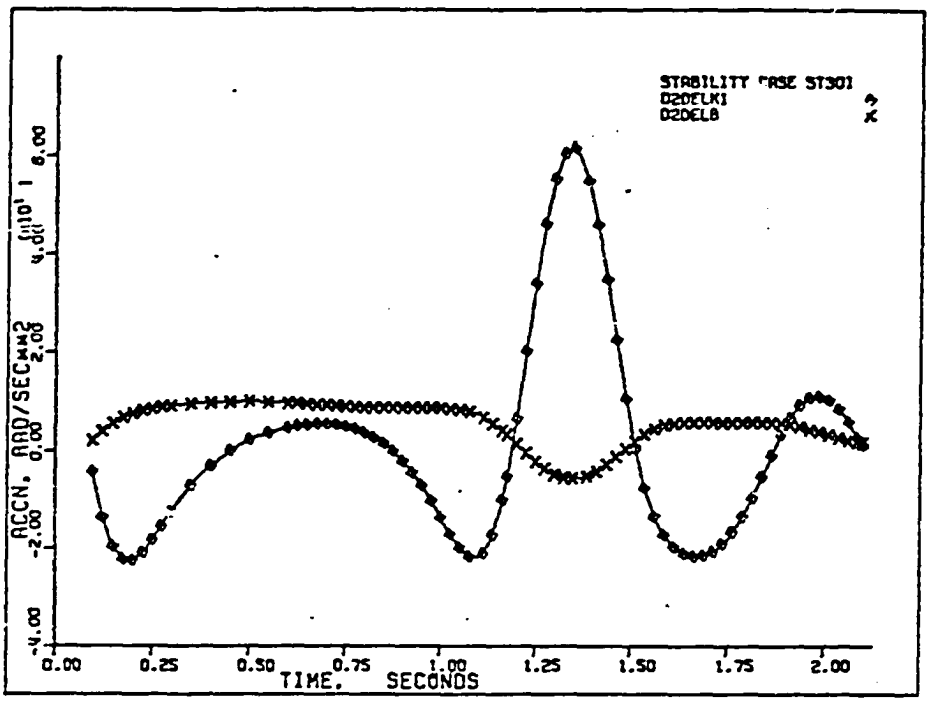

Figure 72. Case ST-30I: accelerations $\ddot{\delta}_k$ and $\ddot{\bar{\delta}}$.

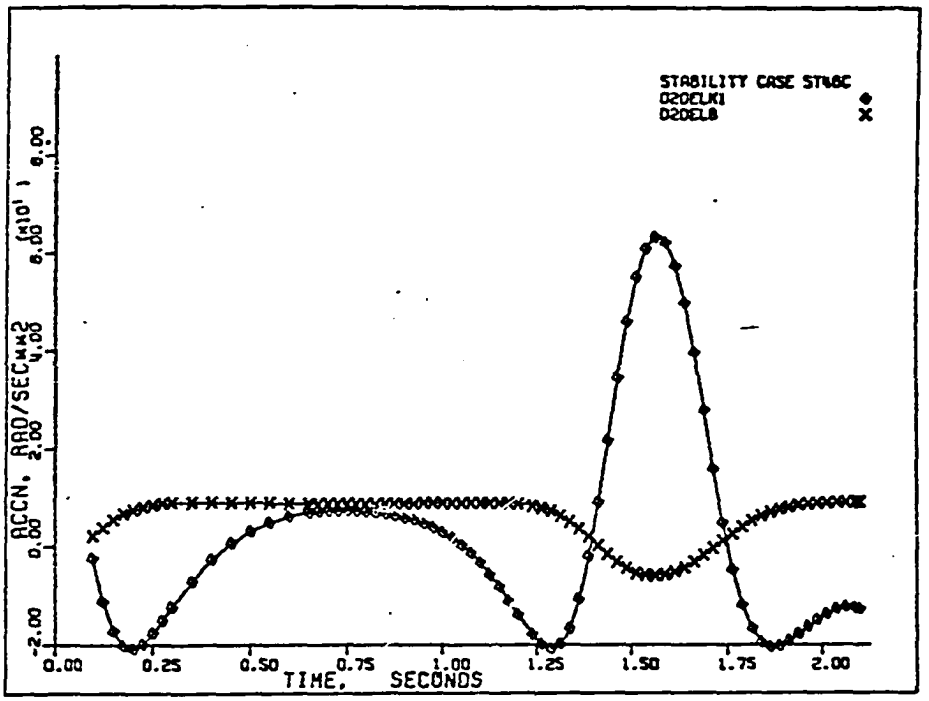

Figure 73. Case ST-46C: accelerations $\ddot{\delta}_k$ and $\ddot{\bar{\delta}}$.

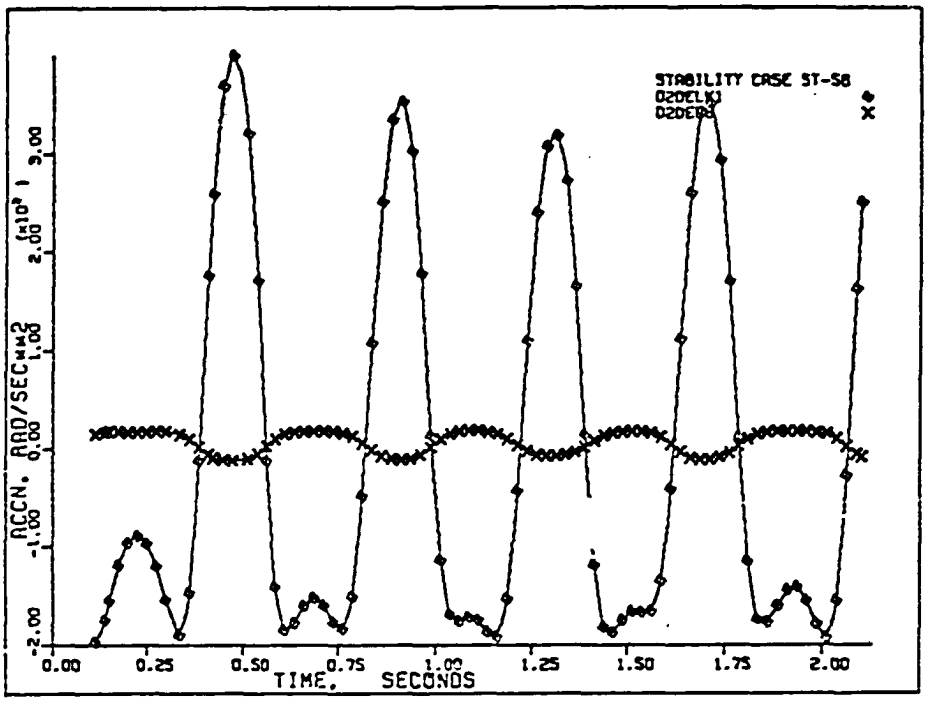

Figure 74. Case ST-56: accelerations $\ddot{\delta}_k$ and $\ddot{\delta}$.

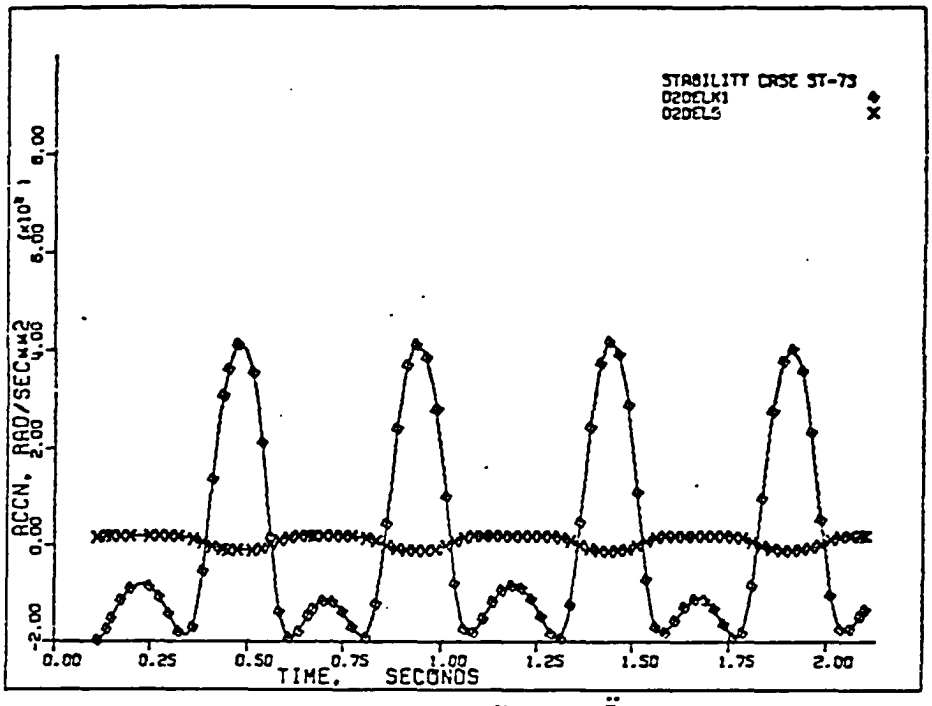

Figure 75. Case ST-73: accelerations $\ddot{\delta}_k$ and $\ddot{\delta}$.

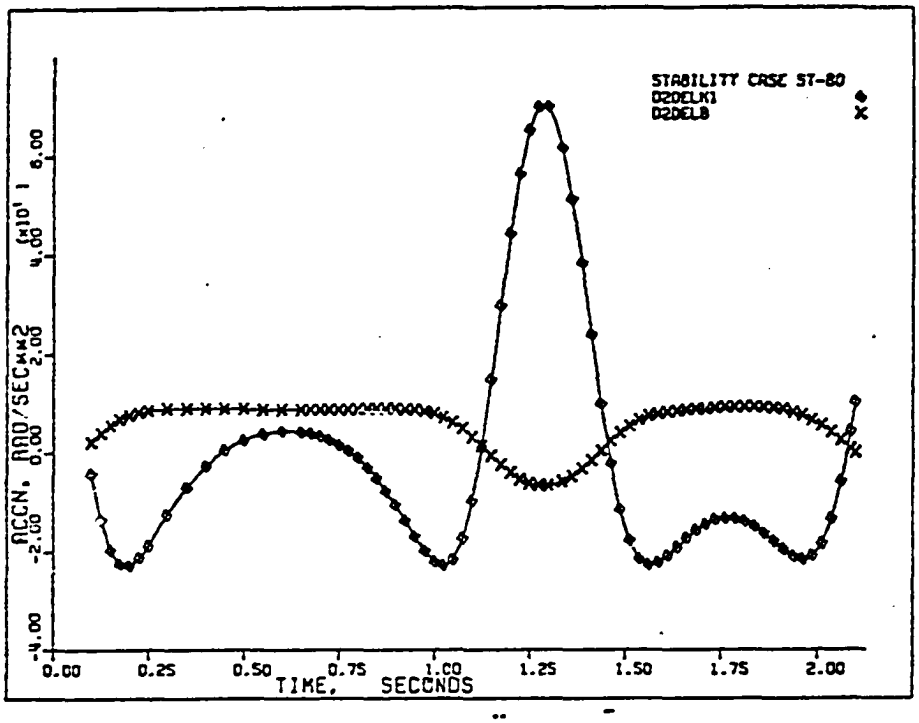

Figure 76. Case ST-80: accelerations $\ddot{\delta}_k$ and $\ddot{\bar{\delta}}$.

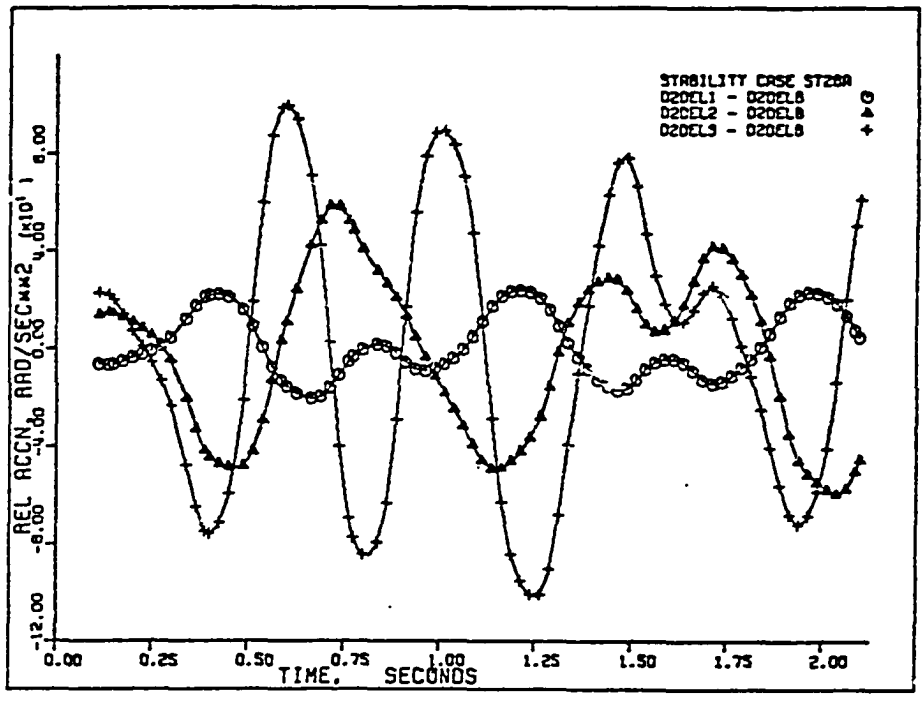

Figure 77. Case ST-26A: relative accelerations $(\ddot{\delta}_1 - \ddot{\bar{\delta}})$, $(\ddot{\delta}_2 - \ddot{\bar{\delta}})$, and $(\ddot{\delta}_3 - \ddot{\bar{\delta}})$.

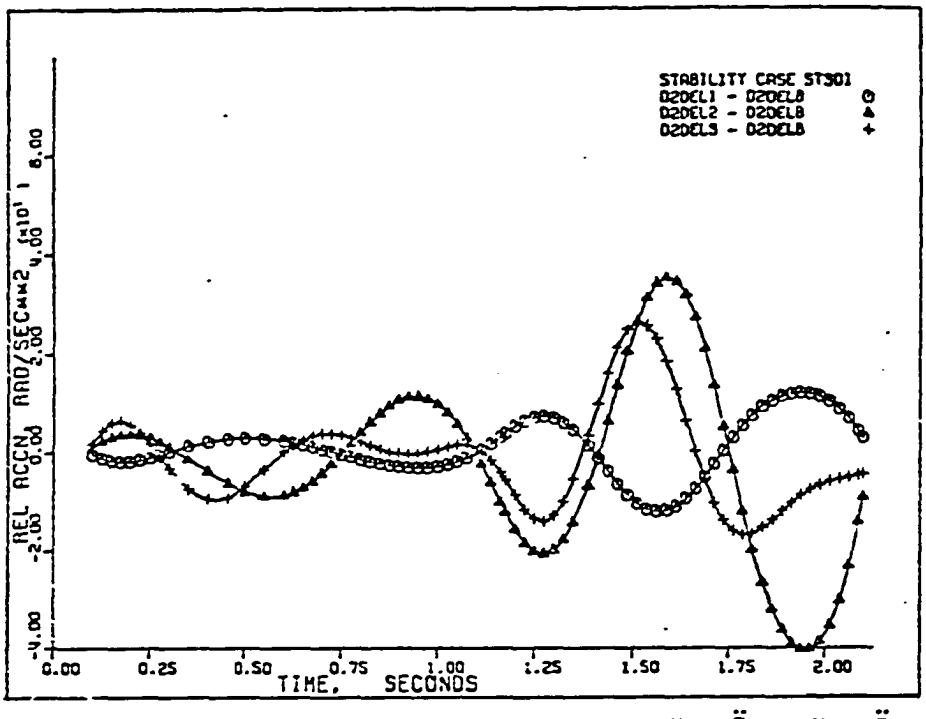

Figure 78. Case ST-30I: relative accelerations $(\ddot{\delta}_1 - \ddot{\bar{\delta}})$, $(\ddot{\delta}_2 - \ddot{\bar{\delta}})$, and $(\ddot{\delta}_3 - \ddot{\bar{\delta}})$.

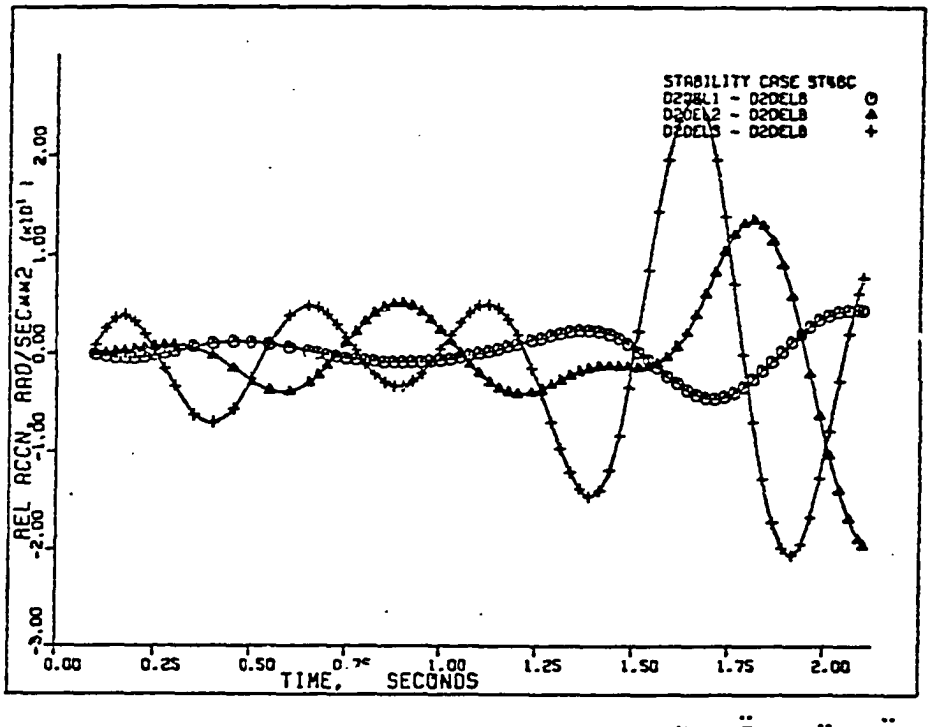

Figure 79. Case ST-46C: relative accelerations $(\ddot{\delta}_1 - \ddot{\bar{\delta}})$, $(\ddot{\delta}_2 - \ddot{\bar{\delta}})$, and $(\ddot{\delta}_3 - \ddot{\bar{\delta}})$.

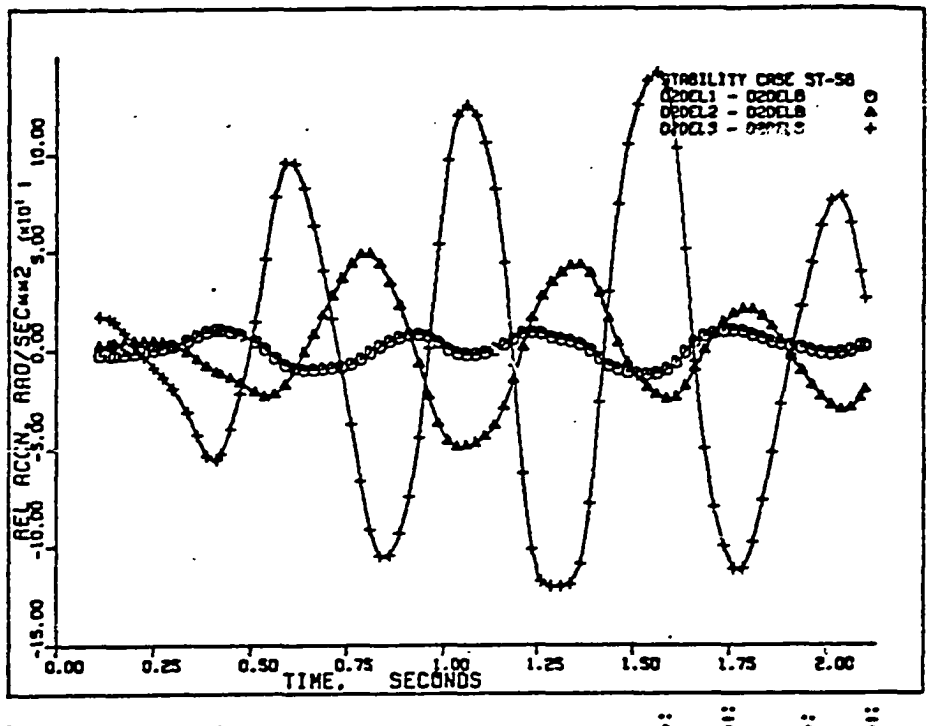

Figure 80. Case ST-56: relative accelerations $(\ddot{\delta}_1 - \ddot{\bar{\delta}})$, $(\ddot{\delta}_2 - \ddot{\bar{\delta}})$, and $(\ddot{\delta}_3 - \ddot{\bar{\delta}})$.

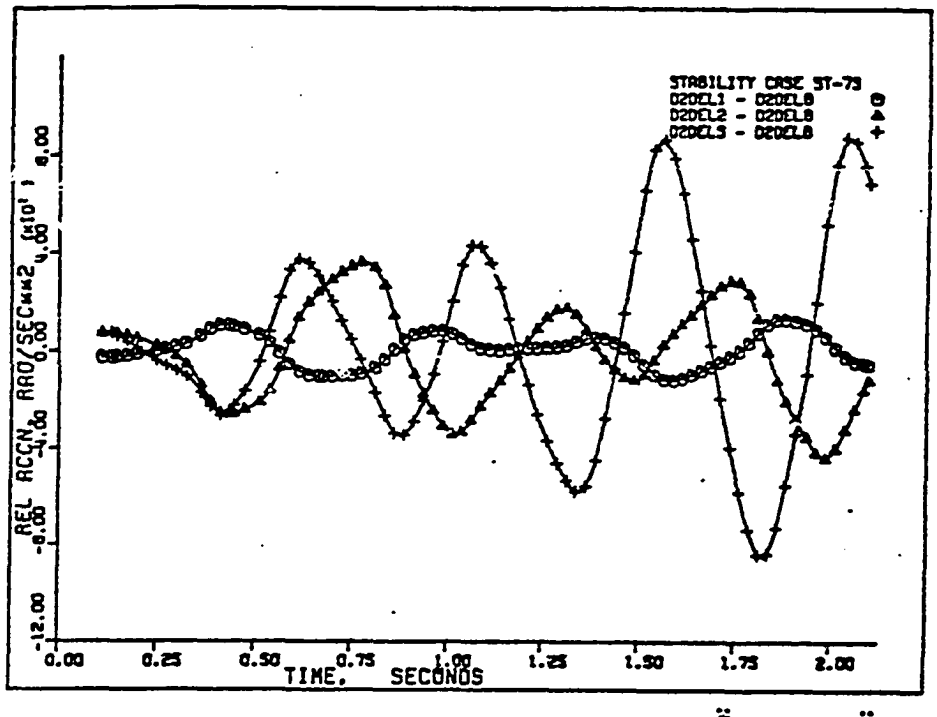

Figure 81. Case ST-73: relative accelerations $(\ddot{\delta}_1 - \ddot{\bar{\delta}})$, $(\ddot{\delta}_2 - \ddot{\bar{\delta}})$, $(\ddot{\delta}_3 - \ddot{\bar{\delta}})$.

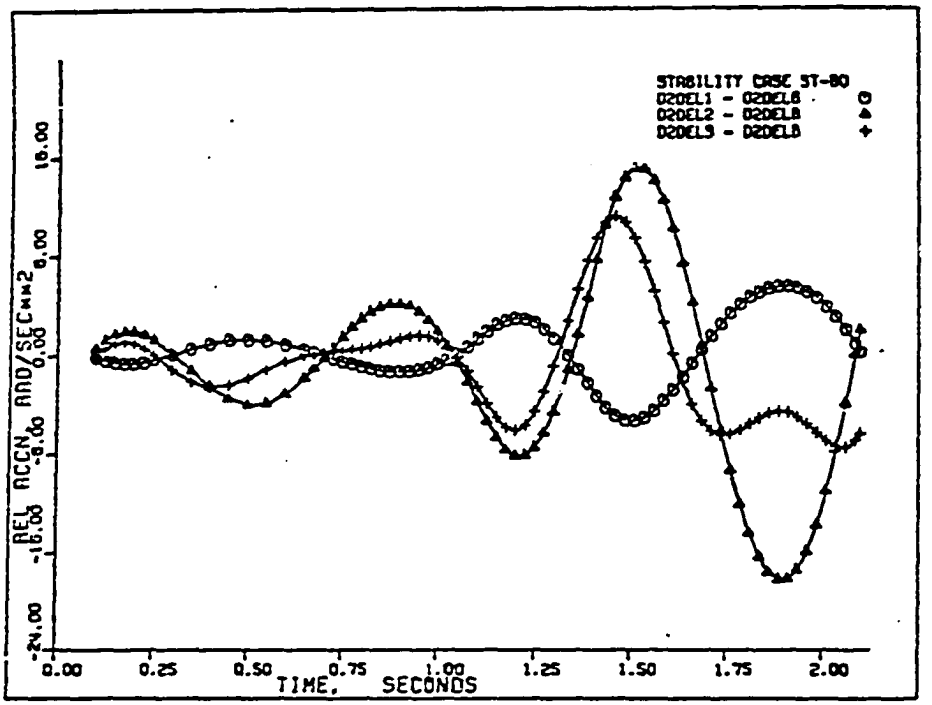

Figure 82. Case ST-80: relative accelerations $(\ddot{\delta}_1 - \ddot{\bar{\delta}})$, $(\ddot{\delta}_2 - \ddot{\bar{\delta}})$, and $(\ddot{\delta}_3 - \ddot{\bar{\delta}})$.

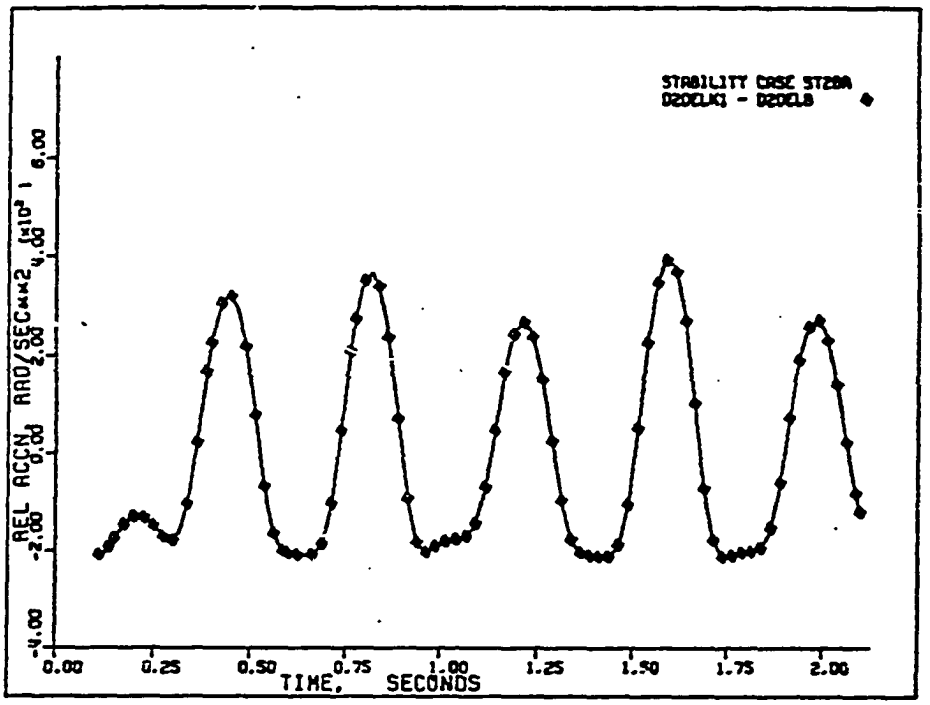

Figure 83. Case ST-26A: relative acceleration $(\ddot{\delta}_k - \ddot{\bar{\delta}})$.

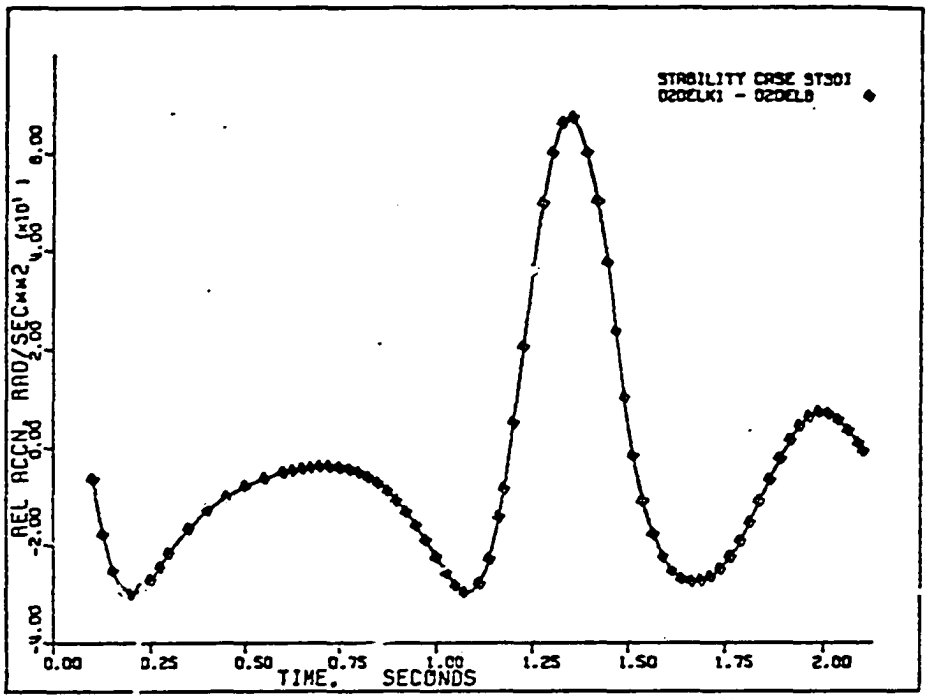

Figure 84. Case ST-30I: relative acceleration $(\ddot{\delta}_k - \ddot{\bar{\delta}})$.

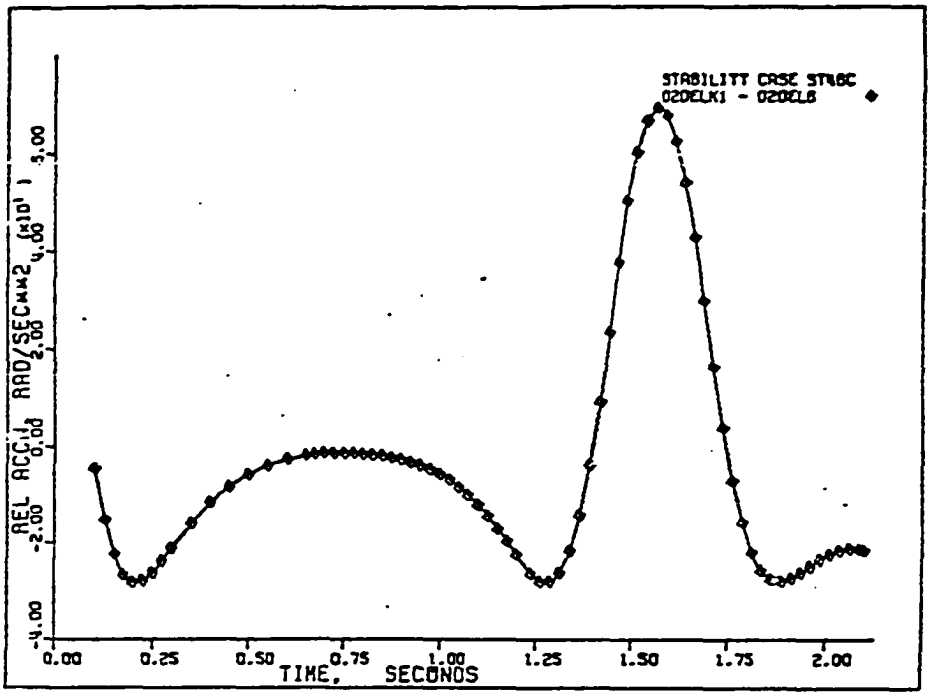

Figure 85. Case ST-46C: relative acceleration $(\ddot{\delta}_k - \ddot{\bar{\delta}})$.

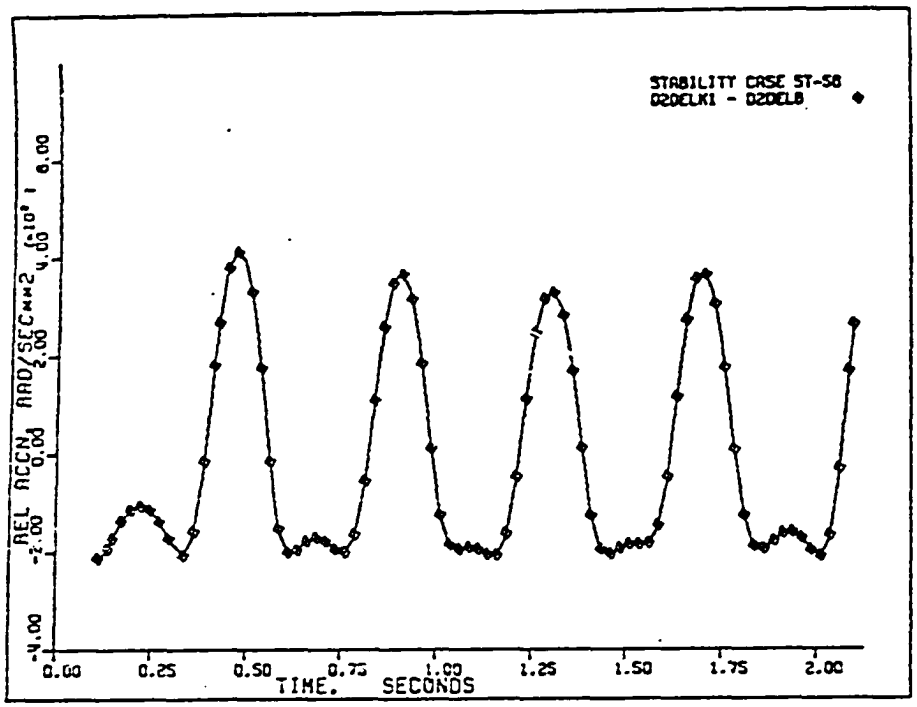

Figure 86. Case ST-56: relative acceleration $(\ddot{\delta}_k - \ddot{\bar{\delta}})$.

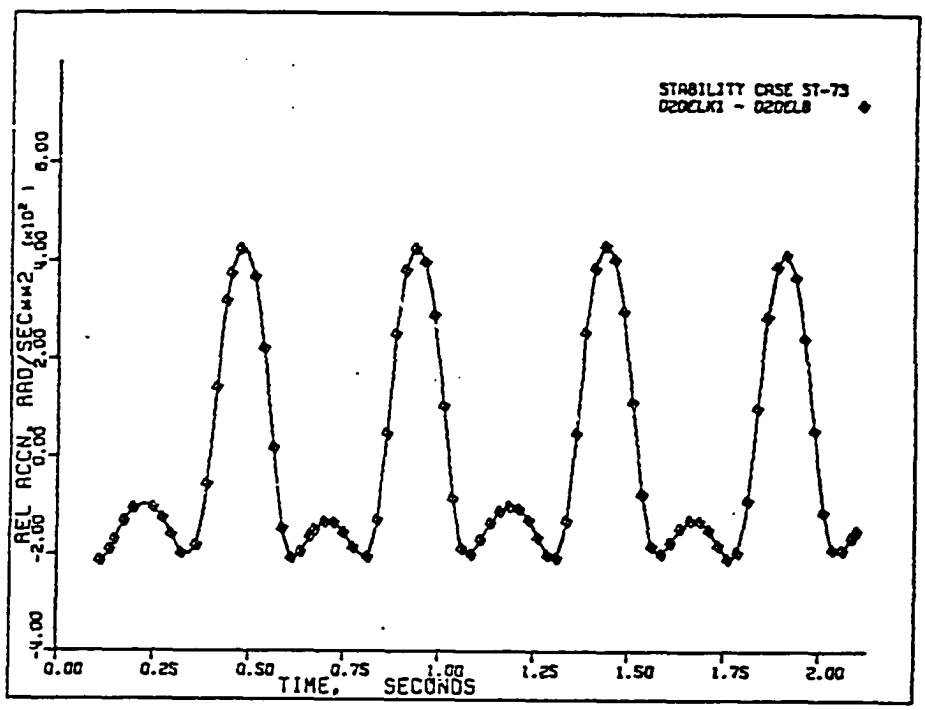

Figure 87. Case ST-73: relative acceleration $(\ddot{\delta}_k - \ddot{\bar{\delta}})$.

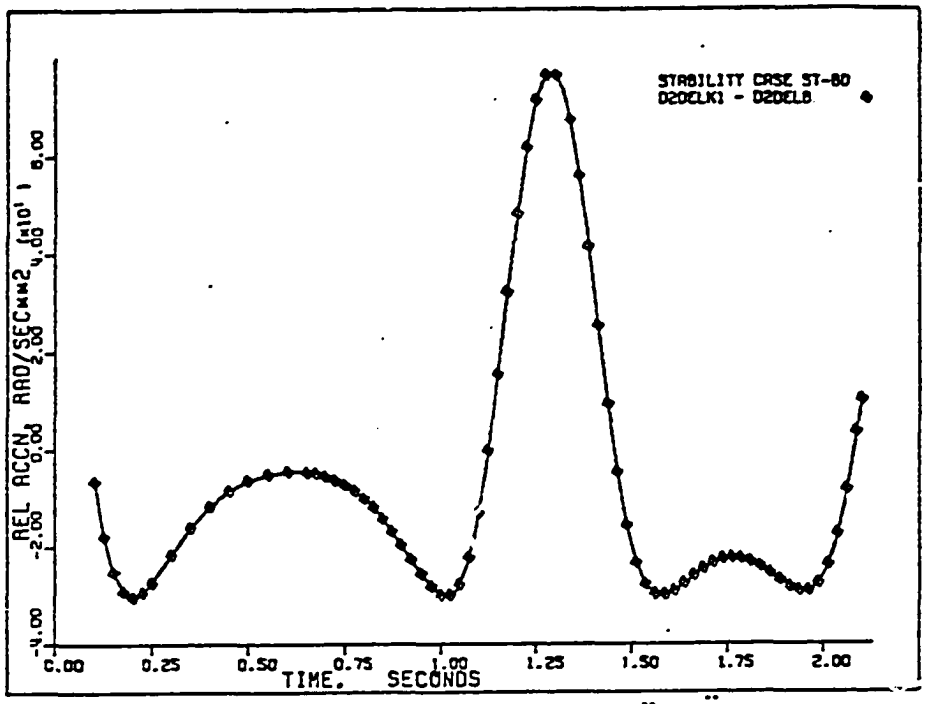

Figure 88. Case ST-80: relative acceleration $(\ddot{\delta}_k - \ddot{\delta})$.

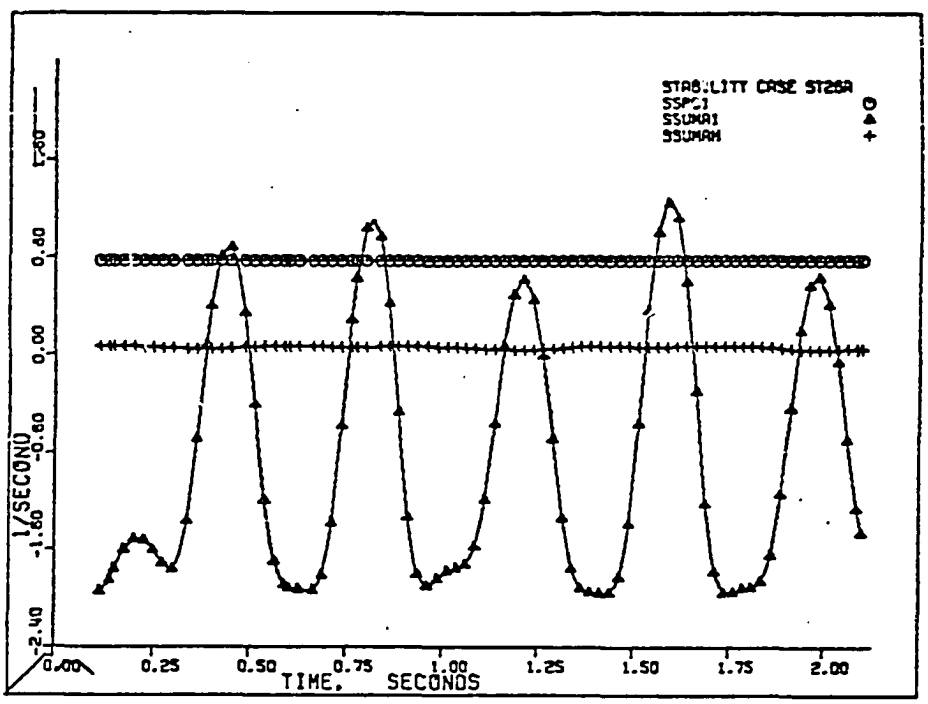

Figure 89. Case ST-26A: terms of equation (4.10).

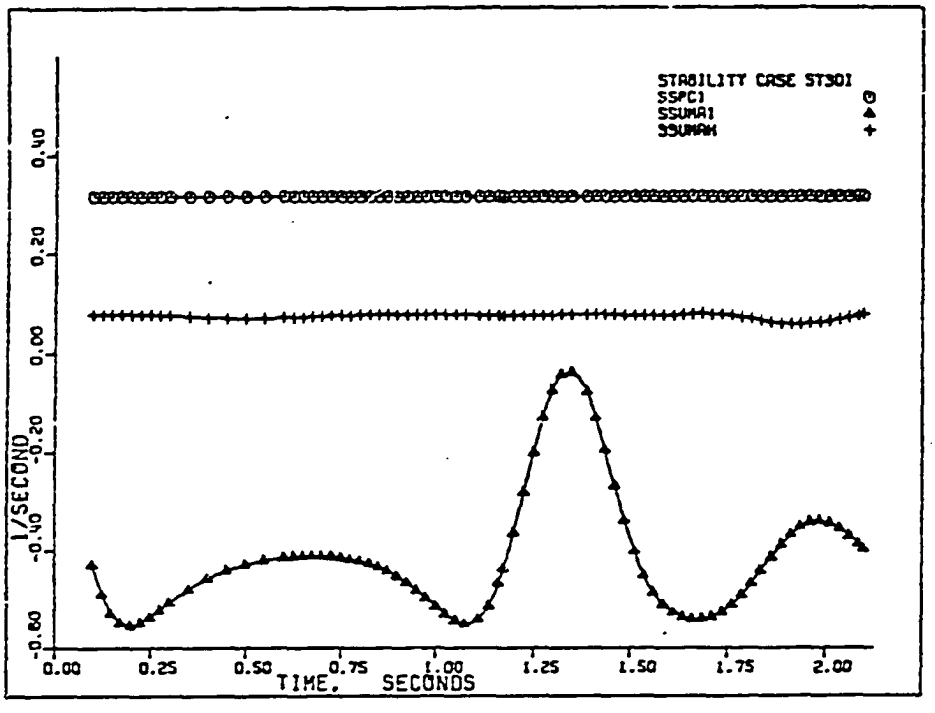

Figure 90. Case ST-30I: terms of equation (4.10).

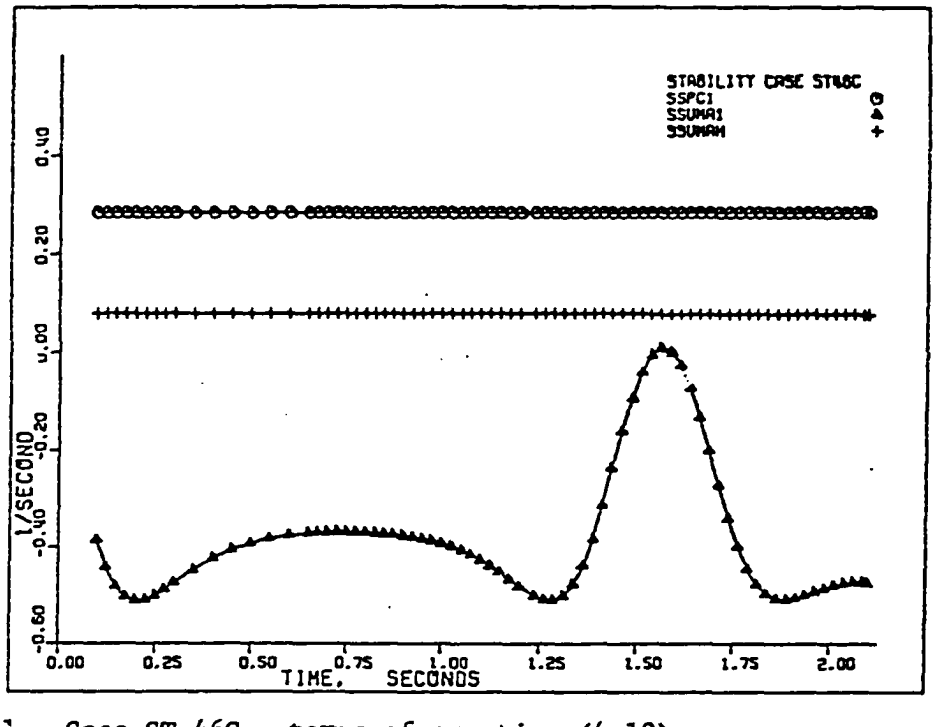

Figure 91. Case ST-46C: terms of equation (4.10).

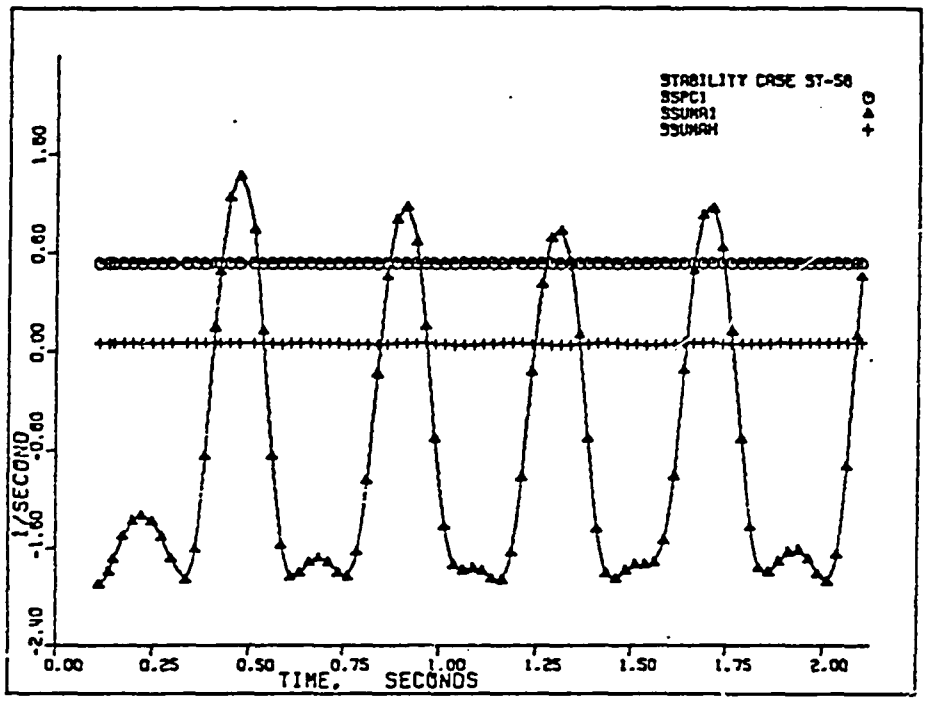

Figure 92. Case ST-56: terms of equation (4.10).

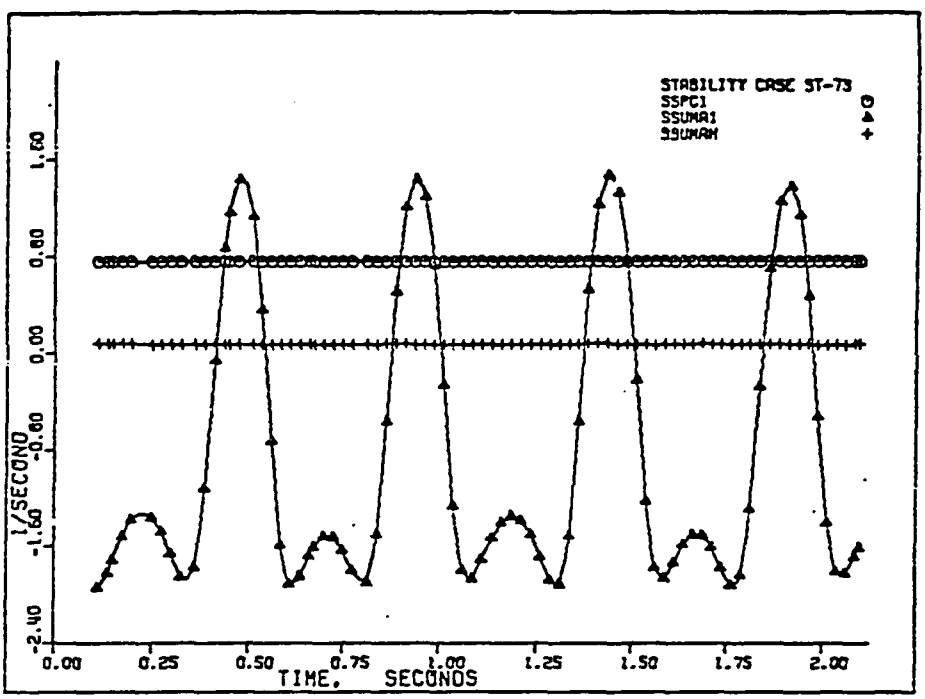

Figure 93. Case ST-73: terms of equation (4.10).

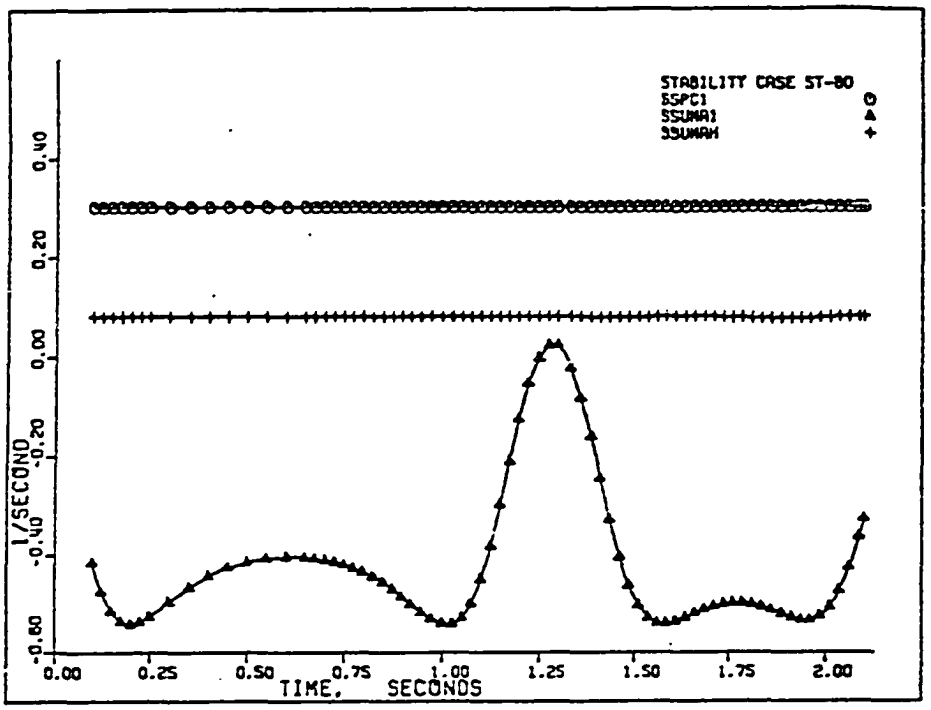

Figure 94. Case ST-80: terms of equation (4.10).

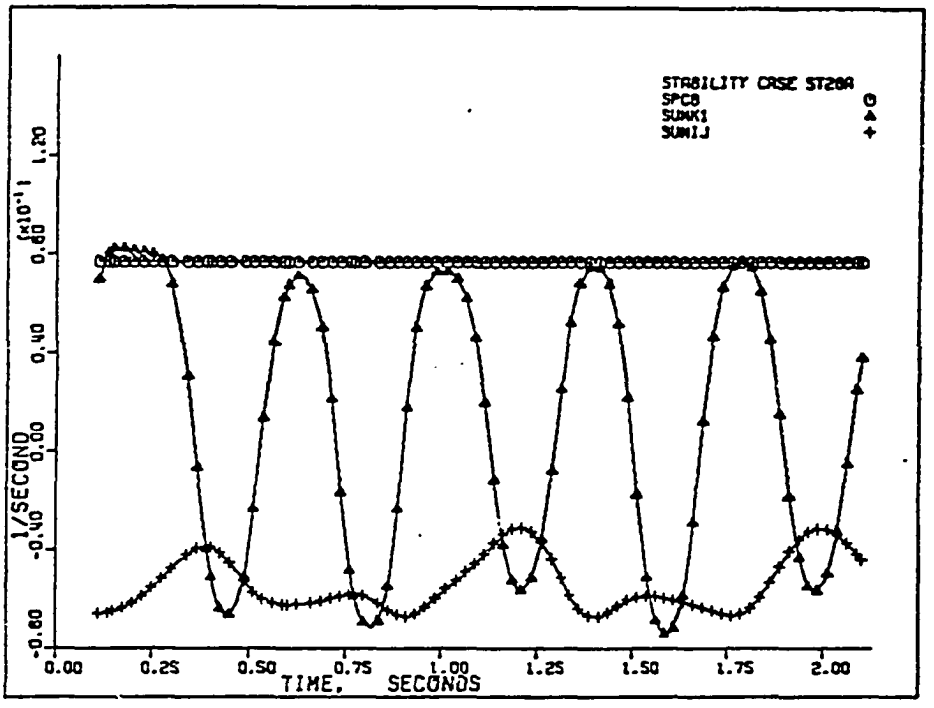

Figure 95. Case ST-26A: terms of equation (4.5).

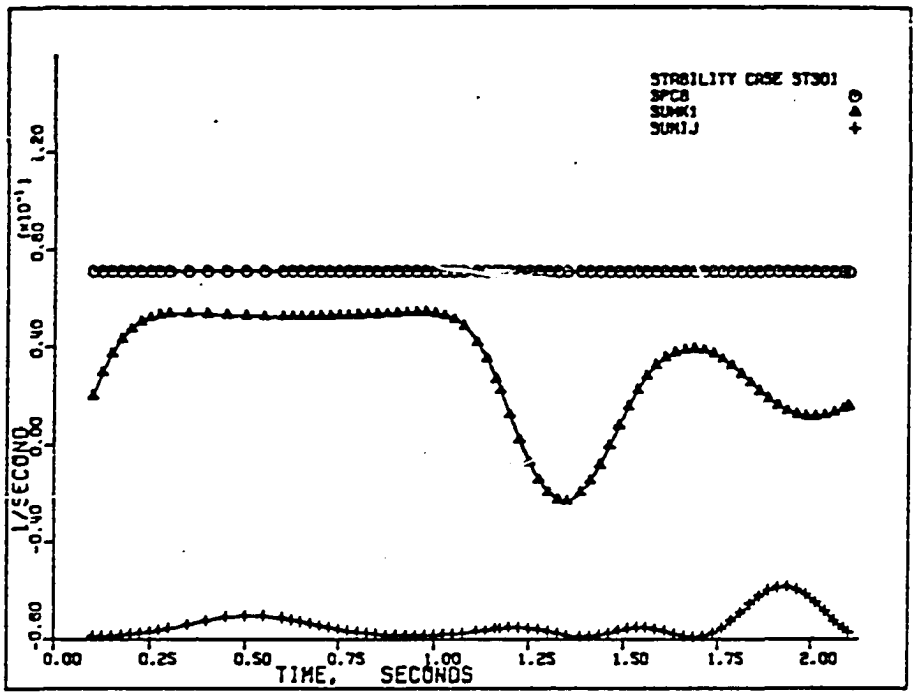

Figure 96. Case ST-30I: terms of equation (4.5).

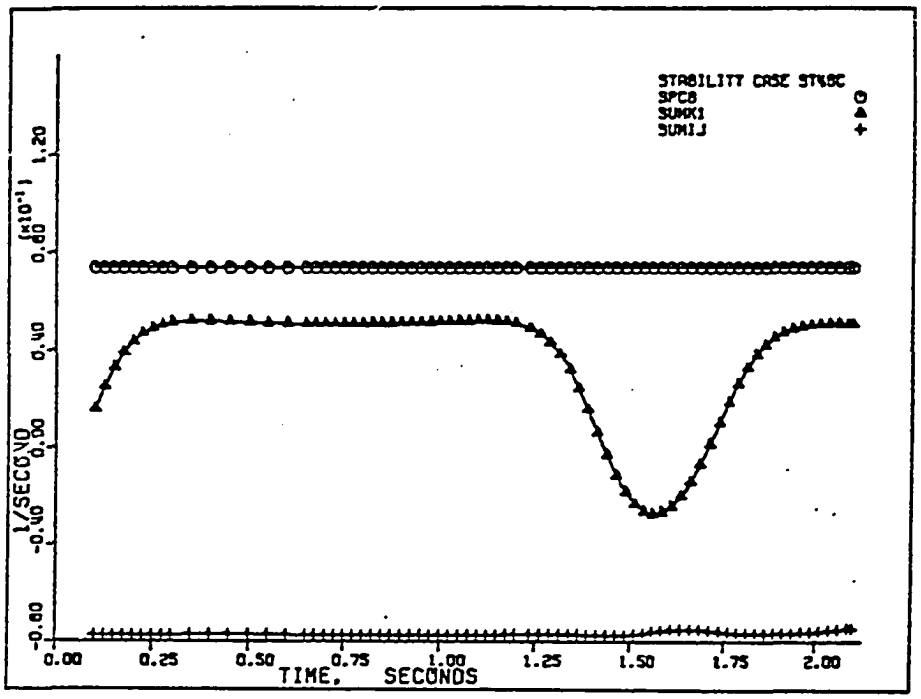

Figure 97. Case ST-46C: terms of equation (4.5).

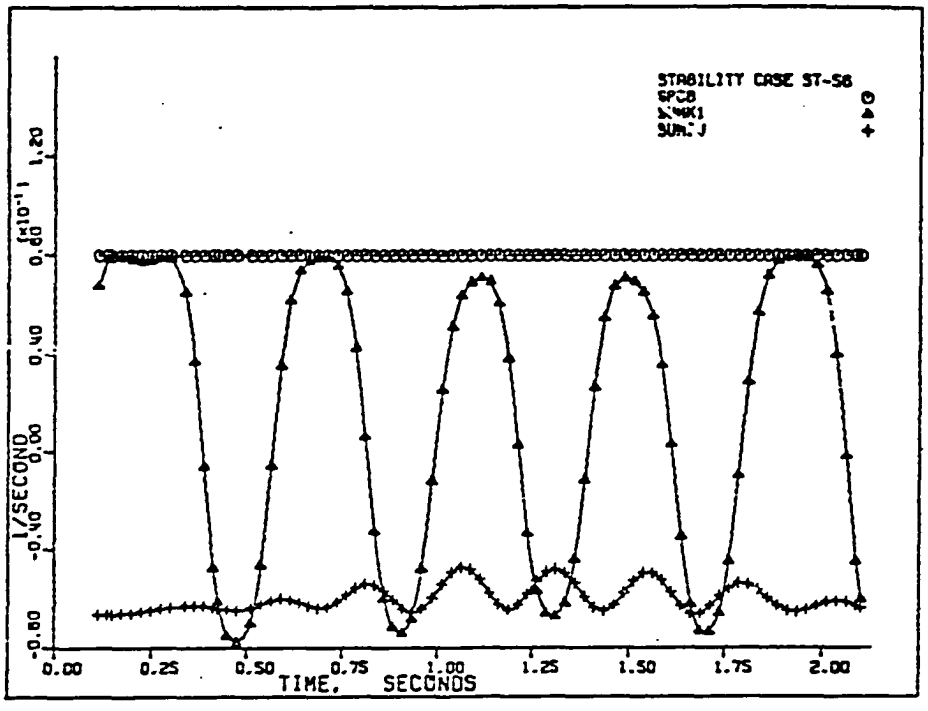

Figure 98. Case ST-56: terms of equation (4.5).

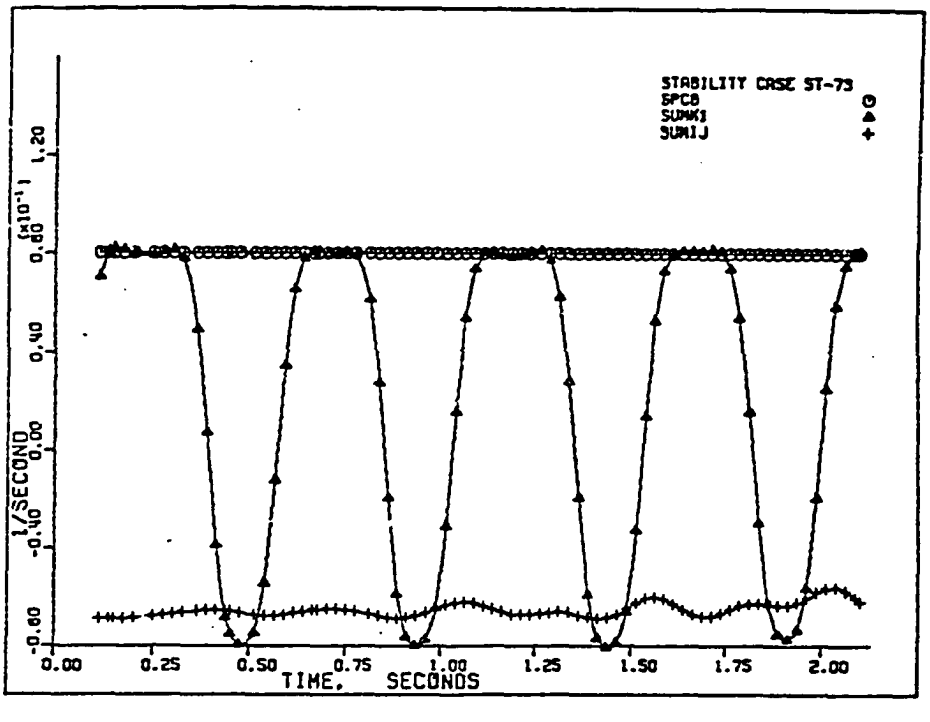

Figure 99. Case ST-73: terms of equation (4.5).

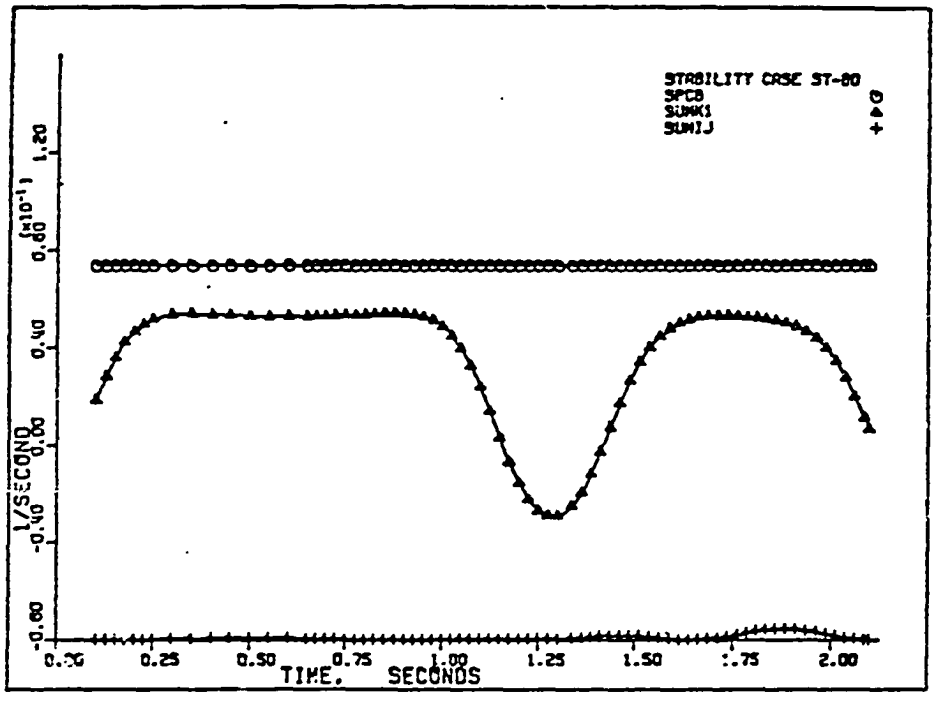

Figure 100. Case ST-80: terms of equation (4.5).

XVI. APPENDIX F: OUTPUT OF STABILITY ANALYSIS COMPUTER PROGRAM FOR REMOTE SYNCHRONOUS GENERATION - VARIATION OF PENETRATION LEVEL

This portion of runs is an addition to the original ST-series (Cases ST-1 through ST-36). The purpose of these runs is to study the effect of variation of penetration level on the dynamic performance of the machines in the existing system and the interaction between the remote machine and the existing machines. The complete list of these runs is listed in Table 7. The output of STANAL computer program for the selected cases in this series is shown via Figures 101 through 211. The variables chosen for demonstration in this series are listed below.

1. Angles δ_1, δ_2, δ_3, and $\bar{\delta}$ (Figures 101 through 111).
2. Angles δ_k and $\bar{\delta}$ (Figures 112 through 122).
3. Relative angles $(\delta_1 - \bar{\delta})$, $(\delta_2 - \bar{\delta})$, and $(\delta_3 - \bar{\delta})$ (Figures 123 through 133).
4. Relative angle $(\delta_k - \bar{\delta})$ (Figures 134 through 144).
5. Accelerations $\ddot{\delta}_1$, $\ddot{\delta}_2$, $\ddot{\delta}_3$, and $\ddot{\bar{\delta}}$ (Figures 145 through 155).
6. Accelerations $\ddot{\delta}_k$ and $\ddot{\bar{\delta}}$ (Figures 156 through 166).
7. Relative accelerations $(\ddot{\delta}_1 - \ddot{\bar{\delta}})$, $(\ddot{\delta}_2 - \ddot{\bar{\delta}})$, and $(\ddot{\delta}_3 - \ddot{\bar{\delta}})$ (Figures 167 through 177).
8. Relative acceleration $(\ddot{\delta}_k - \ddot{\bar{\delta}})$ (Figures 178 through 188).
9. Terms of equation (4.10) (Figures 189 through 198):

$$SSPC = \left(\frac{P_{ck}}{H_k} - \frac{1}{\bar{H}} \sum_{i=1}^{n} P_{ci} \right),$$

$$SSUMA = -\sum_{j=1}^{n}\left[\frac{1}{H_k}A_{kj}\cos(\theta_{kj}-\delta_{kj})+\frac{1}{\bar{H}}A_{kj}\cos(\theta_{kj}+\delta_{kj})\right],$$

$$SSUMAH = \sum_{i=1}^{n-1}\sum_{j=i+1}^{n}\frac{2}{\bar{H}}\hat{A}_{ij}\cos\delta_{ij}.$$

10. Terms of equation (4.13) (Figure 199):

$$SSPC1 = \left(\frac{P_{ck1}}{H_{k1}}-\frac{1}{\bar{H}}\sum_{i=1}^{n}P_{ci}\right),$$

$$SSUMA1 = -\sum_{j=1}^{n}\left[\frac{1}{H_{k1}}A_{k1j}\cos(\theta_{k1j}-\delta_{k1j})-\frac{1}{\bar{H}}A_{k1j}\cos(\theta_{k1j}+\delta_{k1j})\right],$$

$$SSUMAH = \frac{1}{\bar{H}}\sum_{i=1}^{n-1}\sum_{j=i+1}^{n}2\hat{A}_{ij}\cos\delta_{ij},$$

$$SK1K2 = -\frac{1}{H_{k1}}A_{k1k2}\cos(\theta_{k1k2}-\delta_{k1k2}),$$

$$SUMIK2 = \frac{1}{\bar{H}}\sum_{i=1}^{n}A_{ik2}\cos(\theta_{ik2}-\delta_{ik2}).$$

11. Terms of equation (4.14) (Figure 200):

$$SSPC2 = \left(\frac{P_{ck2}}{H_{k2}}-\frac{1}{\bar{H}}\sum_{i=1}^{n}P_{ci}\right),$$

$$SSUMA2 = -\sum_{j=1}^{n}\left[\frac{1}{H_{k2}}A_{k2j}\cos(\theta_{k2j}-\delta_{k2j})-\frac{1}{\bar{H}}A_{k2j}\cos(\theta_{k2j}+\delta_{k2j})\right],$$

$$SSUMAH = \frac{1}{\bar{H}}\sum_{i=1}^{n-1}\sum_{j=i+1}^{n}2\hat{A}_{ij}\cos\delta_{ij},$$

$$SK2K1 = -\frac{1}{H_{k2}}A_{k2k1}\cos(\theta_{k2k1}-\delta_{k2k1}),$$

$$SUMIK1 = \frac{1}{H} \sum_{i=1}^{n} A_{ik1} \cos (\theta_{ik1} - \delta_{ik1}) .$$

12. Terms of equation (4.5) (Figures 201 through 210):

$$SPCB = \frac{1}{H} \sum_{i=1}^{n} P_{ci} ,$$

$$SUMK = -\frac{1}{H} \sum_{i=1}^{n} A_{ik} \cos (\theta_{ik} - \delta_{ik}) ,$$

$$SUMIJ = -\frac{1}{H} \sum_{i=1}^{n} \sum_{\substack{j=1 \\ j \neq i}}^{n} A_{ij} \cos (\theta_{ij} - \delta_{ij}) .$$

13. Terms of equation (4.12) (Figure 211):

$$SPCB = \frac{1}{H} \sum_{i=1}^{n} P_{ci} ,$$

$$SUMK1 = -\frac{1}{H} \sum_{i=1}^{n} A_{ik1} \cos (\theta_{ik1} - \delta_{ik1}) ,$$

$$SUMK2 = -\frac{1}{H} \sum_{i=1}^{n} A_{ik2} \cos (\theta_{ik2} - \delta_{ik2}) ,$$

$$SUMIJ = -\frac{1}{H} \sum_{i=1}^{n} \sum_{\substack{j=1 \\ j \neq i}}^{n} A_{ij} \cos (\theta_{ij} - \delta_{ij}) .$$

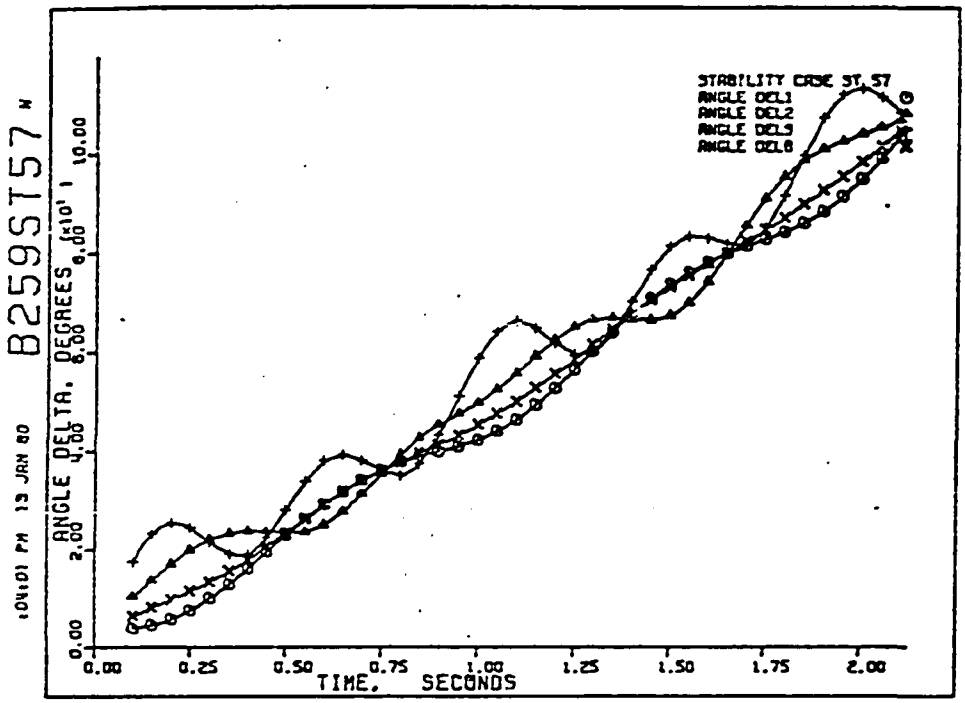

Figure 101. Case ST-57: angles δ_1, δ_2, δ_3, and $\bar{\delta}$.

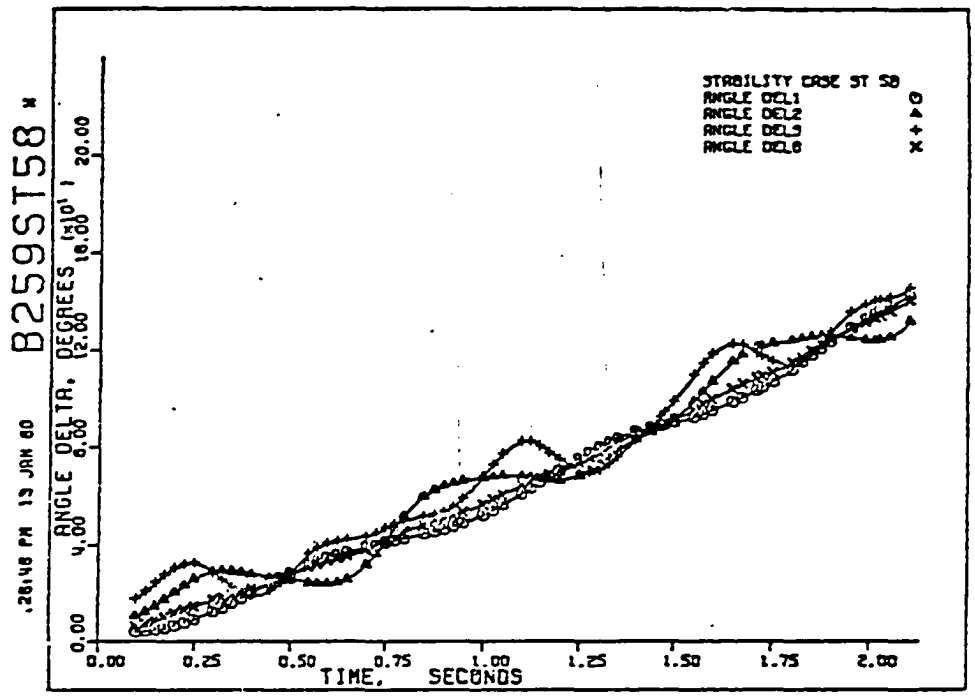

Figure 102. Case ST-58: angles δ_1, δ_2, δ_3, and $\bar{\delta}$.

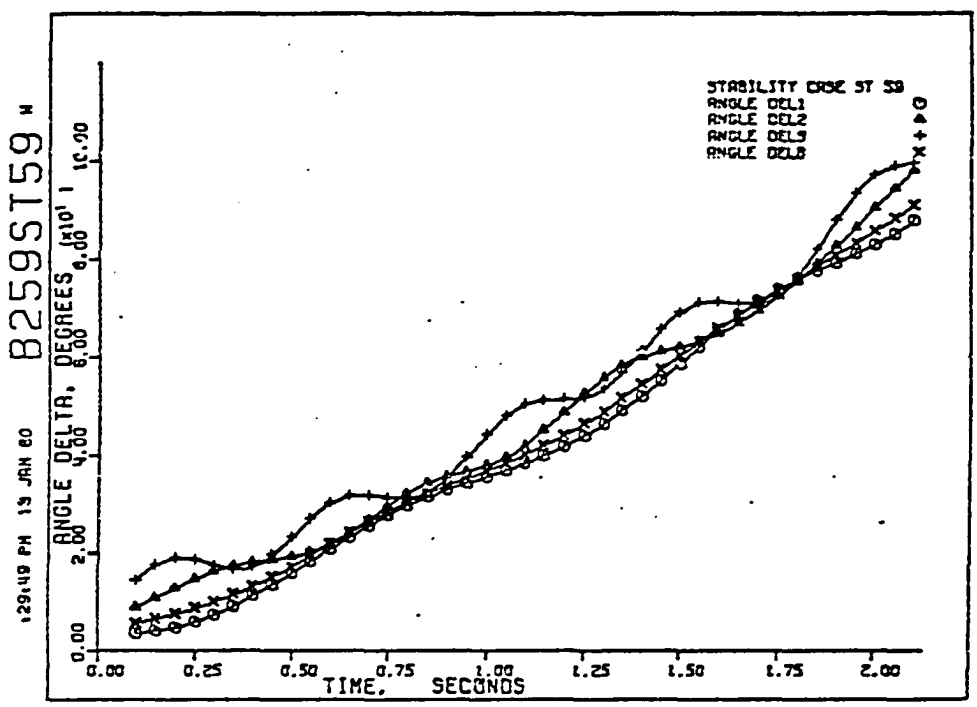

Figure 103. Case ST-59: angles δ_1, δ_2, δ_3, and $\bar{\delta}$.

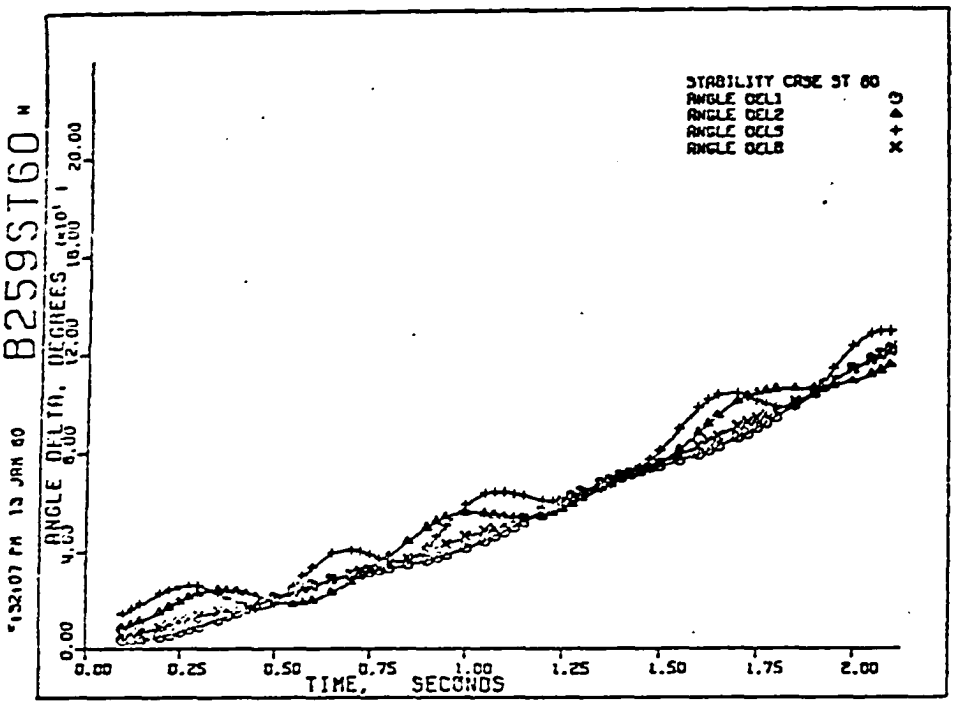

Figure 104. Case ST-60: angles δ_1, δ_2, δ_3, and $\bar{\delta}$.

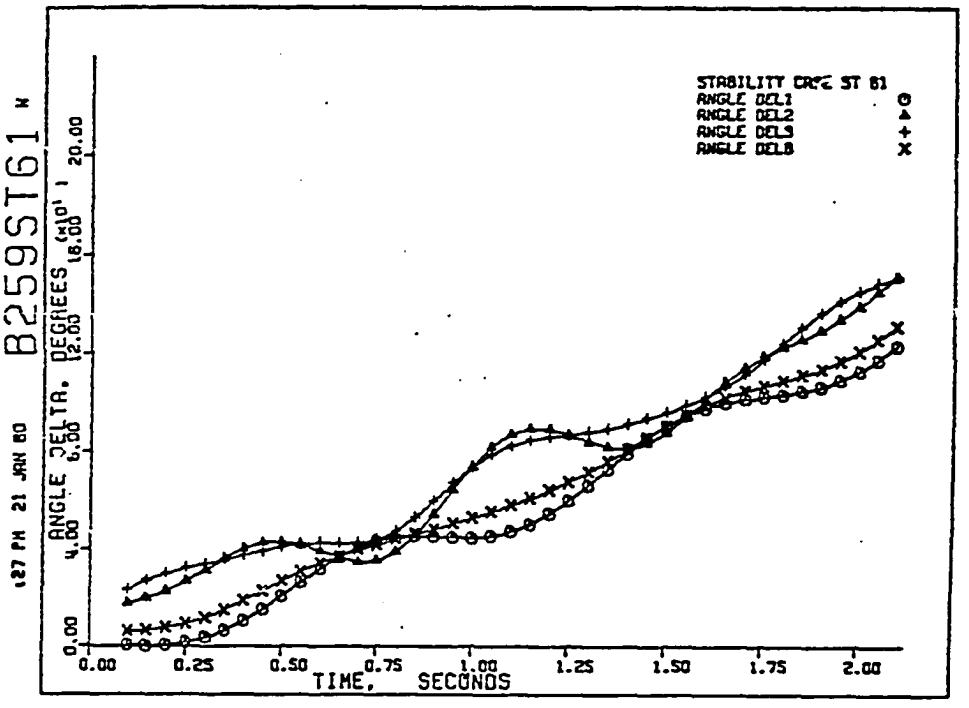

Figure 105. Case ST-61: angles δ_1, δ_2, δ_3, and $\bar{\delta}$.

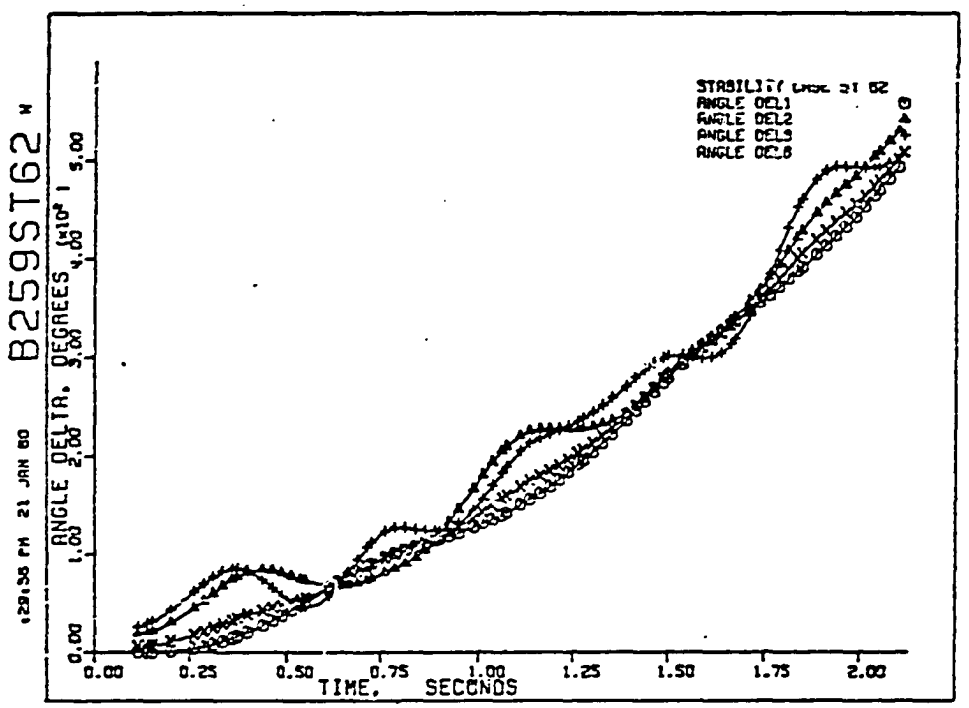

Figure 106. Case ST-62: angles δ_1, δ_2, δ_3, and $\bar{\delta}$.

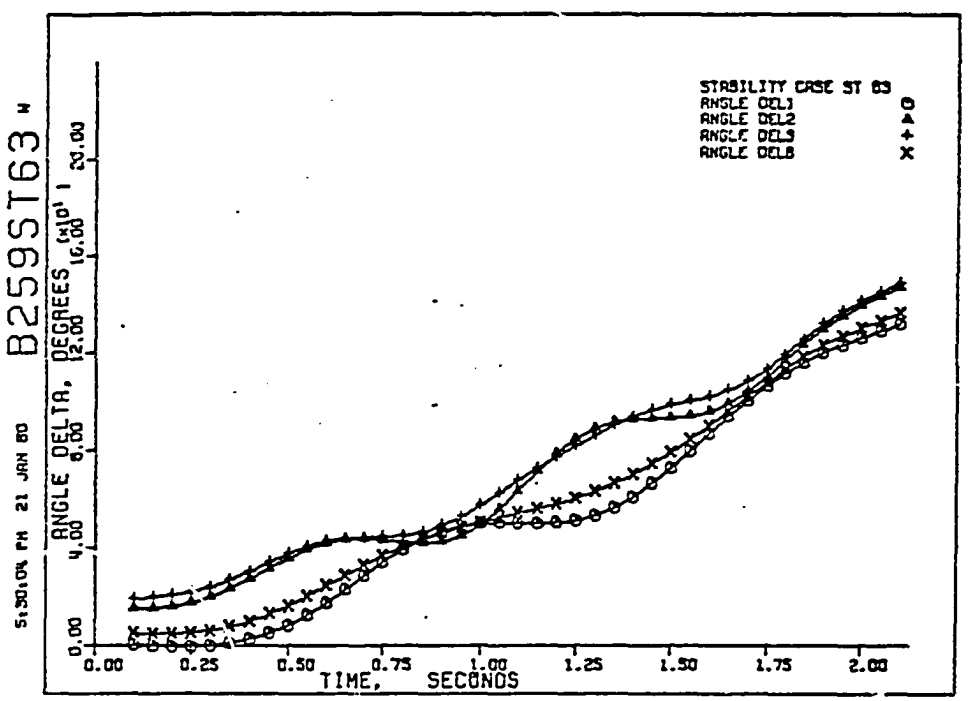

Figure 107. Case ST-63: angles δ_1, δ_2, δ_3, and $\bar{\delta}$.

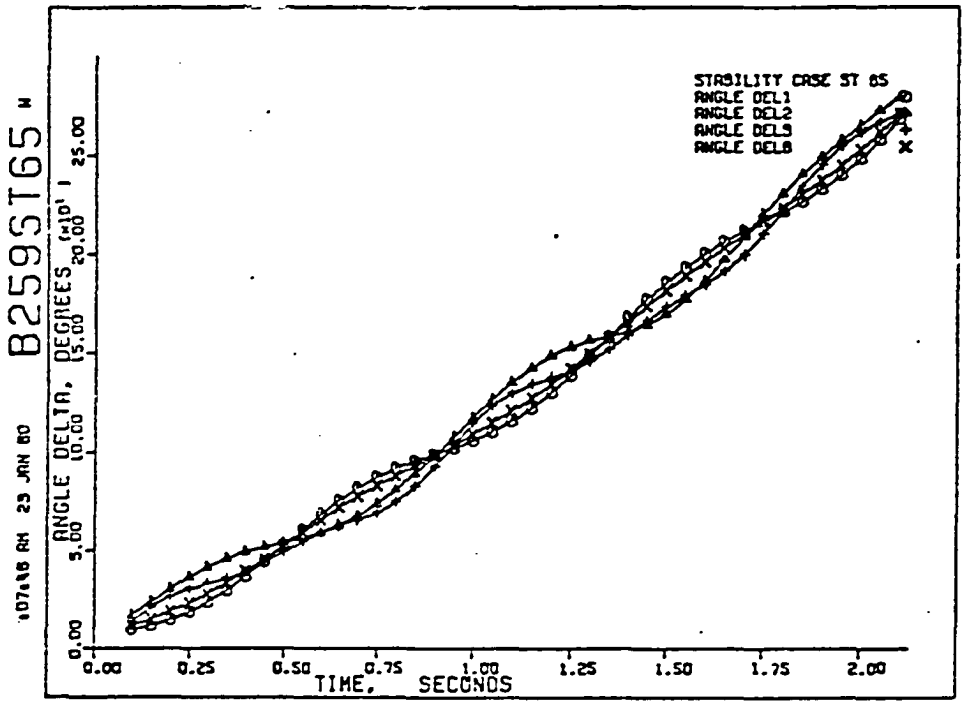

Figure 108. Case ST-65: angles δ_1, δ_2, δ_3, and $\bar{\delta}$.

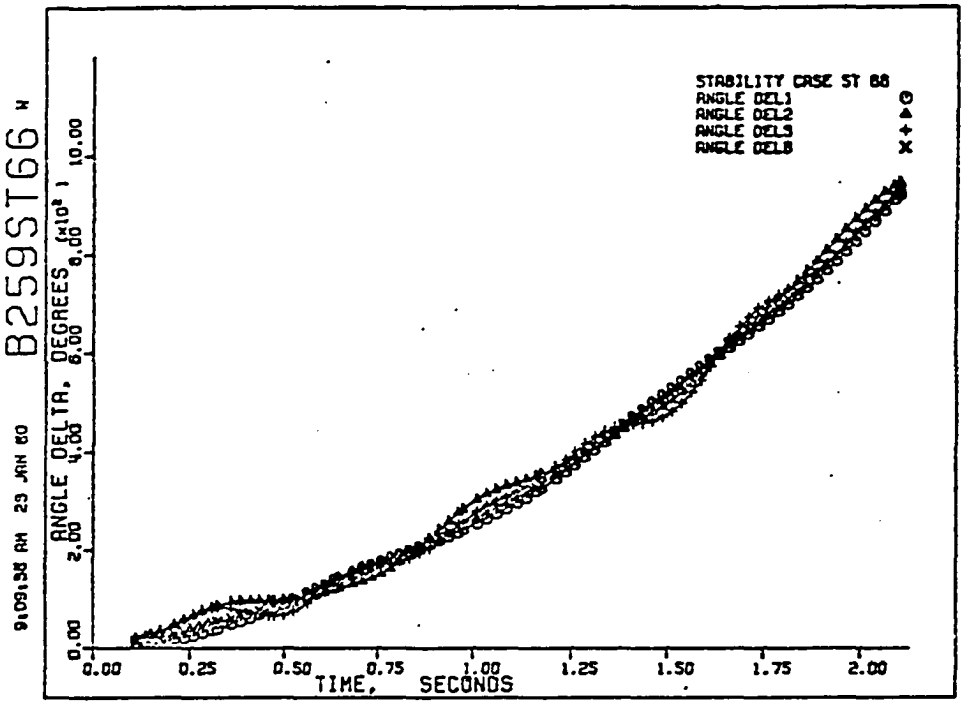

Figure 109. Case ST-66: angles δ_1, δ_2, δ_3, and $\bar{\delta}$.

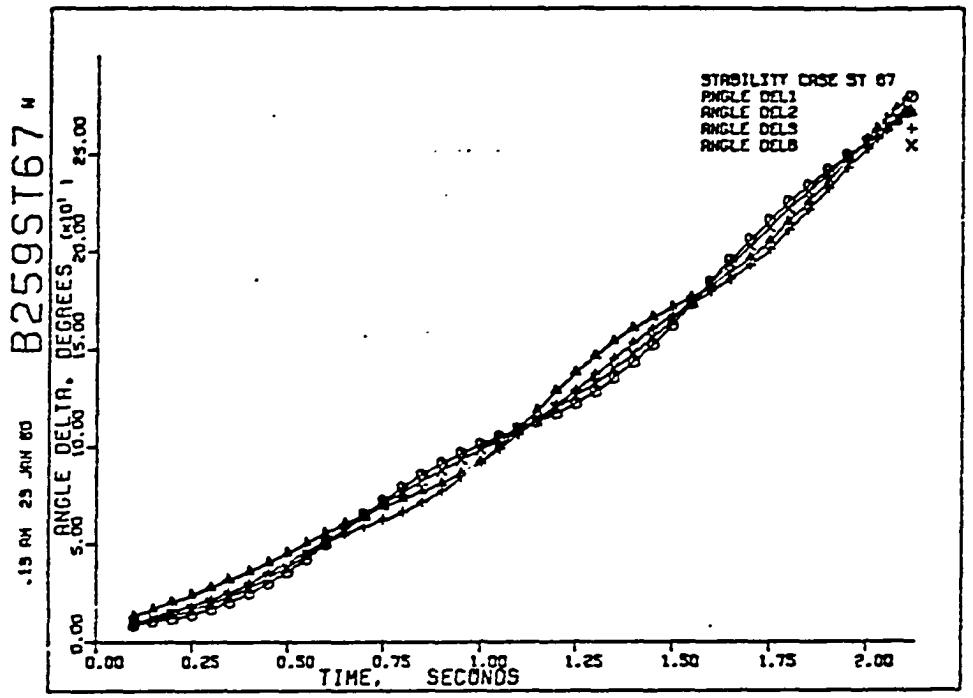

Figure 110. Case ST-67: angles δ_1, δ_2, δ_3, and $\bar{\delta}$.

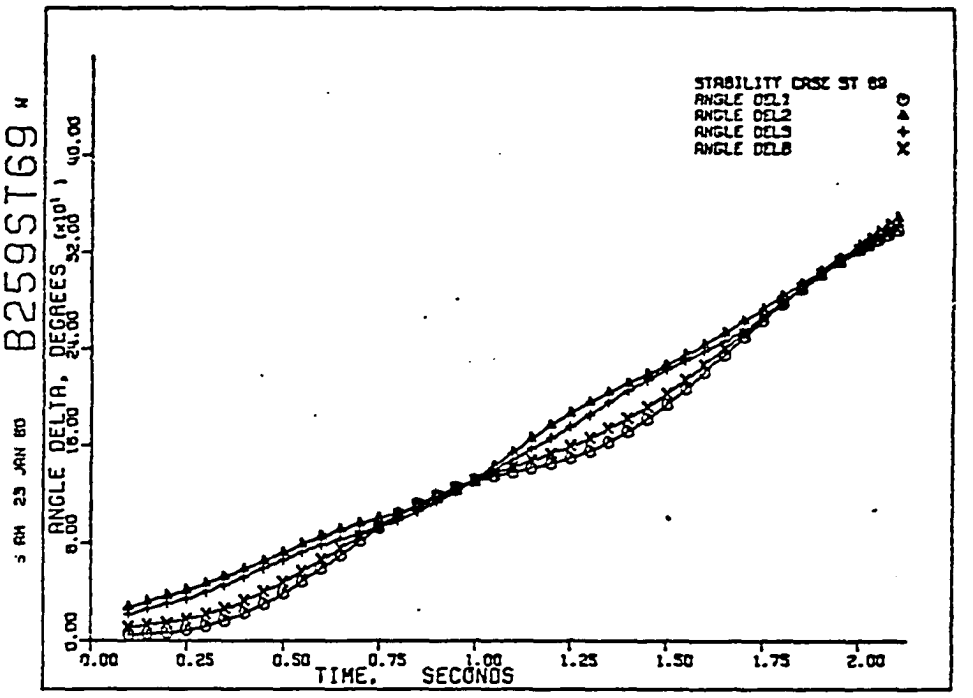

Figure 111. Case ST-69: angles δ_1, δ_2, δ_3, and $\bar{\delta}$.

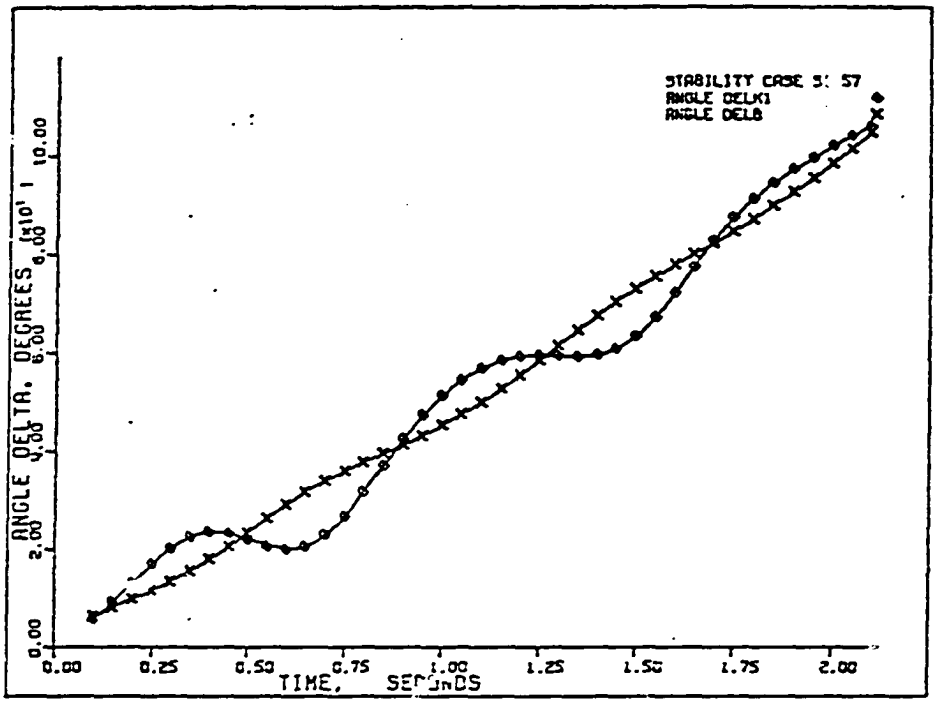

Figure 112. Case ST-57: angles δ_k and $\bar{\delta}$.

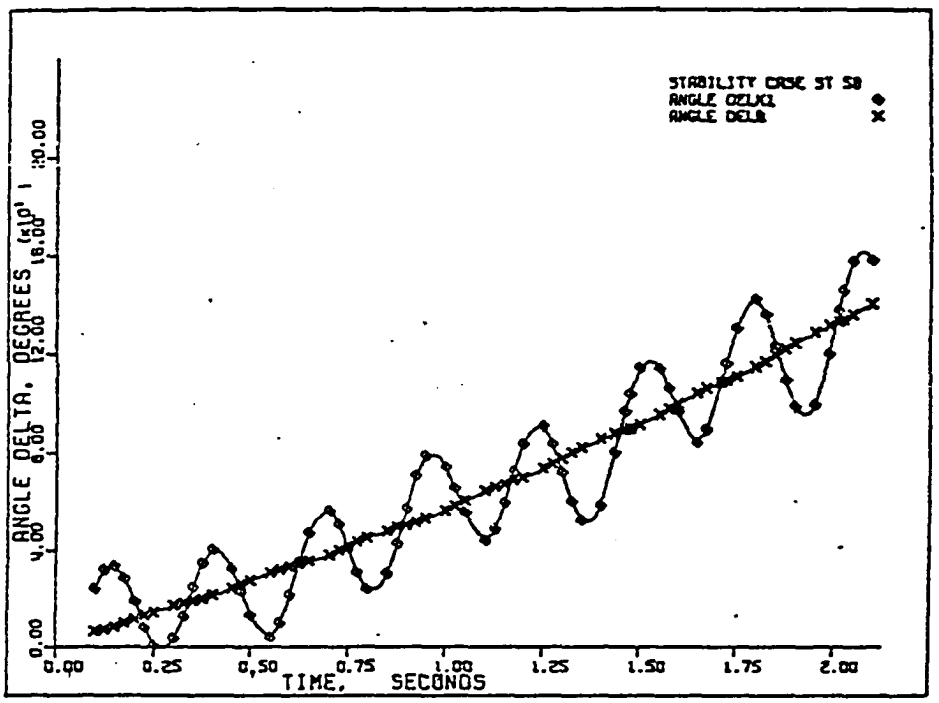

Figure 113. Case ST-58: angles δ_k and $\bar{\delta}$.

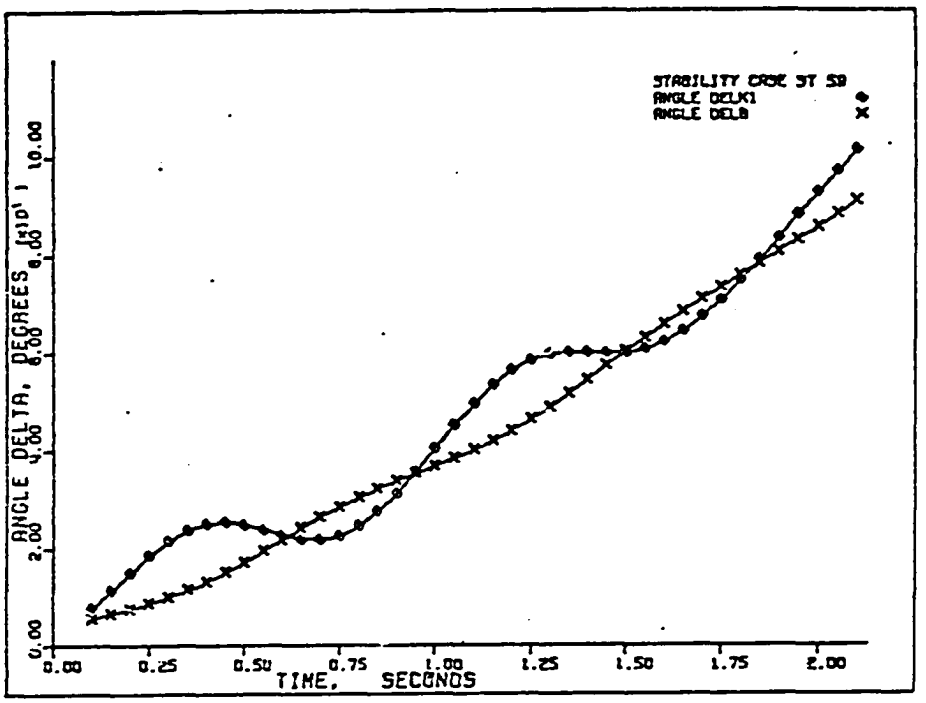

Figure 114. Case ST-59: angles δ_k and $\bar{\delta}$.

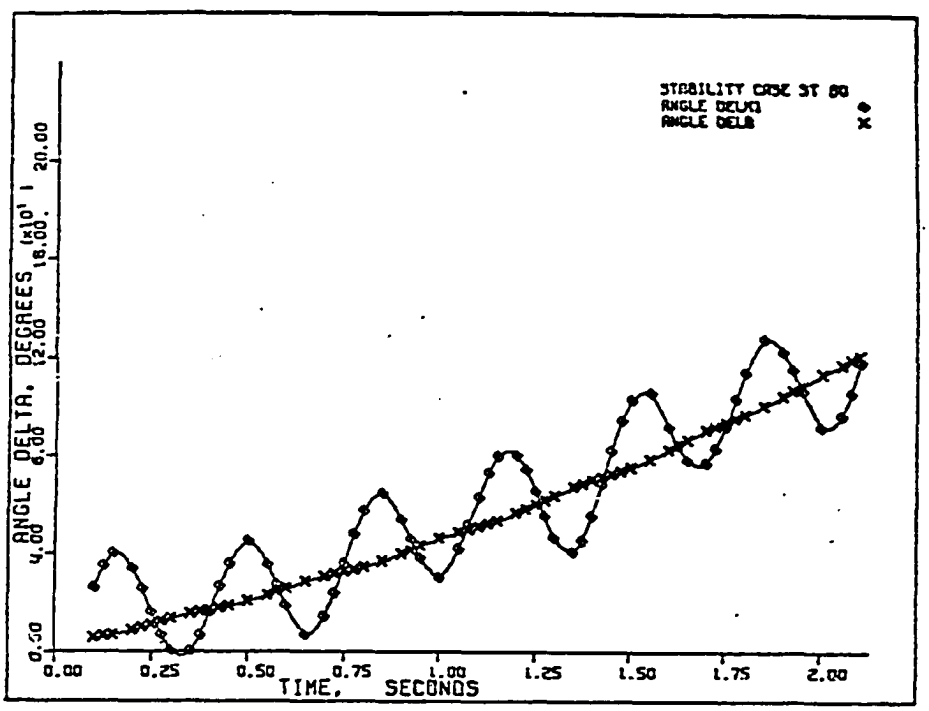

Figure 115. Case ST-60: angles δ_k and $\bar{\delta}$.

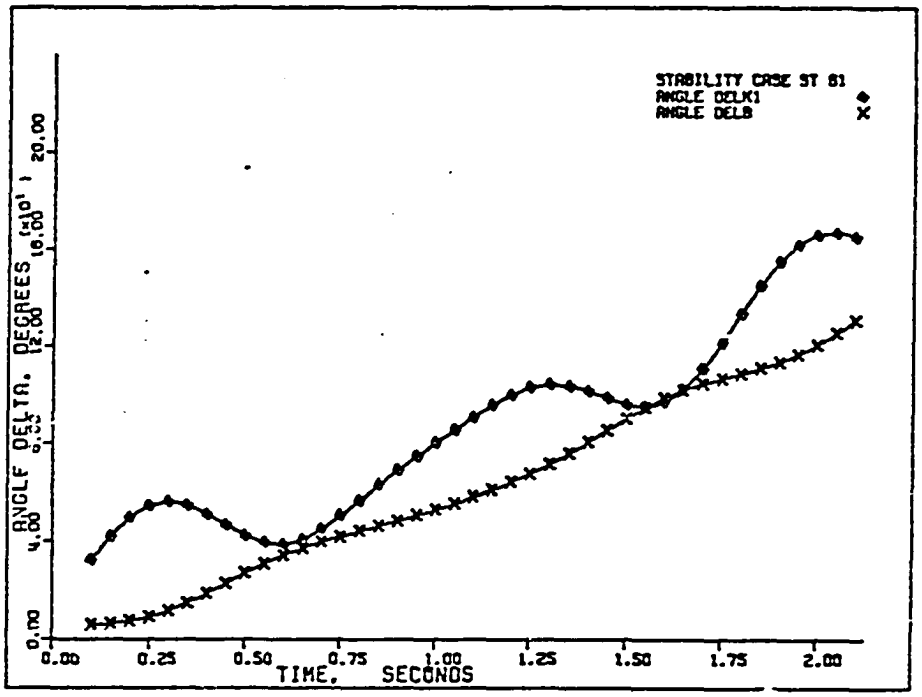

Figure 116. Case ST-61: angles δ_k and $\bar{\delta}$.

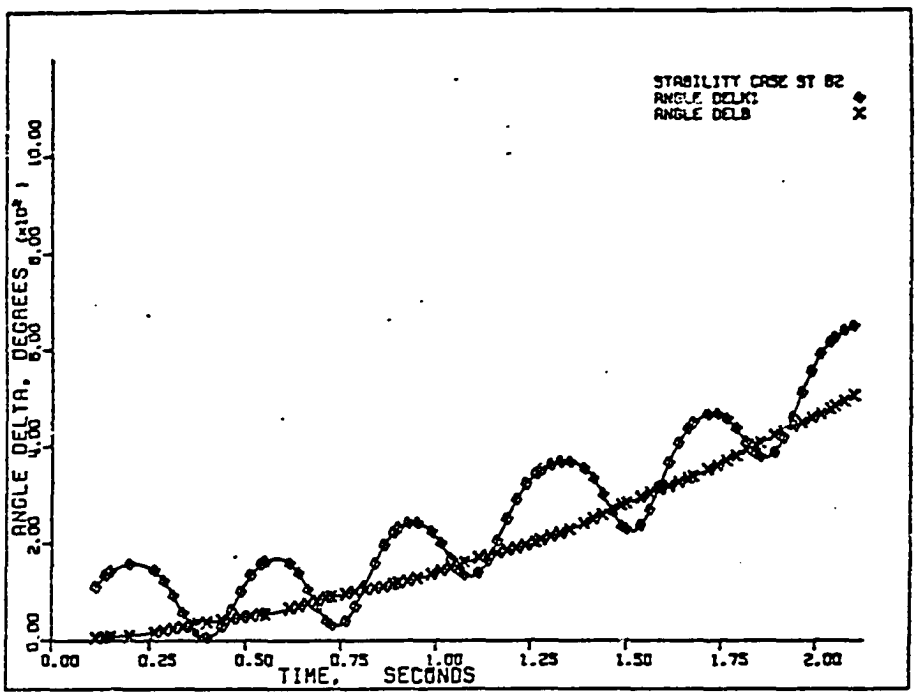

Figure 117. Case ST-62: angles δ_k and $\bar{\delta}$.

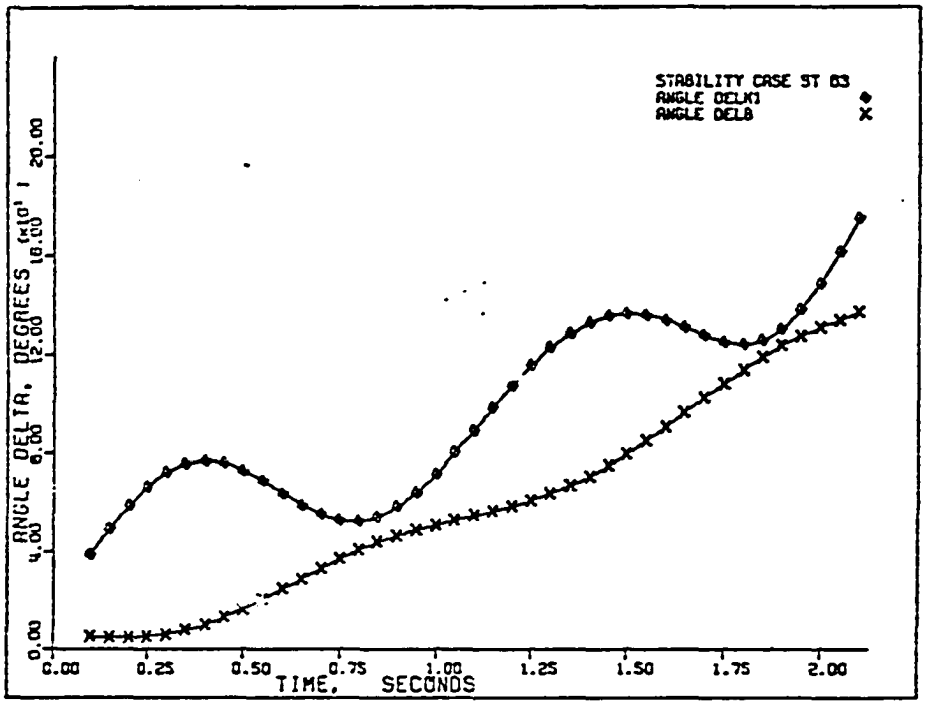

Figure 118. Case ST-63: angles δ_k and $\bar{\delta}$.

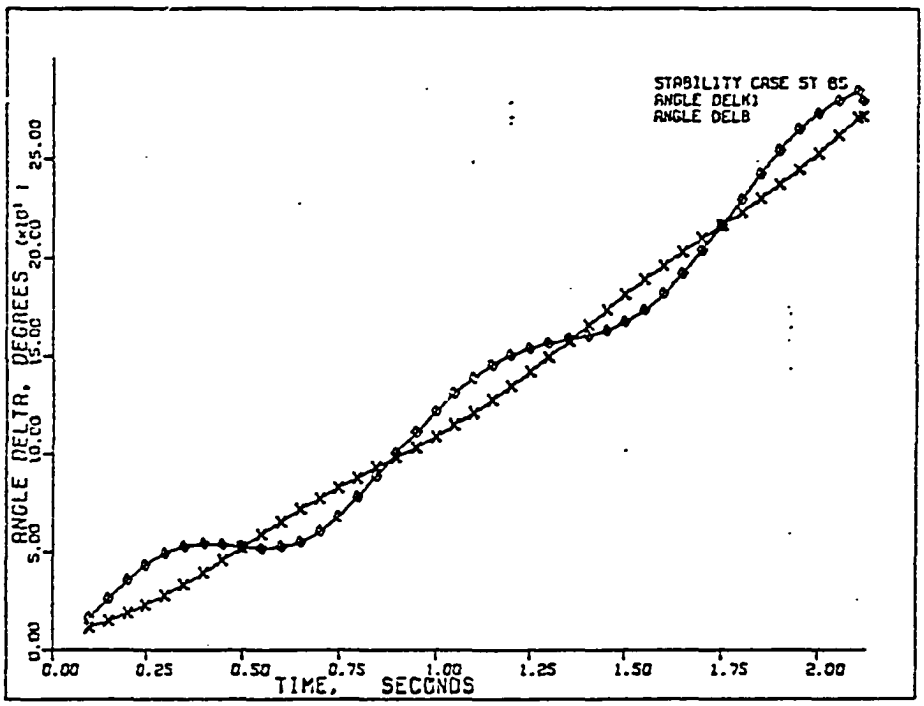

Figure 119. Case ST-65: angles δ_k and $\bar{\delta}$.

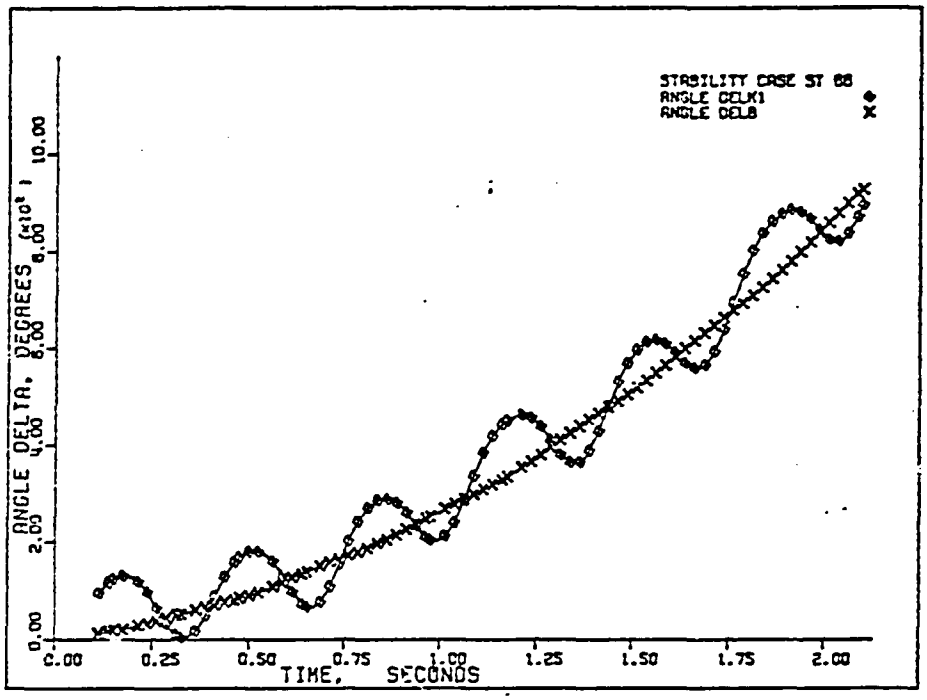

Figure 120. Case ST-66: angles δ_k and $\bar{\delta}$.

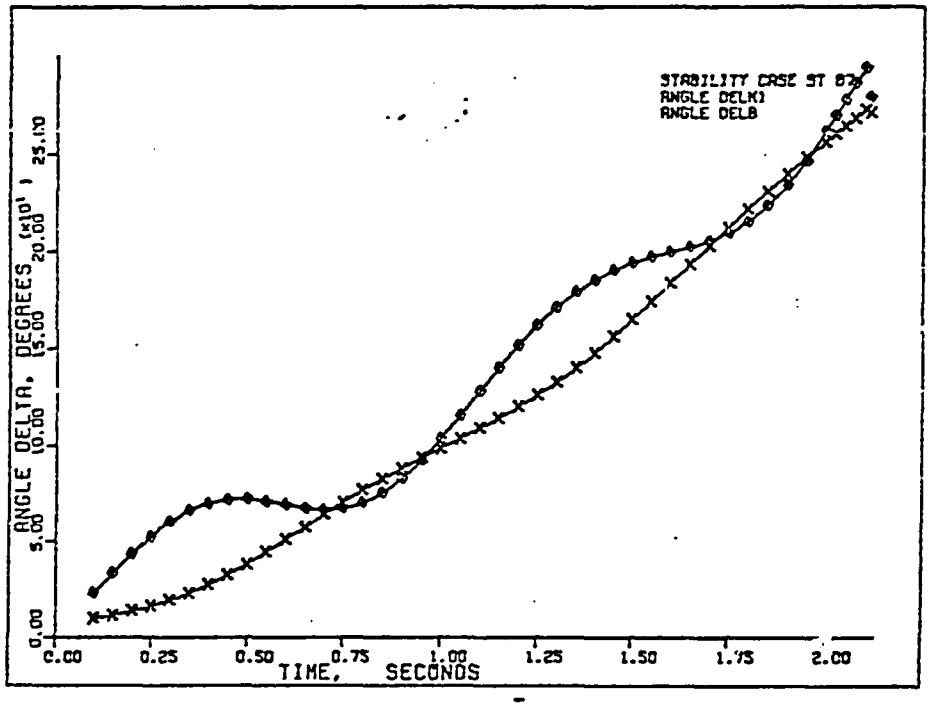

Figure 121. Case ST-67: angles δ_k and $\bar{\delta}$.

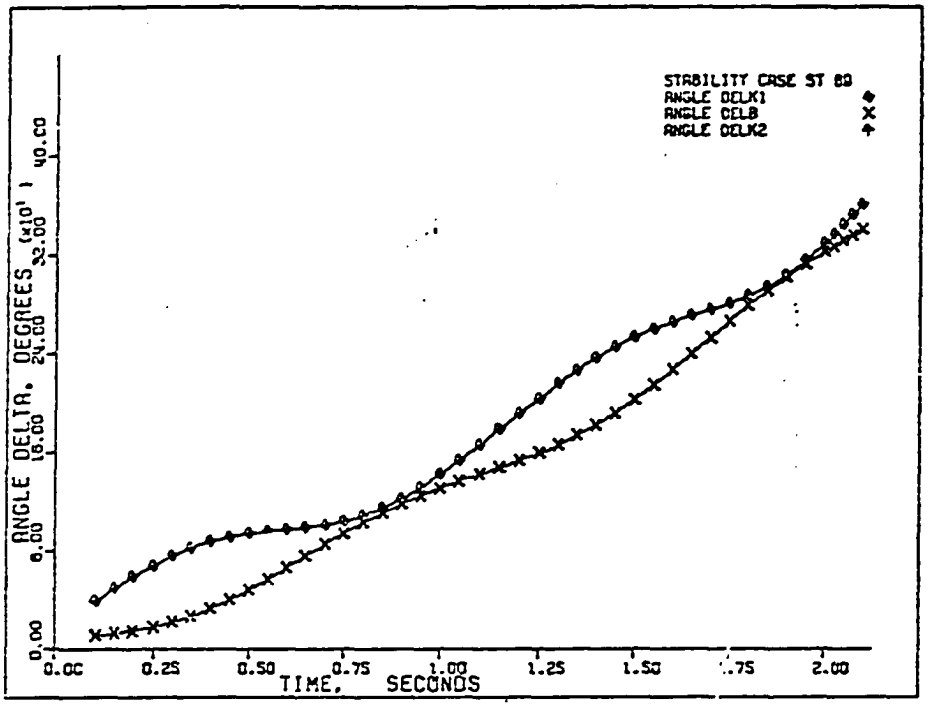

Figure 122. Case ST-69: angles δ_{k1}, δ_{k2}, and $\bar{\delta}$.

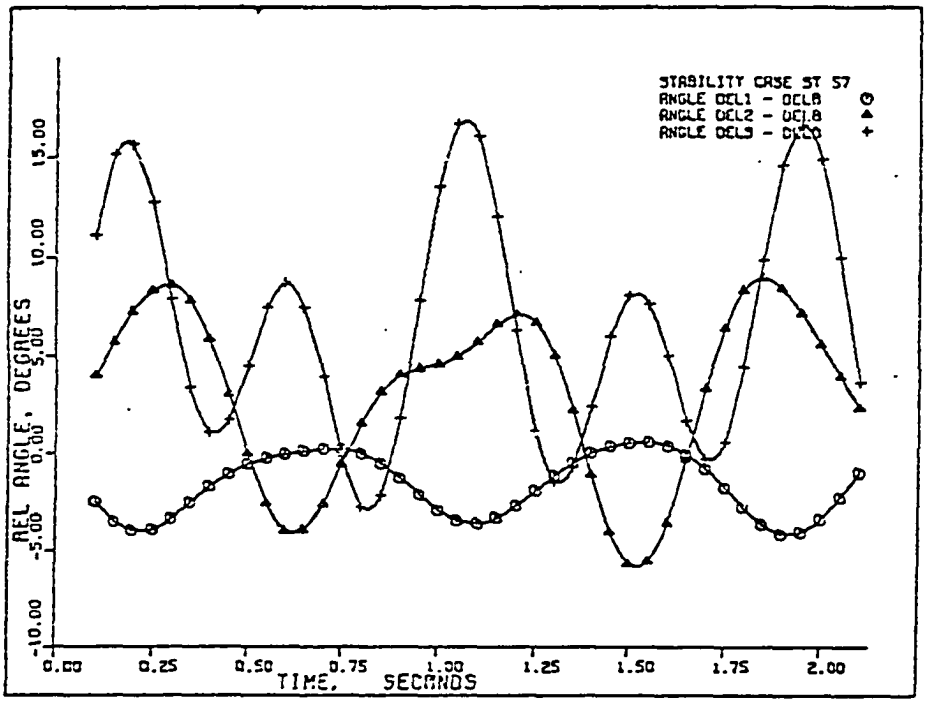

Figure 123. Case ST-57: relative angles $(\delta_1 - \bar{\delta})$, $(\delta_2 - \bar{\delta})$, and $(\delta_3 - \bar{\delta})$.

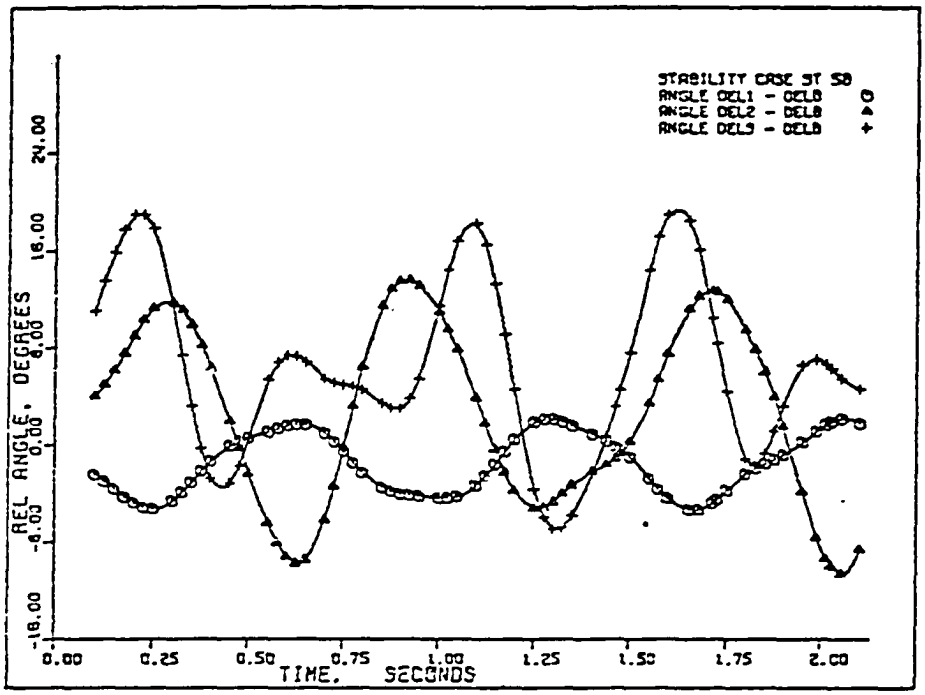

Figure 124. Case ST-58: relative angles $(\delta_1 - \bar{\delta})$, $(\delta_2 - \bar{\delta})$, and $(\delta_3 - \bar{\delta})$.

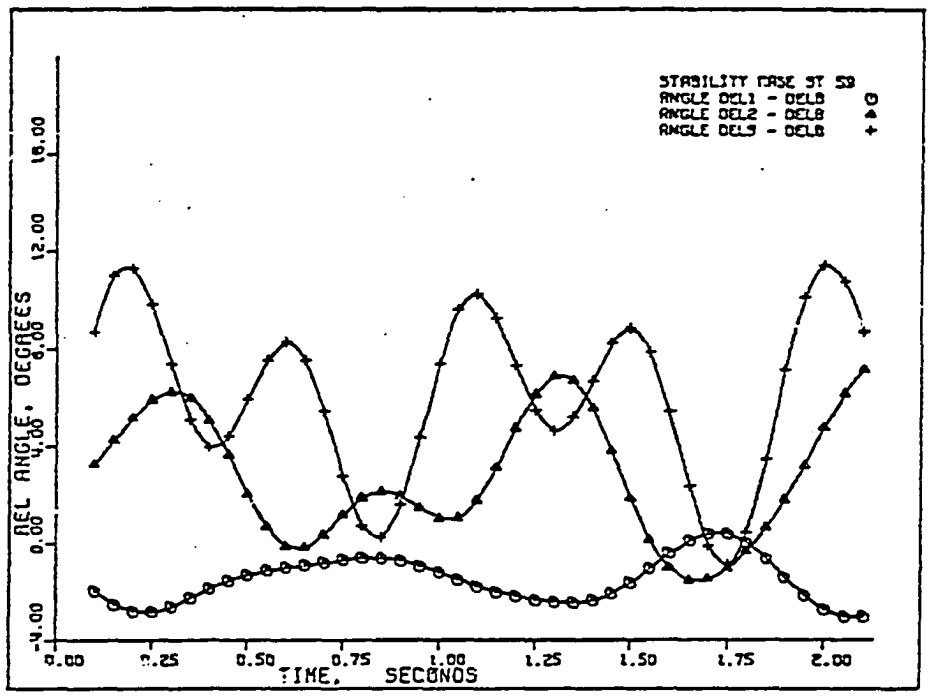

Figure 125. Case ST-59: relative angles $(\delta_1 - \bar{\delta})$, $(\delta_2 - \bar{\delta})$, and $(\delta_3 - \bar{\delta})$.

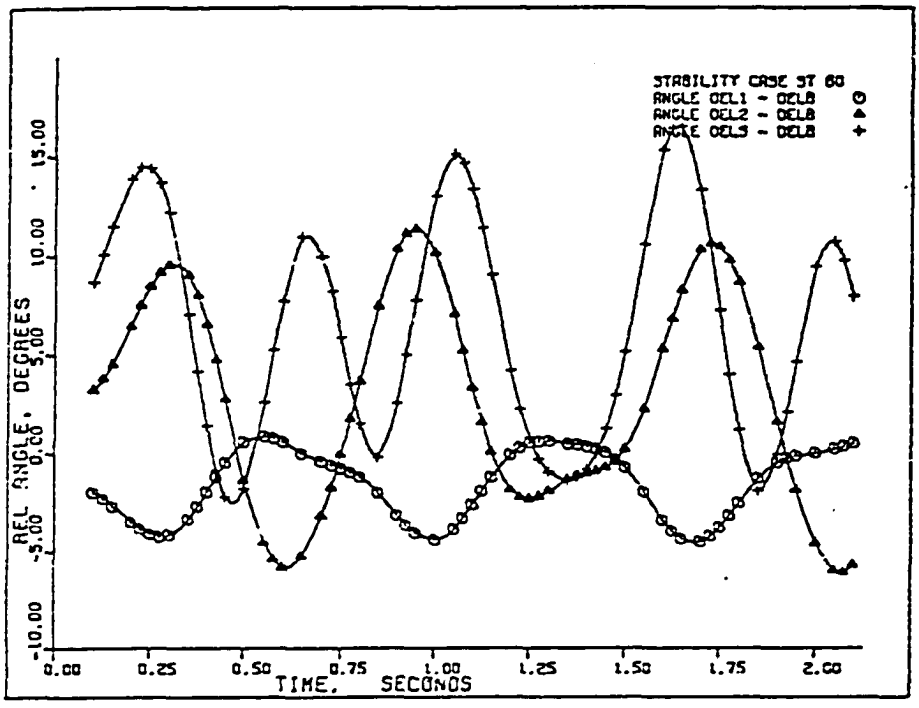

Figure 126. Case ST-60: relative angles $(\delta_1 - \bar{\delta})$, $(\delta_2 - \bar{\delta})$, and $(\delta_3 - \bar{\delta})$.

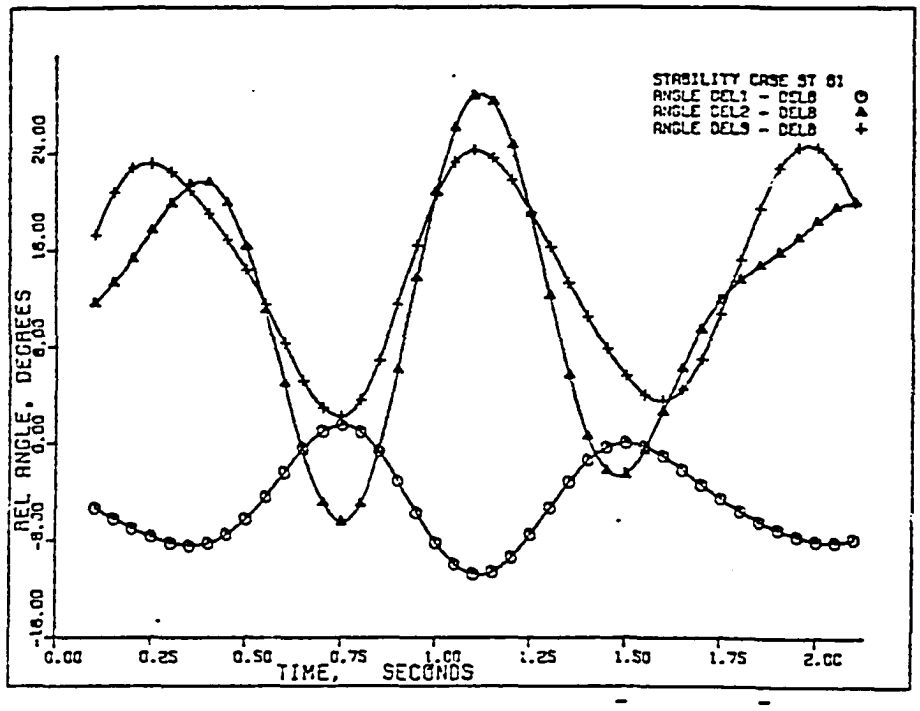

Figure 127. Case ST-61: relative angles $(\delta_1 - \bar{\delta})$, $(\delta_2 - \bar{\delta})$, and $(\delta_3 - \bar{\delta})$.

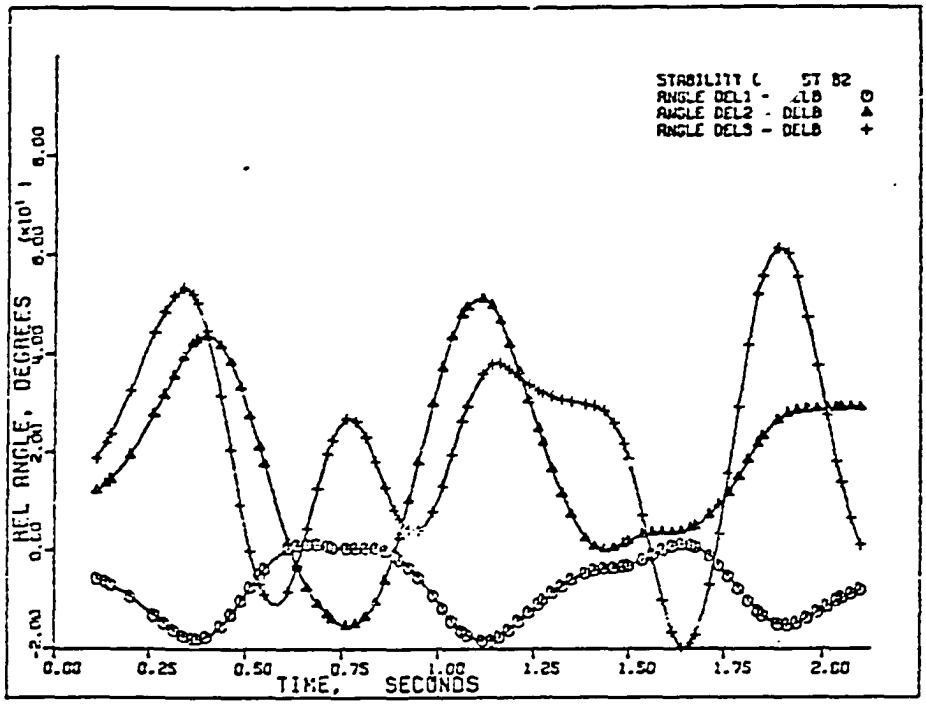

Figure 128. Case ST-62: relative angles $(\delta_1 - \bar{\delta})$, $(\delta_2 - \bar{\delta})$, and $(\delta_3 - \bar{\delta})$.

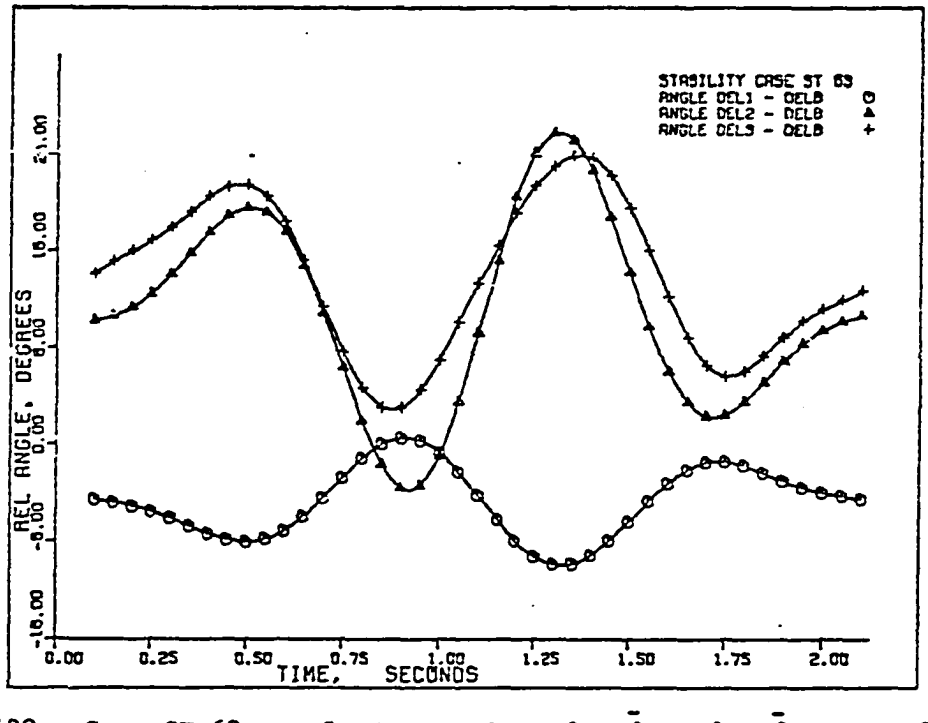

Figure 129. Case ST-63: relative angles $(\delta_1 - \bar{\delta})$, $(\delta_2 - \bar{\delta})$, and $(\delta_3 - \bar{\delta})$.

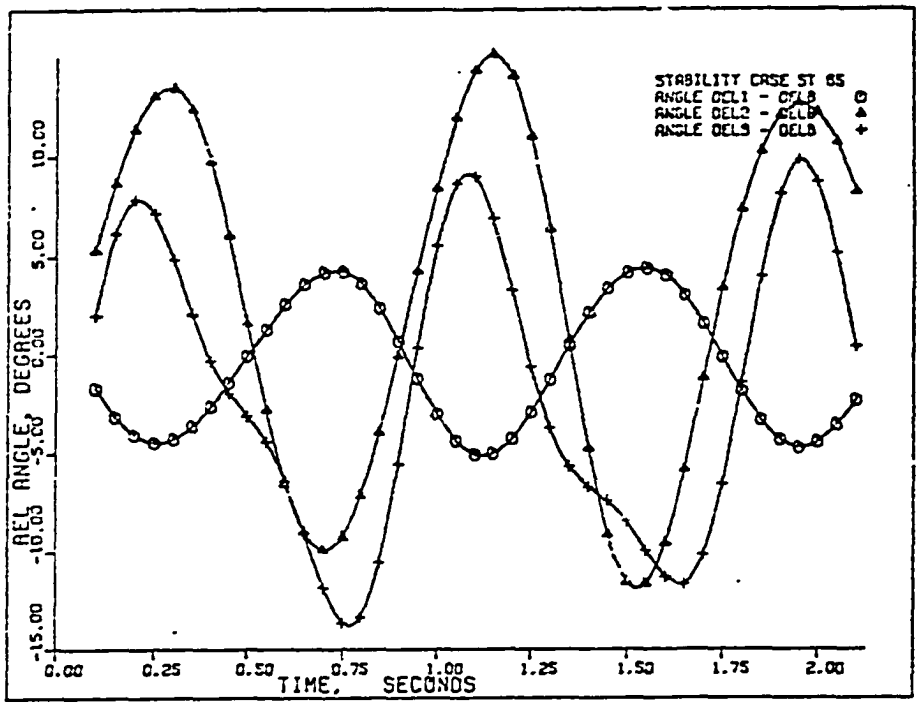

Figure 130. Case ST-65: relative angles $(\delta_1 - \bar{\delta})$, $(\delta_2 - \bar{\delta})$, and $(\delta_3 - \bar{\delta})$.

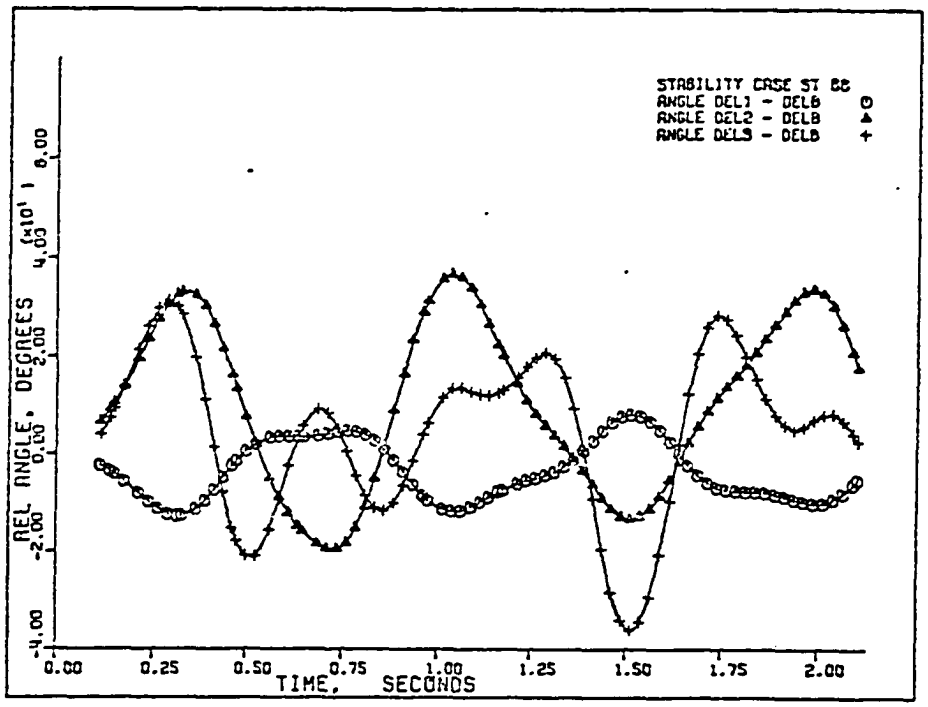

Figure 131. Case ST-66: relative angles $(\delta_1 - \bar{\delta})$, $(\delta_2 - \bar{\delta})$, and $(\delta_3 - \bar{\delta})$.

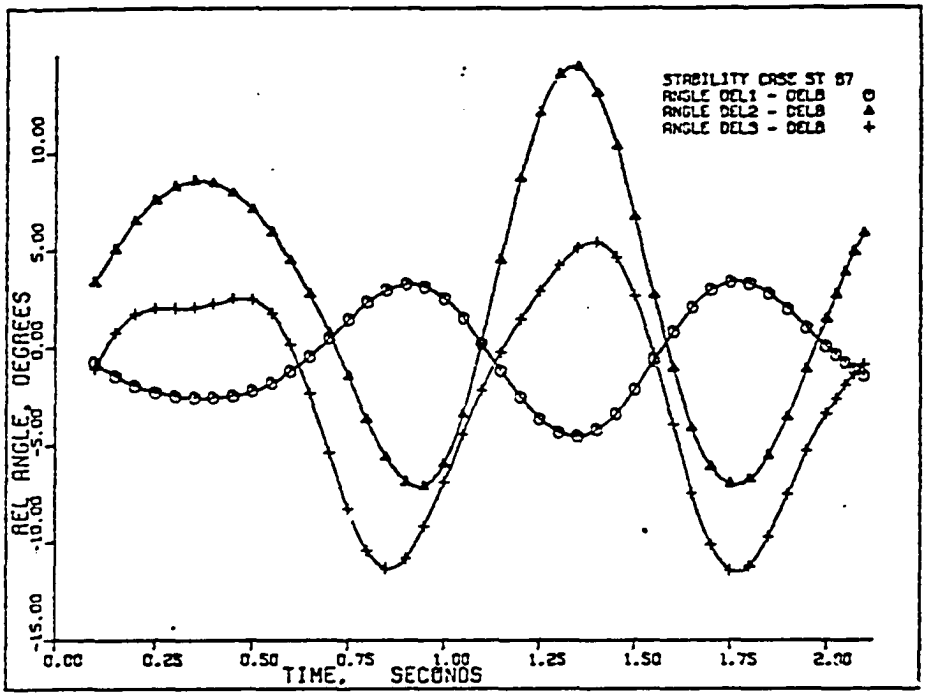

Figure 132. Case ST-67: relative angles $(\delta_1 - \bar{\delta})$, $(\delta_2 - \bar{\delta})$, and $(\delta_3 - \bar{\delta})$.

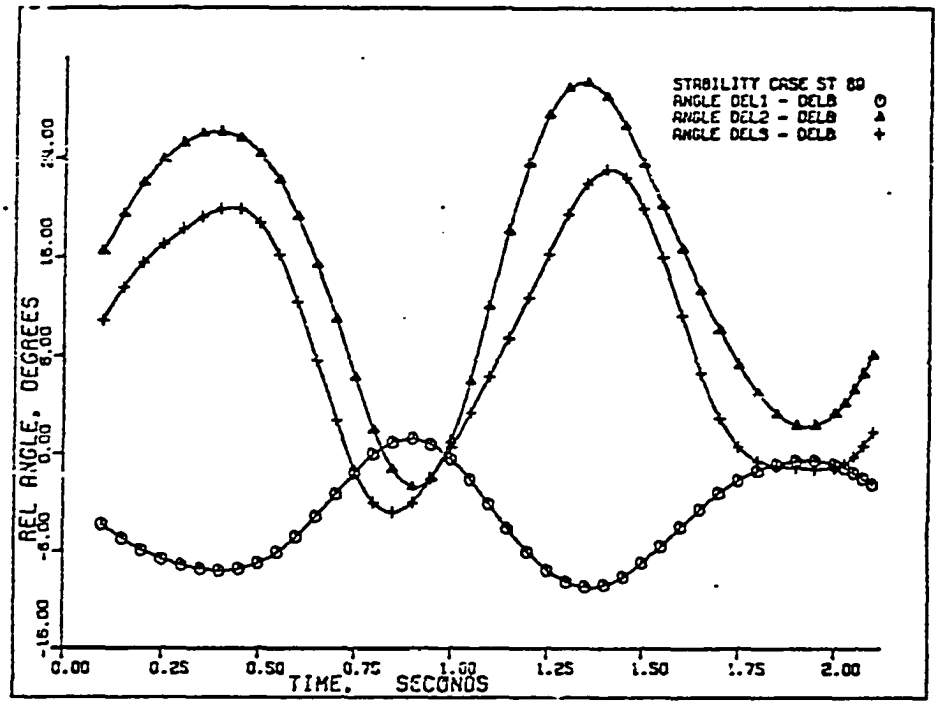

Figure 133. Case ST-69: relative angles $(\delta_1 - \bar{\delta})$, $(\delta_2 - \bar{\delta})$, and $(\delta_3 - \bar{\delta})$.

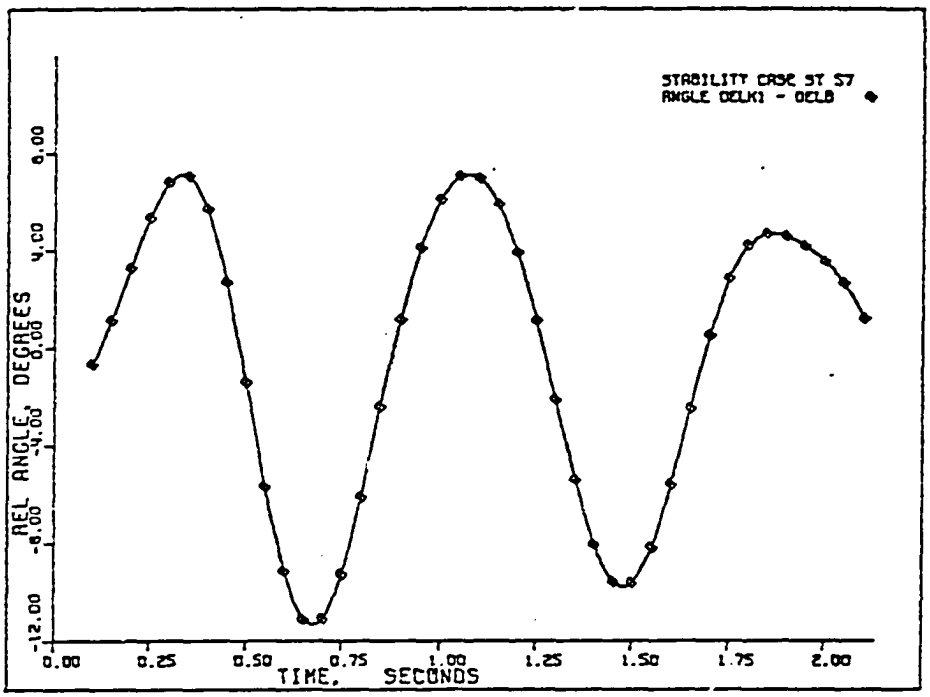

Figure 134. Case ST-57: relative angle $(\delta_k - \bar{\delta})$.

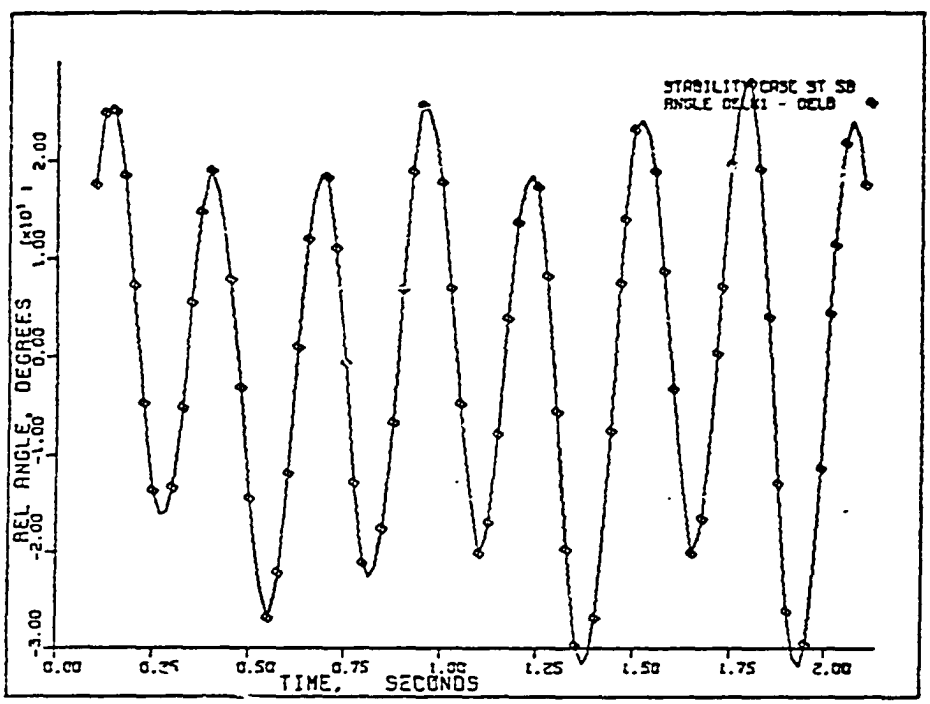

Figure 135. Case ST-58: relative angle $(\delta_k - \bar{\delta})$.

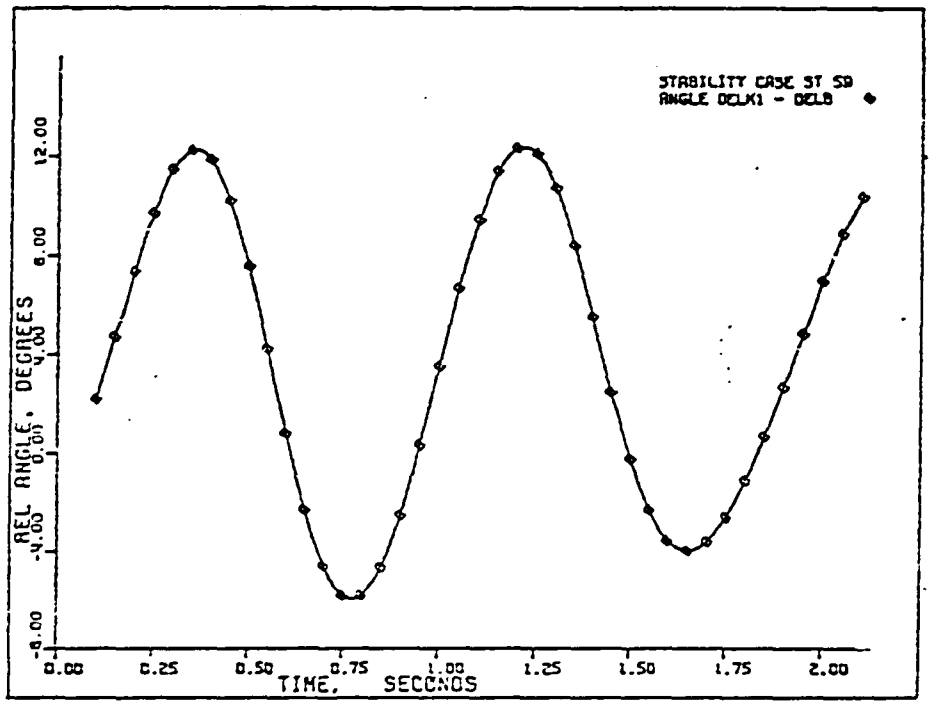

Figure 136. Case ST-59: relative angle $(\delta_k - \bar{\delta})$.

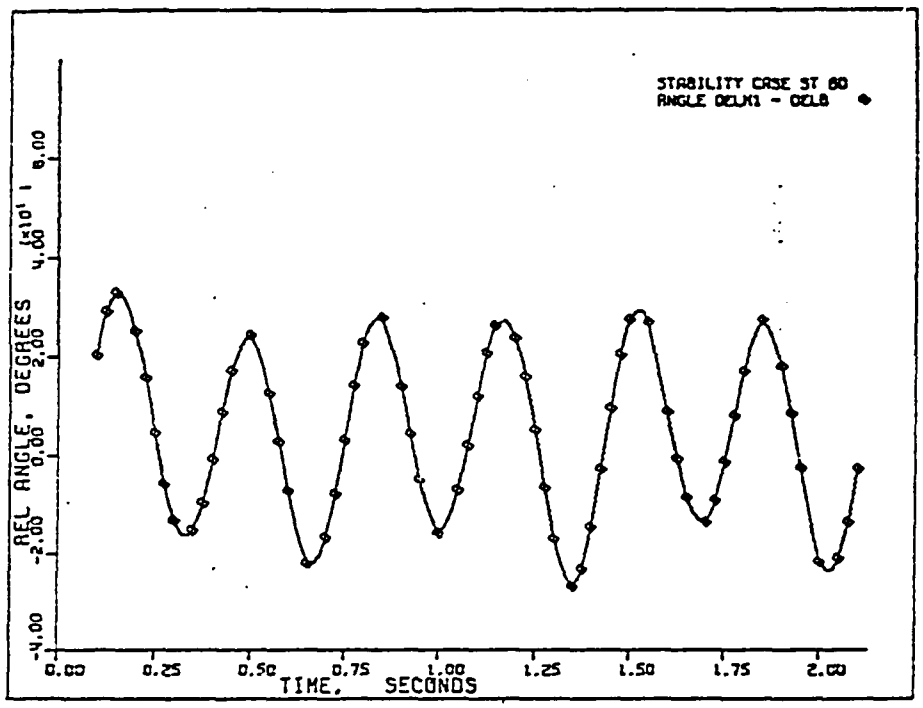

Figure 137. Case ST-60: relative angle $(\delta_k - \bar{\delta})$.

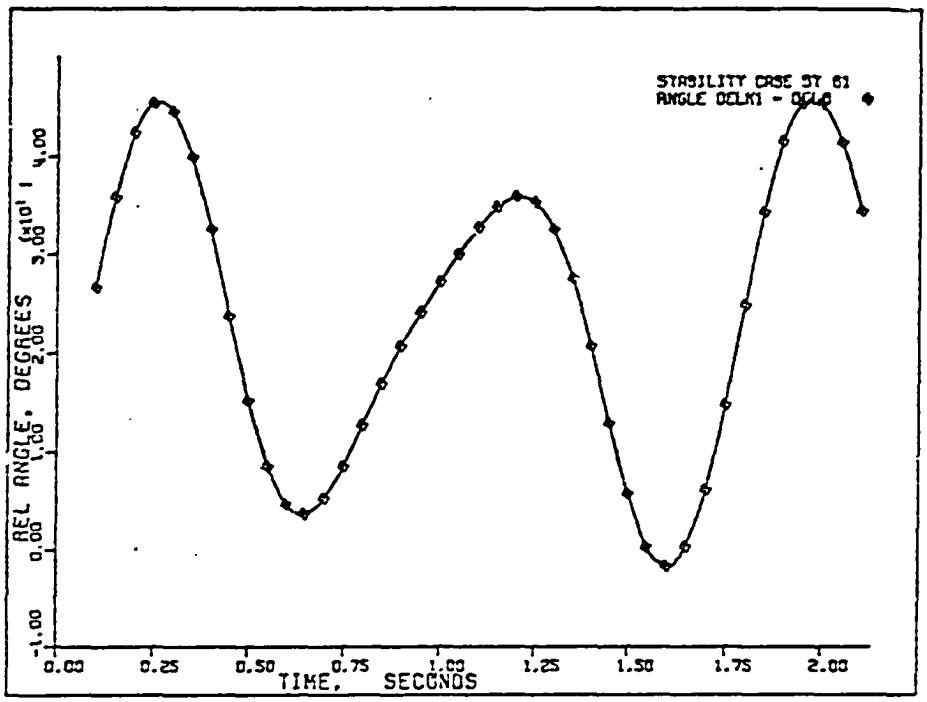

Figure 138. Case ST-61: relative angle $(\delta_k - \bar{\delta})$.

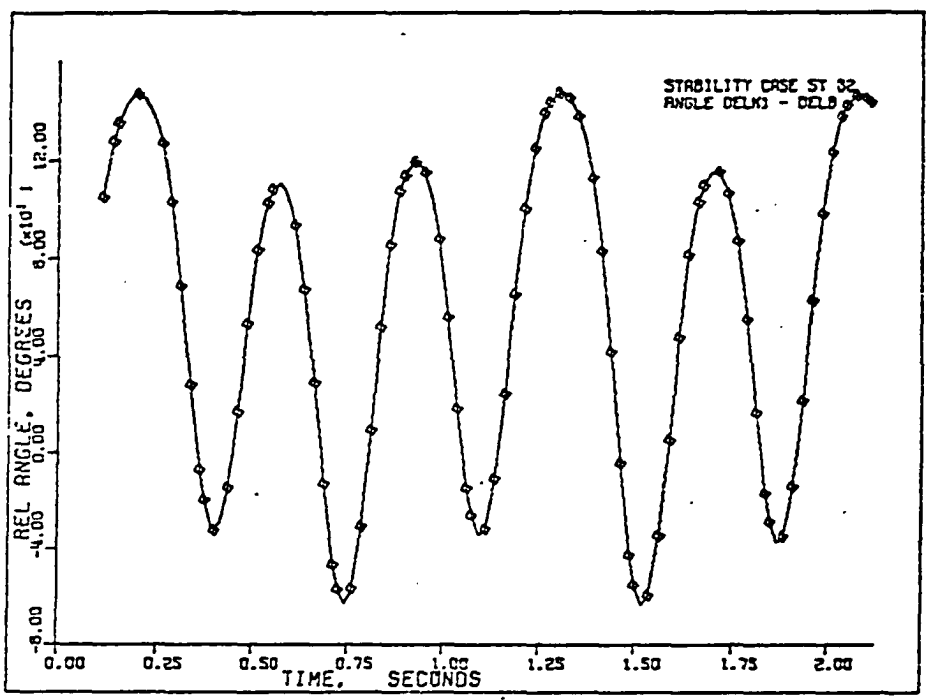

Figure 139. Case ST-62: relative angle $(\delta_k - \bar{\delta})$.

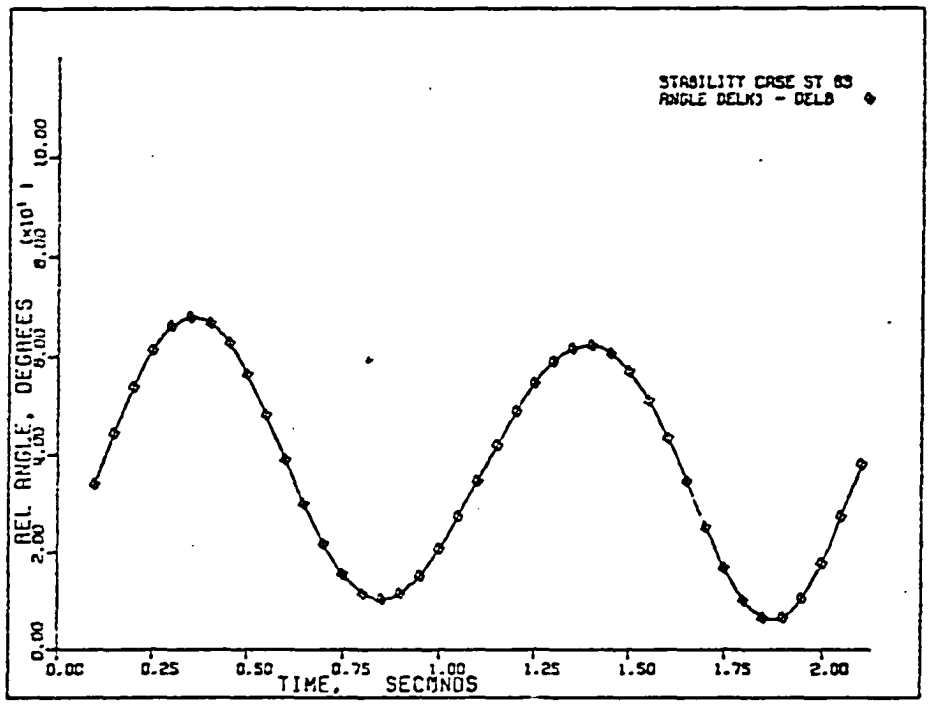

Figure 140. Case ST-63: relative angle $(\delta_k - \bar{\delta})$.

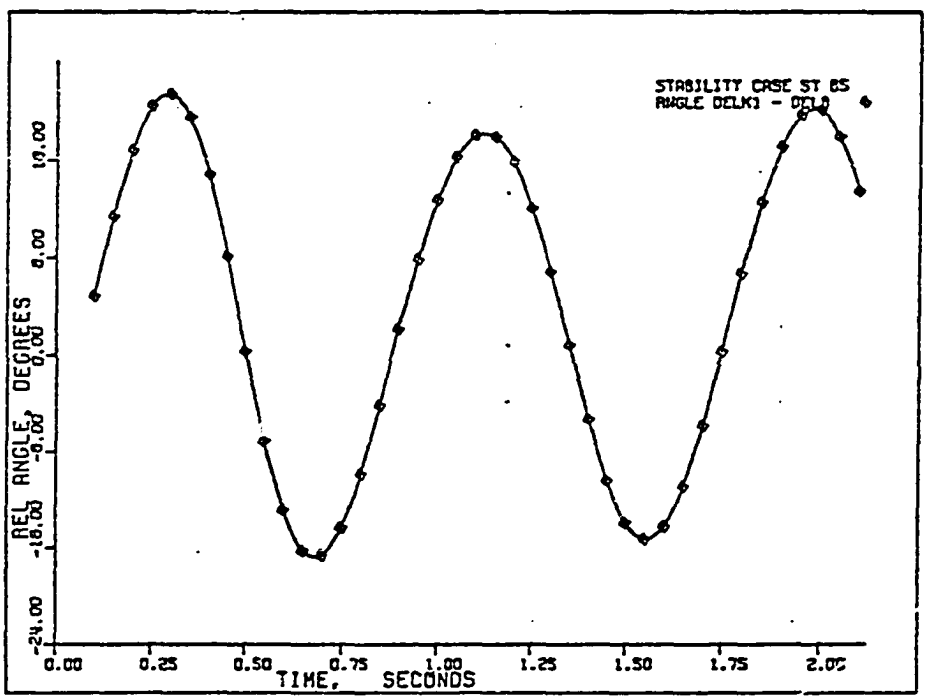

Figure 141. Case ST-65: relative angle $(\delta_k - \bar{\delta})$.

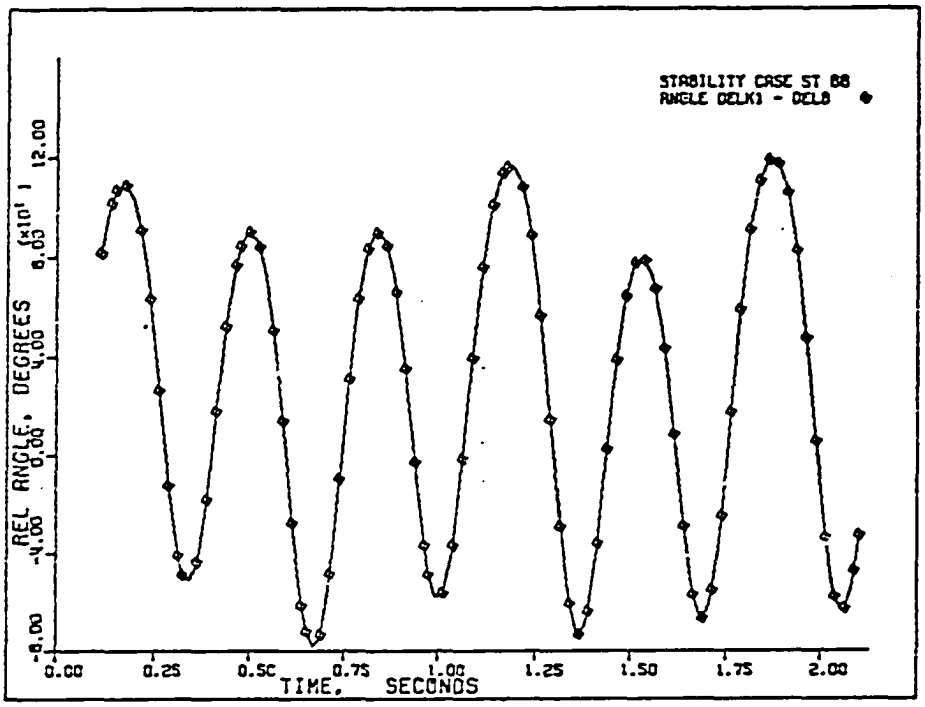

Figure 142. Case ST-66: relative angle $(\delta_k - \bar{\delta})$.

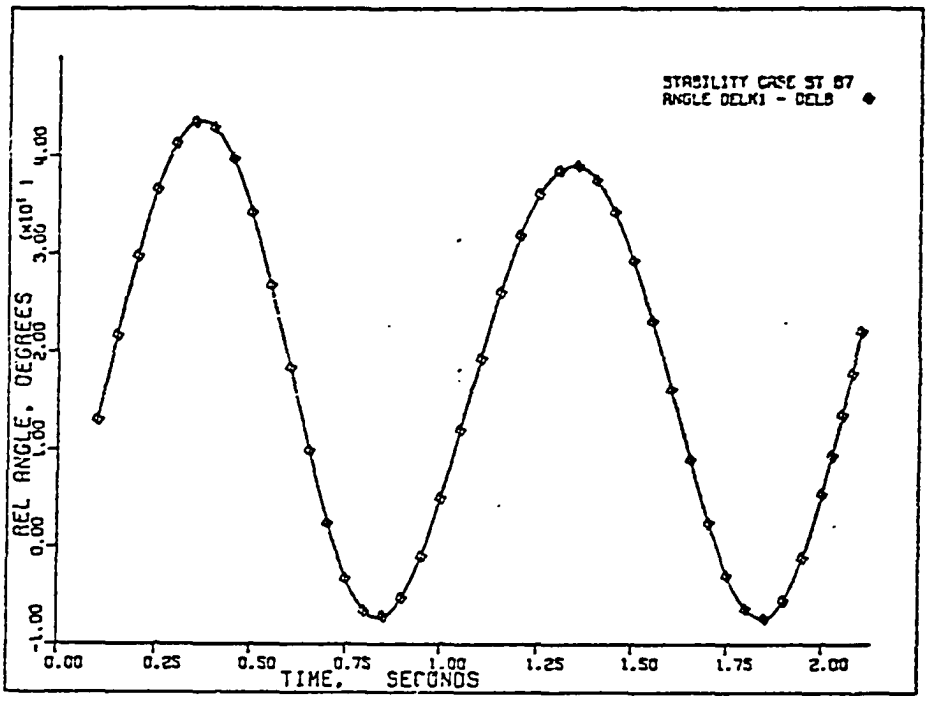

Figure 143. Case ST-67: relative angle $(\delta_k - \bar{\delta})$.

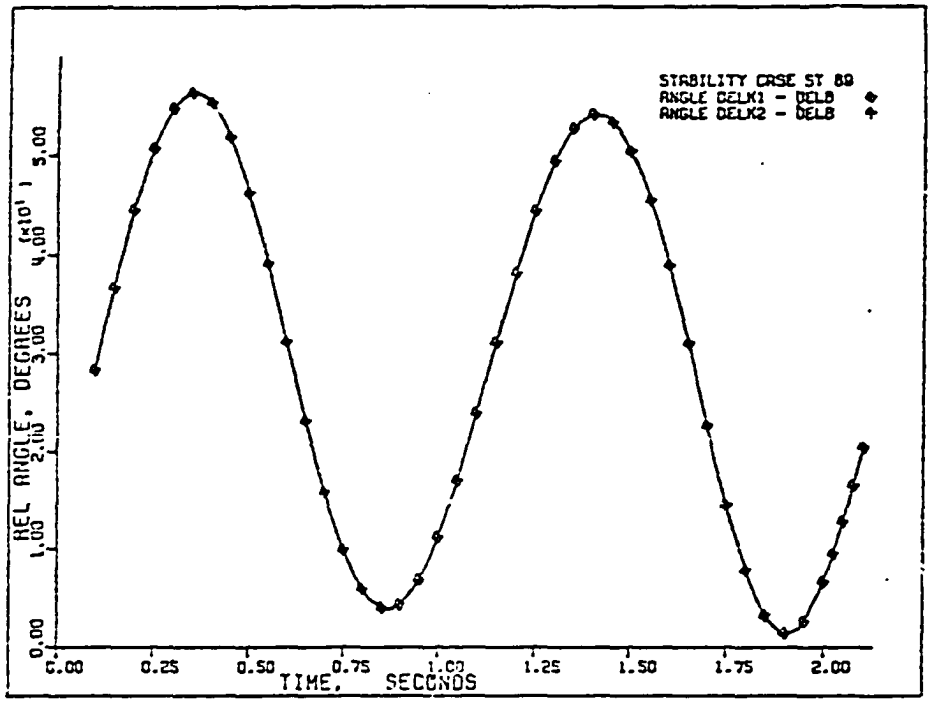

Figure 144. Case ST-69: relative angles $(\delta_{k1} - \bar{\delta})$ and $(\delta_{k2} - \bar{\delta})$.

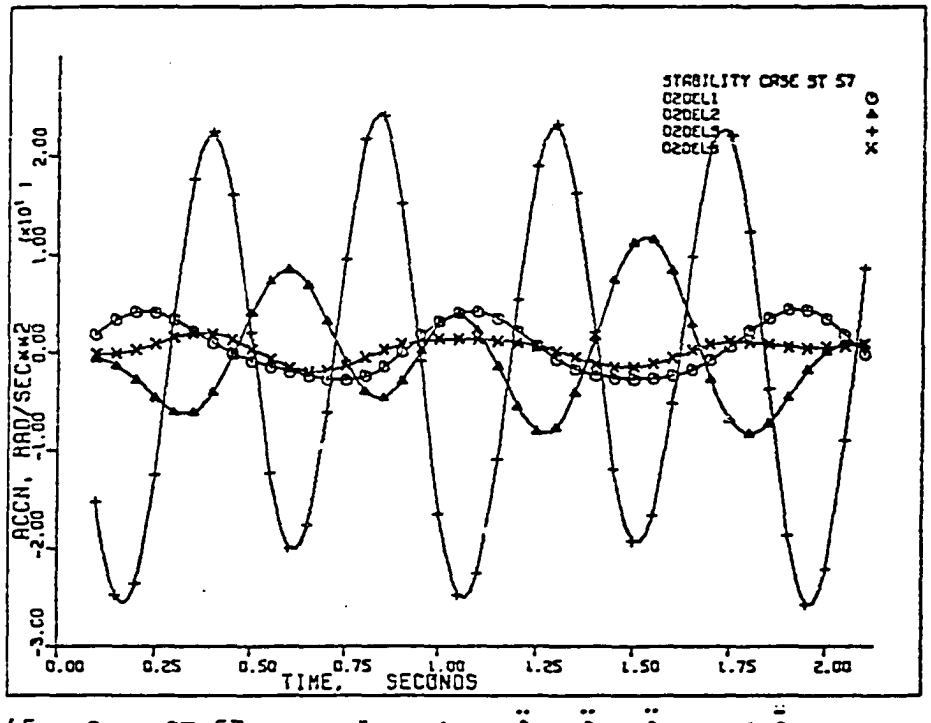

Figure 145. Case ST-57: accelerations $\ddot{\delta}_1$, $\ddot{\delta}_2$, $\ddot{\delta}_3$, and $\ddot{\bar{\delta}}$.

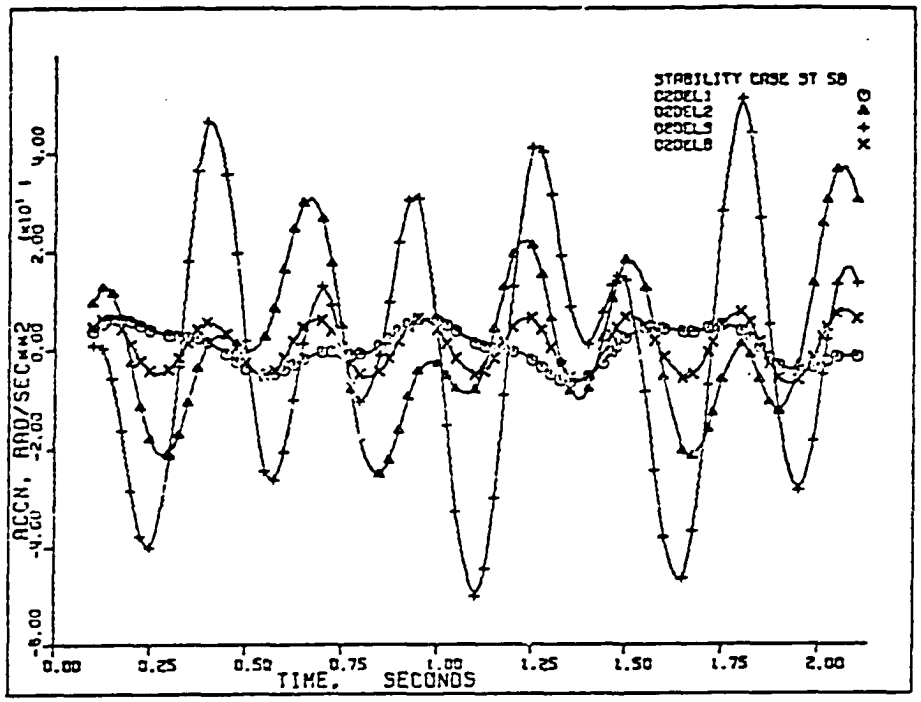

Figure 146. Case ST-58: accelerations $\ddot{\delta}_1$, $\ddot{\delta}_2$, $\ddot{\delta}_3$, and $\ddot{\bar{\delta}}$.

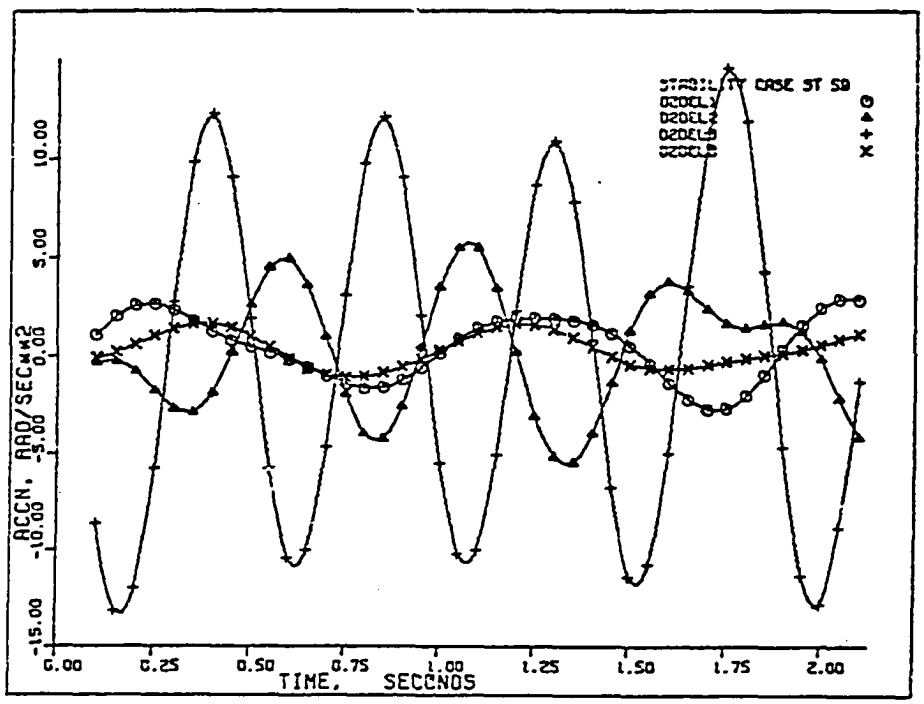

Figure 147. Case ST-59: accelerations $\ddot{\delta}_1$, $\ddot{\delta}_2$, $\ddot{\delta}_3$, and $\ddot{\bar{\delta}}$.

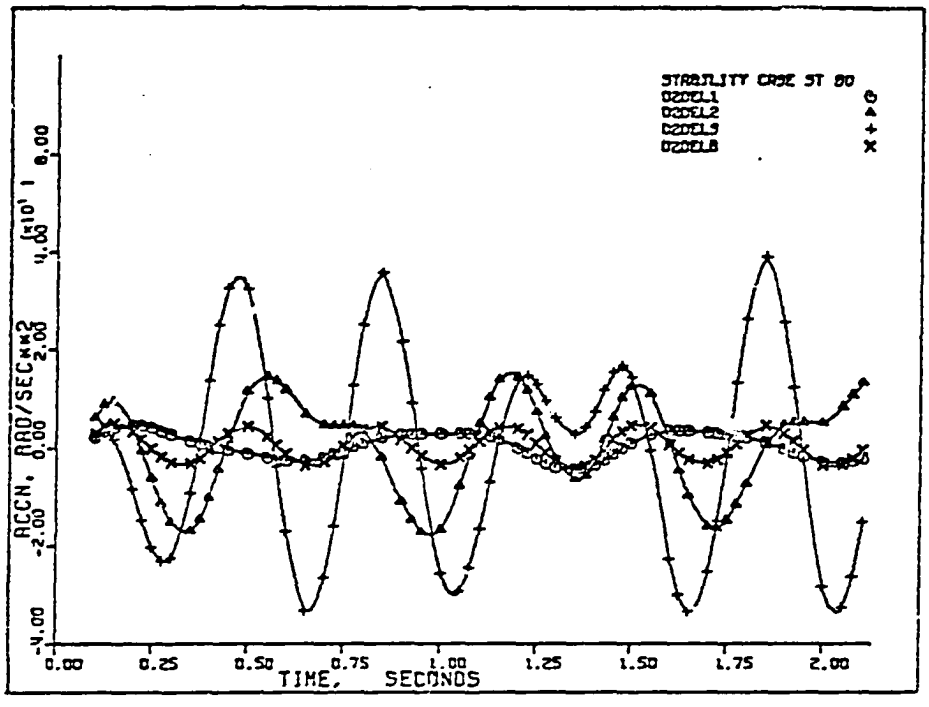

Figure 148. Case ST-60: accelerations $\ddot{\delta}_1$, $\ddot{\delta}_2$, $\ddot{\delta}_3$, and $\ddot{\bar{\delta}}$.

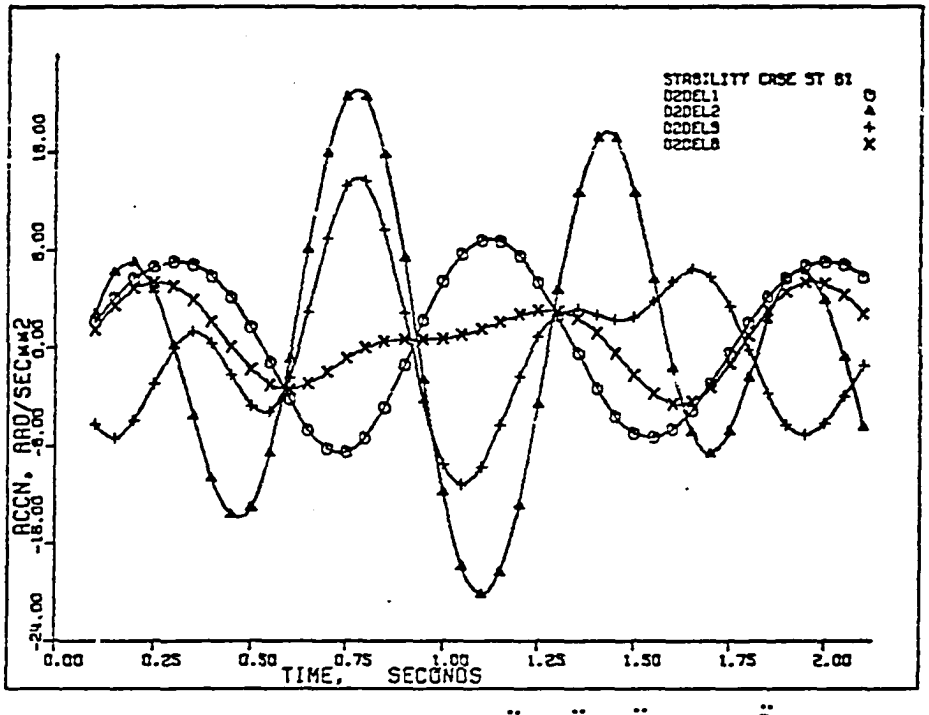

Figure 149. Case ST-61: accelerations $\ddot{\delta}_1$, $\ddot{\delta}_2$, $\ddot{\delta}_3$, and $\ddot{\bar{\delta}}$.

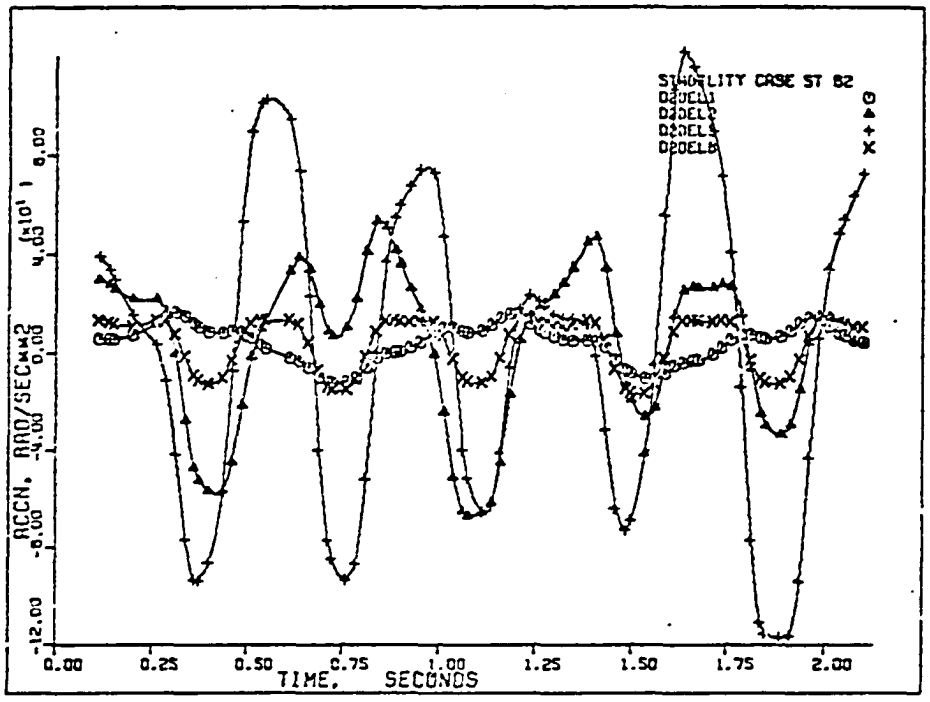

Figure 150. Case ST-62: accelerations $\ddot{\delta}_1$, $\ddot{\delta}_2$, $\ddot{\delta}_3$, and $\ddot{\bar{\delta}}$.

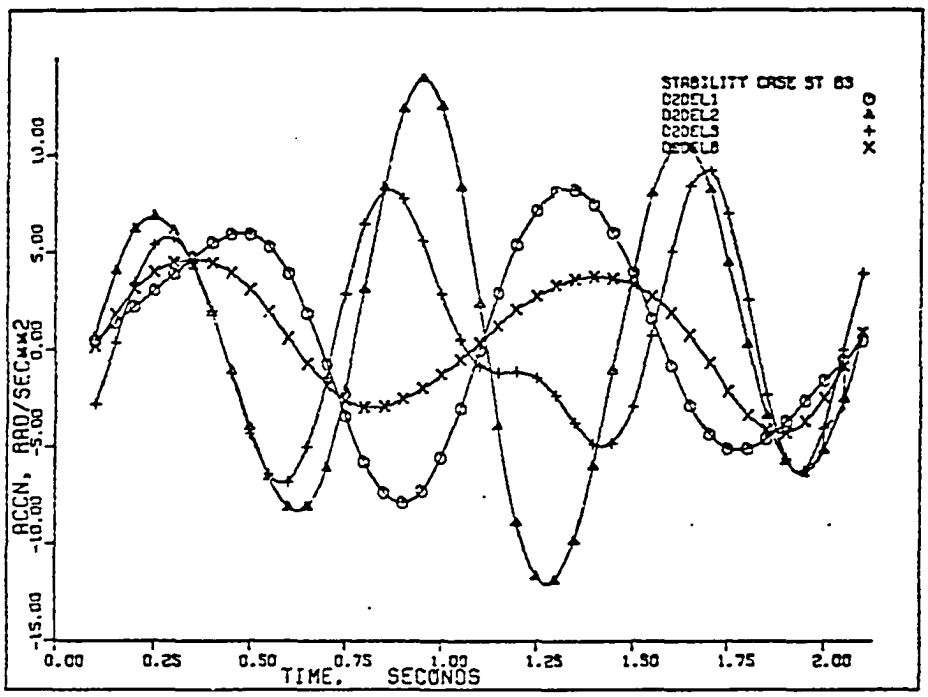

Figure 151. Case ST-63: accelerations $\ddot{\delta}_1$, $\ddot{\delta}_2$, $\ddot{\delta}_3$, and $\ddot{\bar{\delta}}$.

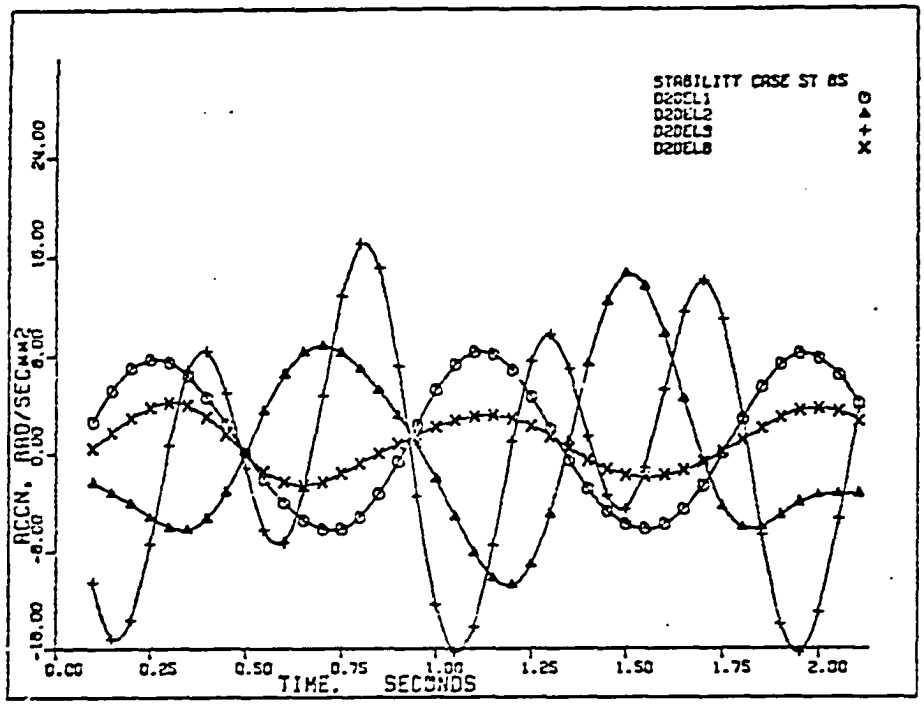

Figure 152. Case ST-65: accelerations $\ddot{\delta}_1$, $\ddot{\delta}_2$, $\ddot{\delta}_3$, and $\ddot{\bar{\delta}}$.

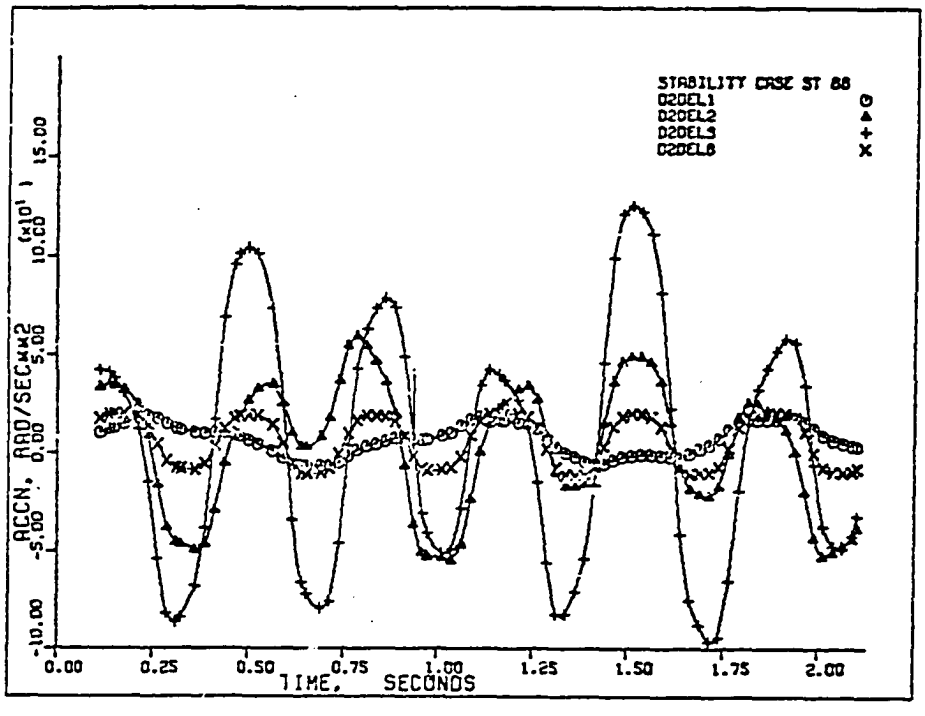

Figure 153. Case ST-66: accelerations $\ddot{\delta}_1$, $\ddot{\delta}_2$, $\ddot{\delta}_3$, and $\ddot{\bar{\delta}}$.

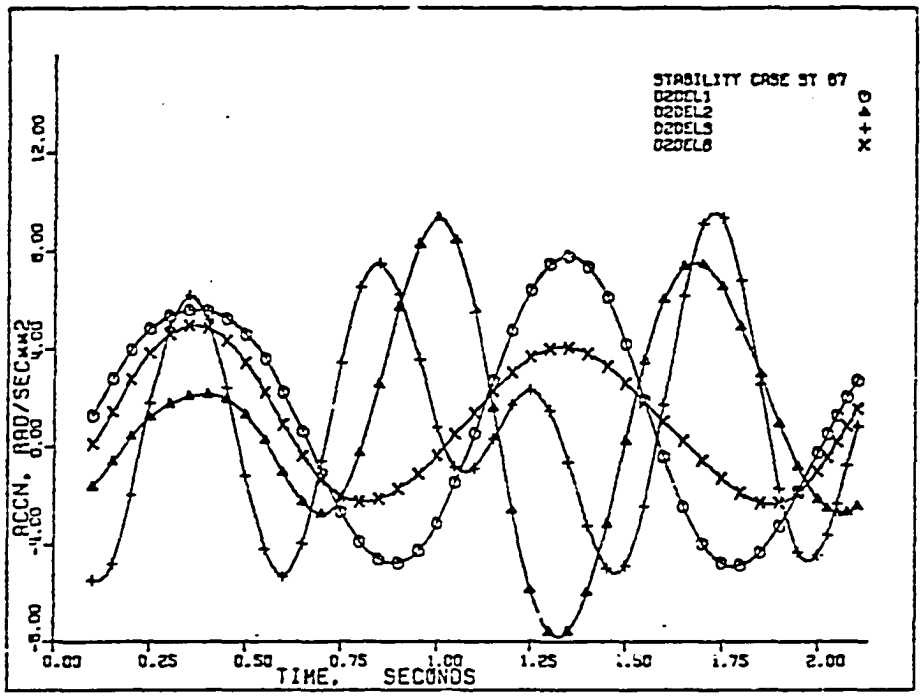

Figure 154. Case ST-67: accelerations $\ddot{\delta}_1$, $\ddot{\delta}_2$, $\ddot{\delta}_3$, and $\ddot{\bar{\delta}}$.

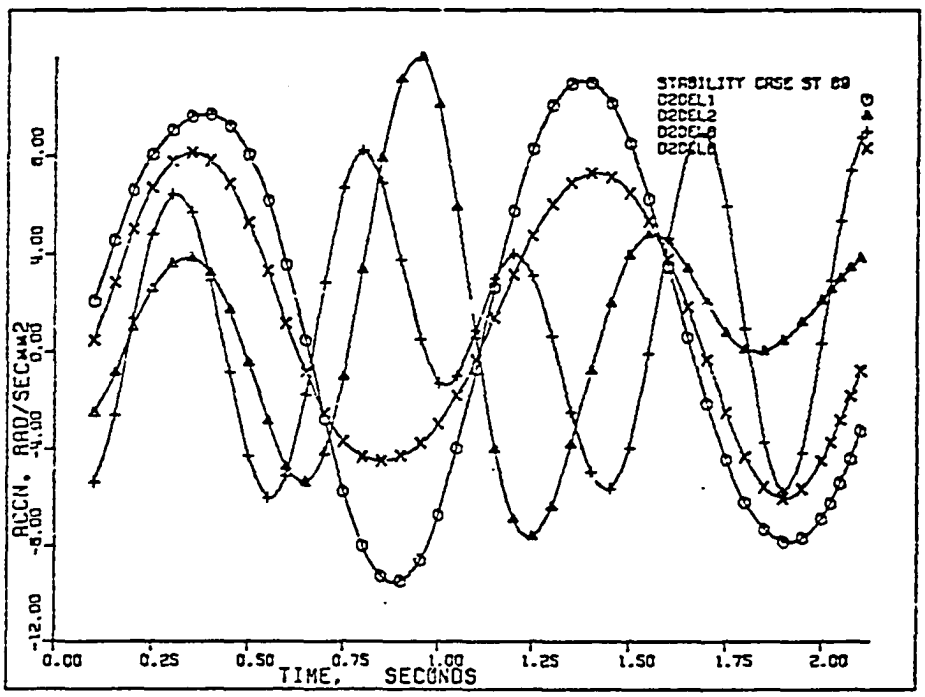

Figure 155. Case ST-69: accelerations $\ddot{\delta}_1$, $\ddot{\delta}_2$, $\ddot{\delta}_3$, and $\ddot{\bar{\delta}}$.

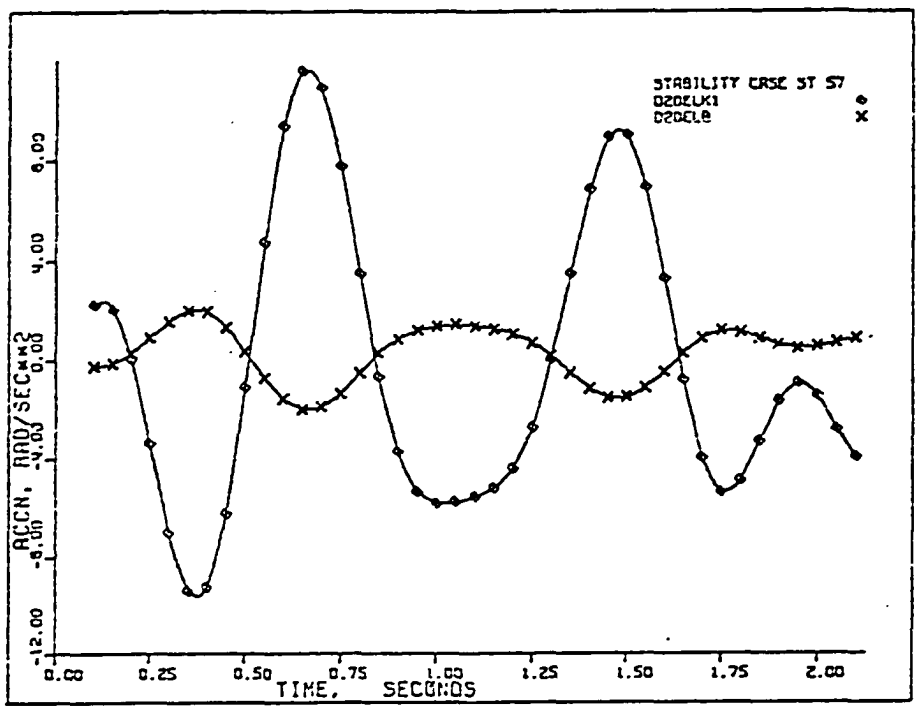

Figure 156. Case ST-57: accelerations $\ddot{\delta}_k$ and $\ddot{\bar{\delta}}$.

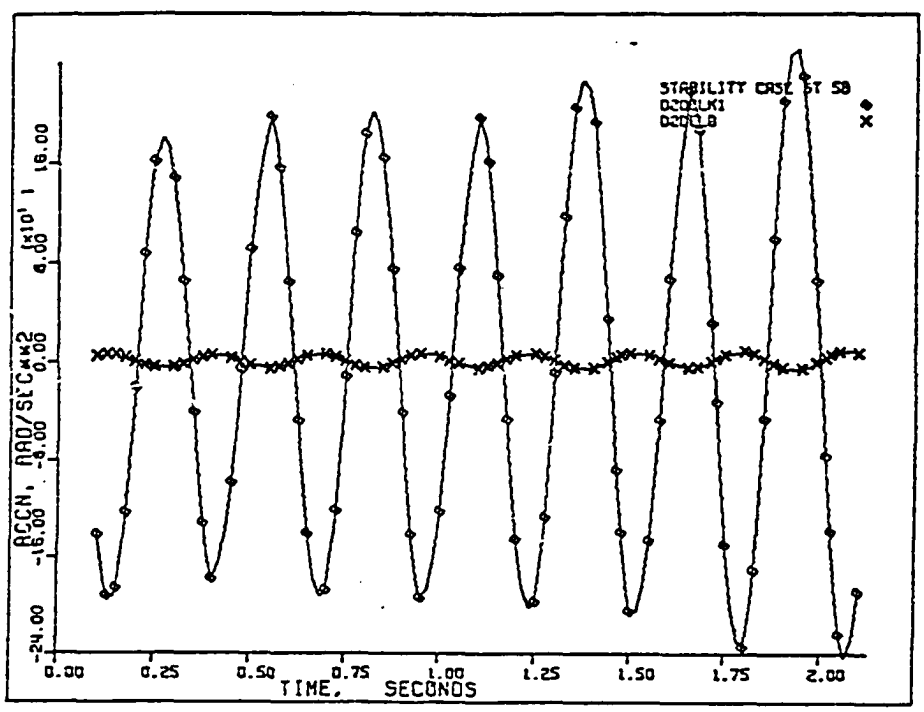

Figure 157. Case ST-58: accelerations $\ddot{\delta}_k$ and $\ddot{\bar{\delta}}$.

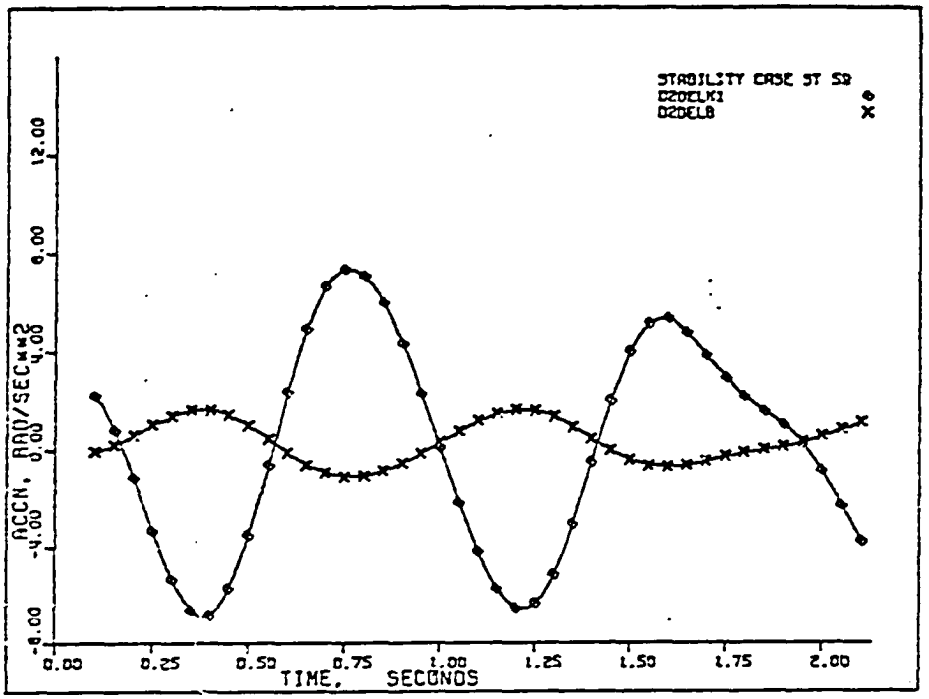

Figure 158. Case ST-59: accelerations $\ddot{\delta}_k$ and $\dddot{\delta}$.

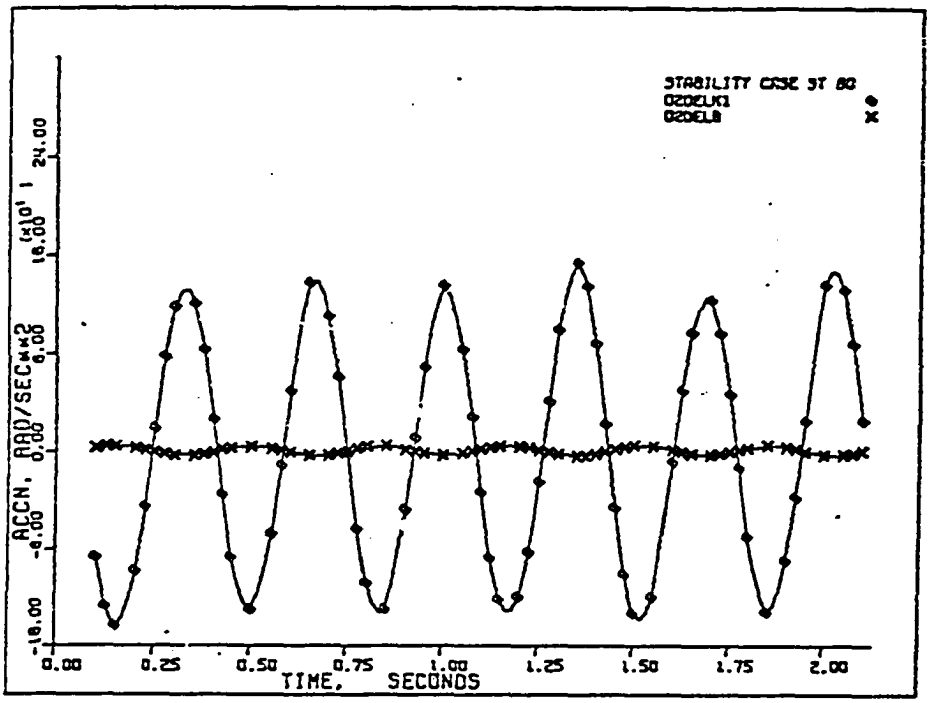

Figure 159. Case ST-60: accelerations $\ddot{\delta}_k$ and $\dddot{\delta}$.

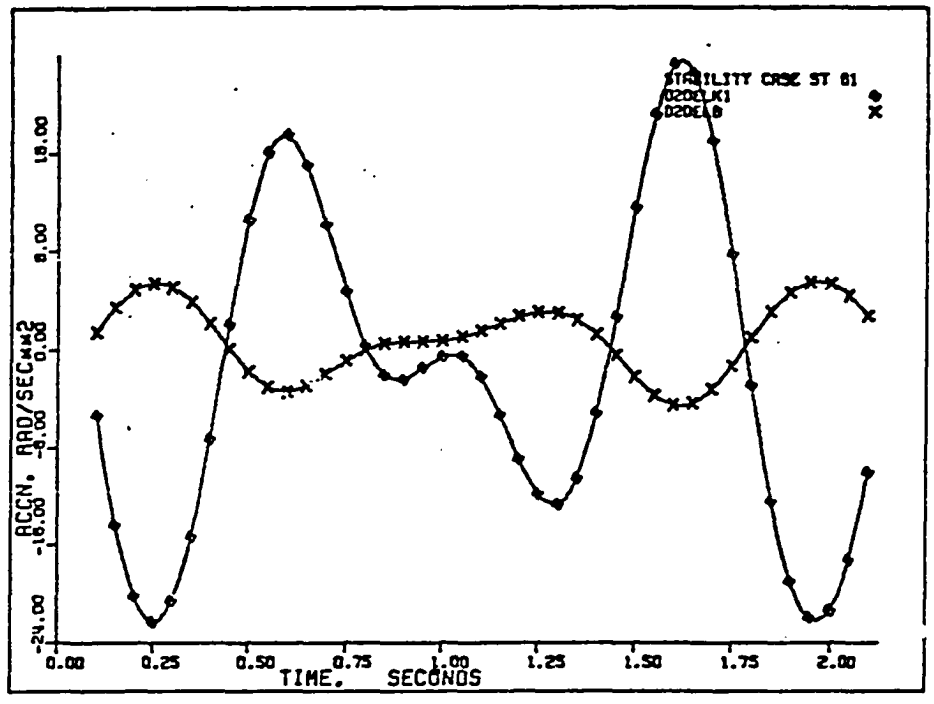

Figure 160. Case ST-61: accelerations $\ddot{\delta}_k$ and $\ddot{\bar{\delta}}$.

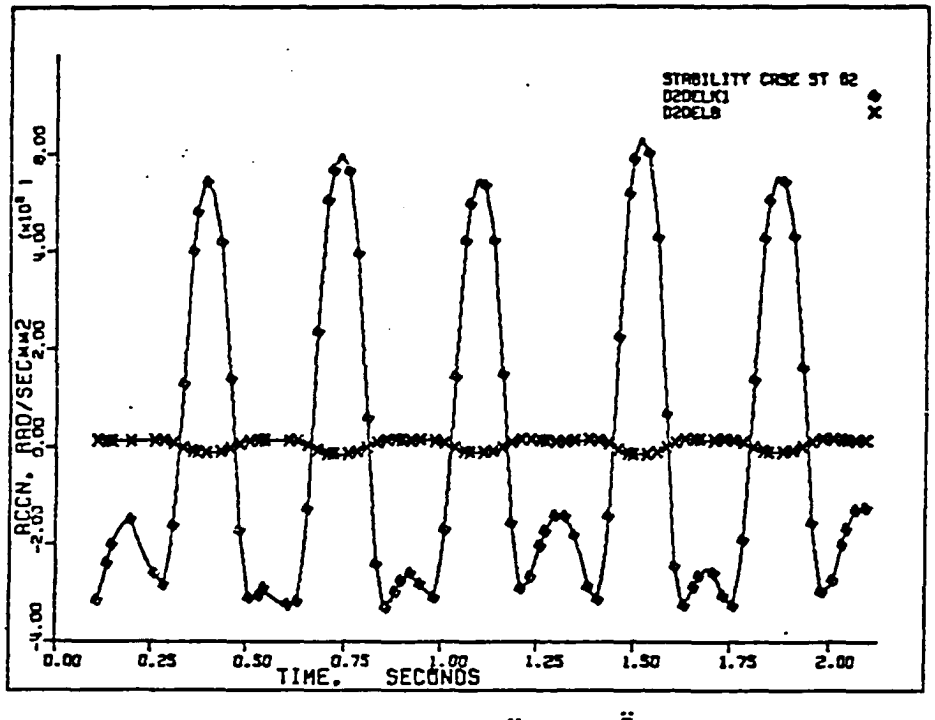

Figure 161. Case ST-62: accelerations $\ddot{\delta}_k$ and $\ddot{\bar{\delta}}$.

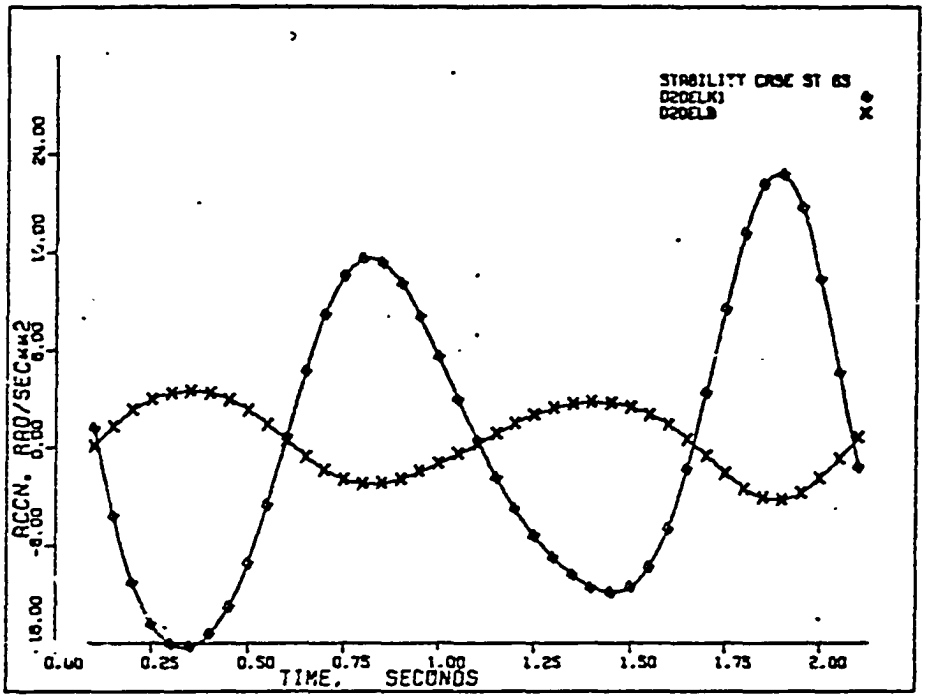

Figure 162. Case ST-63: accelerations $\ddot{\delta}_k$ and $\ddot{\delta}$.

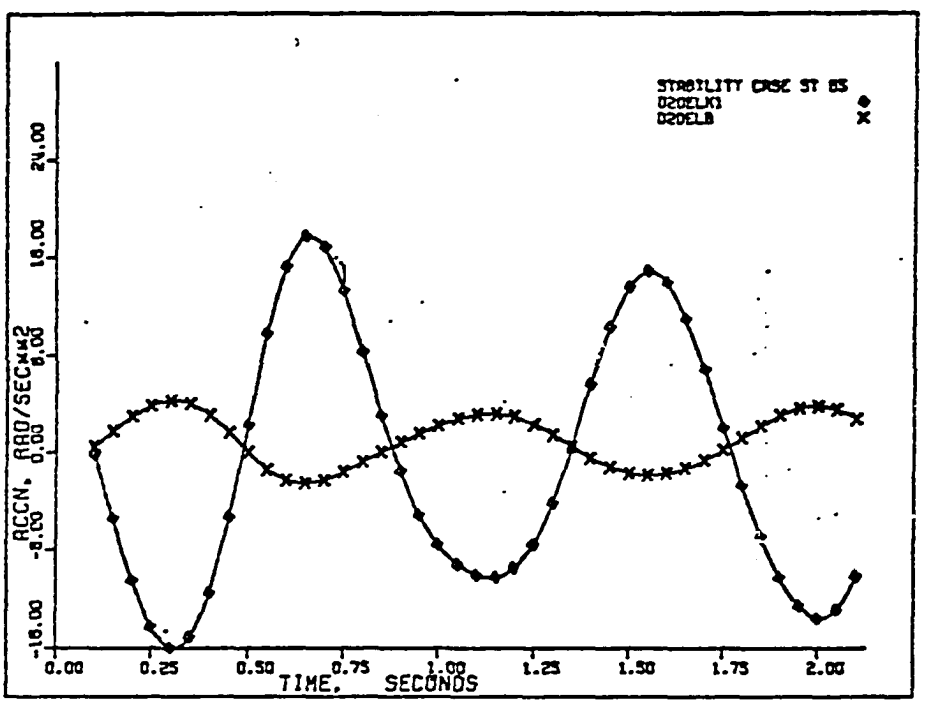

Figure 163. Case ST-65: accelerations $\ddot{\delta}_k$ and $\ddot{\delta}$.

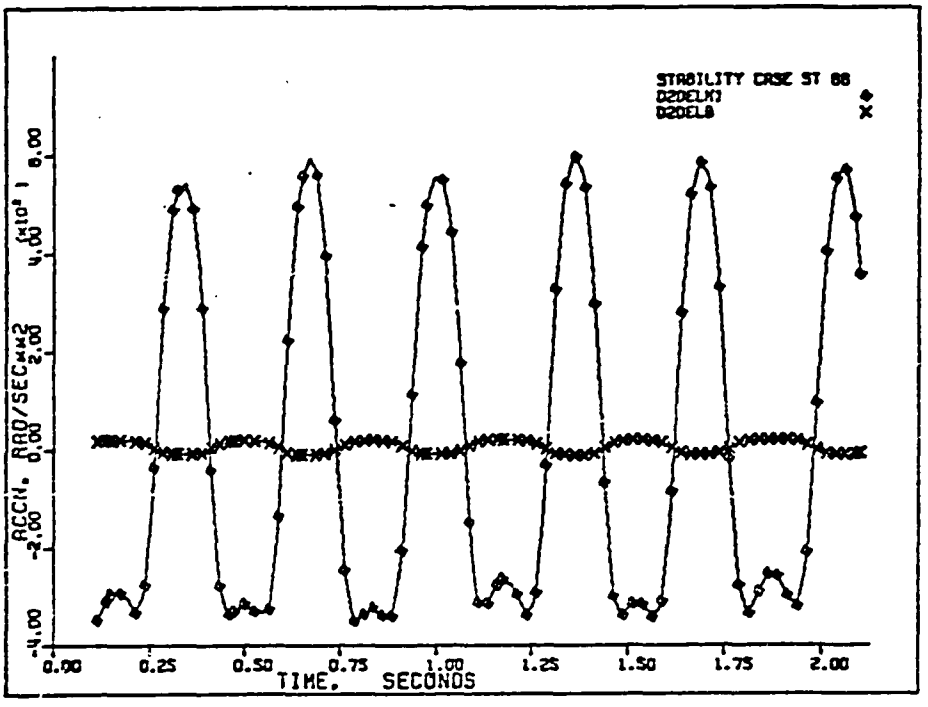

Figure 164. Case ST-66: accelerations $\ddot{\delta}_k$ and $\ddot{\bar{\delta}}$.

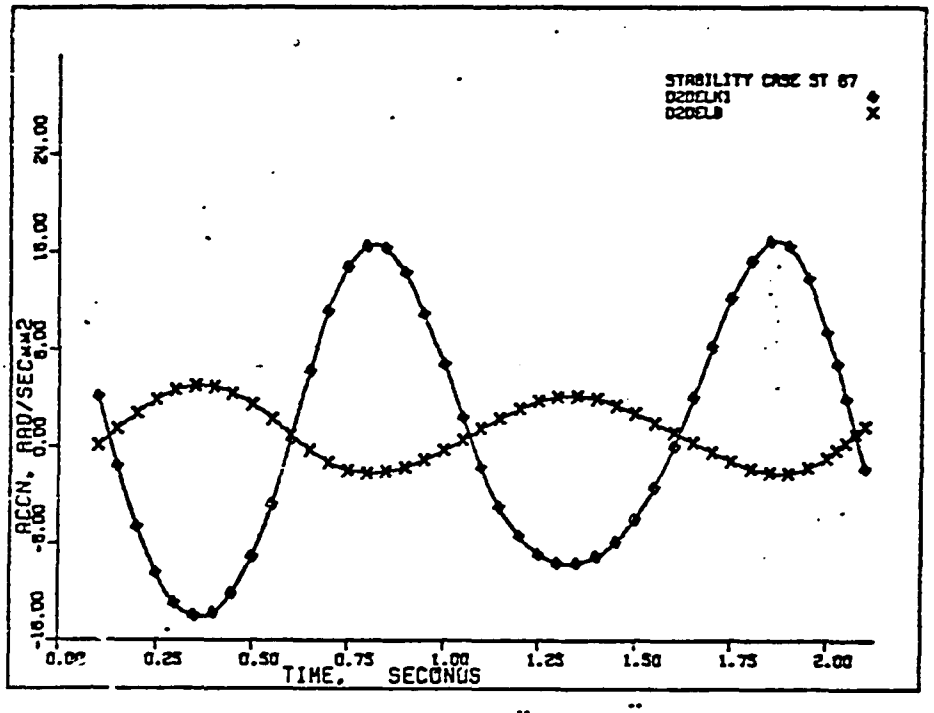

Figure 165. Case ST-67: accelerations $\ddot{\delta}_k$ and $\ddot{\bar{\delta}}$.

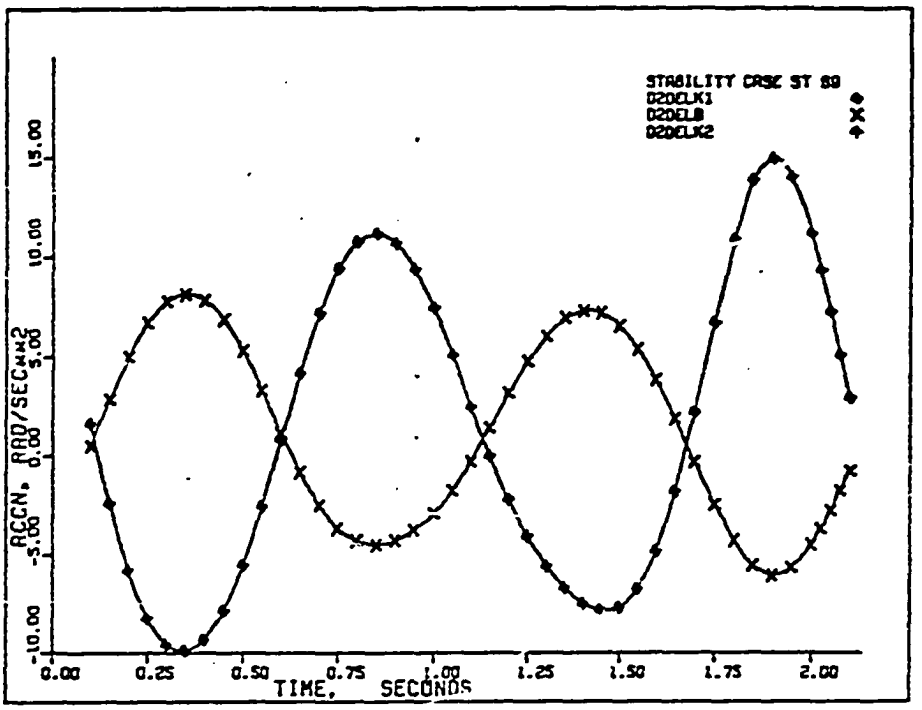

Figure 166. Case ST-69: accelerations $\ddot{\delta}_{k1}$, $\ddot{\delta}_{k2}$, and $\ddot{\bar{\delta}}$.

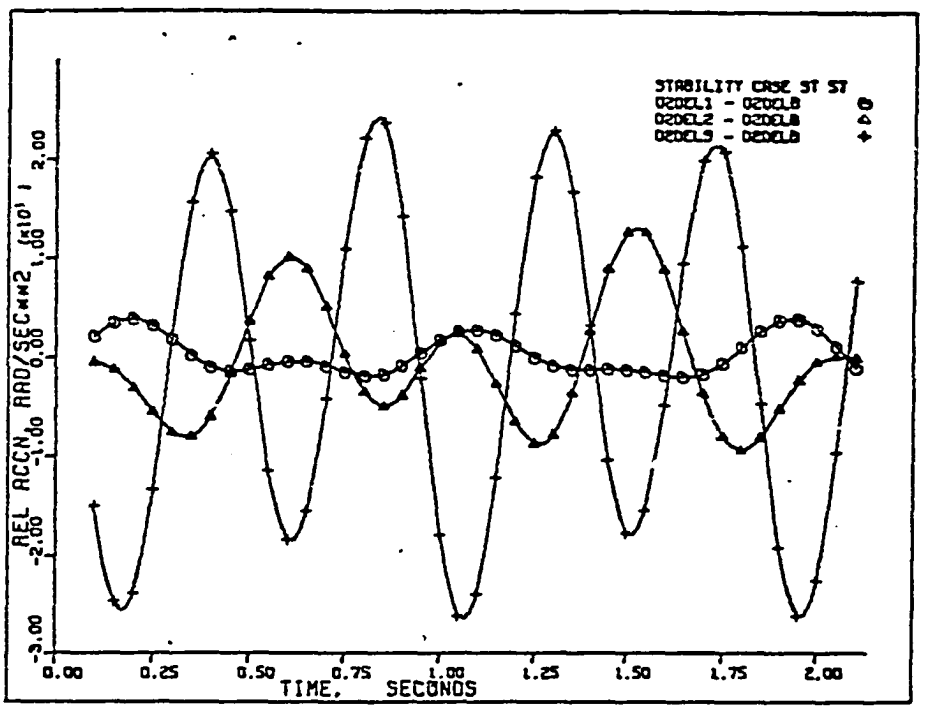

Figure 167. Case ST-57: relative accelerations $(\ddot{\delta}_1 - \ddot{\bar{\delta}})$, $(\ddot{\delta}_2 - \ddot{\bar{\delta}})$, and $(\ddot{\delta}_3 - \ddot{\bar{\delta}})$.

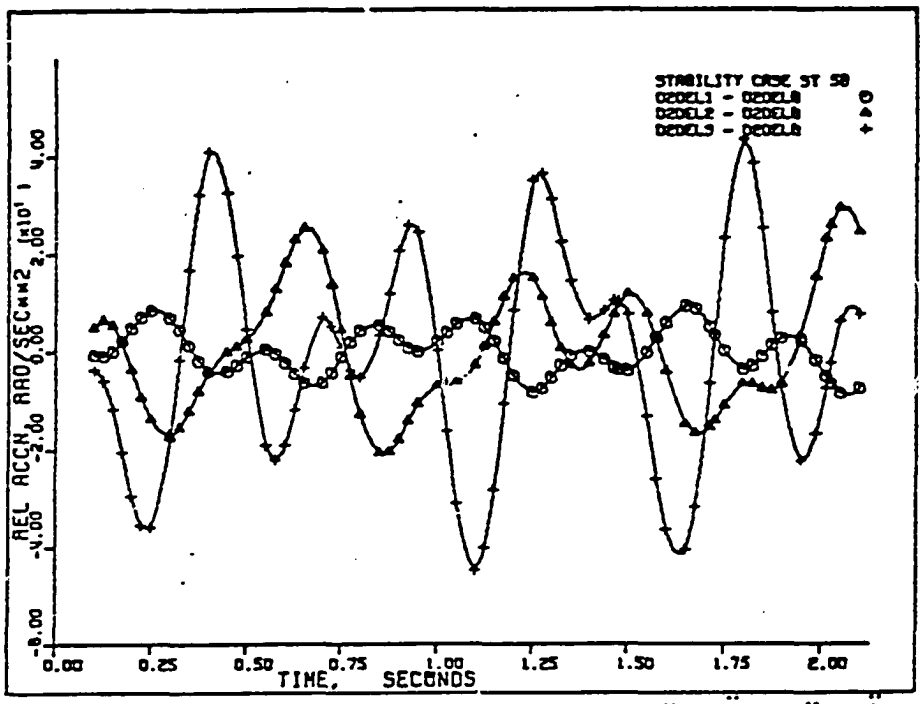

Figure 168. Case ST-58: relative accelerations $(\ddot{\delta}_1 - \ddot{\bar{\delta}})$, $(\ddot{\delta}_2 - \ddot{\bar{\delta}})$, and $(\ddot{\delta}_3 - \ddot{\bar{\delta}})$.

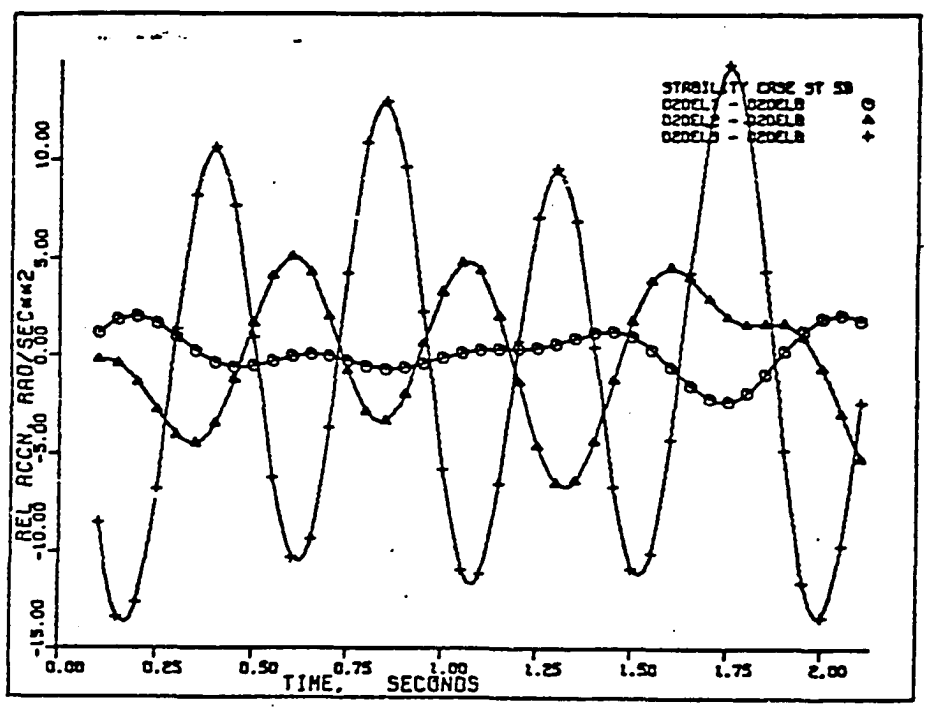

Figure 169. Case ST-59: relative accelerations $(\ddot{\delta}_1 - \ddot{\bar{\delta}})$, $(\ddot{\delta}_2 - \ddot{\bar{\delta}})$, and $(\ddot{\delta}_3 - \ddot{\bar{\delta}})$.

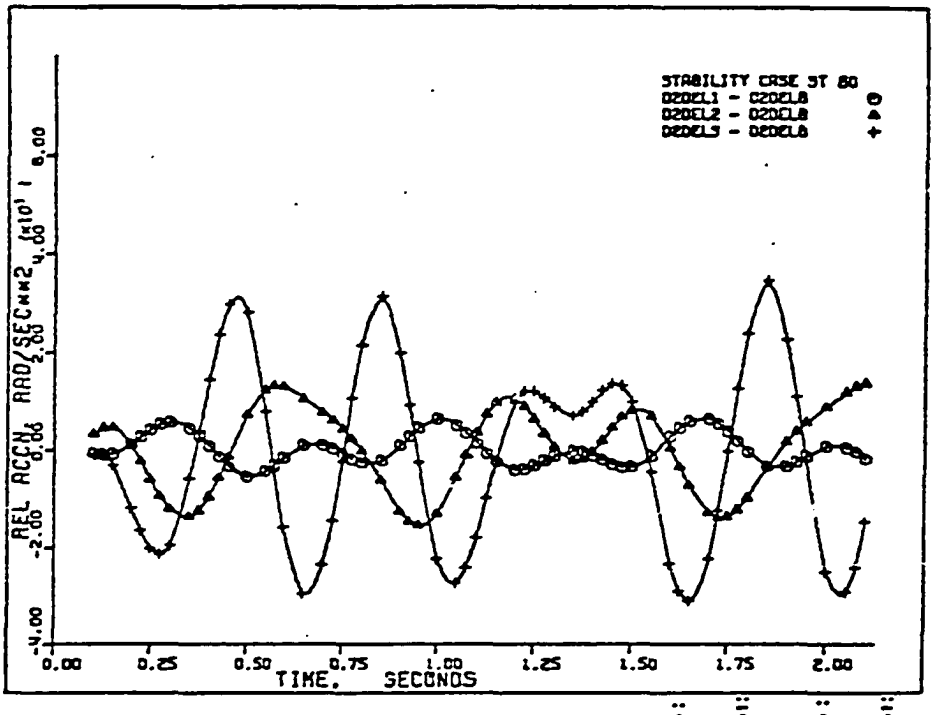

Figure 170. Case ST-60: relative accelerations $(\ddot{\delta}_1 - \ddot{\bar{\delta}})$, $(\ddot{\delta}_2 - \ddot{\bar{\delta}})$, and $(\ddot{\delta}_3 - \ddot{\bar{\delta}})$.

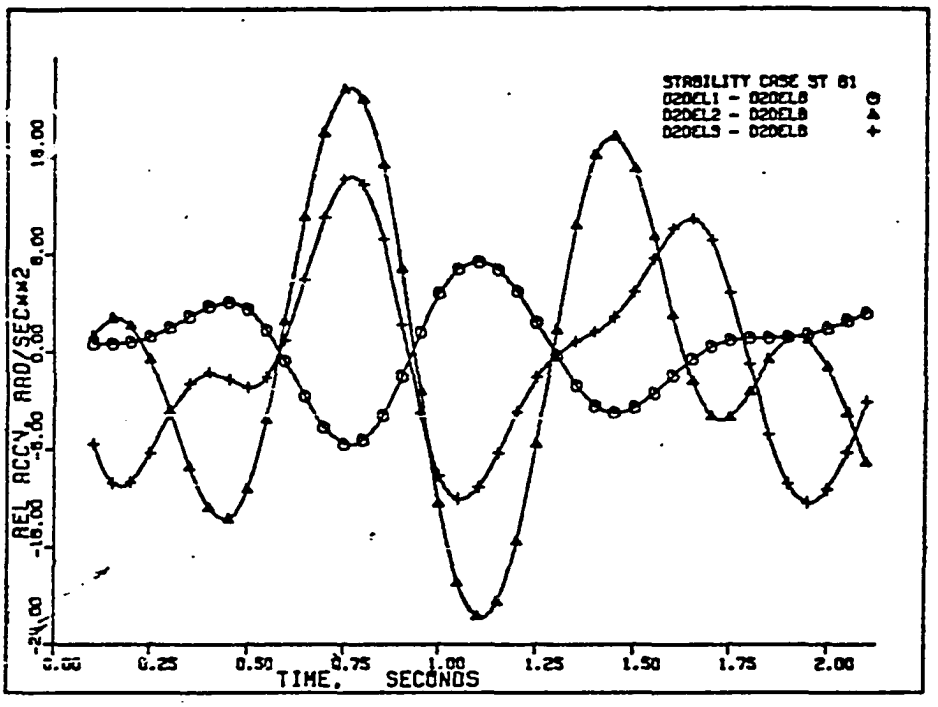

Figure 171. Case ST-61: relative accelerations $(\ddot{\delta}_1 - \ddot{\bar{\delta}})$, $(\ddot{\delta}_2 - \ddot{\bar{\delta}})$, and $(\ddot{\delta}_3 - \ddot{\bar{\delta}})$.

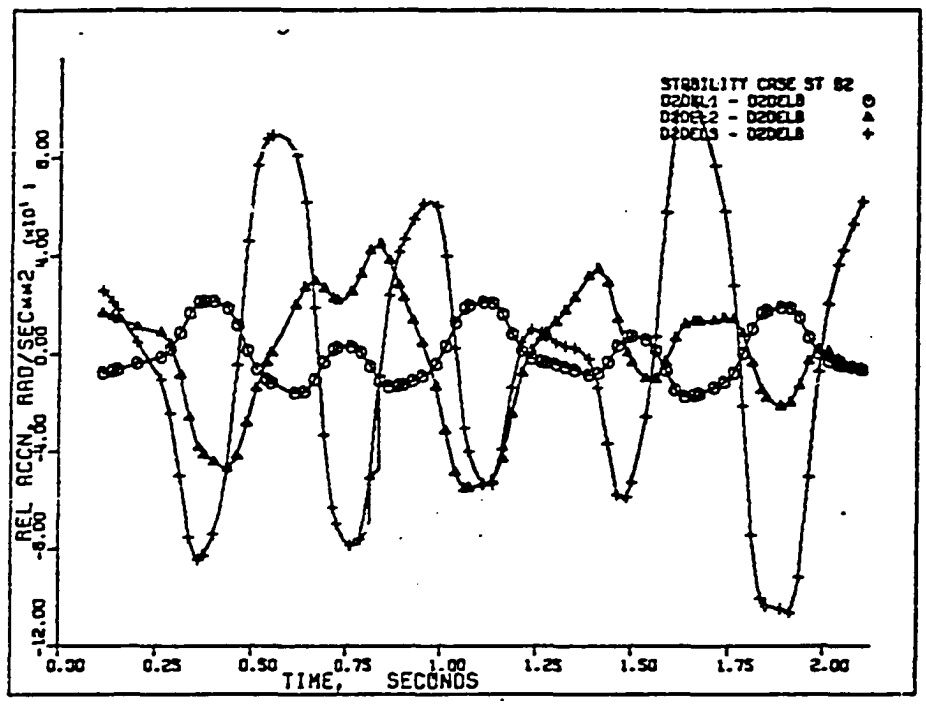

Figure 172. Case ST-62: relative accelerations $(\ddot{\delta}_1 - \ddot{\bar{\delta}})$, $(\ddot{\delta}_2 - \ddot{\bar{\delta}})$, and $(\ddot{\delta}_3 - \ddot{\bar{\delta}})$.

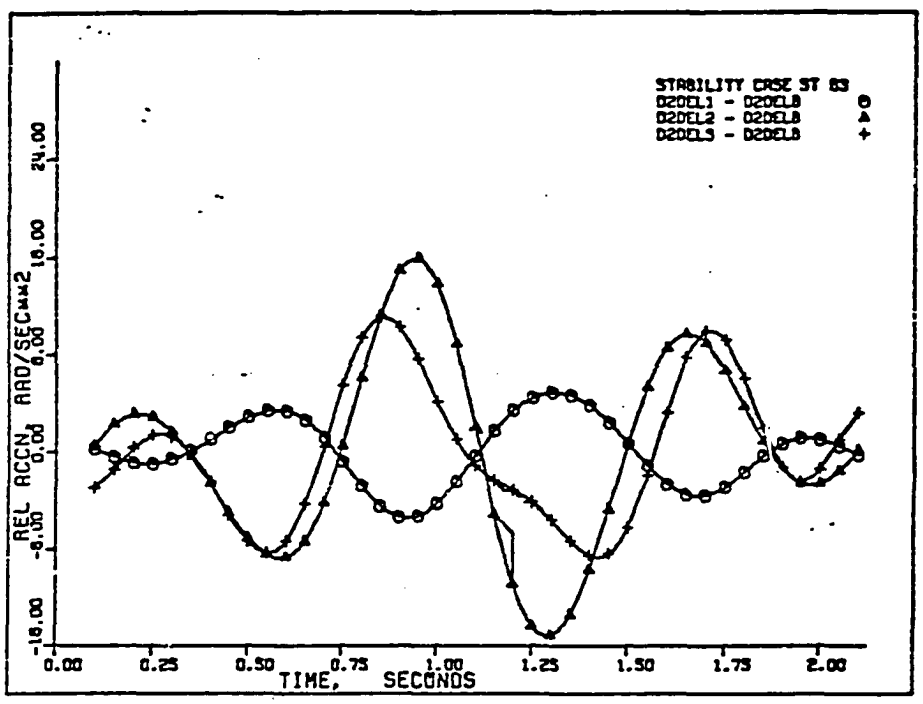

Figure 173. Case ST-63: relative accelerations $(\ddot{\delta}_1 - \ddot{\bar{\delta}})$, $(\ddot{\delta}_2 - \ddot{\bar{\delta}})$, and $(\ddot{\delta}_3 - \ddot{\bar{\delta}})$.

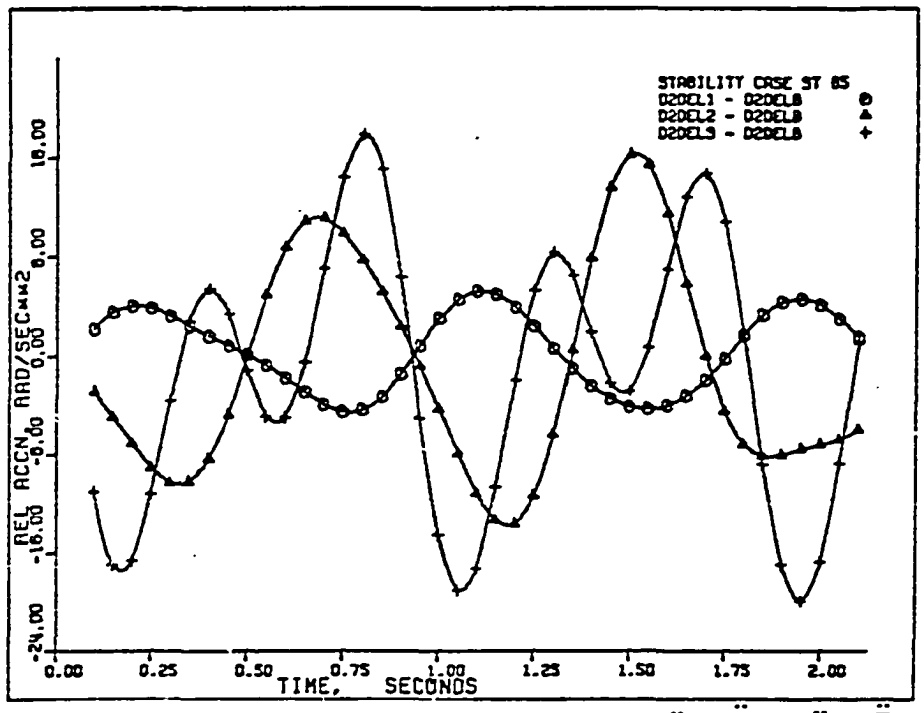

Figure 174. Case ST-65: relative accelerations $(\ddot{\delta}_1 - \ddot{\delta})$, $(\ddot{\delta}_2 - \ddot{\delta})$, and $(\ddot{\delta}_3 - \ddot{\delta})$.

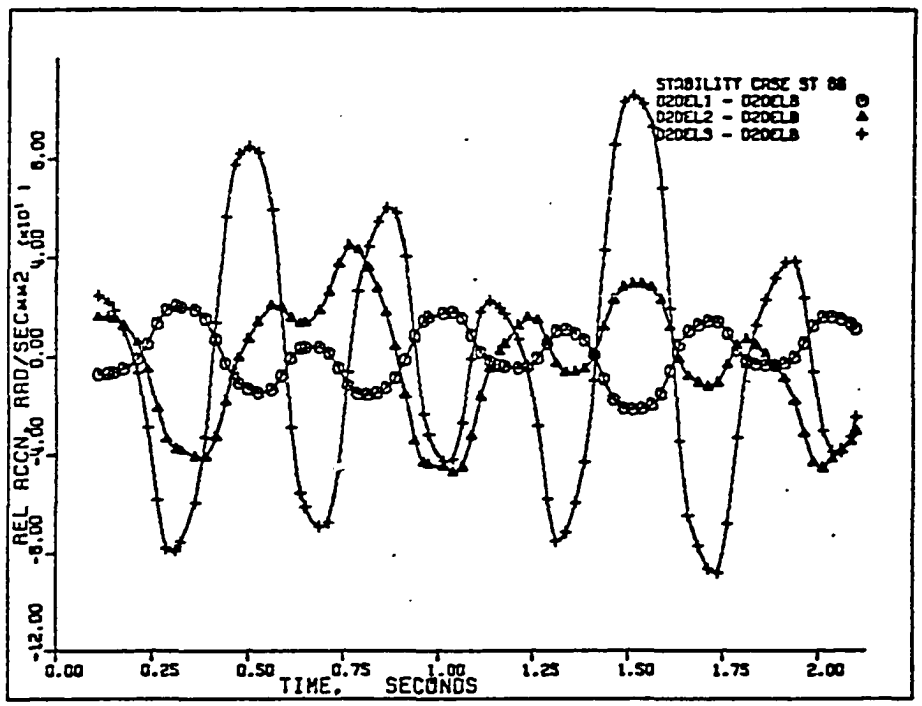

Figure 175. Case ST-66: relative accelerations $(\ddot{\delta}_1 - \ddot{\delta})$, $(\ddot{\delta}_2 - \ddot{\delta})$, and $(\ddot{\delta}_3 - \ddot{\delta})$.

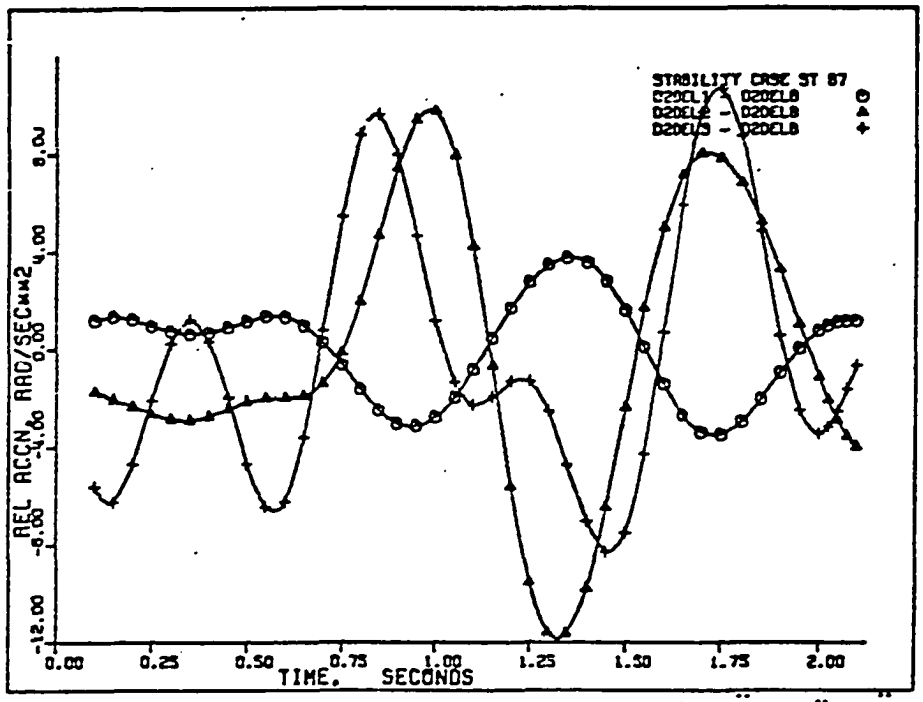

Figure 176. Case SE-67: relative accelerations $(\ddot{\delta}_1 - \ddot{\bar{\delta}})$, $(\ddot{\delta}_2 - \ddot{\bar{\delta}})$, and $(\ddot{\delta}_3 - \ddot{\bar{\delta}})$.

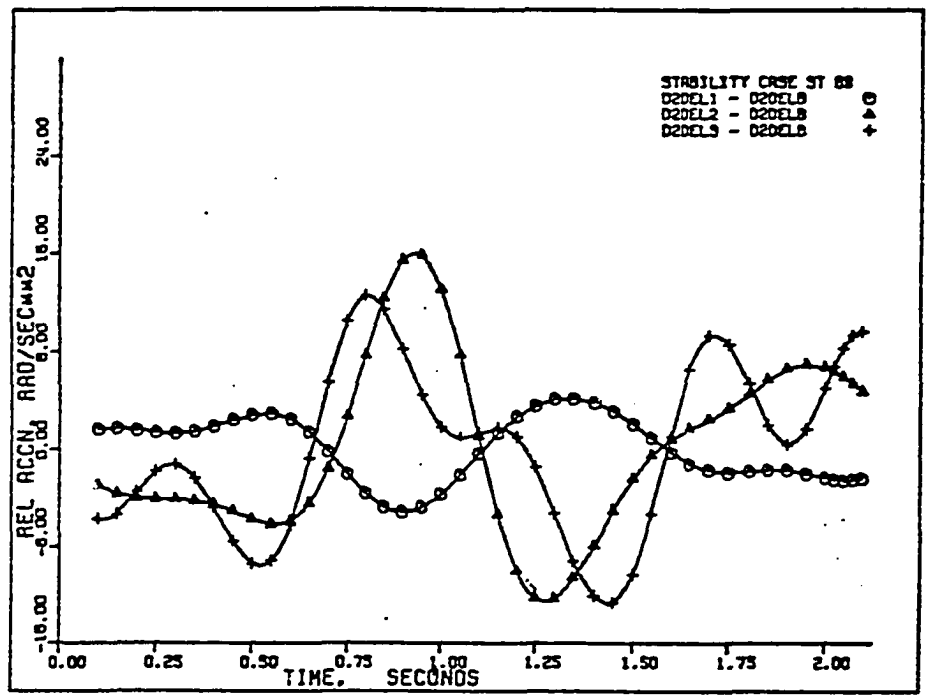

Figure 177. Case ST-69: relative accelerations $(\ddot{\delta}_1 - \ddot{\bar{\delta}})$, $(\ddot{\delta}_2 - \ddot{\bar{\delta}})$, and $(\ddot{\delta}_3 - \ddot{\bar{\delta}})$.

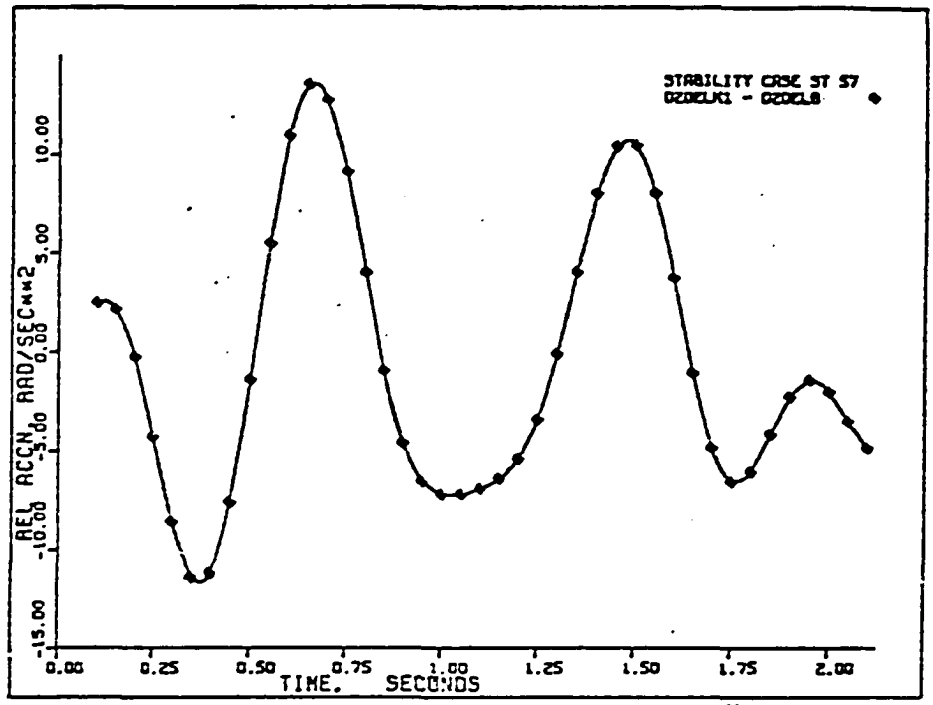

Figure 178. Case ST-57: relative acceleration $(\ddot{\delta}_k - \ddot{\bar{\delta}})$.

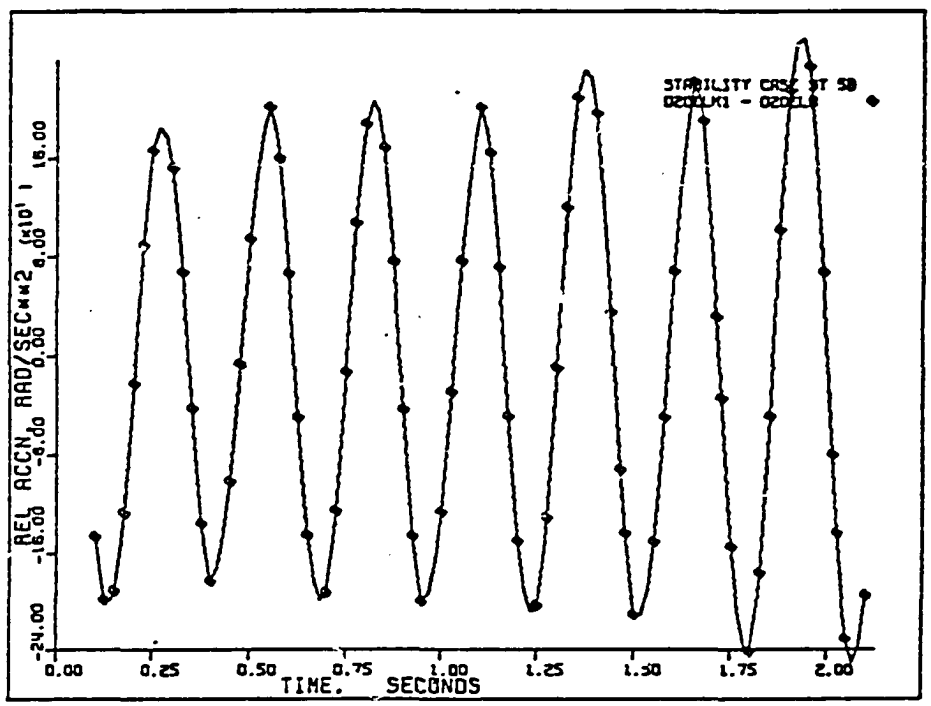

Figure 179. Case ST-58: relative acceleration $(\ddot{\delta}_k - \ddot{\bar{\delta}})$.

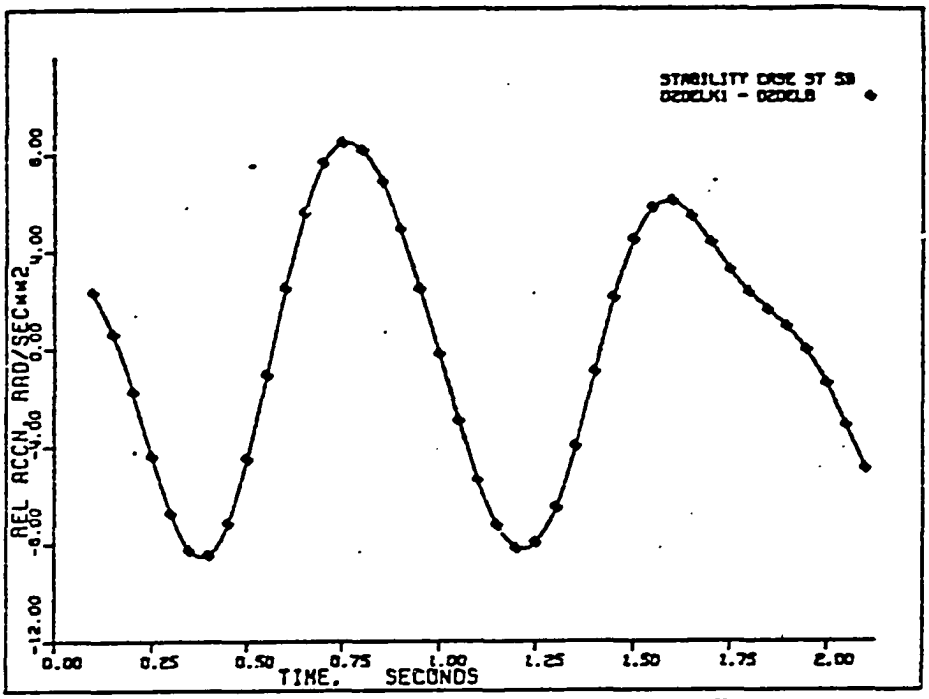

Figure 180. Case ST-59: relative acceleration $(\ddot{\delta}_k - \ddot{\bar{\delta}})$.

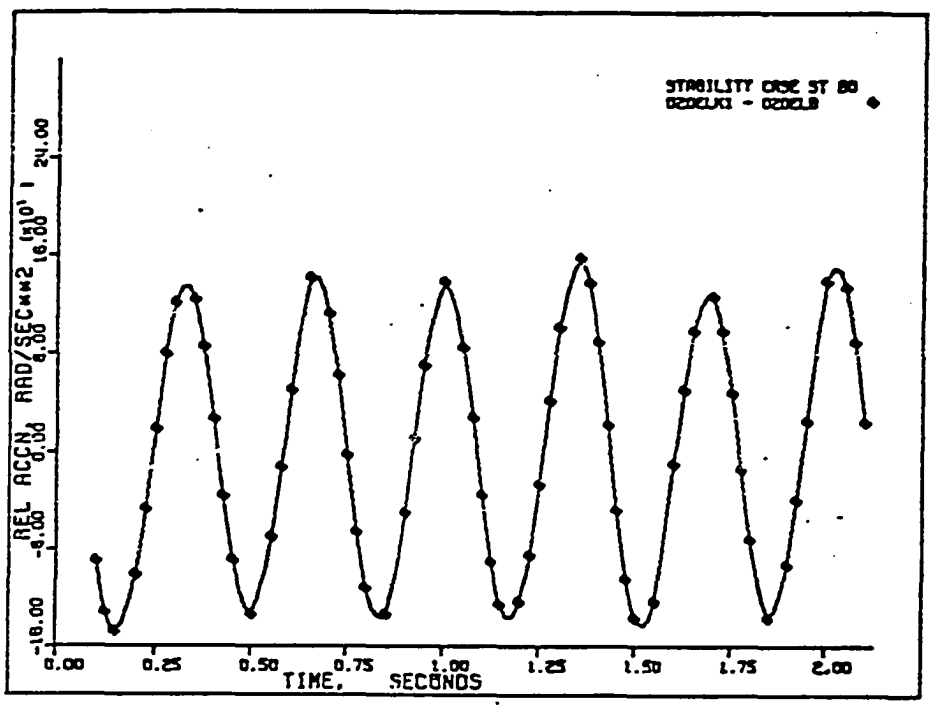

Figure 181. Case ST-60: relative acceleration $(\ddot{\delta}_k - \ddot{\bar{\delta}})$.

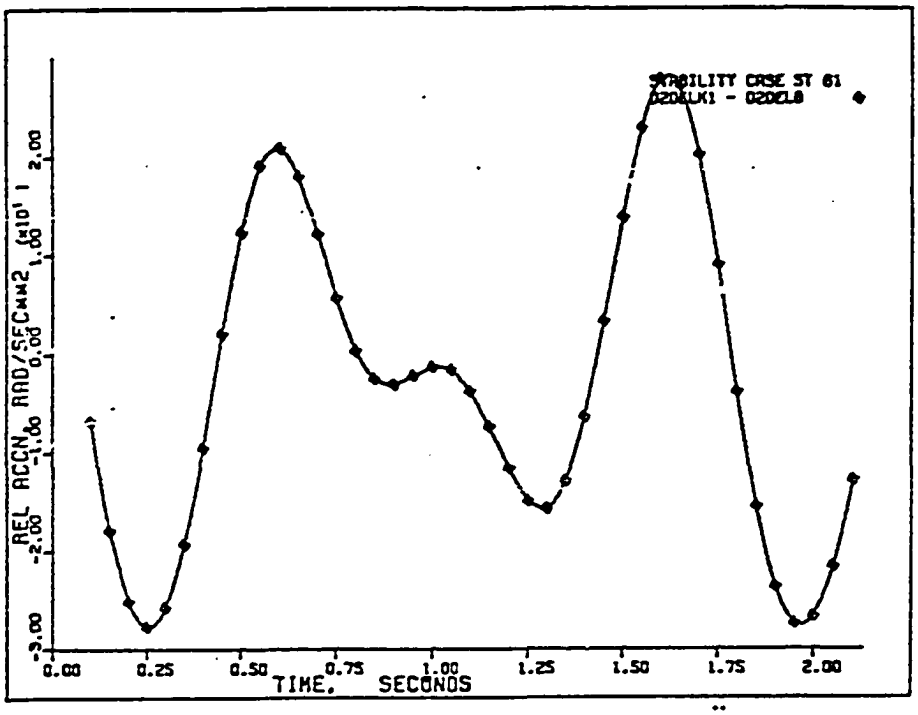

Figure 182. Case ST-61: relative acceleration $(\ddot{\delta}_k - \ddot{\delta})$.

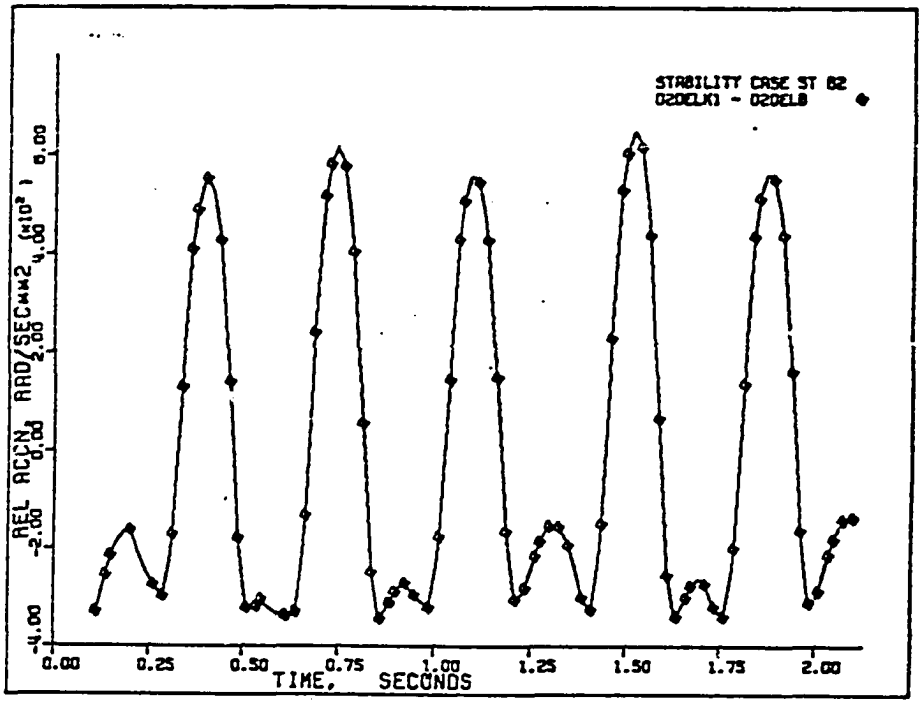

Figure 183. Case ST-62: relative acceleration $(\ddot{\delta}_k - \ddot{\delta})$.

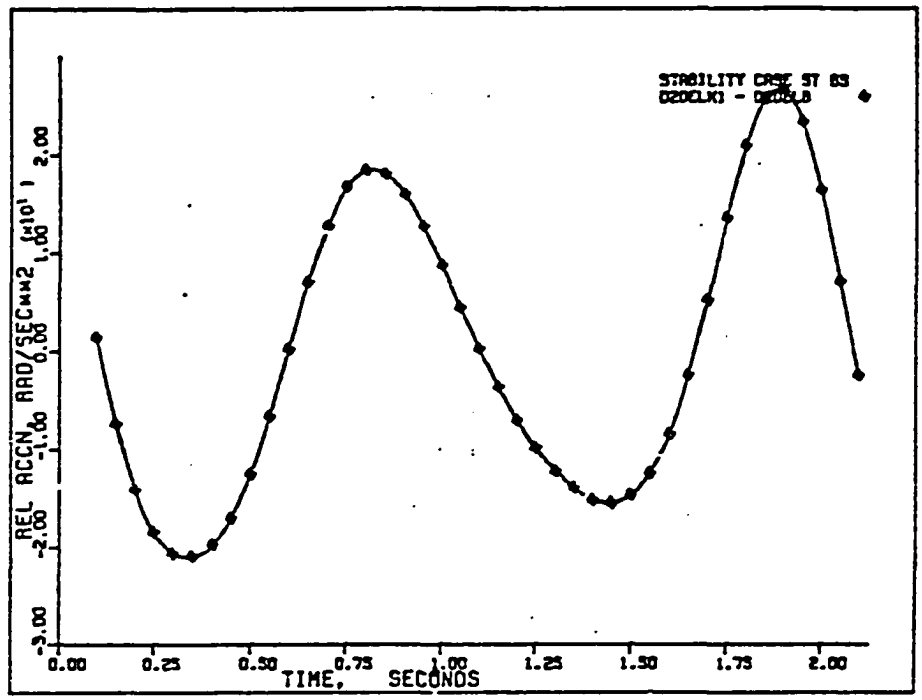

Figure 184. Case ST-63: relative acceleration $(\ddot{\delta}_k - \ddot{\delta})$.

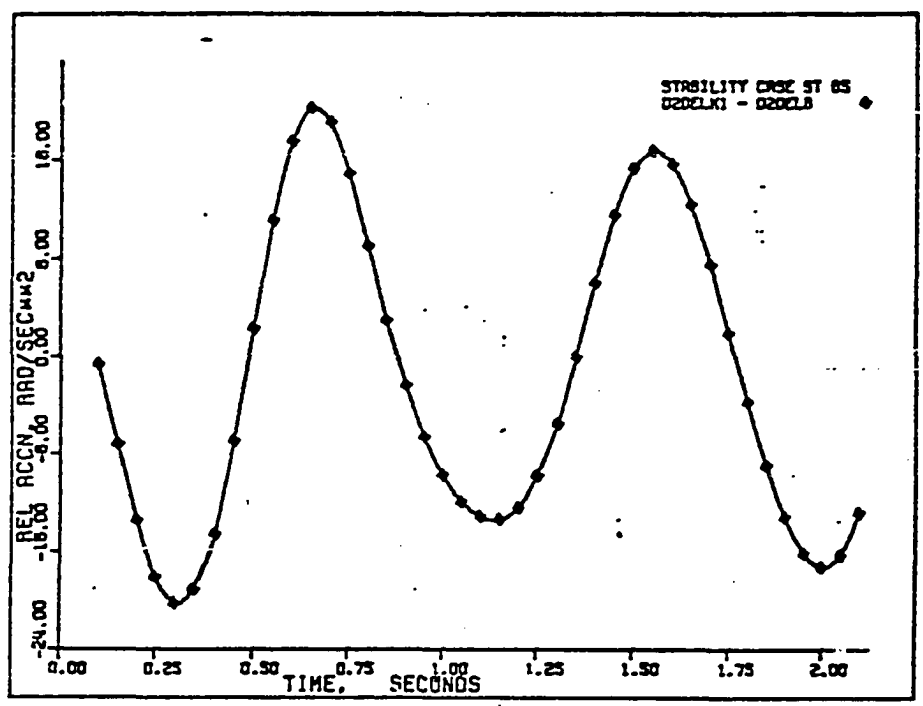

Figure 185. Case ST-65: relative acceleration $(\ddot{\delta}_k - \ddot{\delta})$.

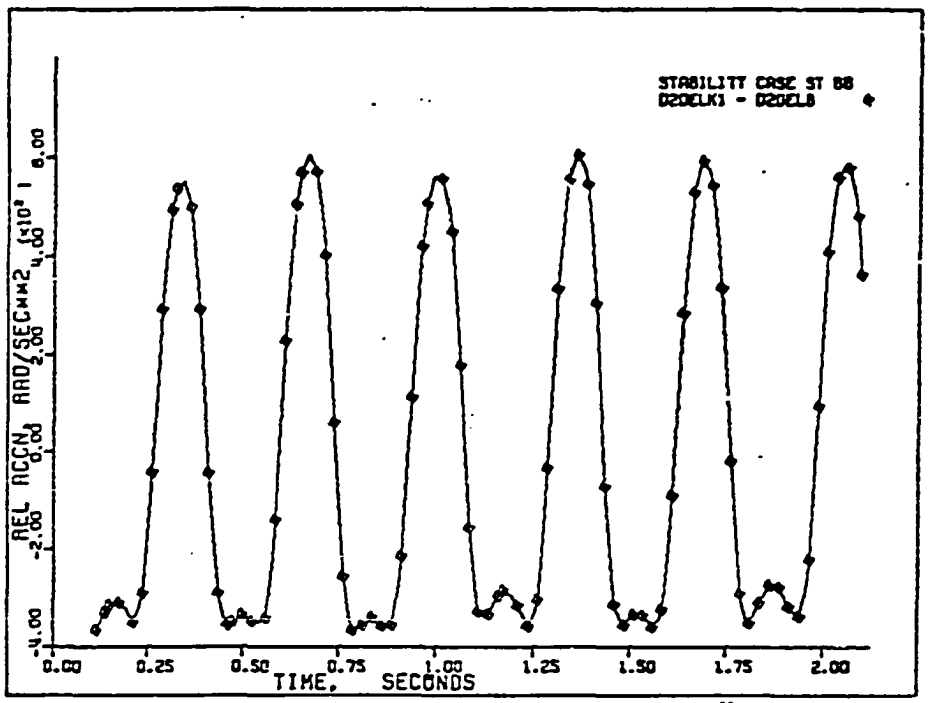

Figure 186. Case ST-66: relative acceleration $(\ddot{\delta}_k - \ddot{\bar{\delta}})$.

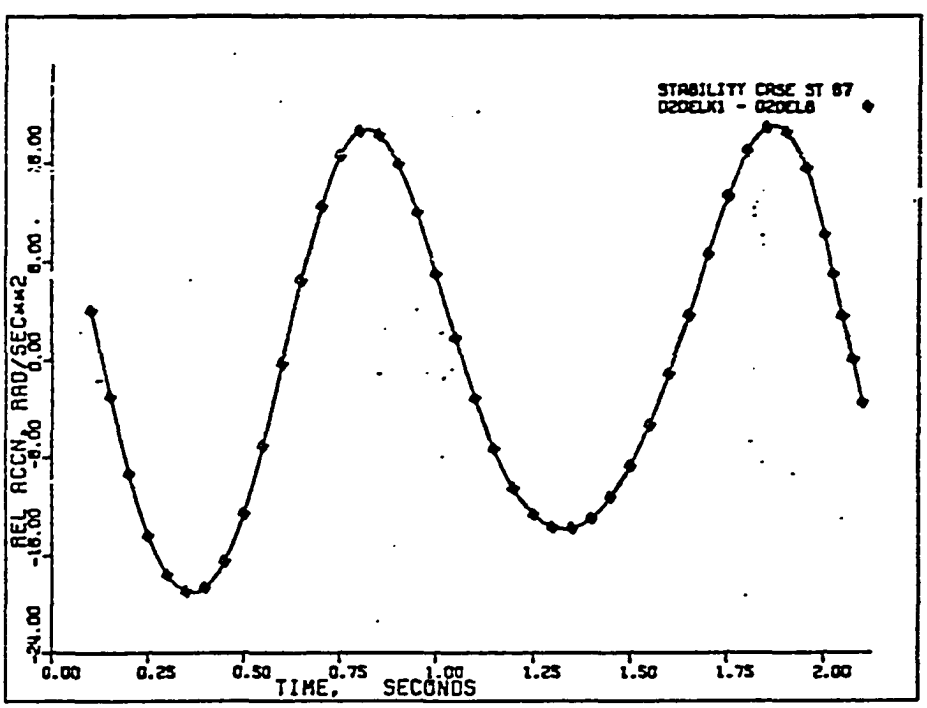

Figure 187. Case ST-67: relative acceleration $(\ddot{\delta}_k - \ddot{\bar{\delta}})$.

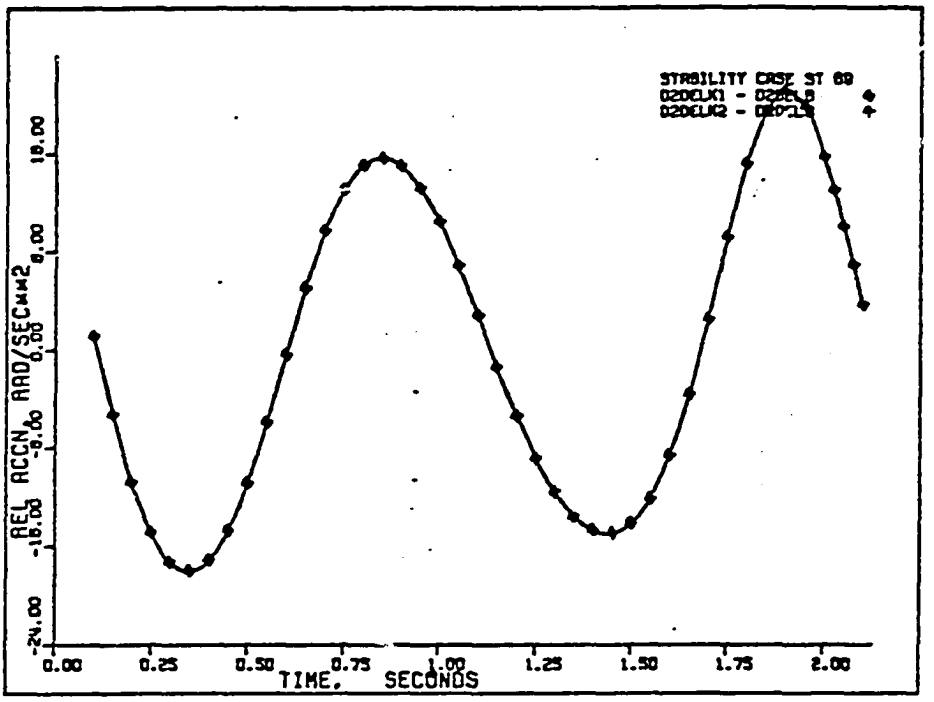

Figure 188. Case ST-69: relative accelerations $(\ddot{\delta}_{k1} - \ddot{\bar{\delta}})$ and $(\ddot{\delta}_{k2} - \ddot{\bar{\delta}})$.

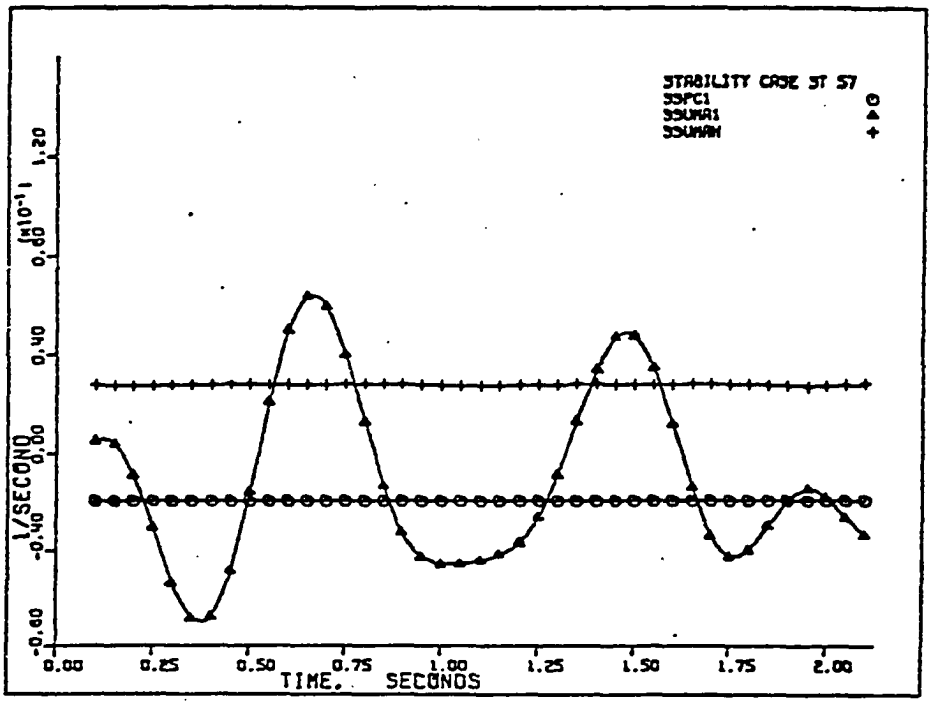

Figure 189. Case ST-57: terms of equation (4.10).

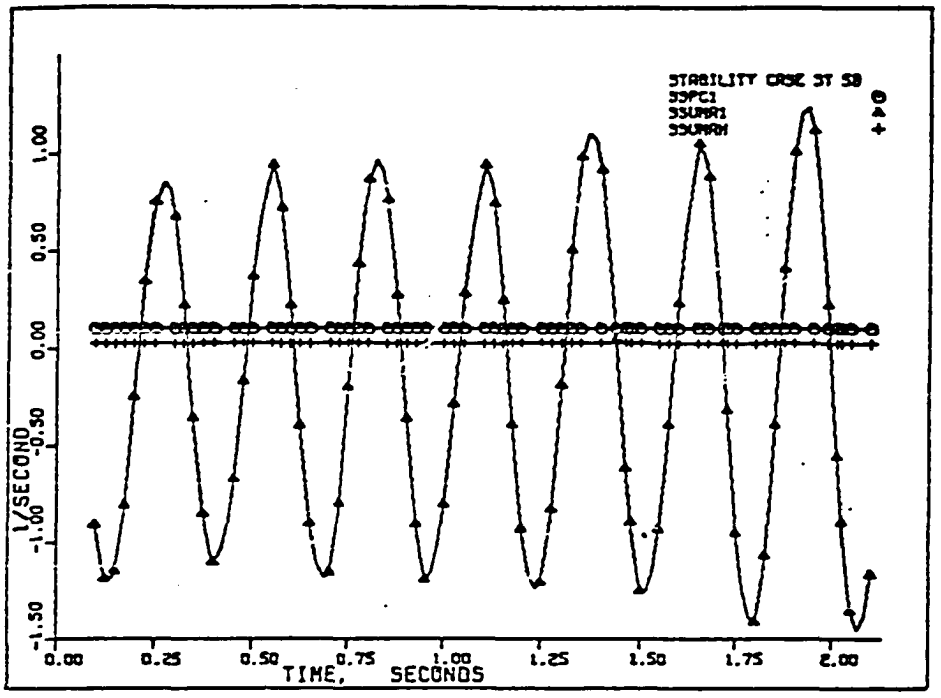

Figure 190. Case ST-58: terms of equation (4.10).

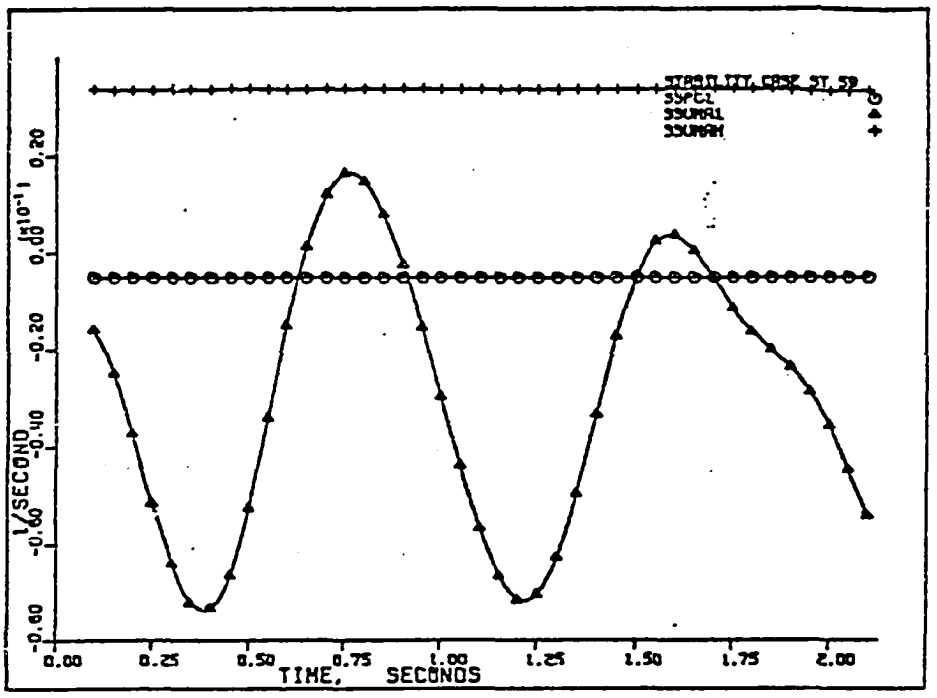

Figure 191. Case ST-59: terms of equation (4.10).

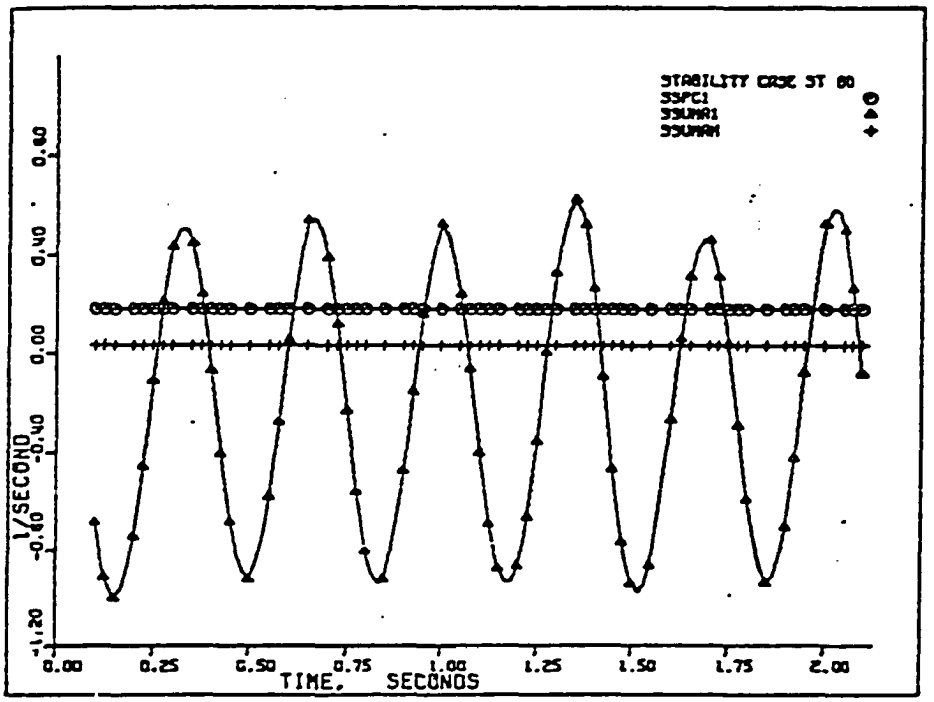

Figure 192. Case ST-60: terms of equation (4.10).

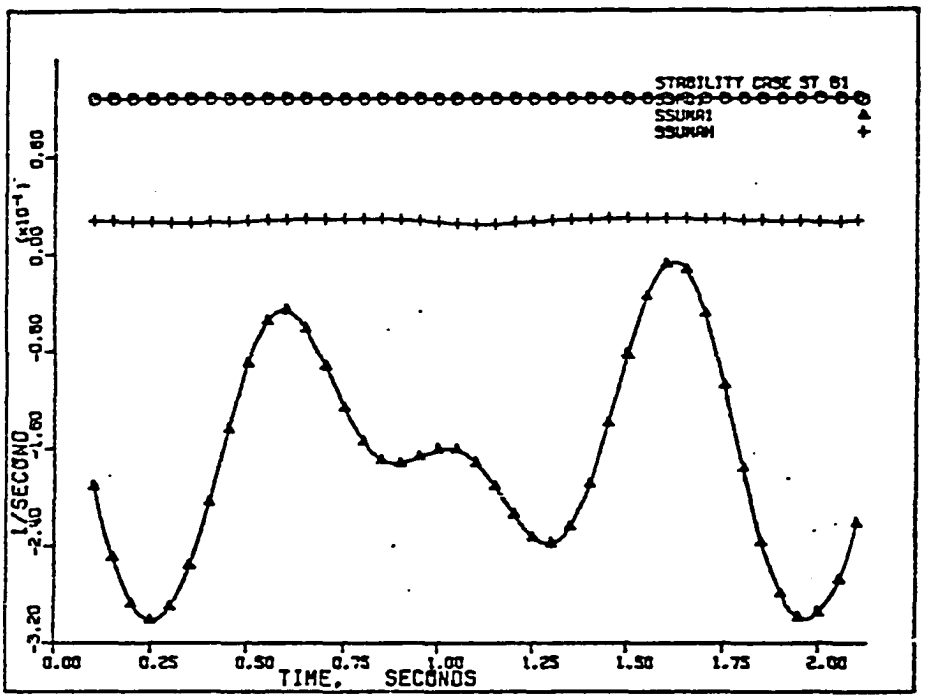

Figure 193. Case ST-61: terms of equation (4.10).

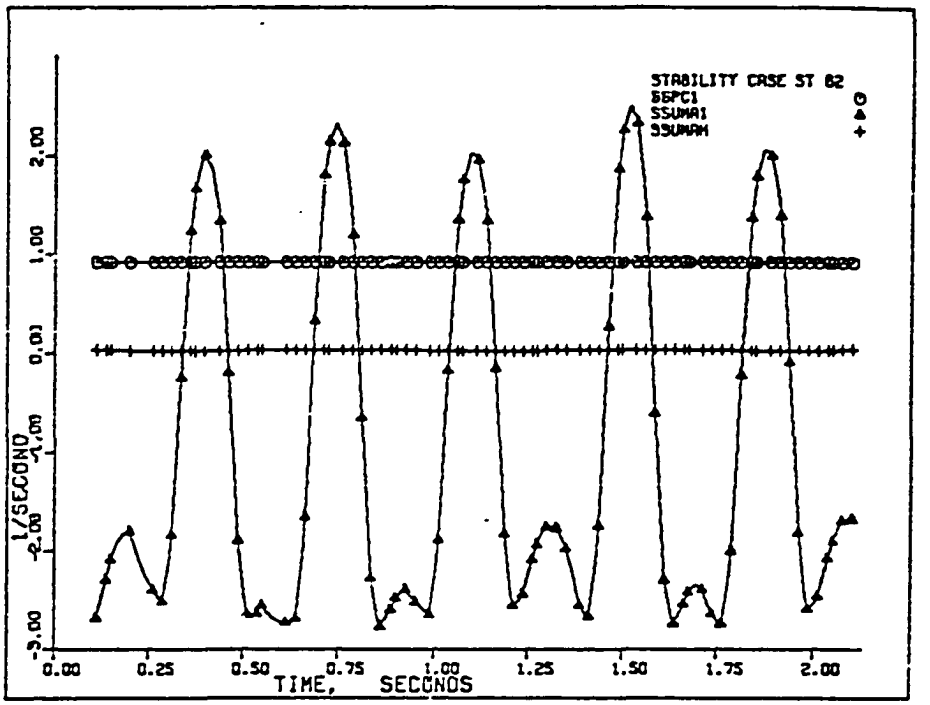

Figure 194. Case ST-62: terms of equation (4.10).

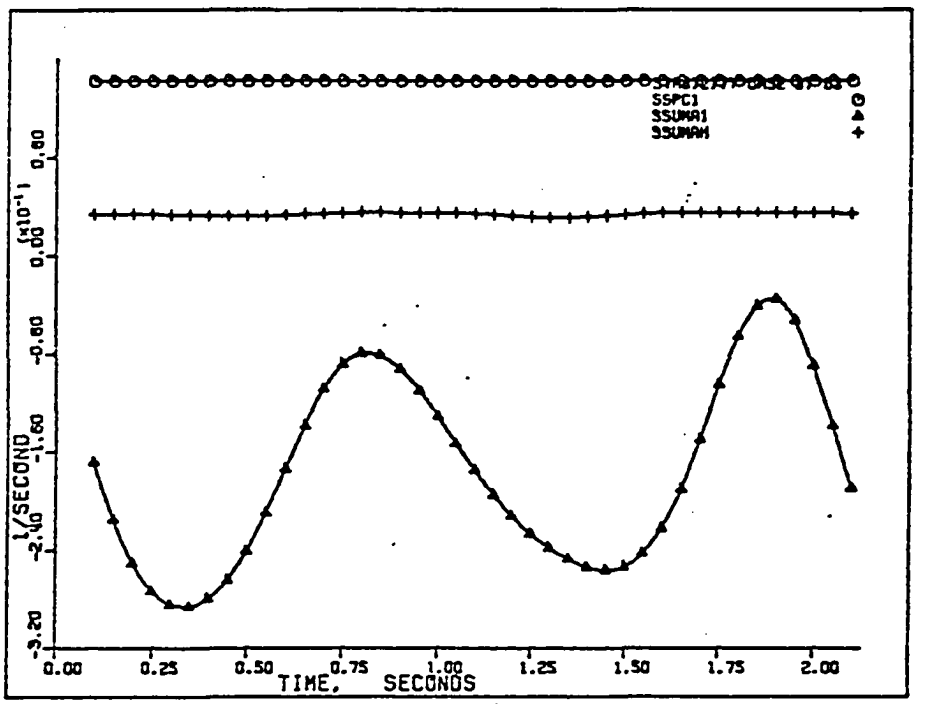

Figure 195. Case ST-63: terms of equation (4.10).

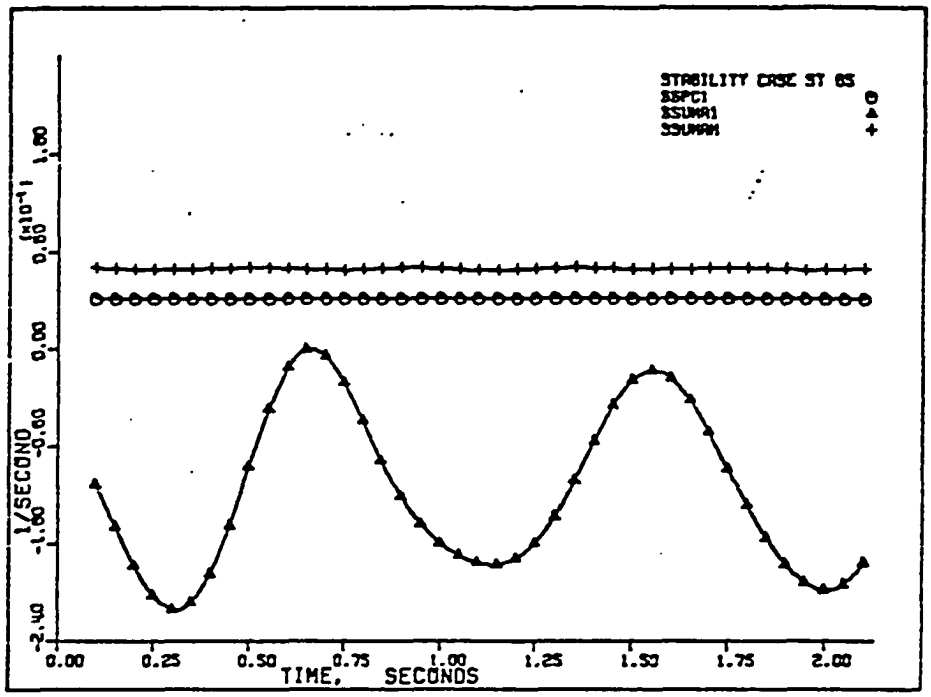

Figure 196. Case ST-65: terms of equation (4.10).

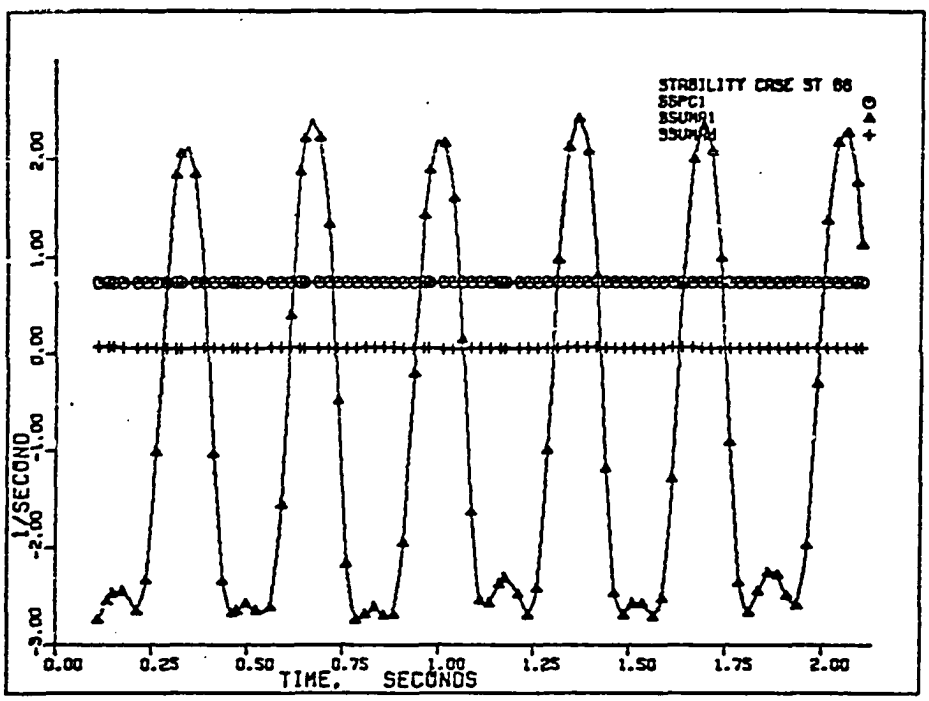

Figure 197. Case ST-66: terms of equation (4.10).

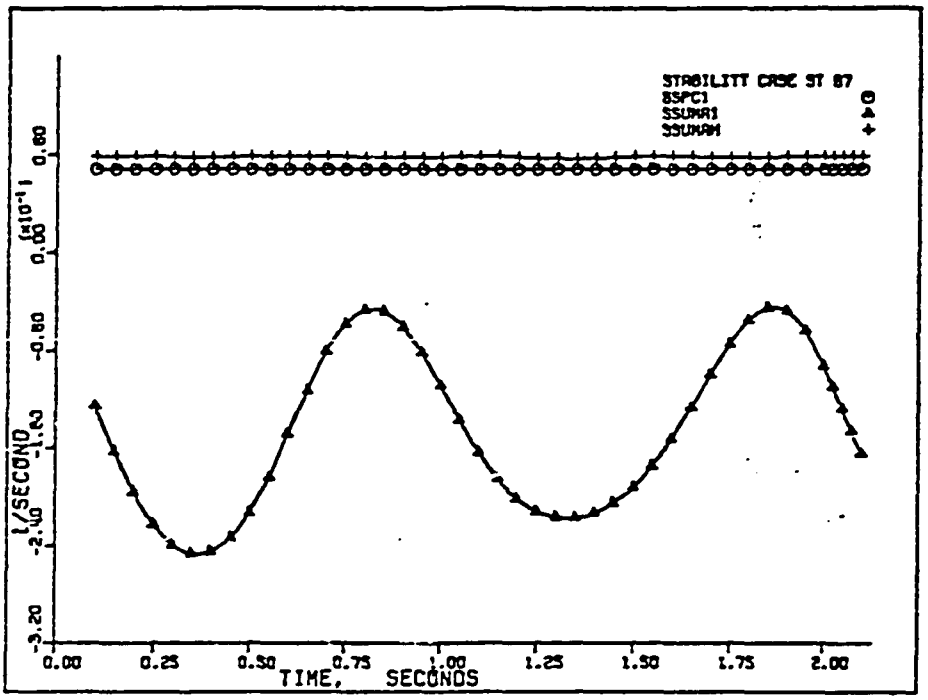

Figure 198. Case ST-67: terms of equation (4.10).

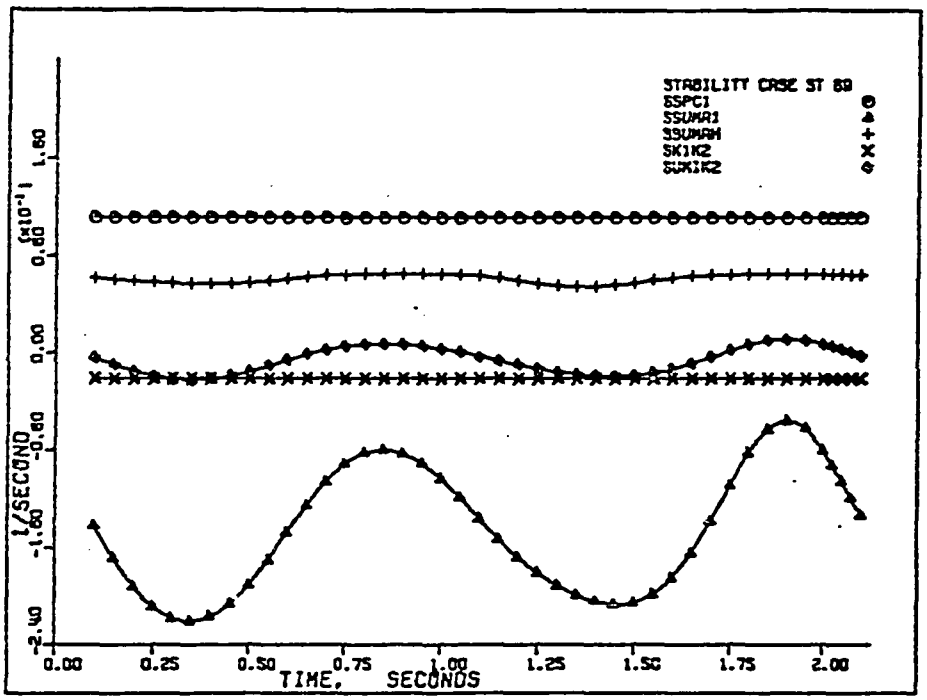

Figure 199. Case ST-69: terms of equation (4.13).

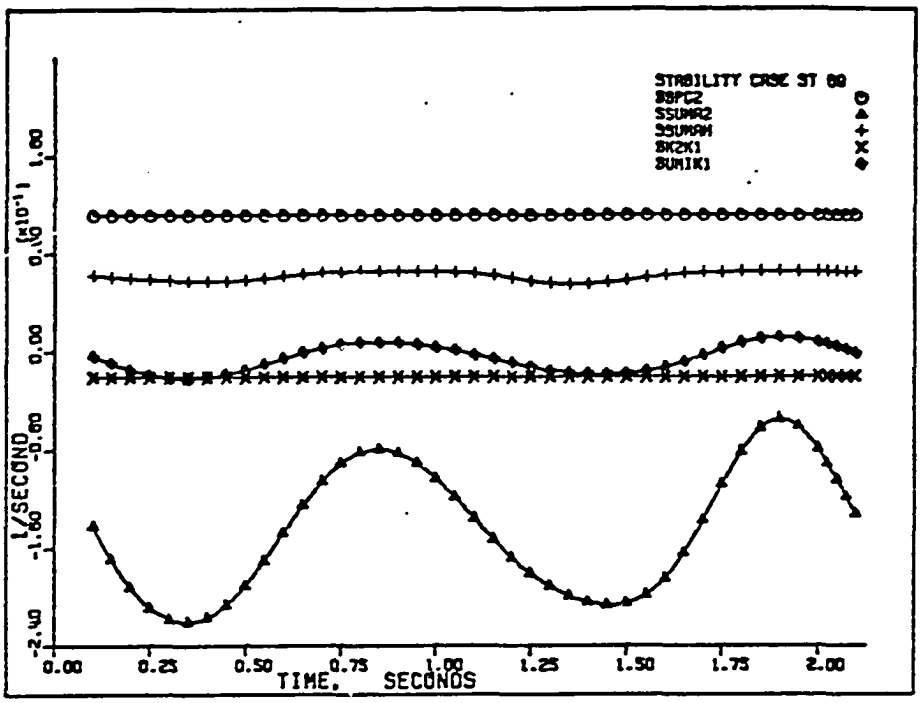

Figure 200. Case ST-69: terms of equation (4.14).

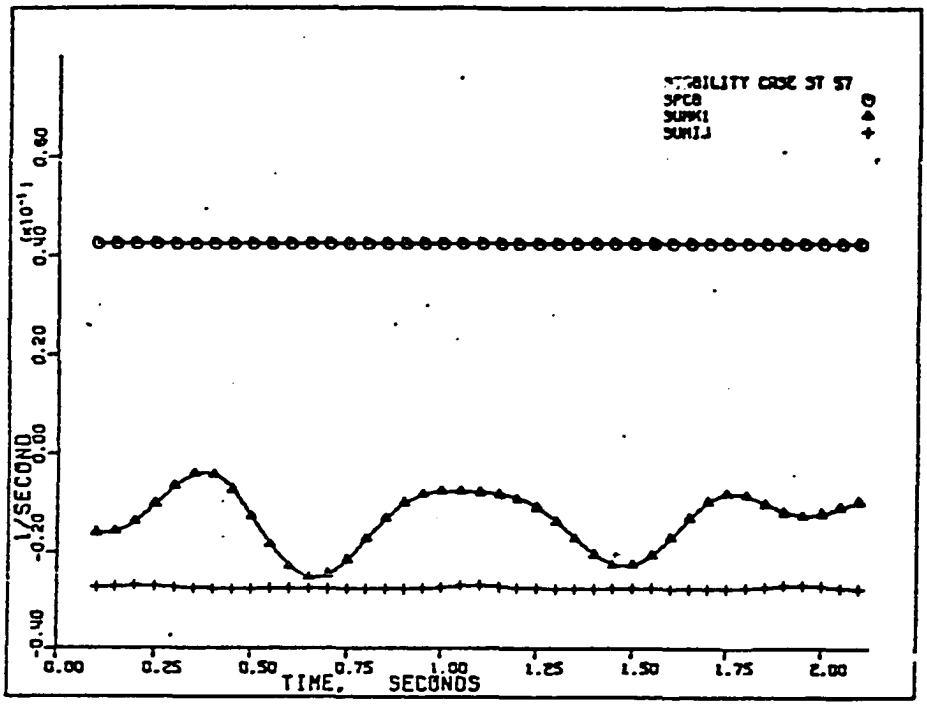

Figure 201. Case ST-57: terms of equation (4.5).

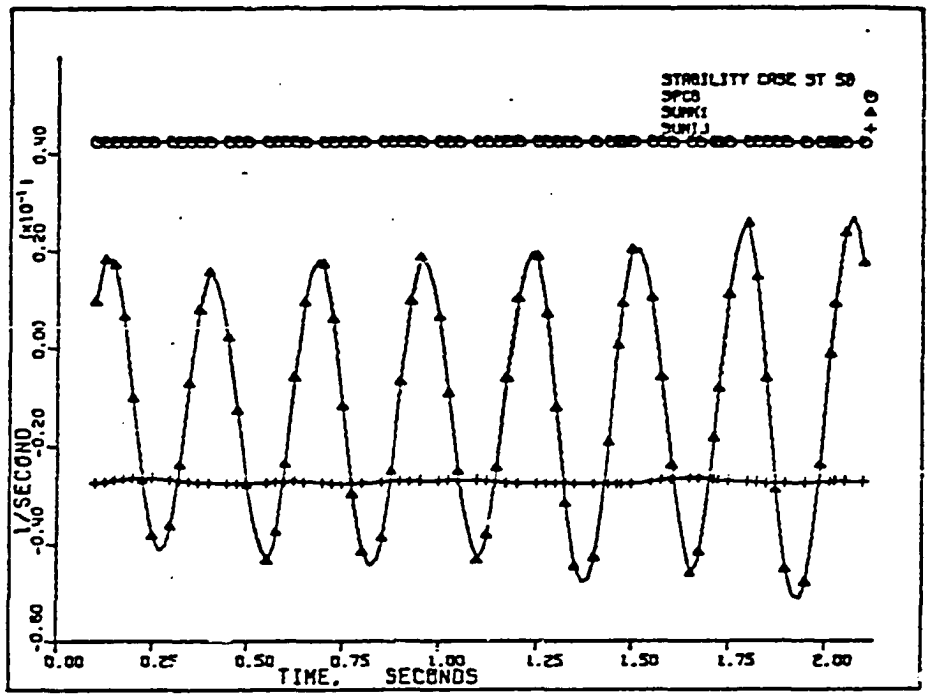

Figure 202. Case ST-58: terms of equation (4.5).

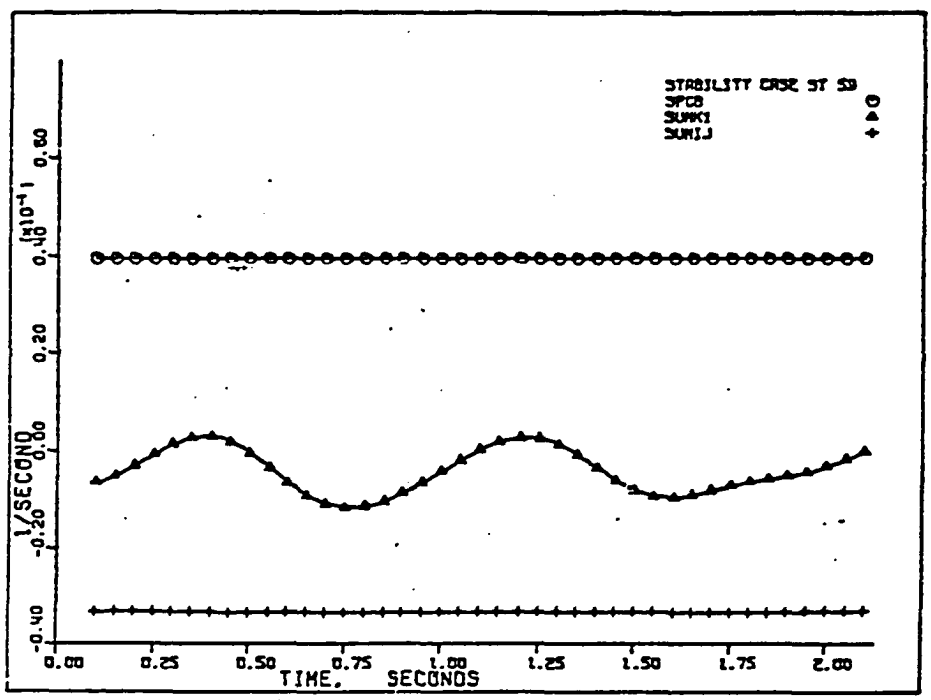

Figure 203. Case ST-59: terms of equation (4.5).

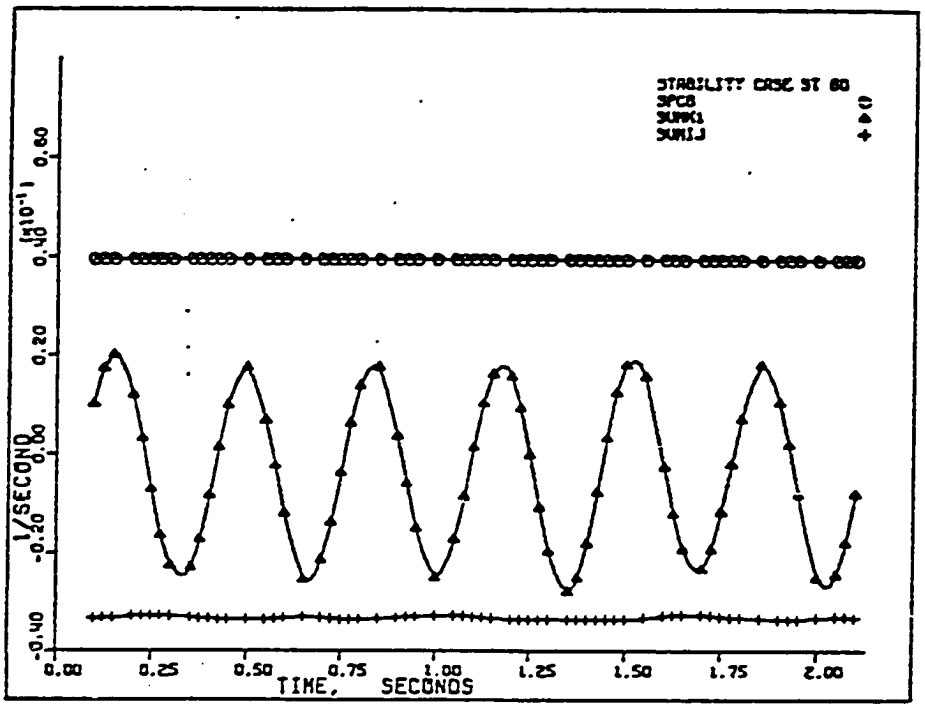

Figure 204. Case ST-60: terms of equation (4.5).

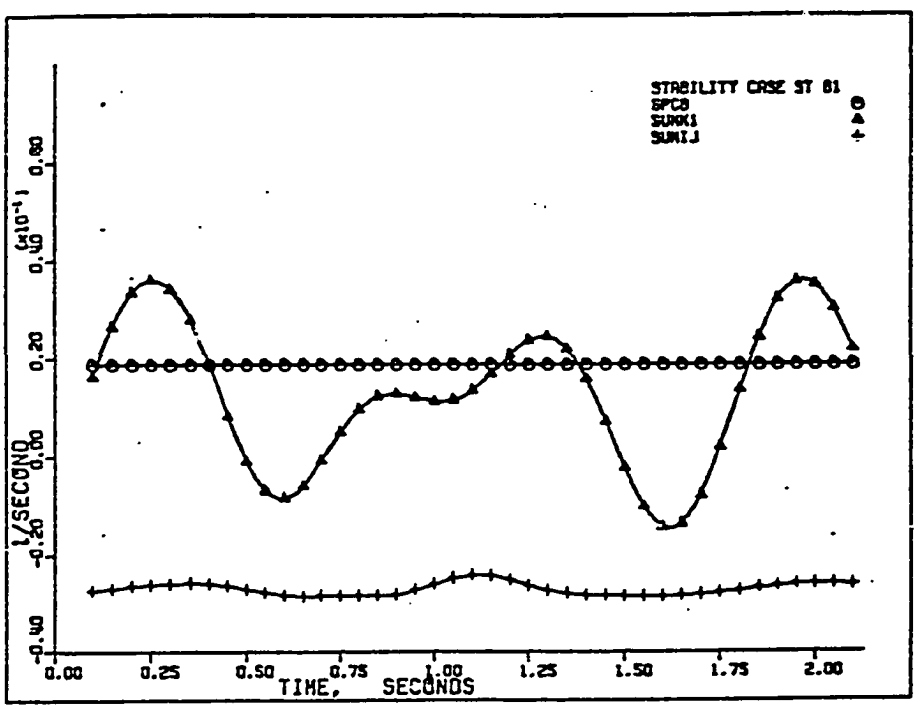

Figure 205. Case ST-61: terms of equation (4.5).

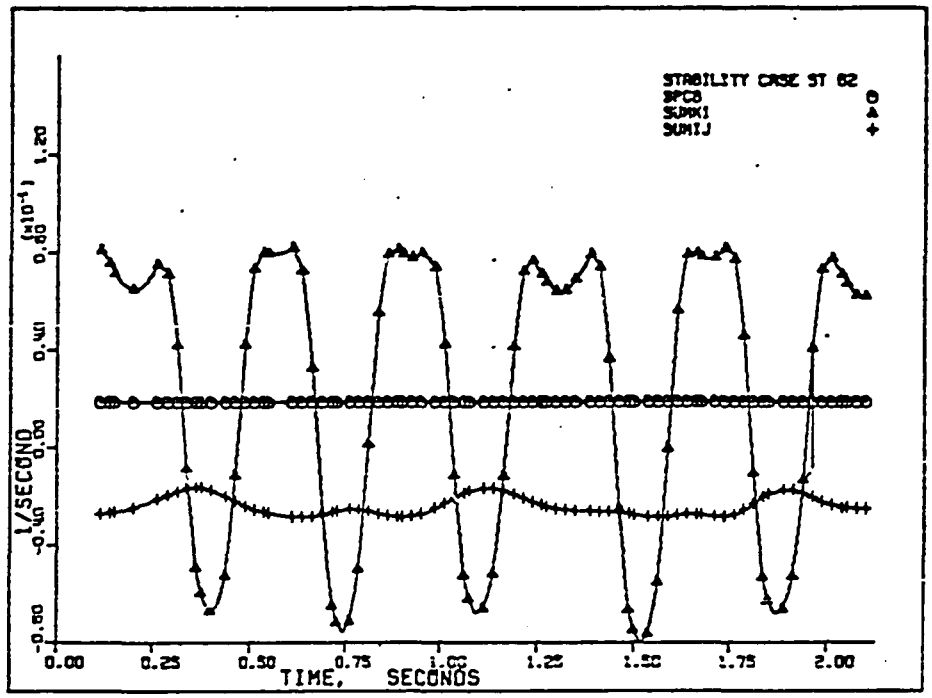

Figure 206. Case ST-62: terms of equation (4.5).

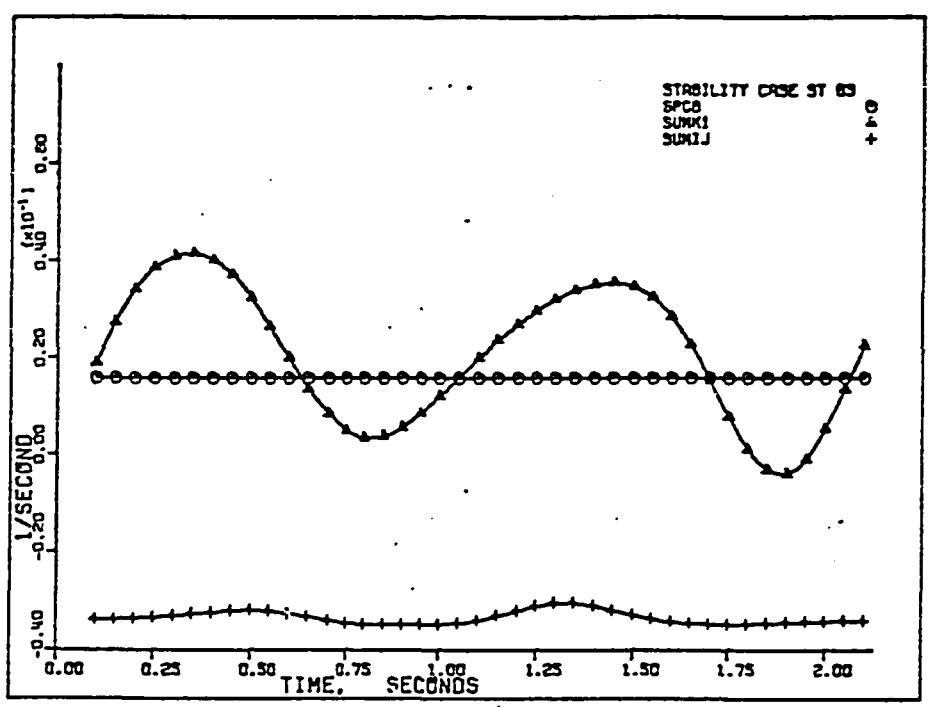

Figure 207. Case ST-63: terms of equation (4.5).

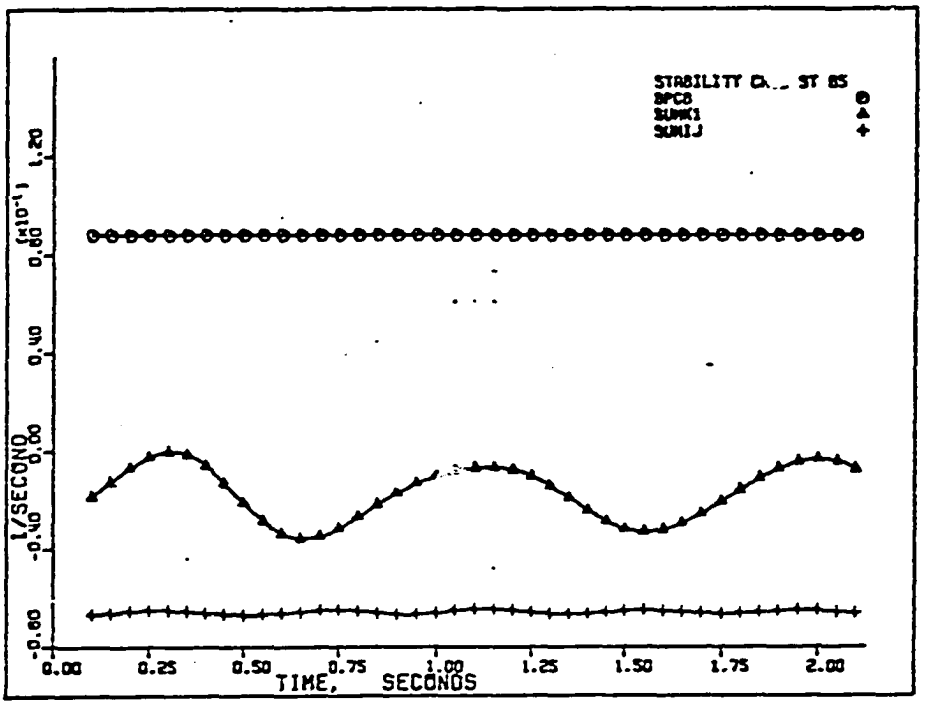

Figure 208. Case ST-65: terms of equation (4.5).

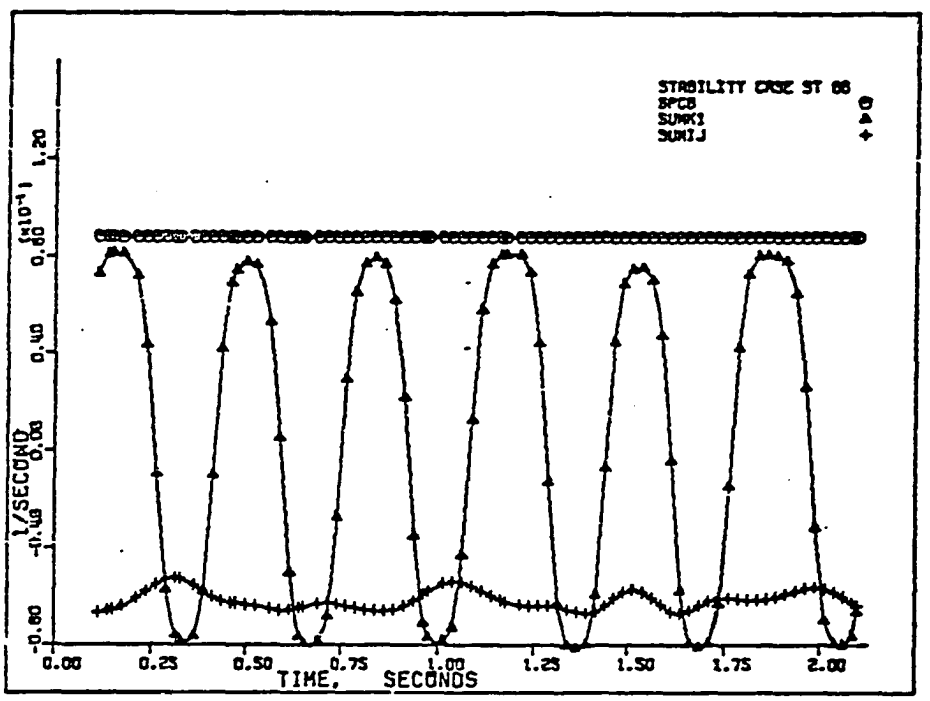

Figure 209. Case ST-66: terms of equation (4.5).

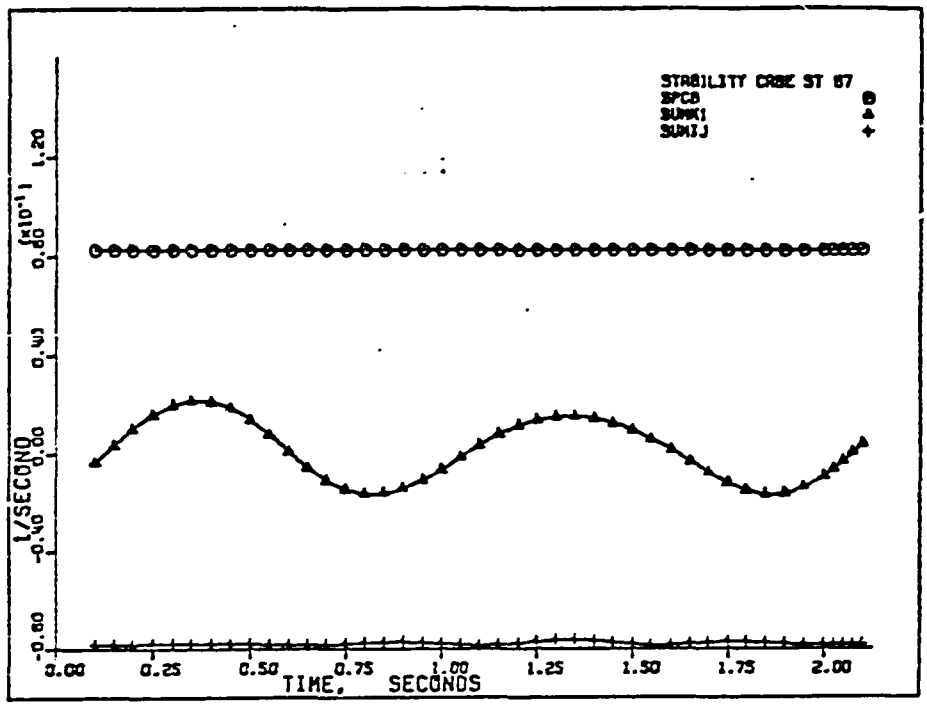

Figure 210. Case ST-67: terms of equation (4.5).

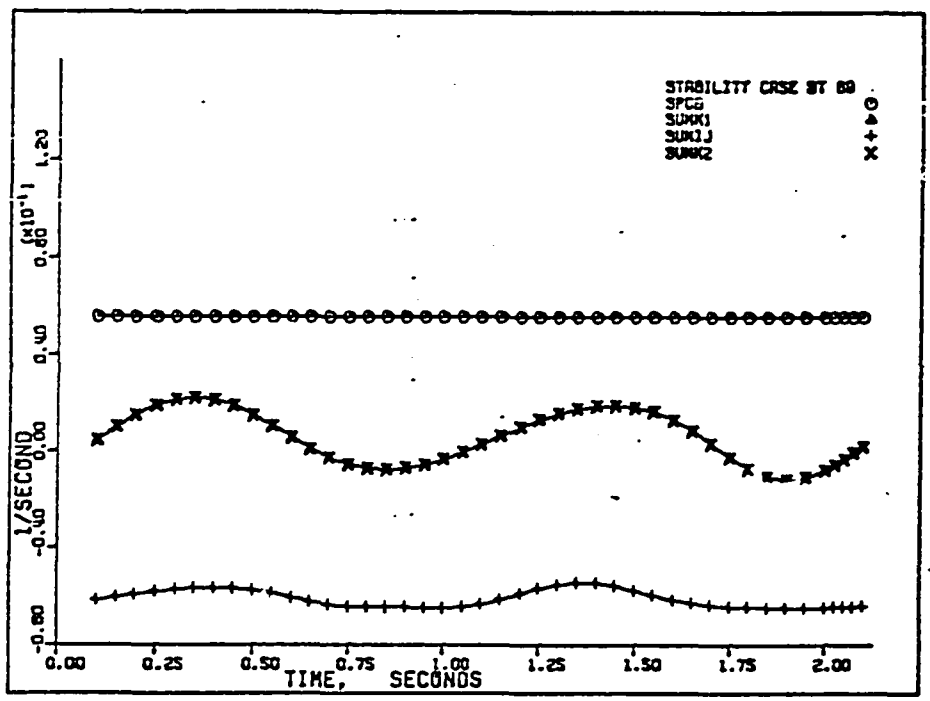

Figure 211. Case ST-69: terms of equation (4.12).

XVII. APPENDIX G: OUTPUT OF STABILITY ANALYSIS COMPUTER PROGRAM FOR REMOTE SYNCHRONOUS GENERATION - FAULTS LOCATED INSIDE THE EXISTING SYSTEM (SR-SERIES)

This series of runs (SR-series) is similar to the original ST-series (Cases ST-1 through ST-36); the only difference is the fault location. In the SR-series, faults are located inside the existing power network rather than in the transmission line joining the remote generation to the existing network as in the ST-series. The complete list of these runs is listed in Table 8. The output of STANAL computer program for the selected cases in this series is shown via Figures 212 through 451. The variables chosen for demonstration in this series are listed below.

1. Angles δ_1, δ_2, δ_3, and $\bar{\delta}$ (Figures 212 through 235).
2. Angles δ_k and $\bar{\delta}$ (Figures 236 through 259).
3. Relative angles $(\delta_1 - \bar{\delta})$, $(\delta_2 - \bar{\delta})$, and $(\delta_3 - \bar{\delta})$ (Figures 260 through 283).
4. Relative angle $(\delta_k - \bar{\delta})$ (Figures 284 through 307).
5. Accelerations $\ddot{\delta}_1$, $\ddot{\delta}_2$, $\ddot{\delta}_3$, and $\ddot{\bar{\delta}}$ (Figures 308 through 331).
6. Accelerations $\ddot{\delta}_k$ and $\ddot{\bar{\delta}}$ (Figures 332 through 355).
7. Relative accelerations $(\ddot{\delta}_1 - \ddot{\bar{\delta}})$, $(\ddot{\delta}_2 - \ddot{\bar{\delta}})$, and $(\ddot{\delta}_3 - \ddot{\bar{\delta}})$ (Figures 356 through 379).
8. Relative acceleration $(\ddot{\delta}_k - \ddot{\bar{\delta}})$ (Figures 380-403).

9. Terms of equation (4.10) (Figures 404-427):

$$SSPC = \frac{P_{ck}}{H_k} - \frac{1}{H} \sum_{i=1}^{n} P_{ci} ,$$

$$SSUMA = - \sum_{j=1}^{n} \left[\frac{1}{H_k} A_{kj} \cos (\theta_{kj} - \delta_{kj}) + \frac{1}{H} A_{kj} \cos (\theta_{kj} + \delta_{kj}) \right] ,$$

$$SSUMAH = \sum_{i=1}^{n-1} \sum_{j=i+1}^{n} \frac{2}{H} \hat{A}_{ij} \cos \delta_{ij} .$$

10. Terms of equation (4.5) (Figures 428-451):

$$SPCB = \frac{1}{H} \sum_{i=1}^{n} P_{ci} ,$$

$$SUMK = - \frac{1}{H} \sum_{i=1}^{n} A_{ij} \cos (\theta_{ij} - \delta_{ij}) ,$$

$$SUMIJ = - \frac{1}{H} \sum_{i=1}^{n} \sum_{\substack{j=1 \\ j \neq i}}^{n} A_{ij} \cos (\theta_{ij} - \delta_{ij}) .$$

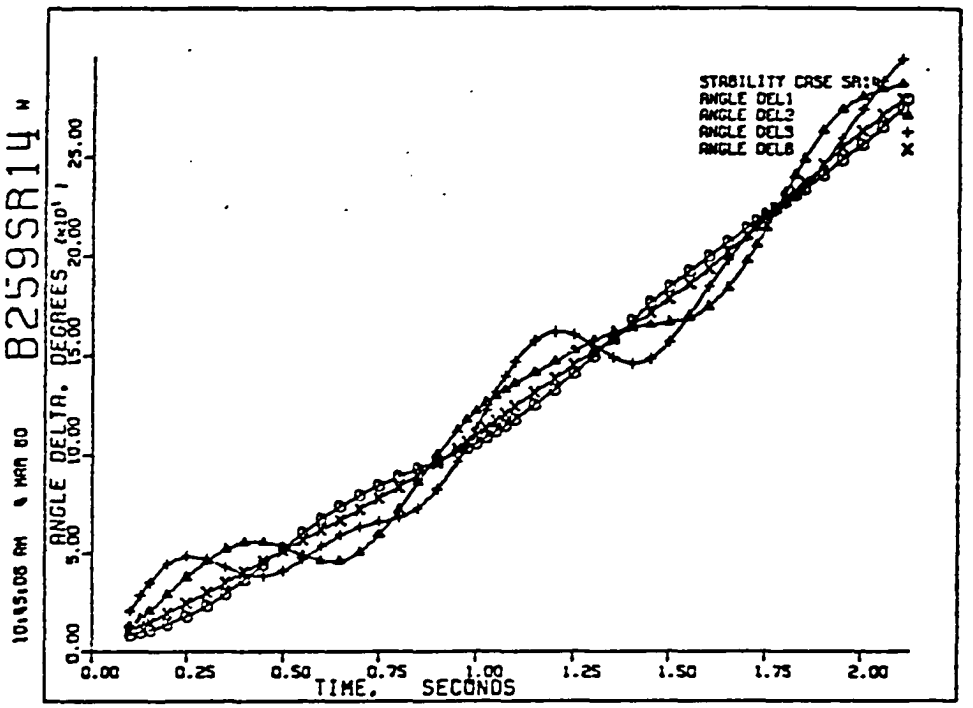

Figure 212. Case SR-14: angles δ_1, δ_2, δ_3, and $\bar{\delta}$.

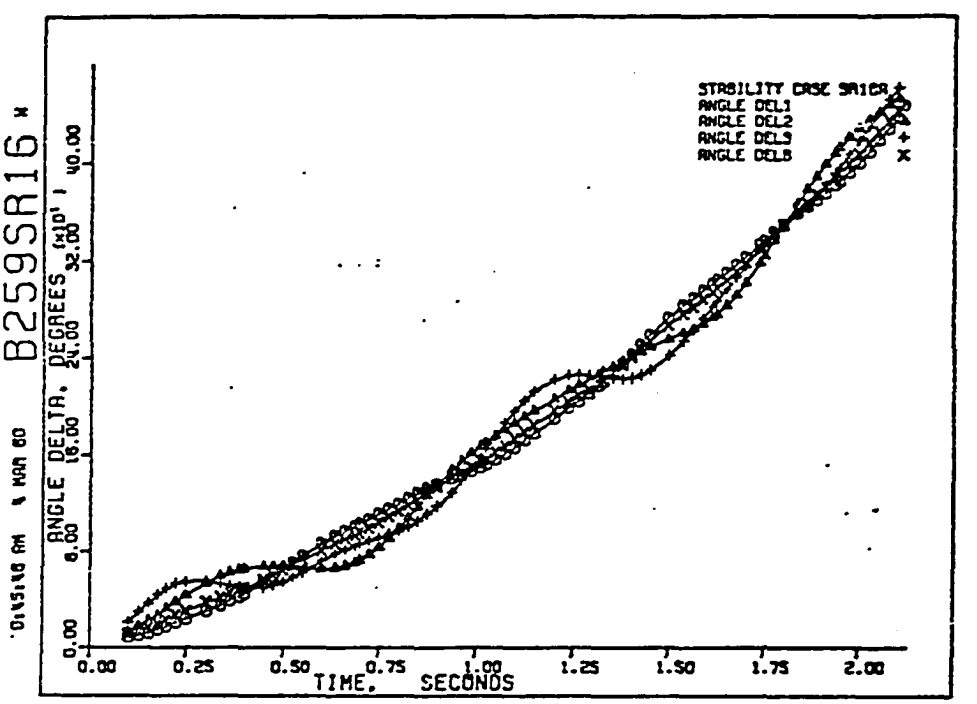

Figure 213. Case SR-16A: angles δ_1, δ_2, δ_3, and $\bar{\delta}$.

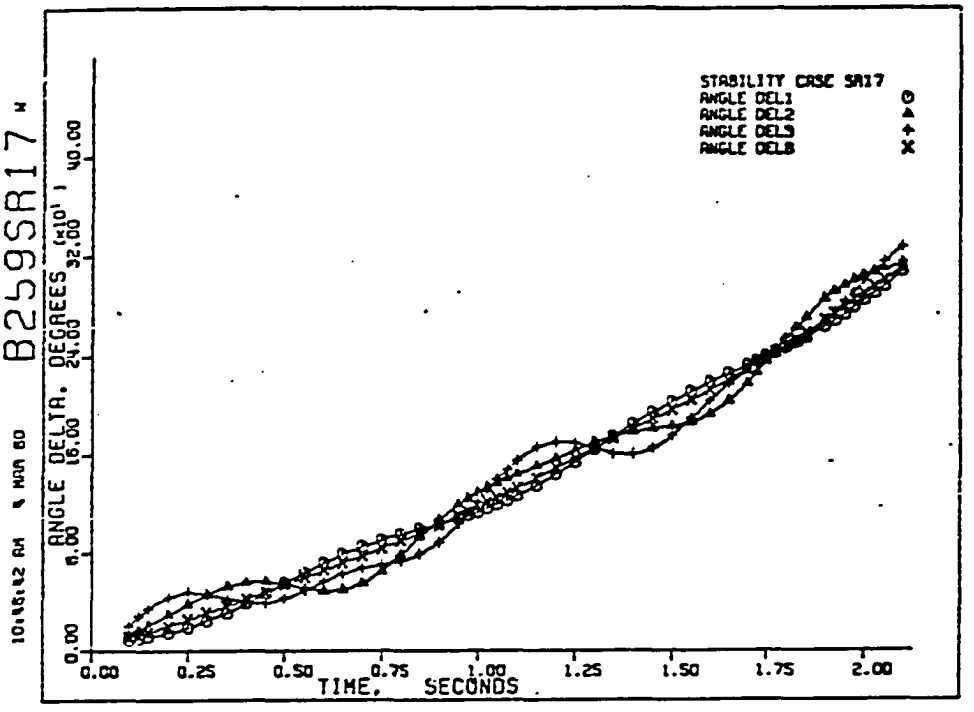

Figure 214. Case SR-17: angles δ_1, δ_2, δ_3, and $\bar{\delta}$.

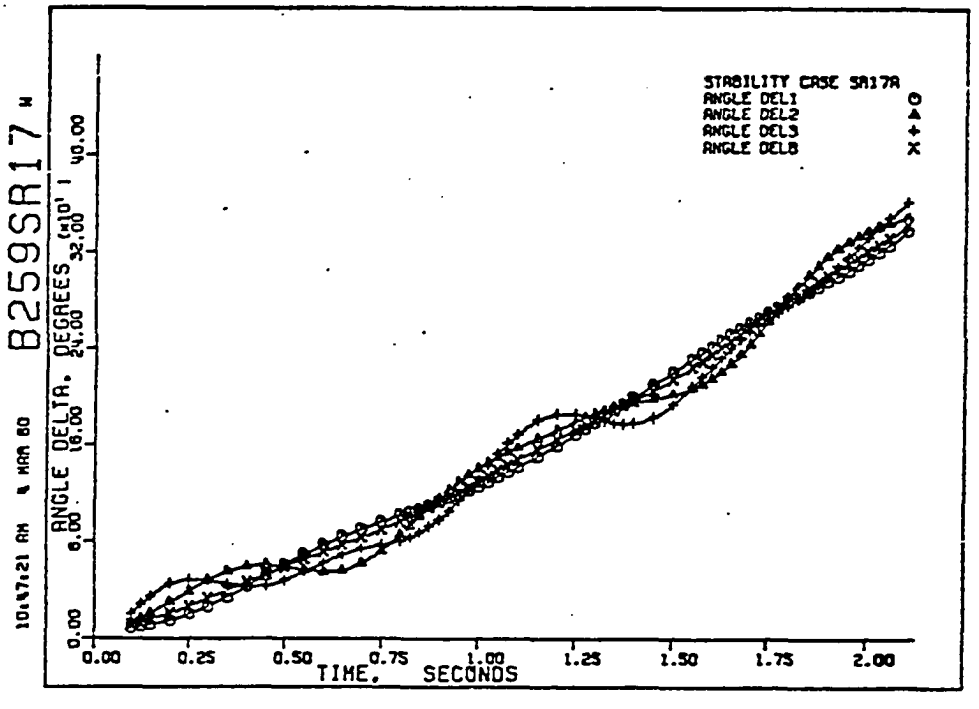

Figure 215. Case SR-17A: angles δ_1, δ_2, δ_3, and $\bar{\delta}$.

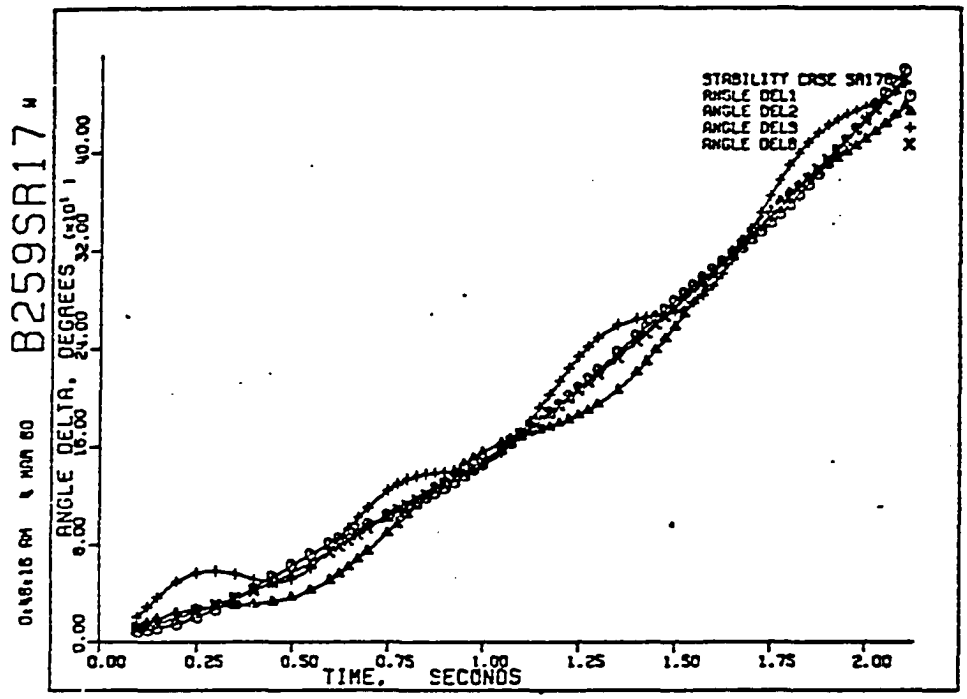

Figure 216. Case SR-17B: angles δ_1, δ_2, δ_3, and $\bar{\delta}$.

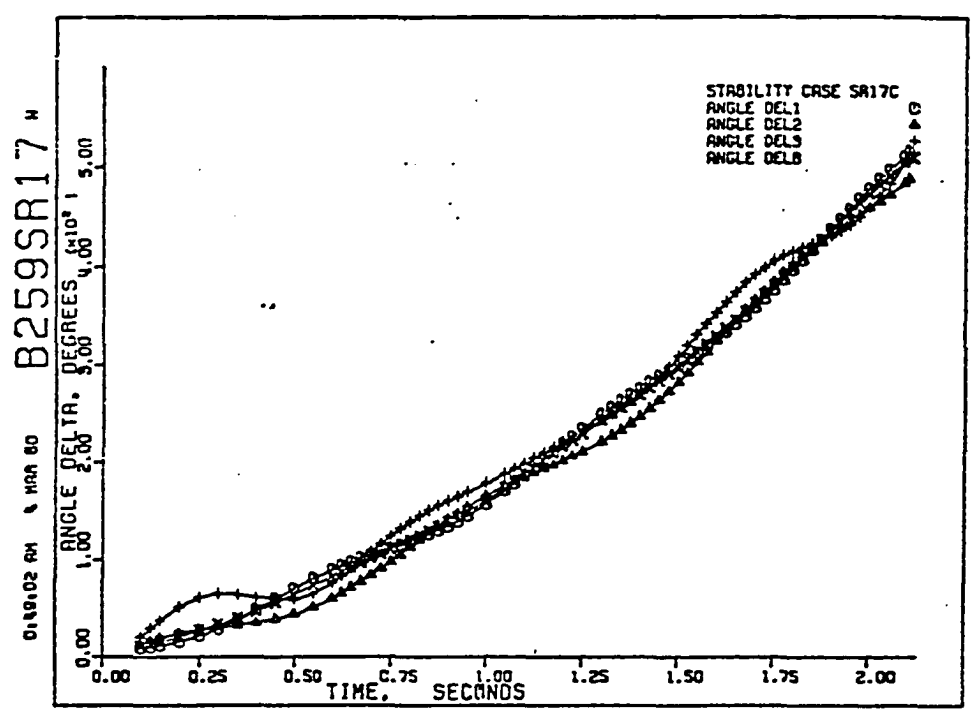

Figure 217. Case SR-17C: angles δ_1, δ_2, δ_3, and $\bar{\delta}$.

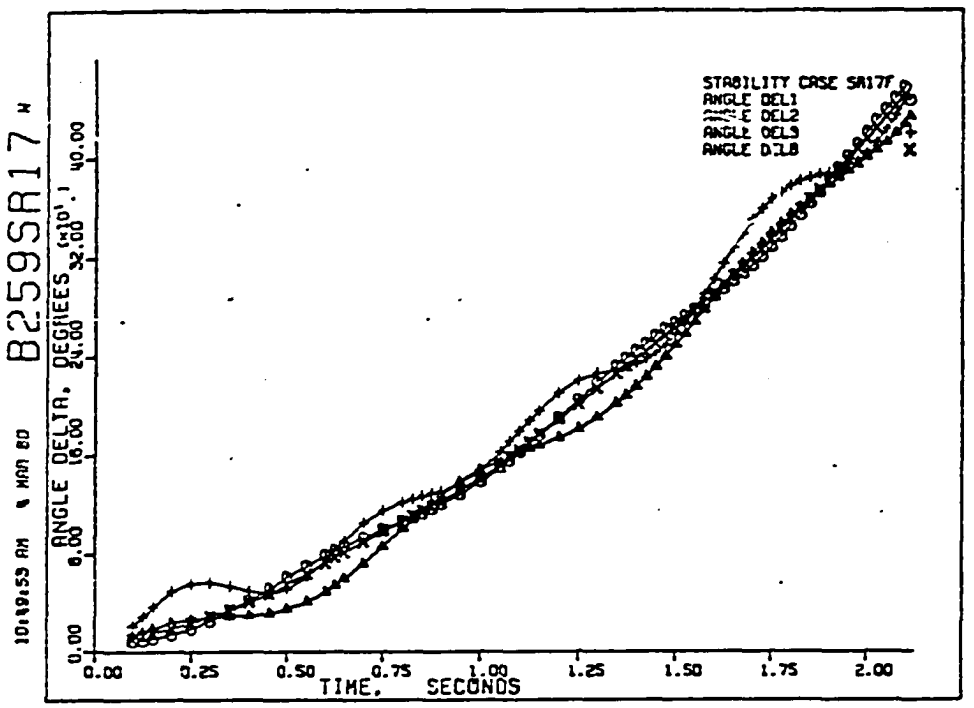

Figure 218. Case SR-17F: angles δ_1, δ_2, δ_3, and $\bar{\delta}$.

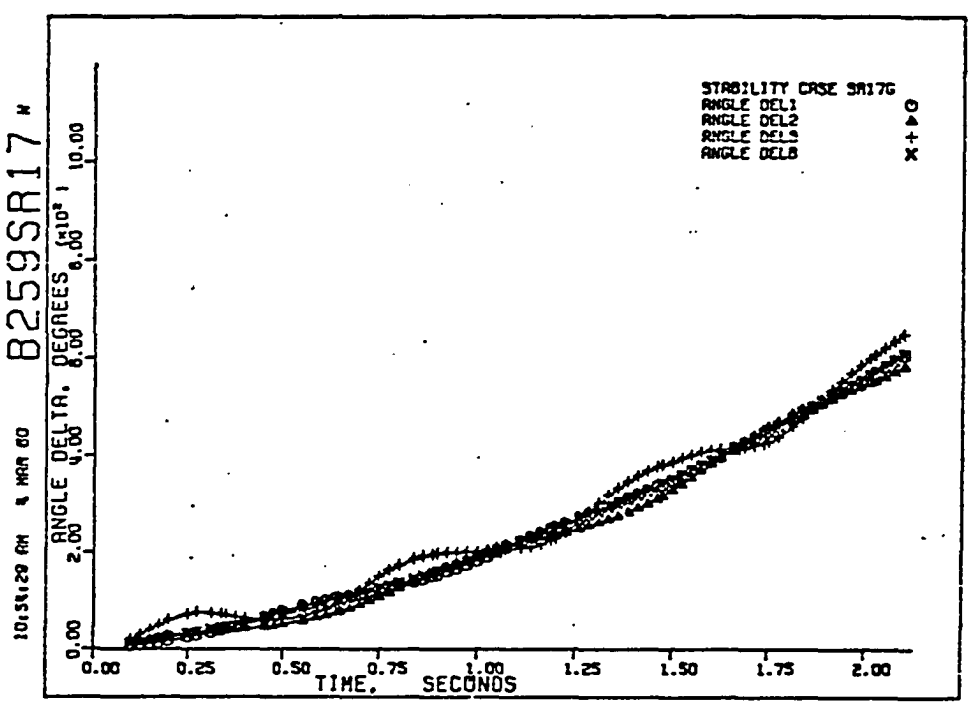

Figure 219. Case SR-17G: angles δ_1, δ_2, δ_3, and $\bar{\delta}$.

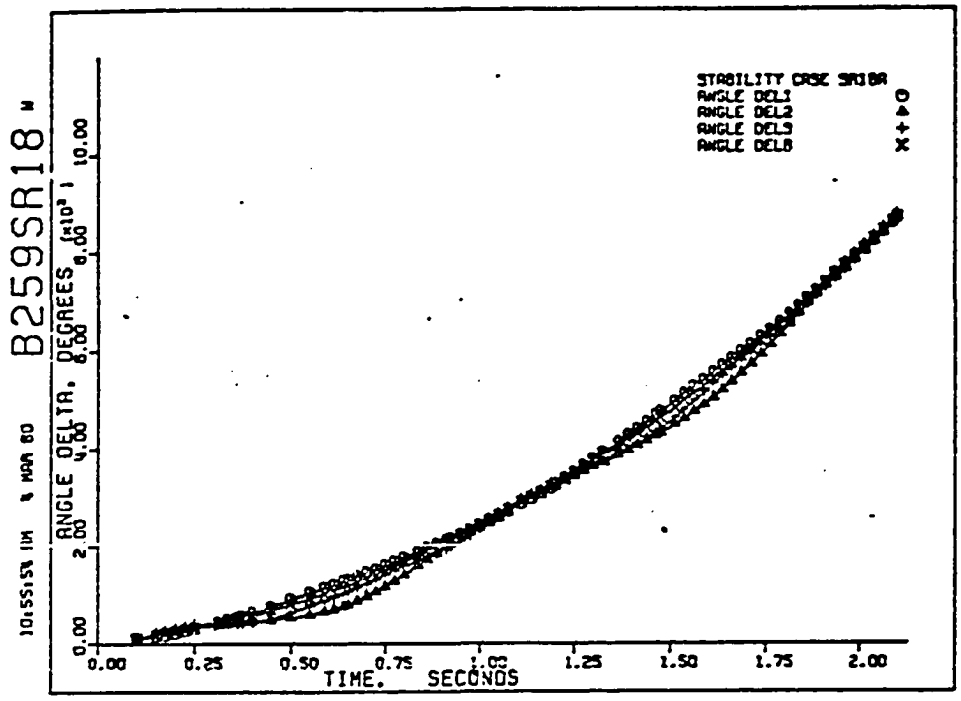

Figure 220. Case SR-18A: angles δ_1, δ_2, δ_3, and $\bar{\delta}$.

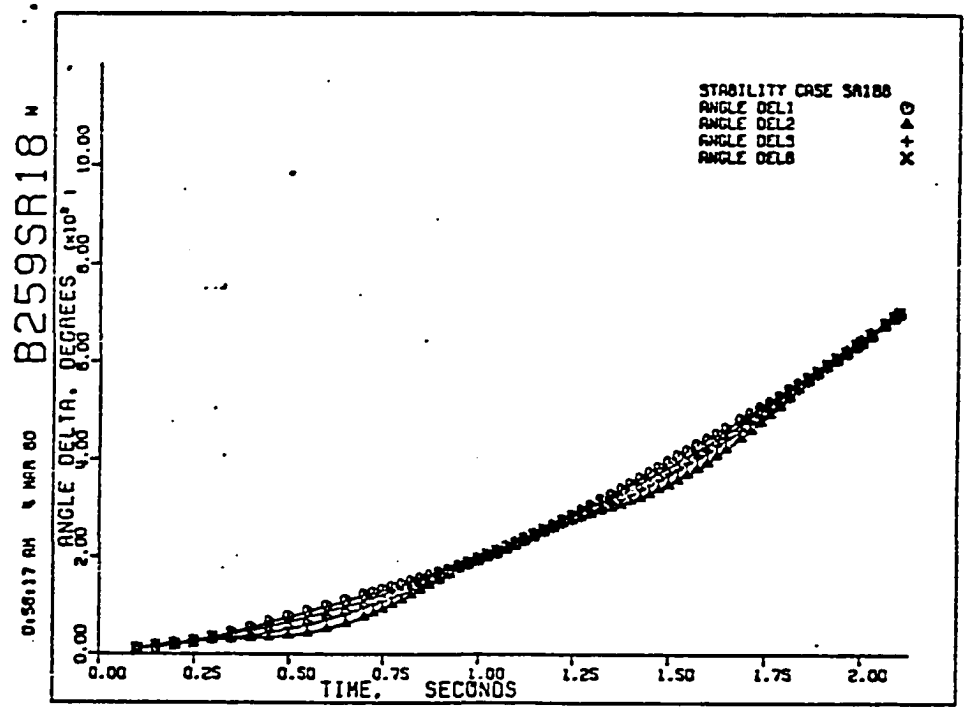

Figure 221. Case SR-18B: angles δ_1, δ_2, δ_3, and $\bar{\delta}$.

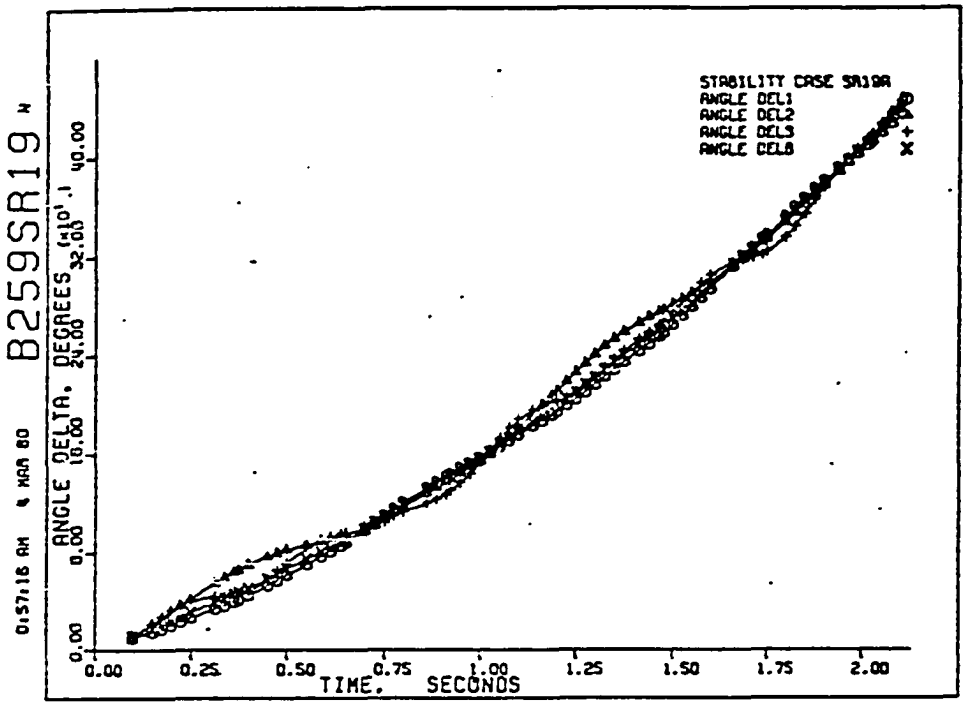

Figure 222. Case SR-19A: angles δ_1, δ_2, δ_3, and $\bar{\delta}$.

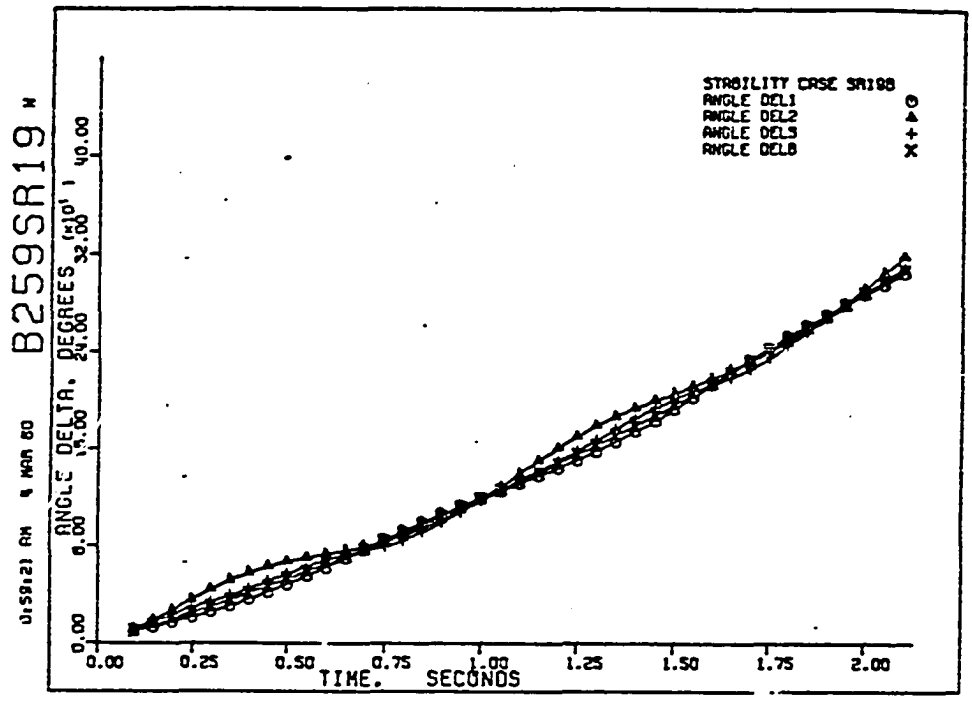

Figure 223. Case SR-19B: angles δ_1, δ_2, δ_3, and $\bar{\delta}$.

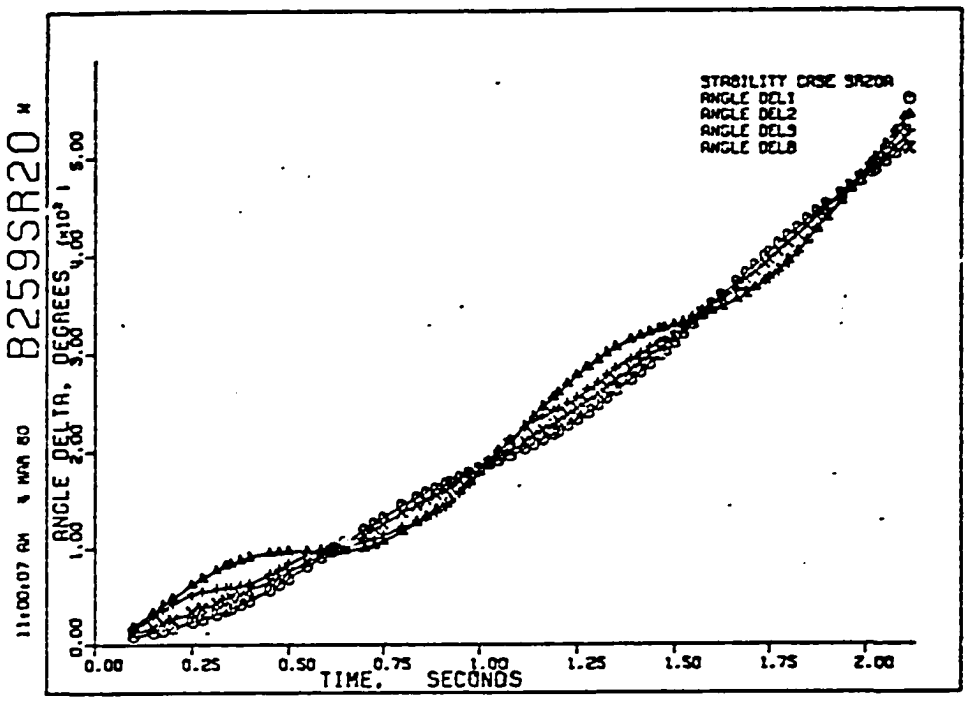

Figure 224. Case SR-20A: angles δ_1, δ_2, δ_3, and $\bar{\delta}$.

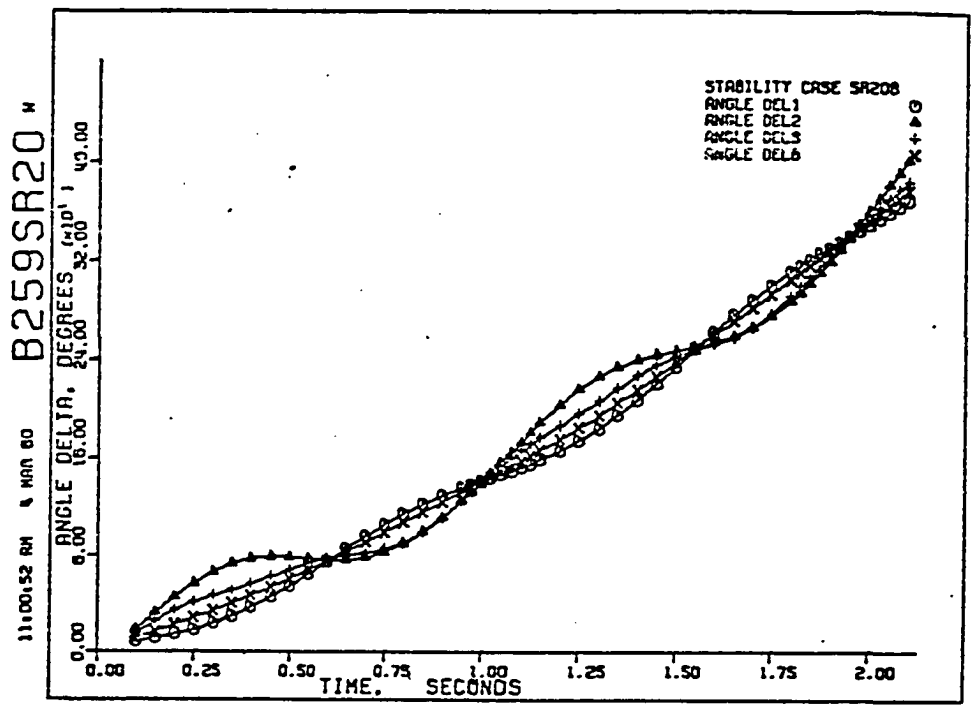

Figure 225. Case SR-20B: angles δ_1, δ_2, δ_3, and $\bar{\delta}$.

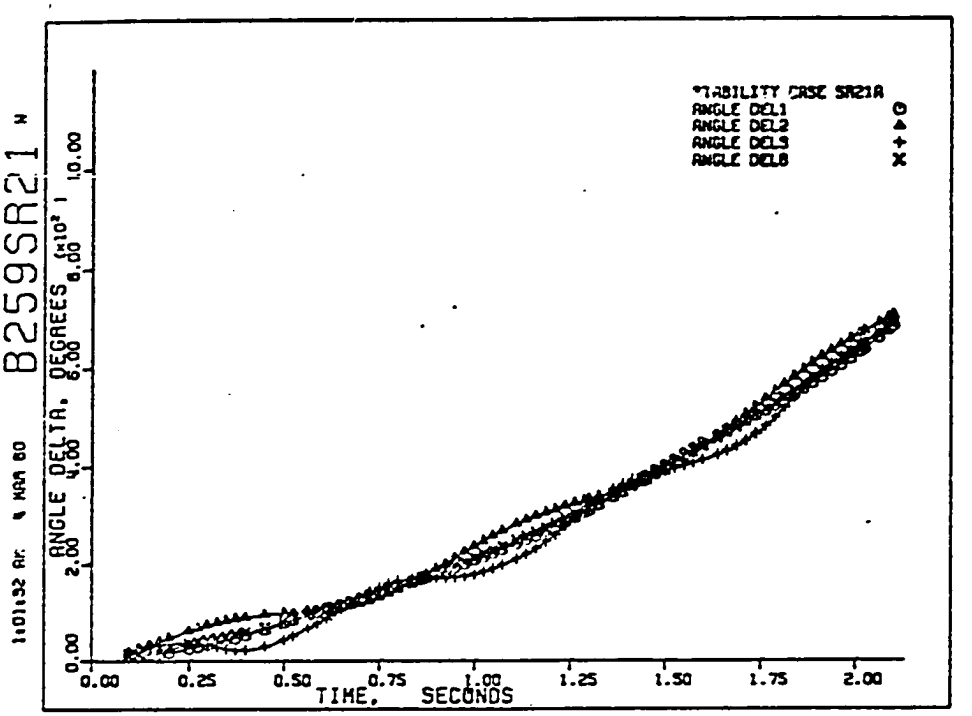

Figure 226. Case SR-21A: angles δ_1, δ_2, δ_3, and $\bar{\delta}$.

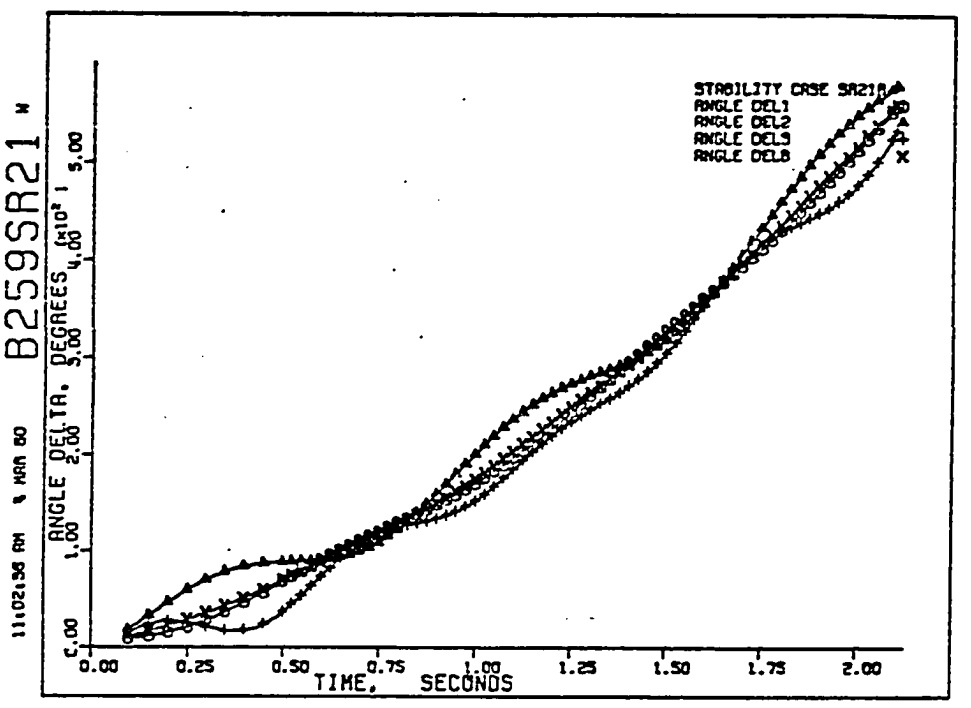

Figure 227. Case SR-21B: angles δ_1, δ_2, δ_3, and $\bar{\delta}$.

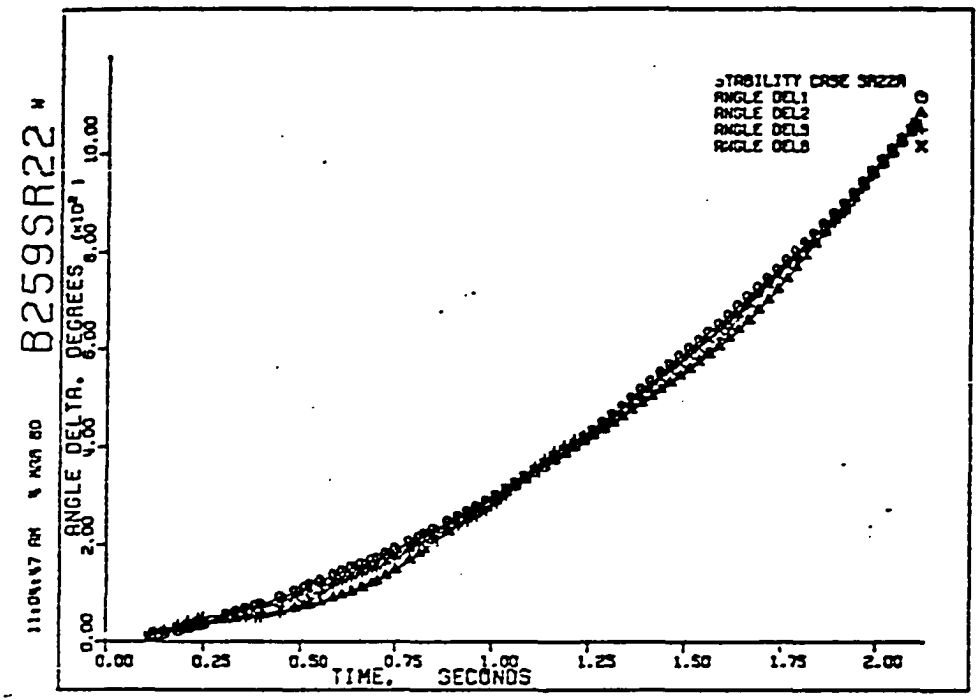

Figure 228. Case SR-22A: angles δ_1, δ_2, δ_3, and $\bar{\delta}$.

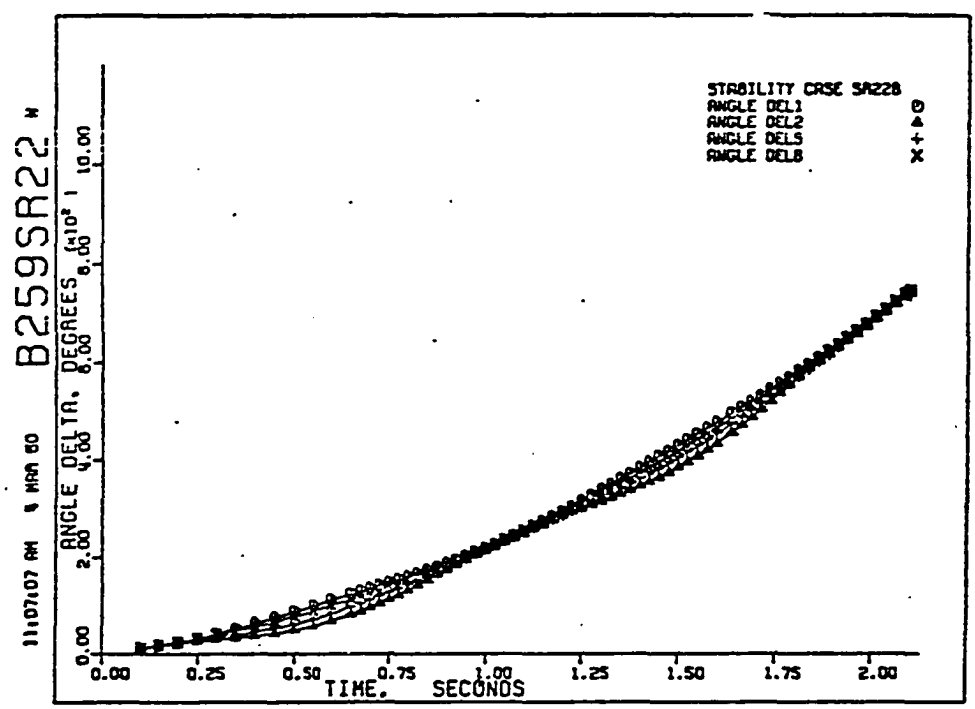

Figure 229. Case SR-22B: angles δ_1, δ_2, δ_3, and $\bar{\delta}$.

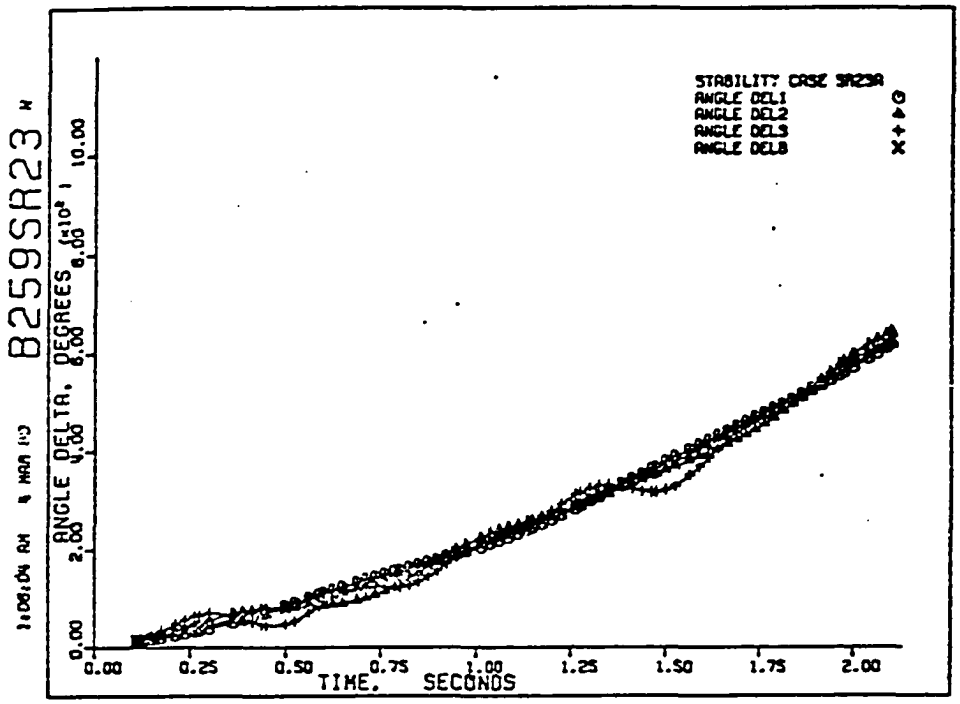

Figure 230. Case SR-23A: angles δ_1, δ_2, δ_3, and $\bar{\delta}$.

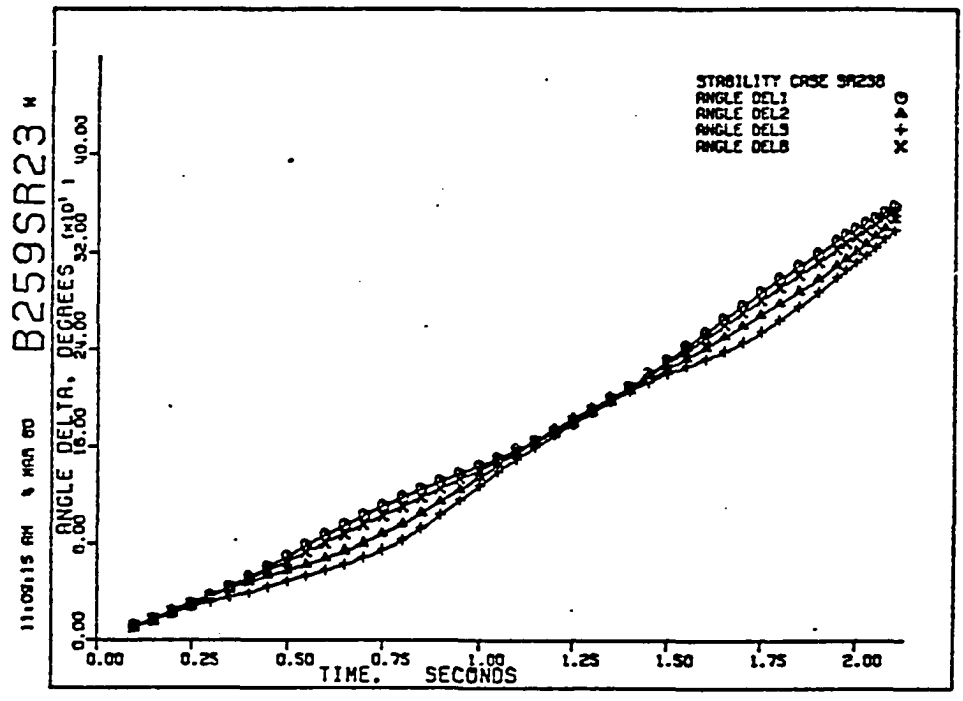

Figure 231. Case SR-23B: angles δ_1, δ_2, δ_3, and $\bar{\delta}$.

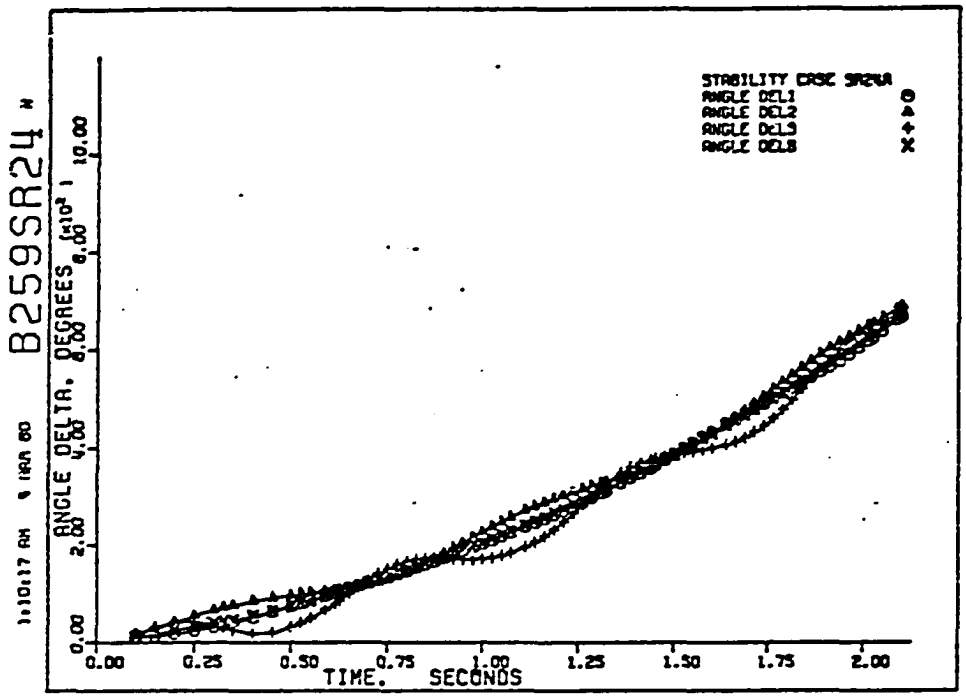

Figure 232. Case SR-24A: angles δ_1, δ_2, δ_3, and $\bar{\delta}$.

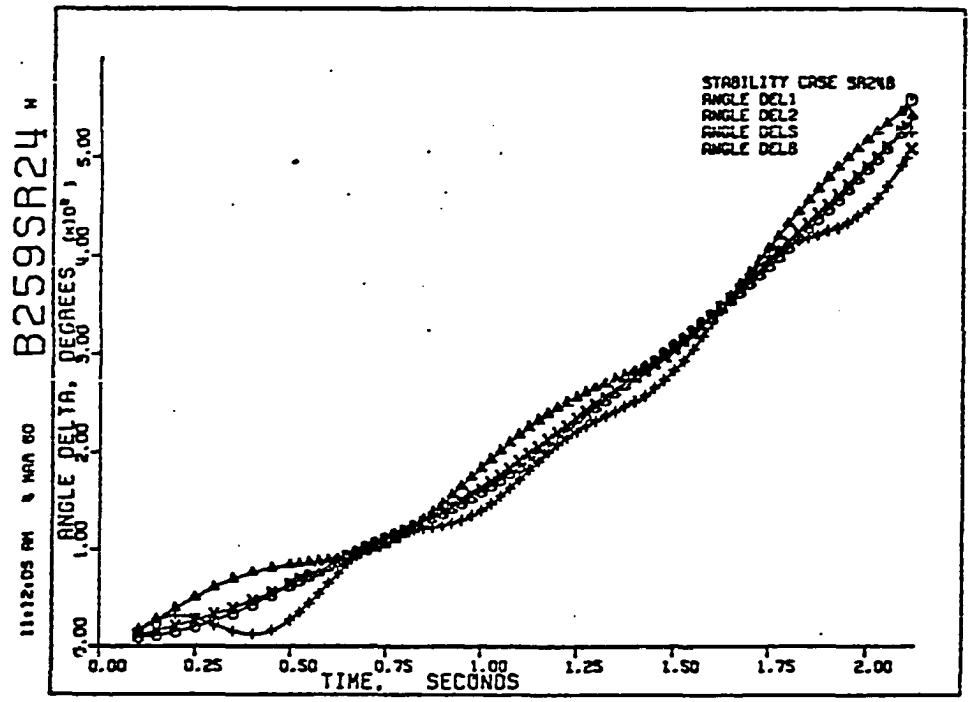

Figure 233. Case SR-24B: angles δ_1, δ_2, δ_3, and $\bar{\delta}$.

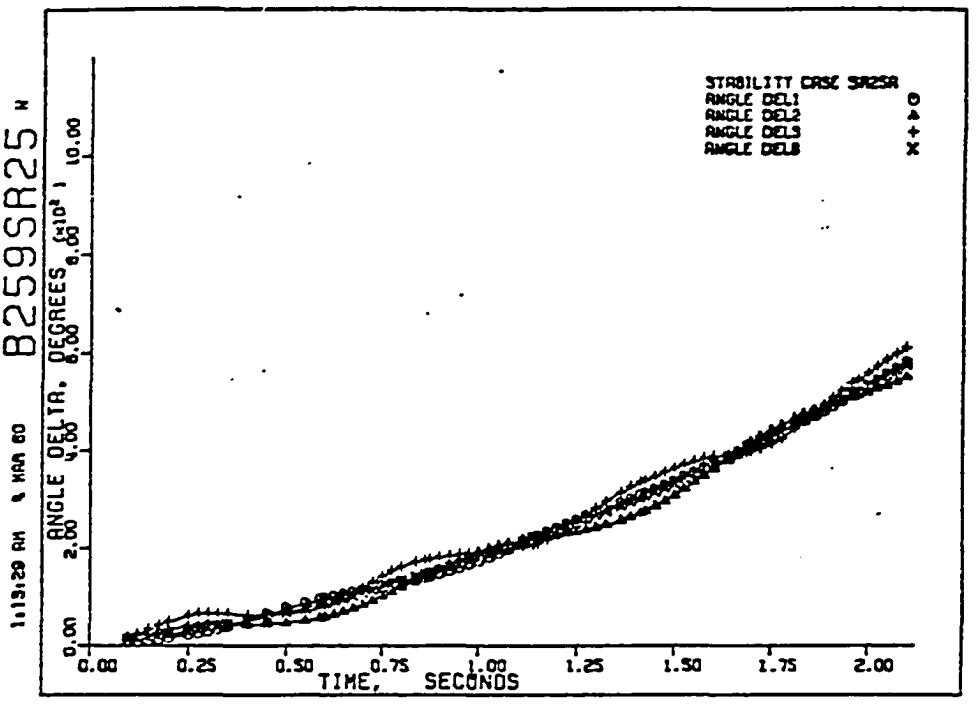

Figure 234. Case SR-25A: angles δ_1, δ_2, δ_3, and $\bar{\delta}$.

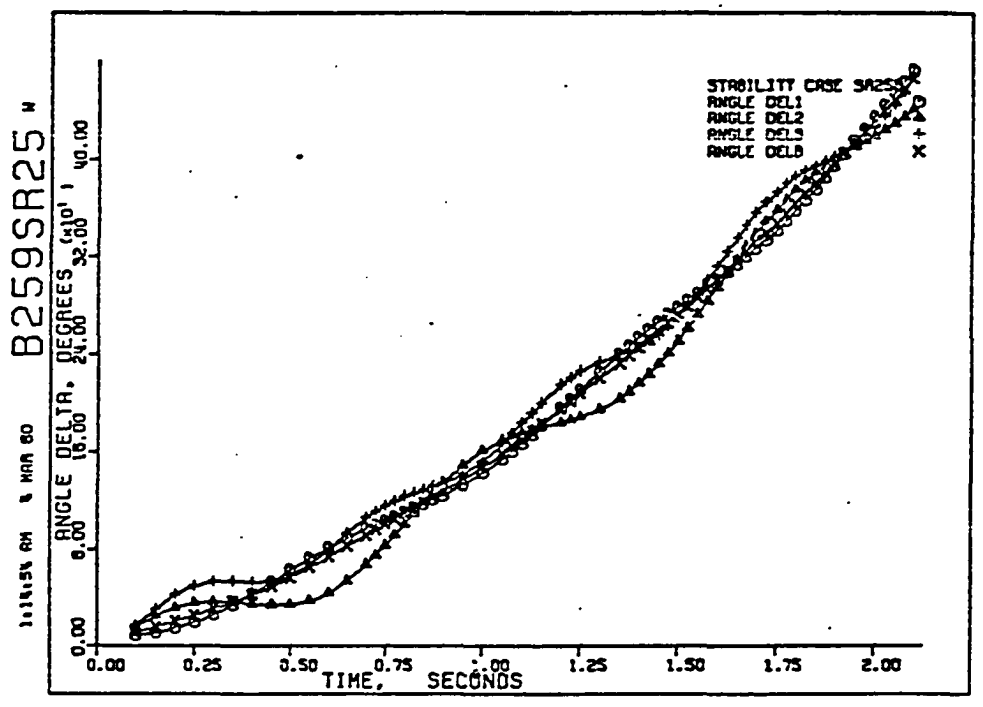

Figure 235. Case SR-25B: angles δ_1, δ_2, δ_3, and $\bar{\delta}$.

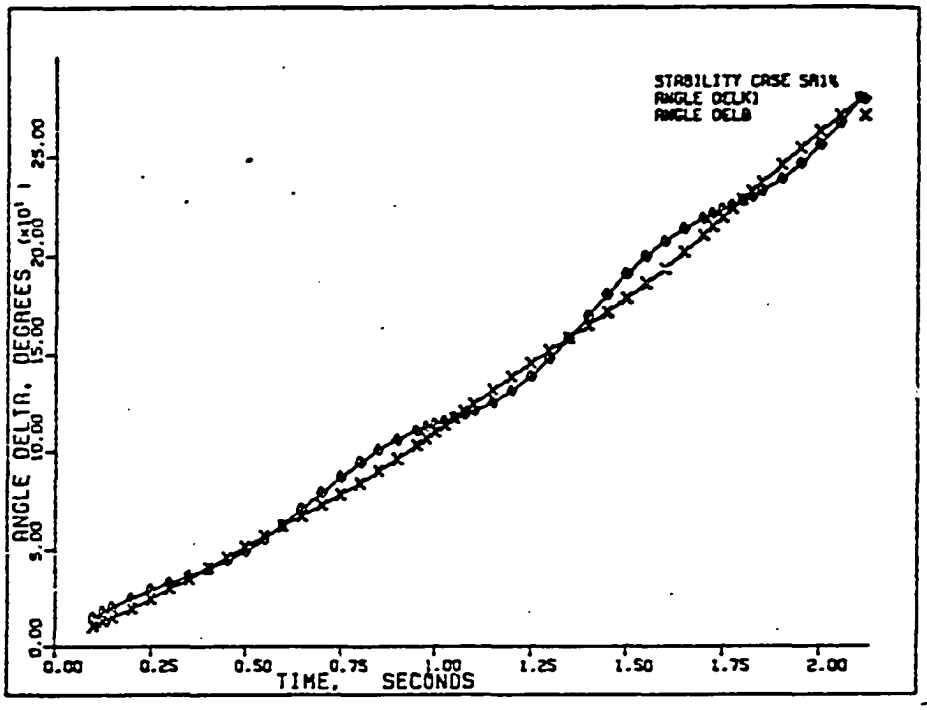

Figure 236. Case SR-14: angles δ_k and $\bar{\delta}$.

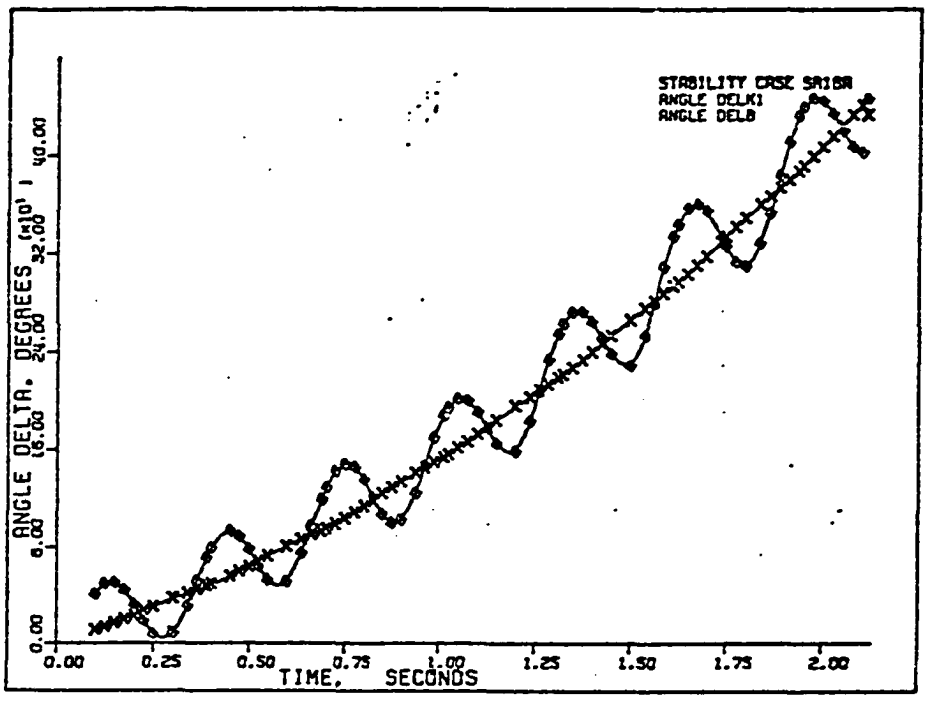

Figure 237. Case SR-16A: angles δ_k and $\bar{\delta}$.

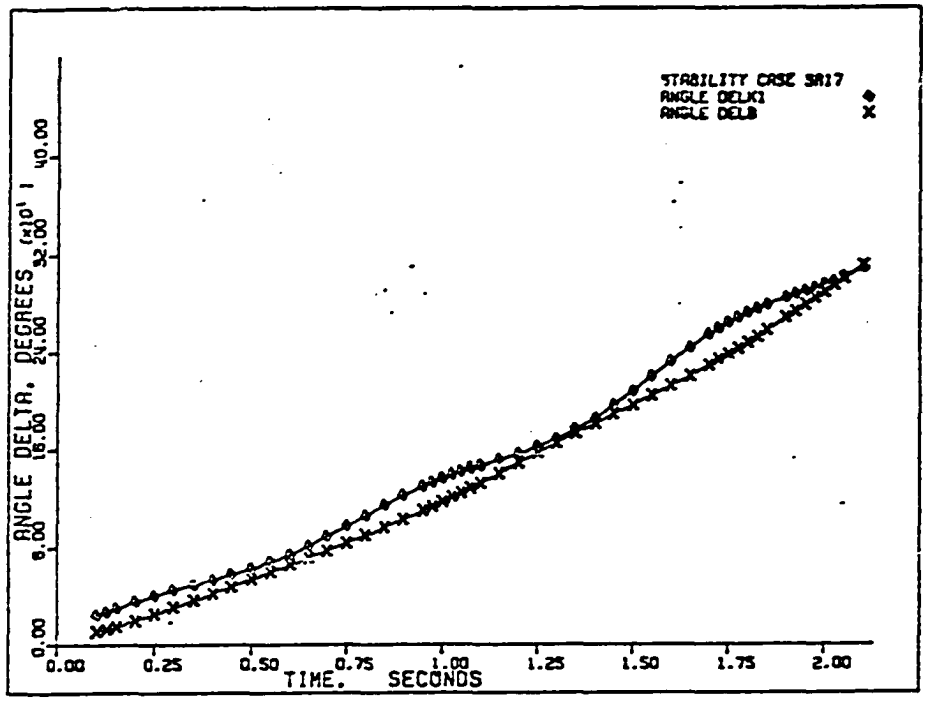

Figure 238. Case SR-17: angles δ_k and $\bar{\delta}$.

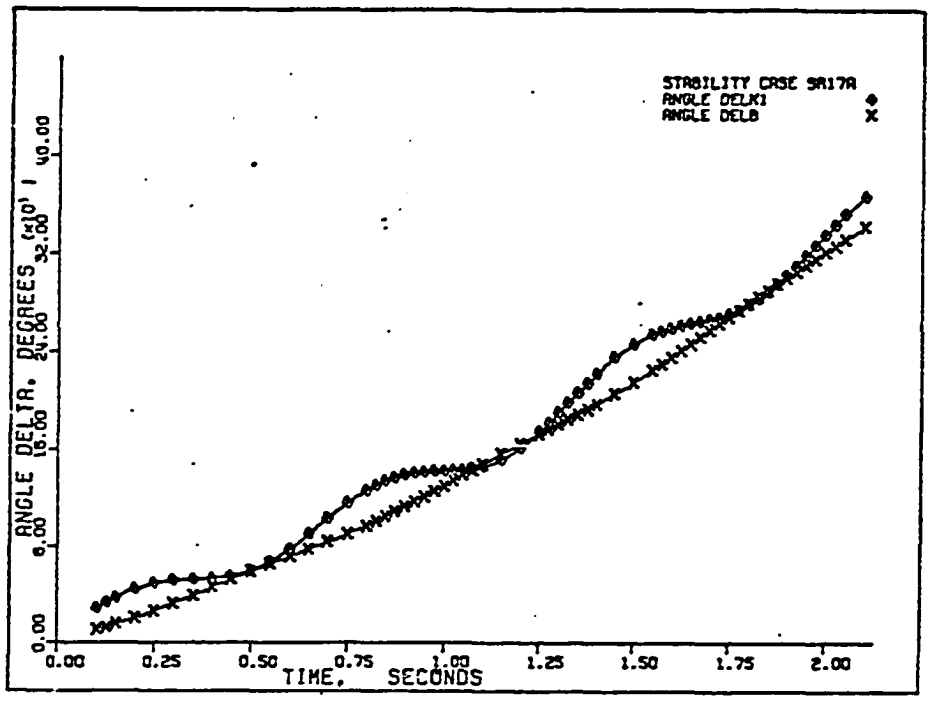

Figure 239. Case SR-17A: angles δ_k and $\bar{\delta}$.

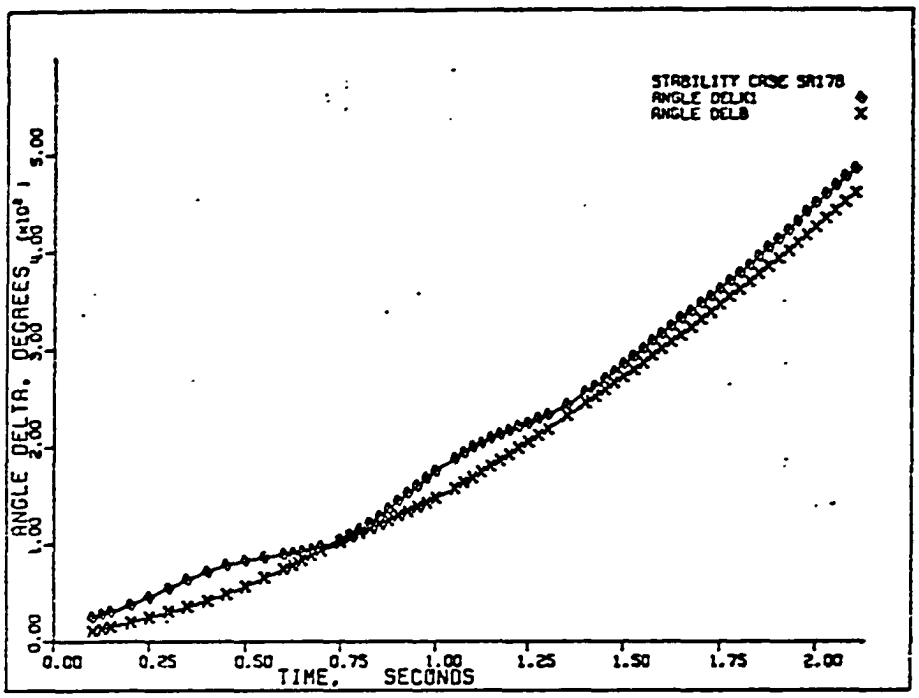

Figure 240. Case SR-17B: angles δ_k and $\bar{\delta}$.

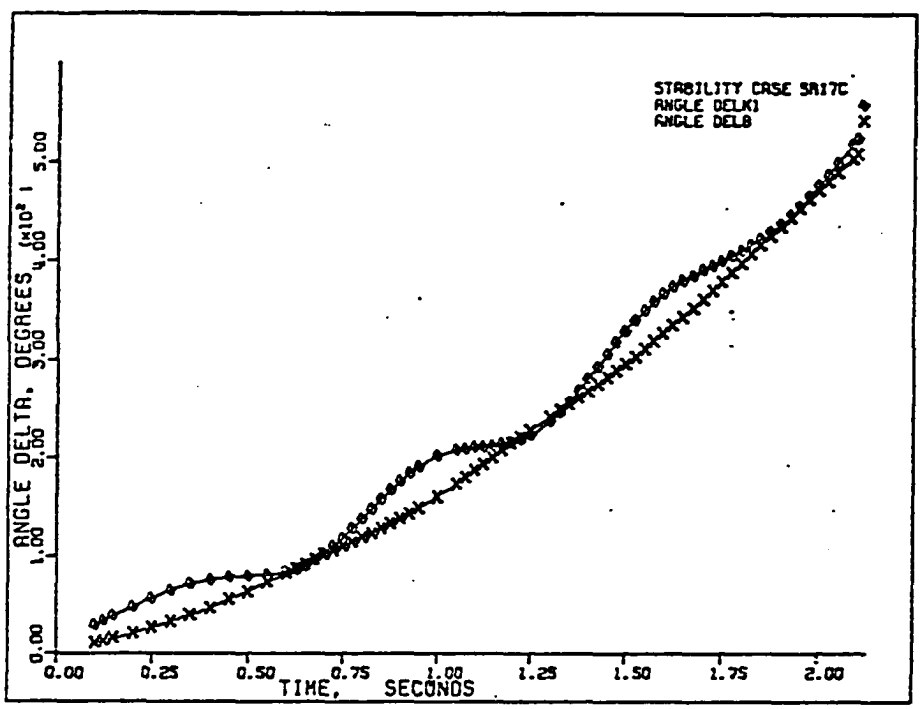

Figure 241. Case SR-17C: angles δ_k and $\bar{\delta}$.

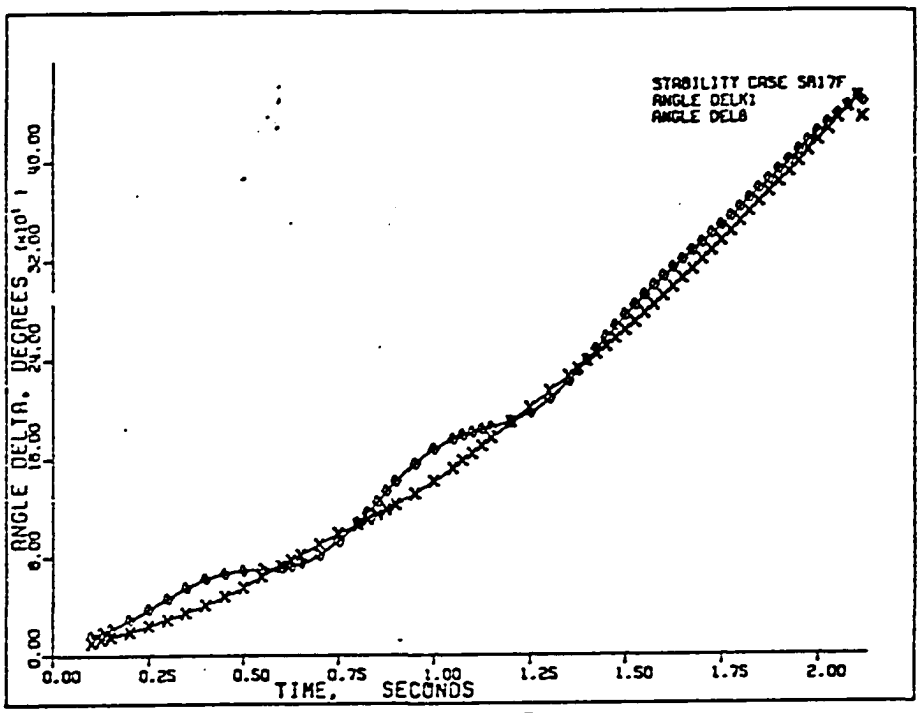

Figure 242. Case SR-17F: angles δ_k and $\bar{\delta}$.

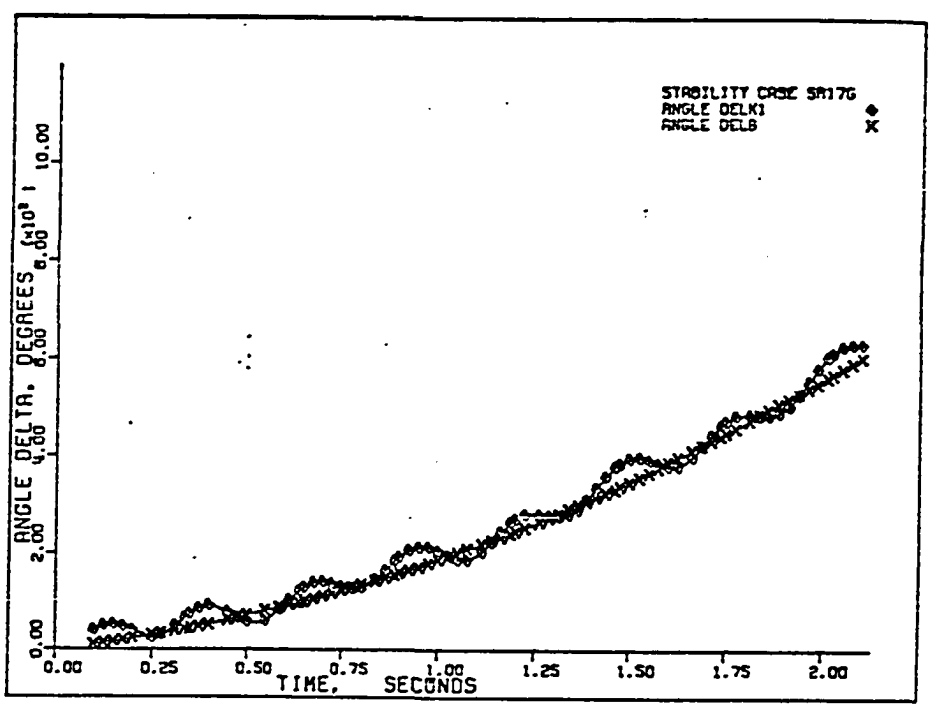

Figure 243. Case SR-17G: angles δ_k and $\bar{\delta}$.

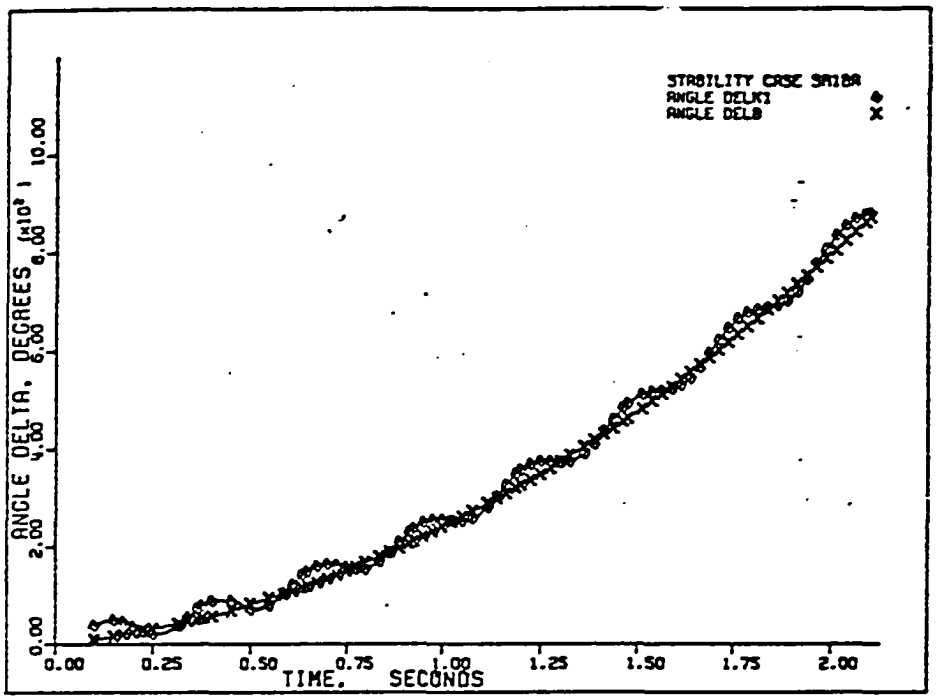

Figure 244. Case SR-18A: angles δ_k and $\bar{\delta}$.

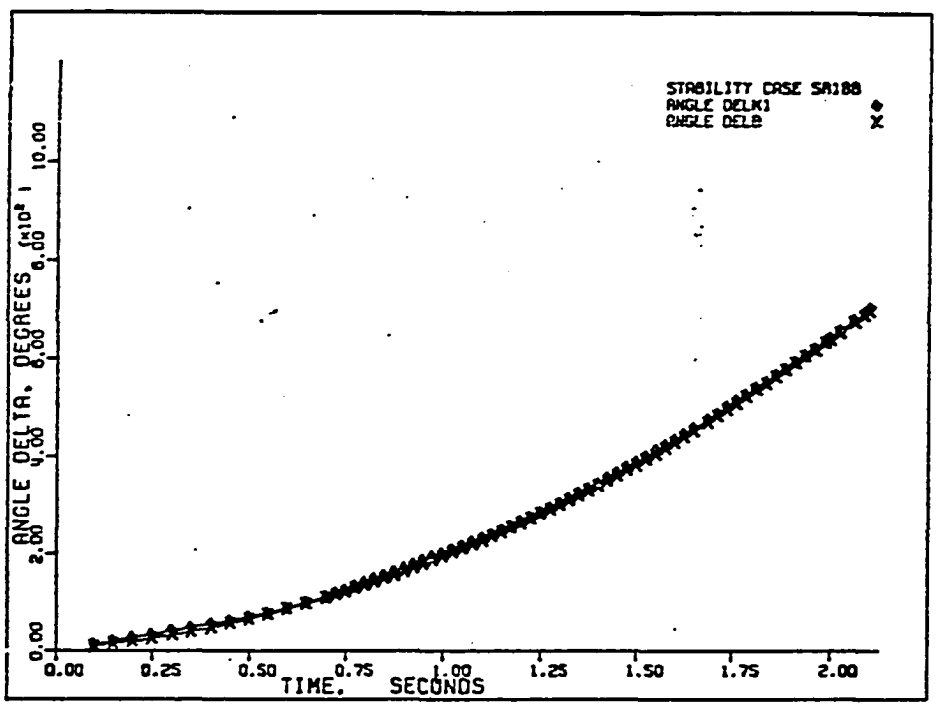

Figure 245. Case SR-18B: angles δ_k and $\bar{\delta}$.

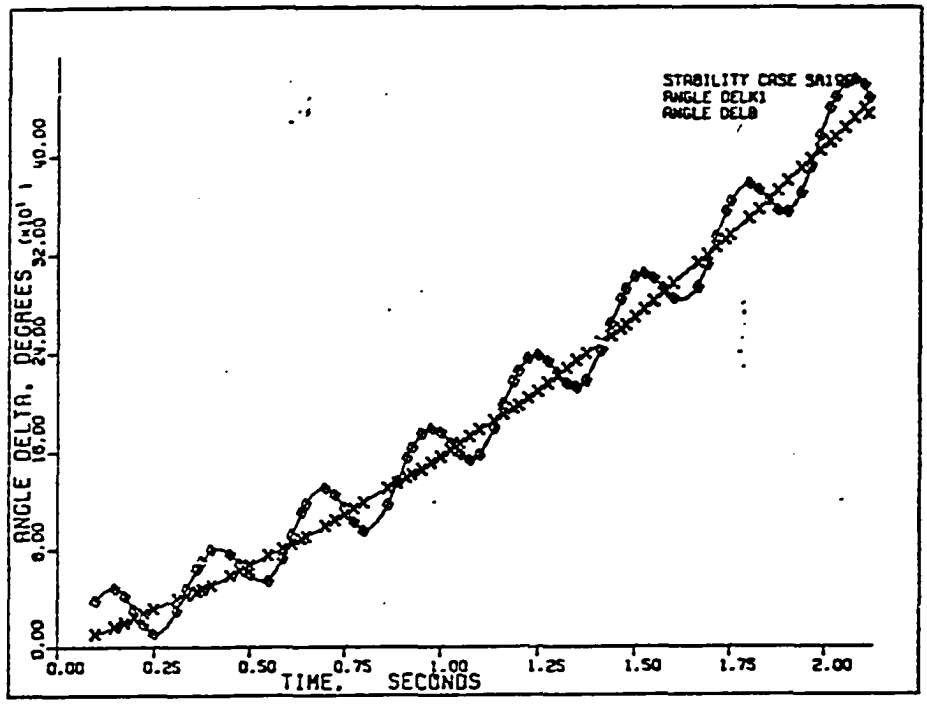

Figure 246. Case SR-19A: angles δ_k and $\bar{\delta}$.

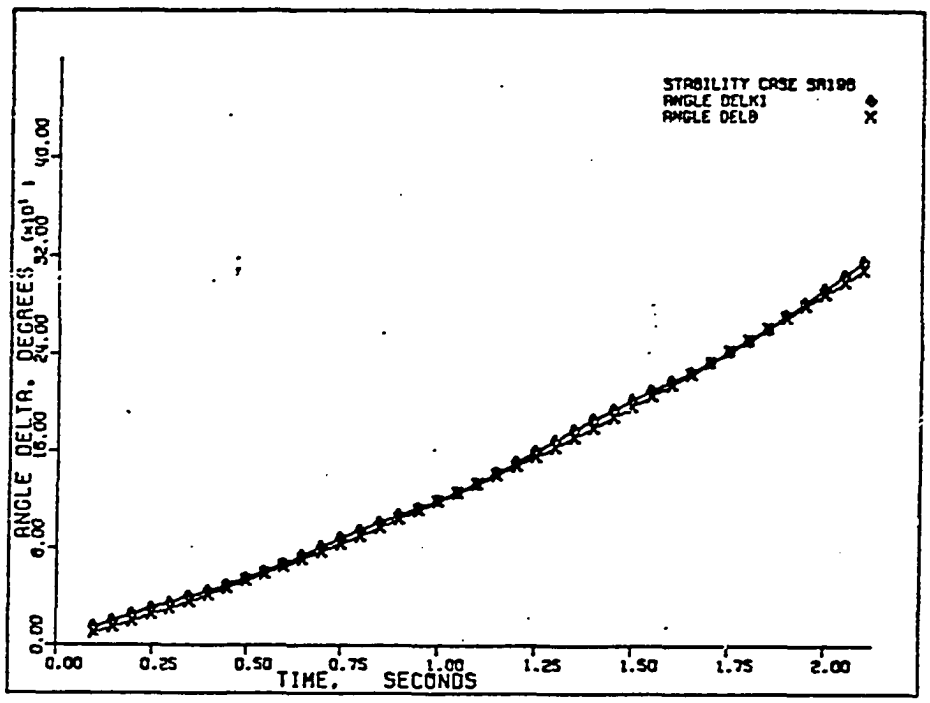

Figure 247. Case SR-19B: angles δ_k and $\bar{\delta}$.

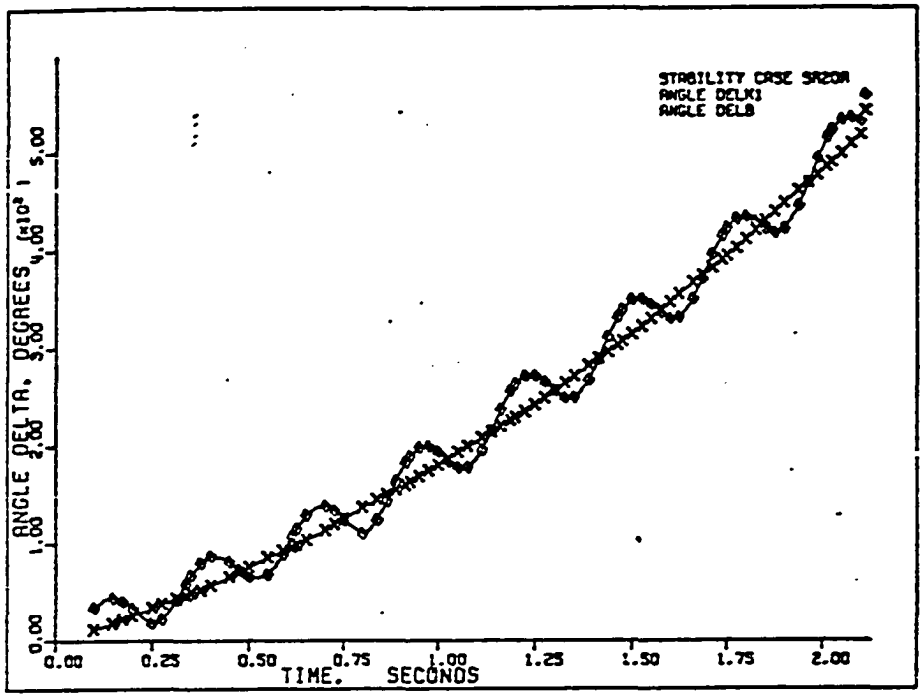

Figure 248. Case SR-20A: angles δ_k and $\bar{\delta}$.

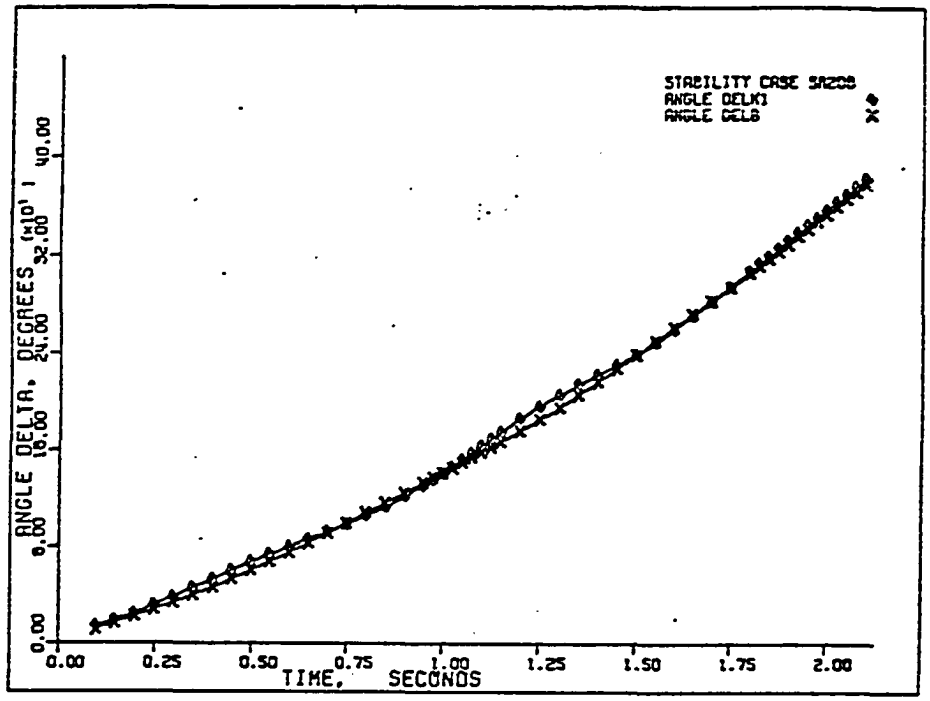

Figure 249. Case SR-20B: angles δ_k and $\bar{\delta}$.

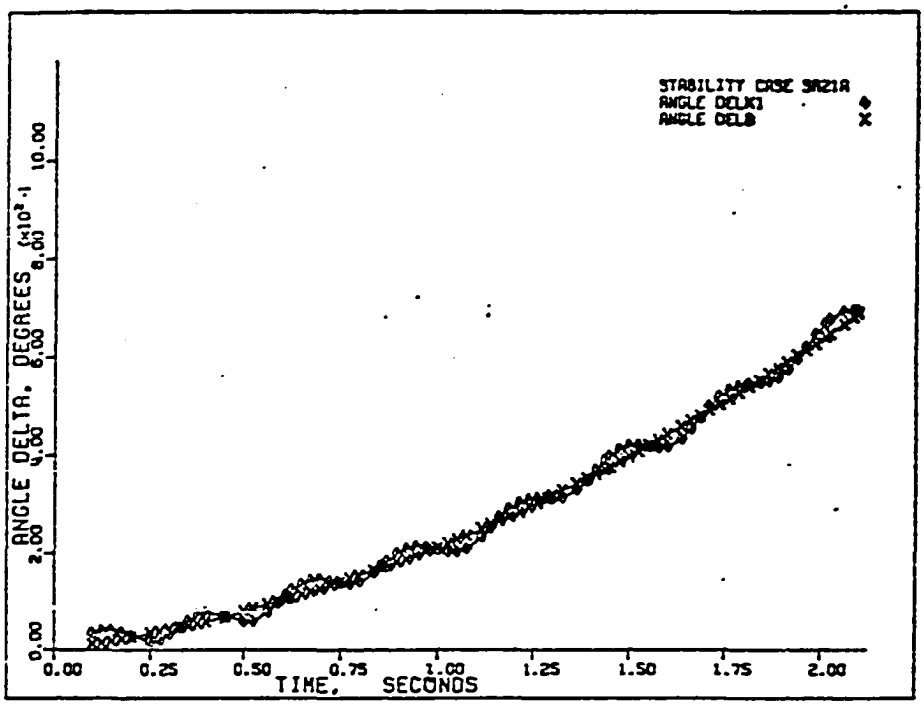

Figure 250. Case SR-21A: angles δ_k and $\bar{\delta}$.

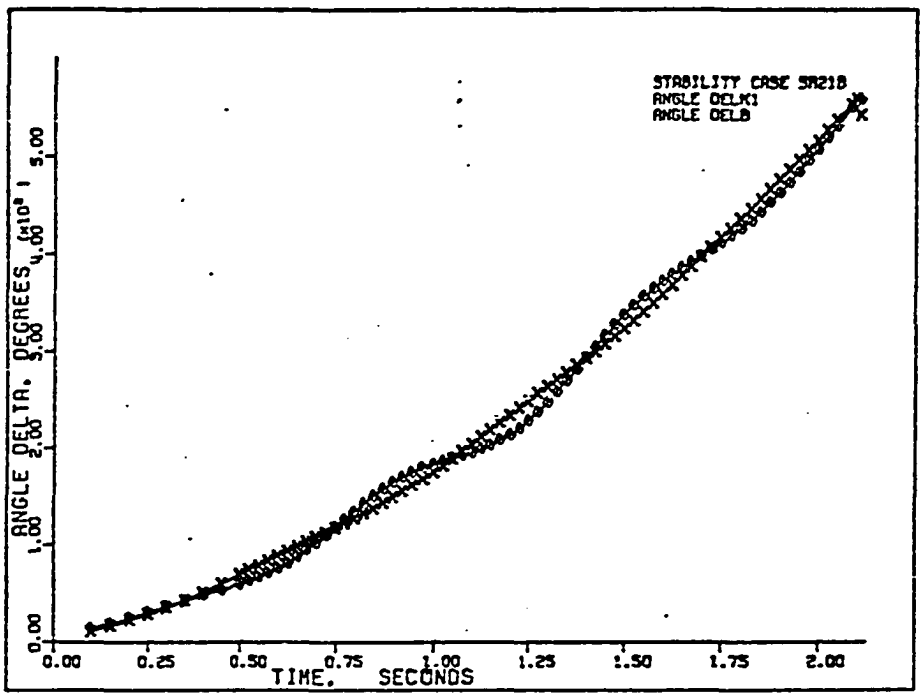

Figure 251. Case SR-21B: angles δ_k and $\bar{\delta}$.

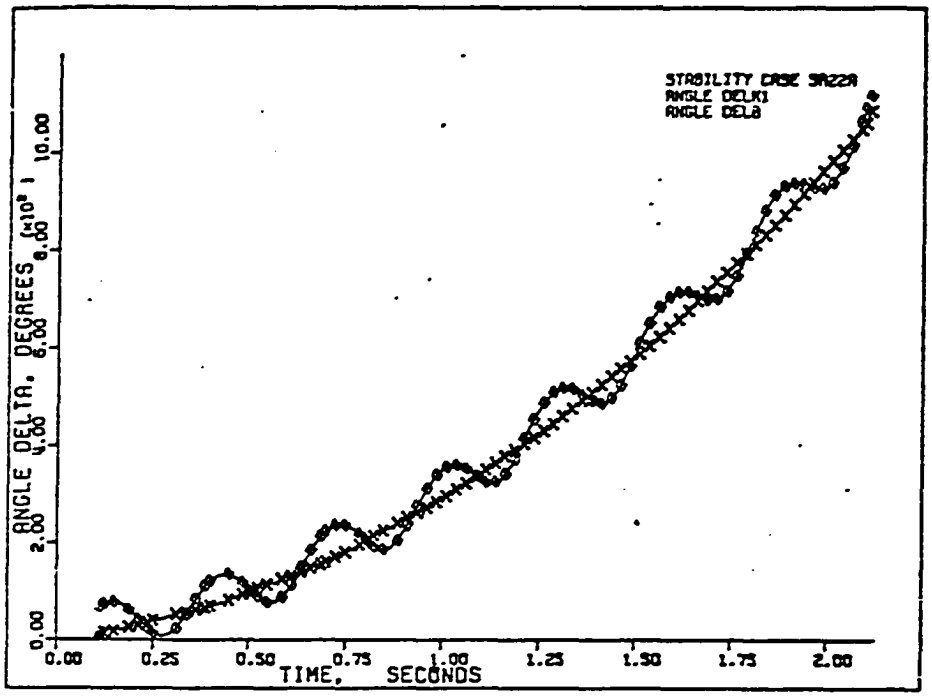

Figure 252. Case SR-22A: angles δ_k and $\bar{\delta}$.

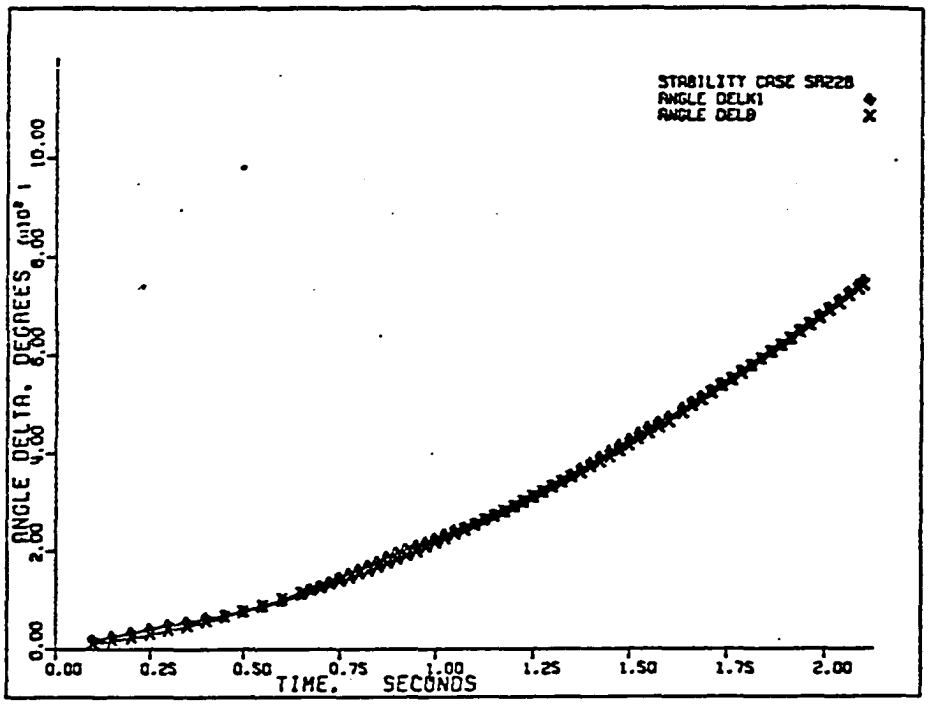

Figure 253. Case SR-22B: angles δ_k and $\bar{\delta}$.

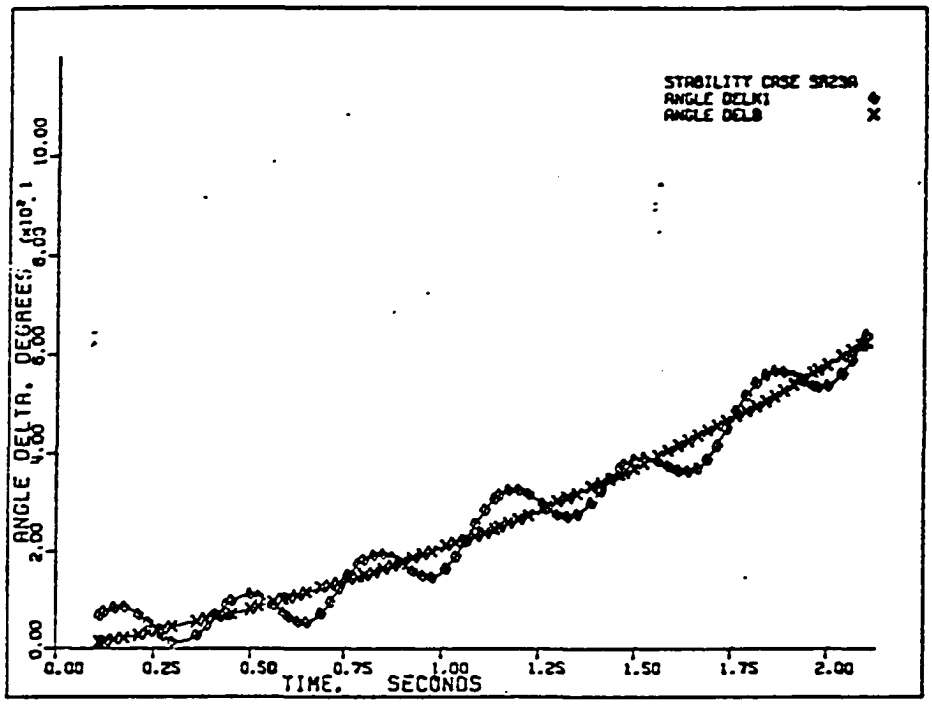

Figure 254. Case SR-23A: angles δ_k and $\bar{\delta}$.

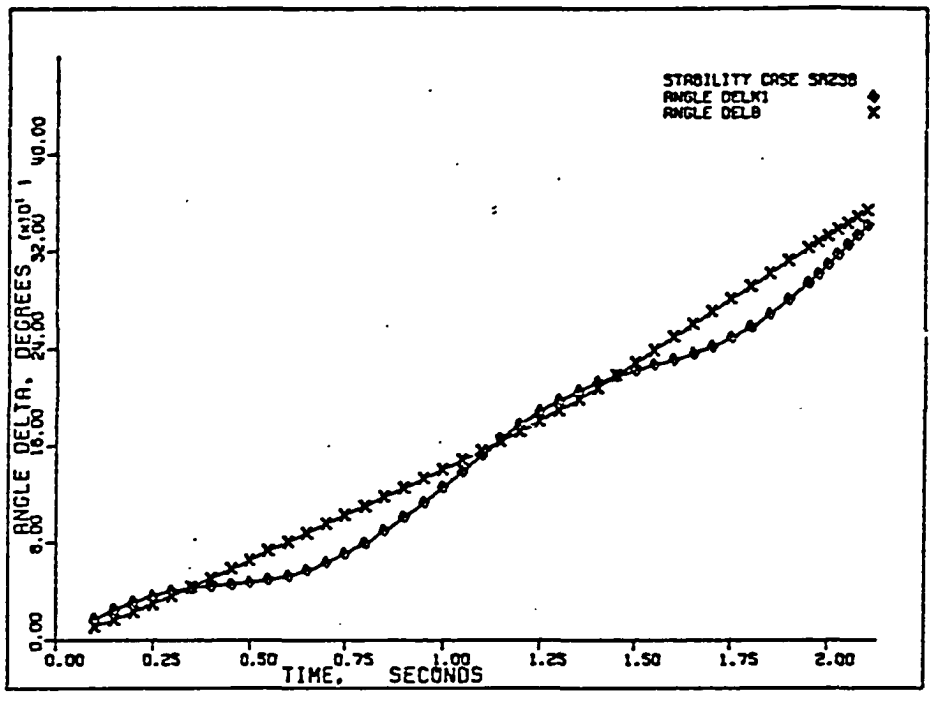

Figure 255. Case SR-23B: angles δ_k and $\bar{\delta}$.

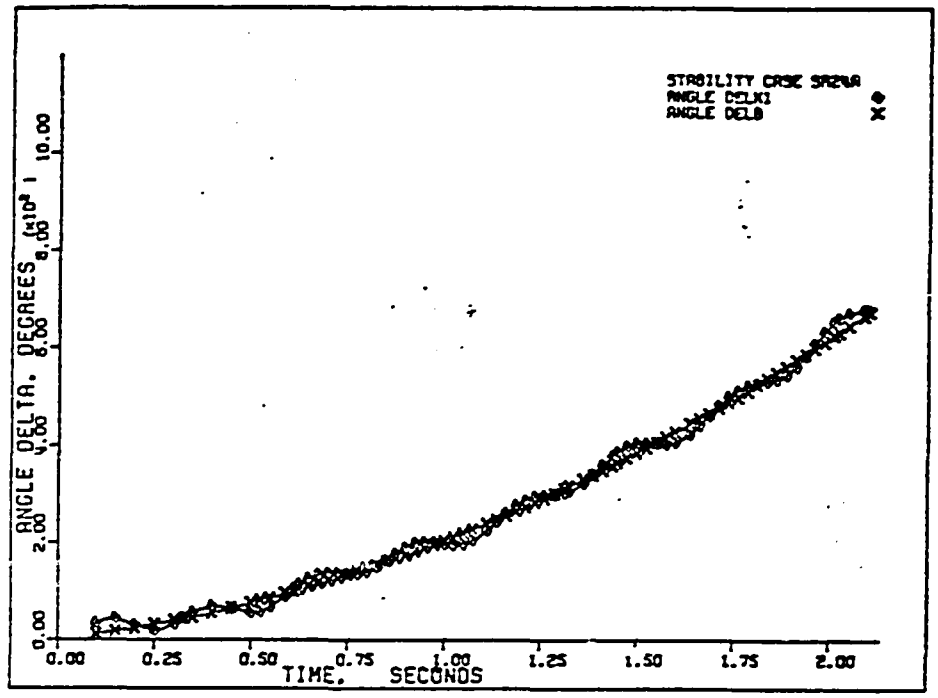

Figure 256. Case SR-24A: angles δ_k and $\bar{\delta}$.

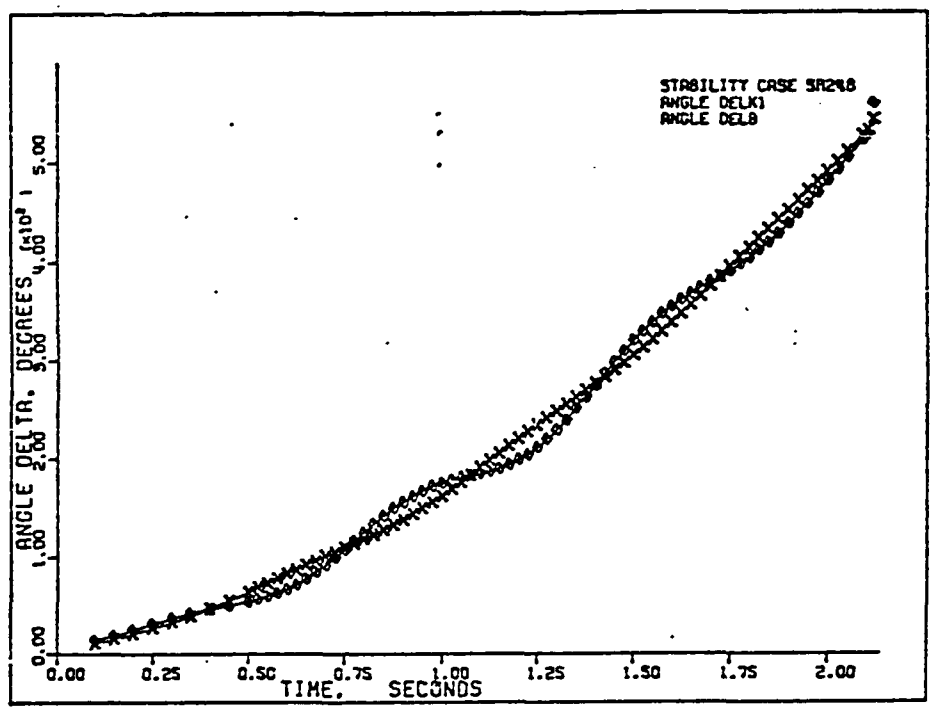

Figure 257. Case SR-24B: angles δ_k and $\bar{\delta}$.

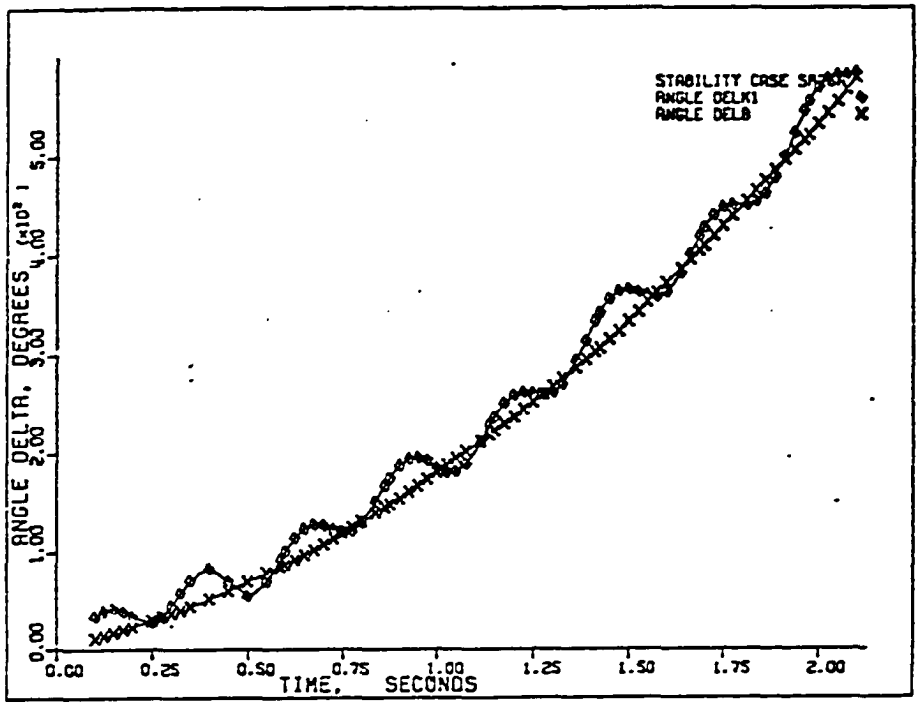

Figure 258. Case SR-25A: angles δ_k and $\bar{\delta}$.

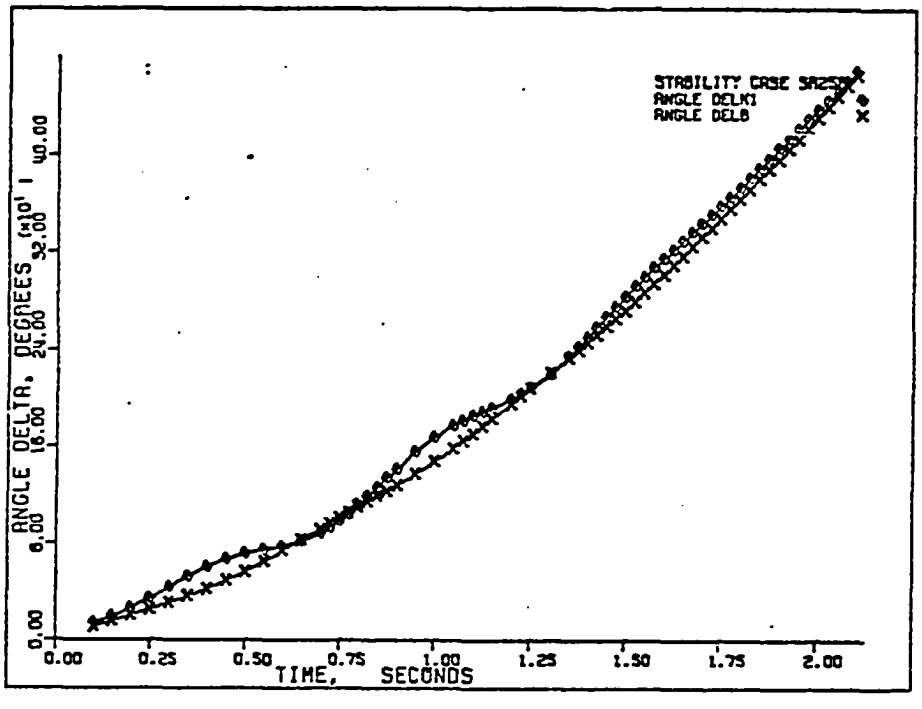

Figure 259. Case SR-25B: angles δ_k and $\bar{\delta}$.

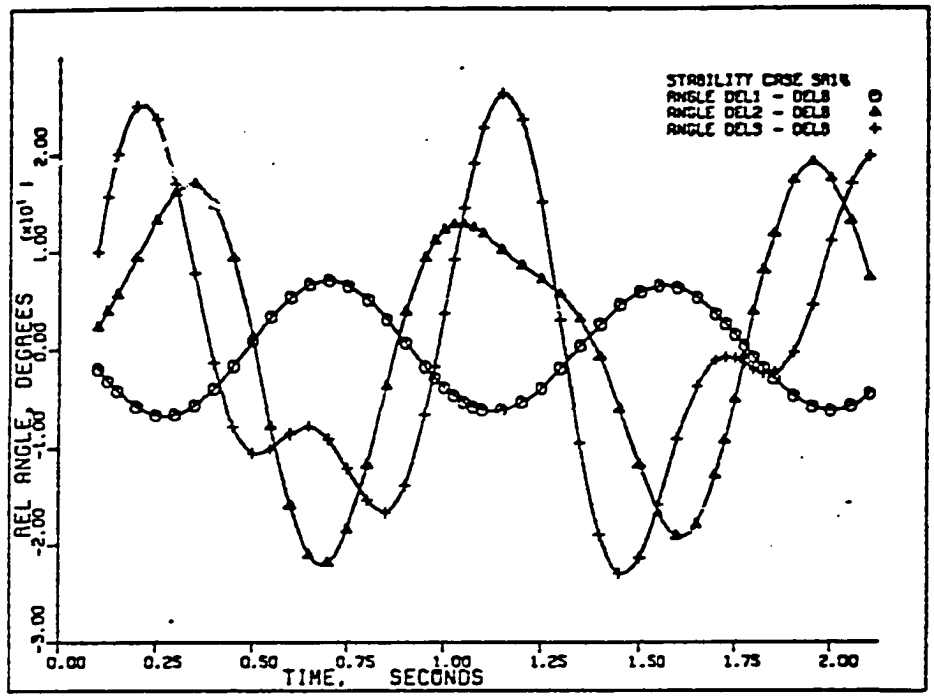

Figure 260. Case SR-14: relative angles $(\delta_1 - \bar{\delta})$, $(\delta_2 - \bar{\delta})$, and $(\delta_3 - \bar{\delta})$.

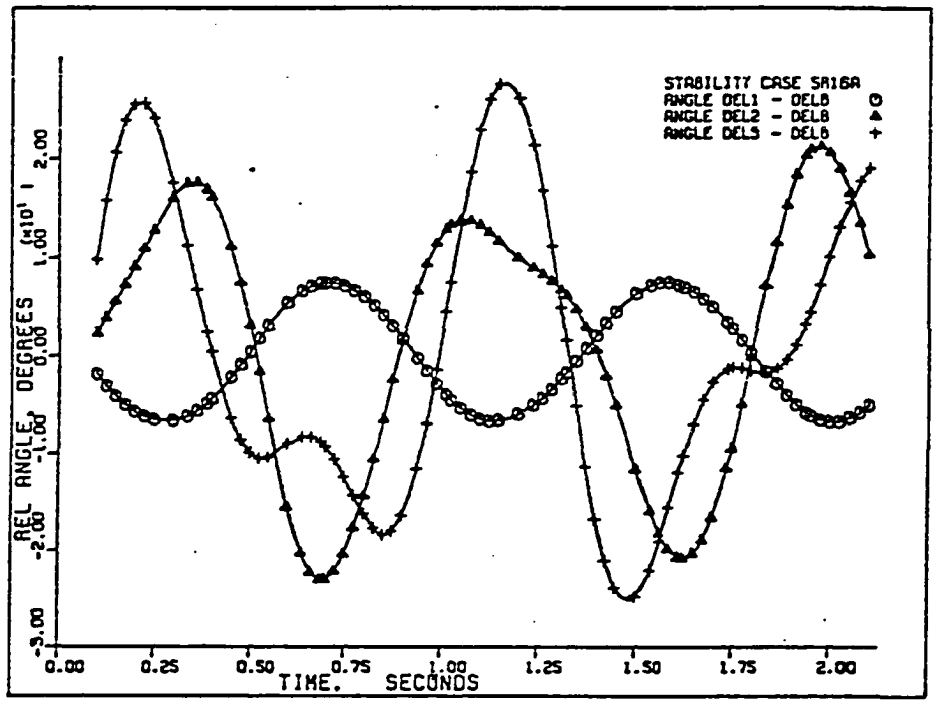

Figure 261. Case SR-16A: relative angles $(\delta_1 - \bar{\delta})$, $(\delta_2 - \bar{\delta})$, and $(\delta_3 - \bar{\delta})$.

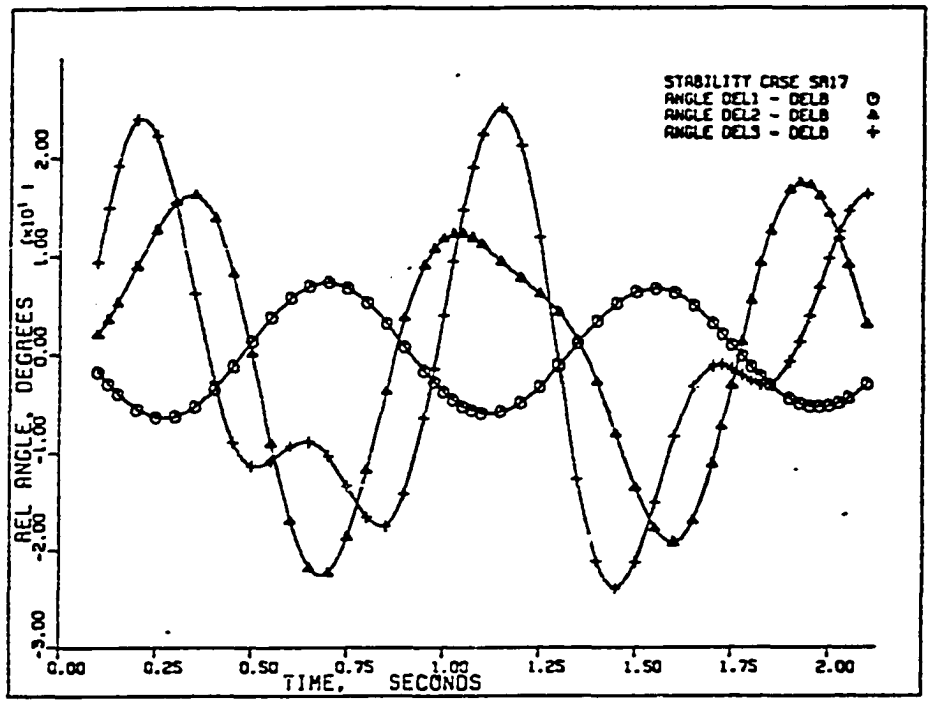

Figure 262. Case SR-17: relative angles $(\delta_1 - \bar{\delta})$, $(\delta_2 - \bar{\delta})$, and $(\delta_3 - \bar{\delta})$.

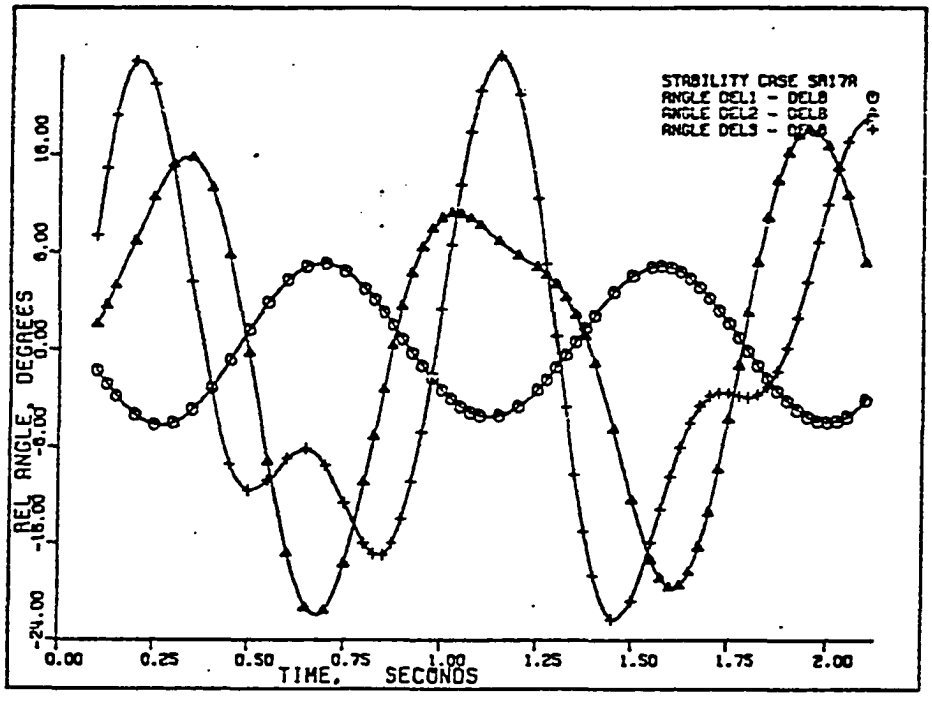

Figure 263. Case SR-17A: relative angles $(\delta_1 - \bar{\delta})$, $(\delta_2 - \bar{\delta})$, and $(\delta_3 - \bar{\delta})$.

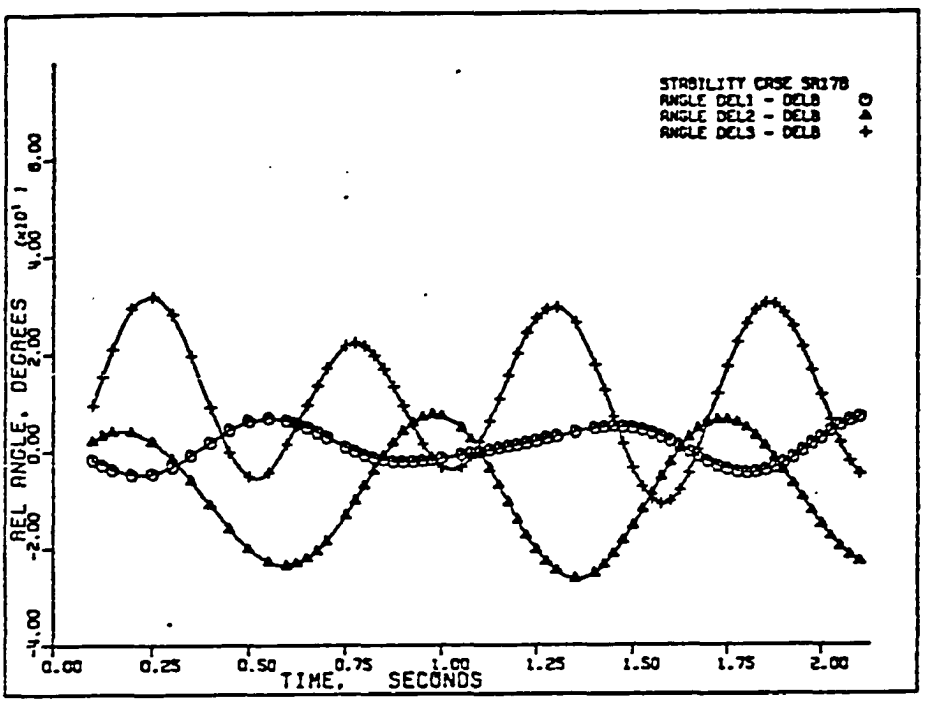

Figure 264. Case SR-17B: relative angles $(\delta_1 - \bar{\delta})$, $(\delta_2 - \bar{\delta})$, and $(\delta_3 - \bar{\delta})$.

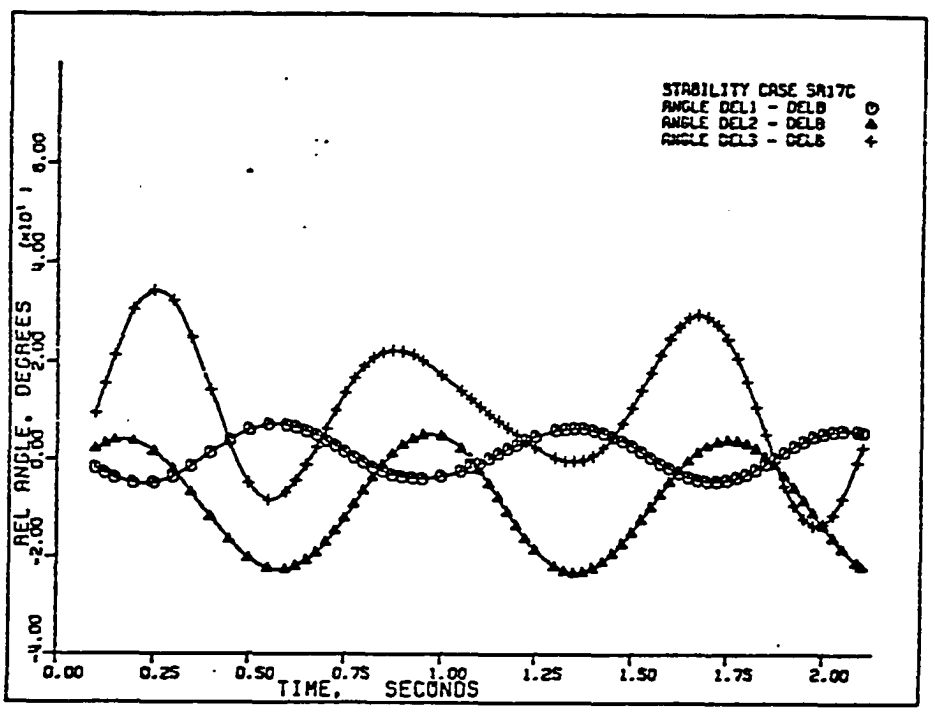

Figure 265. Case SR-17C: relative angles $(\delta_1 - \bar{\delta})$, $(\delta_2 - \bar{\delta})$, and $(\delta_3 - \bar{\delta})$.

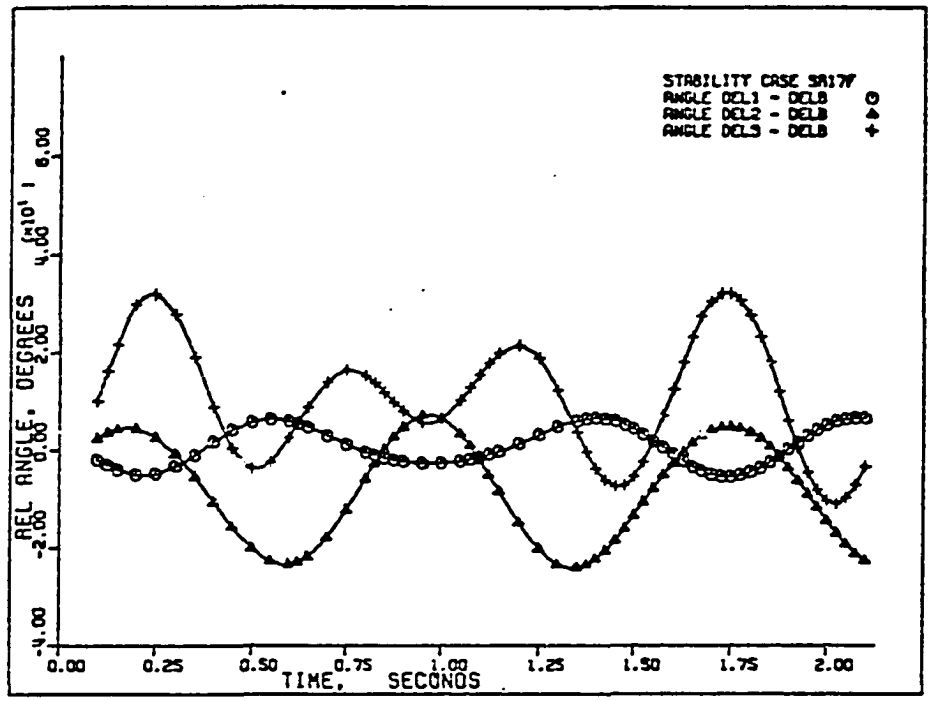

Figure 266. Case SR-17F: relative angles $(\delta_1 - \bar{\delta})$, $(\delta_2 - \bar{\delta})$, and $(\delta_3 - \bar{\delta})$.

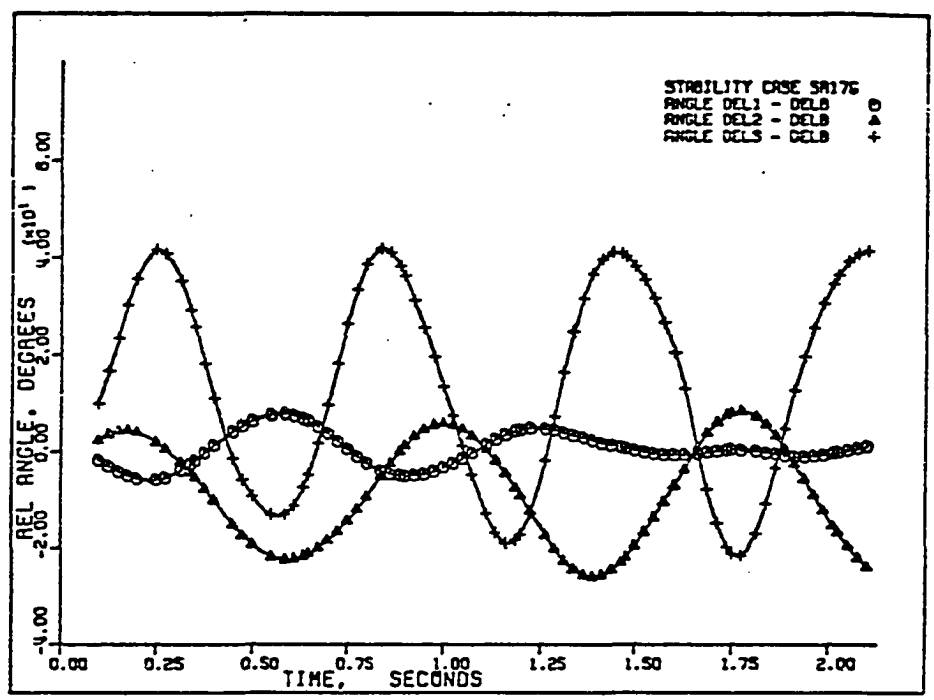

Figure 267. Case SR-17G: relative angles $(\delta_1 - \bar{\delta})$, $(\delta_2 - \bar{\delta})$, and $(\delta_3 - \bar{\delta})$.

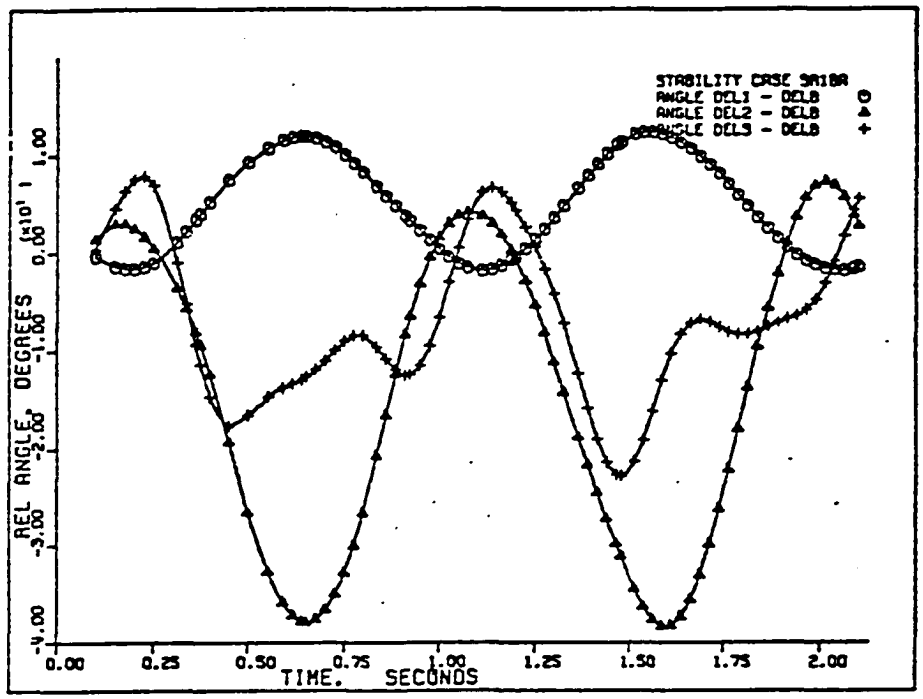

Figure 268. Case SR-18A: relative angles $(\delta_1 - \bar{\delta})$, $(\delta_2 - \bar{\delta})$, and $(\delta_3 - \bar{\delta})$.

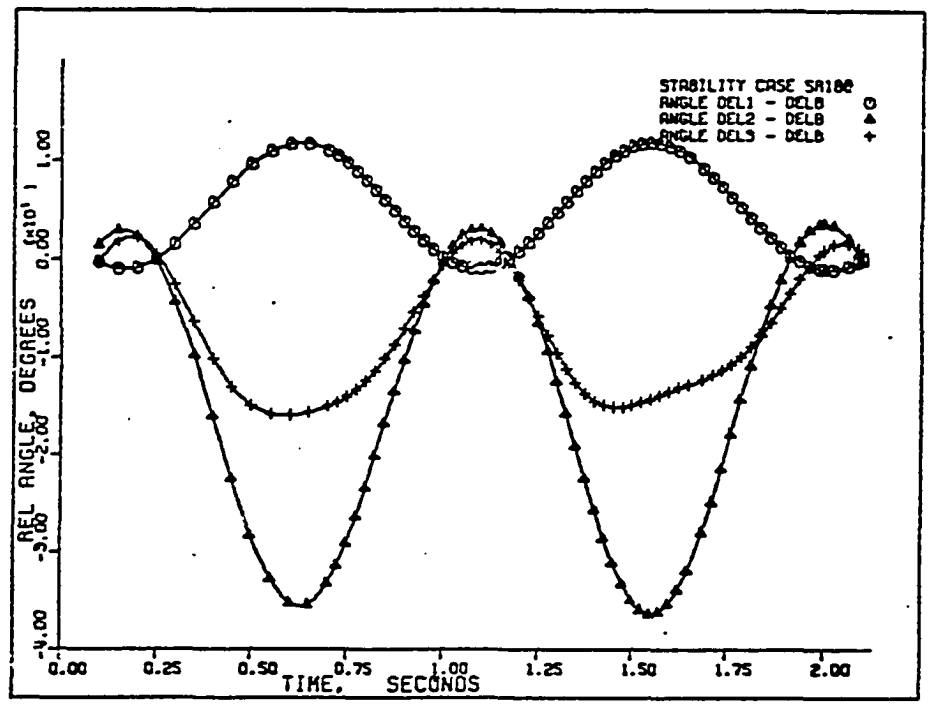

Figure 269. Case SR-18B: relative angles $(\delta_1 - \bar{\delta})$, $(\delta_2 - \bar{\delta})$, and $(\delta_3 - \bar{\delta})$.

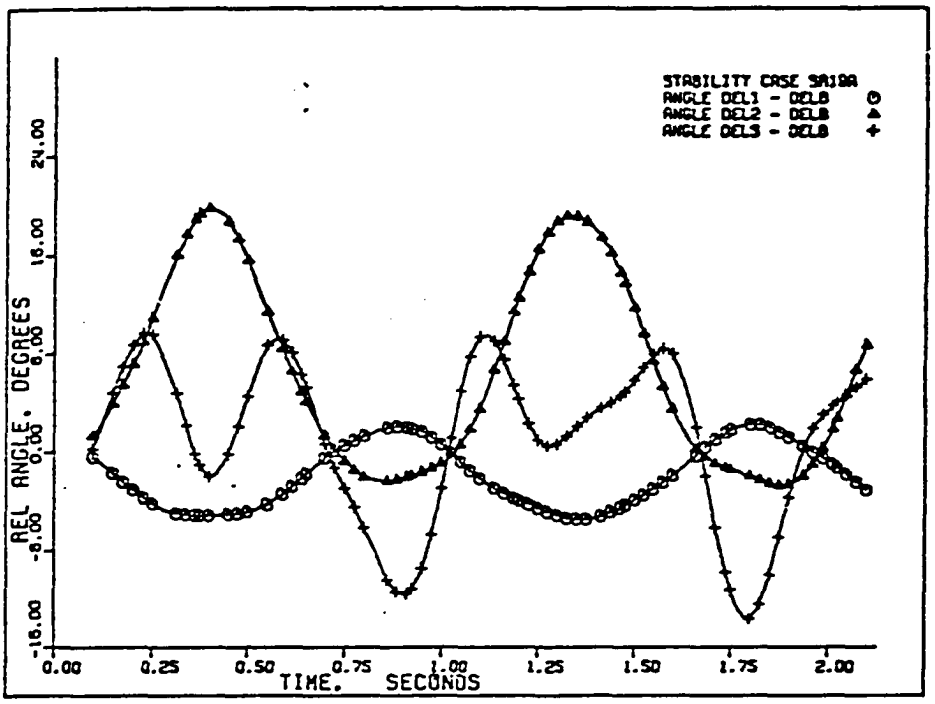

Figure 270. Case SR-19A: relative angles $(\delta_1 - \bar{\delta})$, $(\delta_2 - \bar{\delta})$, and $(\delta_3 - \bar{\delta})$.

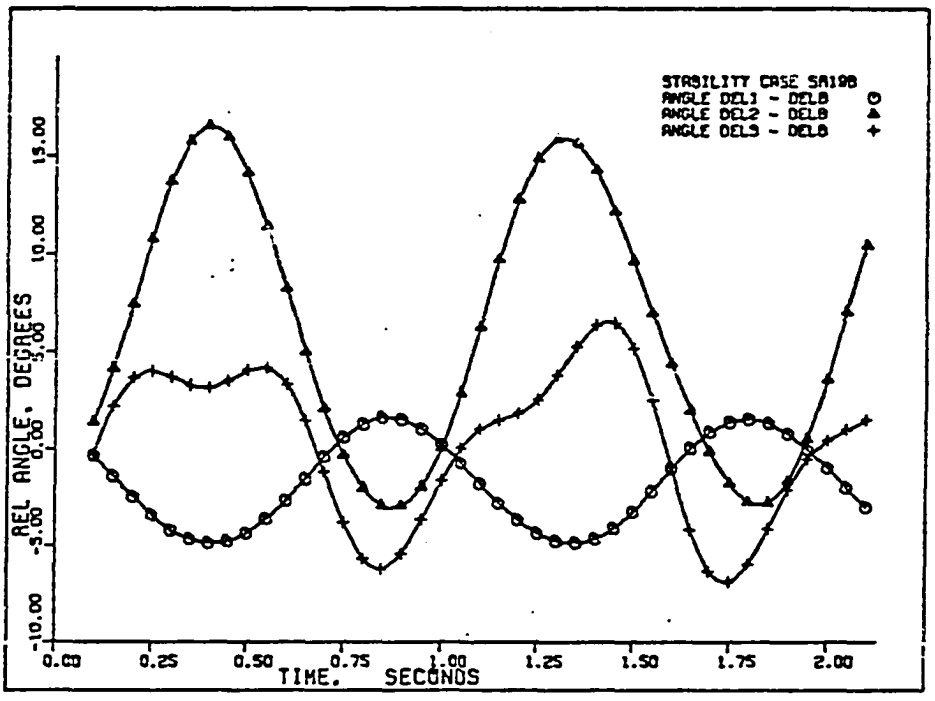

Figure 271. Case SR-19B: relative angles $(\delta_1 - \bar{\delta})$, $(\delta_2 - \bar{\delta})$, and $(\delta_3 - \bar{\delta})$.

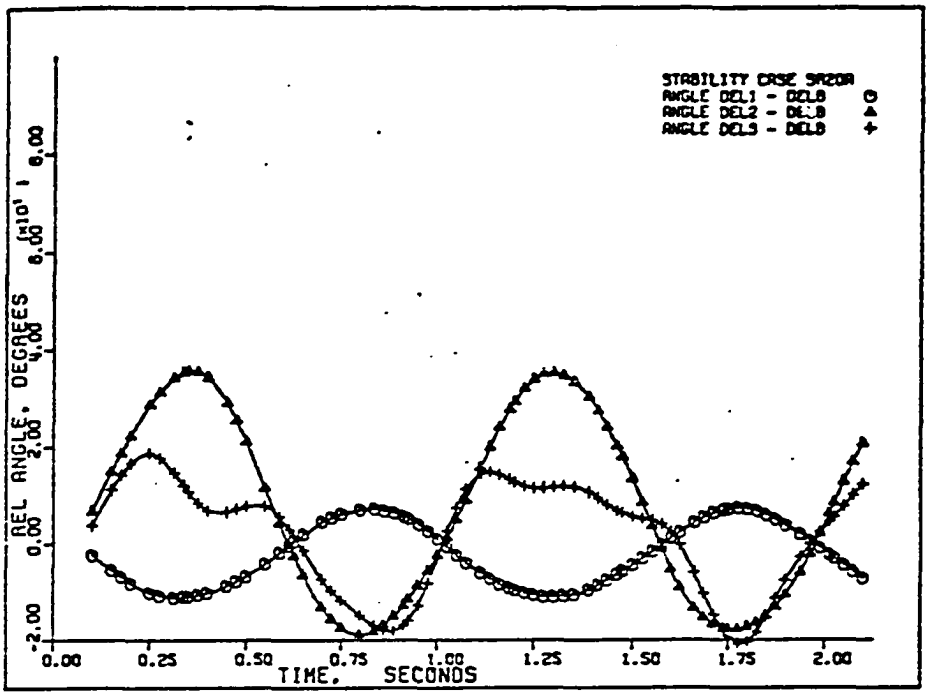

Figure 272. Case SR-20A: relative angles $(\delta_1 - \bar{\delta})$, $(\delta_2 - \bar{\delta})$, and $(\delta_3 - \bar{\delta})$.

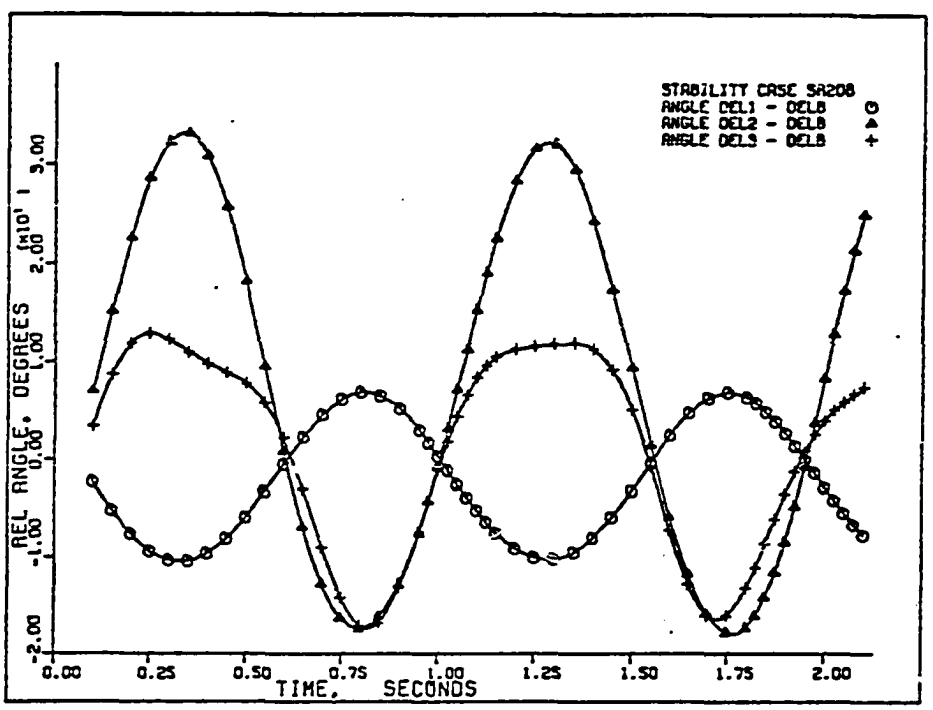

Figure 273. Case SR-20B: relative angles $(\delta_1 - \bar{\delta})$, $(\delta_2 - \bar{\delta})$, and $(\delta_3 - \bar{\delta})$.

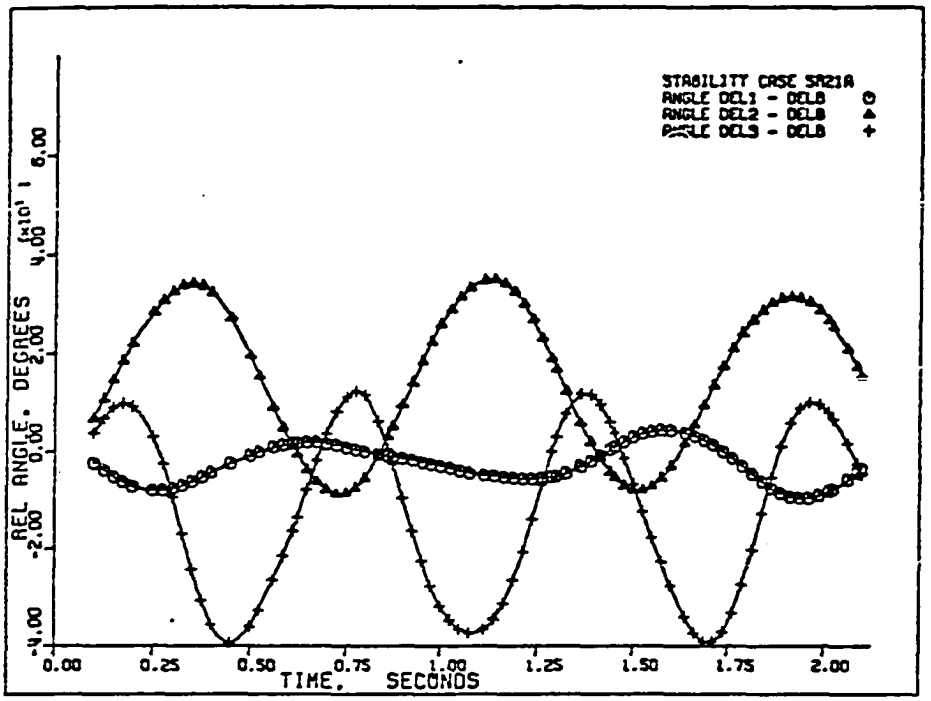

Figure 274. Case SR-21A: relative angles $(\delta_1 - \bar{\delta})$, $(\delta_2 - \bar{\delta})$, and $(\delta_3 - \bar{\delta})$.

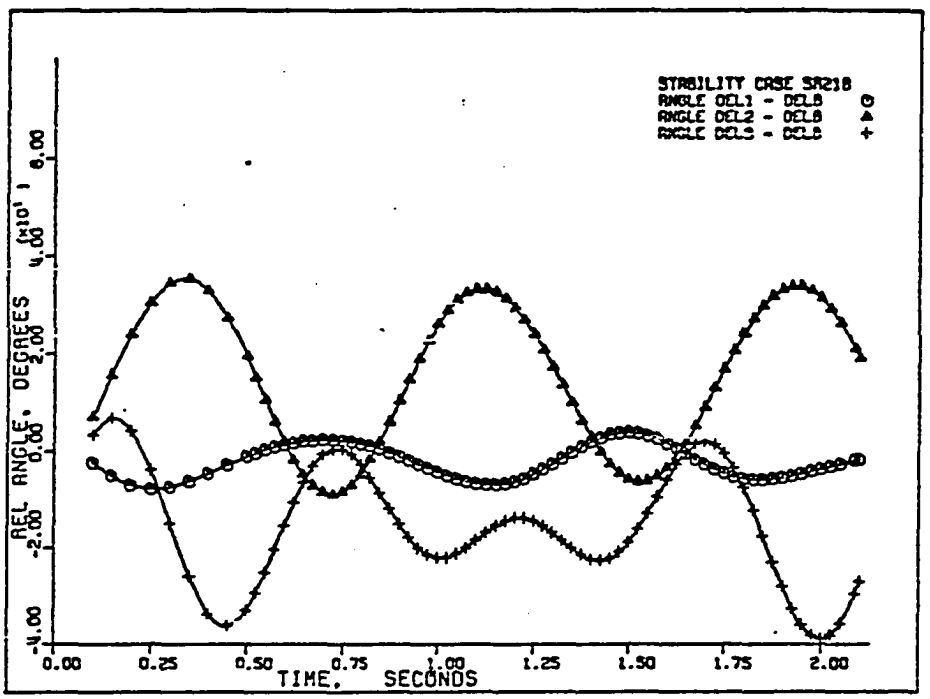

Figure 275. Case SR-21B: relative angles $(\delta_1 - \bar{\delta})$, $(\delta_2 - \bar{\delta})$, and $(\delta_3 - \bar{\delta})$.

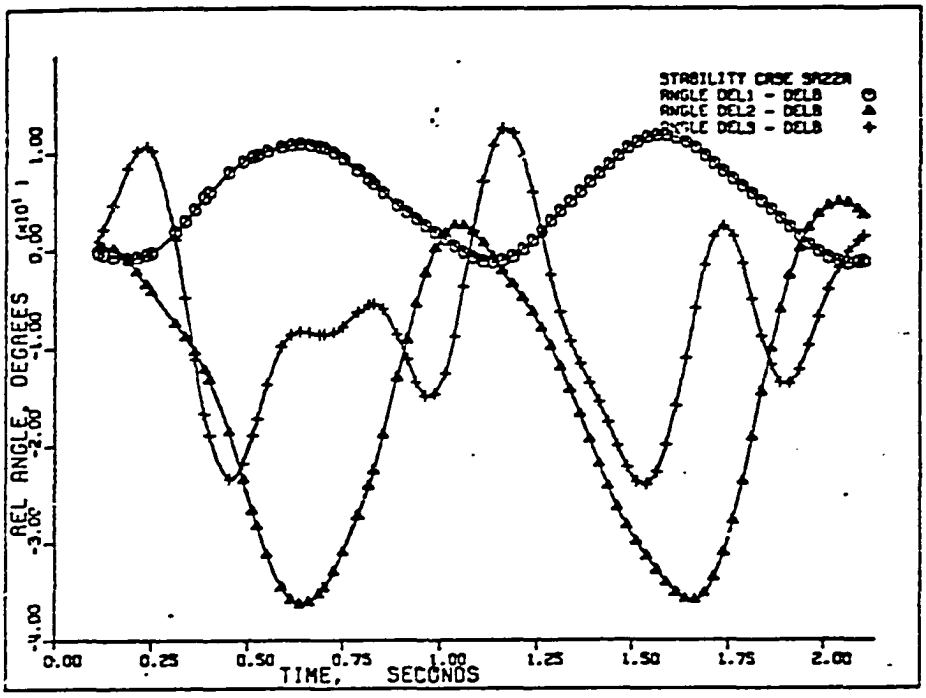

Figure 276. Case SR-22A: relative angles $(\delta_1 - \bar{\delta})$. $(\delta_2 - \bar{\delta})$, and $(\delta_3 - \bar{\delta})$.

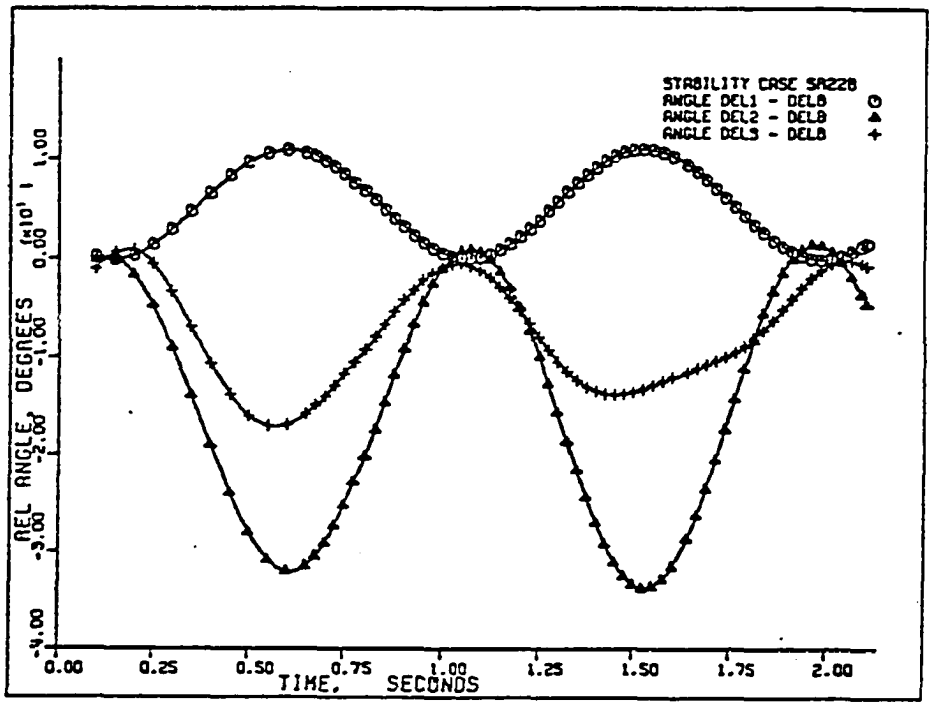

Figure 277. Case SR-22B: relative angles $(\delta_1 - \bar{\delta})$, $(\delta_2 - \bar{\delta})$, and $(\delta_3 - \bar{\delta})$.

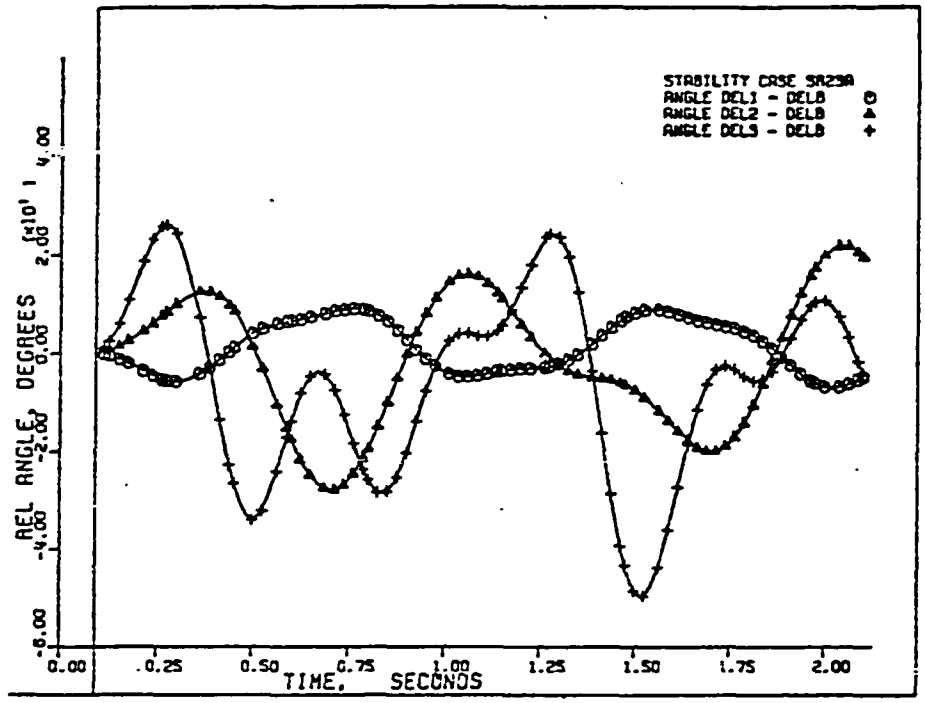

Figure 278. Case SR-23A: relative angles $(\delta_1 - \bar{\delta})$, $(\delta_2 - \bar{\delta})$, and $(\delta_3 - \bar{\delta})$.

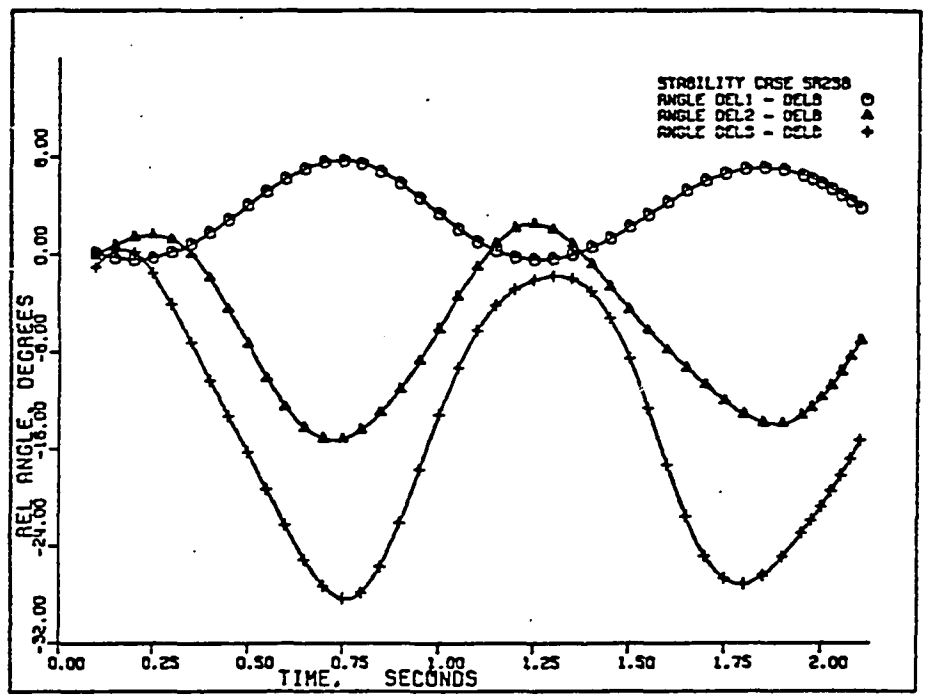

Figure 279. Case SR-23B: relative angles $(\delta_1 - \bar{\delta})$, $(\delta_2 - \bar{\delta})$, and $(\delta_3 - \bar{\delta})$.

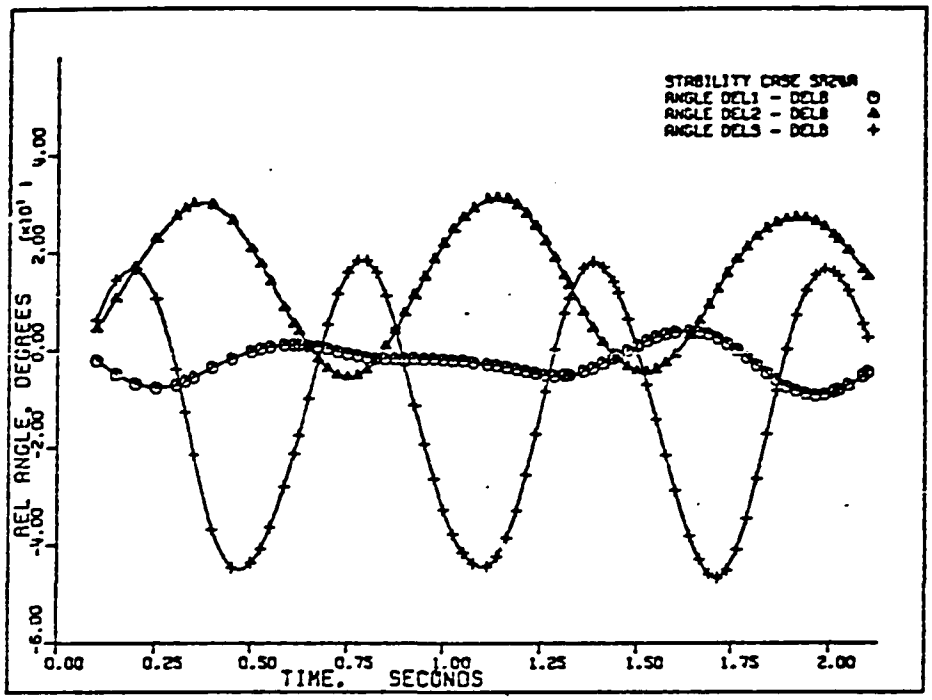

Figure 280. Case SR-24A: relative angles $(\delta_1 - \bar{\delta})$, $(\delta_2 - \bar{\delta})$, and $(\delta_3 - \bar{\delta})$.

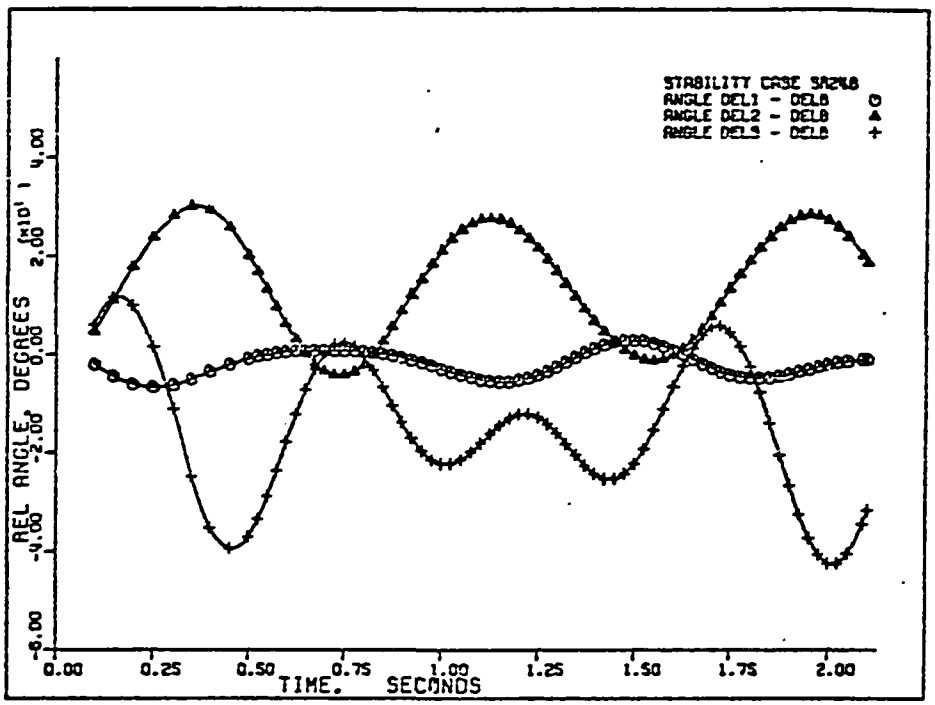

Figure 281. Case SR-24B: relative angles $(\delta_1 - \bar{\delta})$, $(\delta_2 - \bar{\delta})$, and $(\delta_3 - \bar{\delta})$.

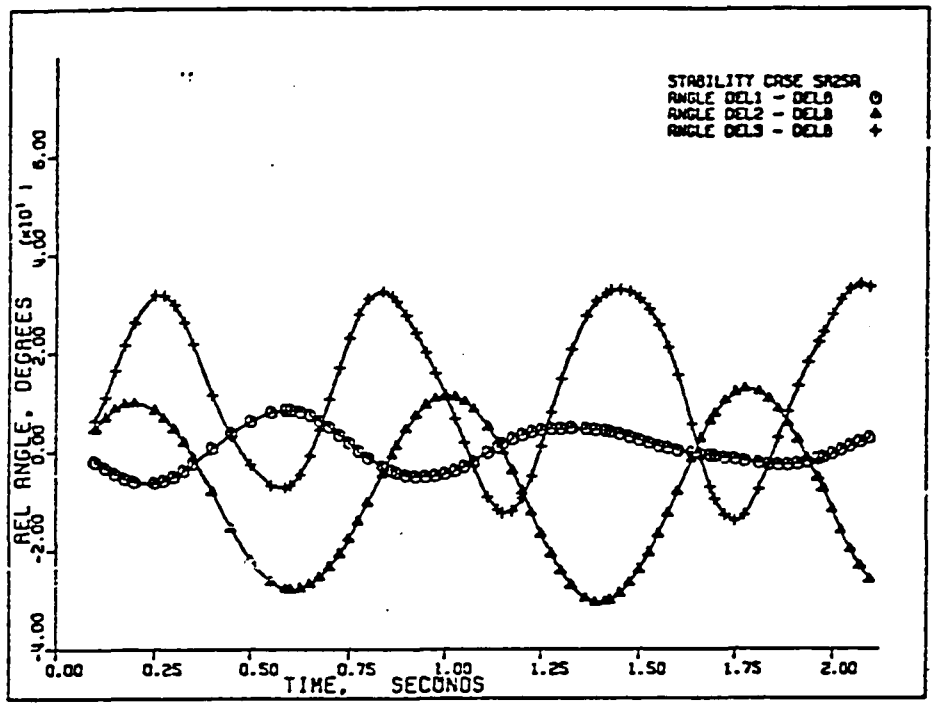

Figure 282. Case SR-25A: relative angles $(\delta_1 - \bar{\delta})$, $(\delta_2 - \bar{\delta})$, and $(\delta_3 - \bar{\delta})$.

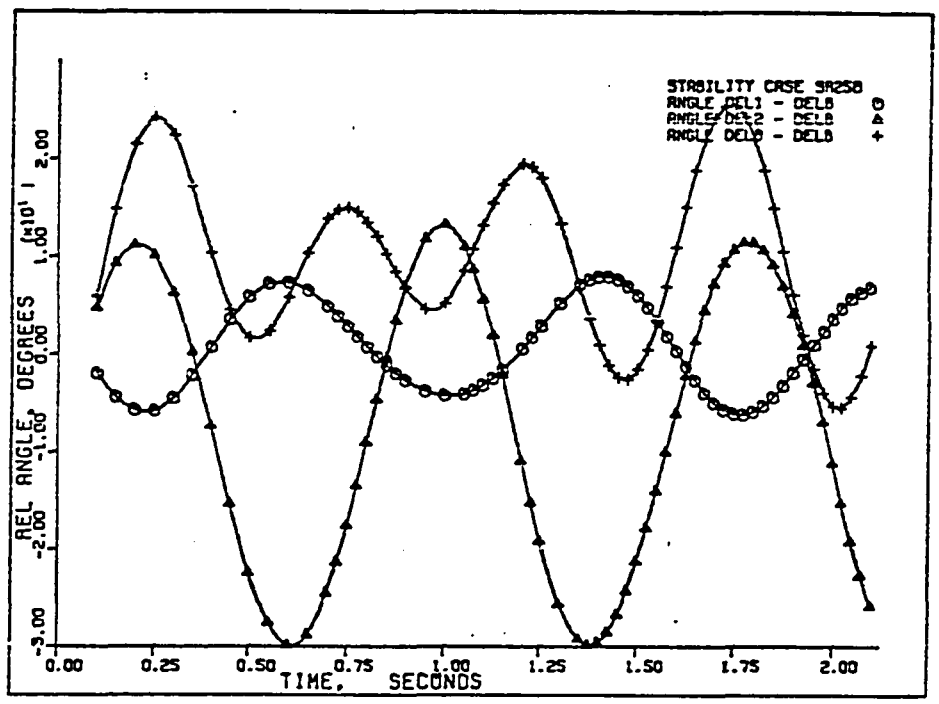

Figure 283. Case SR-25B: relative angles $(\delta_1 - \bar{\delta})$, $(\delta_2 - \bar{\delta})$, and $(\delta_3 - \bar{\delta})$.

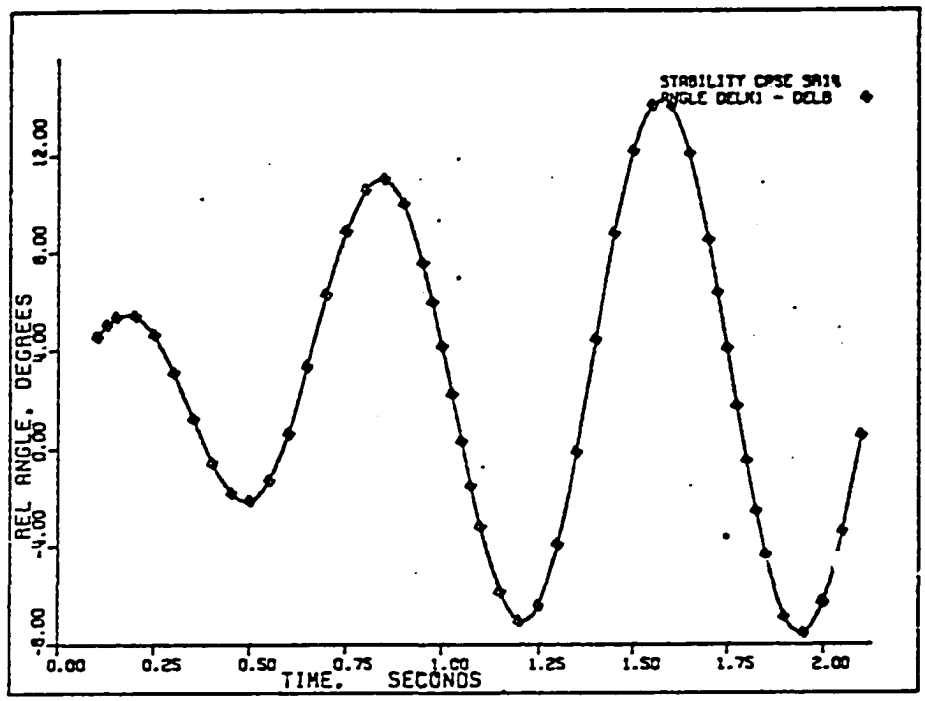

Figure 284. Case SR-14: relative angle $(\delta_k - \bar{\delta})$.

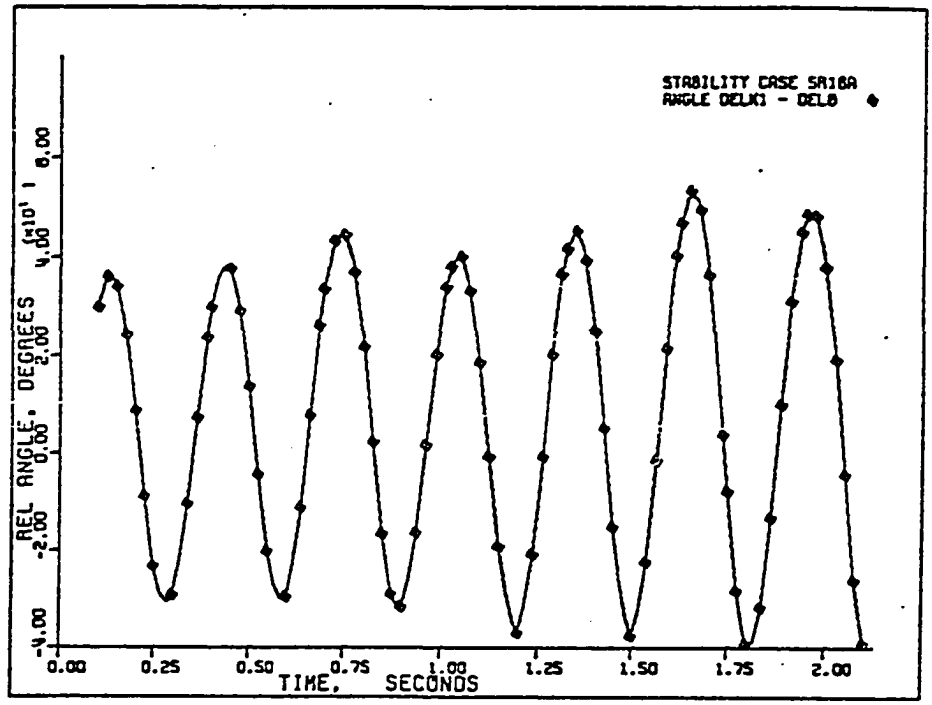

Figure 285. Case SR-16A: relative angle $(\delta_k - \bar{\delta})$.

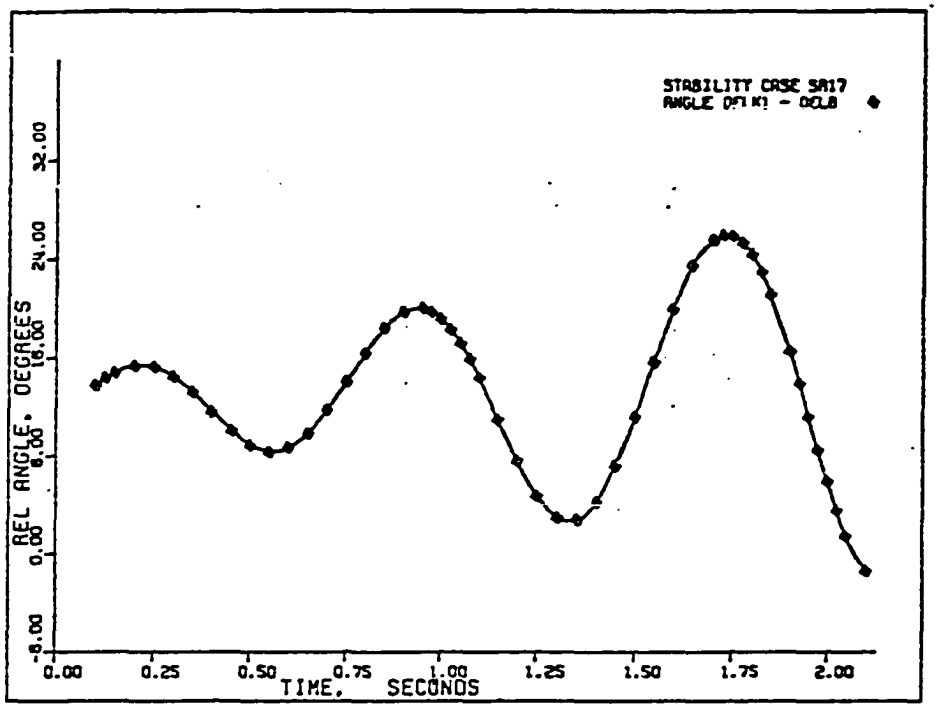

Figure 286. Case SR-17: relative angle $(\delta_k - \bar{\delta})$.

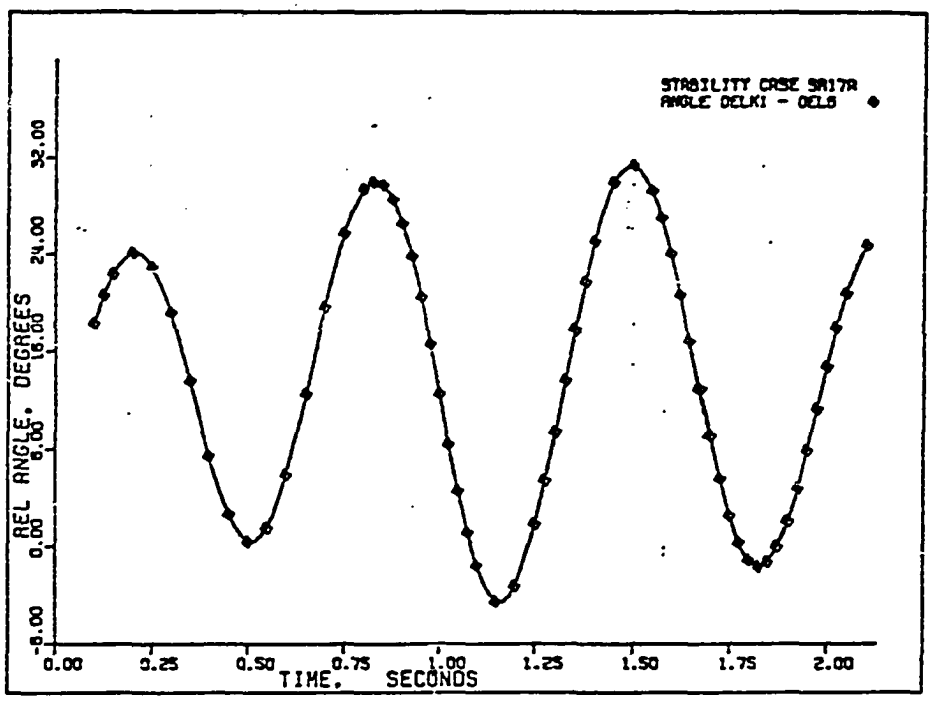

Figure 287. Case SR-17A: relative angle $(\delta_k - \bar{\delta})$.

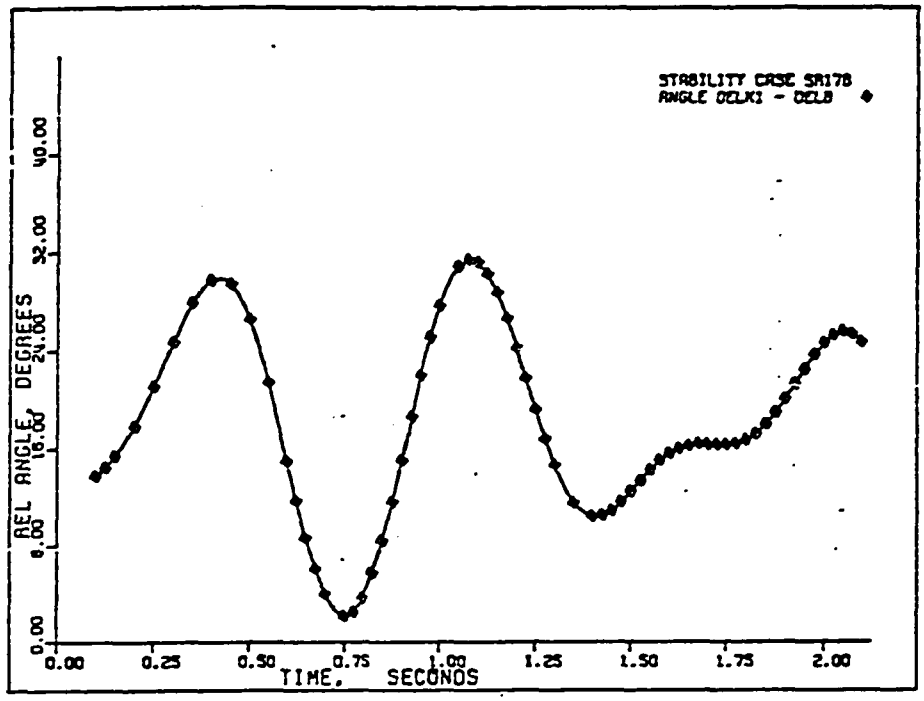

Figure 288. Case SR-17B: relative angle $(\delta_k - \bar{\delta})$.

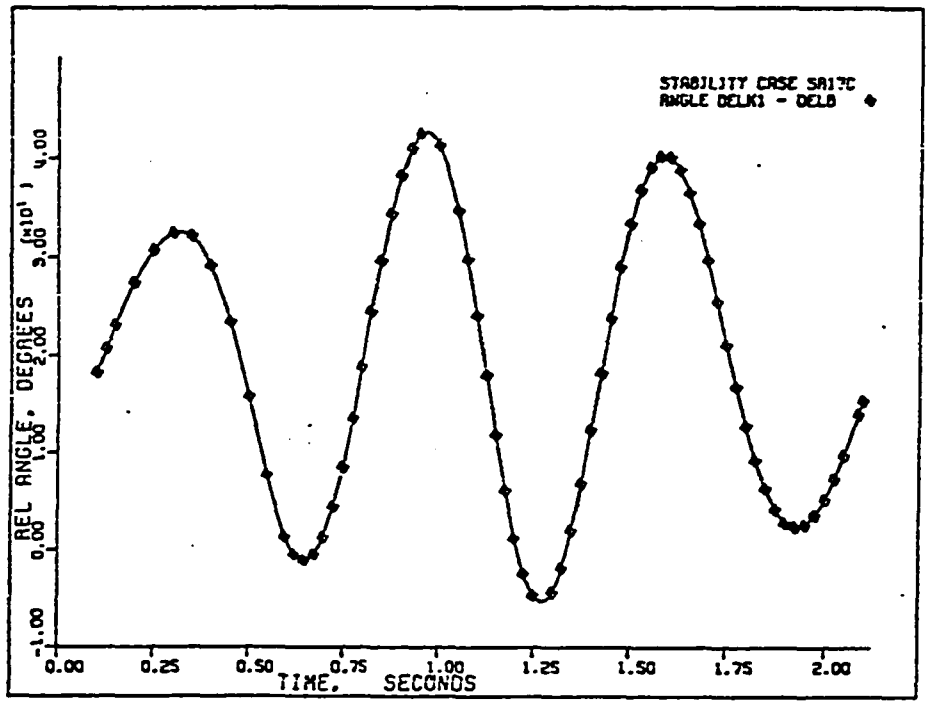

Figure 289. Case SR-17C: relative angle $(\delta_k - \bar{\delta})$.

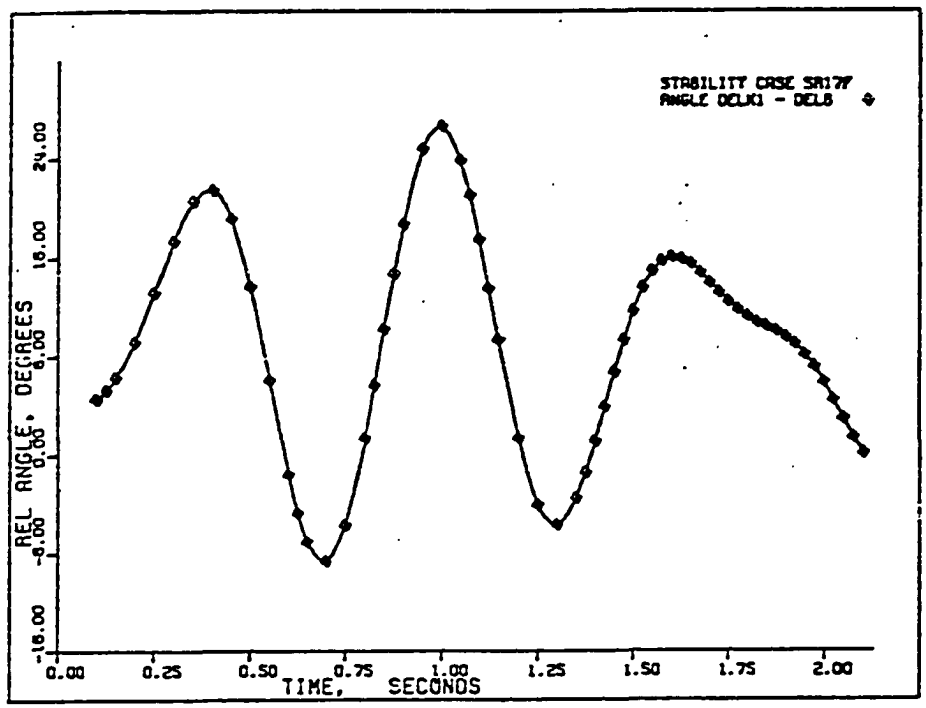

Figure 290. Case SR-17F: relative angle $(\delta_k - \bar{\delta})$.

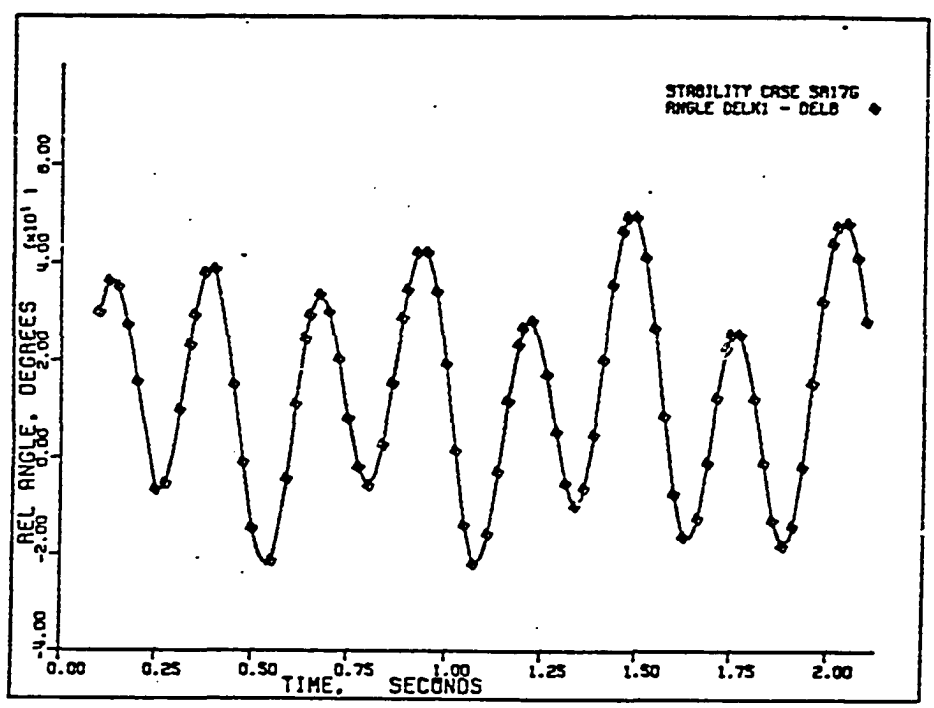

Figure 291. Case SR-17G: relative angle $(\delta_k - \bar{\delta})$.

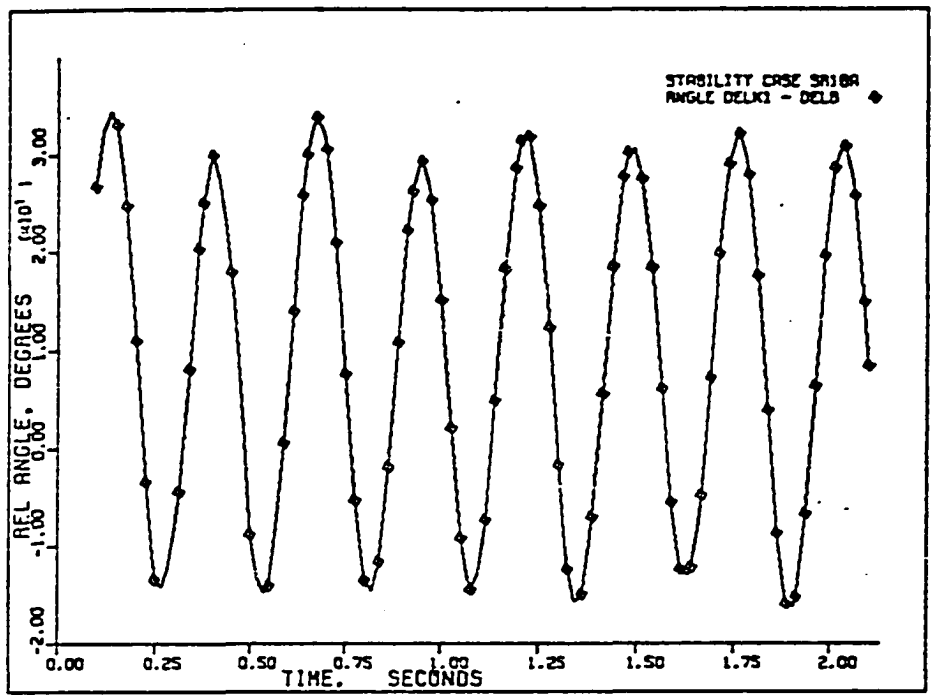

Figure 292. Case SR-18A: relative angle $(\delta_k - \bar{\delta})$.

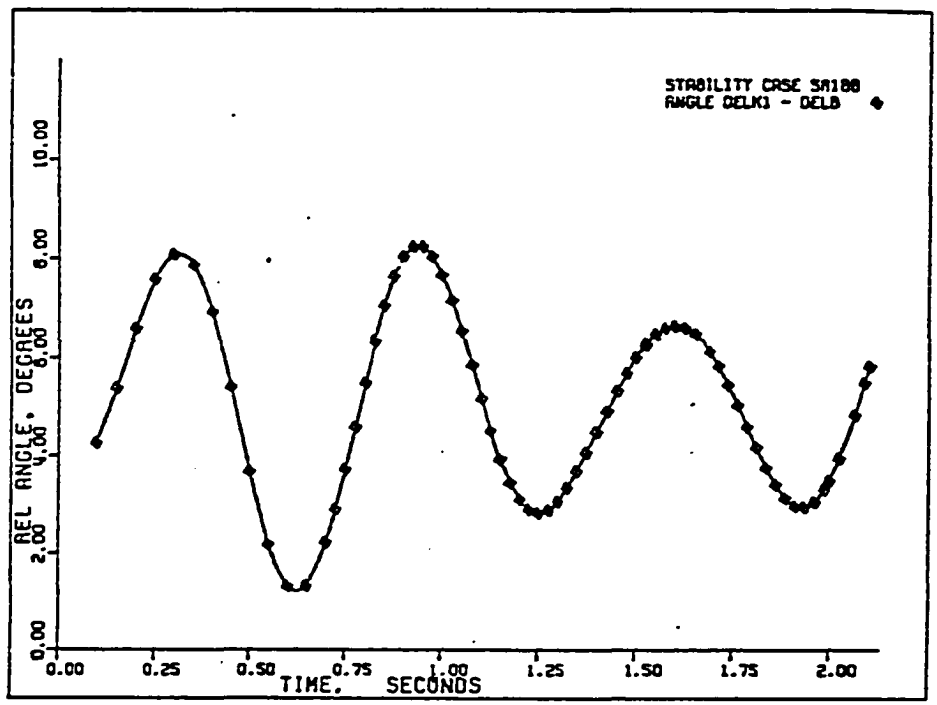

Figure 293. Case SR-18B: relative angle $(\delta_k - \bar{\delta})$.

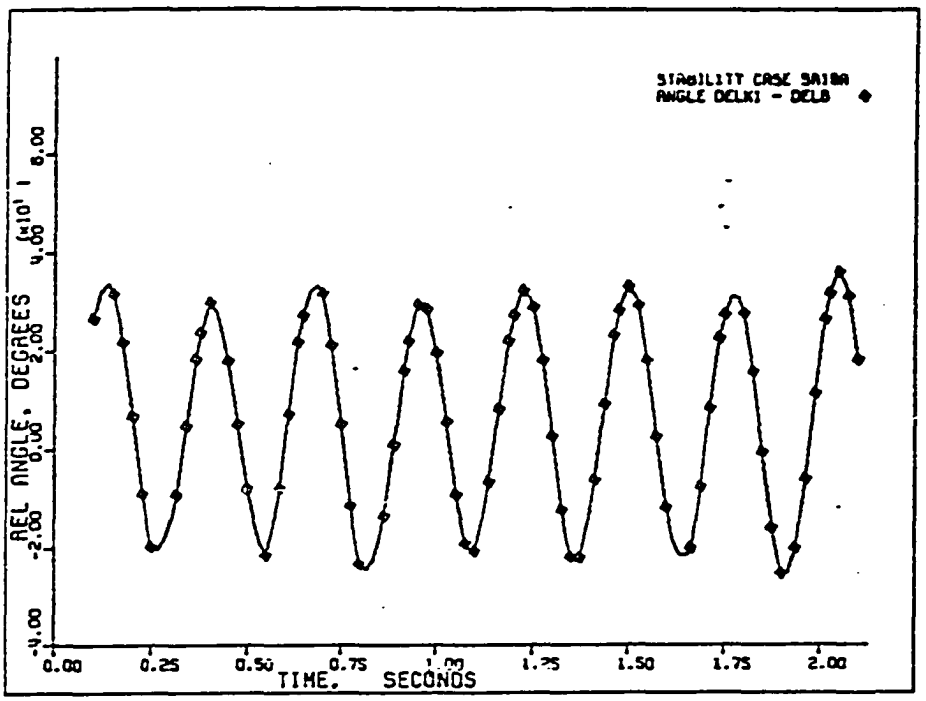

Figure 294. Case SR-19A: relative angle $(\delta_k - \bar{\delta})$.

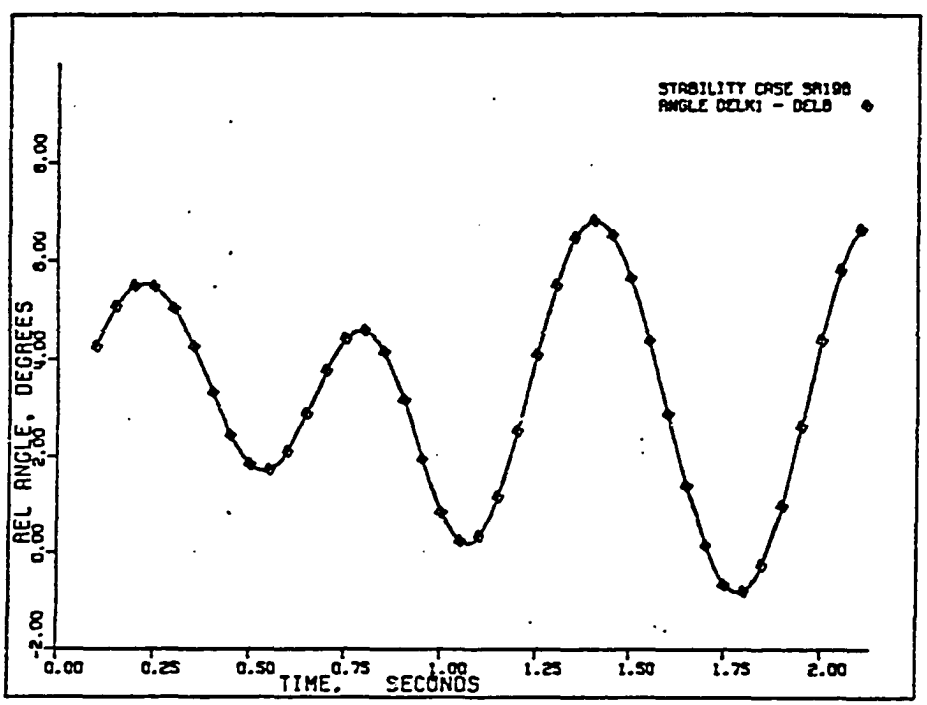

Figure 295. Case SR-19B: relative angle $(\delta_k - \bar{\delta})$.

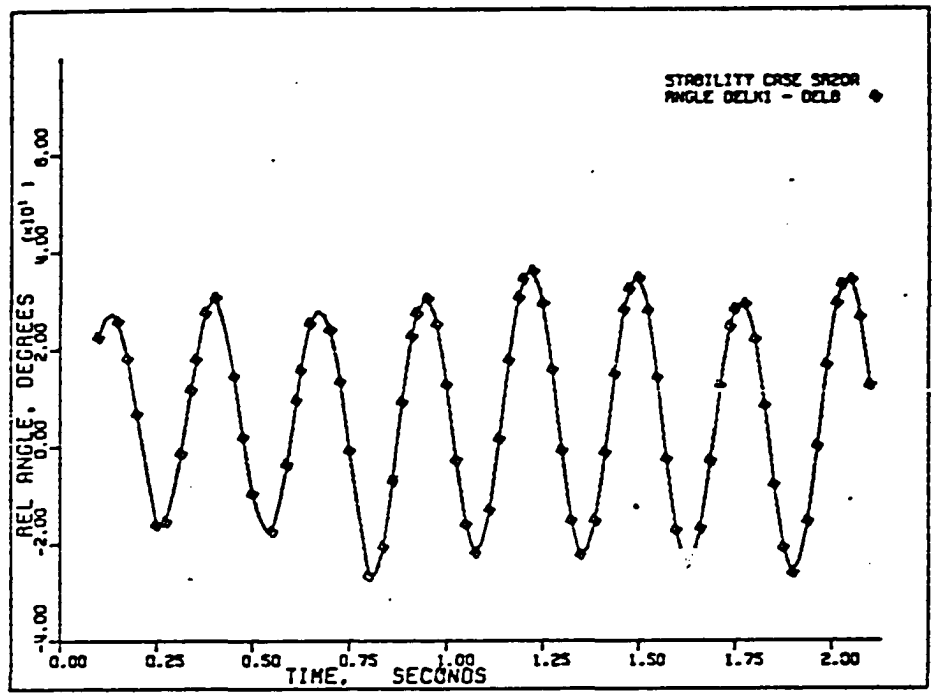

Figure 296. Case SR-20A: relative angle $(\delta_k - \bar{\delta})$.

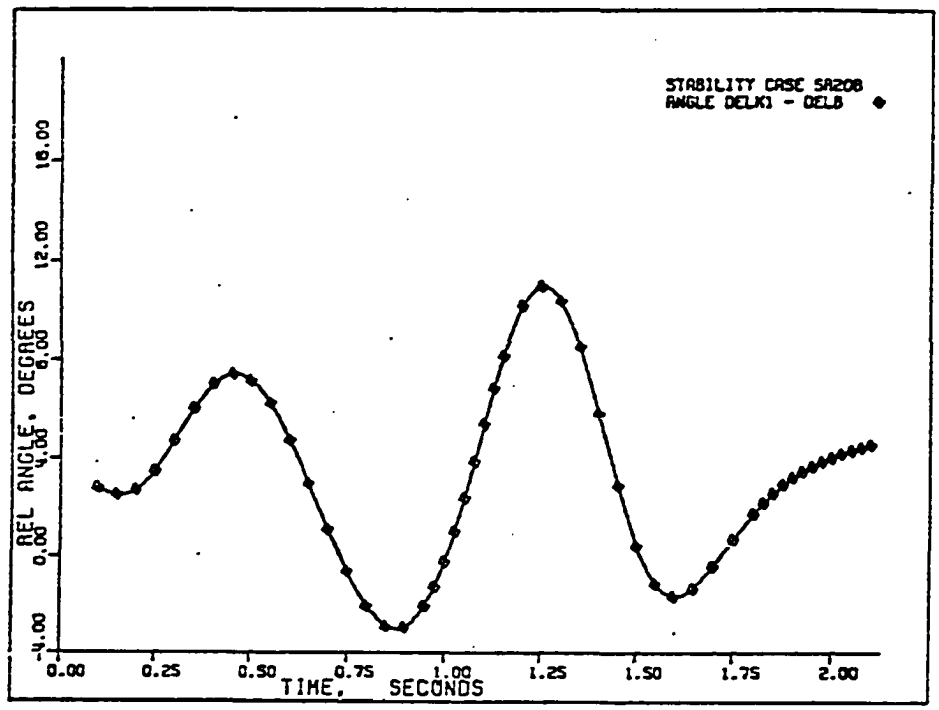

Figure 297. Case SR-20B: relative angle $(\delta_k - \bar{\delta})$.

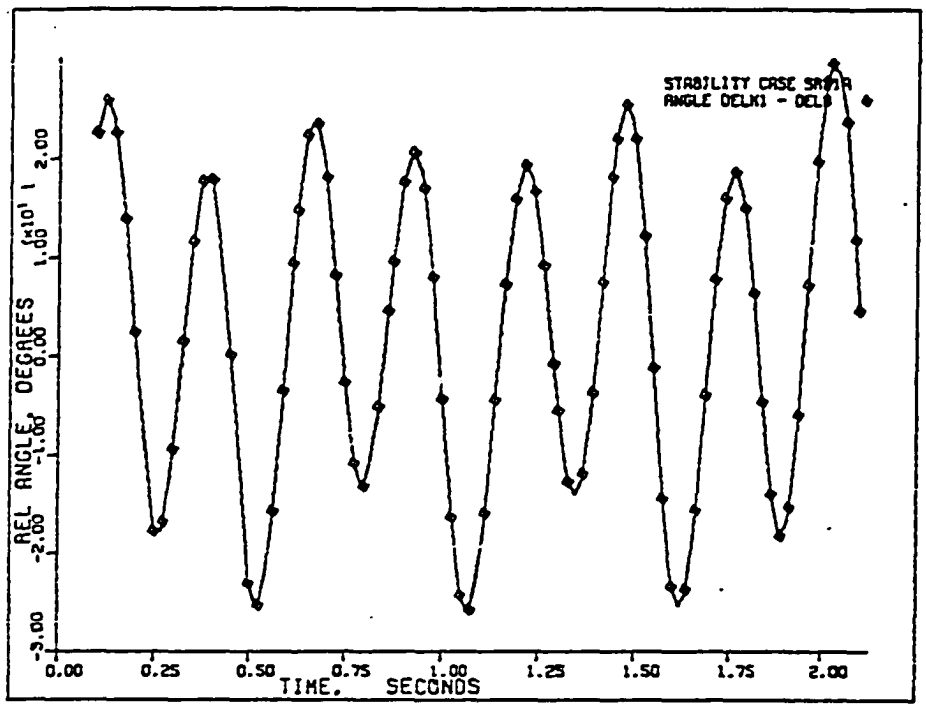

Figure 298. Case SR-21A: relative angle $(\delta_k - \bar{\delta})$.

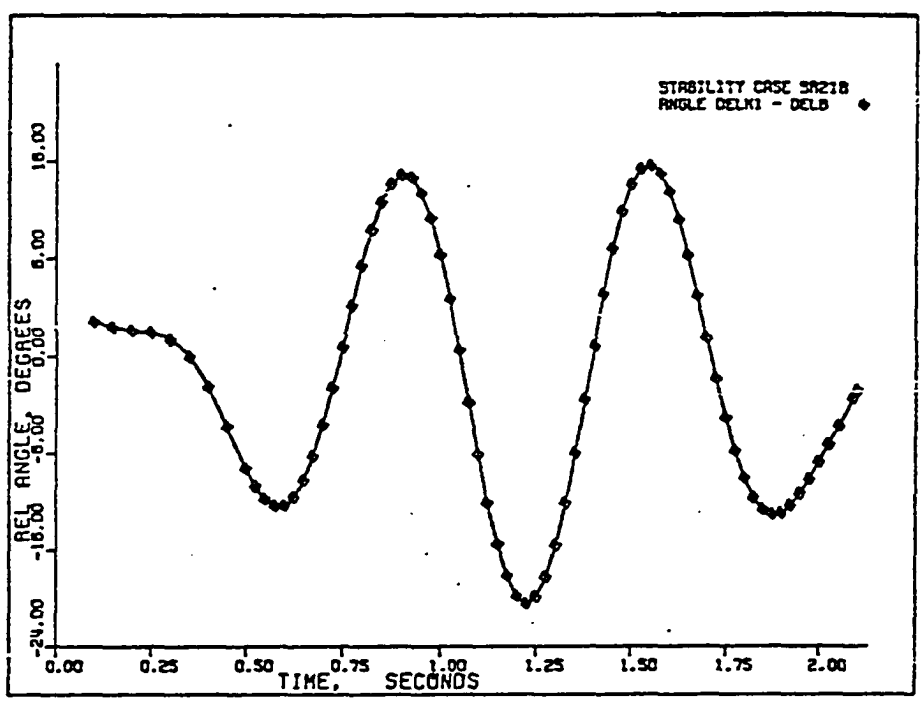

Figure 299. Case SR-21B: relative angle $(\delta_k - \bar{\delta})$.

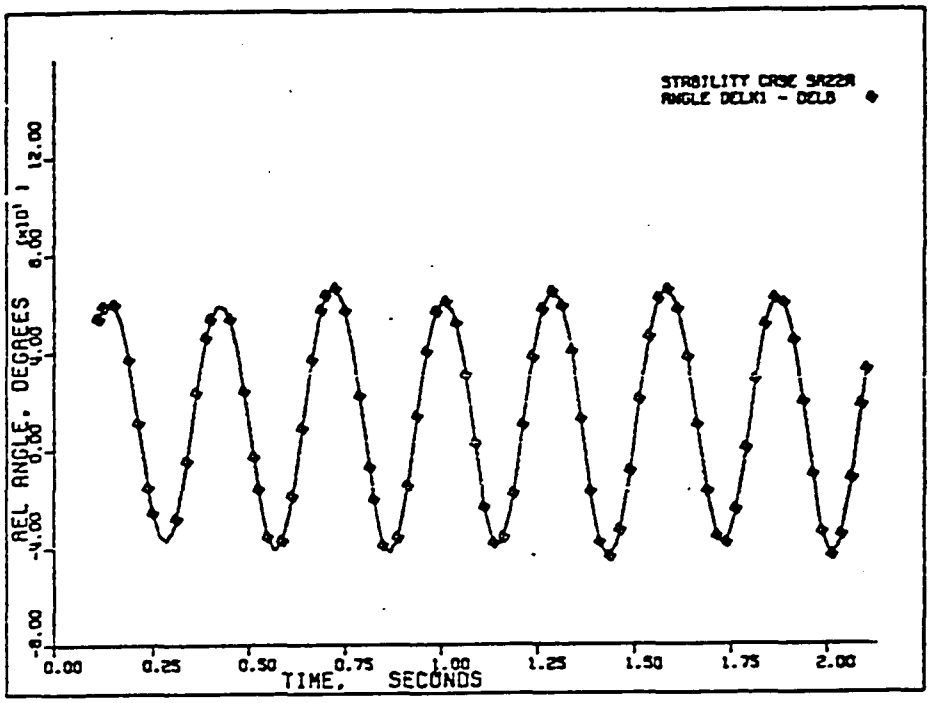

Figure 300. Case SR-22A: relative angle $(\delta_k - \bar{\delta})$.

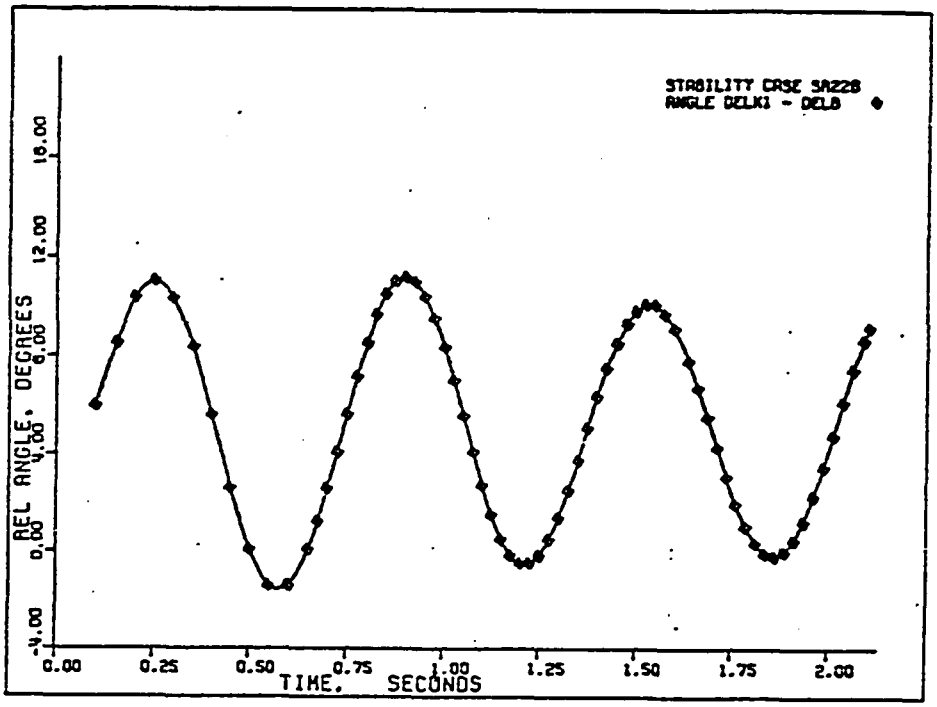

Figure 301. Case SR-22B: relative angle $(\delta_k - \bar{\delta})$.

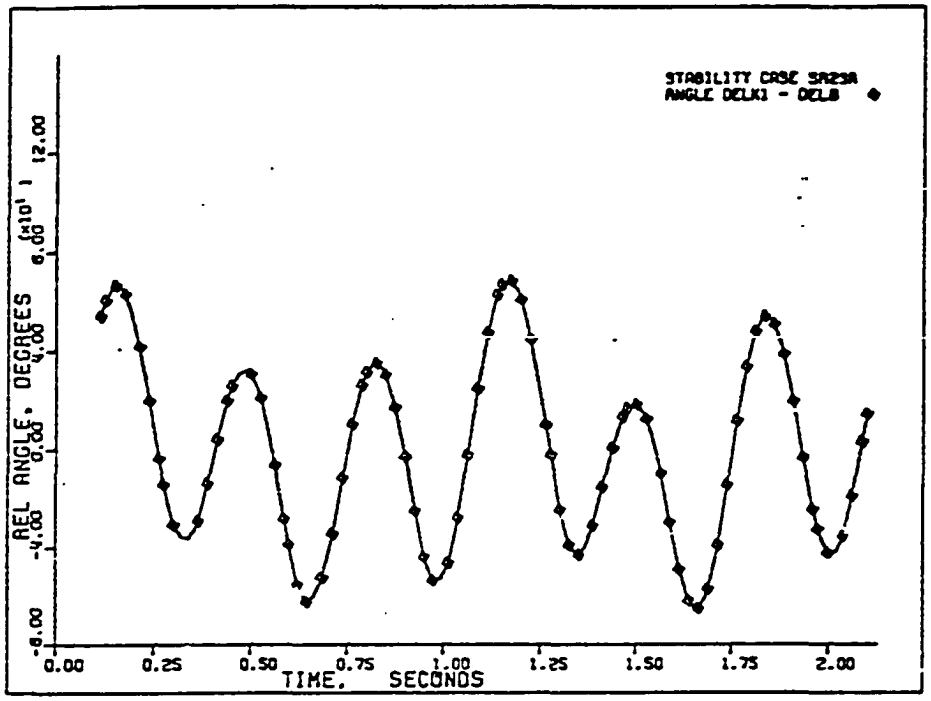

Figure 302. Case SR-23A: relative angle $(\delta_k - \bar{\delta})$.

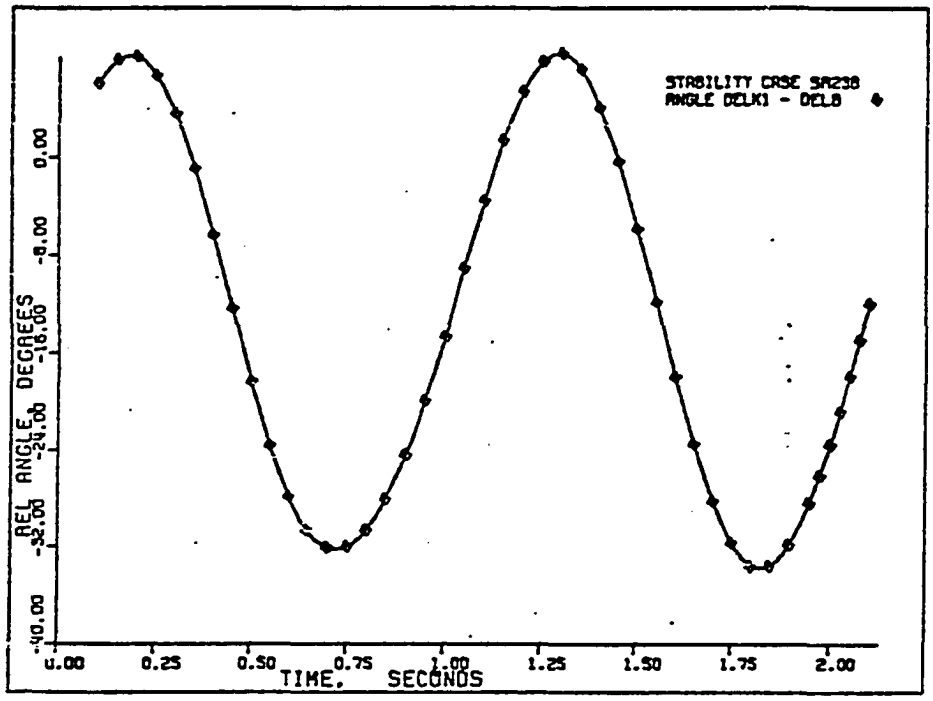

Figure 303. Case SR-23B: relative angle $(\delta_k - \bar{\delta})$.

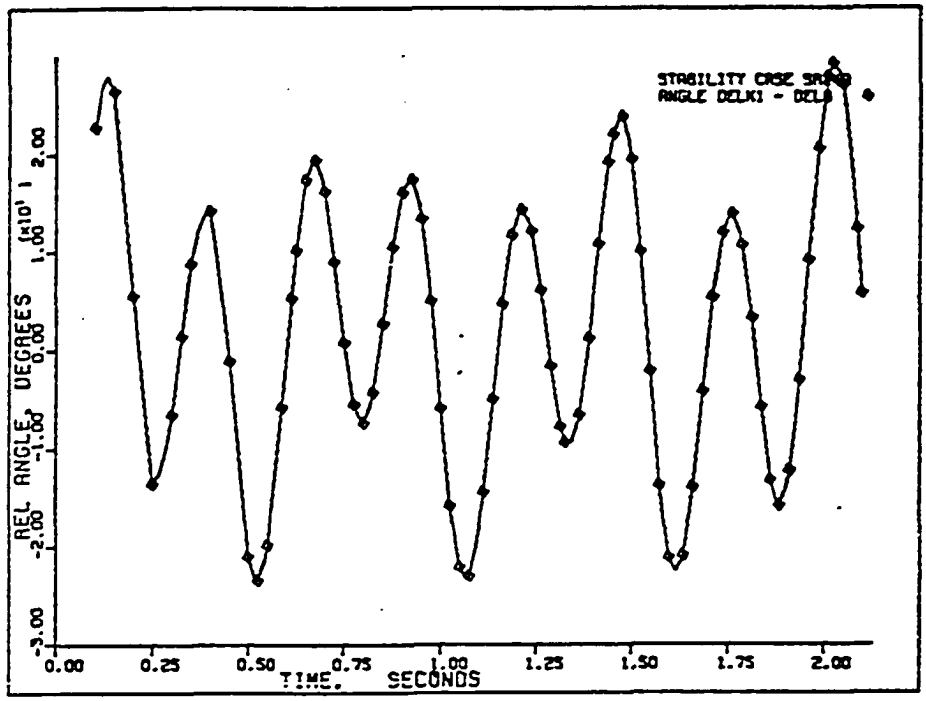

Figure 304. Case SR-24A: relative angle $(\delta_k - \bar{\delta})$.

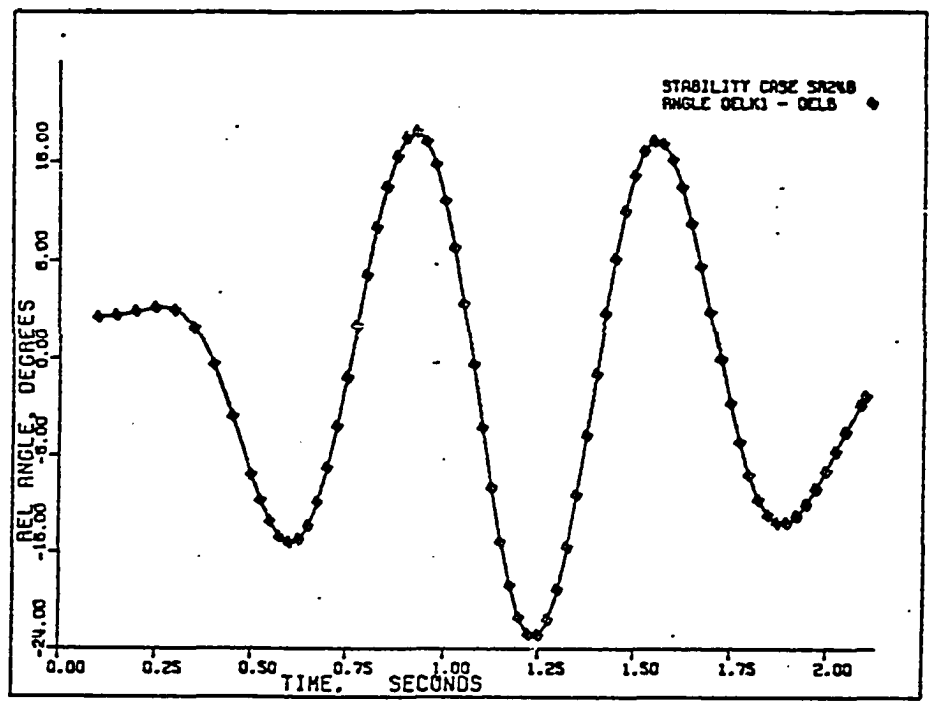

Figure 305. Case SR-24B: relative angle $(\delta_k - \bar{\delta})$.

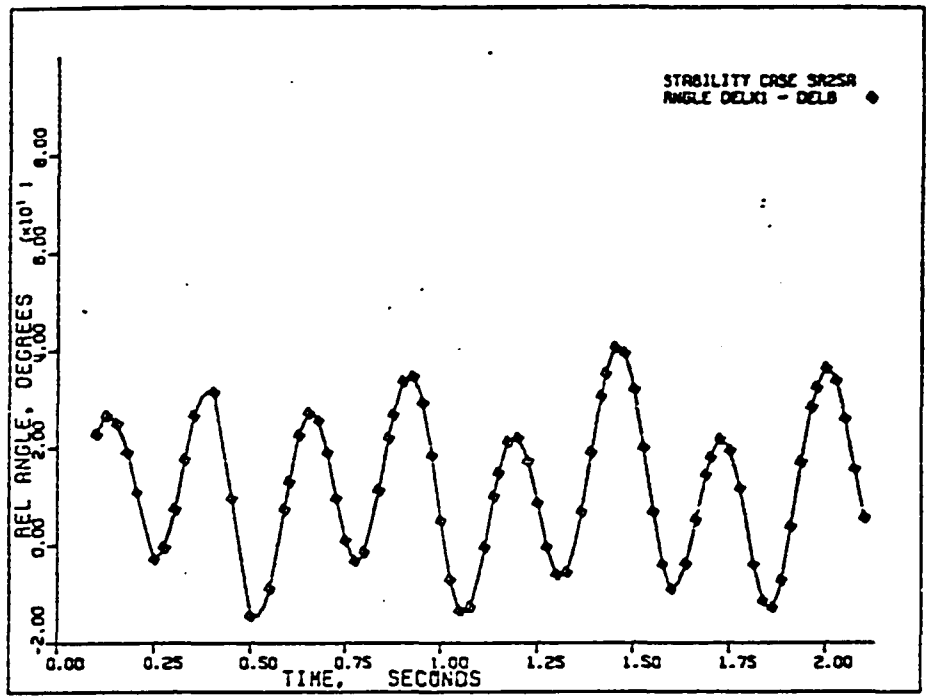

Figure 306. Case SR-25A: relative angle $(\delta_k - \bar{\delta})$.

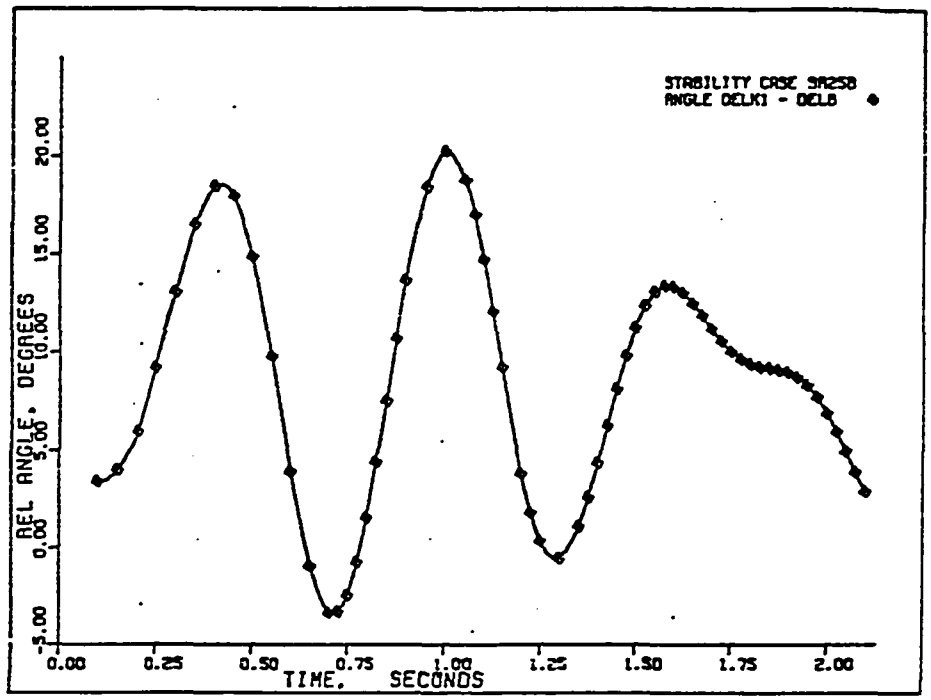

Figure 307. Case SR-25B: relative angle $(\delta_k - \bar{\delta})$.

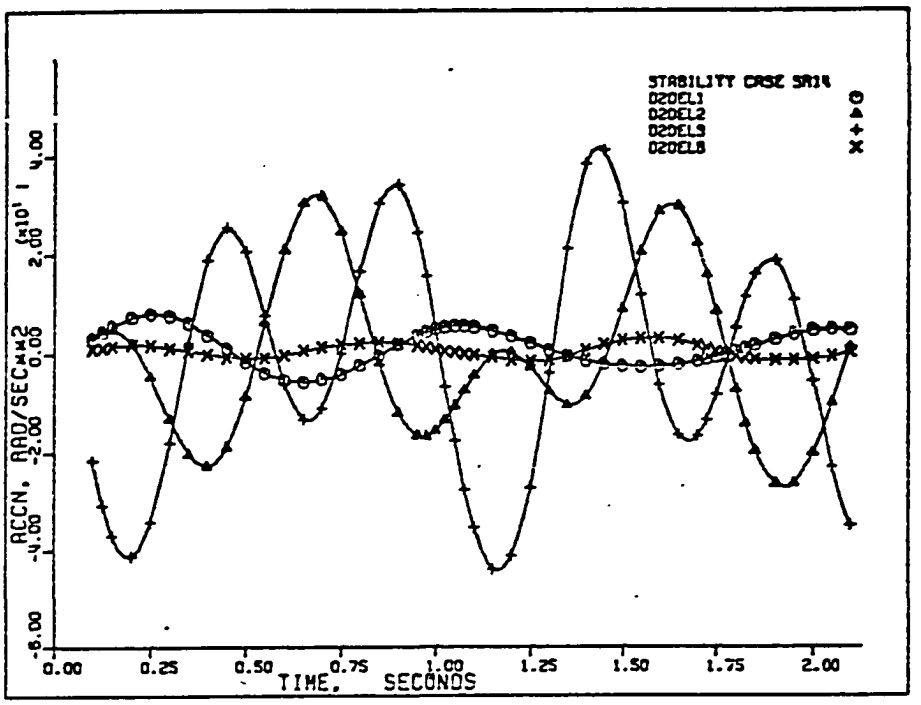

Figure 308. Case SR-14: accelerations $\ddot{\delta}_1$, $\ddot{\delta}_2$, $\ddot{\delta}_3$, and $\ddot{\ddot{\delta}}$.

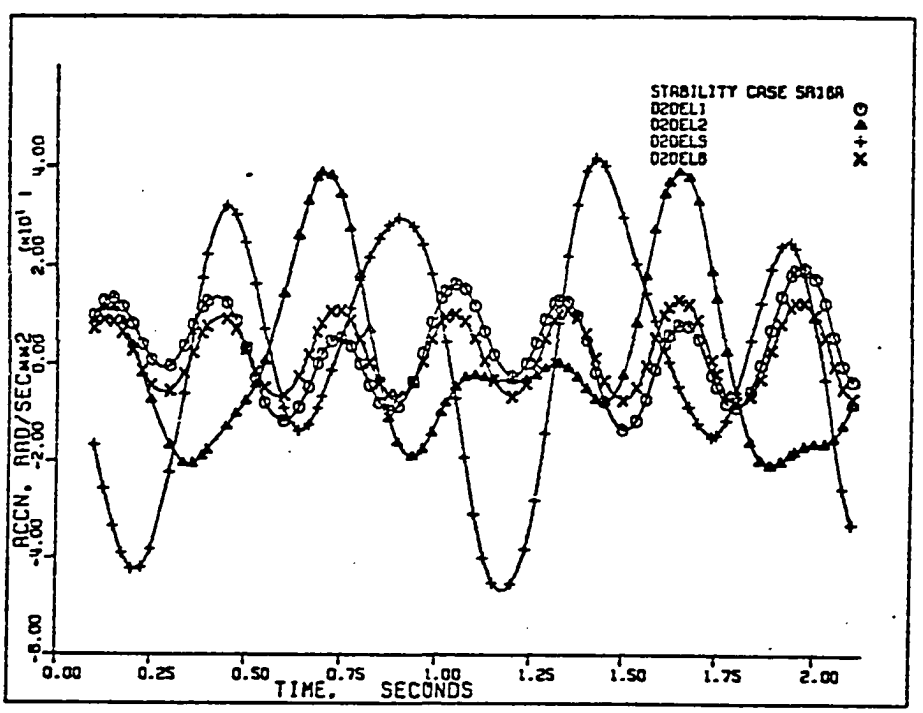

Figure 309. Case SR-16A: accelerations $\ddot{\delta}_1$, $\ddot{\delta}_2$, $\ddot{\delta}_3$, and $\ddot{\ddot{\delta}}$.

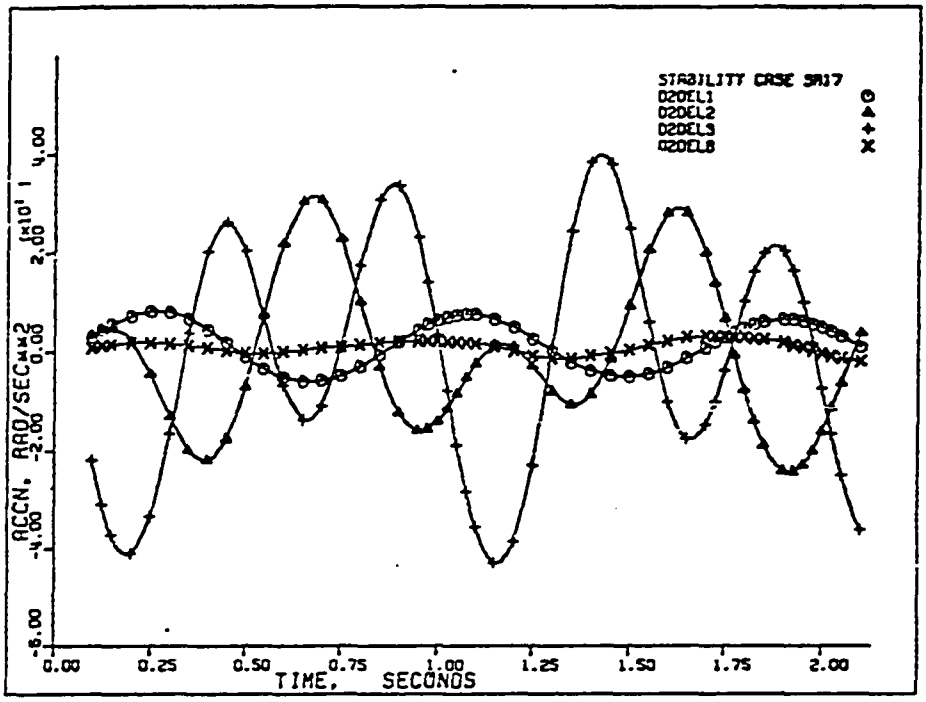

Figure 310. Case SR-17: accelerations $\ddot{\delta}_1$, $\ddot{\delta}_2$, $\ddot{\delta}_3$, and $\bar{\delta}$.

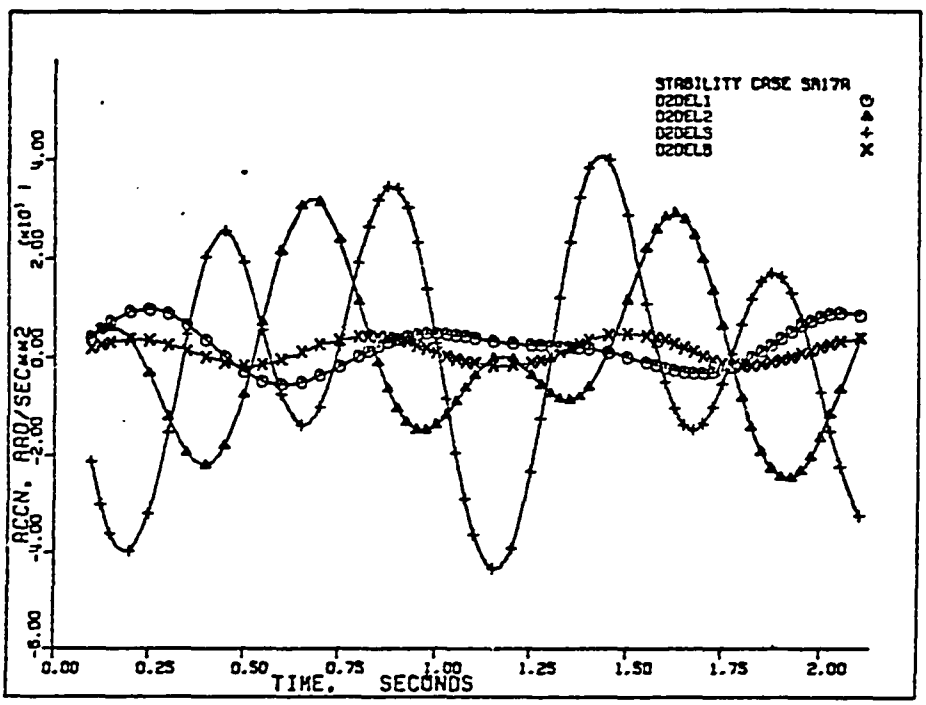

Figure 311. Case SR-17A: accelerations $\ddot{\delta}_1$, $\ddot{\delta}_2$, $\ddot{\delta}_3$, and $\bar{\bar{\delta}}$.

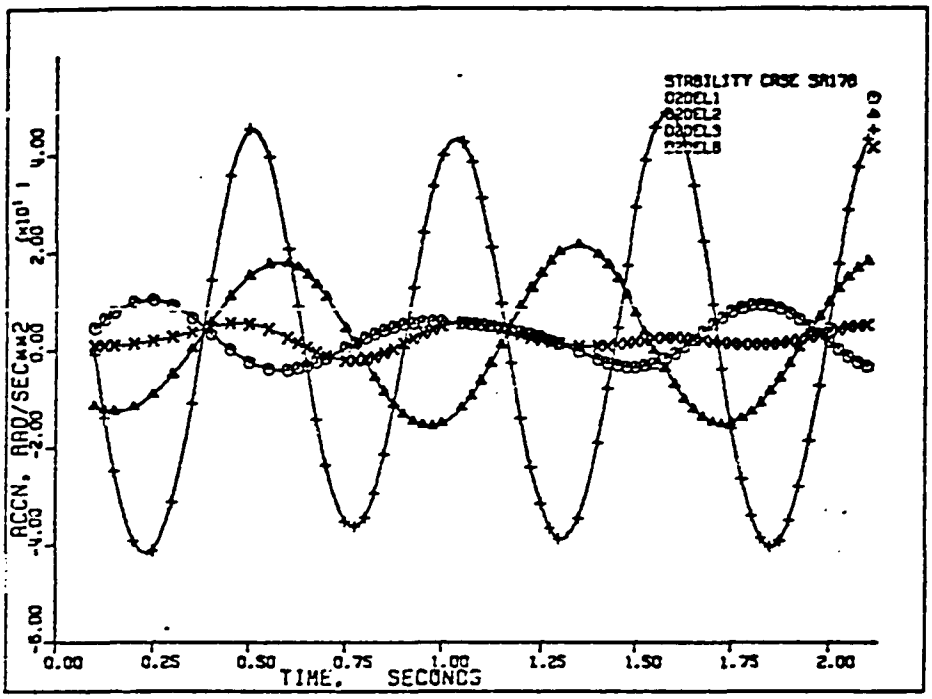

Figure 312. Case SR-17B: accelerations $\ddot{\delta}_1$, $\ddot{\delta}_2$, $\ddot{\delta}_3$, and $\ddot{\bar{\delta}}$.

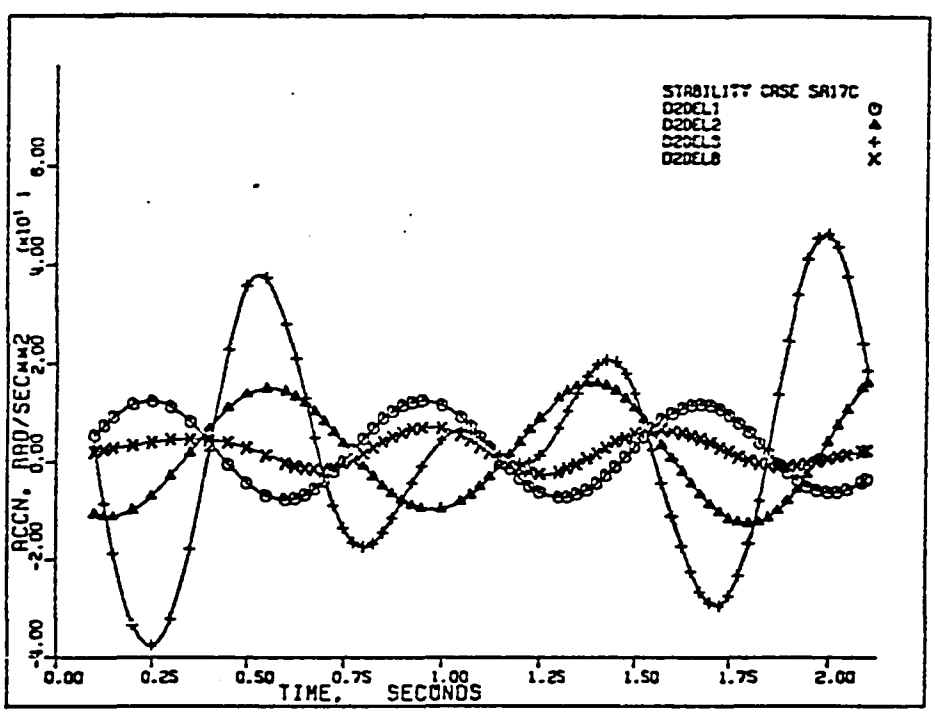

Figure 313. Case SR-17C: accelerations $\ddot{\delta}_1$, $\ddot{\delta}_2$, $\ddot{\delta}_3$, and $\ddot{\bar{\delta}}$.

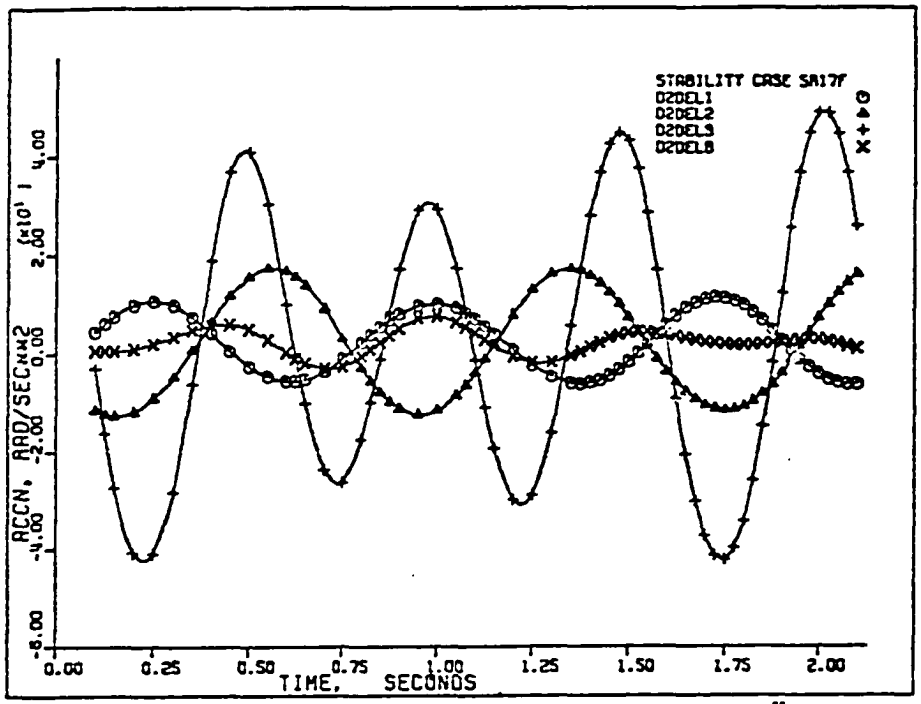

Figure 314. Case SR-17F: accelerations $\ddot{\delta}_1$, $\ddot{\delta}_2$, $\ddot{\delta}_3$, and $\ddot{\bar{\delta}}$.

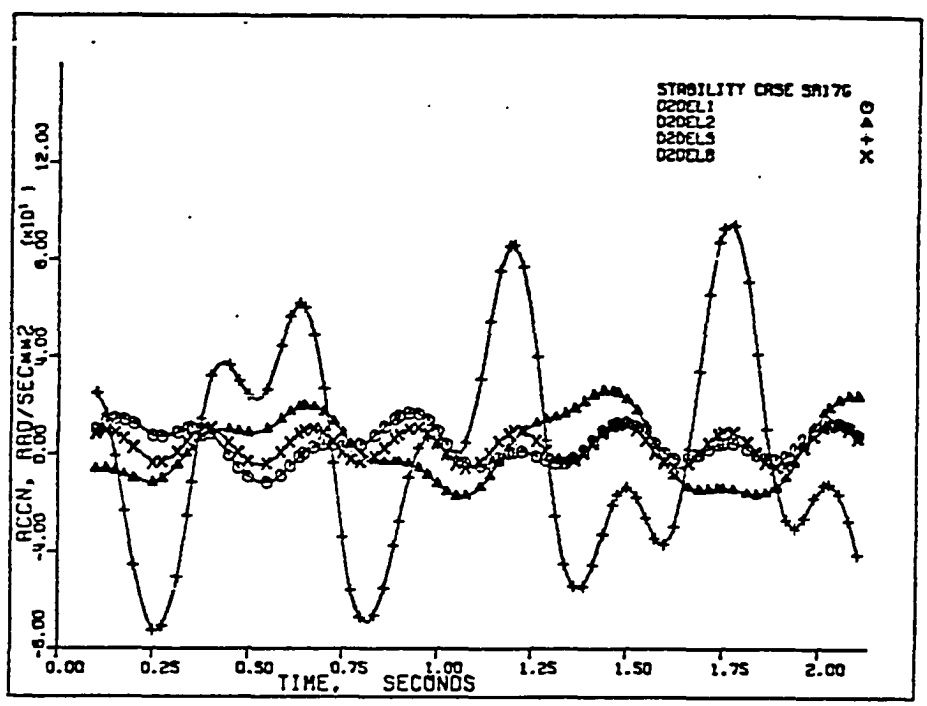

Figure 315. Case SR-17G: accelerations $\ddot{\delta}_1$, $\ddot{\delta}_2$, $\ddot{\delta}_3$, and $\ddot{\bar{\delta}}$.

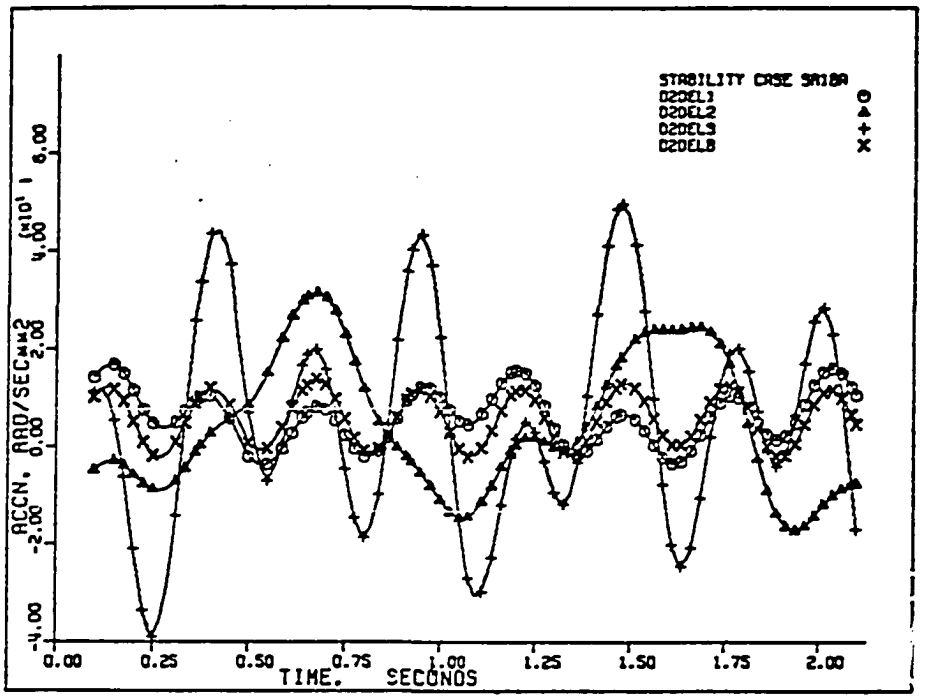

Figure 316. Case SR-18A: accelerations $\ddot{\delta}_1$, $\ddot{\delta}_2$, $\ddot{\delta}_3$, and $\bar{\delta}$.

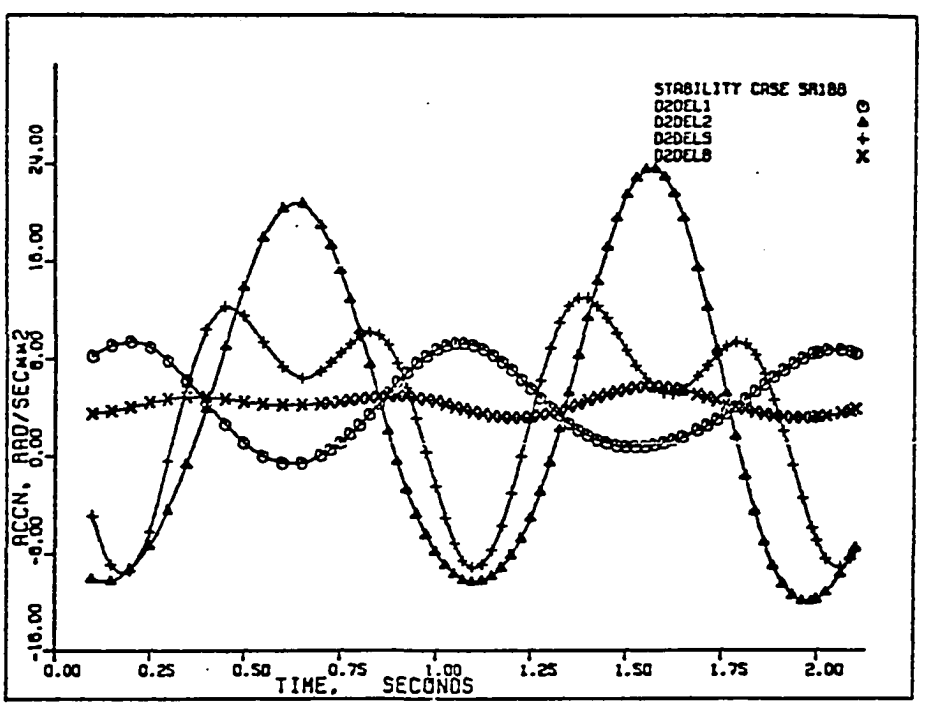

Figure 317. Case SR-18B: accelerations $\ddot{\delta}_1$, $\ddot{\delta}_2$, $\ddot{\delta}_3$, and $\ddot{\bar{\delta}}$.

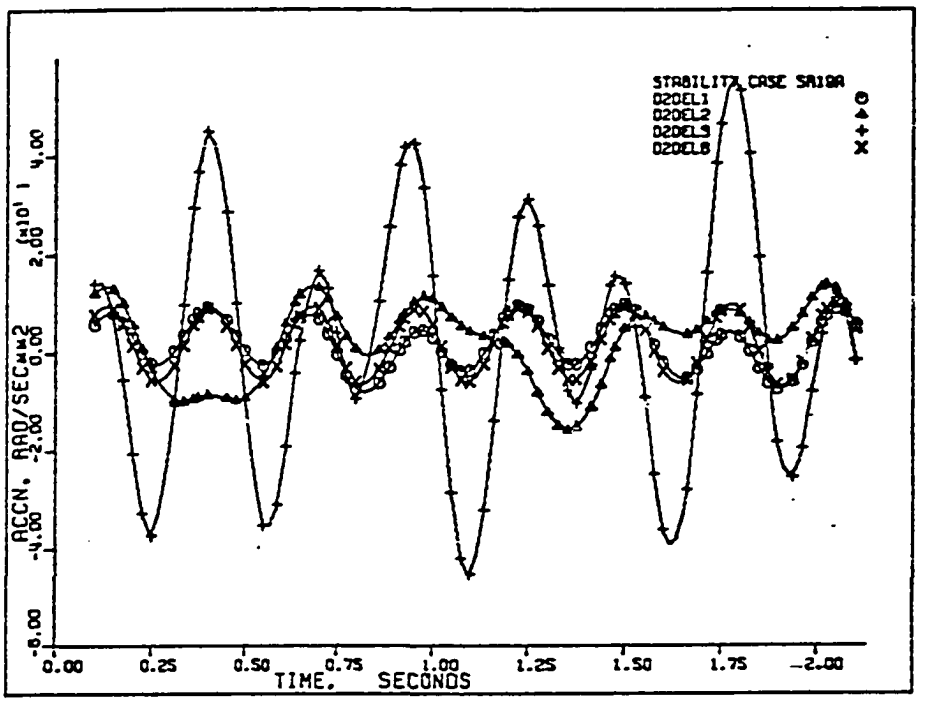

Figure 318. Case SR-19A: accelerations $\ddot{\delta}_1$, $\ddot{\delta}_2$, $\ddot{\delta}_3$, and $\bar{\ddot{\delta}}$.

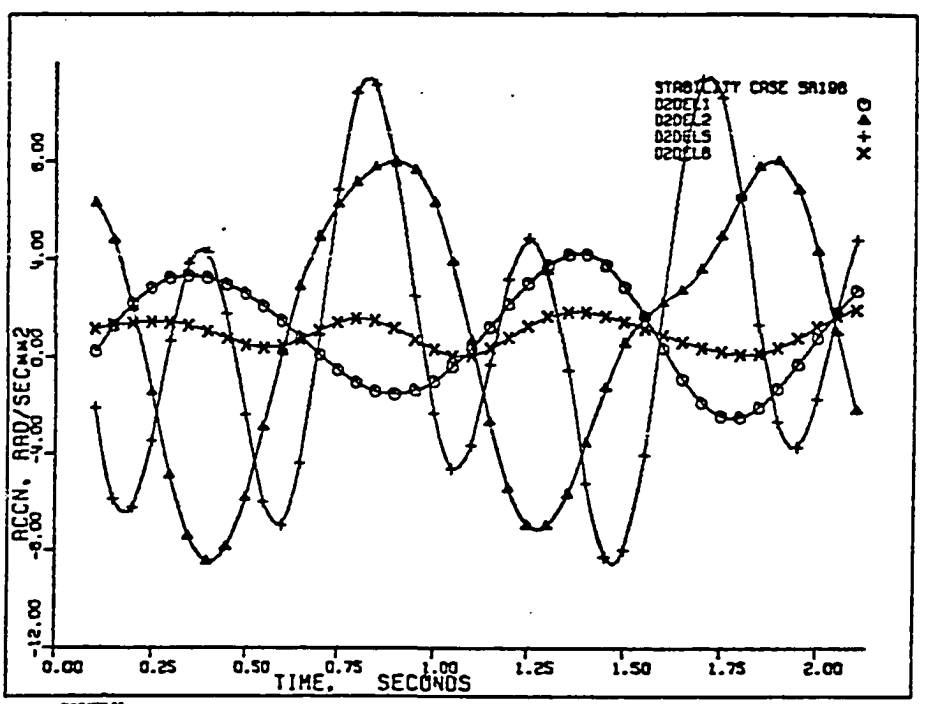

Figure 319. Case SR-19B: accelerations $\ddot{\delta}_1$, $\ddot{\delta}_2$, $\ddot{\delta}_3$, and $\bar{\ddot{\delta}}$.

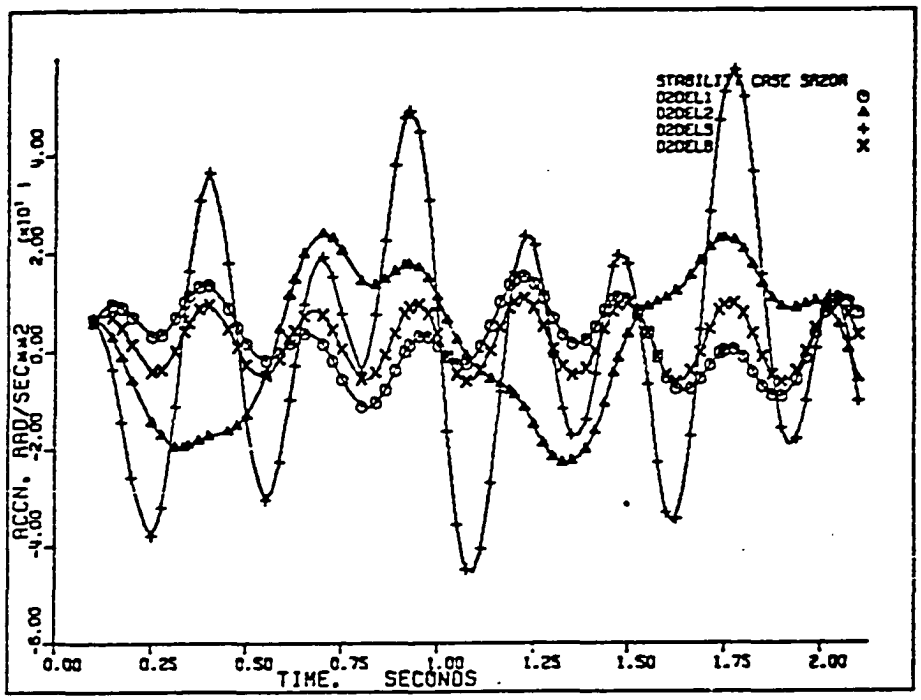

Figure 320. Case SR-20A: accelerations $\ddot{\delta}_1$, $\ddot{\delta}_2$, $\ddot{\delta}_3$, and $\ddot{\bar{\delta}}$.

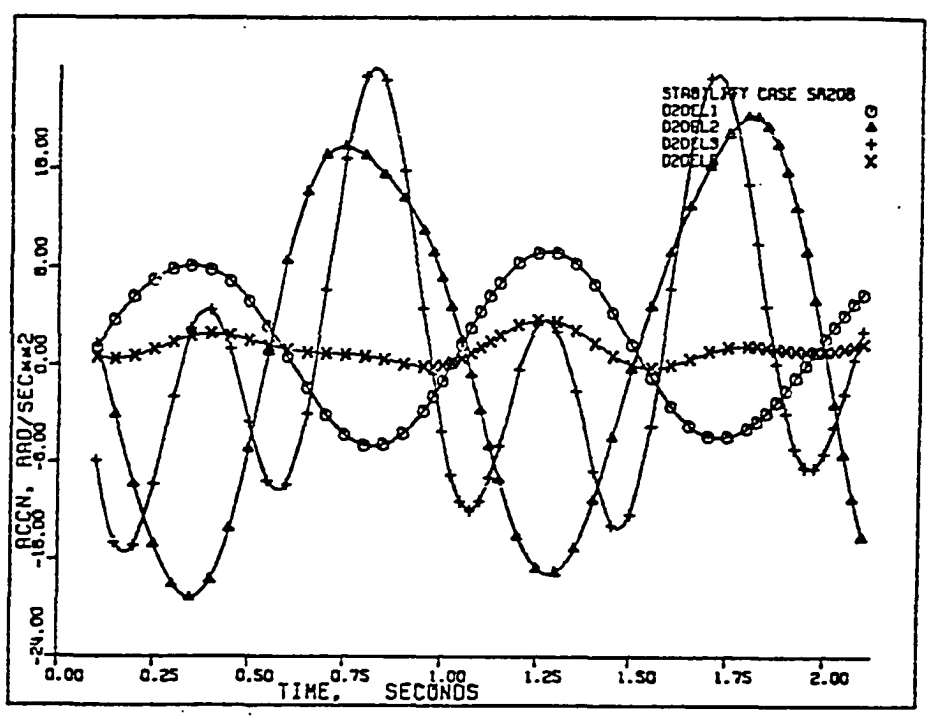

Figure 321. Case SR-20B: accelerations $\ddot{\delta}_1$, $\ddot{\delta}_2$, $\ddot{\delta}_3$, and $\ddot{\bar{\delta}}$.

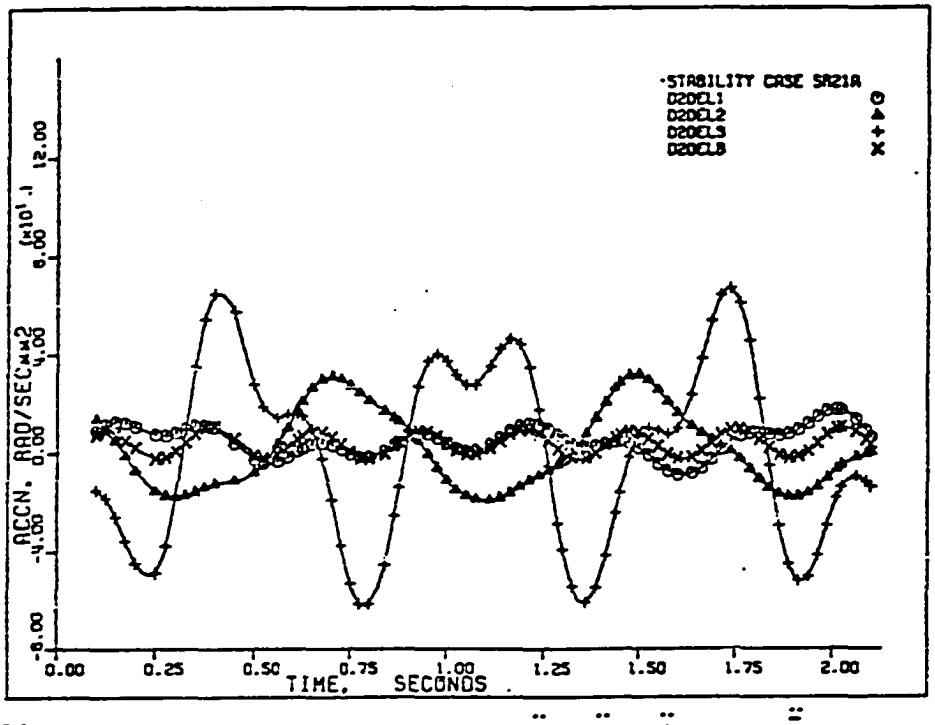

Figure 322. Case SR-21A: accelerations $\ddot{\delta}_1$, $\ddot{\delta}_2$, $\ddot{\delta}_3$, and $\ddot{\bar{\delta}}$.

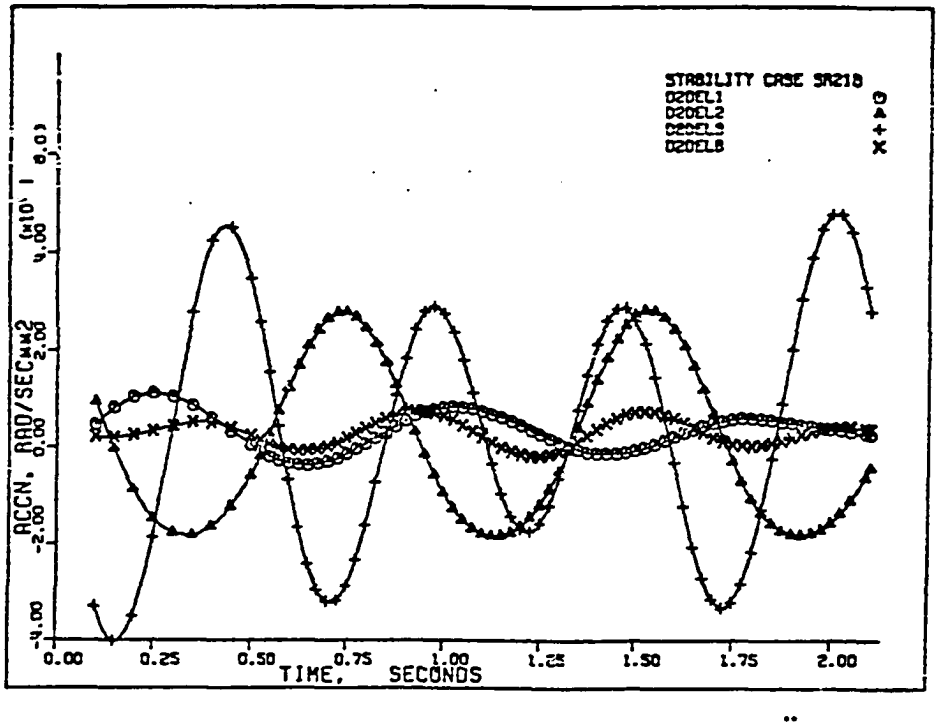

Figure 323. Case SR-21B: accelerations $\ddot{\delta}_1$, $\ddot{\delta}_2$, $\ddot{\delta}_3$, and $\ddot{\bar{\delta}}$.

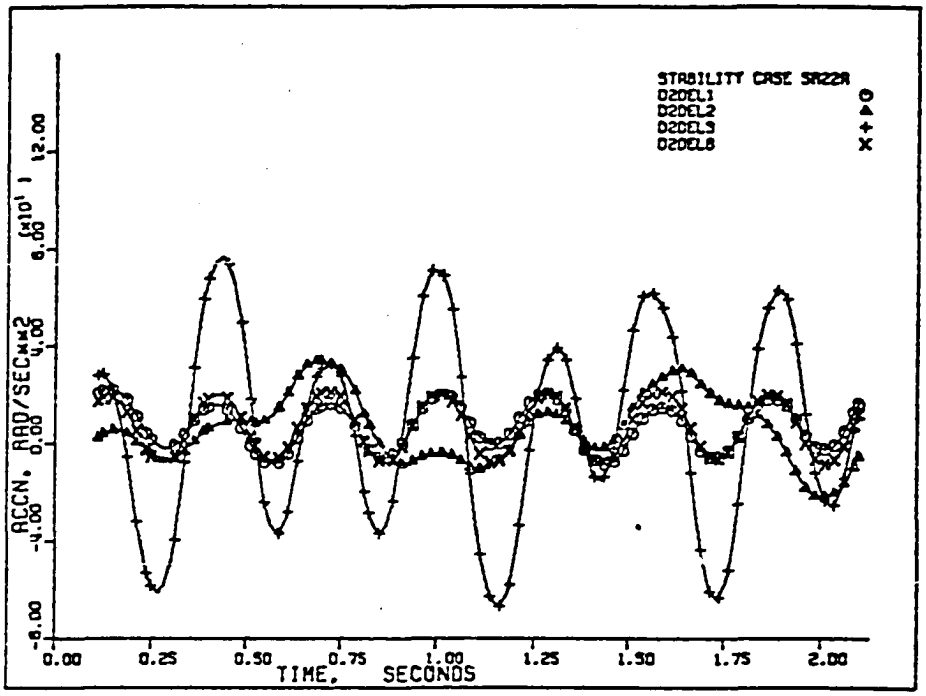

Figure 324. Case SR-22A: accelerations $\ddot{\delta}_1$, $\ddot{\delta}_2$, $\ddot{\delta}_3$, and $\ddot{\bar{\delta}}$.

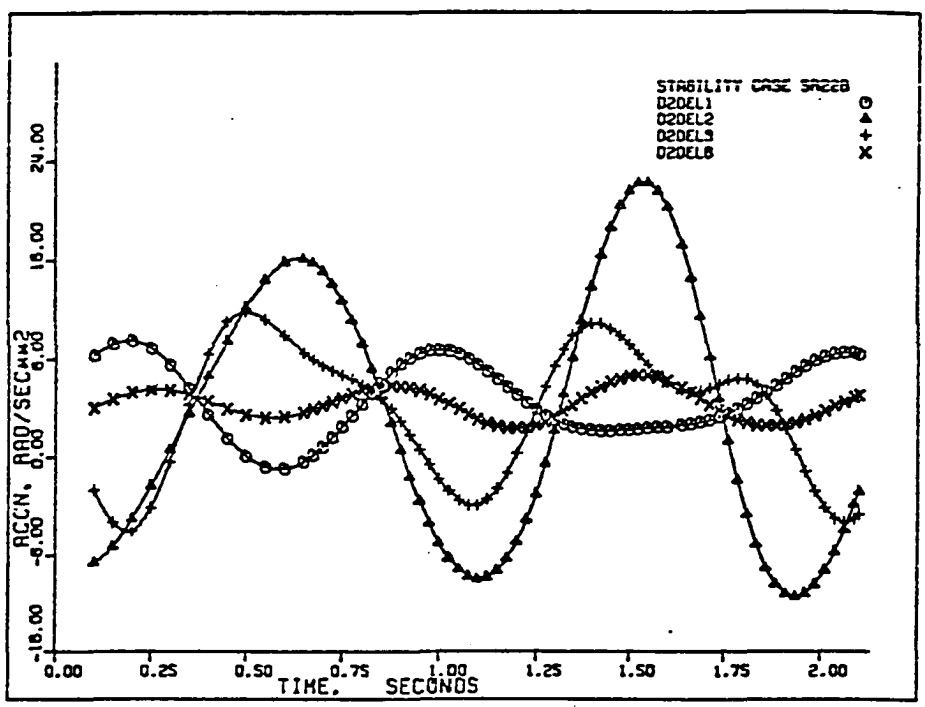

Figure 325. Case SR-22B: accelerations $\ddot{\delta}_1$, $\ddot{\delta}_2$, $\ddot{\delta}_3$, and $\ddot{\bar{\delta}}$.

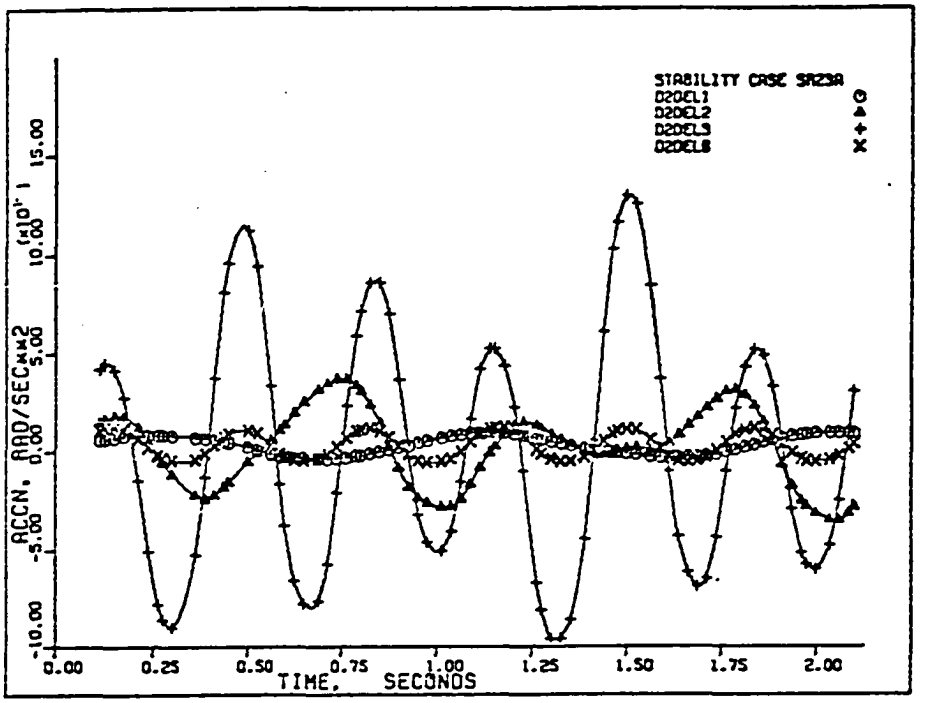

Figure 326. Case SR-23A: accelerations $\ddot{\delta}_1$, $\ddot{\delta}_2$, $\ddot{\delta}_3$, and $\ddot{\bar{\delta}}$.

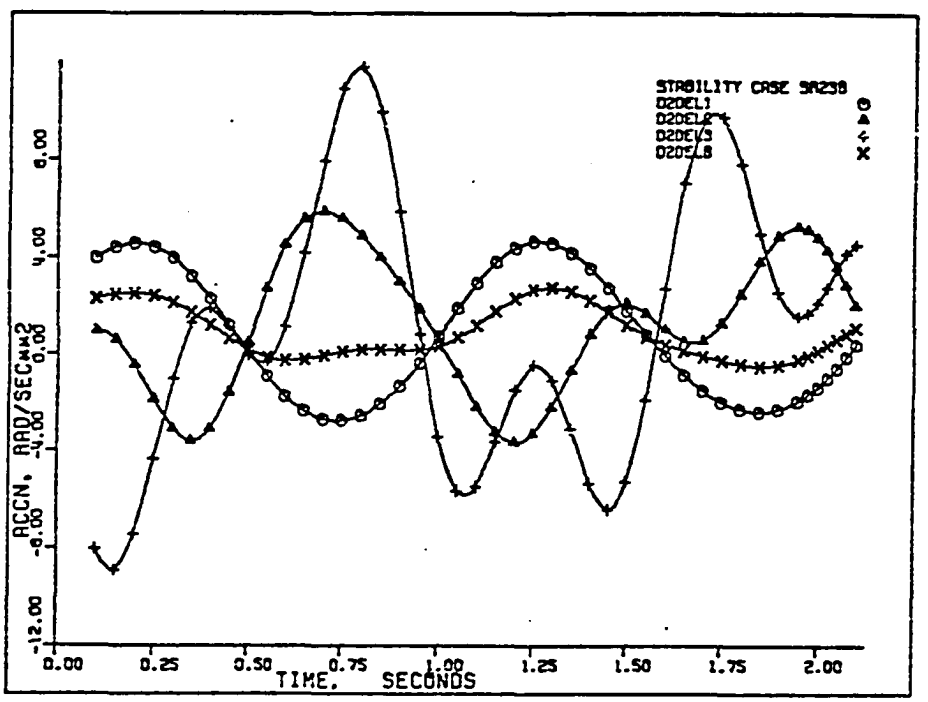

Figure 327. Case SR-23B: accelerations $\ddot{\delta}_1$, $\ddot{\delta}_2$, $\ddot{\delta}_3$, and $\ddot{\bar{\delta}}$.

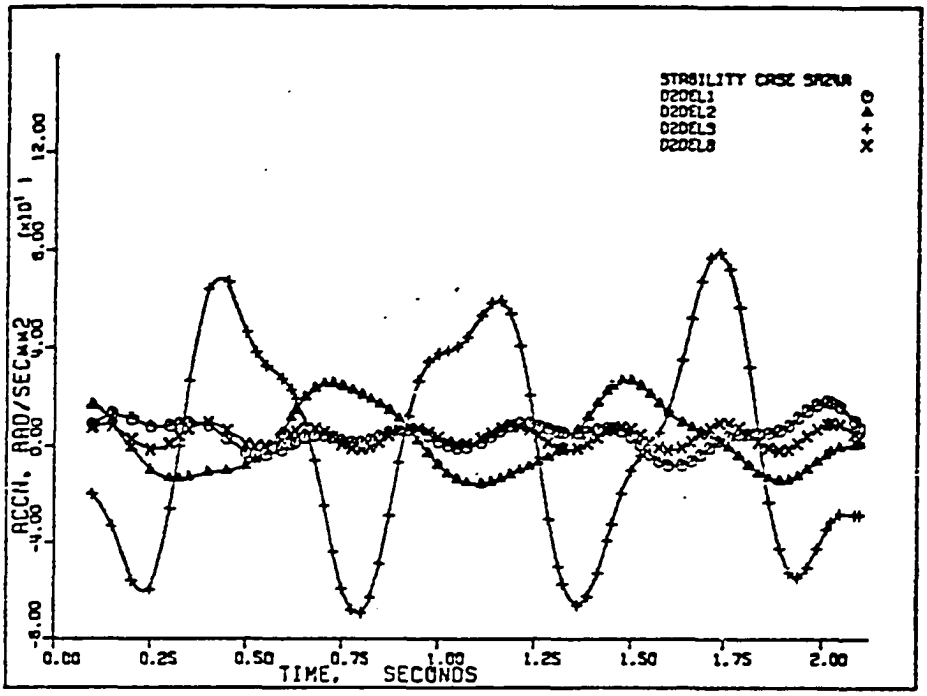

Figure 328. Case SR-24A: accelerations $\ddot{\delta}_1$, $\ddot{\delta}_2$, $\ddot{\delta}_3$, and $\dddot{\delta}$.

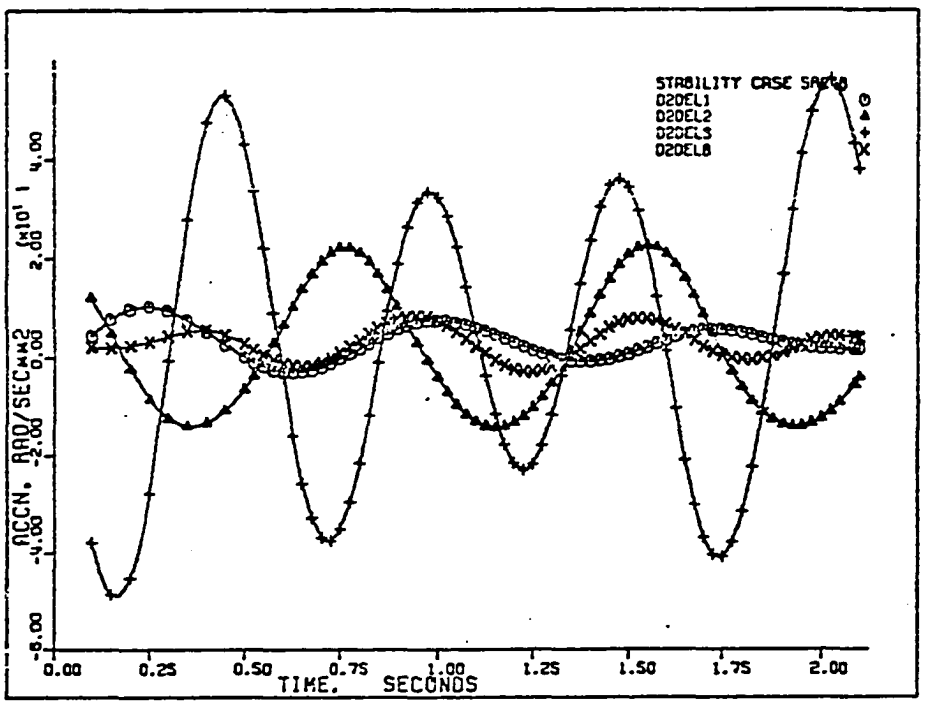

Figure 329. Case SR-24B: accelerations $\ddot{\delta}_1$, $\ddot{\delta}_2$, $\ddot{\delta}_3$, and $\dddot{\delta}$.

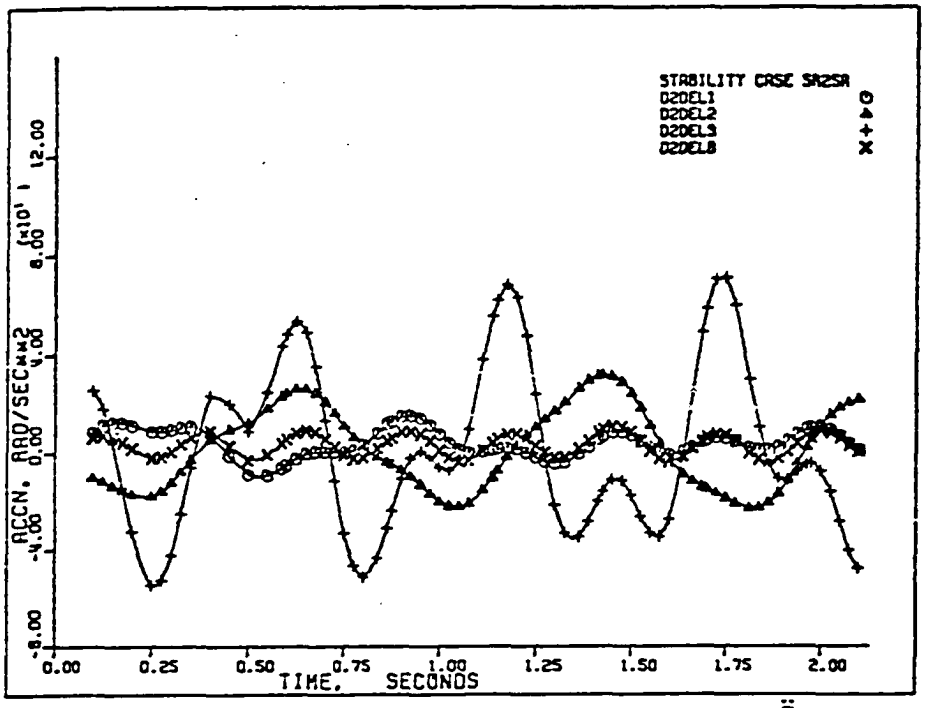

Figure 330. Case SR-25A: accelerations $\ddot{\delta}_1$, $\ddot{\delta}_2$, $\ddot{\delta}_3$, and $\ddot{\delta}$.

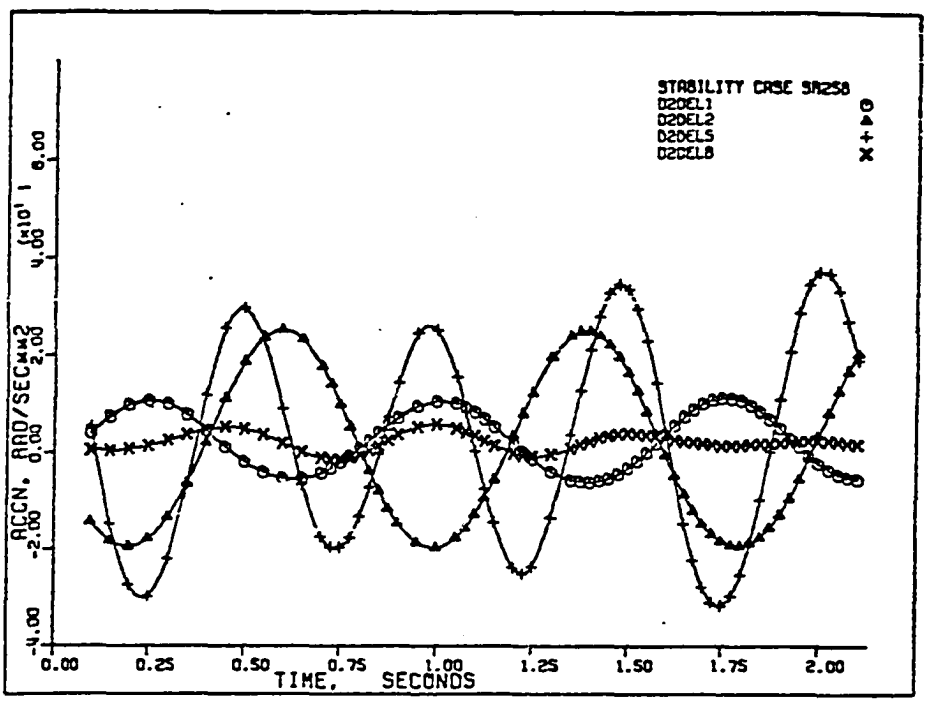

Figure 331. Case SR-25B: accelerations $\ddot{\delta}_1$, $\ddot{\delta}_2$, $\ddot{\delta}_3$, and $\ddot{\delta}$.

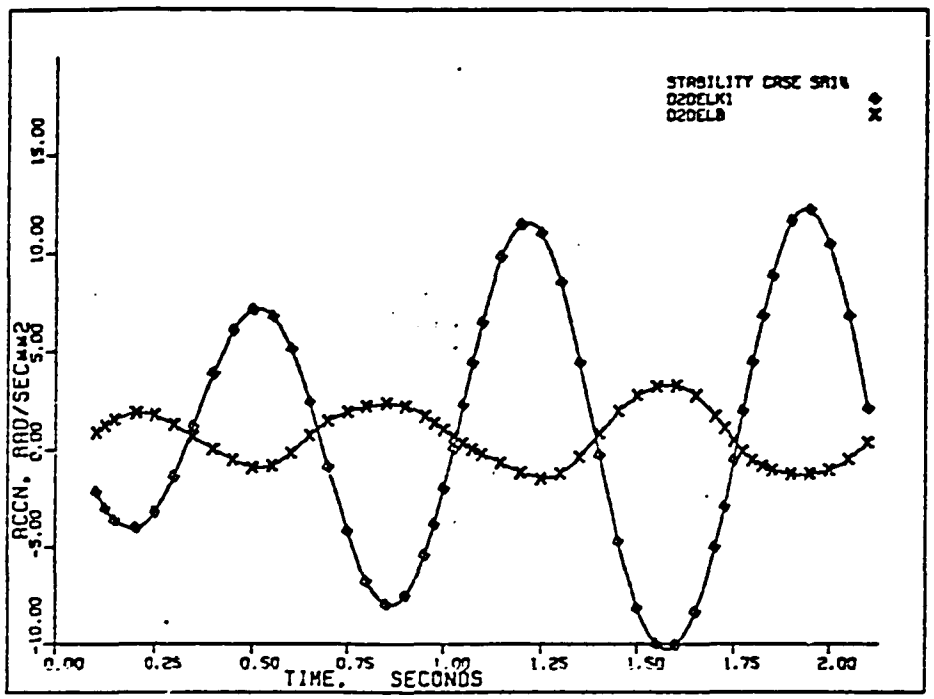

Figure 332. Case SR-14. accelerations $\ddot{\delta}_k$ and $\ddot{\delta}$.

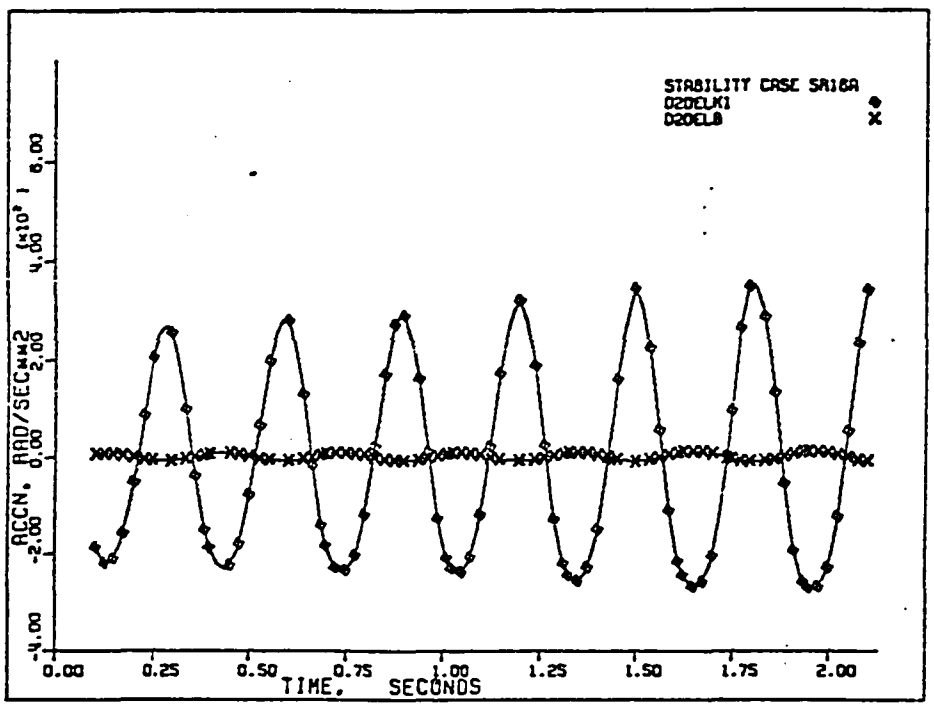

Figure 333. Case SR-16A: accelerations $\ddot{\delta}_k$ and $\ddot{\delta}$.

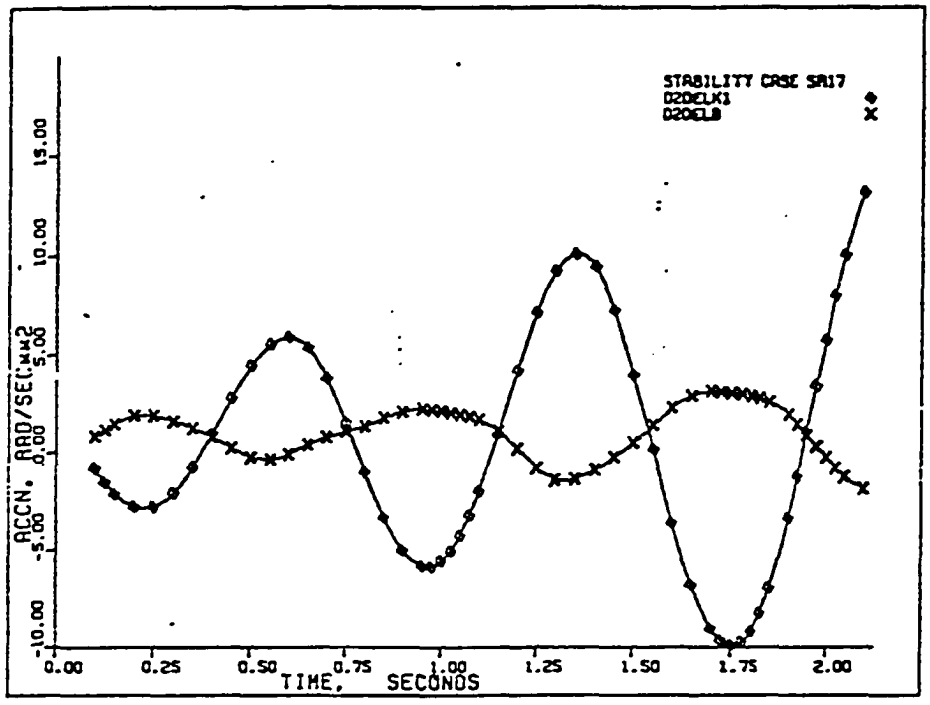

Figure 334. Case SR-17: accelerations $\ddot{\delta}_k$ and $\ddot{\bar{\delta}}$.

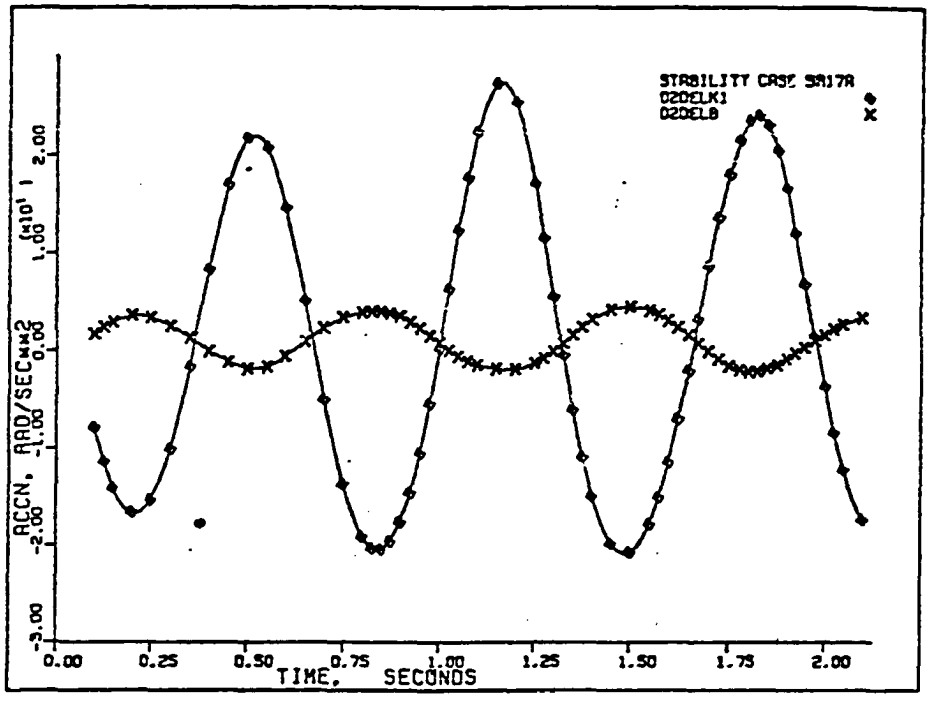

Figure 335. Case SR-17A: accelerations $\ddot{\delta}_k$ and $\ddot{\bar{\delta}}$.

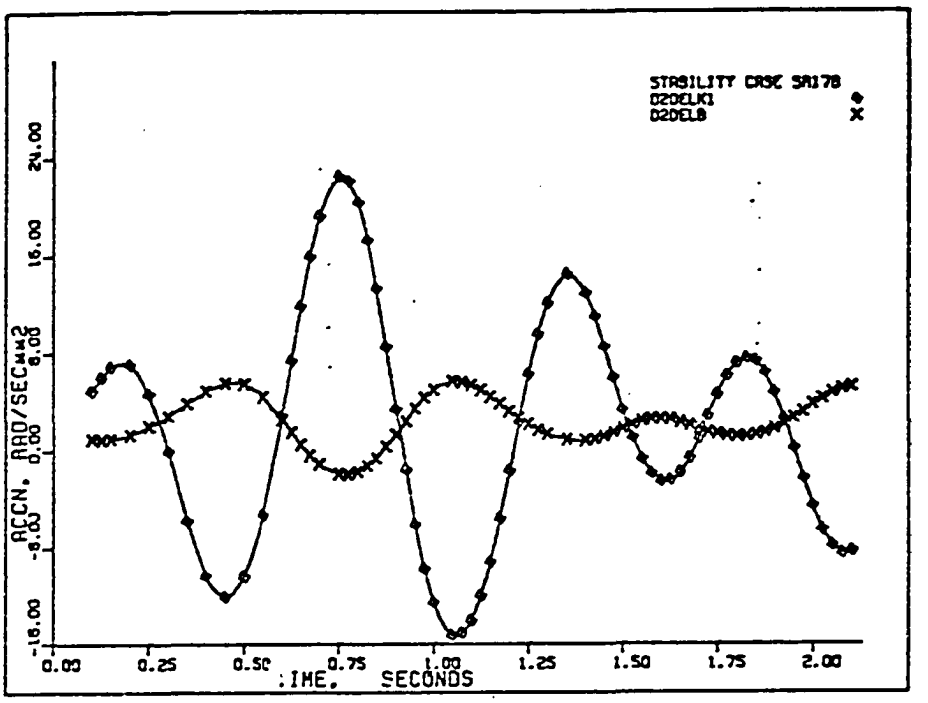

Figure 336. Case SR-17B: accelerations $\ddot{\delta}_k$ and $\ddot{\bar{\delta}}$.

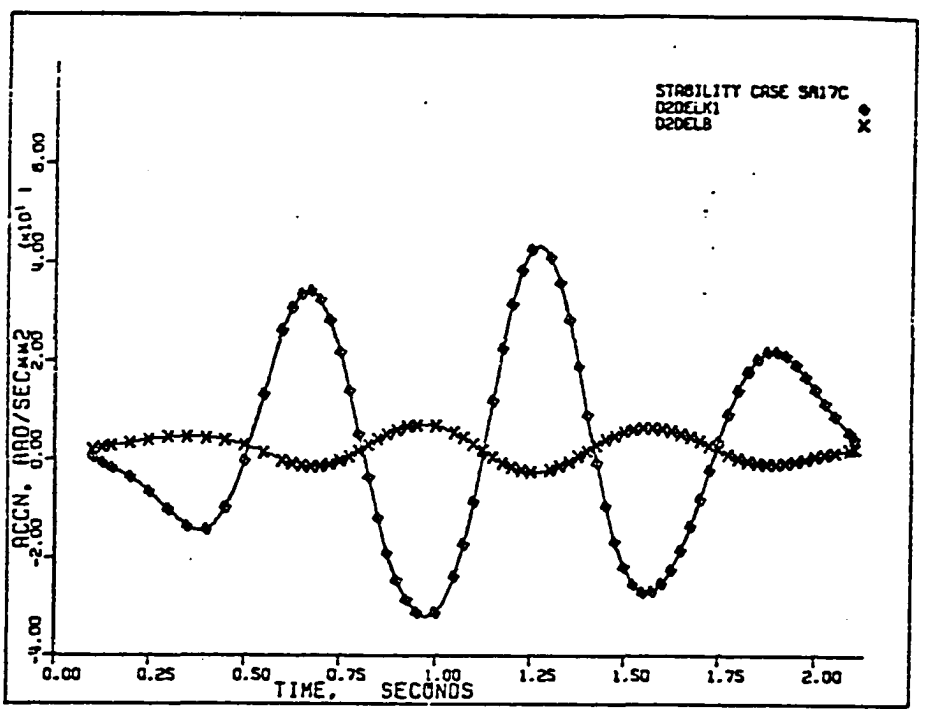

Figure 337. Case SR-17C: accelerations $\ddot{\delta}_k$ and $\ddot{\bar{\delta}}$.

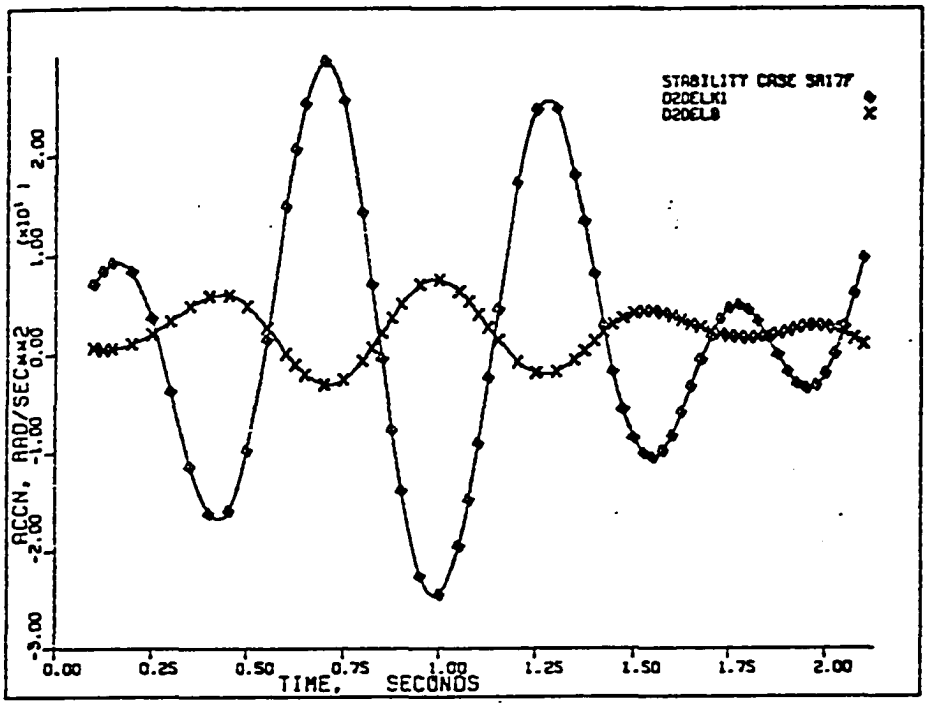

Figure 338. Case SR-17F: accelerations $\ddot{\delta}_k$ and $\ddot{\bar{\delta}}$.

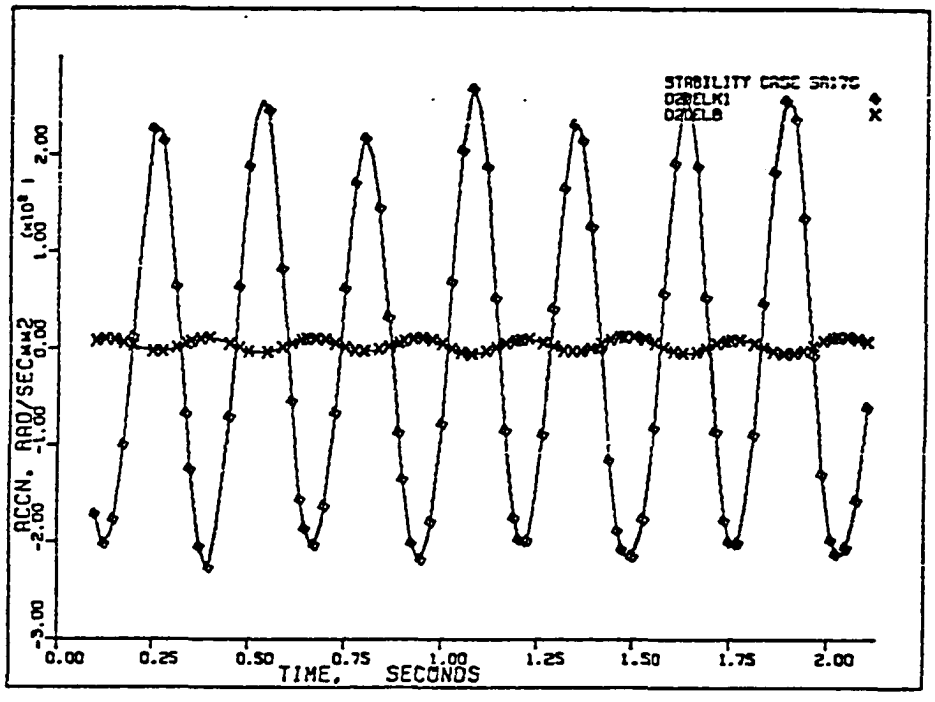

Figure 339. Case SR-17G: accelerations $\ddot{\delta}_k$ and $\ddot{\bar{\delta}}$.

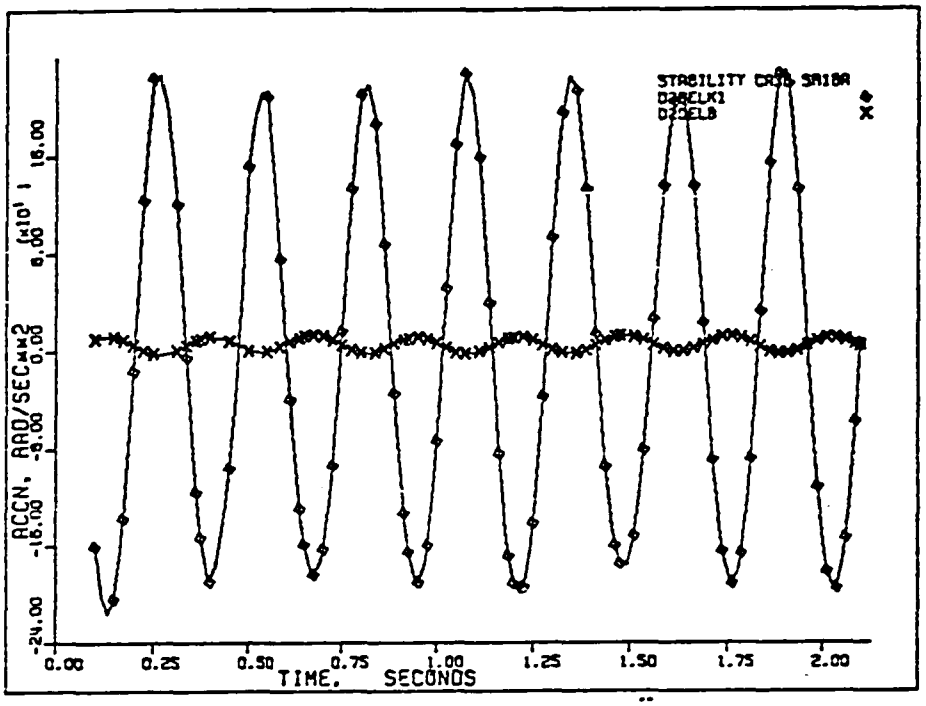

Figure 340. Case SR-18A: accelerations $\ddot{\delta}_k$ and $\ddot{\bar{\delta}}$.

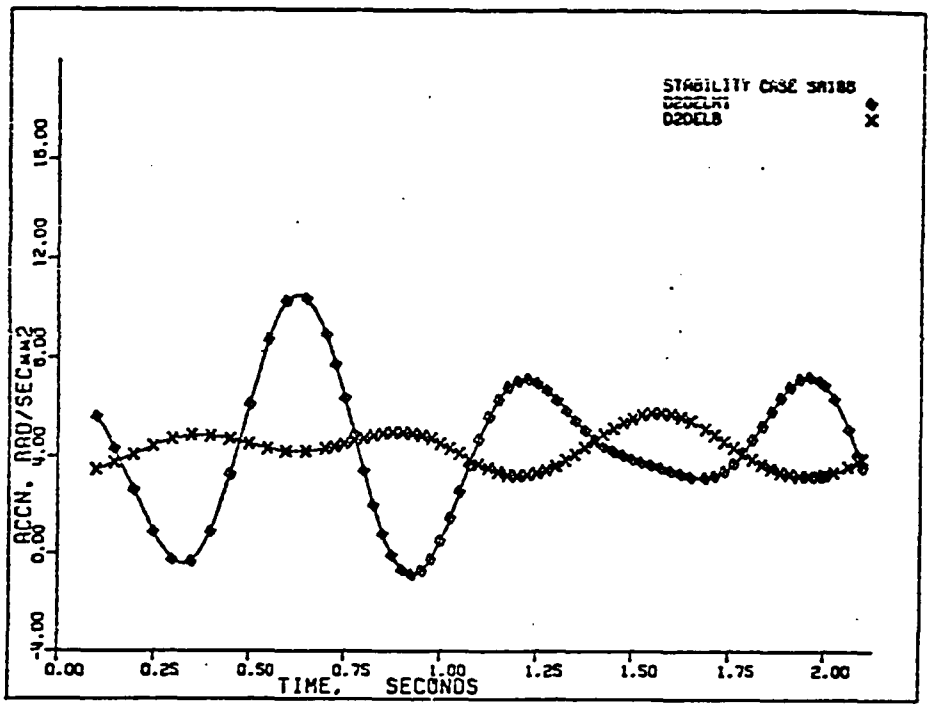

Figure 341. Case SR-18B: accelerations $\ddot{\delta}_k$ and $\ddot{\bar{\delta}}$.

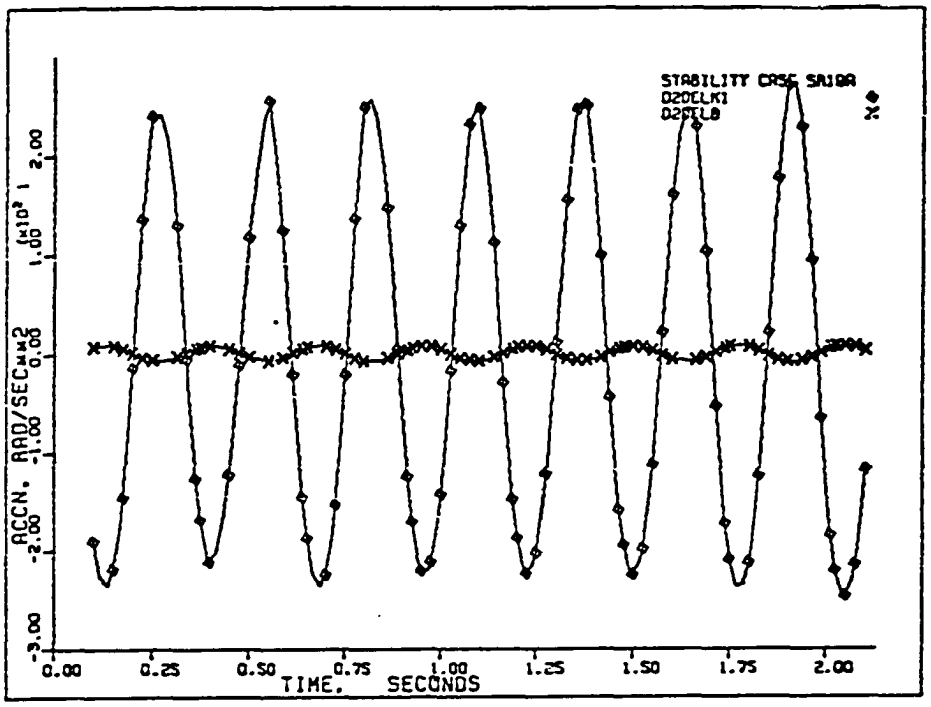

Figure 342. Case SR-19A: accelerations $\ddot{\delta}_k$ and $\ddot{\bar{\delta}}$.

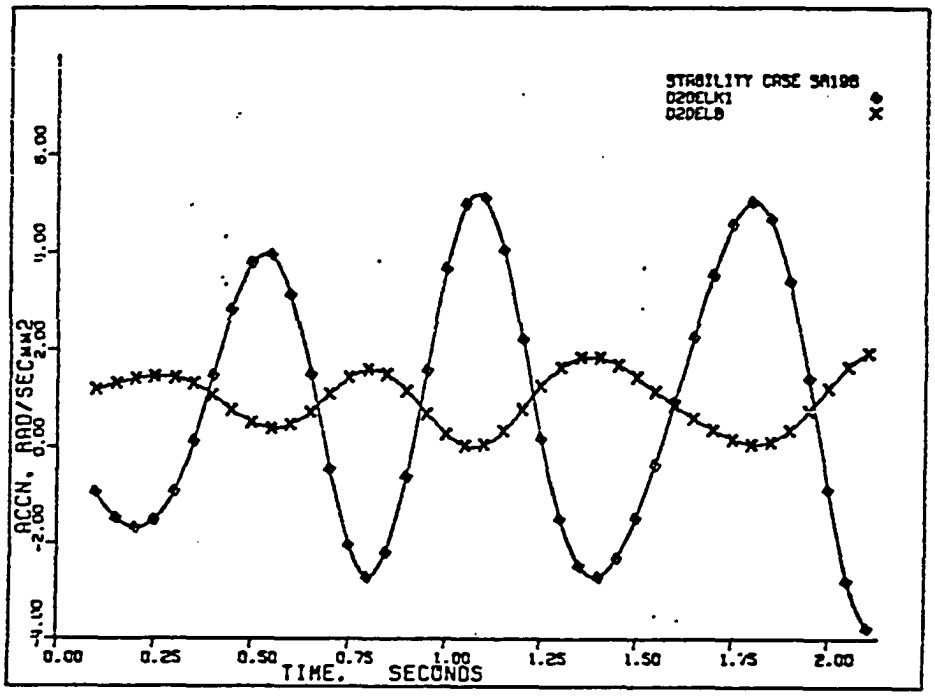

Figure 343. Case SR-19B: accelerations $\ddot{\delta}_k$ and $\ddot{\bar{\delta}}$.

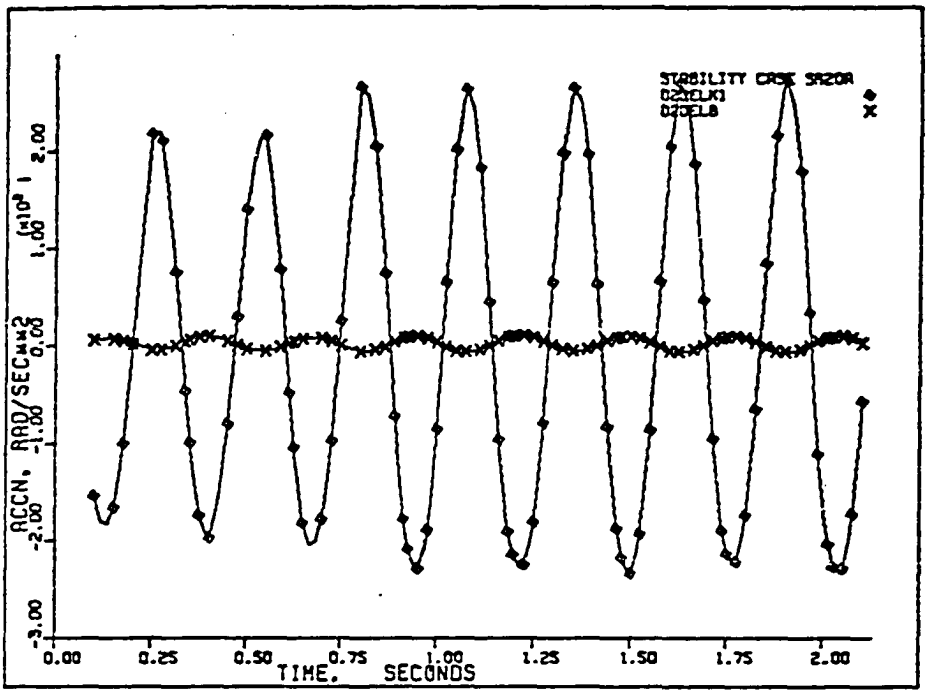

Figure 344. Case SR-20A: accelerations $\ddot{\delta}_k$ and $\ddot{\bar{\delta}}$.

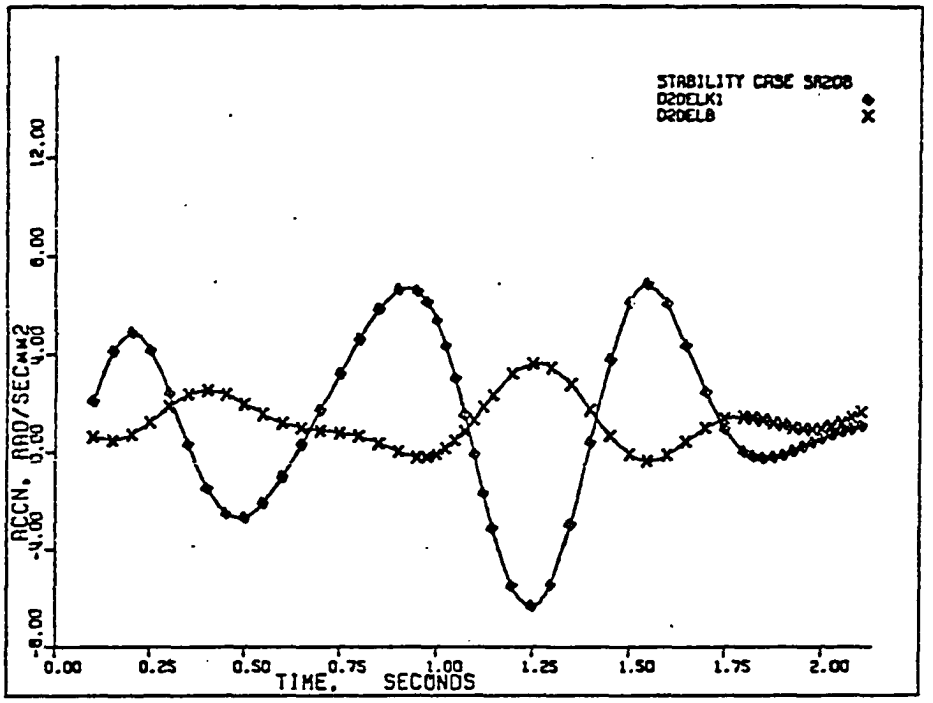

Figure 345. Case SR-20B: accelerations $\ddot{\delta}_k$ and $\ddot{\bar{\delta}}$.

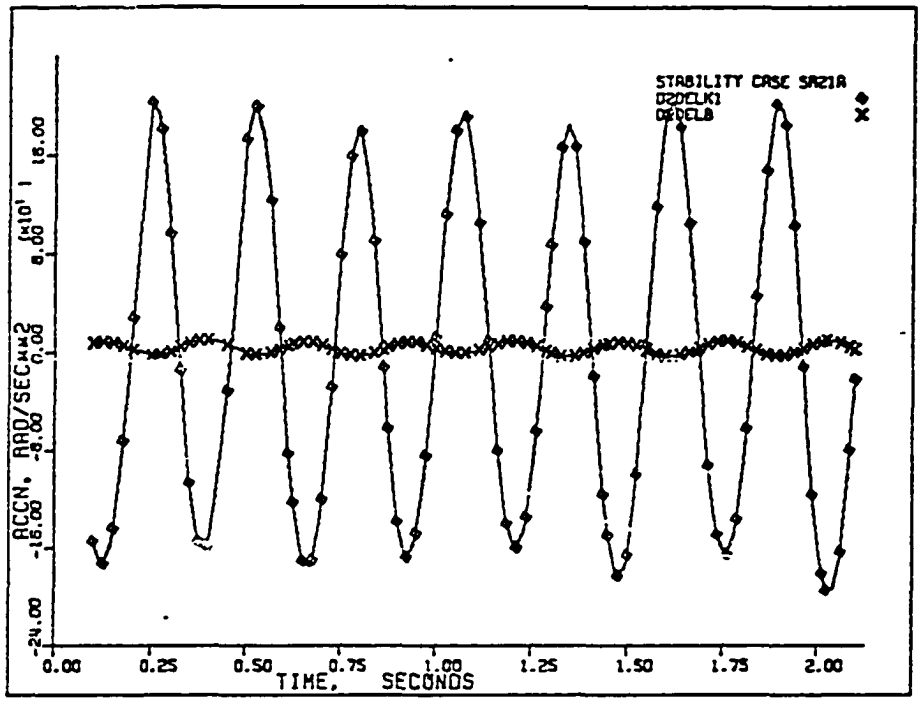

Figure 346. Case SR-21A: accelerations $\ddot{\delta}_k$ and $\ddot{\bar{\delta}}$.

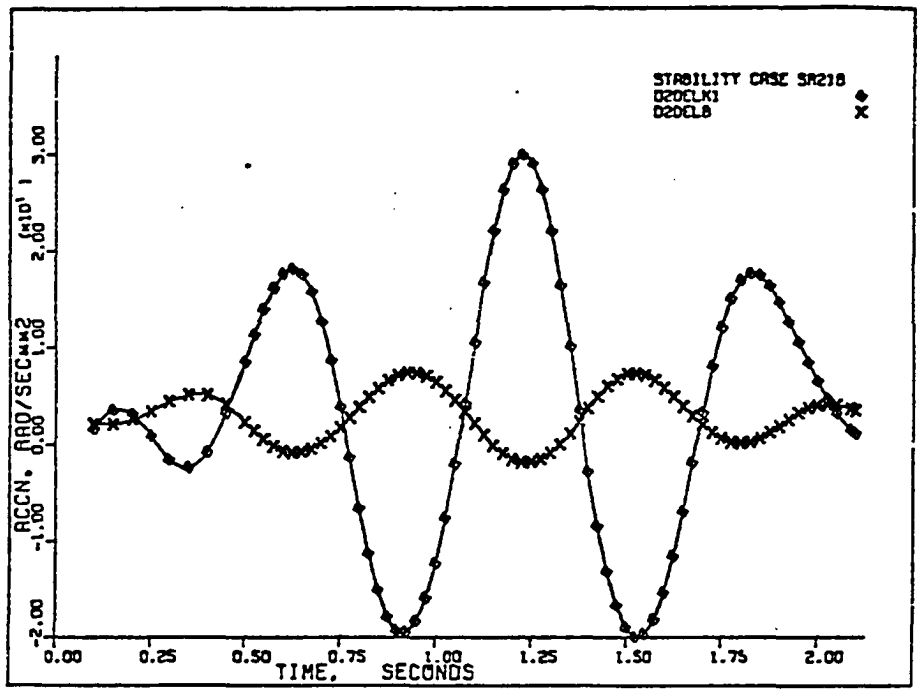

Figure 347. Case SR-21B: accelerations $\ddot{\delta}_k$ and $\ddot{\bar{\delta}}$.

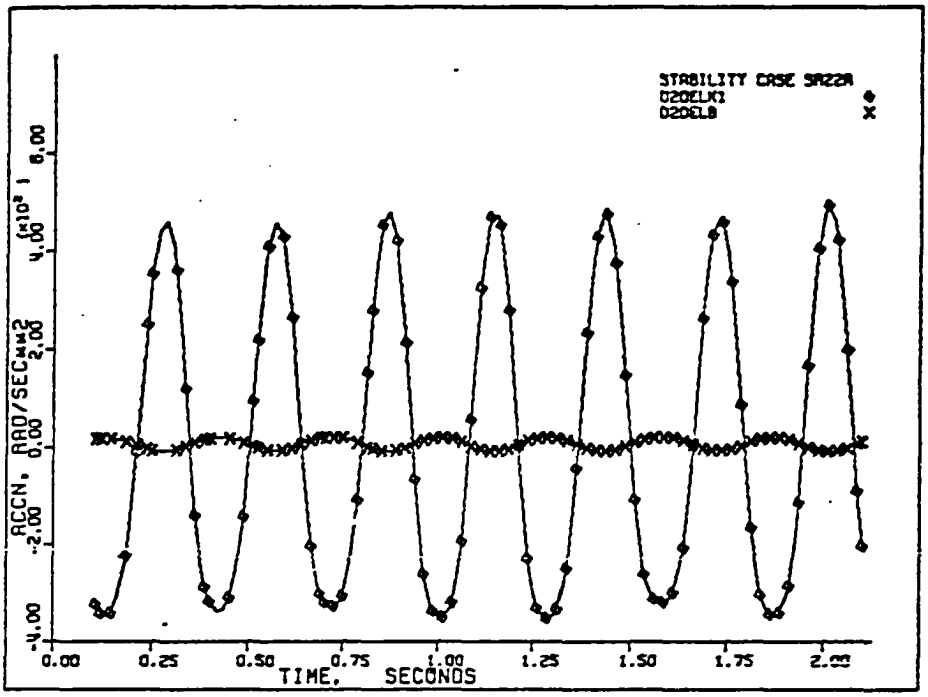

Figure 348. Case SR-22A: accelerations $\ddot{\delta}_k$ and $\ddot{\delta}$.

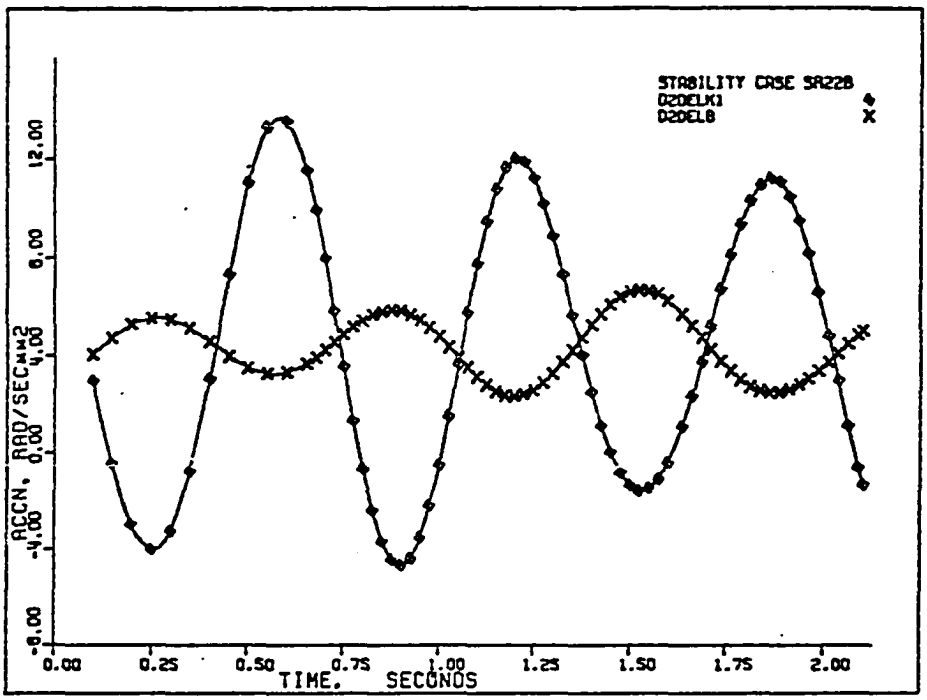

Figure 349. Case SR-22B: accelerations $\ddot{\delta}_k$ and $\ddot{\delta}$.

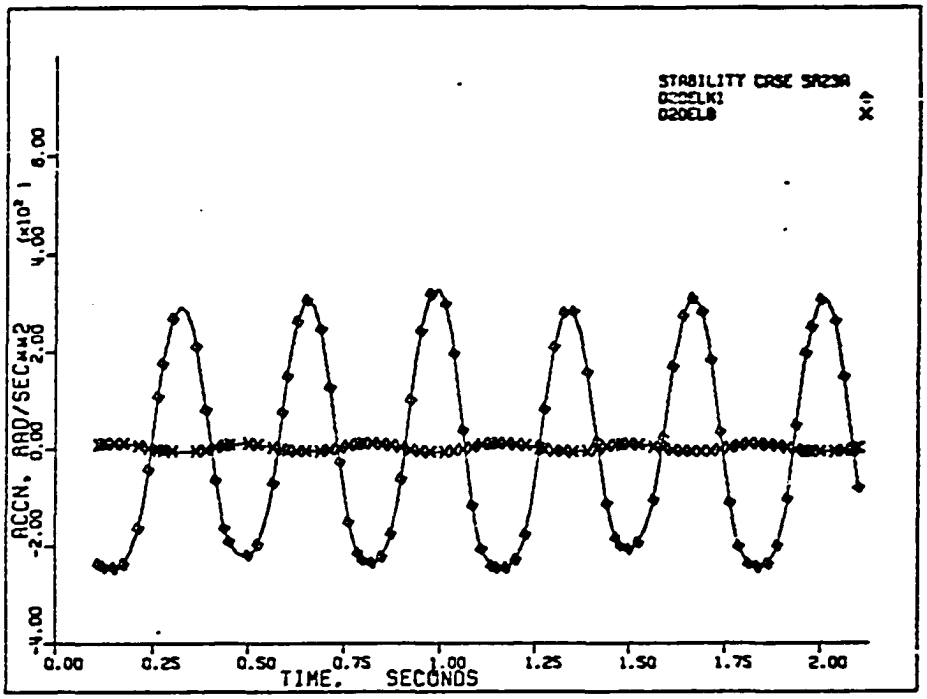

Figure 350. Case SR-23A: accelerations $\ddot{\delta}_k$ and $\ddot{\delta}$.

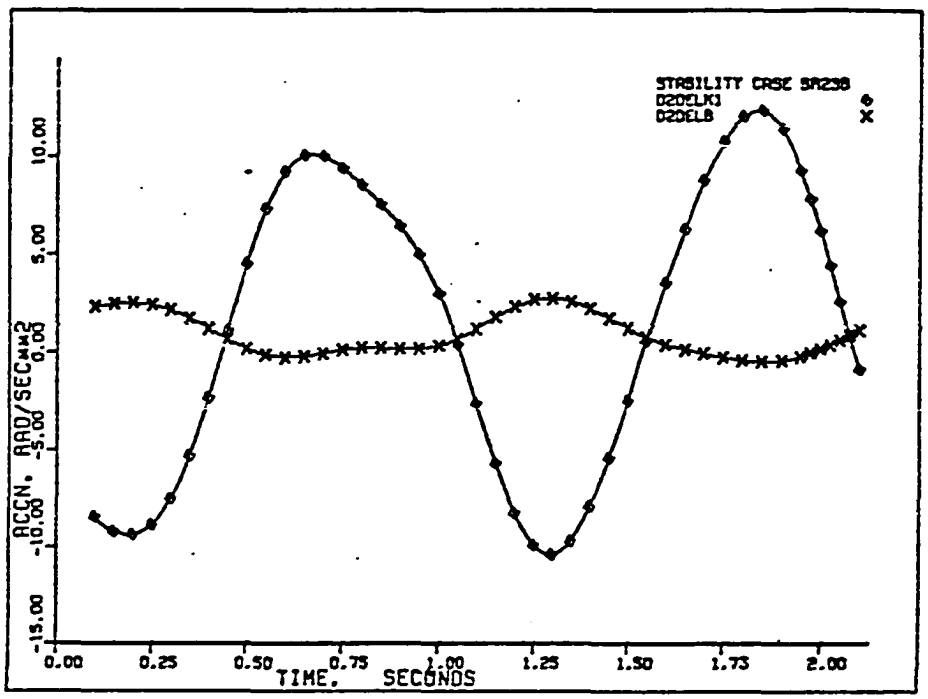

Figure 351. Case SR-23B: accelerations $\ddot{\delta}_k$ and $\ddot{\delta}$.

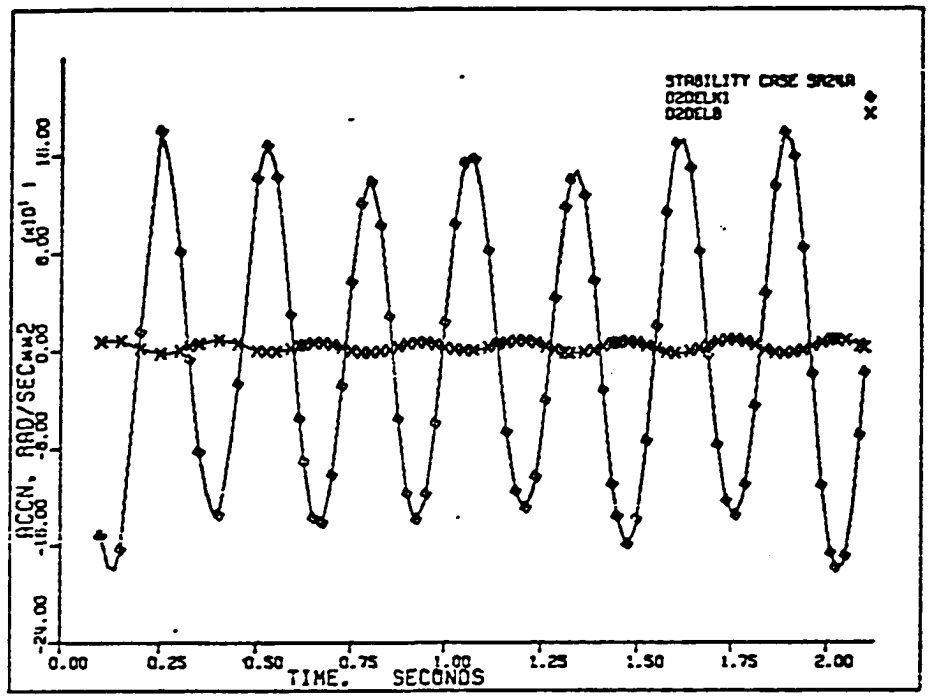

Figure 352. Case SR-24A: accelerations $\ddot{\delta}_k$ and $\ddot{\bar{\delta}}$.

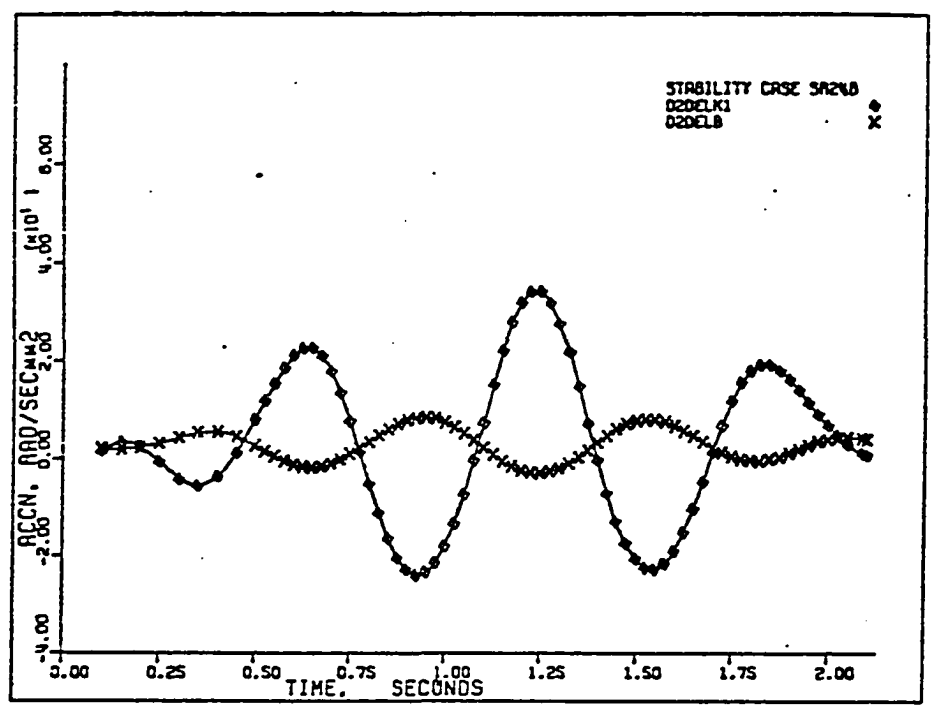

Figure 353. Case SR-24B: accelerations $\ddot{\delta}_k$ and $\ddot{\bar{\delta}}$.

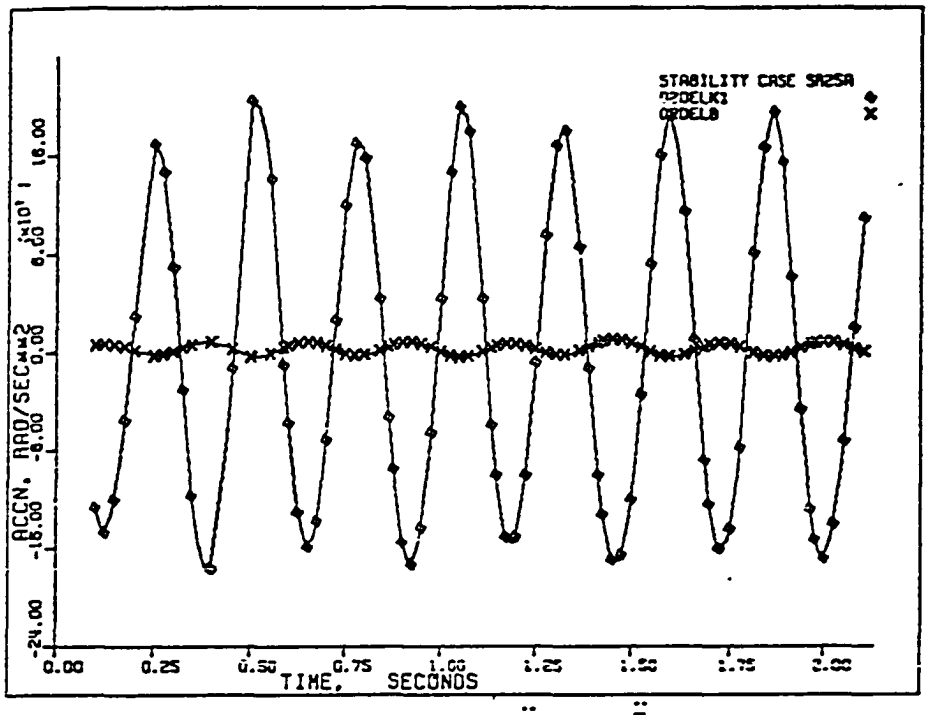

Figure 354. Case SR-25A: accelerations $\ddot{\delta}_k$ and $\ddot{\bar{\delta}}$.

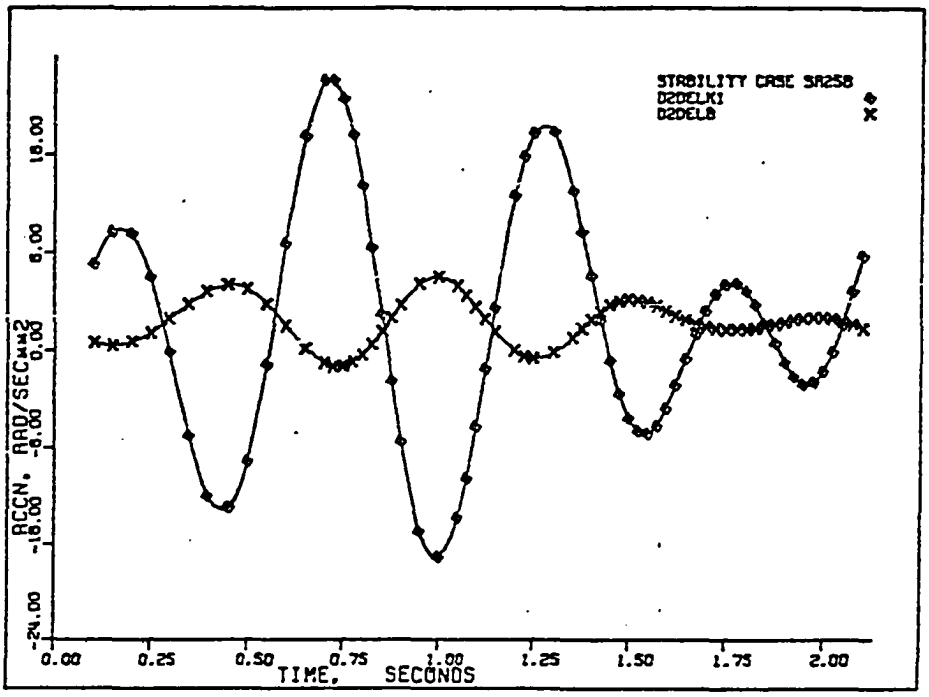

Figure 355. Case SR-25B: accelerations $\ddot{\delta}_k$ and $\ddot{\bar{\delta}}$.

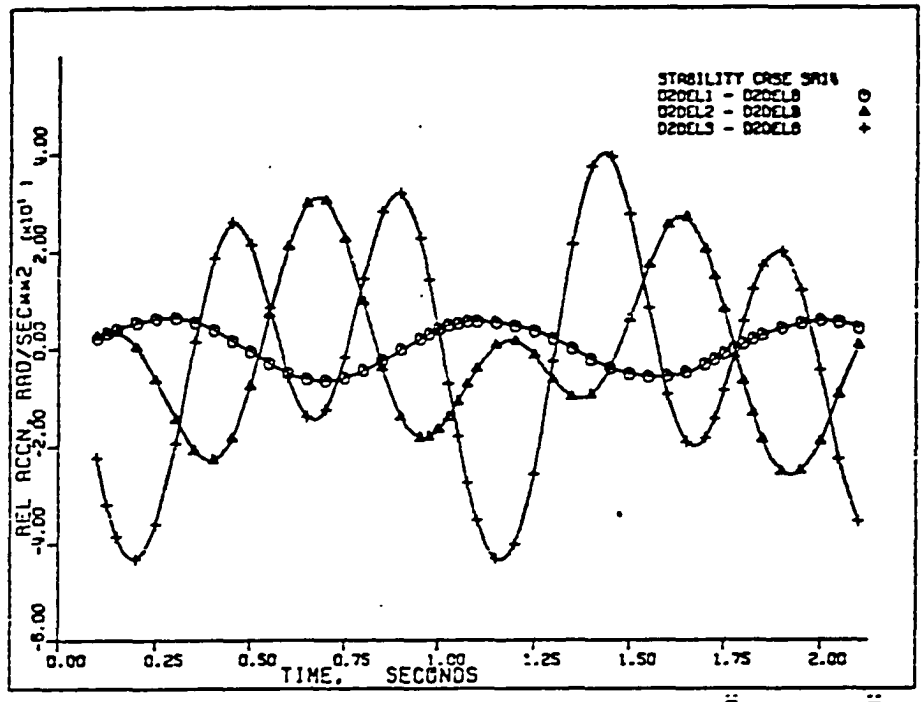

Figure 356. Case SR-14: relative accelerations $(\ddot{\delta}_1 - \ddot{\bar{\delta}})$, $(\ddot{\delta}_2 - \ddot{\bar{\delta}})$, and $(\ddot{\delta}_3 - \ddot{\bar{\delta}})$.

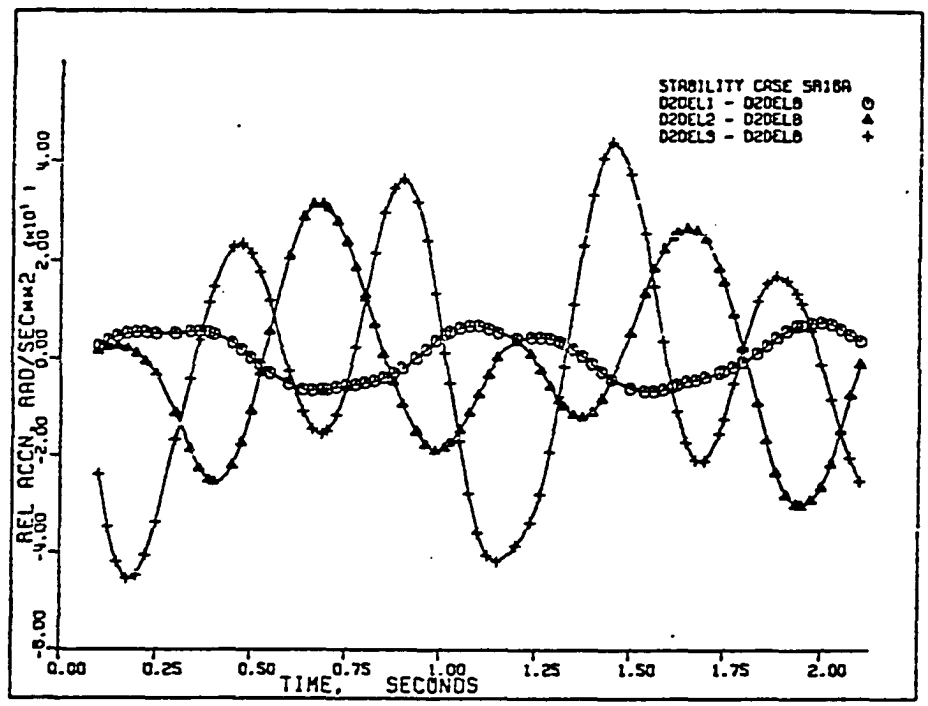

Figure 357. Case SR-16A: relative accelerations $(\ddot{\delta}_1 - \ddot{\bar{\delta}})$, $(\ddot{\delta}_2 - \ddot{\bar{\delta}})$, and $(\ddot{\delta}_3 - \ddot{\bar{\delta}})$.

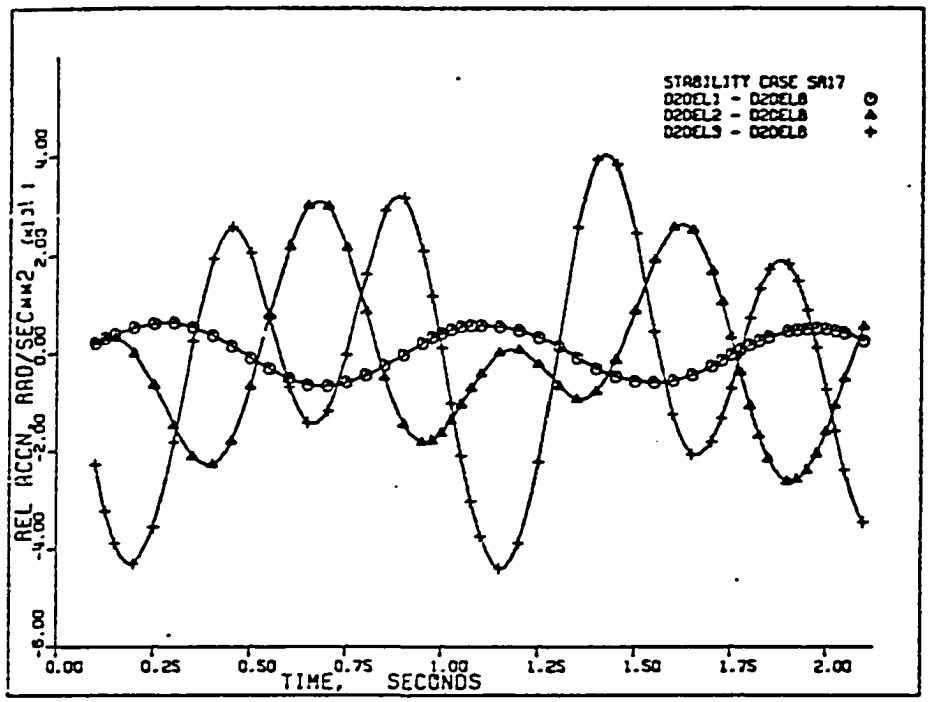

Figure 358. Case SR-17: relative accelerations $(\ddot{\delta}_1 - \ddot{\delta})$, $(\ddot{\delta}_2 - \ddot{\delta})$, and $(\ddot{\delta}_3 - \ddot{\delta})$.

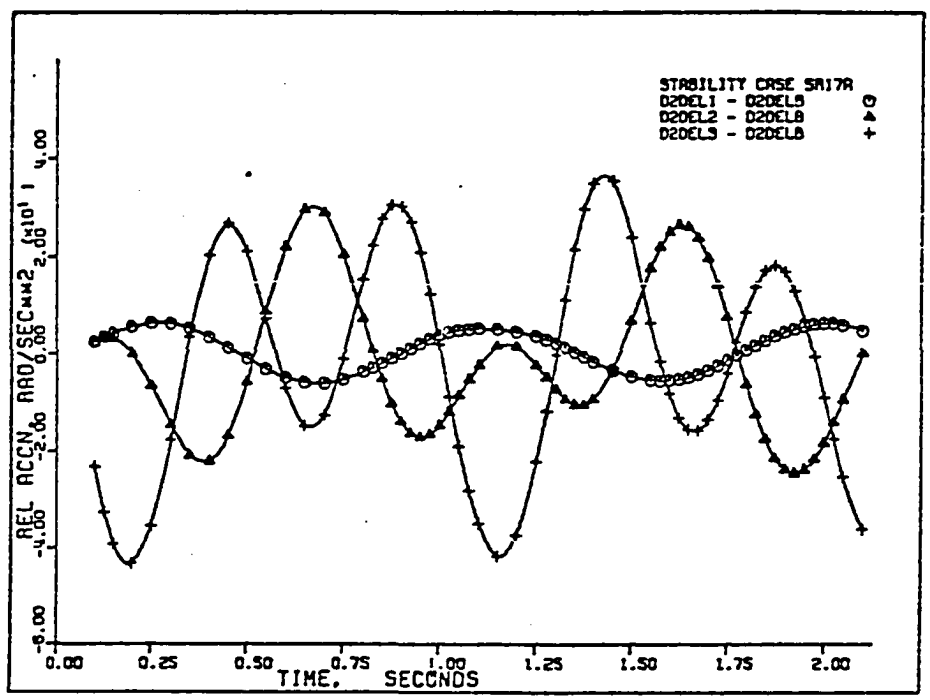

Figure 359. Case SR-17A: relative accelerations $(\ddot{\delta}_1 - \ddot{\delta})$, $(\ddot{\delta}_2 - \ddot{\delta})$, and $(\ddot{\delta}_3 - \ddot{\delta})$.

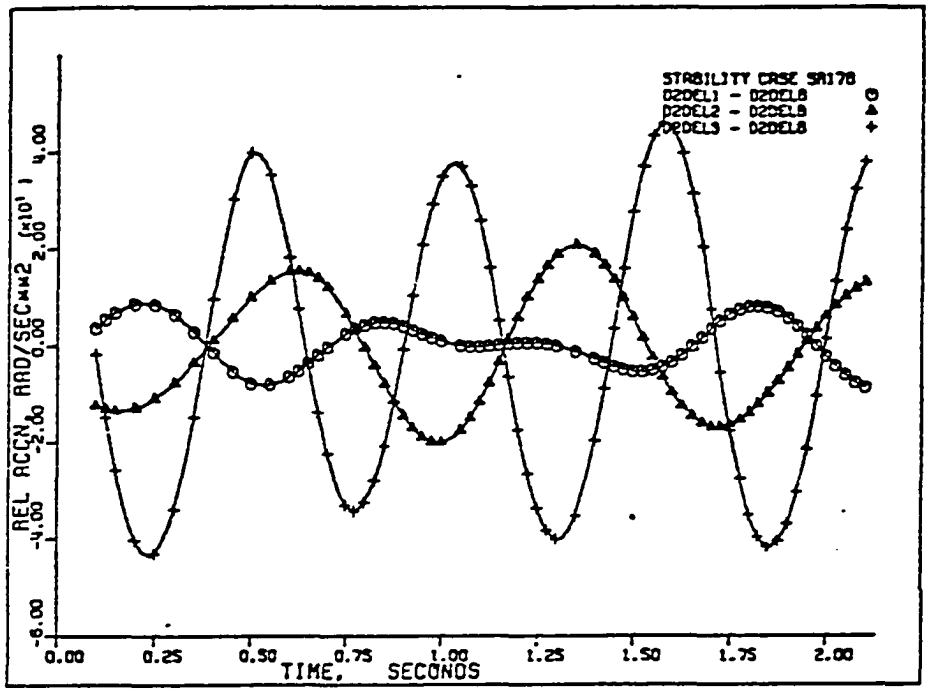

Figure 360. Case SR-17B: relative accelerations $(\ddot{\delta}_1 - \ddot{\bar{\delta}})$, $(\ddot{\delta}_2 - \ddot{\bar{\delta}})$, and $(\ddot{\delta}_3 - \ddot{\bar{\delta}})$.

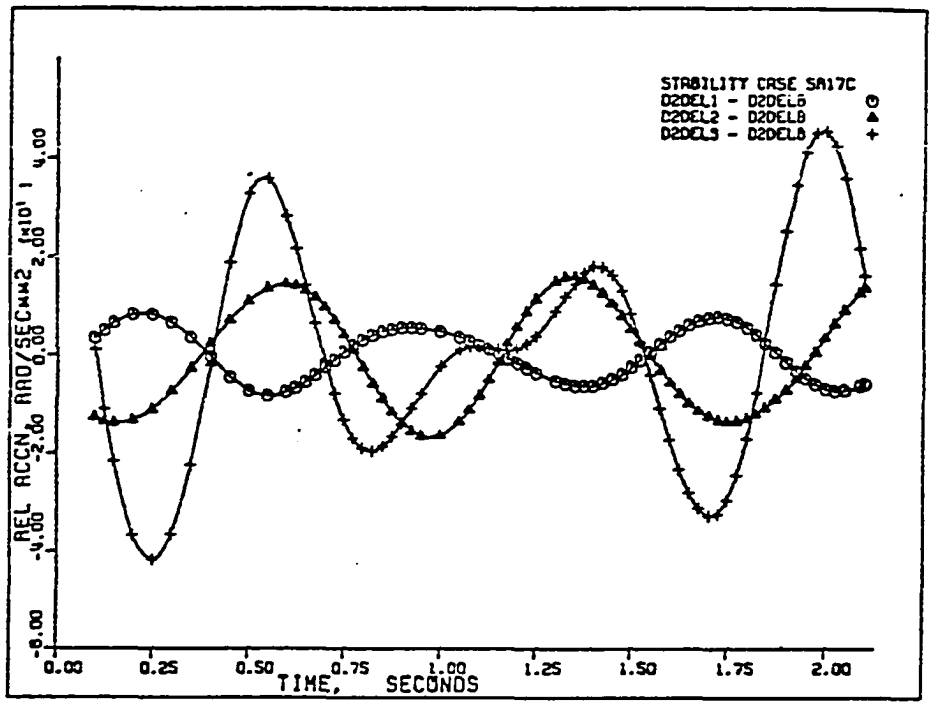

Figure 361. Case SR-17C: relative accelerations $(\ddot{\delta}_1 - \ddot{\bar{\delta}})$, $(\ddot{\delta}_2 - \ddot{\bar{\delta}})$, and $(\ddot{\delta}_3 - \ddot{\bar{\delta}})$.

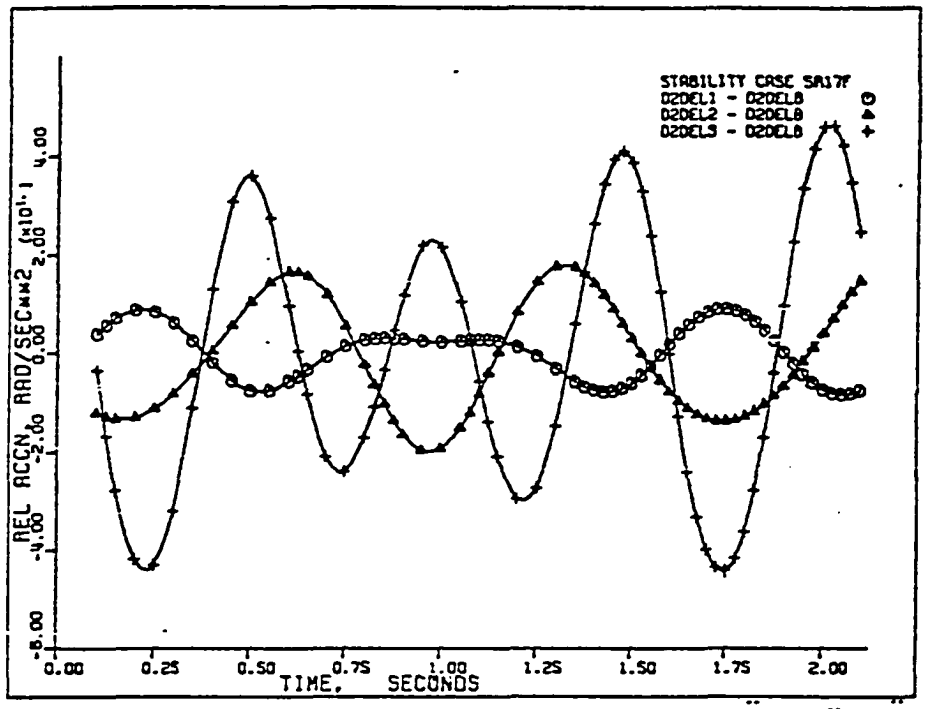

Figure 362. Case SR-17F: relative accelerations $(\ddot{\delta}_1 - \ddot{\bar{\delta}})$, $(\ddot{\delta}_2 - \ddot{\bar{\delta}})$, and $(\ddot{\delta}_3 - \ddot{\bar{\delta}})$.

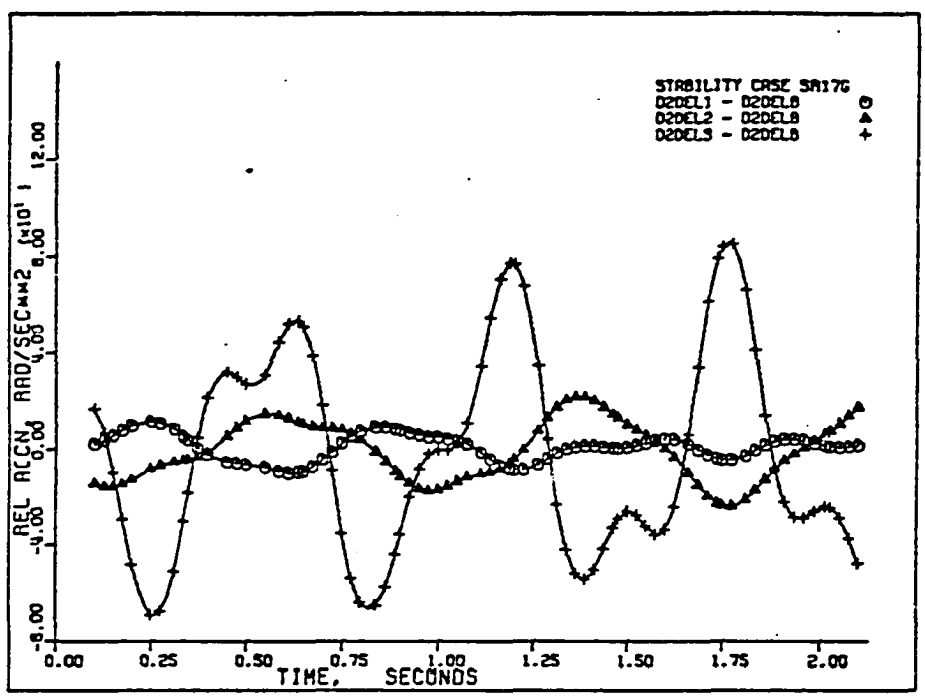

Figure 363. Case SR-17G: relative accelerations $(\ddot{\delta}_1 - \ddot{\bar{\delta}})$, $(\ddot{\delta}_2 - \ddot{\bar{\delta}})$, and $(\ddot{\delta}_3 - \ddot{\bar{\delta}})$.

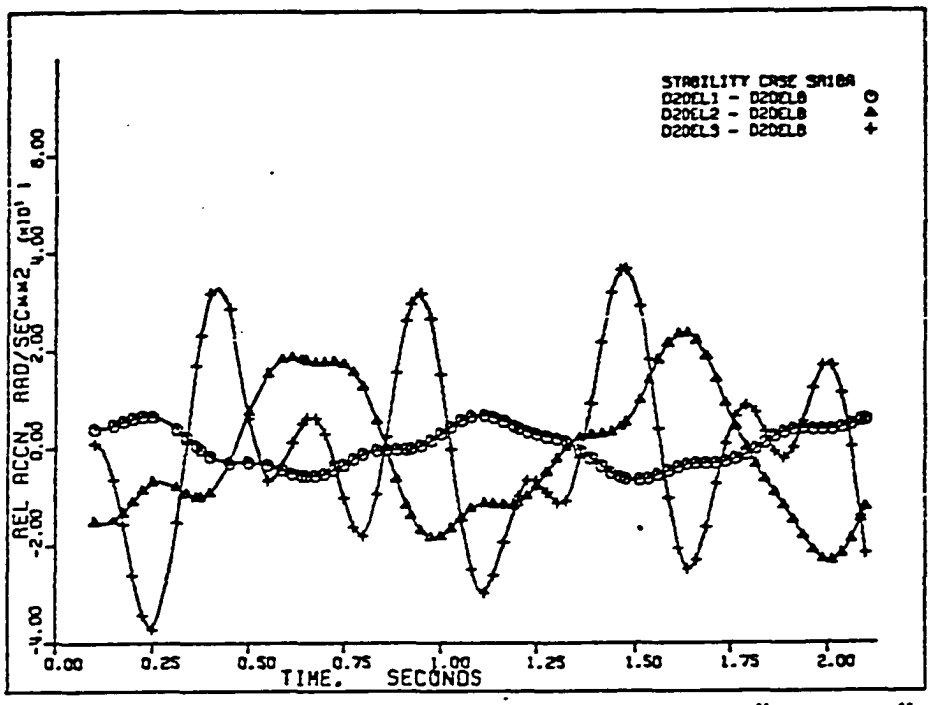

Figure 364. Case SR-18A: relative accelerations $(\ddot{\delta}_1 - \ddot{\delta})$, $(\ddot{\delta}_2 - \ddot{\delta})$, and $(\ddot{\delta}_3 - \ddot{\delta})$.

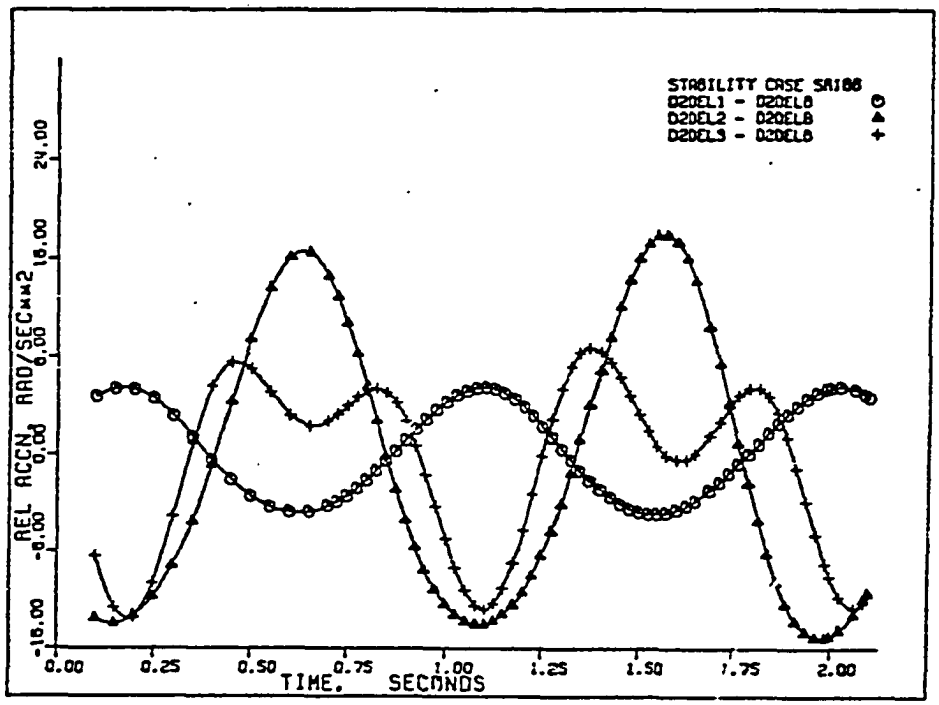

Figure 365. Case SR-18B: relative accelerations $(\ddot{\delta}_1 - \ddot{\delta})$, $(\ddot{\delta}_2 - \ddot{\delta})$, and $(\ddot{\delta}_3 - \ddot{\delta})$.

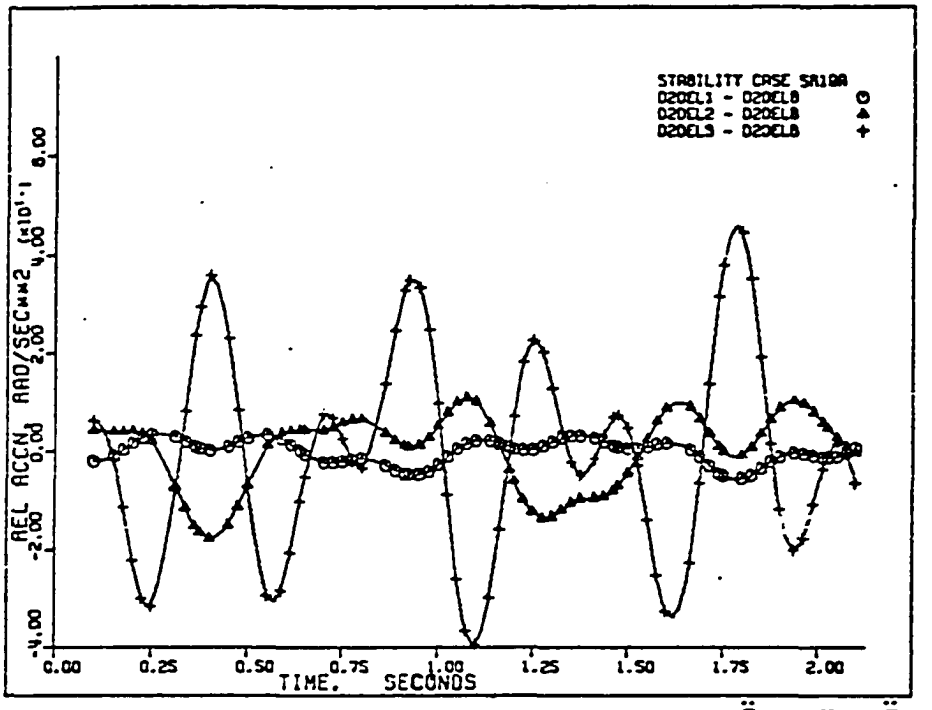

Figure 366. Case SR-19A: relative accelerations $(\ddot{\delta}_1 - \ddot{\bar{\delta}})$, $(\ddot{\delta}_2 - \ddot{\bar{\delta}})$, and $(\ddot{\delta}_3 - \ddot{\bar{\delta}})$.

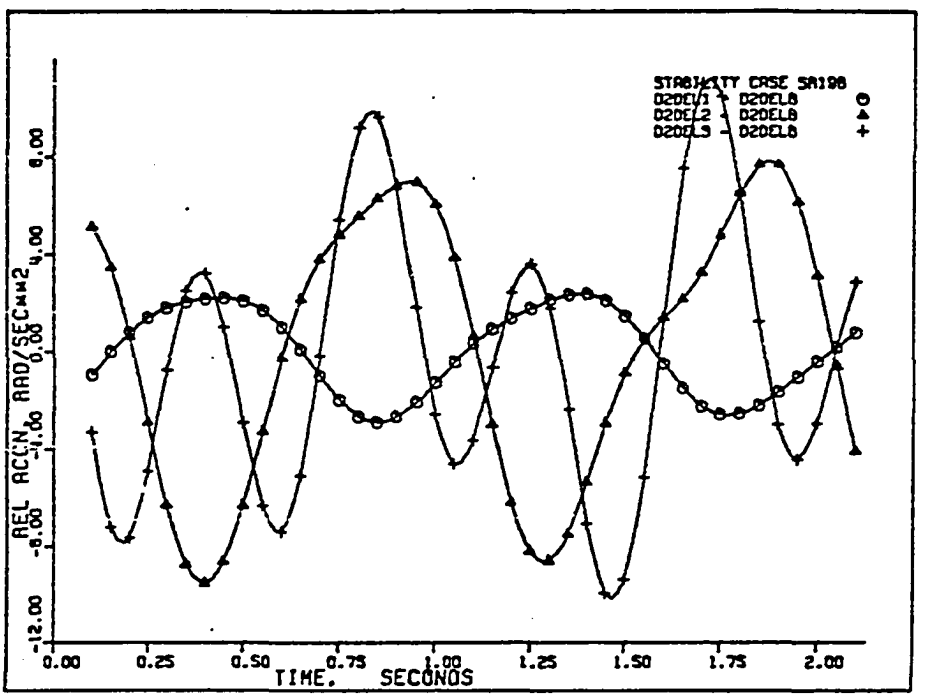

Figure 367. Case SR-19B: relative accelerations $(\ddot{\delta}_1 - \ddot{\bar{\delta}})$, $(\ddot{\delta}_2 - \ddot{\bar{\delta}})$, and $(\ddot{\delta}_3 - \ddot{\bar{\delta}})$.

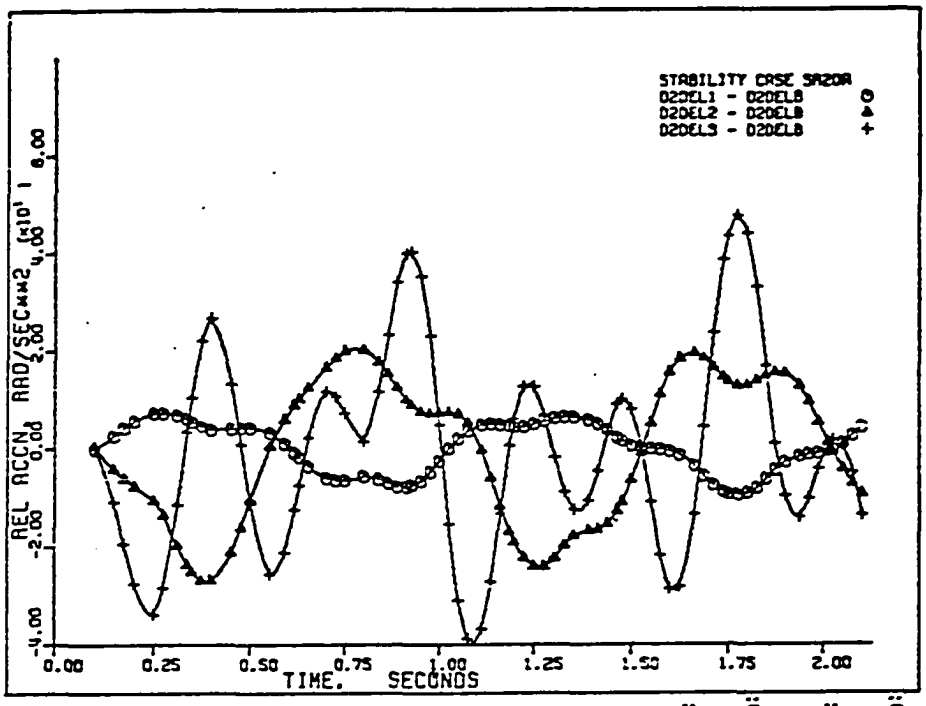

Figure 368. Case SR-20A: relative accelerations $(\ddot{\delta}_1 - \ddot{\bar{\delta}})$, $(\ddot{\delta}_2 - \ddot{\bar{\delta}})$, and $(\ddot{\delta}_3 - \ddot{\bar{\delta}})$.

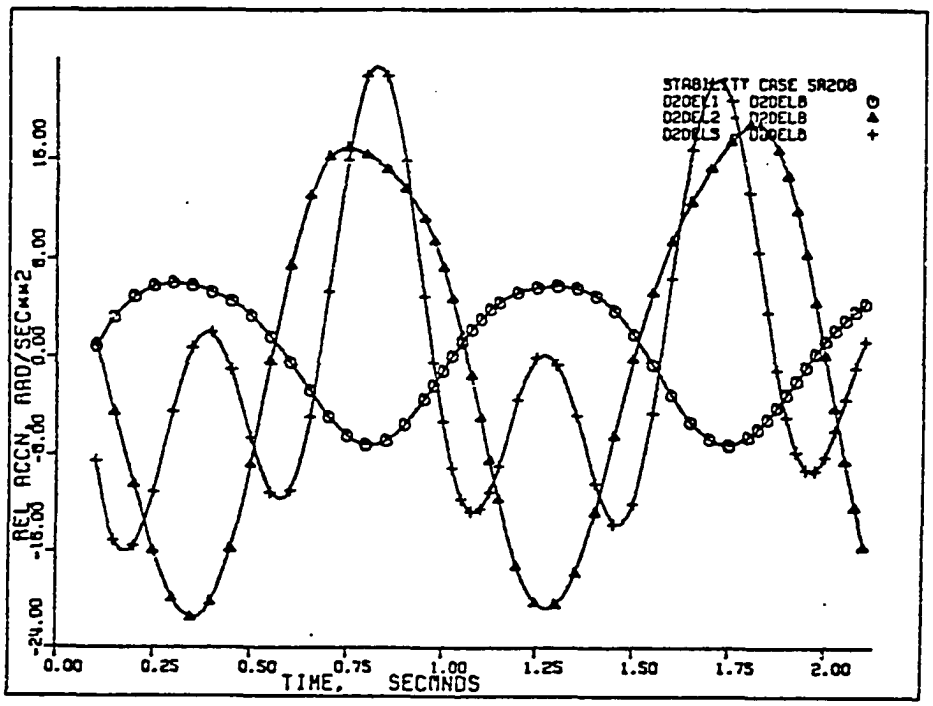

Figure 369. Case SR-20B: relative accelerations $(\ddot{\delta}_1 - \ddot{\bar{\delta}})$, $(\ddot{\delta}_2 - \ddot{\bar{\delta}})$, and $(\ddot{\delta}_3 - \ddot{\bar{\delta}})$.

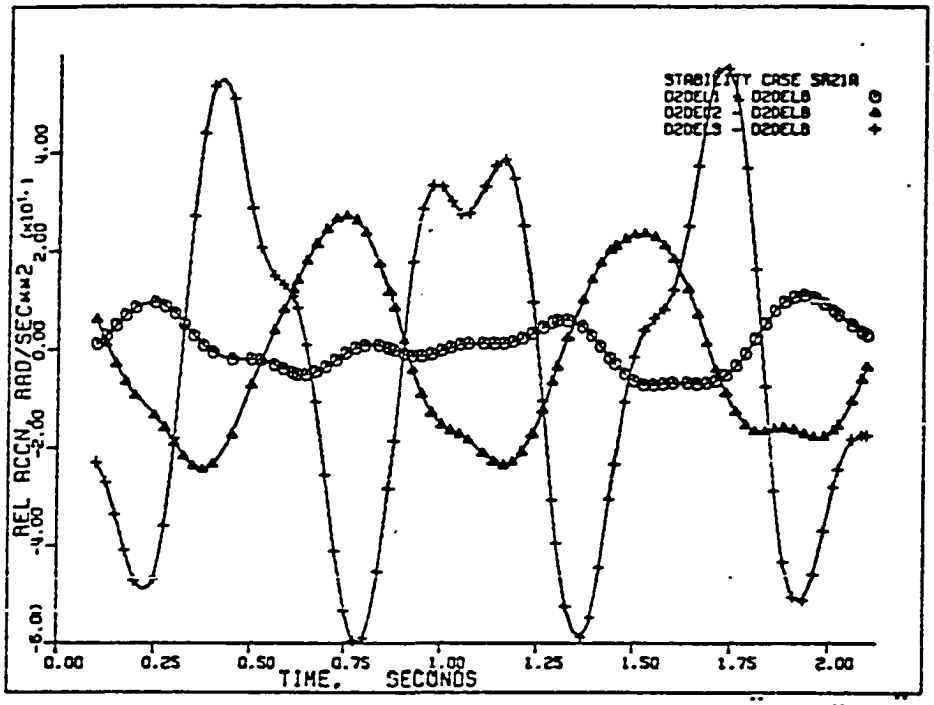

Figure 370. Case SR-21A: relative accelerations $(\ddot{\delta}_1 - \ddot{\bar{\delta}})$, $(\ddot{\delta}_2 - \ddot{\bar{\delta}})$, and $(\ddot{\delta}_3 - \ddot{\bar{\delta}})$.

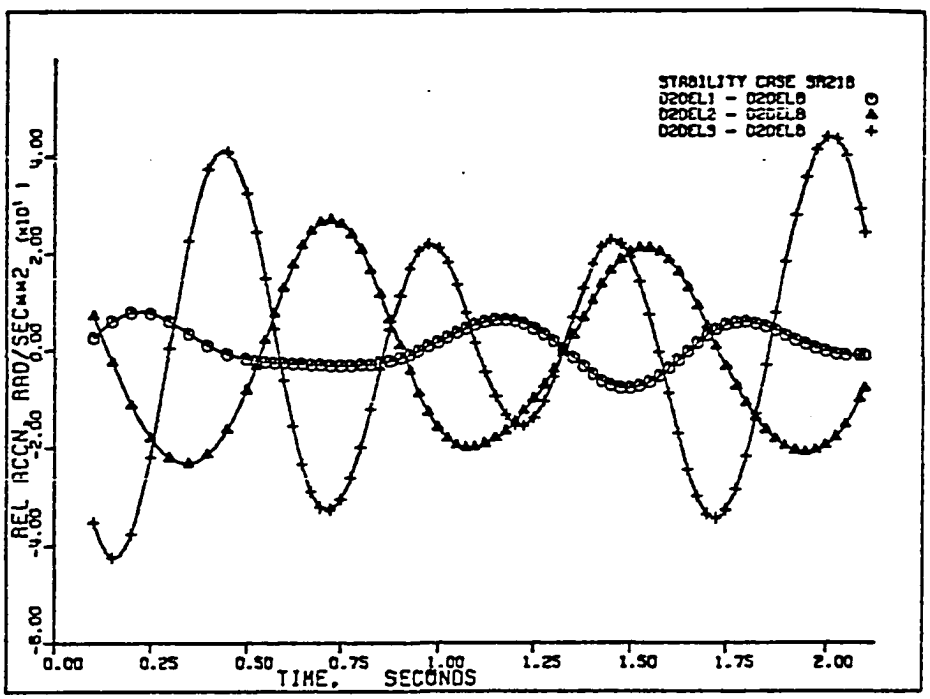

Figure 371. Case SR-21B: relative accelerations $(\ddot{\delta}_1 - \ddot{\bar{\delta}})$, $(\ddot{\delta}_2 - \ddot{\bar{\delta}})$, and $(\ddot{\delta}_3 - \ddot{\bar{\delta}})$.

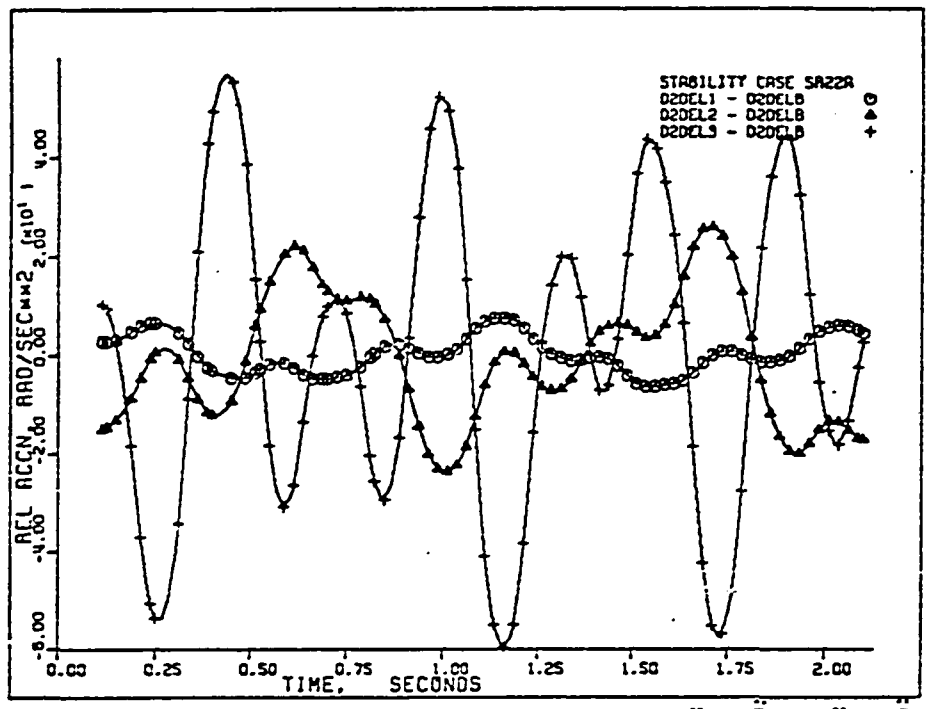

Figure 372. Case SR-22A: relative accelerations $(\ddot{\delta}_1 - \ddot{\bar{\delta}})$, $(\ddot{\delta}_2 - \ddot{\bar{\delta}})$, and $(\ddot{\delta}_3 - \ddot{\bar{\delta}})$.

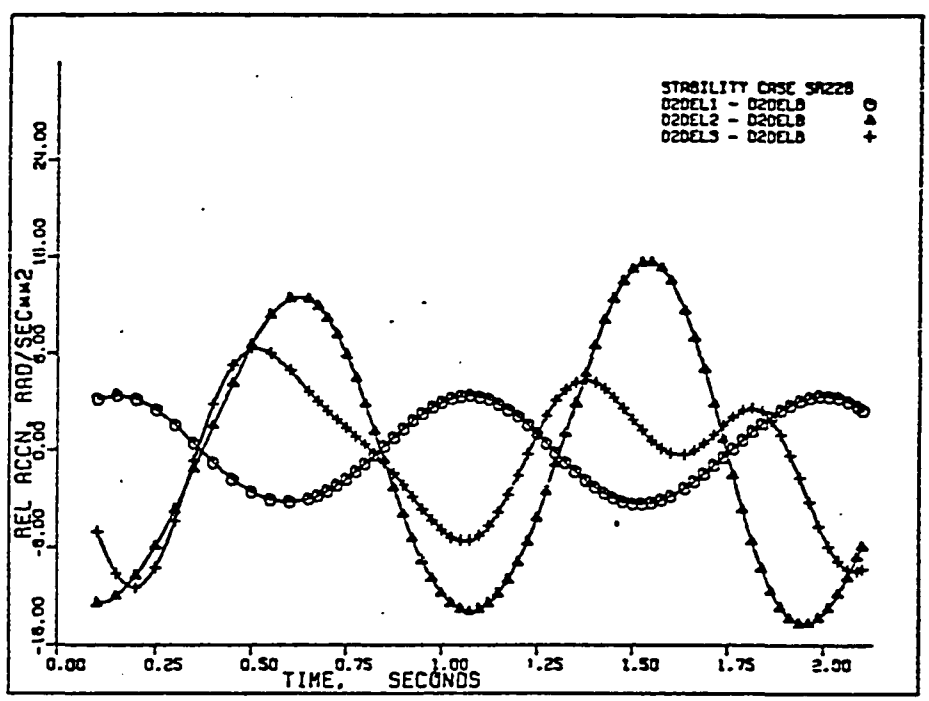

Figure 373. Case SR-22B: relative accelerations $(\ddot{\delta}_1 - \ddot{\bar{\delta}})$, $(\ddot{\delta}_2 - \ddot{\bar{\delta}})$, and $(\ddot{\delta}_3 - \ddot{\bar{\delta}})$.

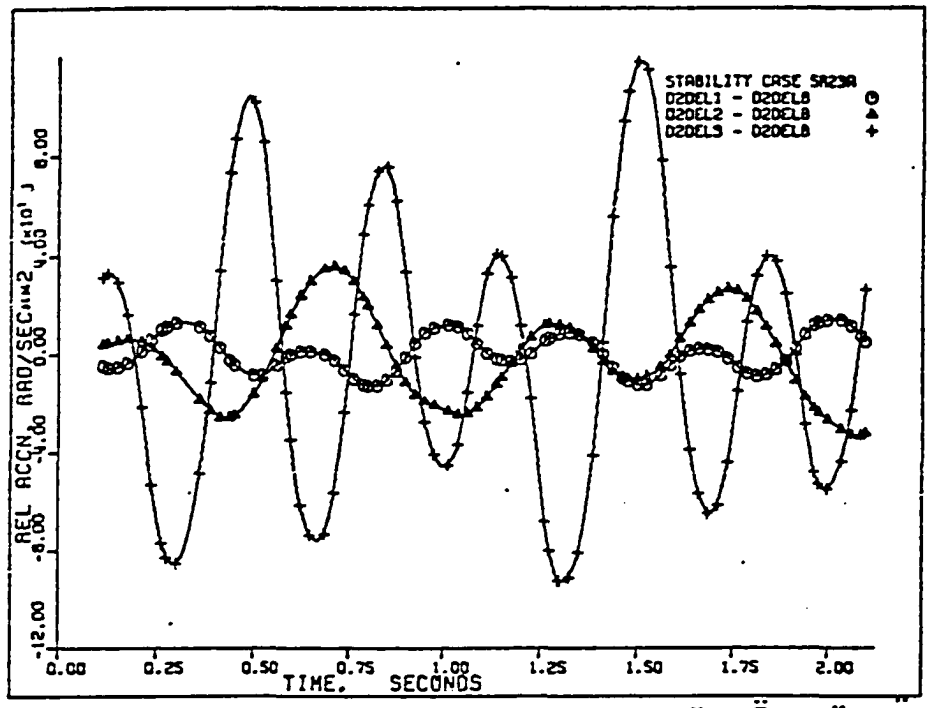

Figure 374. Case SR-23A: relative accelerations $(\ddot{\delta}_1 - \ddot{\bar{\delta}})$, $(\ddot{\delta}_2 - \ddot{\bar{\delta}})$, and $(\ddot{\delta}_3 - \ddot{\bar{\delta}})$.

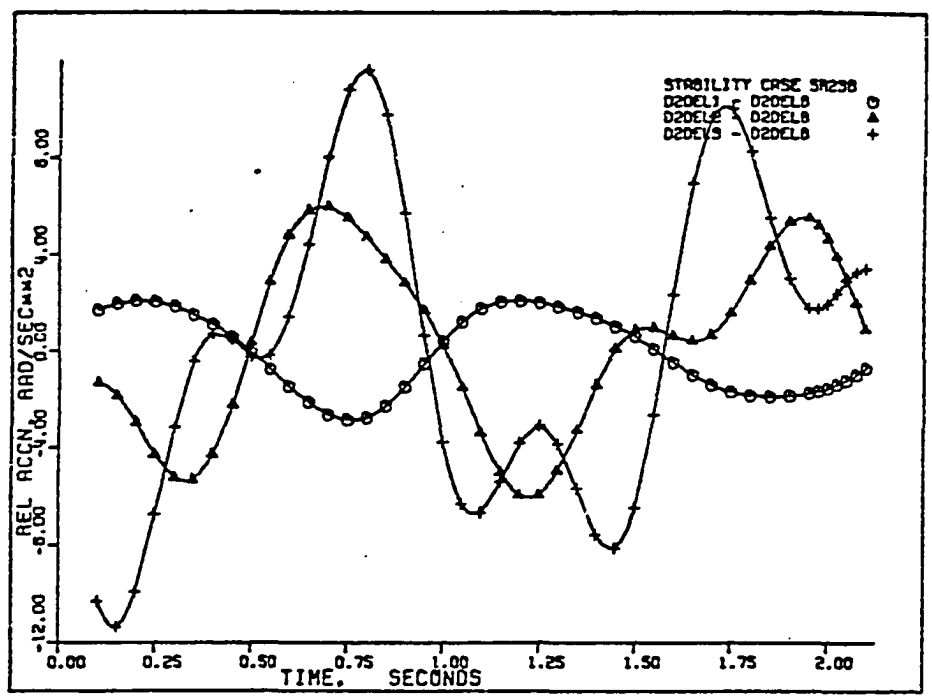

Figure 375. Case SR-23B: relative accelerations $(\ddot{\delta}_1 - \ddot{\bar{\delta}})$, $(\ddot{\delta}_2 - \ddot{\bar{\delta}})$, and $(\ddot{\delta}_3 - \ddot{\bar{\delta}})$.

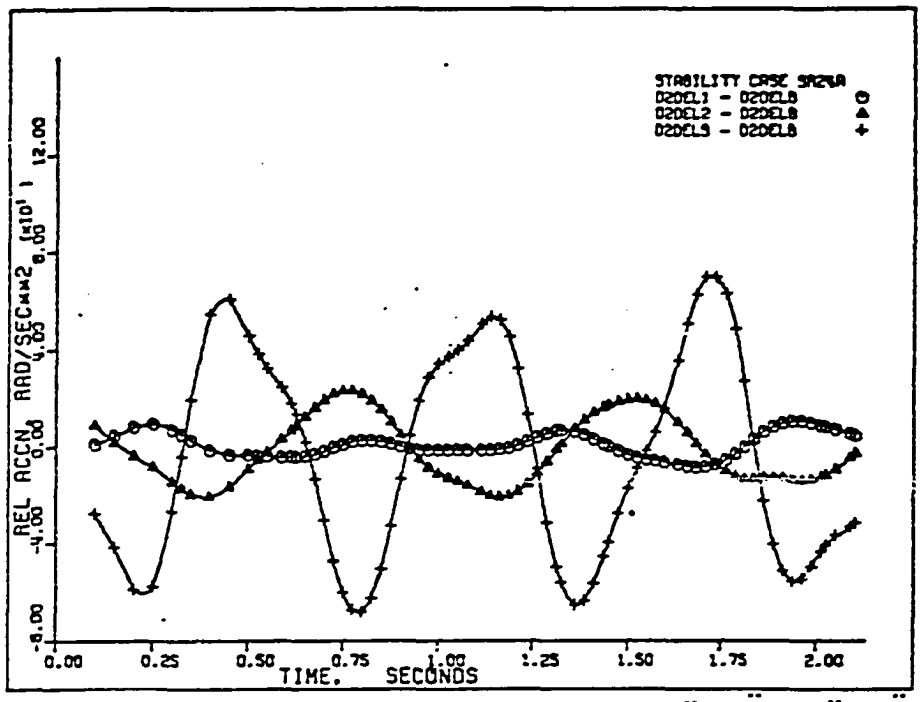

Figure 376. Case SR-24A: relative accelerations $(\ddot{\delta}_1 - \ddot{\bar{\delta}})$, $(\ddot{\delta}_2 - \ddot{\bar{\delta}})$, and $(\ddot{\delta}_3 - \ddot{\bar{\delta}})$.

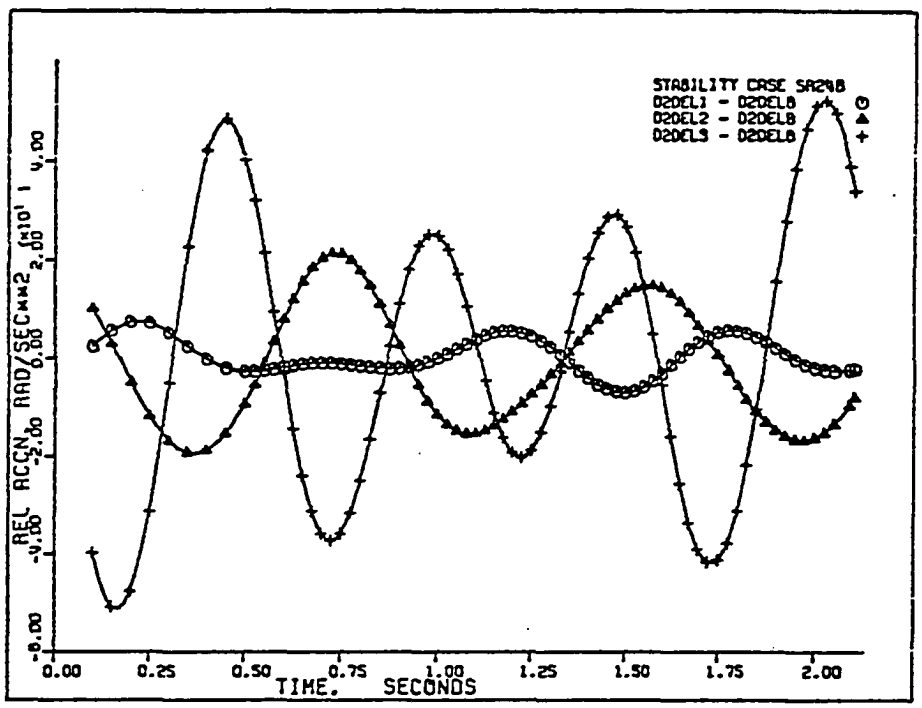

Figure 377. Case SR-24B: relative accelerations $(\ddot{\delta}_1 - \ddot{\bar{\delta}})$, $(\ddot{\delta}_2 - \ddot{\bar{\delta}})$, and $(\ddot{\delta}_3 - \ddot{\bar{\delta}})$.

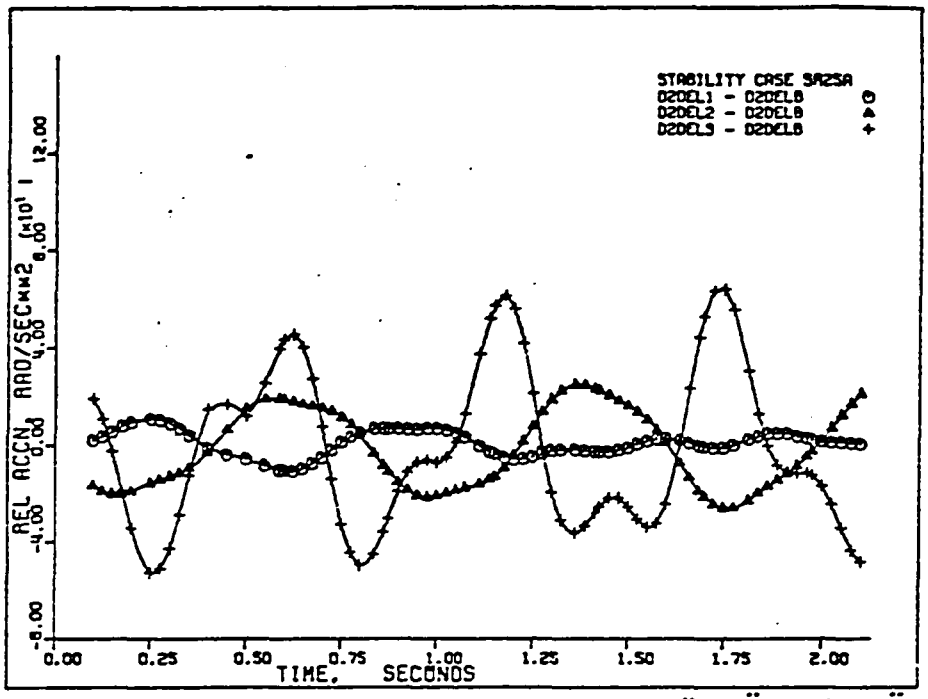

Figure 378. Case SR-25A: relative accelerations $(\ddot{\delta}_1 - \ddot{\bar{\delta}})$, $(\ddot{\delta}_2 - \ddot{\bar{\delta}})$, and $(\ddot{\delta}_3 - \ddot{\bar{\delta}})$.

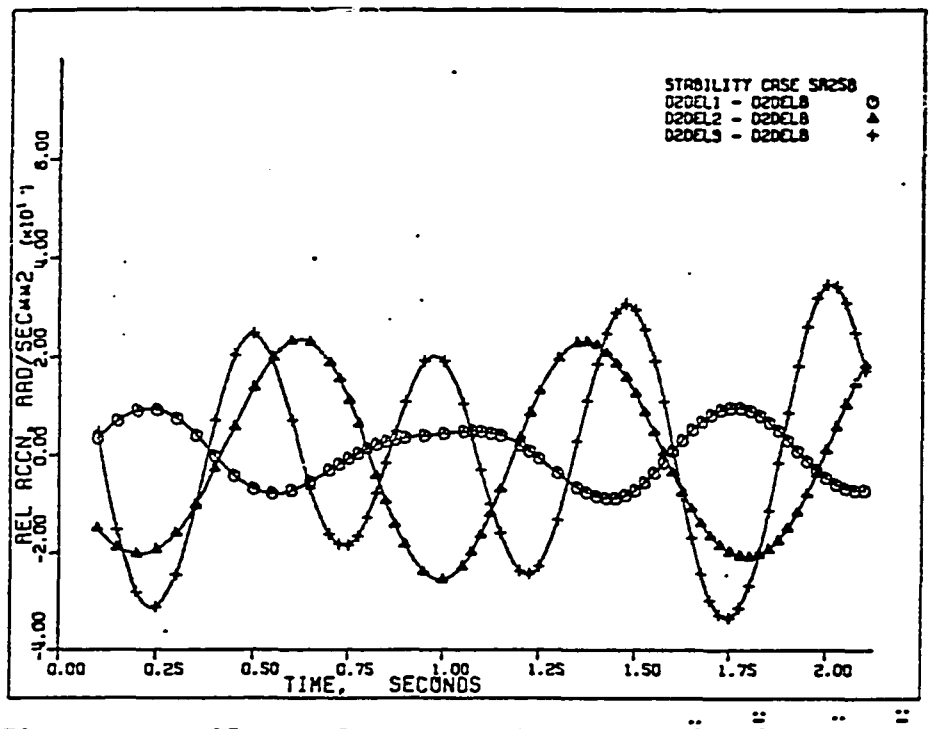

Figure 379. Case SR-25B: relative accelerations $(\ddot{\delta}_1 - \ddot{\bar{\delta}})$, $(\ddot{\delta}_2 - \ddot{\bar{\delta}})$, and $(\ddot{\delta}_3 - \ddot{\bar{\delta}})$.

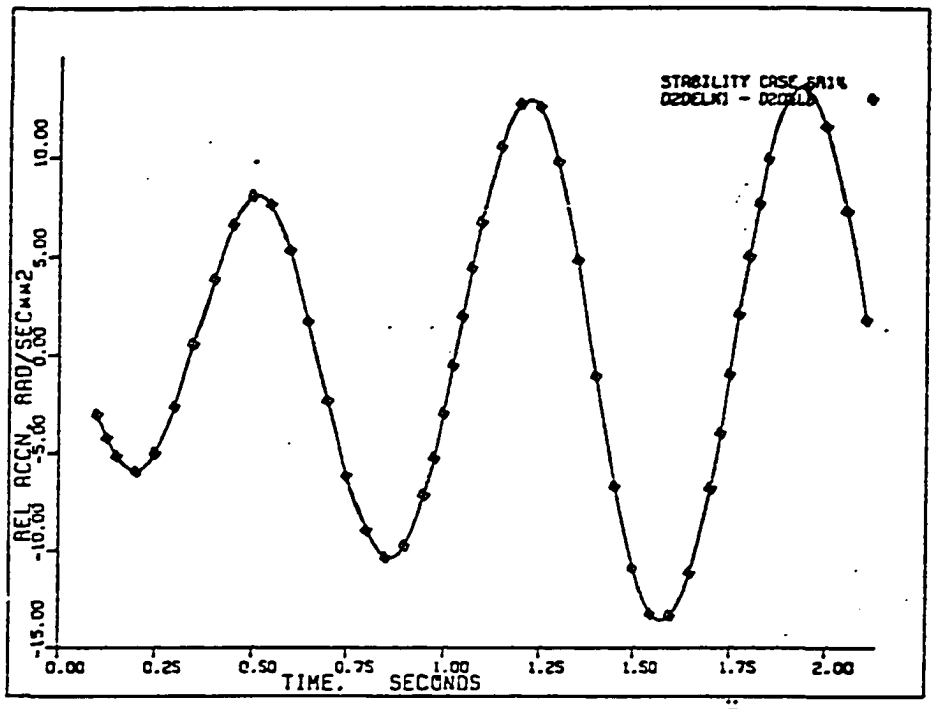

Figure 380. Case SR-14: relative acceleration $(\ddot{\delta}_k - \ddot{\bar{\delta}})$.

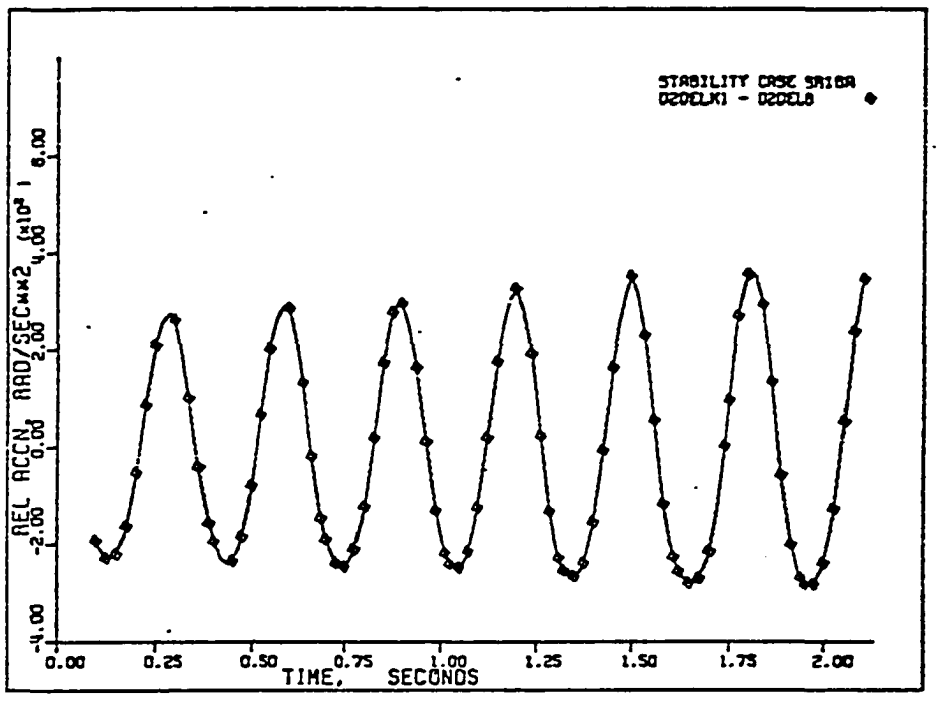

Figure 381. Case SR-16A: relative acceleration $(\ddot{\delta}_k - \ddot{\bar{\delta}})$.

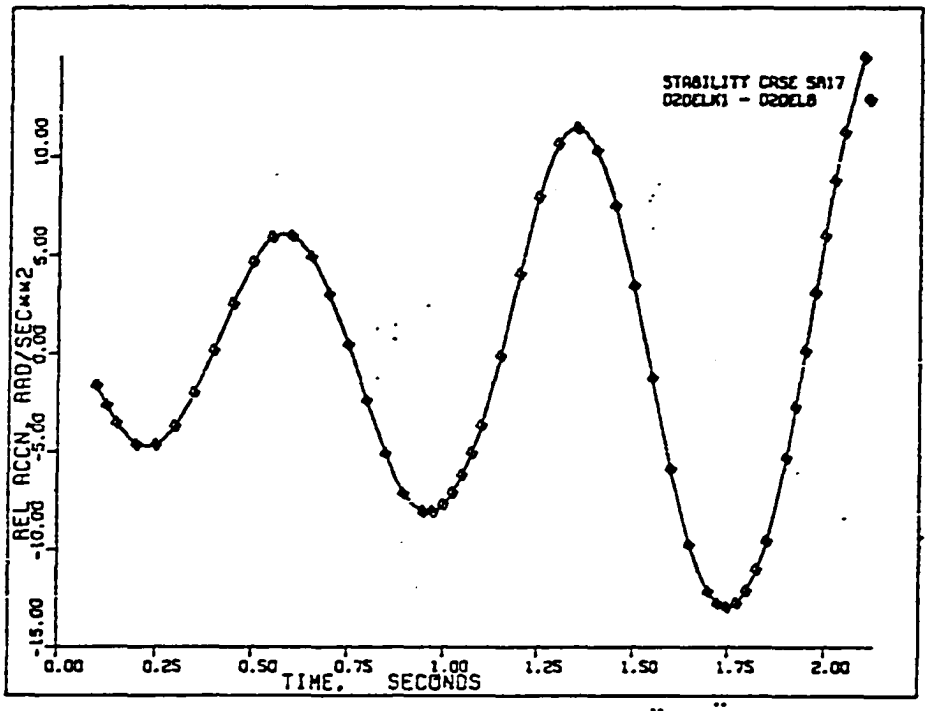

Figure 382. Case SR-17: relative acceleration $(\ddot{\delta}_k - \ddot{\bar{\delta}})$.

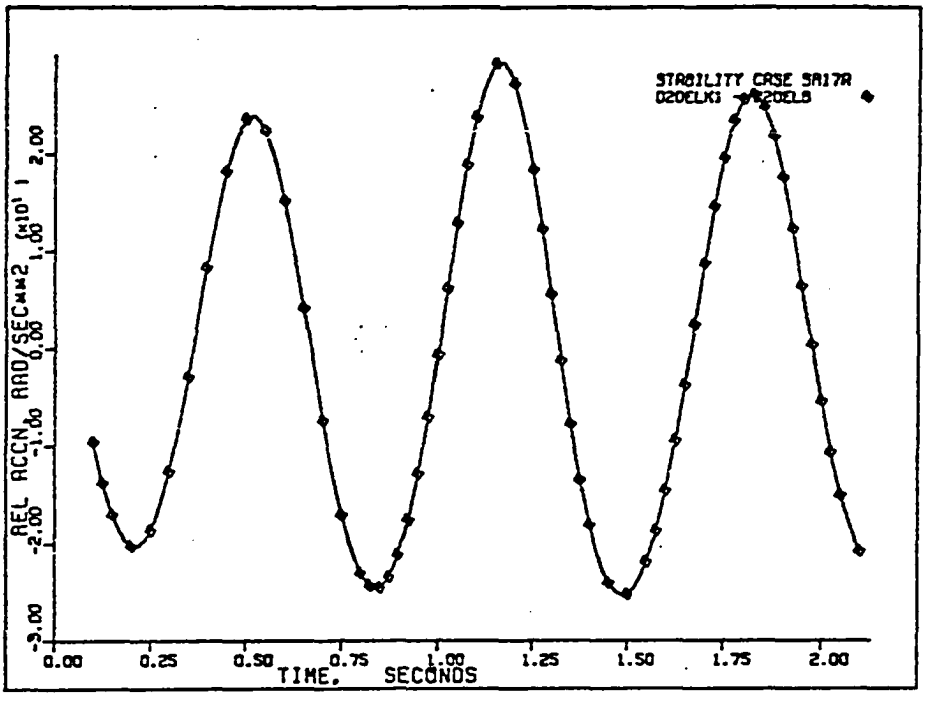

Figure 383. Case SR-17A: relative acceleration $(\ddot{\delta}_k - \ddot{\bar{\delta}})$.

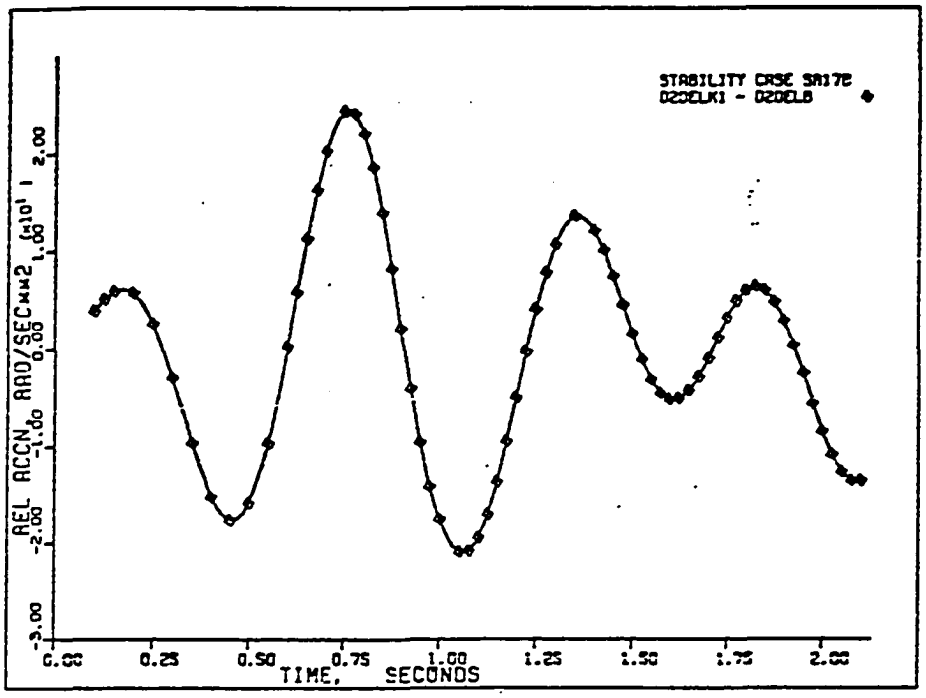

Figure 384. Case SR-17B: relative acceleration $(\ddot{\delta}_k - \ddot{\bar{\delta}})$.

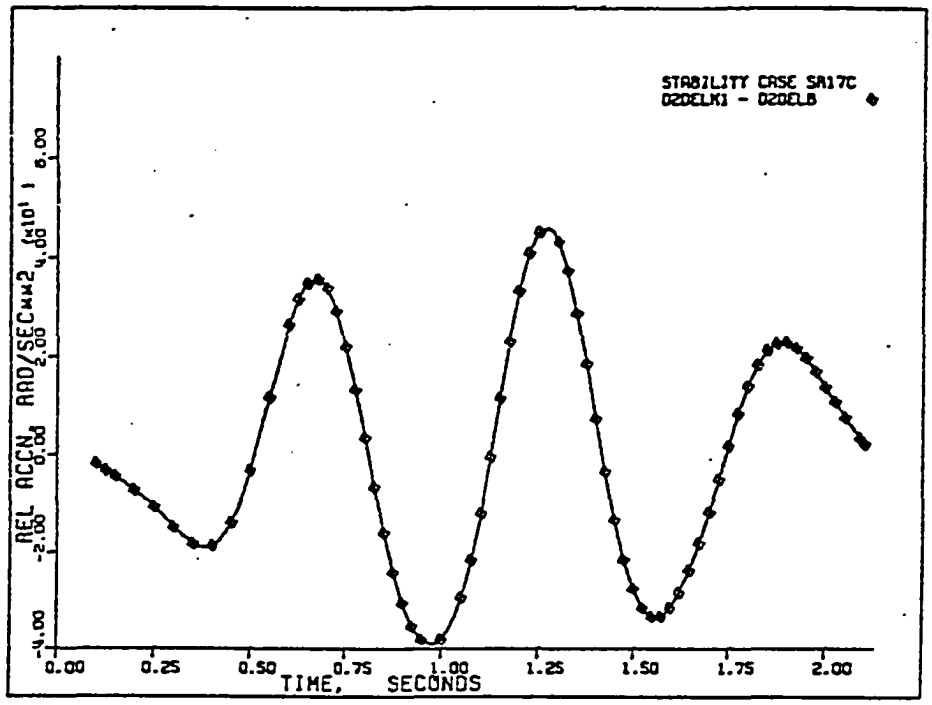

Figure 385. Case SR-17C: relative acceleration $(\ddot{\delta}_k - \ddot{\bar{\delta}})$.

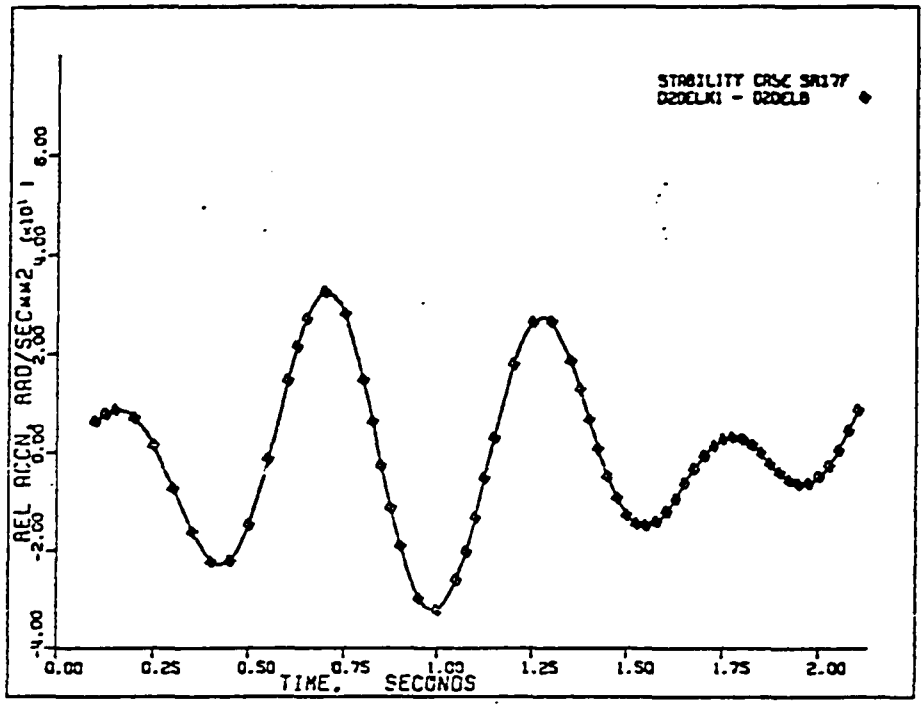

Figure 386. Case SR-17F: relative acceleration $(\ddot{\delta}_k - \ddot{\bar{\delta}})$.

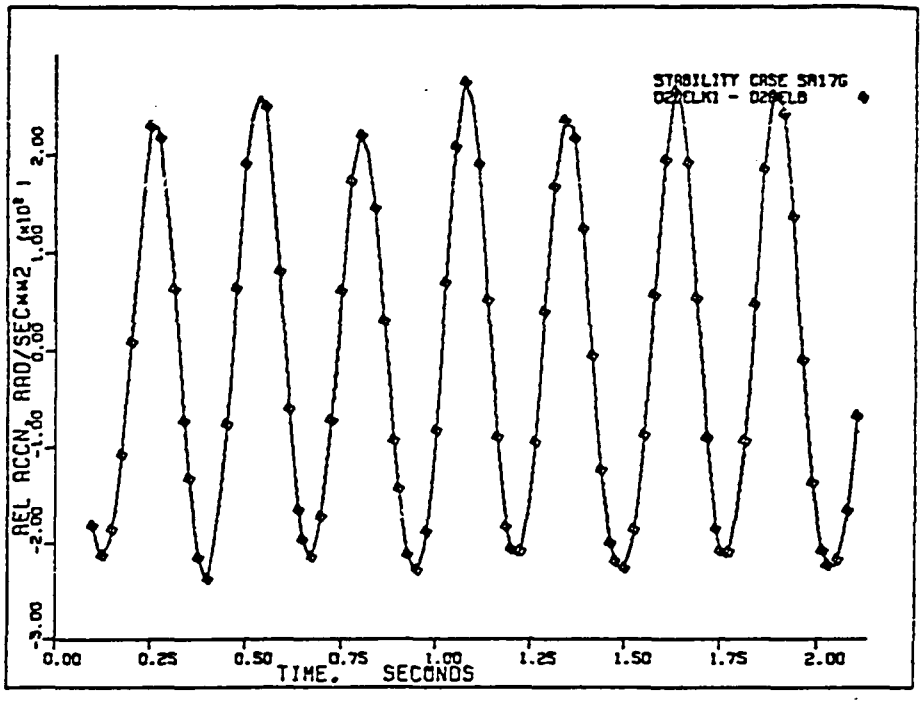

Figure 387. Case SR-17G: relative acceleration $(\ddot{\delta}_k - \ddot{\bar{\delta}})$.

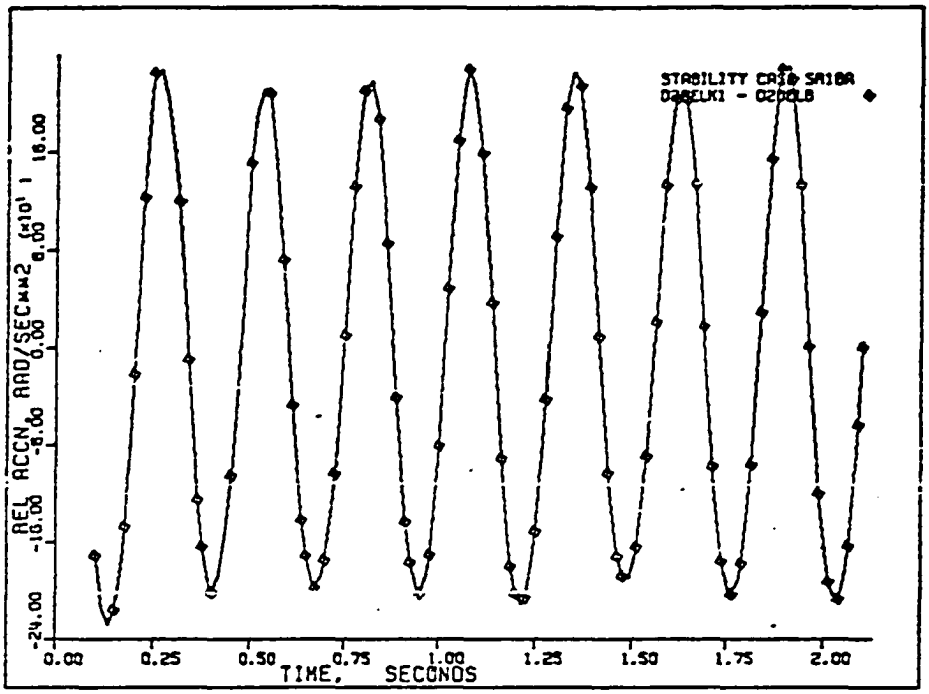

Figure 388. Case SR-18A: relative acceleration $(\ddot{\delta}_k - \ddot{\bar{\delta}})$.

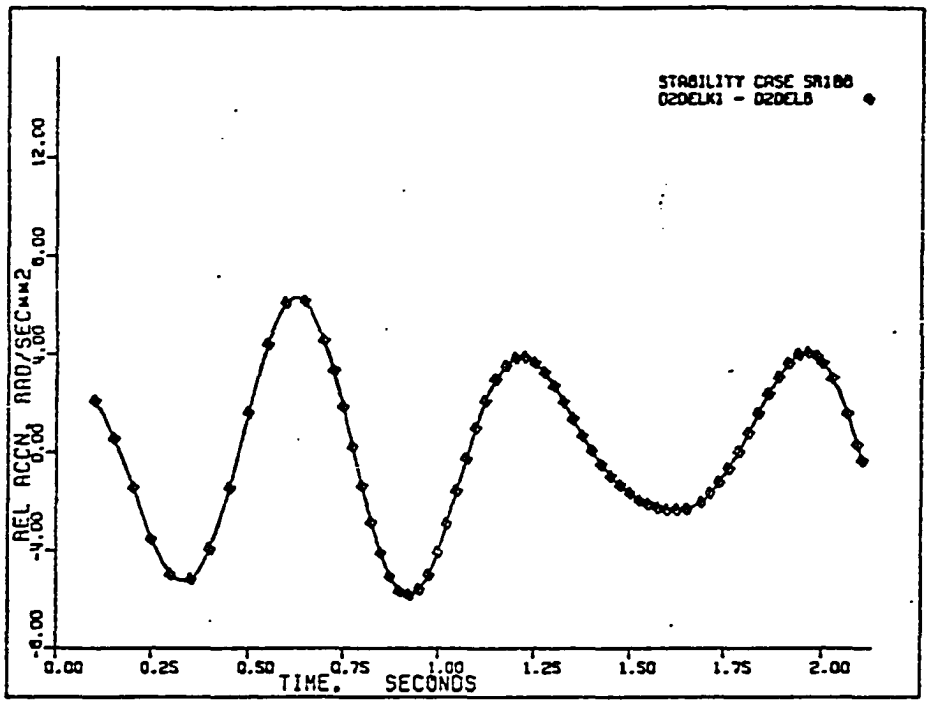

Figure 389. Case SR-18B: relative acceleration $(\ddot{\delta}_k - \ddot{\bar{\delta}})$.

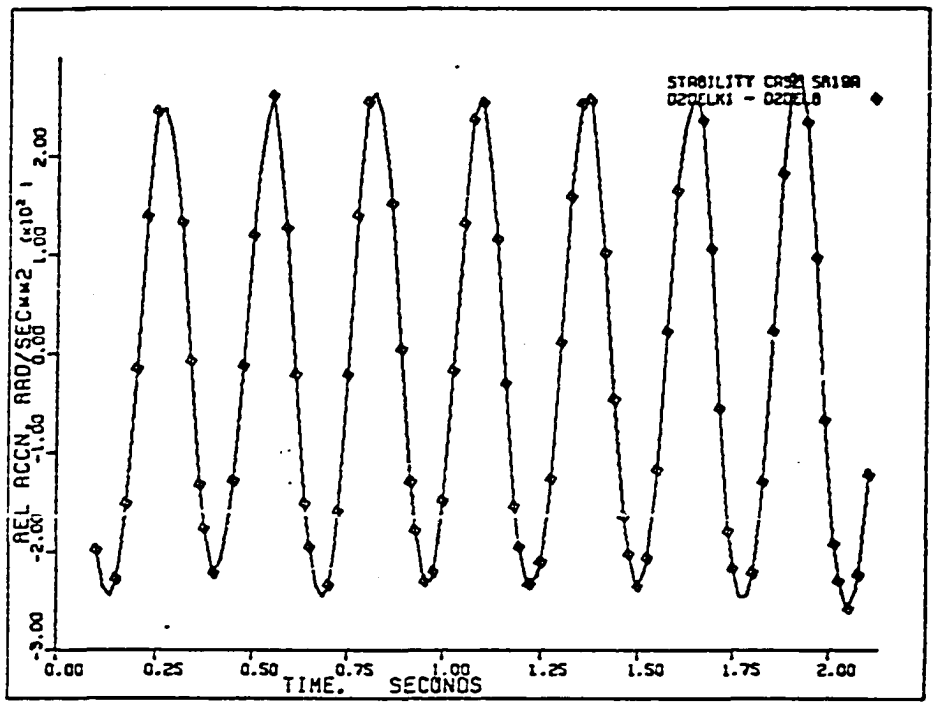

Figure 390. Case SR-19A: relative acceleration $(\ddot{\delta}_k - \ddot{\bar{\delta}})$.

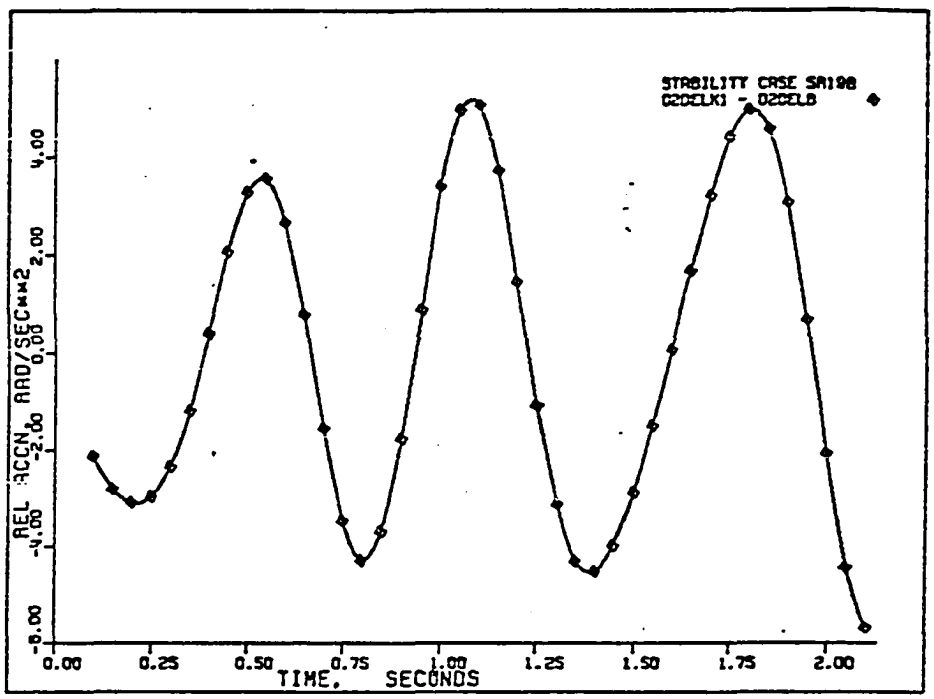

Figure 391. Case SR-19B: relative acceleration $(\ddot{\delta}_k - \ddot{\bar{\delta}})$.

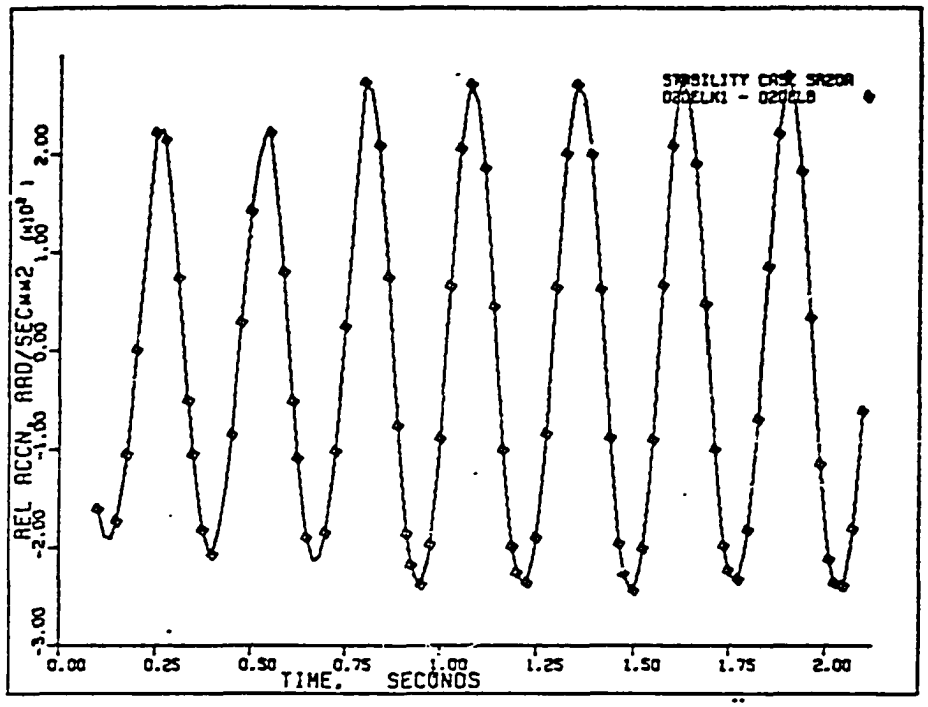

Figure 392. Case SR-20A: relative acceleration $(\ddot{\delta}_k - \ddot{\bar{\delta}})$.

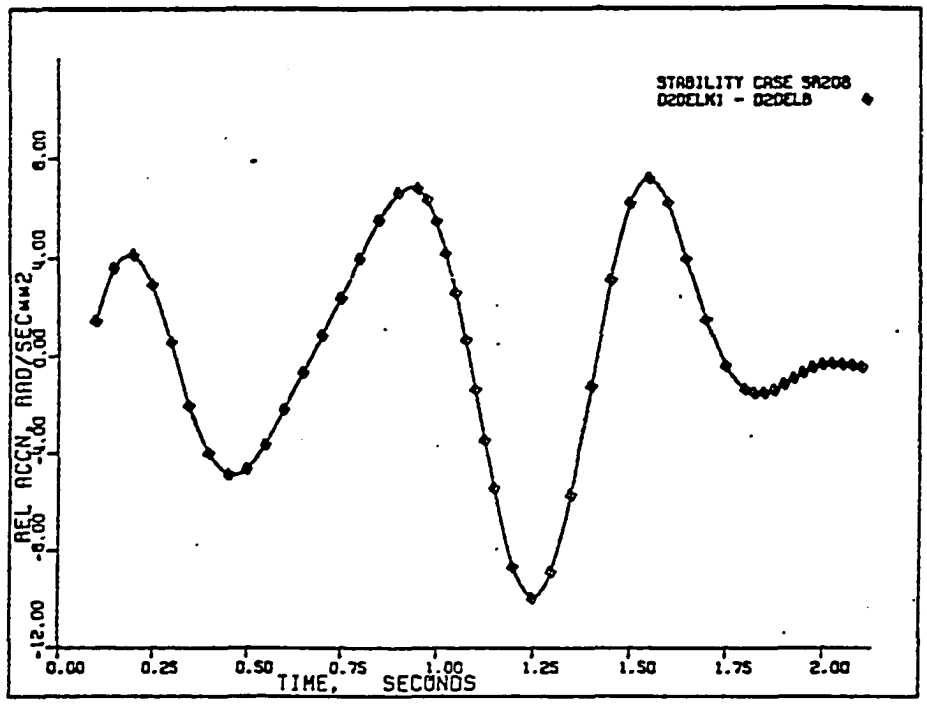

Figure 393. Case SR-20B: relative acceleration $(\ddot{\delta}_k - \ddot{\bar{\delta}})$.

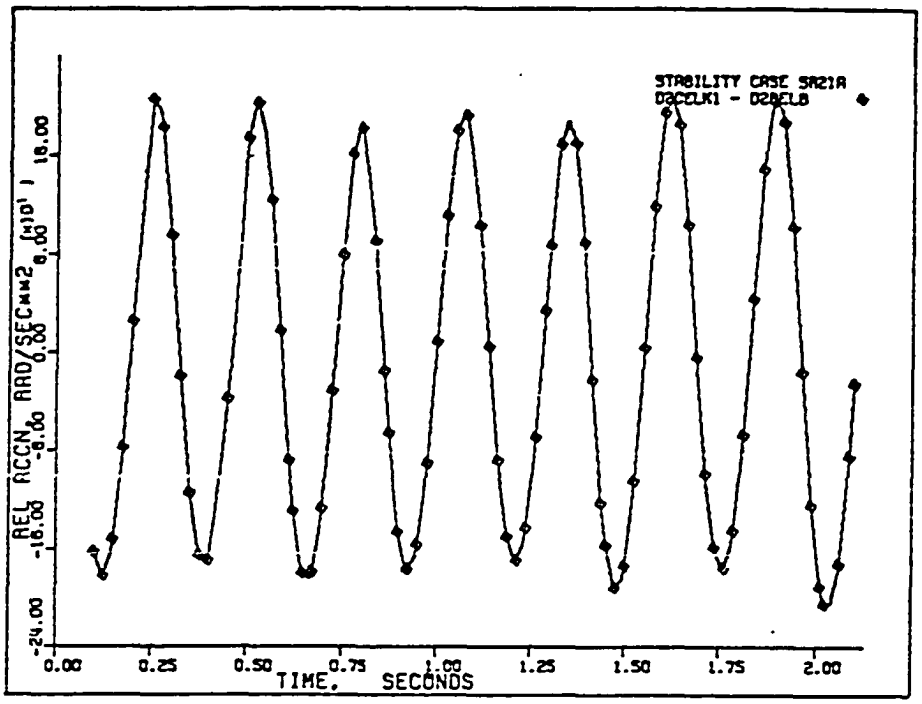

Figure 394. Case SR-21A: relative acceleration $(\ddot{\delta}_k - \ddot{\bar{\delta}})$.

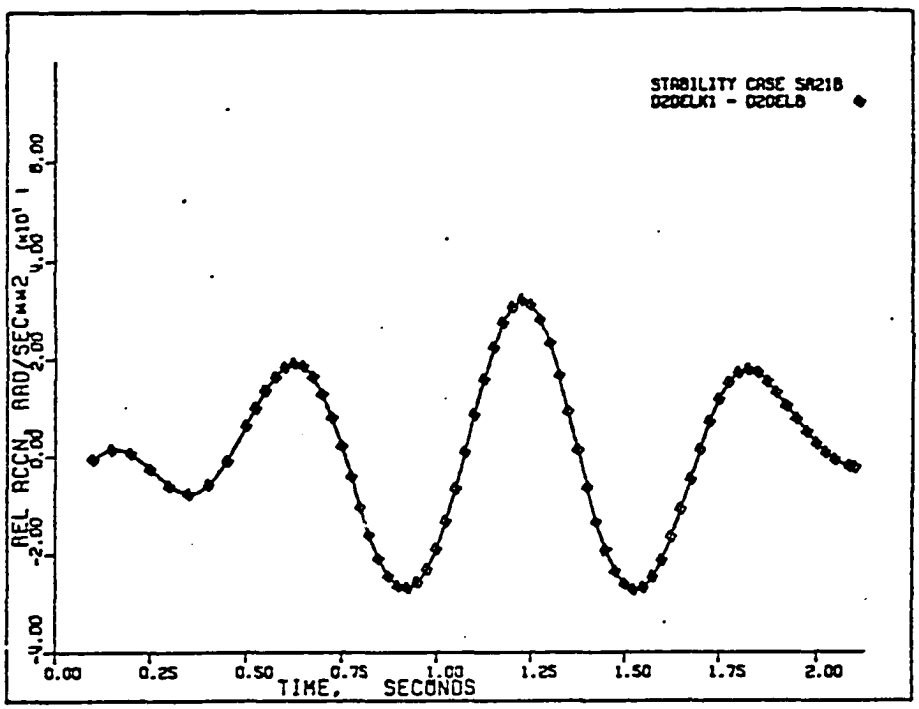

Figure 395. Case SR-21B: relative acceleration $(\ddot{\delta}_k - \ddot{\bar{\delta}})$.

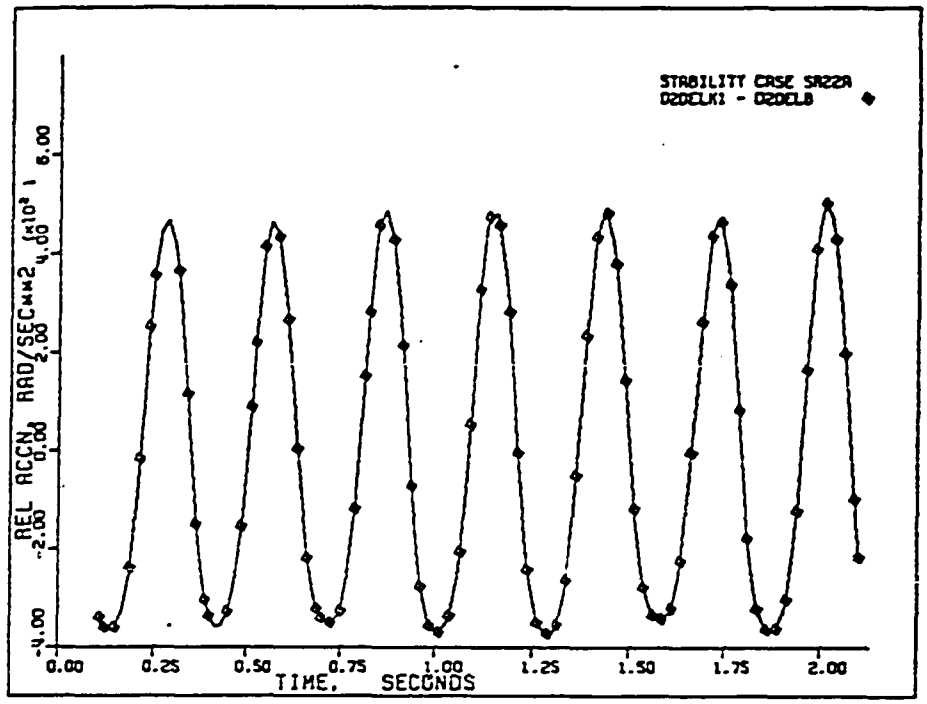

Figure 396. Case SR-22A: relative acceleration $(\ddot{\delta}_k - \ddot{\bar{\delta}})$.

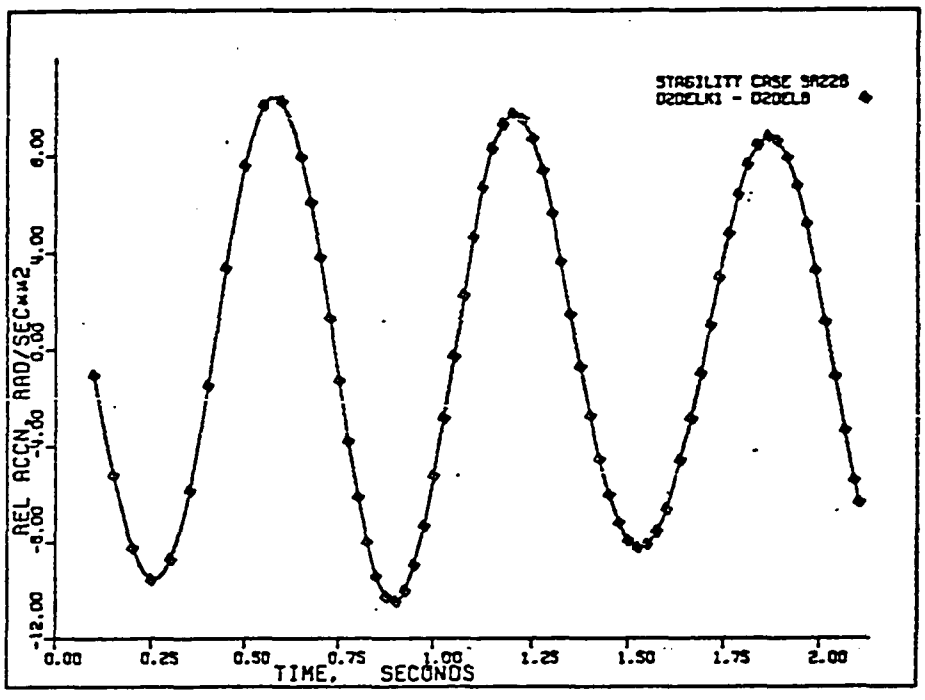

Figure 397. Case SR-22B: relative acceleration $(\ddot{\delta}_k - \ddot{\bar{\delta}})$.

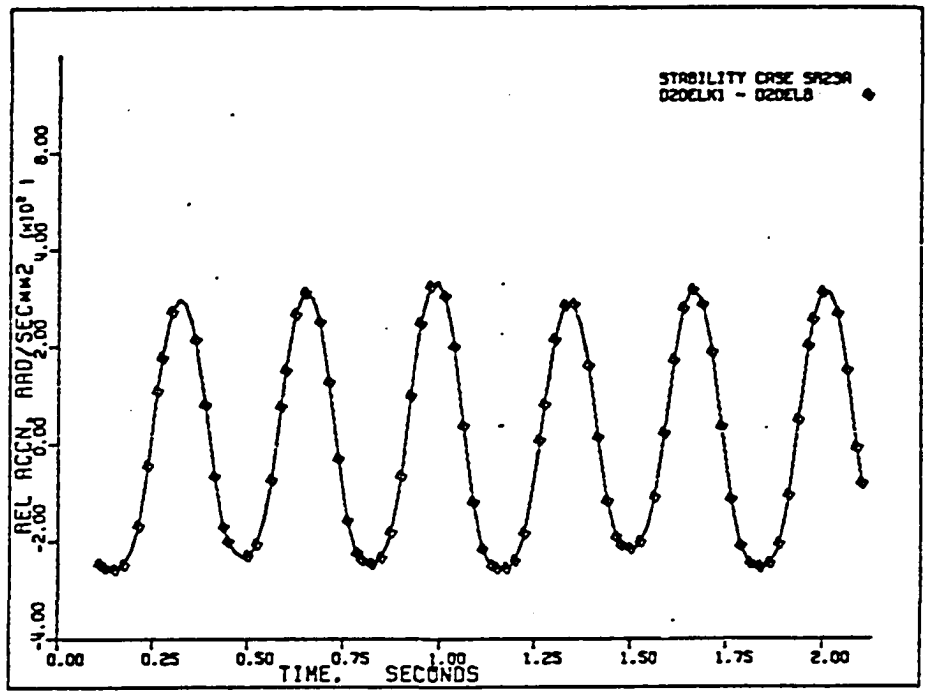

Figure 398. Case SR-23A: relative acceleration $(\ddot{\delta}_k - \ddot{\bar{\delta}})$.

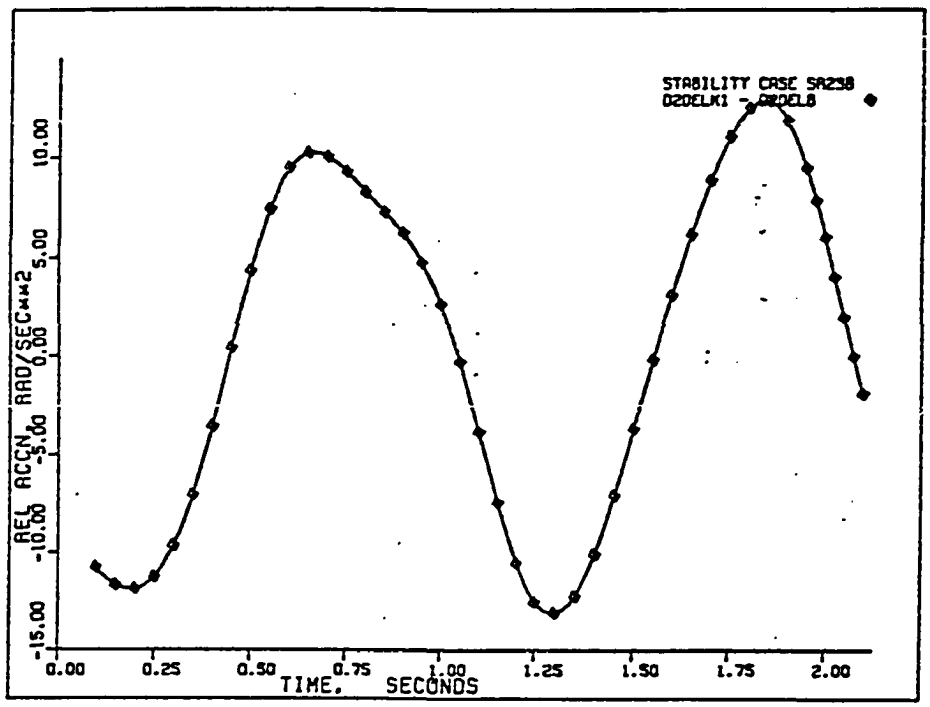

Figure 399. Case SR-23B: relative acceleration $(\ddot{\delta}_k - \ddot{\bar{\delta}})$.

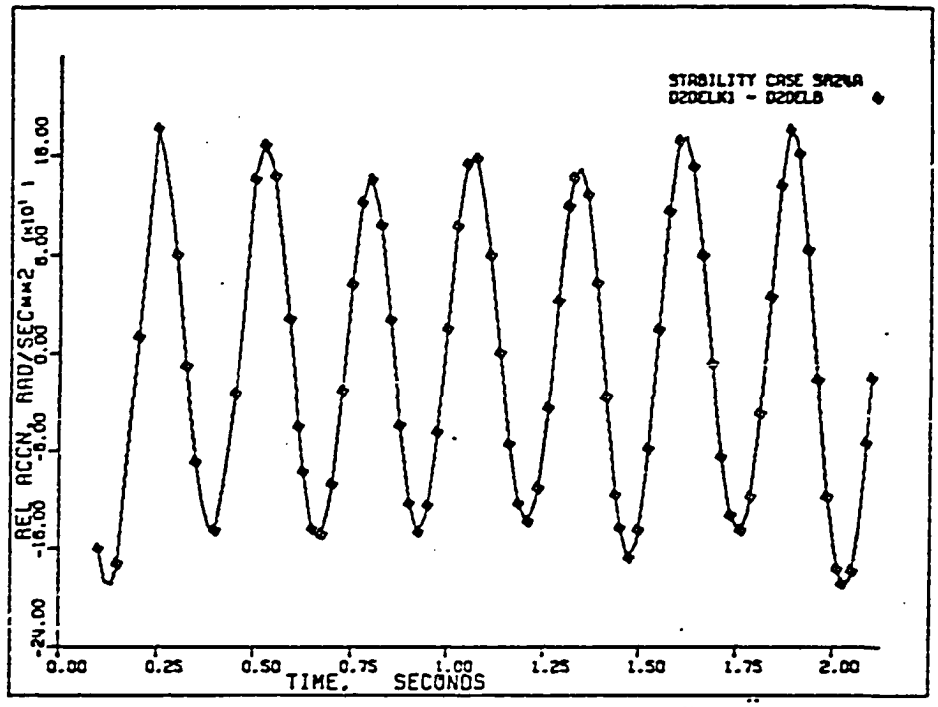

Figure 400. Case SR-24A: relative acceleration $(\ddot{\delta}_k - \ddot{\bar{\delta}})$.

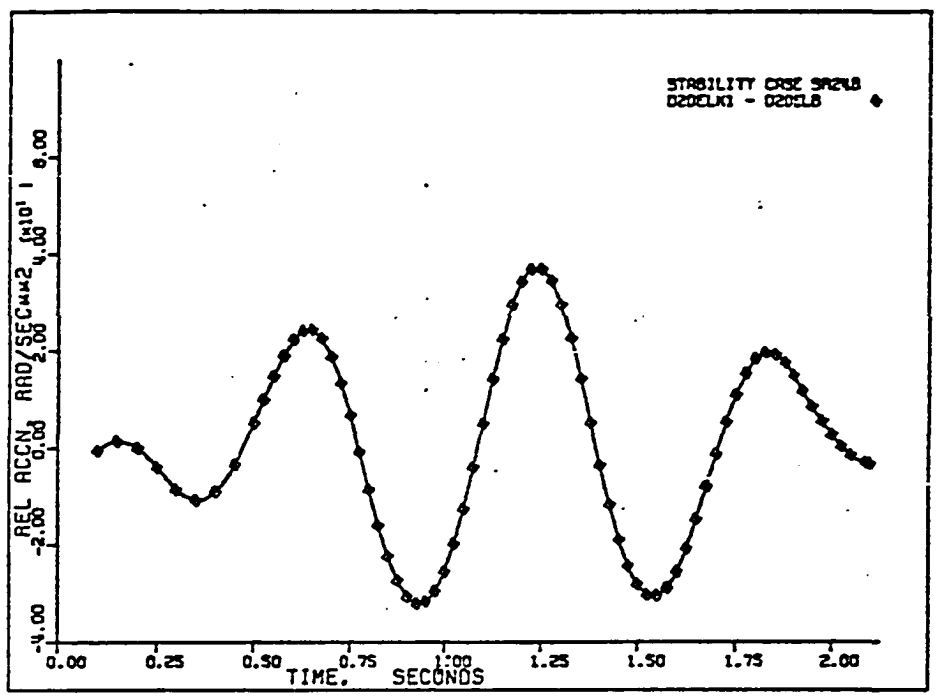

Figure 401. Case SR-24B: relative acceleration $(\ddot{\delta}_k - \ddot{\bar{\delta}})$.

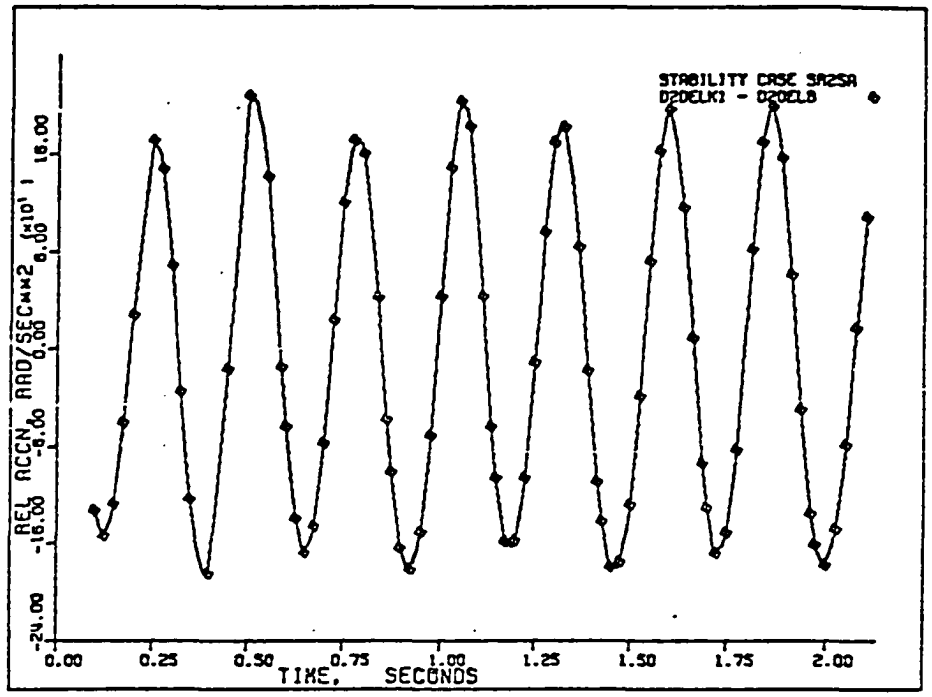

Figure 402. Case SR-25A: relative acceleration $(\ddot{\delta}_k - \ddot{\bar{\delta}})$.

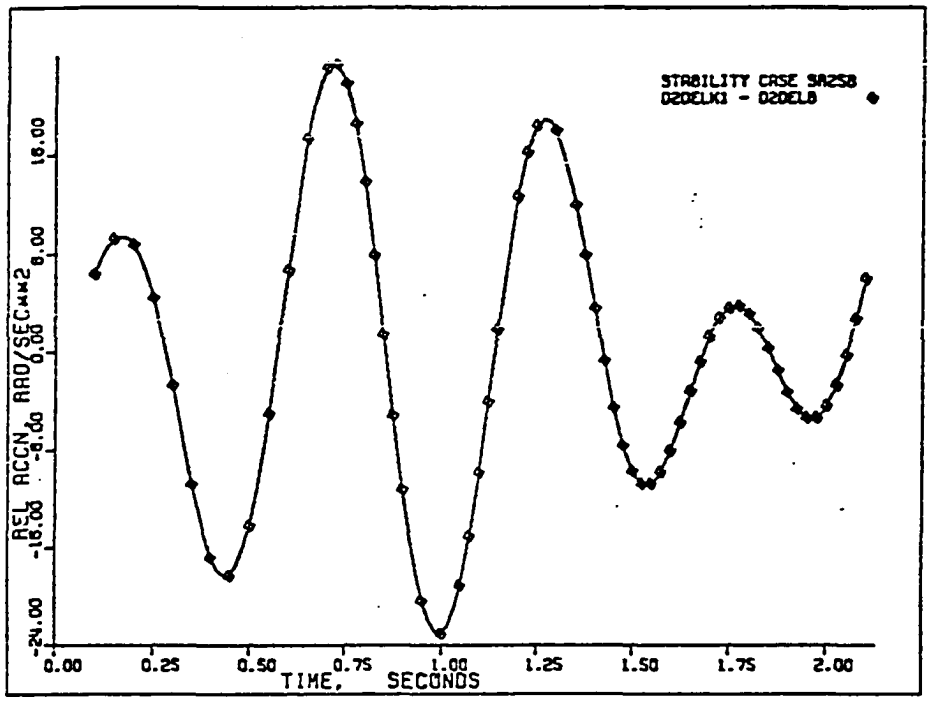

Figure 403. Case SR-25B: relative acceleration $(\ddot{\delta}_k - \ddot{\bar{\delta}})$.

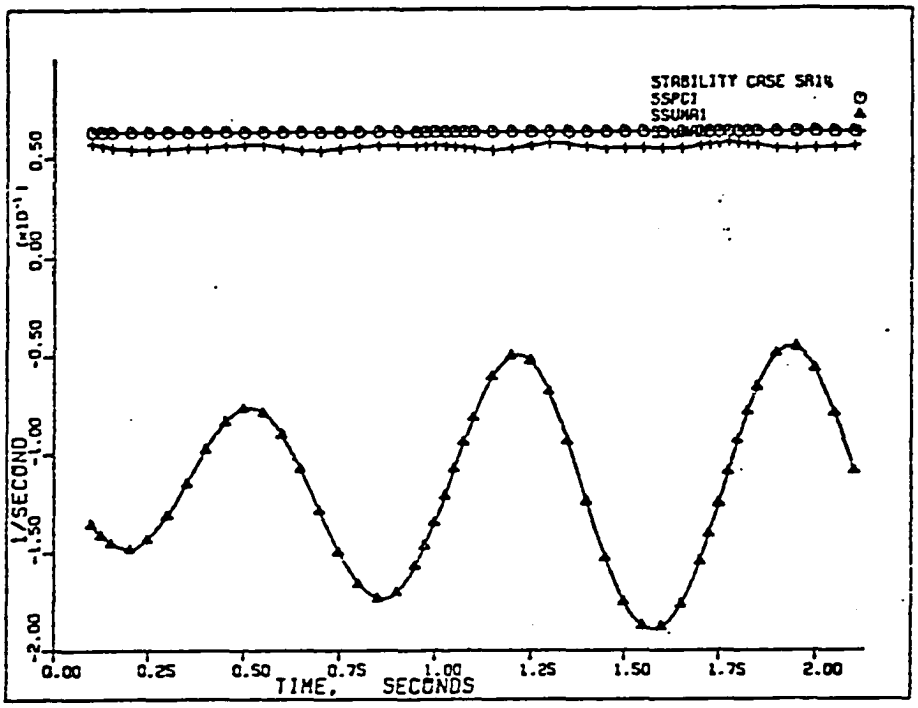

Figure 404. Case SR-14: terms of equation (4.10).

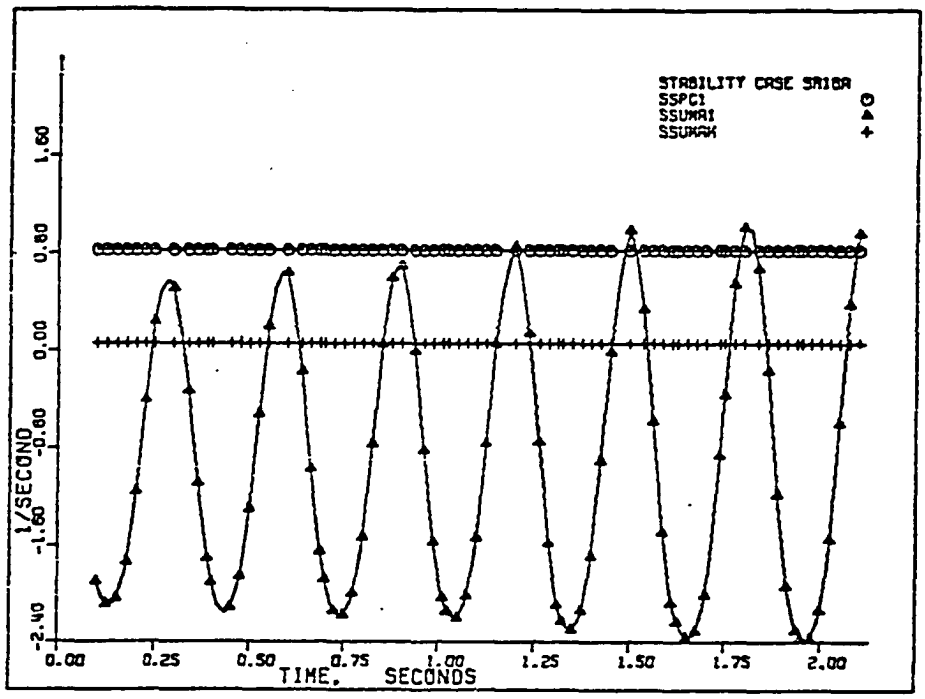

Figure 405. Case SR-16A: terms of equation (4.10).

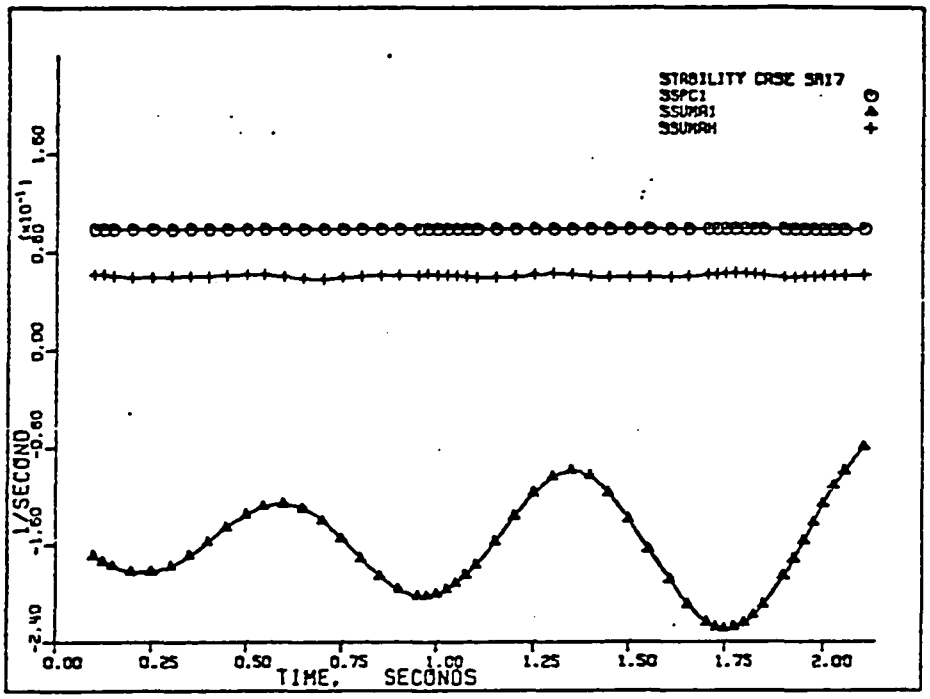

Figure 406. Case SR-17: terms of equation (4.10).

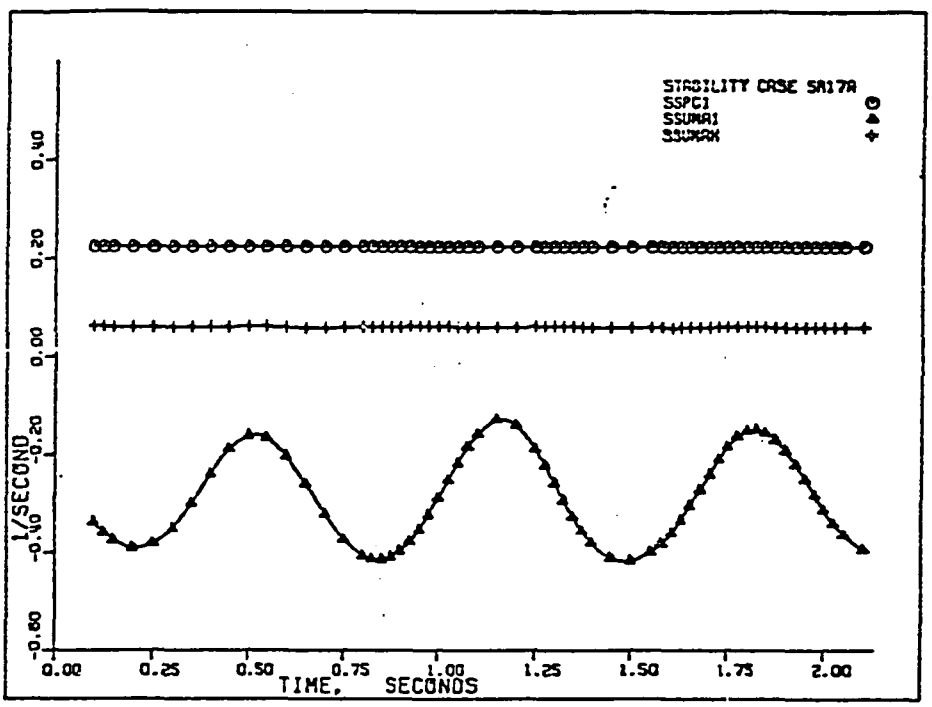

Figure 407. Case SR-17A: terms of equation (4.10).

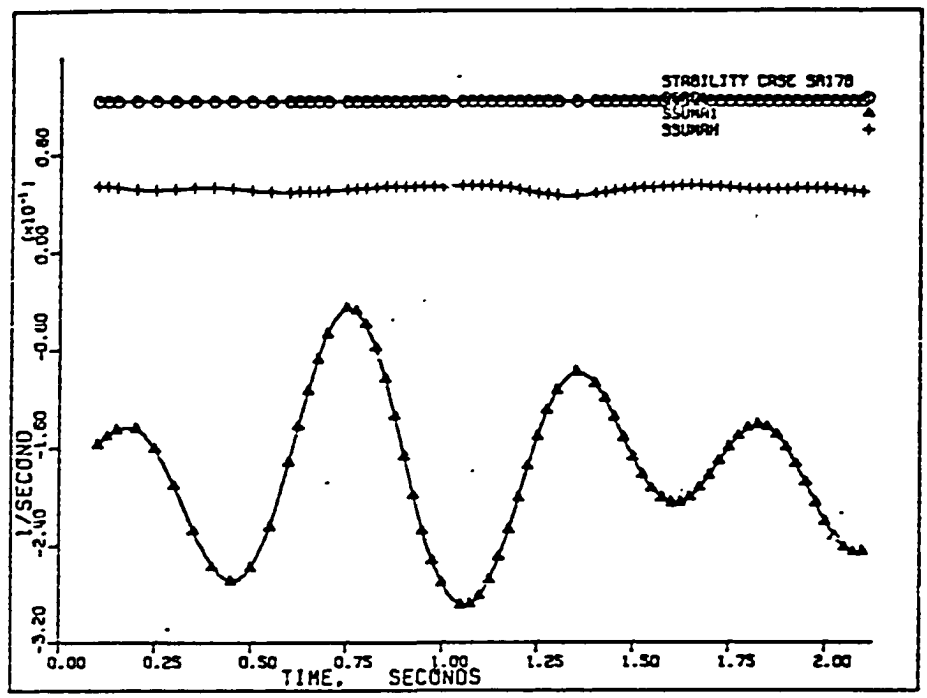

Figure 408. Case SR-17B: terms of equation (4.10).

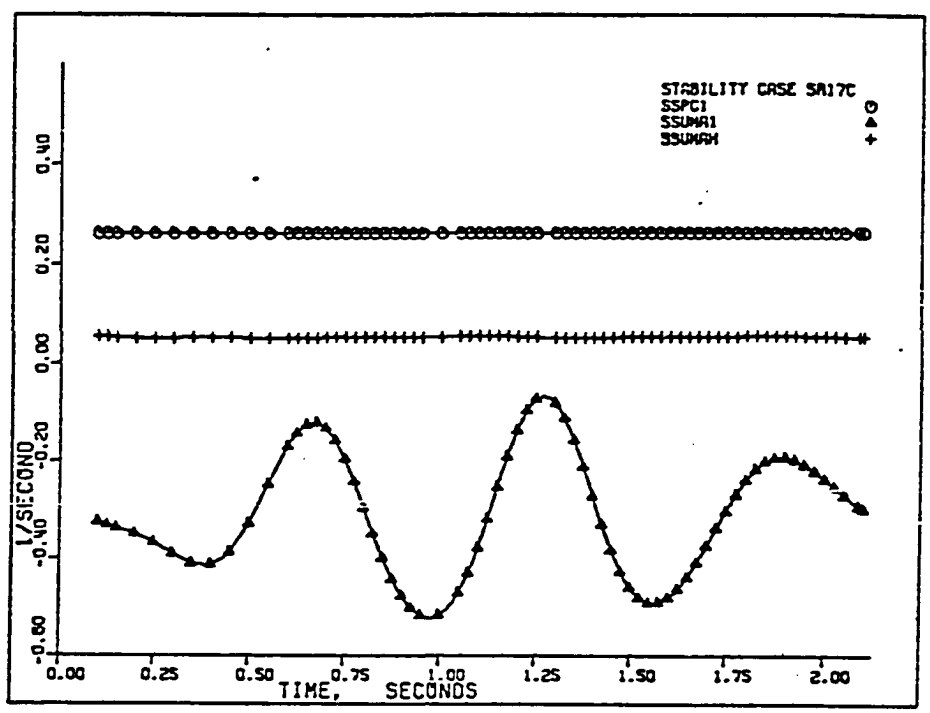

Figure 409. Case SR-17C: terms of equation (4.10).

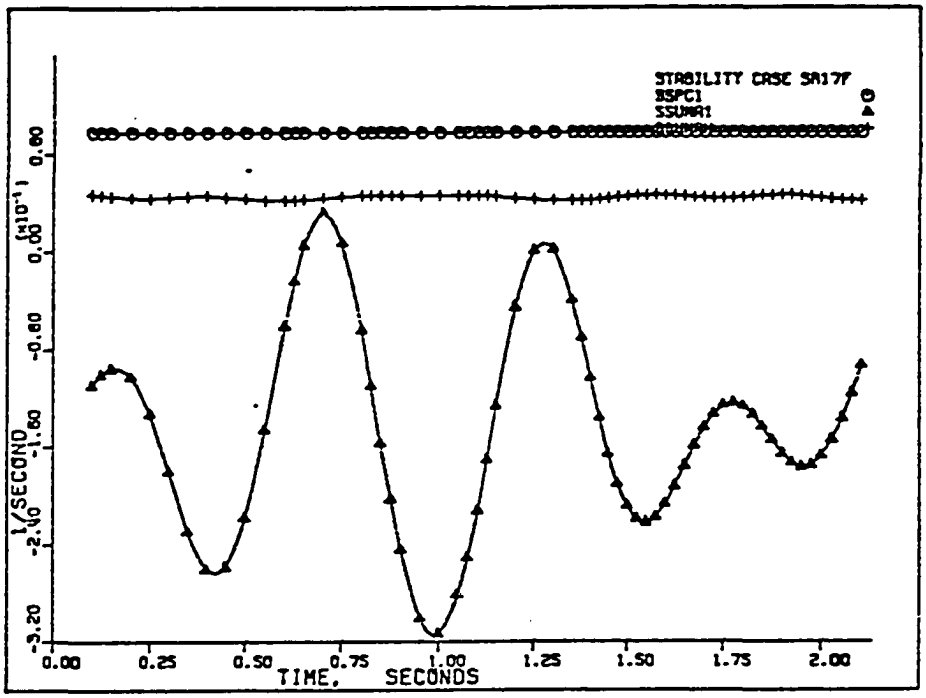

Figure 410. Case SR-17F: terms of equation (4.10).

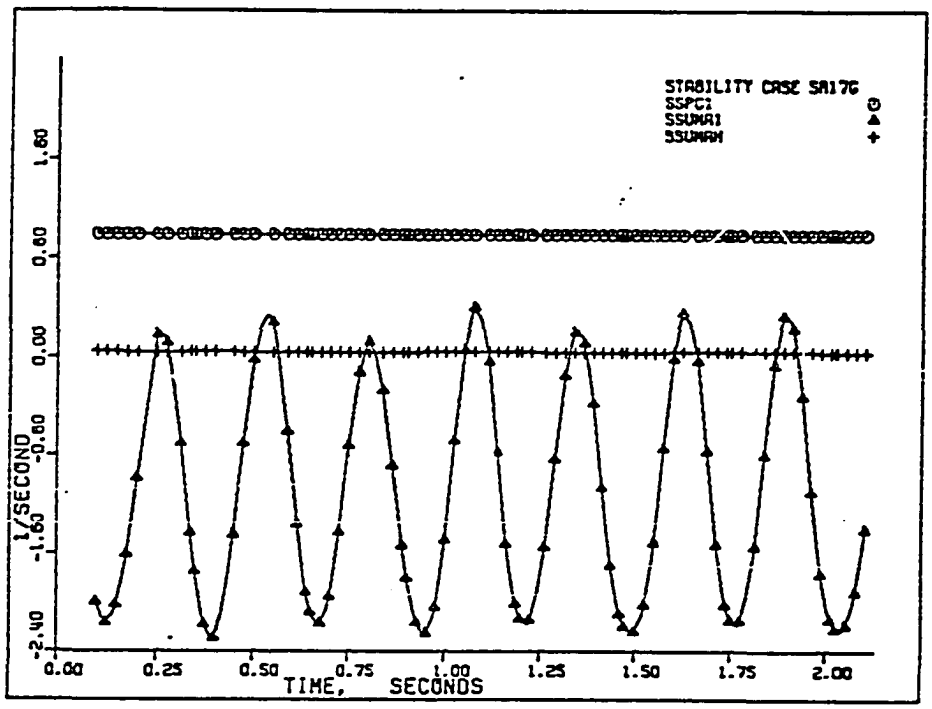

Figure 411. Case SR-17G: terms of equation (4.10).

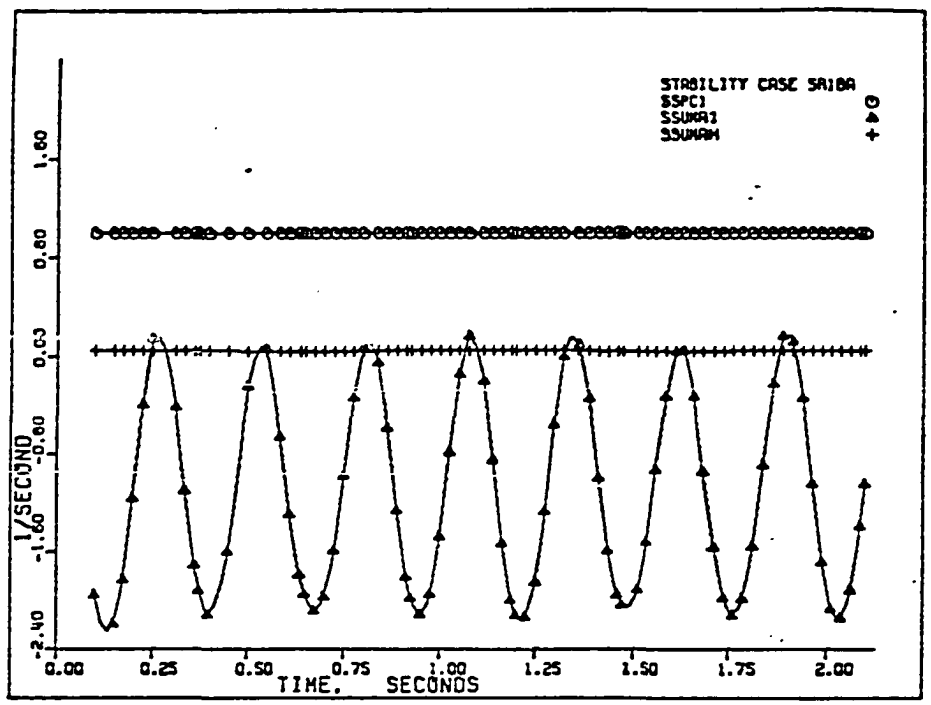

Figure 412. Case SR-18A: terms of equation (4.10).

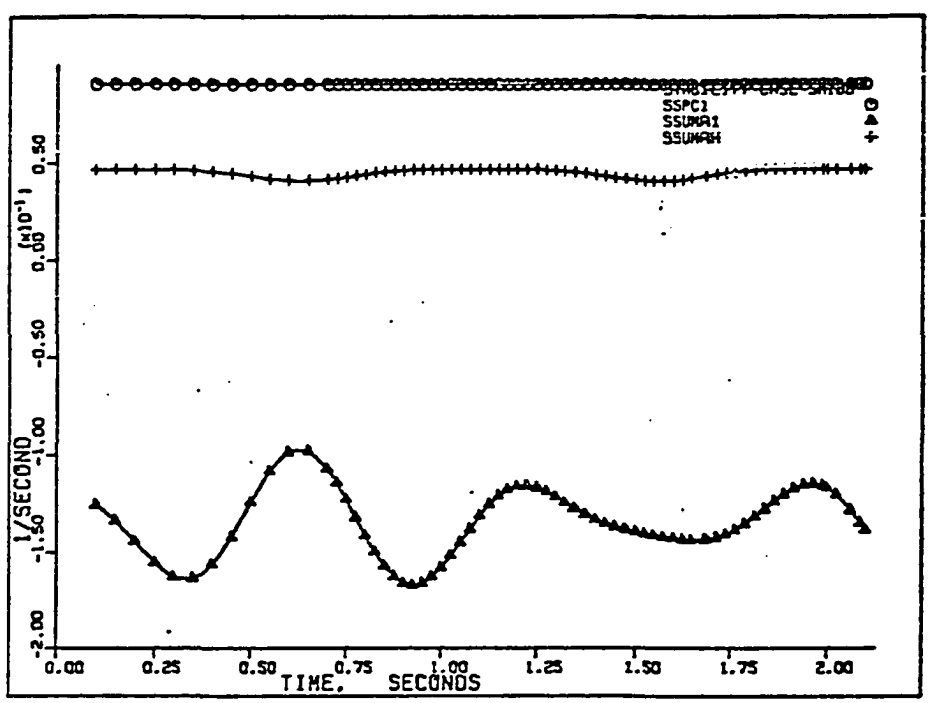

Figure 413. Case SR-18B: terms of equation (4.10).

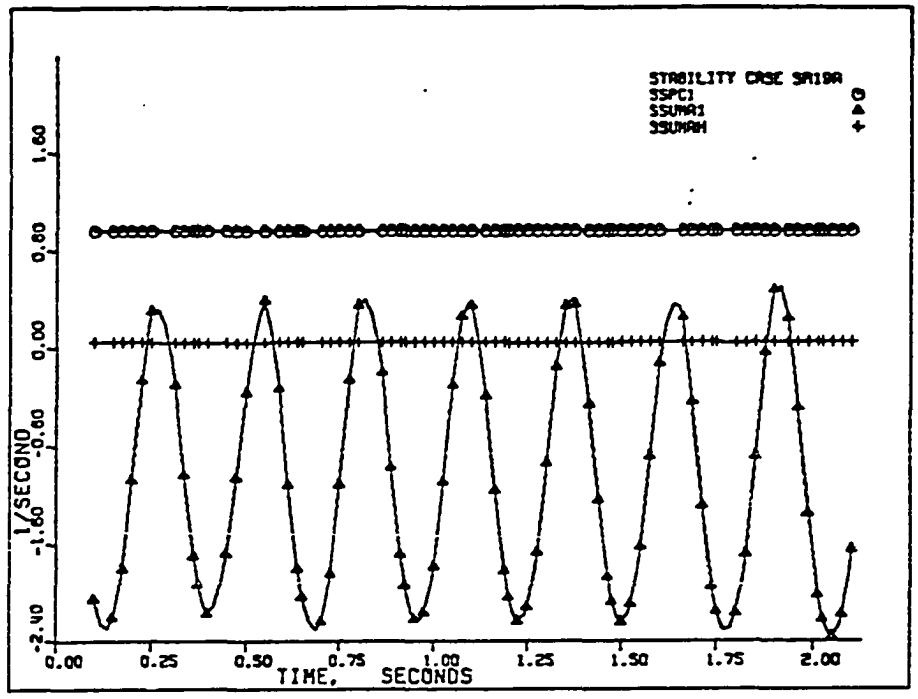

Figure 414. Case SR-19A: terms of equation (4.10).

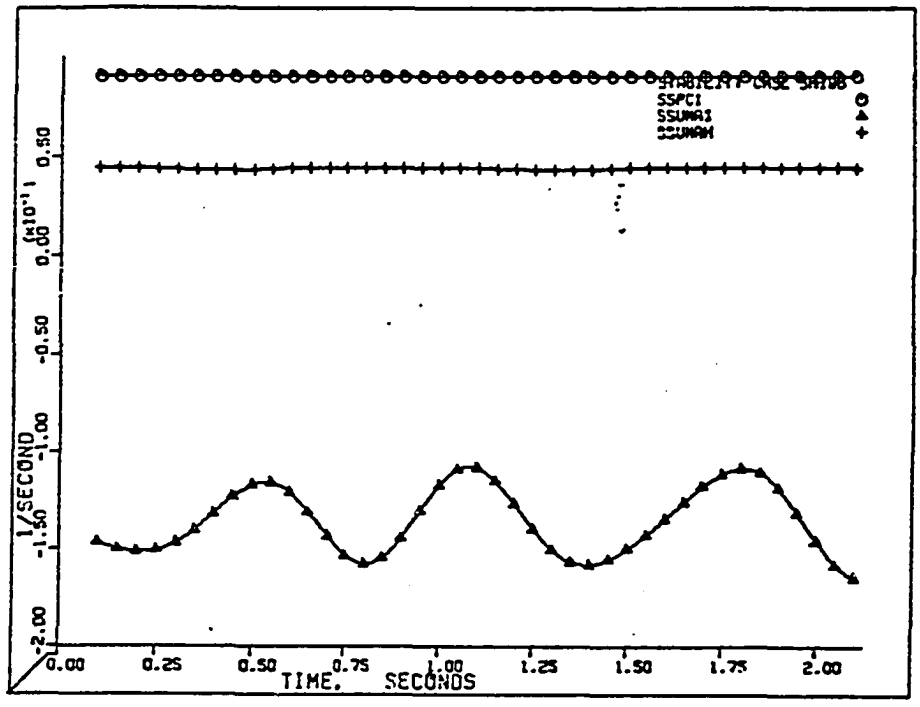

Figure 415. Case SR-19B: terms of equation (4.10).

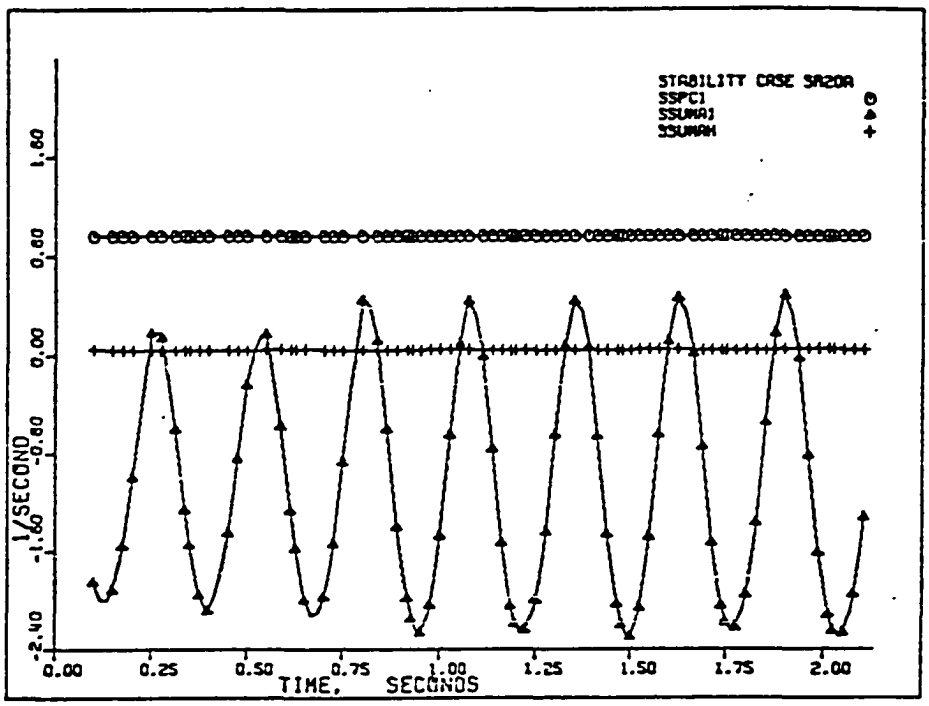

Figure 416. Case SR-20A: terms of equation (4.10).

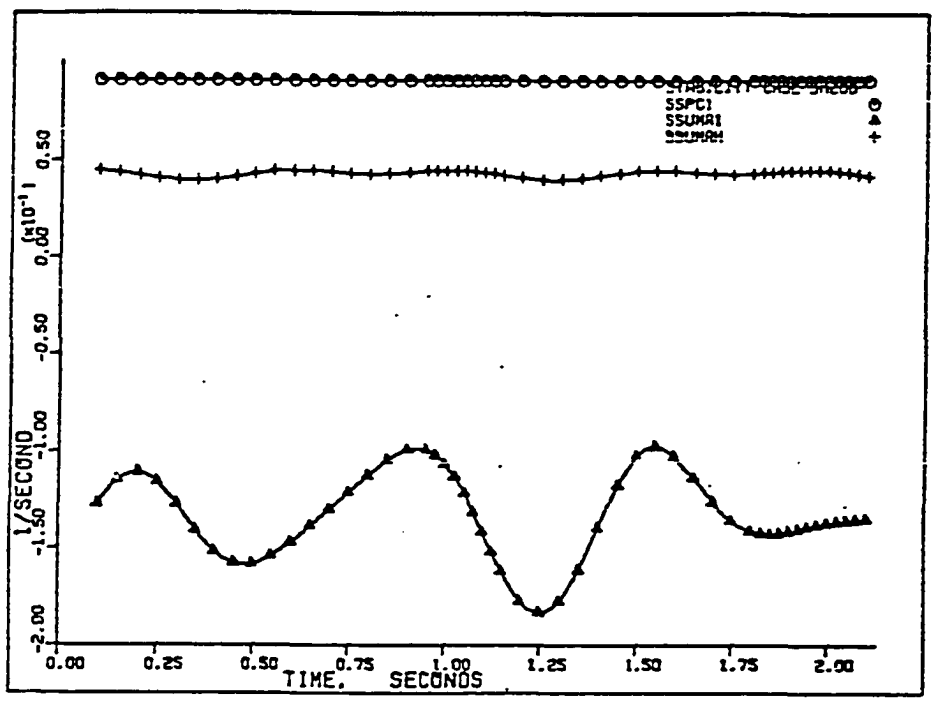

Figure 417. Case SR-20B: terms of equation (4.10).

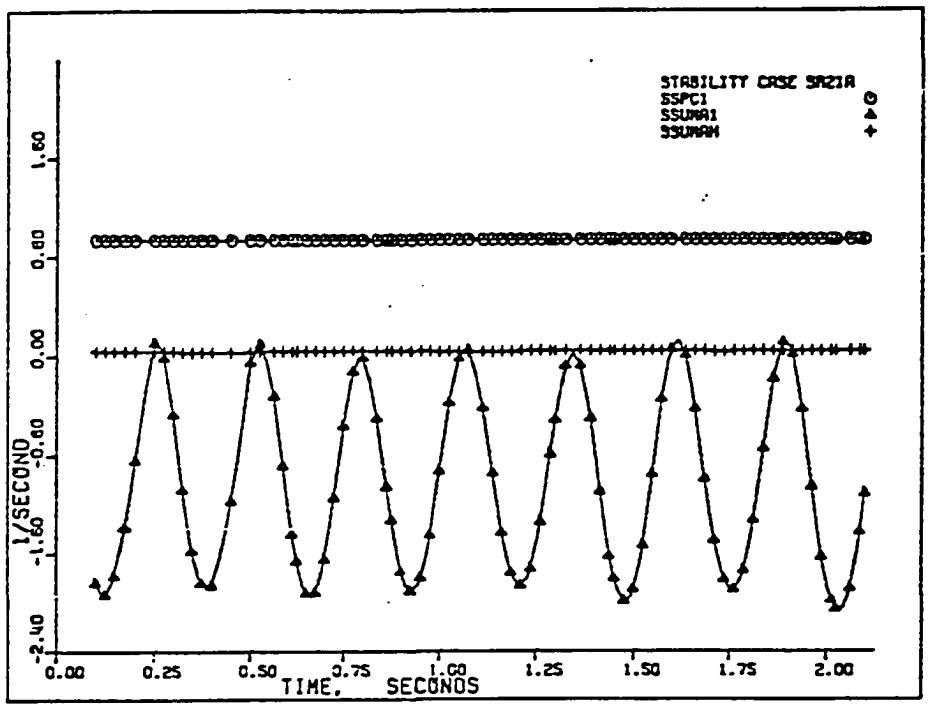

Figure 418. Case SR-21A: terms of equation (4.10).

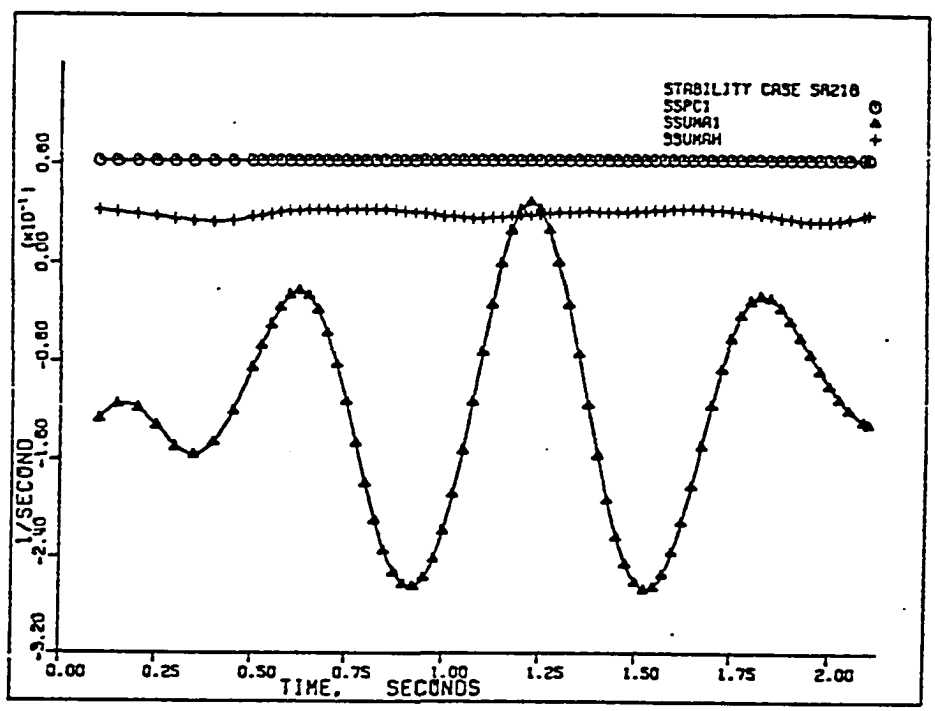

Figure 419. Case SR-21B: terms of equation (4.10).

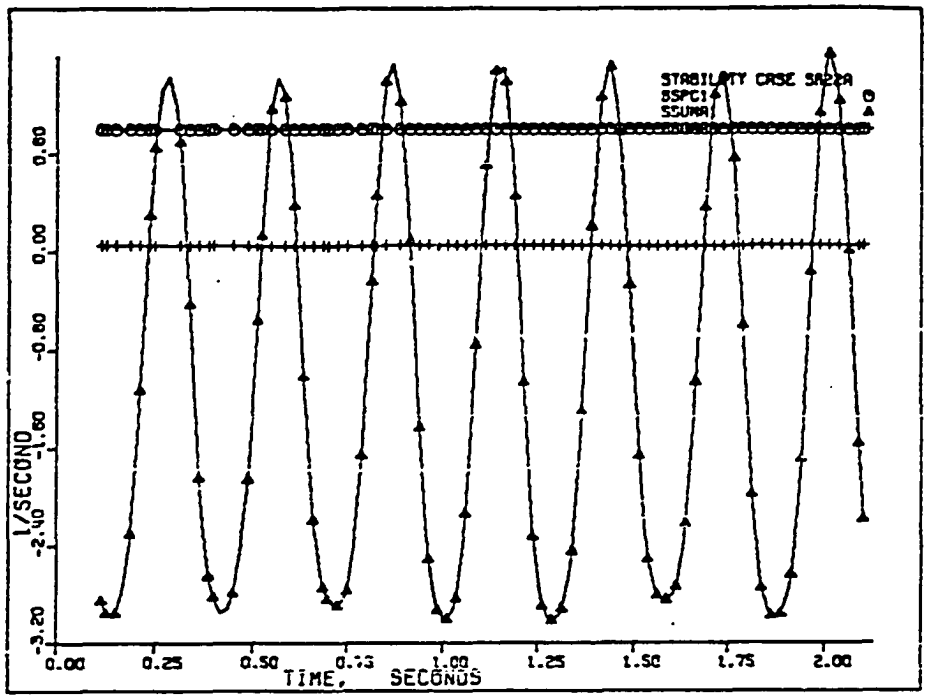

Figure 420. Case SR-22A: terms of equation (4.10).

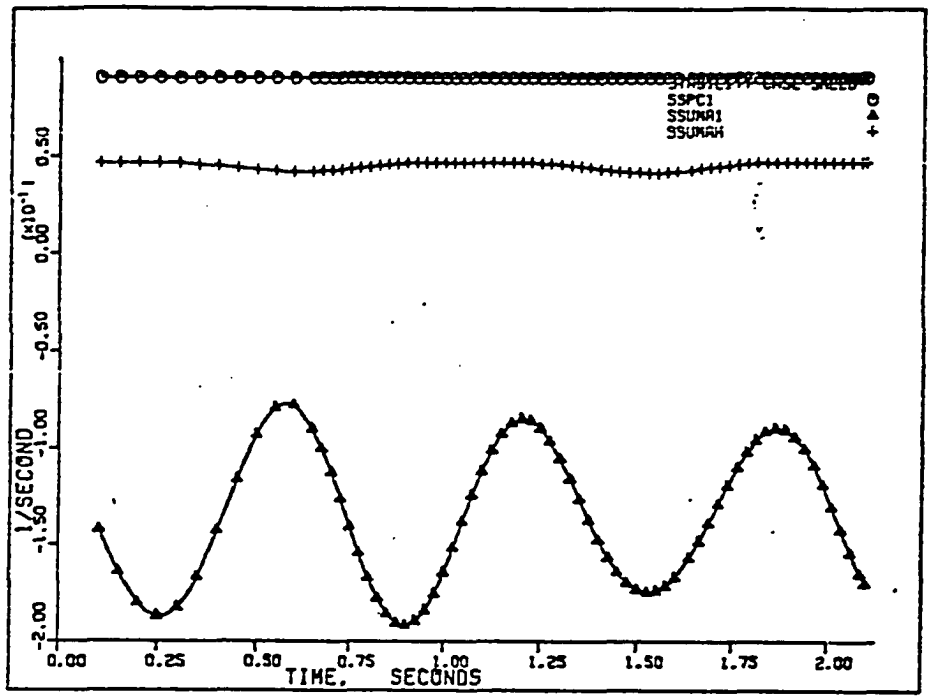

Figure 421. Case SR-22B: terms of equation (4.10).

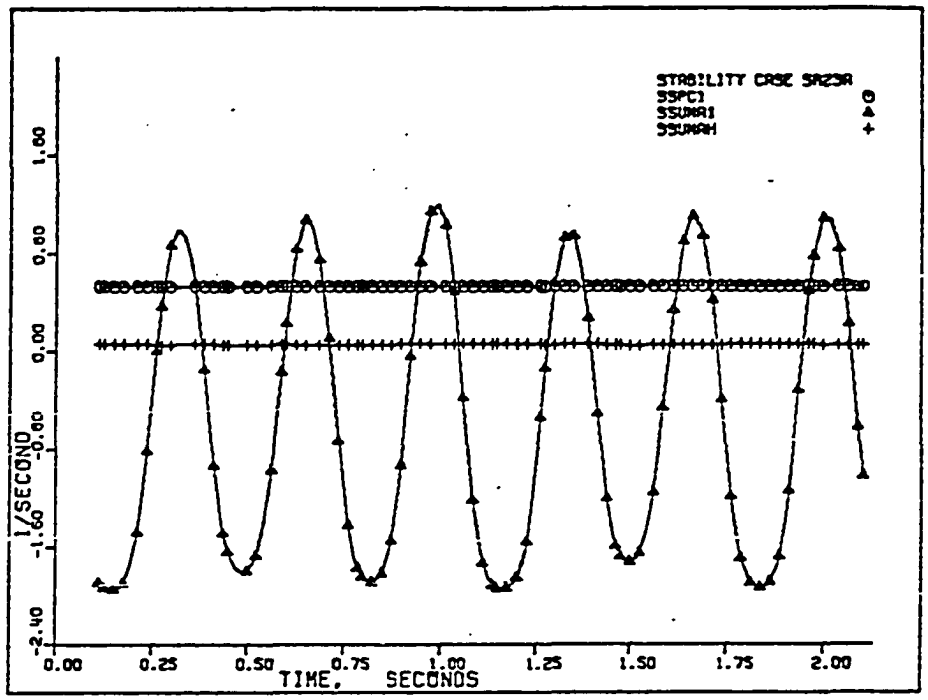

Figure 422. Case SR-23A: terms of equation (4.10).

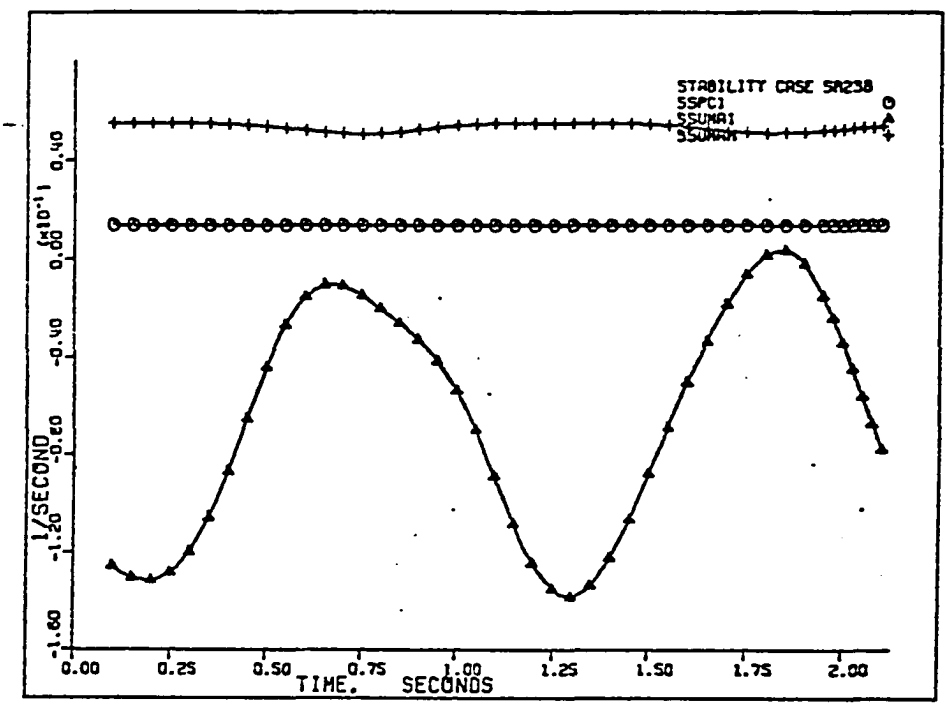

Figure 423. Case SR-23B: terms of equation (4.10).

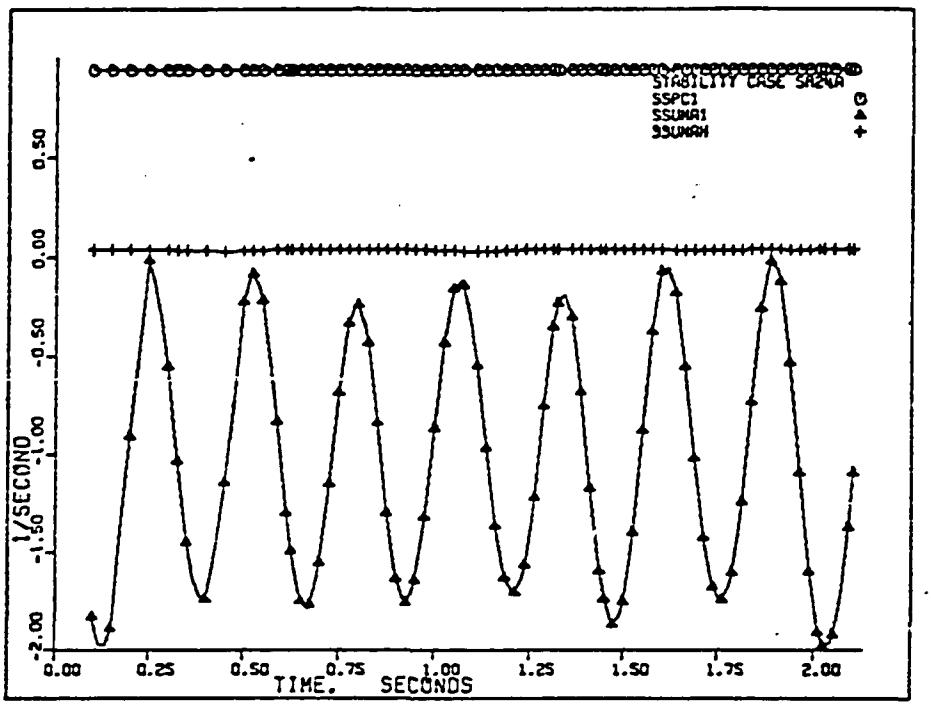

Figure 424. Case SR-24A: terms of equation (4.10).

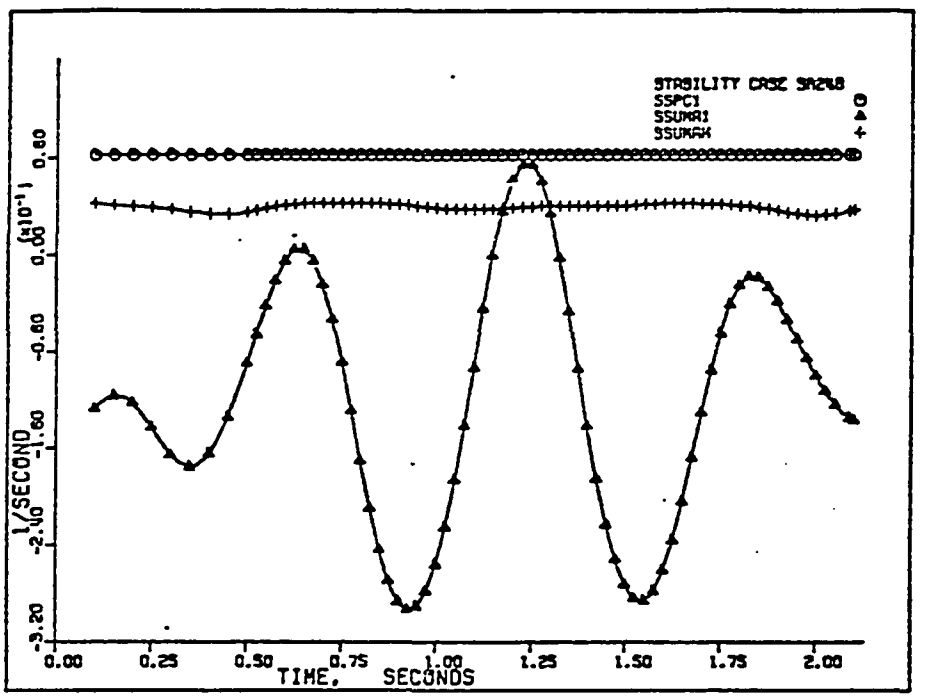

Figure 425. Case SR-24B: terms of equation (4.10).

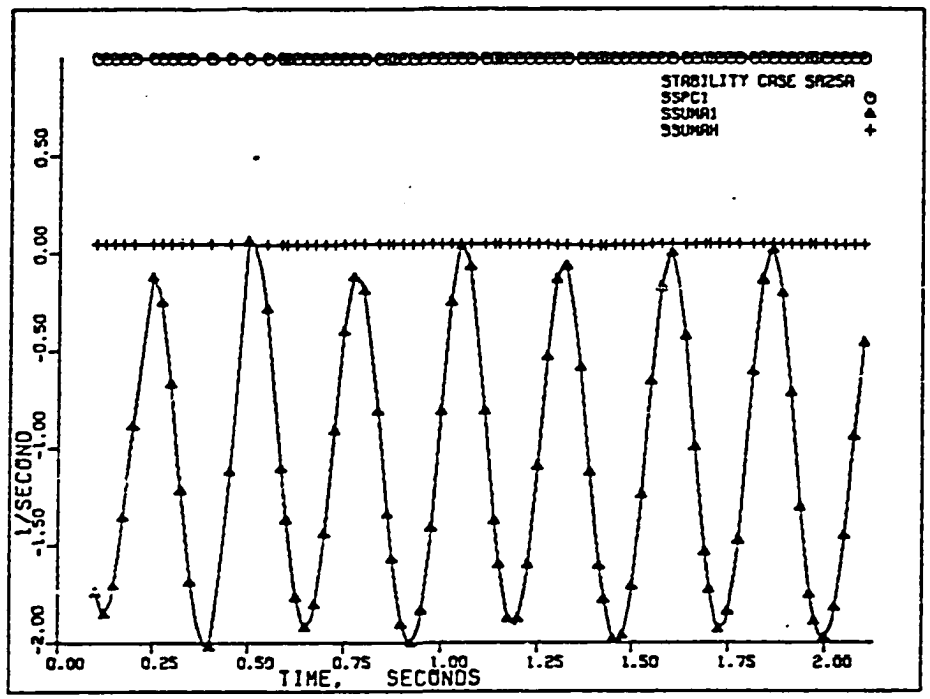

Figure 426. Case SR-25A: terms of equation (4.10).

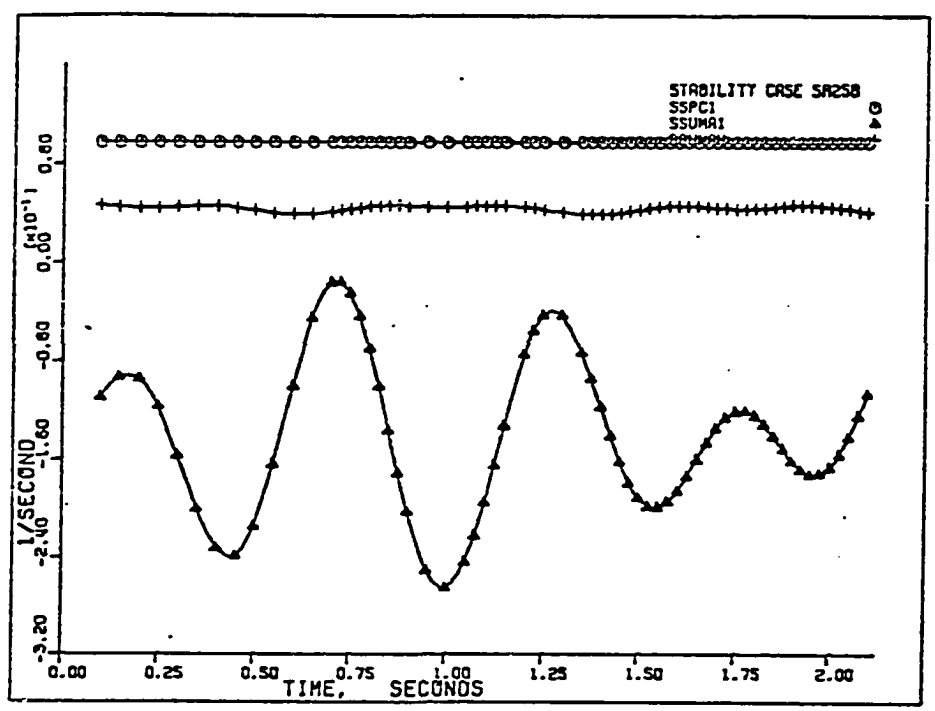

Figure 427. Case SR-25B: terms of equation (4.10).

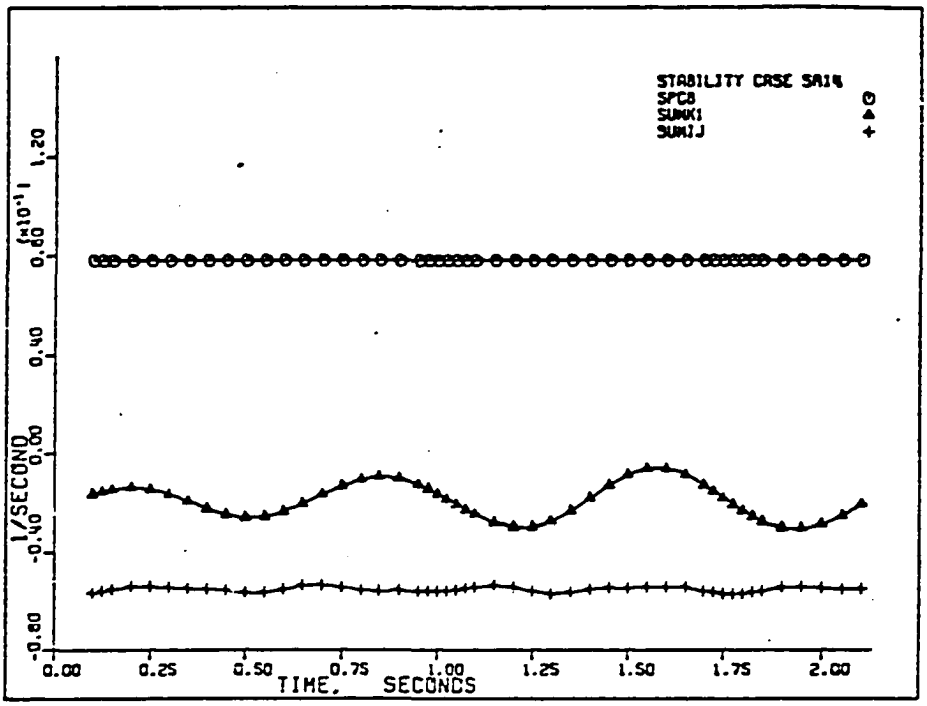

Figure 428. Case SR-14: terms of equation (4.5).

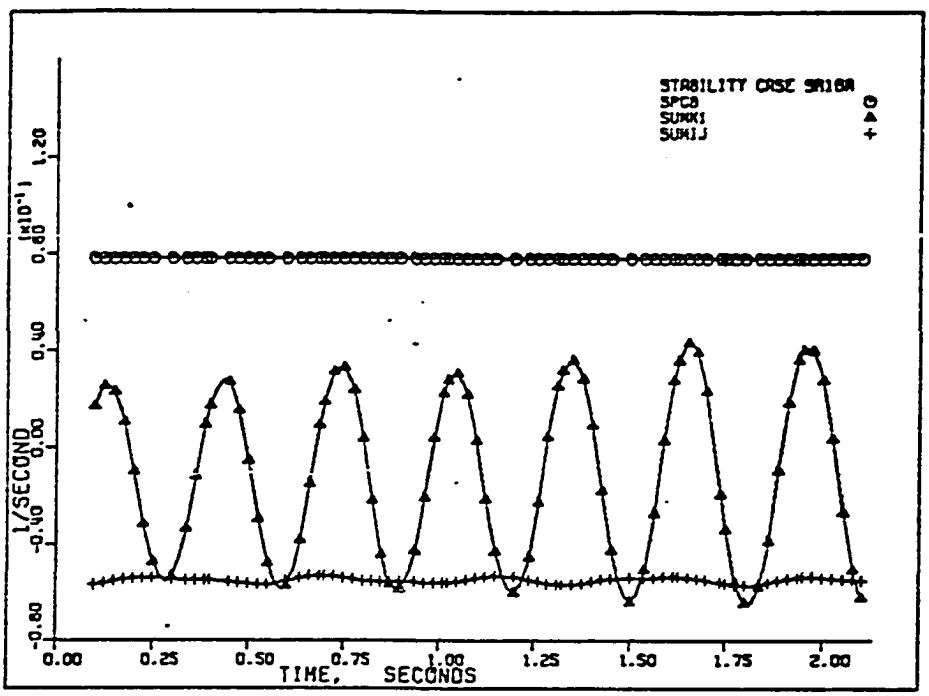

Figure 429. Case SR-16A: terms of equation (4.5).

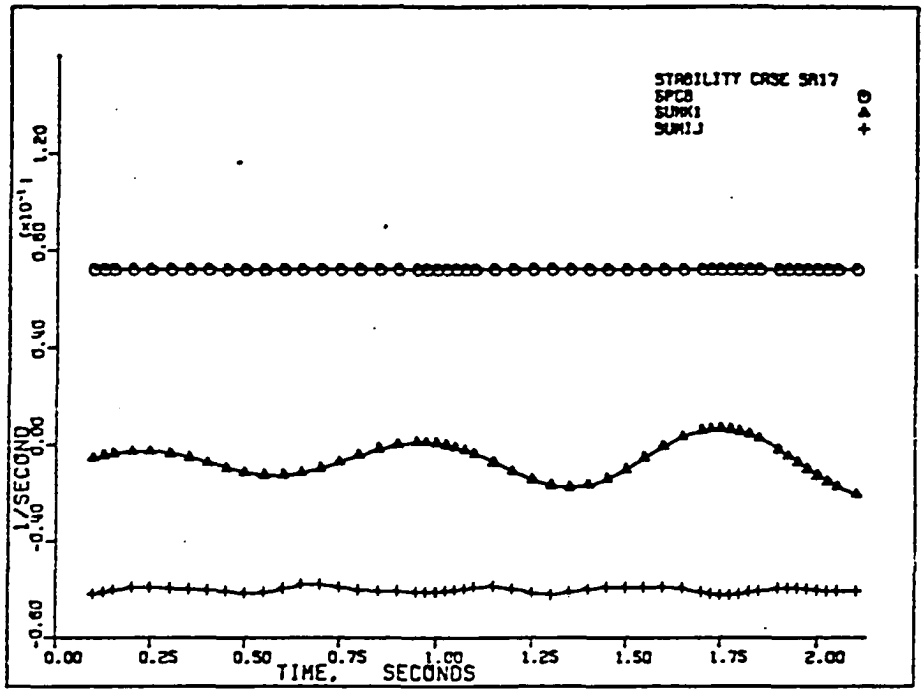

Figure 430. Case SR-17: terms of equation (4.5).

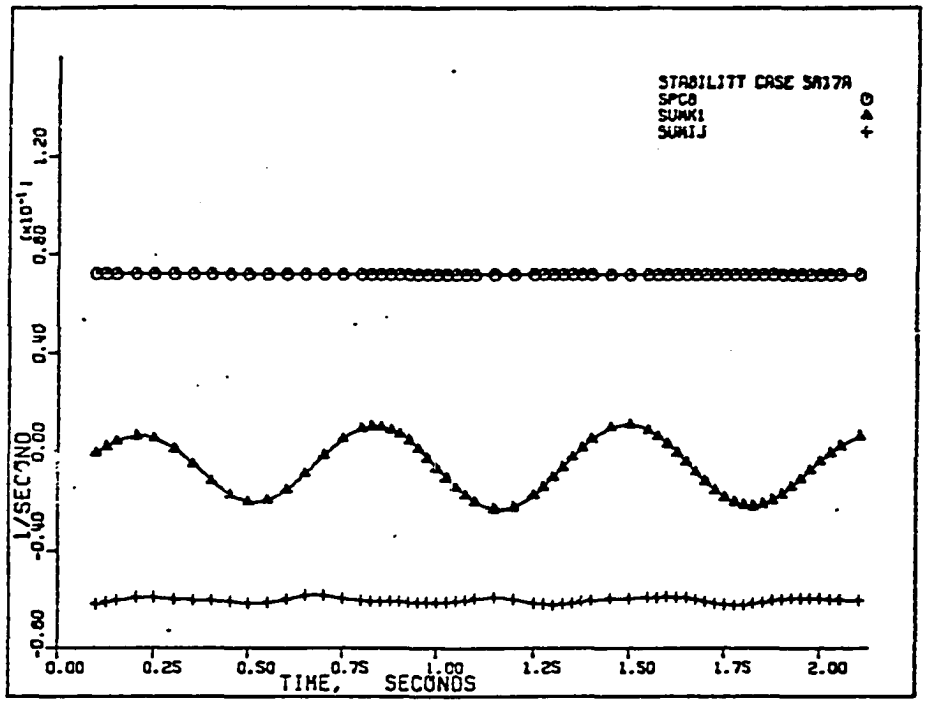

Figure 431. Case SR-17A: terms of equation (4.5).

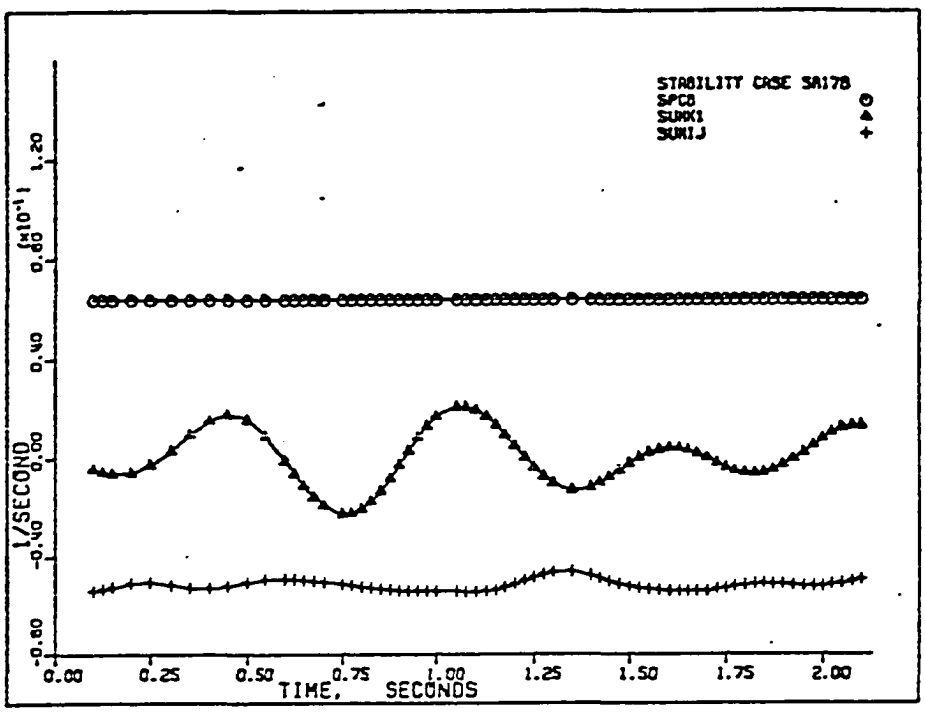

Figure 432. Case SR-17B: terms of equation (4.5).

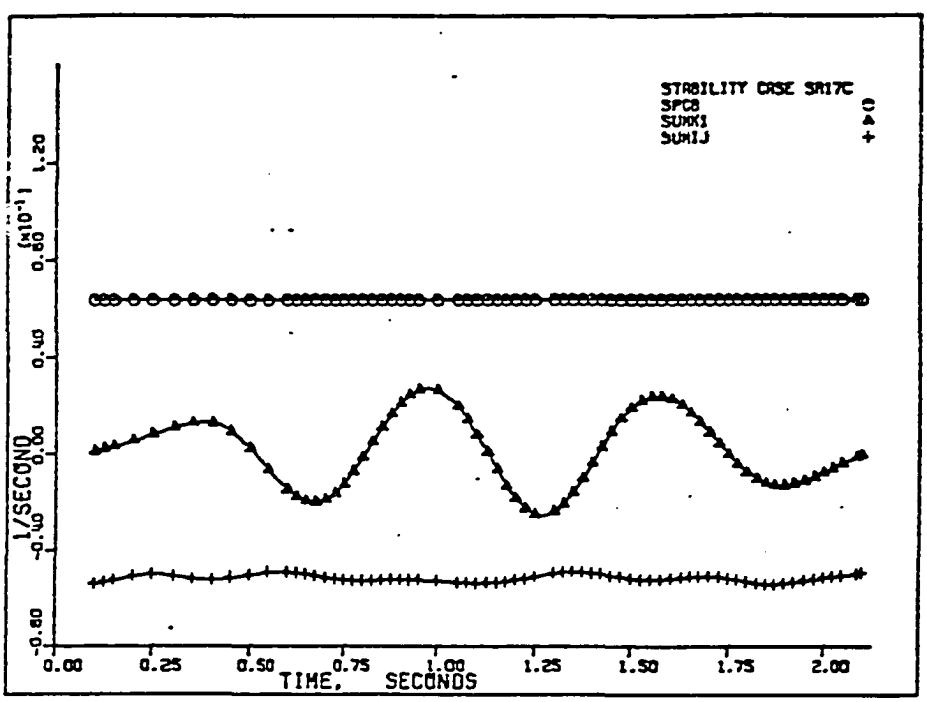

Figure 433. Case SR-17C: terms of equation (4.5).

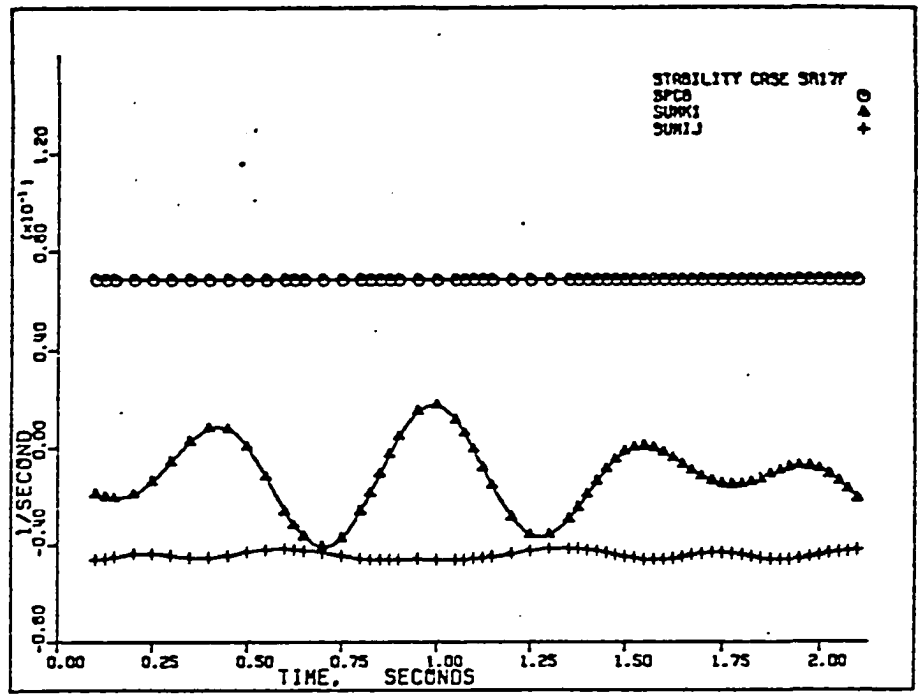

Figure 434. Case SR-17F: terms of equation (4.5).

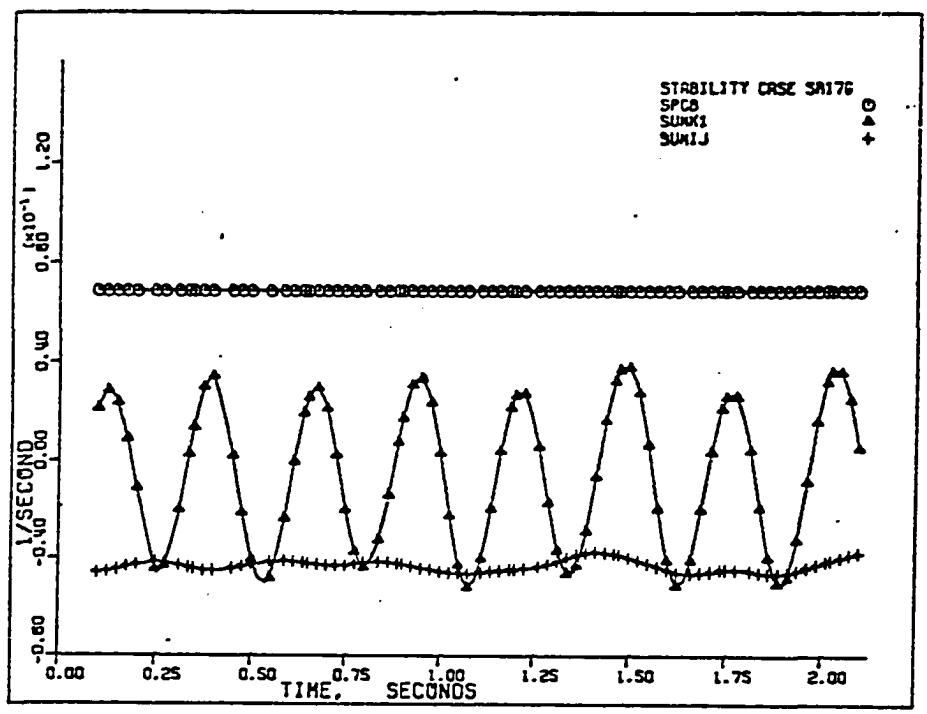

Figure 435. Case SR-17G: terms of equation (4.5).

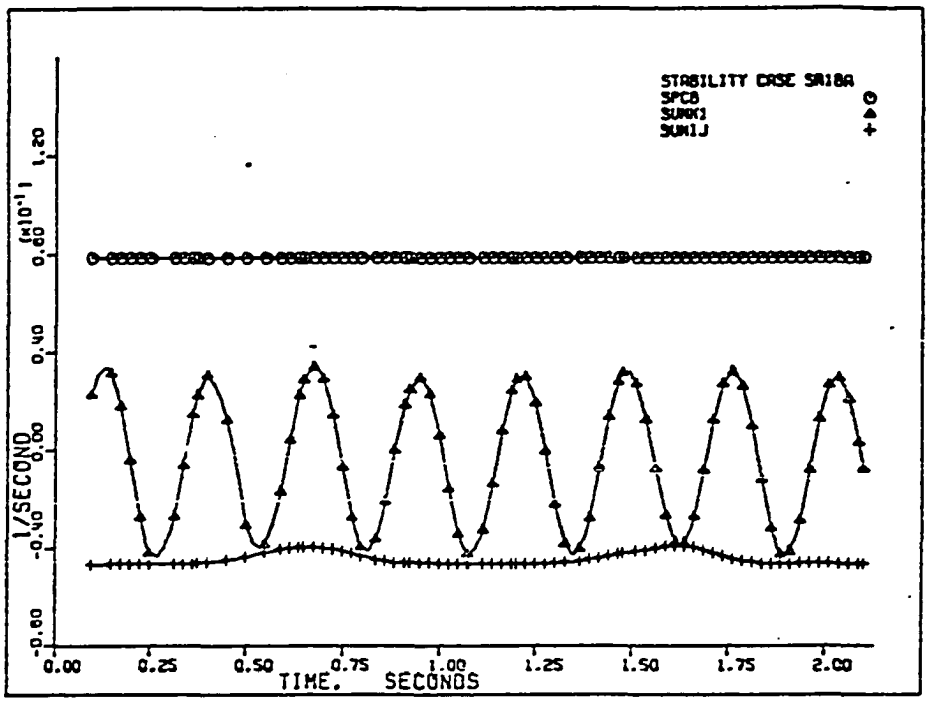

Figure 436. Case SR-18A: terms of equation (4.5).

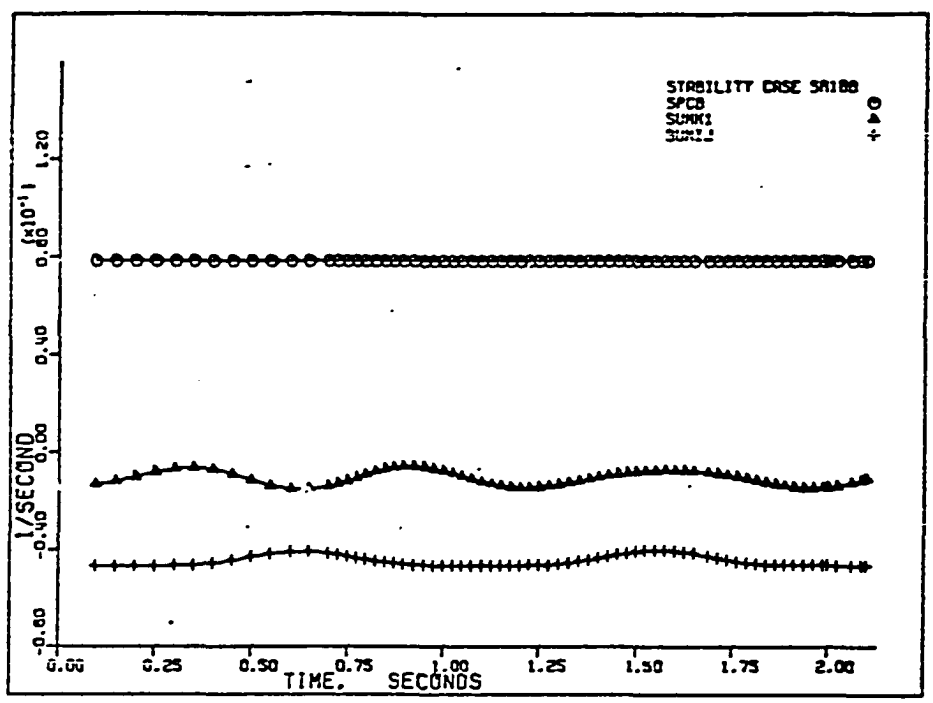

Figure 437. Case SR-18B: terms of equation (4.5).

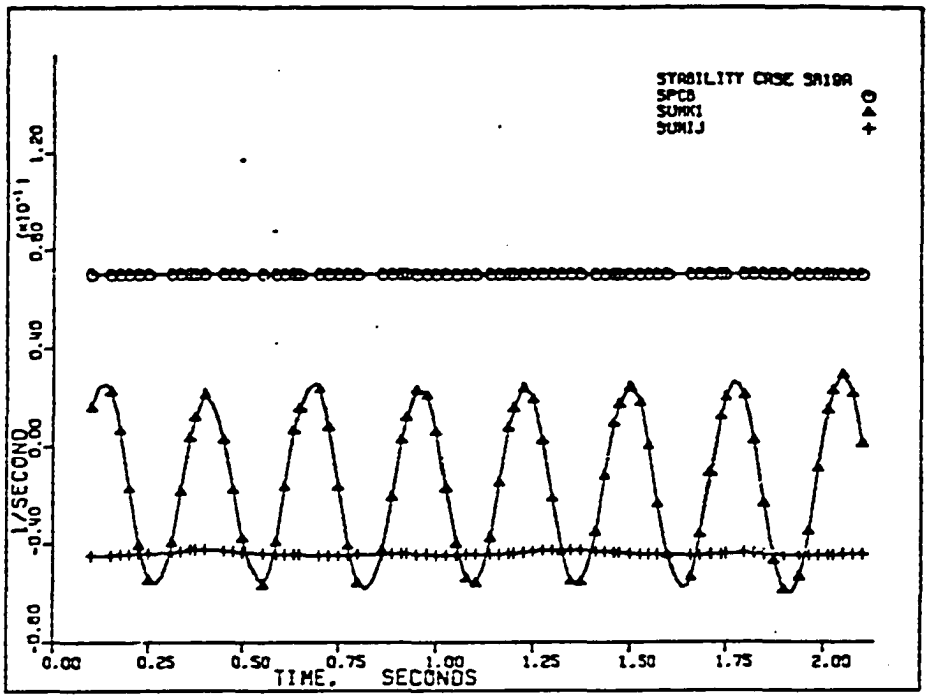

Figure 438. Case SR-19A: terms of equation (4.5).

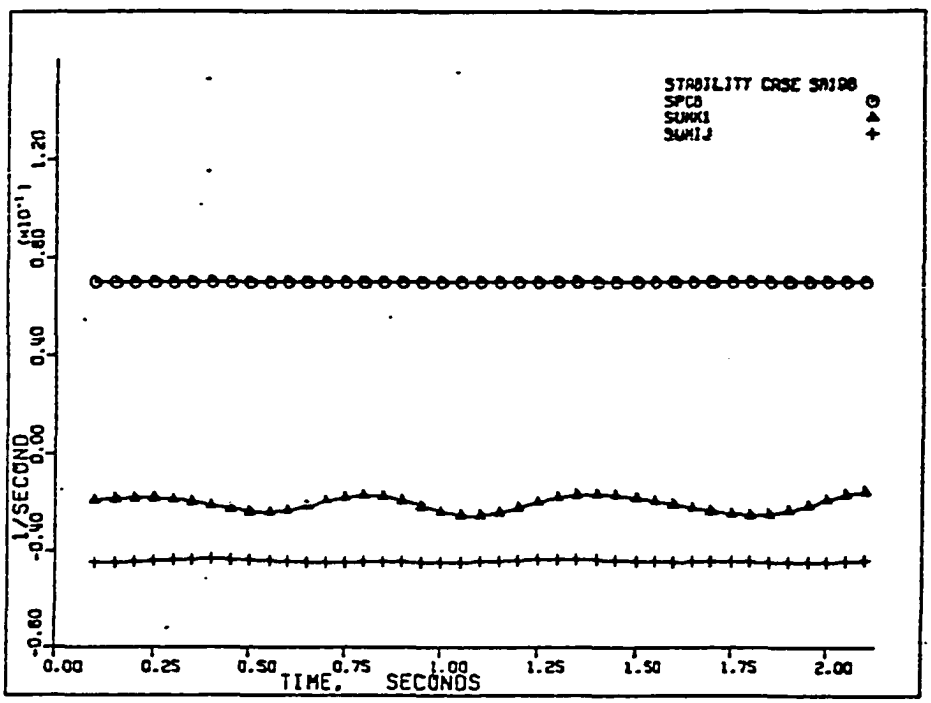

Figure 439. Case SR-19B: terms of equation (4.5).

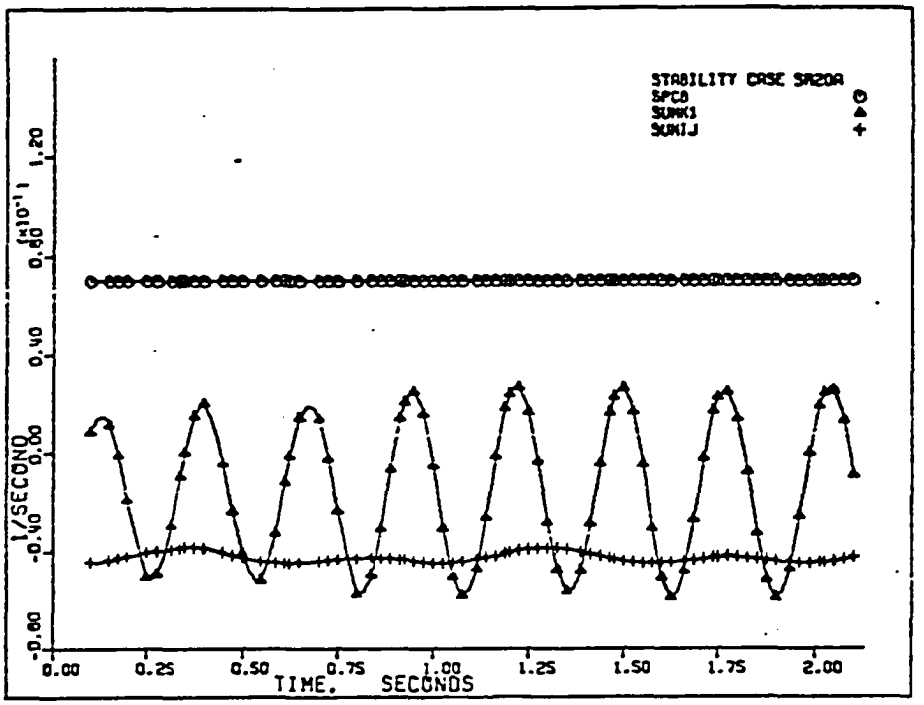

Figure 440. Case SR-20A: terms of equation (4.5).

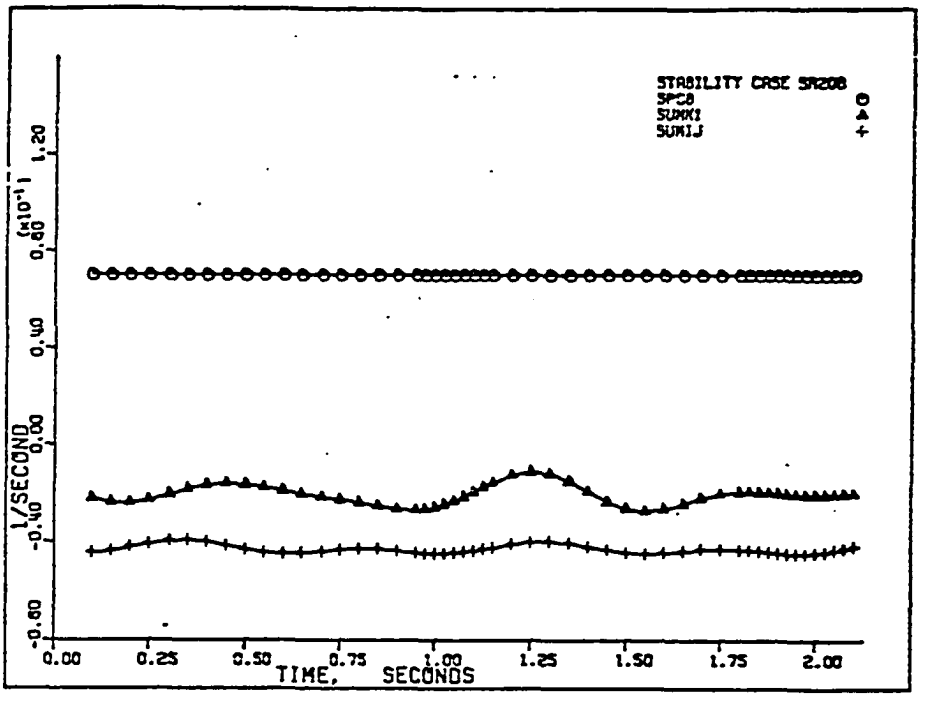

Figure 441. Case SR-20B: terms of equation (4.5).

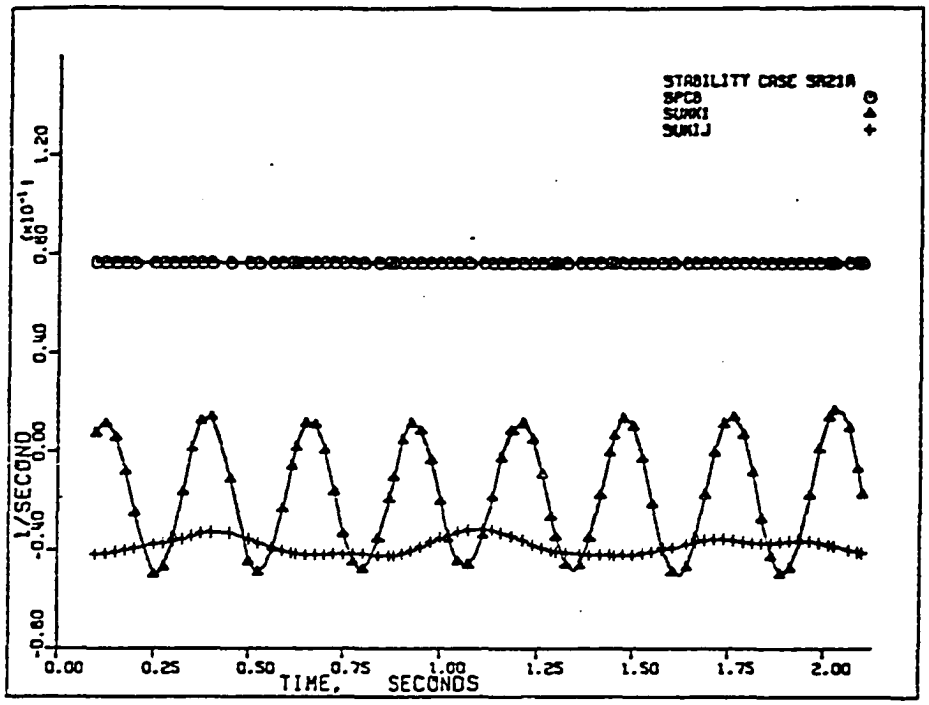

Figure 442. Case SR-21A: terms of equation (4.5).

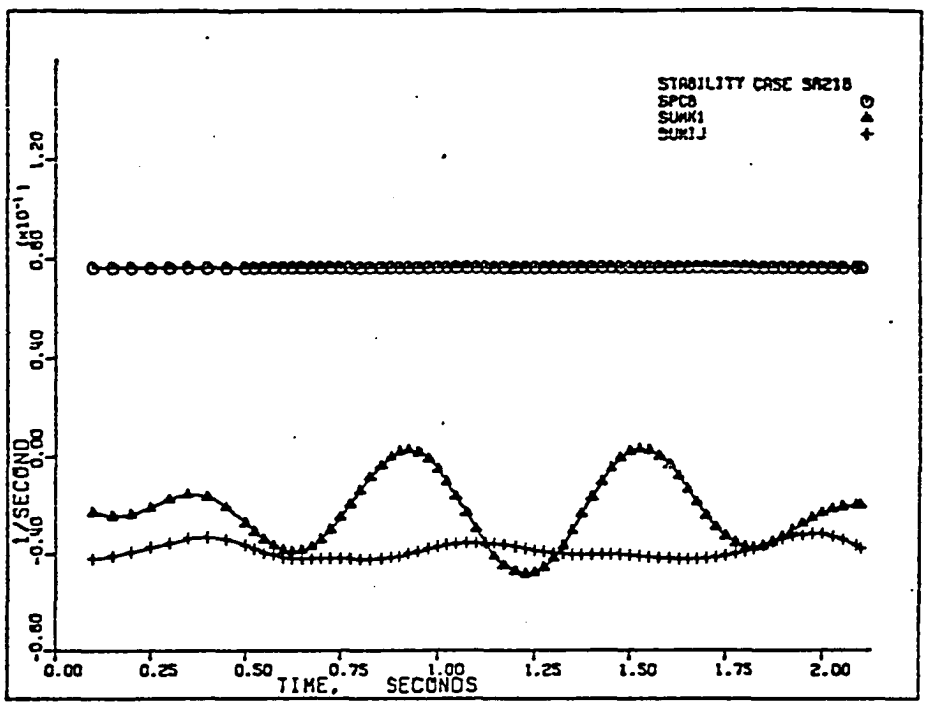

Figure 443. Case SR-21B: terms of equation (4.5).

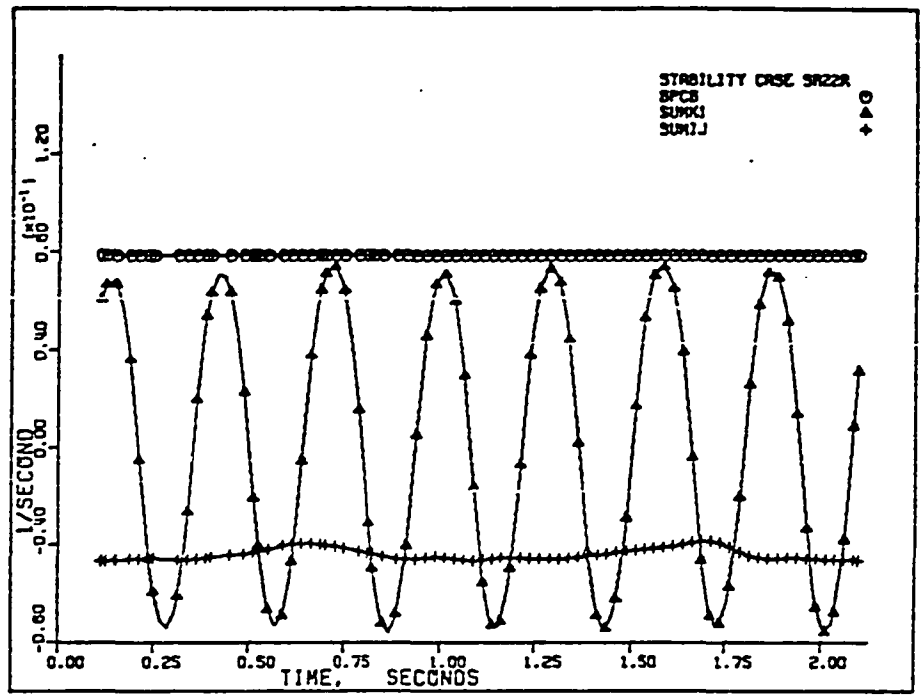

Figure 444. Case SR-22A: terms of equation (4.5).

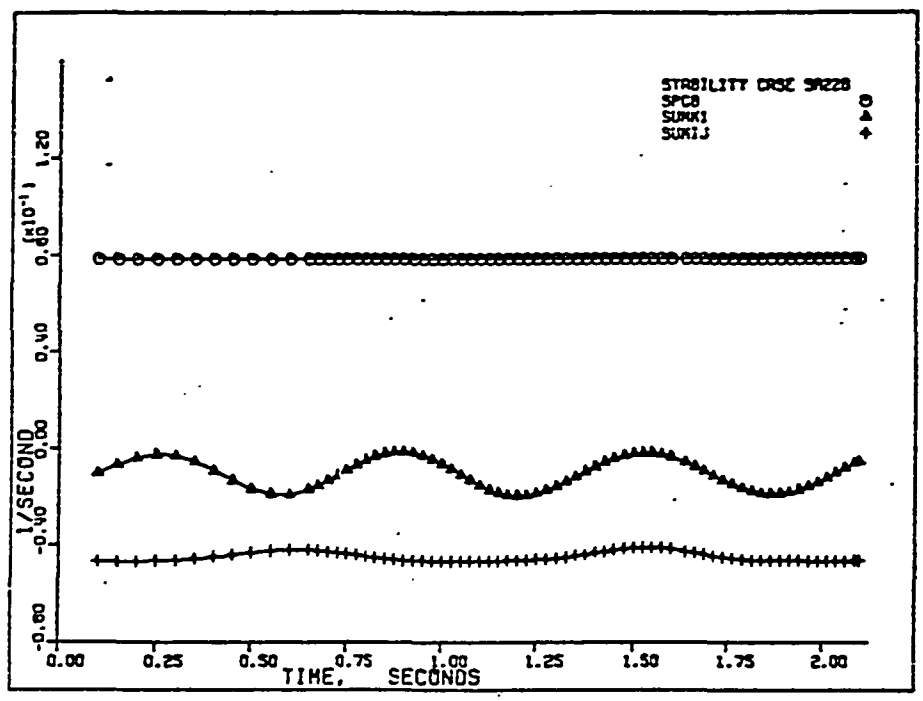

Figure 445. Case SR-22B: terms of equation (4.5).

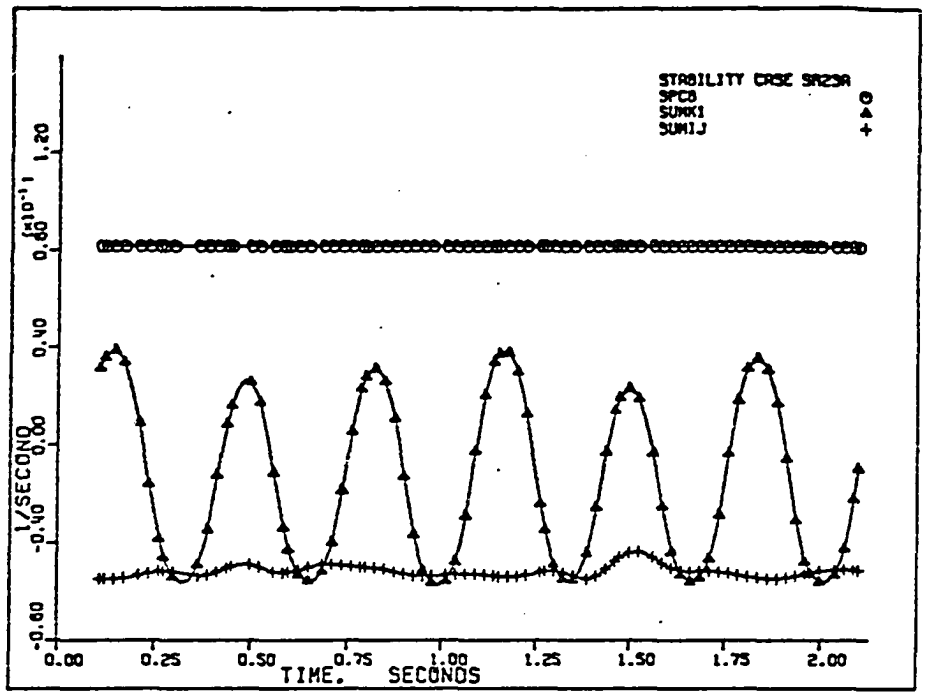

Figure 446. Case SR-23A: terms of equation (4.5).

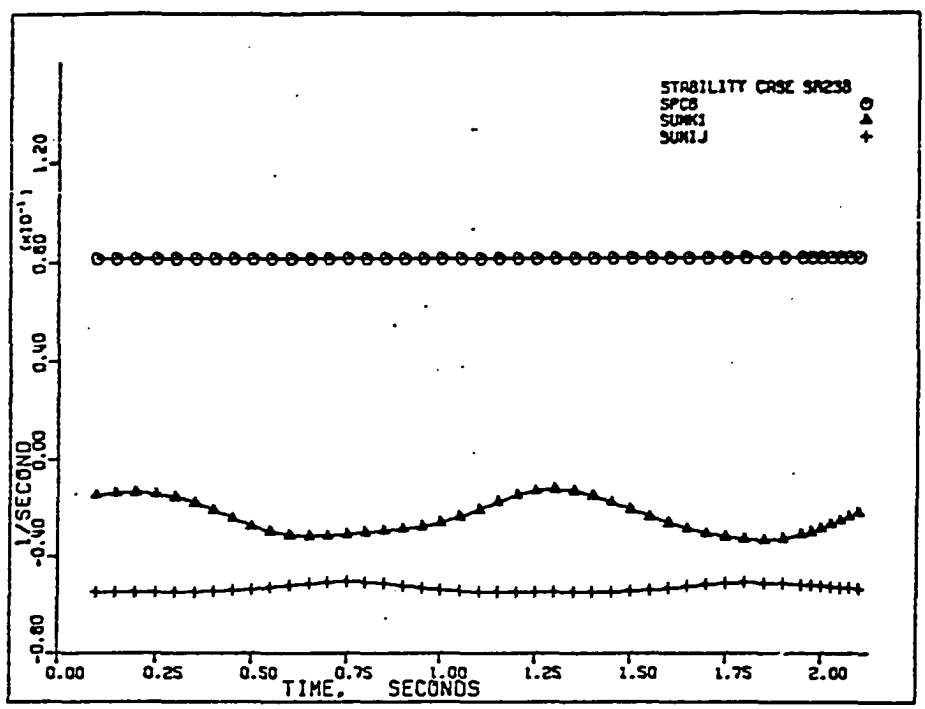

Figure 447. Case SR-23B: terms of equation (4.5).

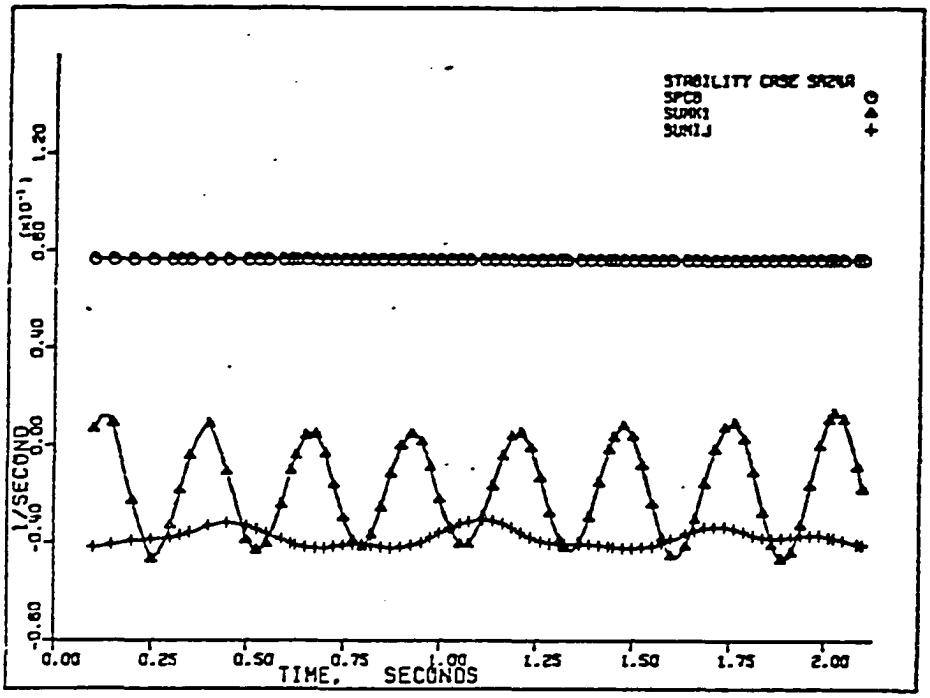

Figure 448. Case SR-24A: terms of equation (4.5).

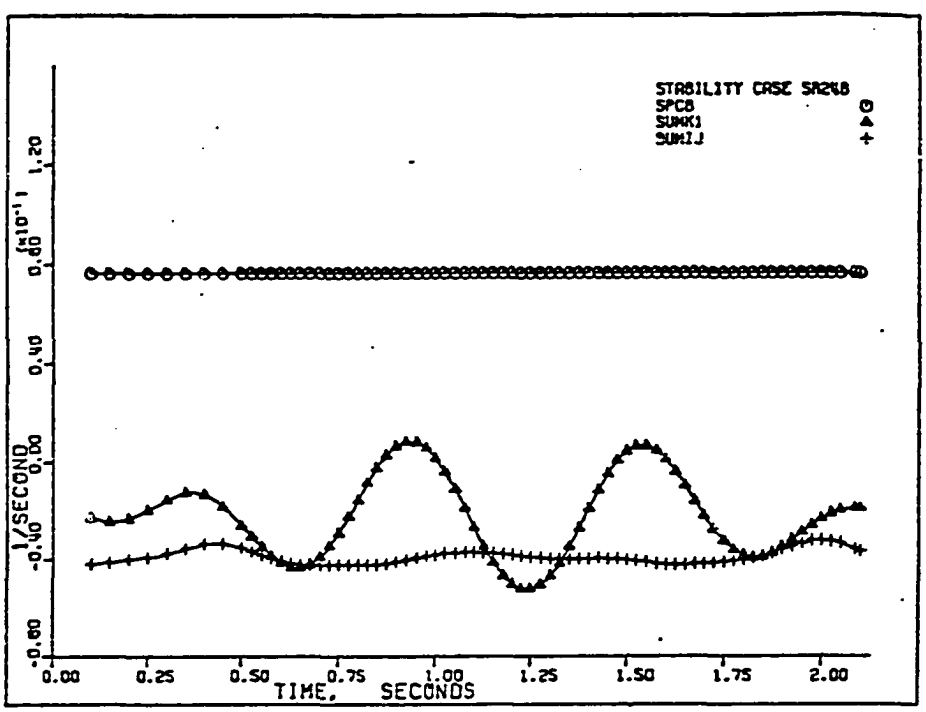

Figure 449. Case SR-24B: terms of equation (4.5).

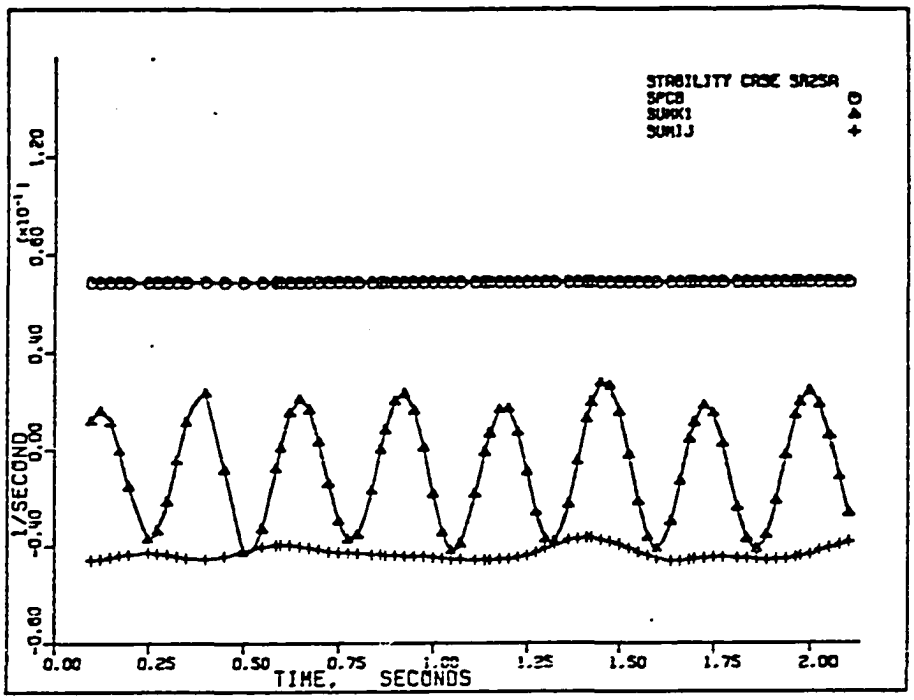

Figure 450. Case SR-25A: terms of equation (4.5).

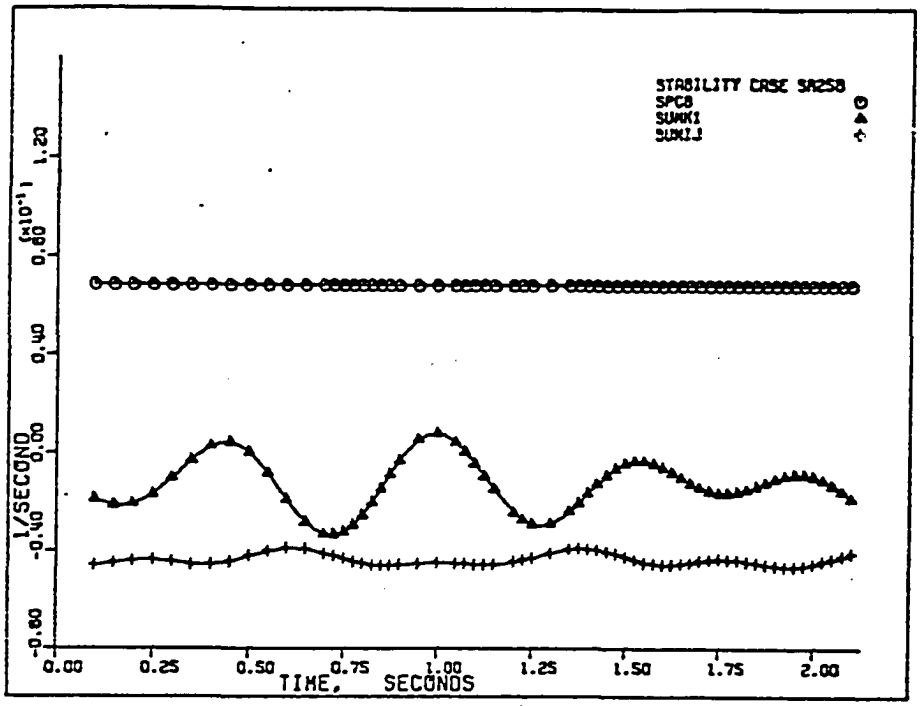

Figure 451. Case SR-25B: terms of equation (4.5).